

MCP/83

**MONASH UNIVERSITY
'THESIS ACCEPTED' IN SATISFACTION OF THE
REQUIREMENTS FOR THE DEGREE OF
DOCTOR OF PHILOSOPHY**

ON..... 8 February 2005.....
.....

Sec. Research Graduate School Committee

Under the Copyright Act 1968, this thesis must be used only under the normal conditions of scholarly fair dealing for the purposes of research, criticism or review. In particular no results or conclusions should be extracted from it, nor should it be copied or closely paraphrased in whole or in part without the written consent of the author. Proper written acknowledgement should be made for any assistance obtained from this thesis.

**ENHANCEMENT OF THE
PERCUTANEOUS ABSORPTION
OF THE OPIOID ANALGESIC FENTANYL**

A thesis submitted for the degree of

DOCTOR OF PHILOSOPHY

By

Brigette Danielle Traversa B.Pharm.(Hons)

Department of Pharmaceutics,
Victorian College of Pharmacy, Monash University
381 Royal Parade, Parkville
Victoria, Australia 3052

June 2004

CONTENTS

Abstract	i
Statement of originality	iii
Acknowledgments	iv
Communications	v
Abbreviations and symbols	vi

CHAPTER 1: INTRODUCTION

1.1. STRUCTURE AND FUNCTION OF THE SKIN	1
1.1.1 Epidermis	3
1.1.1.1. Stratum basale	4
1.1.1.2. Stratum spinosum	5
1.1.1.3. Stratum granulosm	6
1.1.1.4. Final stages of keratinocyte differentiation	6
1.1.1.5. Other cells in the epidermis	7
1.1.2 Dermis	8
1.1.3 Hypodermis	8
1.1.4 Vascular, lymphatic and neural systems within the skin	9
1.1.5 Skin appendages	10
1.1.5.1. Hair	10
1.1.5.2. Sebaceous glands	11
1.1.5.3. Sweat glands	11
1.1.5.4. Nails	12
1.2. STRUCTURE, DYNAMICS AND BARRIER FUNCTION OF THE STRATUM CORNEUM	13
1.2.1. Assignment of the stratum corneum as the main rate-limiting barrier of the skin	13
1.2.2. Components of the stratum corneum	14
1.2.2.1. Corneocytes	14
1.2.2.2. Cornified cell envelope	15
1.2.2.3. Corneodesmosomes	17
1.2.2.4. Intercellular lipids	17
1.2.3. Relationship between stratum corneum microstructure and barrier function	21
1.2.4. Desquamation	23

1.2.5. Repair of barrier function following perturbation	24
1.3. PRINCIPLES OF PERCUTANEOUS DRUG ABSORPTION	24
1.3.1. Drug absorption through the skin	24
1.3.2. Transport pathways through the stratum corneum	27
1.3.3. Factors affecting percutaneous drug absorption	29
1.3.3.1. Biological factors	29
1.3.3.1.1. Anatomical site	29
1.3.3.1.2. Age, sex and race	29
1.3.3.1.3. Dermal blood supply	30
1.3.3.1.4. Exercise, humidity and temperature	31
1.3.3.1.5. Skin condition	31
1.3.3.1.6. Cutaneous metabolism	31
1.3.3.1.7. Species differences	32
1.3.3.2. Physicochemical determinants	33
1.3.3.2.1. Drug-vehicle interactions	35
1.3.3.2.2. Vehicle-skin interactions	36
1.3.3.2.3. Drug-skin interactions	36
1.4. PASSIVE ENHANCEMENT STRATEGIES IN PERCUTANEOUS DRUG ABSORPTION	38
1.4.1. Strategies that influence thermodynamic activity	38
1.4.1.1. Supersaturation	39
1.4.2. Strategies that improve drug solubility in the stratum corneum	40
1.4.3. Strategies that reduce the barrier function of the stratum corneum	40
1.4.3.1. Occlusion	40
1.4.3.2. Chemical penetration enhancers	41
1.5. TRANSDERMAL DRUG DELIVERY OF OPIOID ANALGESICS	46
1.5.1. Rationale	46
1.5.2. Technical feasibility	47
1.5.2.1. Drug candidate selection	48
1.5.2.2. Transdermal delivery system	52
1.6. OBJECTIVES OF THIS THESIS	52
1.7. REFERENCES	54

CHAPTER 2: DEVELOPMENT OF A SUITABLE MODEL FOR STUDYING *IN VITRO* FENTANYL PERCUTANEOUS ABSORPTION

2.1. INTRODUCTION	65
2.2. OBJECTIVES	67
2.3. MATERIALS AND METHODS	68
2.3.1. Materials	68
2.3.2. Fentanyl saturated solubility studies	68
2.3.3. <i>In vitro</i> skin diffusion studies	68
2.3.3.1. Skin preparation	68
2.3.3.2. <i>In vitro</i> skin diffusion studies	69
2.3.4. Stratum corneum-water partitioning studies	70
2.3.4.1. Isolation of human stratum corneum	70
2.3.4.2. Stratum corneum-water partitioning studies	71
2.3.5. Analytical methods	72
2.3.6. Mathematical analysis	73
2.3.6.1. Fentanyl diffusional parameters	73
2.3.6.2. Stratum corneum-water partition coefficient	74
2.3.6.3. Enhancement ratios generated by octisalate pretreatment	74
2.3.7. Statistical analysis	74
2.4. RESULTS AND DISCUSSION	75
2.4.1. Fentanyl solubility and sink conditions	75
2.4.2. Effect of an ethanolic receptor solution on fentanyl percutaneous absorption	77
2.4.3. Effect of an ethanolic receptor solution on fentanyl partitioning between isolated human stratum corneum and water	81
2.4.4. Effect of an ethanolic receptor solution on the mechanism(s) by which octisalate enhances fentanyl percutaneous absorption	83
2.5. CONCLUSIONS	87
2.6. REFERENCES	88

CHAPTER 3: THE EFFECTS OF OCTISALATE AND PADIMATE O ON FENTANYL PERMEATION FROM A "FINITE DOSE"

3.1. INTRODUCTION	92
3.2. OBJECTIVES	94
3.3. MATERIALS AND METHODS	95

3.3.1. Materials	95
3.3.2. Saturated solubility studies	95
3.3.3. Initial screening for the effect(s) of octisalate and padimate O on fentanyl permeation: <i>In vitro</i> finite dose skin diffusion studies using shed snake skin as the model membrane	96
3.3.3.1. Skin preparation	96
3.3.3.2. <i>In vitro</i> skin diffusion studies	96
3.3.4. <i>In vitro</i> "finite dose" skin diffusion studies using human epidermis as the model membrane	98
3.3.4.1. Skin preparation	98
3.3.4.2. <i>In vitro</i> skin diffusion studies	98
3.3.5. Analytical methods	99
3.3.6. Mathematical analysis	99
3.3.6.1. Shed snake skin as the model membrane	99
3.3.6.2. Human epidermis as the model membrane	99
3.3.7. Statistical analysis	100
3.4. RESULTS AND DISCUSSION	100
3.4.1. Fentanyl solubility in ethanol, octisalate and padimate O	100
3.4.2. Initial screening for the effect(s) of octisalate and padimate O: Percutaneous absorption of fentanyl through shed snake skin	101
3.4.2.1. Use of shed snake skin as a model membrane for predicting fentanyl permeation through human epidermis, and the effects of octisalate and padimate O, under "finite dosing" conditions	103
3.4.3. The effects of octisalate and padimate O on the <i>in vitro</i> percutaneous absorption of fentanyl through human epidermis under "finite dosing" conditions	108
3.4.3.1. Fentanyl permeation through human epidermis under "finite dosing" conditions	108
3.4.3.2. Kinetics of fentanyl permeation through human epidermis under "finite dosing" conditions and the effects(s) of octisalate and padimate O	111
3.5. CONCLUSIONS	119
3.6. REFERENCES	121

CHAPTER 4: THE EFFECTS OF OCTISALATE AND PADIMATE O ON FENTANYL PERMEATION, PARTITIONING AND DIFFUSION

4.1. INTRODUCTION	128
4.2. OBJECTIVES	132
4.3. MATERIALS AND METHODS	133
4.3.1. Materials	133
4.3.2. "Infinite dose" <i>in vitro</i> skin diffusion studies	133
4.3.2.1. Skin preparation	133
4.3.2.2. "Infinite dose" skin diffusion studies	133
4.3.3. Stratum corneum-water partitioning studies	134
4.3.3.1. Isolation of human stratum corneum	134
4.3.3.2. Stratum corneum-water partitioning studies	134
4.3.3.3. Surface wipe procedure	136
4.3.3.3.1. Surface wipe procedure	136
4.3.3.3.2. Validation of the surface wipe procedure	136
4.3.3.3.2.1. Surface wipe samples	136
4.3.3.3.2.2. Surface wipe standards	136
4.3.3.3.2.3. Recovery, accuracy, and precision	136
4.3.4. Fentanyl partitioning between liquid organic phases and water	139
4.3.5. Saturated solubility studies	139
4.3.5.1. Saturated solubility of fentanyl in isopropyl myristate and octanol	139
4.3.5.2. Saturated solubility of octisalate and padimate O in octanol	
4.3.6. Analytical methods	140
4.3.6.1. Chromatographic assays for fentanyl quantification in permeation, partitioning and saturated solubility samples	140
4.3.6.2. Chromatographic assays for octisalate and padimate O quantification in surface wipe and saturated solubility samples	140
4.3.7. Mathematical analysis	142
4.3.7.1. Fentanyl diffusional parameters derived from "infinite dose" skin diffusion studies	142
4.3.7.2. Partition coefficient of fentanyl between human stratum corneum and water	143
4.3.7.3. Partition coefficients of fentanyl between liquid organic phases and water	144
4.3.8. Statistical analysis	144

4.4. RESULTS AND DISCUSSION	145
4.4.1. Diffusional parameters derived from "infinite dose" skin diffusion studies	145
4.4.2. Fentanyl partitioning between isolated human stratum corneum and water	155
4.4.3. Fentanyl solubility in liquid organic phases	158
4.4.4. Fentanyl partitioning between liquid organic phases and water	164
4.4.5. The effects of octisalate and padimate O on fentanyl partitioning between isopropyl myristate and water	167
4.4.6. Factors governing the partitioning of fentanyl into human stratum corneum	170
4.4.6.1. Physical and chemical constraints within the stratum corneum	171
4.4.6.2. Possible differences between interactions with octisalate or padimate O and the stratum corneum	173
4.4.6.3. Other mechanisms by which octisalate and padimate O may enhance fentanyl partitioning into the stratum corneum	175
4.5. CONCLUSIONS	176
4.6. REFERENCES	179

CHAPTER 5: THE EFFECTS OF OCTISALATE AND PADIMATE O ON FENTANYL DISTRIBUTION ACROSS HUMAN STRATUM CORNEUM

5.1. INTRODUCTION	187
5.2. OBJECTIVES	190
5.3. MATERIALS AND METHODS	190
5.3.1. Materials	190
5.3.2. Skin preparation	190
5.3.3. Tape stripping procedure	191
5.3.4. Surface wipe procedure and extraction	192
5.3.4.1. Surface wipe procedure	192
5.3.4.2. Extraction of fentanyl, octisalate and padimate O from surface wipes	193
5.3.4.3. Validation of the surface wipe procedure	193
5.3.4.3.1. Surface wipe samples	193
5.3.4.3.2. Surface wipe standards	194
5.3.4.3.3. Recovery, accuracy, and precision	194

5.3.5. Tape strip extraction	195
5.3.5.1. Extraction of fentanyl, octisalate, and padimate O from tape strips	195
5.3.5.2. Validation of fentanyl, octisalate, and padimate O extraction from tape strips	196
5.3.5.2.1. Tape strip samples	196
5.3.5.2.2. Tape strip standards	196
5.3.5.2.3. Recovery, accuracy, and precision	197
5.3.6. Analytical methods	198
5.3.7. Mathematical analysis	199
5.3.7.1. Normalisation of stratum corneum depth and fentanyl concentrations within the stratum corneum	199
5.3.7.2. Areas under the fentanyl distribution profiles	200
5.3.7.3. Kinetic modeling of stratum corneum surface clearance	201
5.3.8. Statistical analysis	201
5.4. RESULTS AND DISCUSSION	201
5.4.1. Vehicle and time dependent effects on stratum corneum weight removed	201
5.4.2. Fentanyl distribution across human stratum corneum	204
5.4.3. Areas under the fentanyl distribution profiles and clearance of fentanyl from the stratum corneum surface	208
5.4.4. Dose accountability	214
5.5. CONCLUSIONS	223
5.6. REFERENCES	224

CHAPTER 6: DISTRIBUTION OF OCTISALATE AND PADIMATE O ACROSS HUMAN STRATUM CORNEUM

6.1. INTRODUCTION	230
6.2. OBJECTIVES	234
6.3. MATERIALS AND METHODS	234
6.3.1. Materials	234
6.3.2. Determination of octisalate and padimate O distribution across human stratum corneum <i>in vitro</i>	234
6.3.2.1. Skin preparation	235
6.3.2.2. Tape stripping procedure	235

6.3.2.3. Analytical methods	236
6.3.2.3.1. Chromatographic analysis of octisalate and padimate O	236
6.3.2.3.2. Spectroscopic analysis of octisalate and padimate O	236
6.3.2.3.2.1. Acquisition of ATR-FTIR spectra	236
6.3.2.3.2.2. Identification of infrared absorbances arising from octisalate and padimate O	237
6.3.2.3.2.3. Assay validation	241
6.3.3. Determination of octisalate and padimate O distribution across human stratum corneum <i>in vivo</i>	246
6.3.3.1. Participants	246
6.3.3.2. Study design	247
6.3.3.3. Skin irritation	249
6.3.3.4. Analytical methods	250
6.3.3.4.1. Chromatographic analysis of octisalate	250
6.3.3.4.2. Spectroscopic analysis of octisalate	250
6.3.3.4.2.1. Acquisition of ATR-FTIR spectra	250
6.3.3.4.2.2. Identification of infrared absorbances arising from octisalate	252
6.3.3.4.2.3. Assay validation	252
6.3.4. Mathematical analysis	257
6.3.4.1. Normalisation of stratum corneum depth and octisalate and padimate O concentrations within the stratum corneum	257
6.3.4.2. Areas under the octisalate and padimate O distribution profiles	258
6.3.4.3. Kinetic modeling of clearance from the stratum corneum surface	258
6.3.5. Statistical analysis	258
6.4. RESULTS AND DISCUSSION	259
6.4.1. Distribution of octisalate and padimate O across human stratum corneum <i>in vitro</i>	259
6.4.2. Distribution of octisalate across human stratum corneum <i>in vivo</i>	266
6.4.3. Correlation between the <i>in vitro</i> and <i>in vivo</i> distribution of octisalate across human stratum corneum	266
6.4.4. Correlation between the octisalate and padimate O distribution profiles determined by HPLC/UV and ATR-FTIR	275
6.5. CONCLUSIONS	277

CHAPTER 7: THE EFFECTS OF OCTISALATE AND PADIMATE O ON HUMAN STRATUM CORNEUM LIPIDS

7.1. INTRODUCTION	284
7.2. OBJECTIVES	287
7.3. MATERIALS AND METHODS	288
7.3.1. Materials	288
7.3.2. Skin preparation	288
7.3.3. Determination of the effects of octisalate and padimate O on lipids located within the superficial layers of the stratum corneum	288
7.3.3.1. Concentration-dependent studies	288
7.3.3.2. Time-dependent studies	289
7.3.4. Determination of the concentration-dependent effects of octisalate and padimate O on lipids located within the different layers of the stratum corneum	289
7.3.5. Analytical methods	290
7.3.5.1. Acquisition of ATR-FTIR spectra	290
7.3.5.2. Spectral analysis	291
7.3.5.2.1. Deconvolution of the C-H stretching	291
7.3.5.2.2. Determination of peak frequency maxima	
7.3.5.2.3. Effects of octisalate and padimate O on the conformational order of the stratum corneum lipid bilayers	293
7.3.5.2.4. Effects of octisalate and padimate O on stratum corneum lipid content	294
7.3.5.2.5. Uptake of octisalate and padimate O into the superficial layers of the stratum corneum	295
7.3.6. Statistical analysis	296
7.4. RESULTS AND DISCUSSION	297
7.4.1. The effects of octisalate and padimate O on lipids located within the superficial layers of the stratum corneum	297
7.4.1.1. Concentration-dependent effects	297
7.4.1.1.1. Stratum corneum lipid content	297
7.4.1.1.2. Conformational order of the stratum corneum lipid	

bilayers	301
7.4.1.1.3. Uptake of octisalate and padimate O into the superficial layers of the stratum corneum	308
7.4.1.2. Time-related effects	310
7.4.1.2.1. Stratum corneum lipid content	310
7.4.1.2.2. Conformation order of the stratum corneum lipid bilayers	313
7.4.1.2.3. Uptake of octisalate and padimate O into the superficial layers of the stratum corneum	316
7.4.2. The concentration-dependent effects of octisalate and padimate O on lipids located within different layers of the stratum corneum	319
7.4.2.1. Effects of octisalate and padimate O on stratum corneum lipid content	319
7.4.2.2. Effects of octisalate on the conformational order of stratum corneum lipids	322
7.4.2.3. Changes in the properties of the stratum corneum as a function of increasing depth	324
7.5. CONCLUSIONS	329
7.6. REFERENCES	331

CHAPTER 8: SUMMARY OF MAJOR FINDINGS AND CONCLUDING REMARKS

8.1. POSSIBLE MECHANISMS BY WHICH OCTISALATE AND PADIMATE O ENHANCE THE PERCUTANEOUS ABSORPTION OF FENTANYL <i>IN VITRO</i> UNDER "FINITE DOSE" CONDITIONS	337
8.2. SUGGESTIONS FOR FUTURE RESEARCH	346
8.3. REFERENCES	349

APPENDICES

Appendix I	350
Appendix II	354

ABSTRACT

The primary objective of this research was to investigate the mechanism(s) by which two investigational chemical penetration enhancers, octisalate (OS) and padimate O (PO), enhance the *in vitro* percutaneous absorption of the opioid analgesic, fentanyl, under predicted conditions of use *in vivo*. The percutaneous absorption of fentanyl *in vitro* was determined using a flow-through diffusion cell design. In order to simulate the dosing conditions that would prevail *in vivo*, finite dose diffusion studies were conducted by applying fentanyl 5%w/v in ethanol alone or ethanolic solutions containing 5%w/v fentanyl and 1 to 10%w/v of OS or PO to either shed snake skin or human female abdominal epidermis. From these studies, it was found that OS significantly enhanced the percutaneous absorption of fentanyl at all concentrations investigated ($p < 0.05$ compared with control (ethanol alone)) and that its enhancing capabilities were linearly related to its applied concentration. On the other hand, a parabolic relationship was observed between fentanyl permeation enhancement and the applied concentration of PO such that significant enhancement was only observed at concentrations between 2.5 to 7.5%w/v ($p < 0.05$ compared with control). It was also found that the application of fentanyl with high ($> 5\%$ w/v) concentrations of OS and PO resulted in the maintenance of optimal fentanyl flux across the skin over prolonged periods of time and that the enhancing capability of OS was generally superior to that of PO.

As it is often difficult to derive diffusional parameters from finite dose diffusion data, infinite dose diffusion studies were conducted using human female abdominal epidermis. Saturated aqueous solutions of fentanyl (2000 μ l) were applied to untreated skin (control) or skin pretreated with ethanol alone or ethanolic solutions containing 1 to 10% w/v of OS or PO. Under these conditions, both OS and PO significantly enhanced the permeability coefficient of fentanyl at all concentrations investigated ($p < 0.05$ compared with untreated skin). Again, the enhancing effects of OS appeared to be linearly related to its applied concentration whereas a parabolic relationship was evident between fentanyl permeation enhancement and the applied concentration of PO. As similar concentration-dependent trends were evident for the enhancement of the partition coefficient of fentanyl between the stratum corneum (SC) and the vehicle, it appeared that a major mechanism by which OS and PO enhance fentanyl permeation is by increasing its partitioning into the SC. As i) the saturated solubility of fentanyl in OS and

PO was found to be higher than its solubility in model liquid organic phases (octanol (OCT) and isopropyl myristate (IPM)) and ii) both OS and PO enhanced the intrinsic partition coefficient of fentanyl free base between IPM and water in a concentration-dependent manner, it appears that OS and PO enhance fentanyl partitioning into the SC by, or partly by, increasing its solubility in the SC lipids.

To further investigate the effects of OS and PO on fentanyl permeation under finite dose conditions, tape-stripping experiments were conducted. Ethanol alone or ethanolic solutions containing 5%w/v of fentanyl and 5%w/v of either OS or PO were applied to the SC surface of 1 x 5 cm pieces of full-thickness human female abdominal skin and after a predetermined exposure time, excess solution was wiped from the skin surface and the SC was sequentially removed by adhesive tape stripping. From these studies, it was evident that, compared with ethanol alone, both OS and PO modified the distribution of fentanyl across the SC such that relatively high concentrations of fentanyl were maintained in the upper regions of the SC over prolonged exposure times. However, discernible differences were apparent between the distribution phenomena of fentanyl and the distribution phenomena of OS and PO. Differences were also found between the distribution of OS across human SC *in vitro* and *in vivo*, which highlights the need to conduct further mechanistic studies *in vivo*.

Attenuated total reflectance Fourier transform infrared (ATR-FTIR) investigations into the effects of OS and PO on human SC lipids *in vitro* were also conducted in order to gain further insight into the possibility that OS and PO increase the diffusivity of fentanyl within the SC. After a finite dose application to the skin for 2 h, both OS and PO significantly reduced the areas and heights of SC-lipid derived CH₂ asymmetric and symmetric stretching frequencies at concentrations above 5%w/v and 1%w/v respectively ($p < 0.05$ compared with untreated skin and skin treated with ethanol alone). While the apparent lipid-reducing effects of OS appeared to be related to its applied concentration and the amount taken up into the SC, the effects of PO appeared to be saturated within a concentration range between 1 and 10%w/v. Furthermore, OS, but not PO, appeared to shift the CH₂ asymmetric and symmetric stretching frequencies to higher wavenumbers, which may indicate that it reduces the conformational order of the SC lipid bilayers. However, this effect requires further investigation.

STATEMENT OF ORIGINALITY

The Registrar
Victorian College of Pharmacy
Monash University

The work contained in this thesis has been performed solely by the candidate under the supervision of Dr. B.C. Finnin and Prof. B.L. Reed. No portion of this thesis has been submitted by the candidate for the award of any other degree or diploma. To the best of the candidate's knowledge, this thesis contains no material that has been previously published or written by any other person, except where due reference is made in the text of the thesis.



Brigette Traversa
June 2004

ACKNOWLEDGMENTS

First, I would like to thank my supervisors, Dr. Barrie Finnin and Prof. Barry Reed, because I would never have pursued this opportunity if it wasn't for their initial encouragement. Both of them have offered tremendous support and encouragement throughout my PhD and they are continual sources of inspiration and infinite wisdom. I am particularly grateful for the time and effort that have recently been spent on "proof reading" this thesis.

I would also like to thank my mum and dad, who are the two most important people in my life. On so many occasions, they sacrificed their time – even if that time was *very* late at night – to come into uni with me. They have both been incredibly supportive, understanding and patient even though I've been a nightmare to live with lately. I sincerely can't express in words how grateful I am for everything they've done for me.

Thank you to my grandparents for being so loving and caring – and for the prayers!

Thanks to everyone in the Pharmaceutics department for their friendship and help and for making my time at VCP a happy and memorable experience. A special thanks to Joe ("my little brother") and Nina ("my big sister") for the laughs, support, and words of wisdom – especially when I needed it! Thanks also to Dr. Kate Klose, not only for her friendship but also for her guidance and wisdom when I first started this research.

Thanks to my friends outside VCP, who have all been supportive along the way. I would also like to say a big "thank you" to Brendan, who has been the most patient and understanding boyfriend a girl doing her PhD could have! I think the past couple of years have been as enduring for him as they have been for me!

I would like to acknowledge the financial support of Acrux Ltd. and to everyone there for their friendship, help and advice.

Finally, I would like to thank Tri, Phil, Brunda, Donna, and Catherine for giving up their time and their skin (!) for the *in vivo* studies that were conducted.

This research was supported by an Australian Postgraduate Award.

COMMUNICATIONS

Traversa, B.D., Reed, B.L., Finnin, B.C.: Transdermal delivery of opioid analgesics. Australian Pharmaceutical Sciences Association, Annual Conference, Melbourne, Australia, 9 – 12 December, 2001*

Traversa, B.D., Reed, B.L., Finnin, B.C.: Enhancement of the percutaneous penetration of the opioid analgesic fentanyl by octyl salicylate and padimate O. Perspectives in Percutaneous Penetration, Eighth International Conference, Antibes/Juan-les-Pins, France, 2 – 6 April, 2002

Traversa, B.D., Reed, B.L., Finnin, B.C.: Spectroscopic and chromatographic determination of octyl salicylate and fentanyl distribution across human stratum corneum. Australian Pharmaceutical Sciences Association, Annual Conference, Melbourne, Australia, 8 – 11 December, 2002*

Traversa, B.D., Reed, B.L., Finnin, B.C.: An ATR-FTIR spectroscopic investigation on the effect of octyl salicylate and padimate O on stratum corneum surface lipids. Australian Pharmaceutical Sciences Association, Annual Conference, Melbourne, Australia, 8 – 11 December, 2002

* Awarded best poster presentation in pharmaceuticals

ABBREVIATIONS AND SYMBOLS

α	hydrogen bond donor strength
ATR-FTIR	attenuated total reflectance Fourier transform infrared spectroscopy
AUC	area under the curve
AZ	Azone® (laurocapram)
β	hydrogen bond acceptor strength
CER	ceramide
CPE	chemical penetration enhancer
CL _T	total body clearance
CV	coefficient of variation (%)
C _v	concentration of drug in vehicle
D	apparent diffusion coefficient of solute within the stratum corneum
DSC	differential scanning calorimetry
ER	enhancement ratio
EtOH	ethanol
h	stratum corneum thickness
h (time reference)	hours
HPLC	high performance liquid chromatography
IPB pH 7.4, 0.1%NaN ₃	isotonic phosphate buffer pH 7.4, 0.1%w/v sodium azide
IPM	isopropyl myristate
J	solute flux across the skin
K _{IPM/W}	apparent partition coefficient between isopropyl myristate and water
K _{OCT/W}	apparent partition coefficient between octanol and water
K _{ORG/W}	apparent partition coefficient between a specified organic phase and water
K _{ORG/W (INT)}	intrinsic partition coefficient between a specified organic phase and water
K _{OS/W}	apparent partition coefficient between octisalate and water
K _{POW}	apparent partition coefficient between padimate O and water
K _{SC/V}	apparent partition coefficient between human stratum corneum and a vehicle
K _{SC/W}	apparent partition coefficient between human stratum corneum and water
K _{SC/W (INT)}	intrinsic partition coefficient between human stratum corneum and water

K_p	permeability coefficient
LD_{50}/ED_{50}	therapeutic safety index: the ratio of the dosage of drug required to produce death in 50% of the tested population to the dosage required to produce the designated (desired) effect in 50% of the tested population
min	minutes
MW	molecular weight
MP	melting point
OA	oleic acid
OCT	octanol, n-octanol
OS	octisalate (formerly octyl salicylate)
PG	propylene glycol
PO	padimate O
Q_t	cumulative amount of drug penetrating the skin at time, t.
δ	Hildebrand solubility parameter
δ_T	Hansen total solubility parameter
δ_D	Hansen dispersion solubility parameter
δ_P	Hansen polar solubility parameter
δ_H	Hansen hydrogen bonding (or ion-exchange) solubility parameter
SC	stratum corneum, isolated human stratum corneum
SD	standard deviation of the mean
sec	seconds
SEM	standard error of the mean (standard deviation/square root of sample size)
S_{SC}	solubility of drug in the stratum corneum
S_v	solubility of drug in vehicle
TC	Transcutol®
TDD	transdermal drug delivery
TDR	transdermal delivery rate
TEWL	transepidermal water loss
t_{lag}	lag time
$t_{1/2\beta}$	elimination half life
TTS	transdermal therapeutic system
UV	ultraviolet
ZnSe	zinc selenide

CHAPTER 1

INTRODUCTION

1.1. STRUCTURE AND FUNCTION OF THE SKIN

The skin is the largest organ of the body, accounting for more than 10% of total body mass (1). It essentially consists of four different layers: the stratum corneum, the viable epidermis, the dermis, and the hypodermis (or subcutaneous tissue) (Figure 1.1). Several appendages also exist in the skin including hair follicles, sebaceous glands, sweat glands, nails, and sensory receptors.

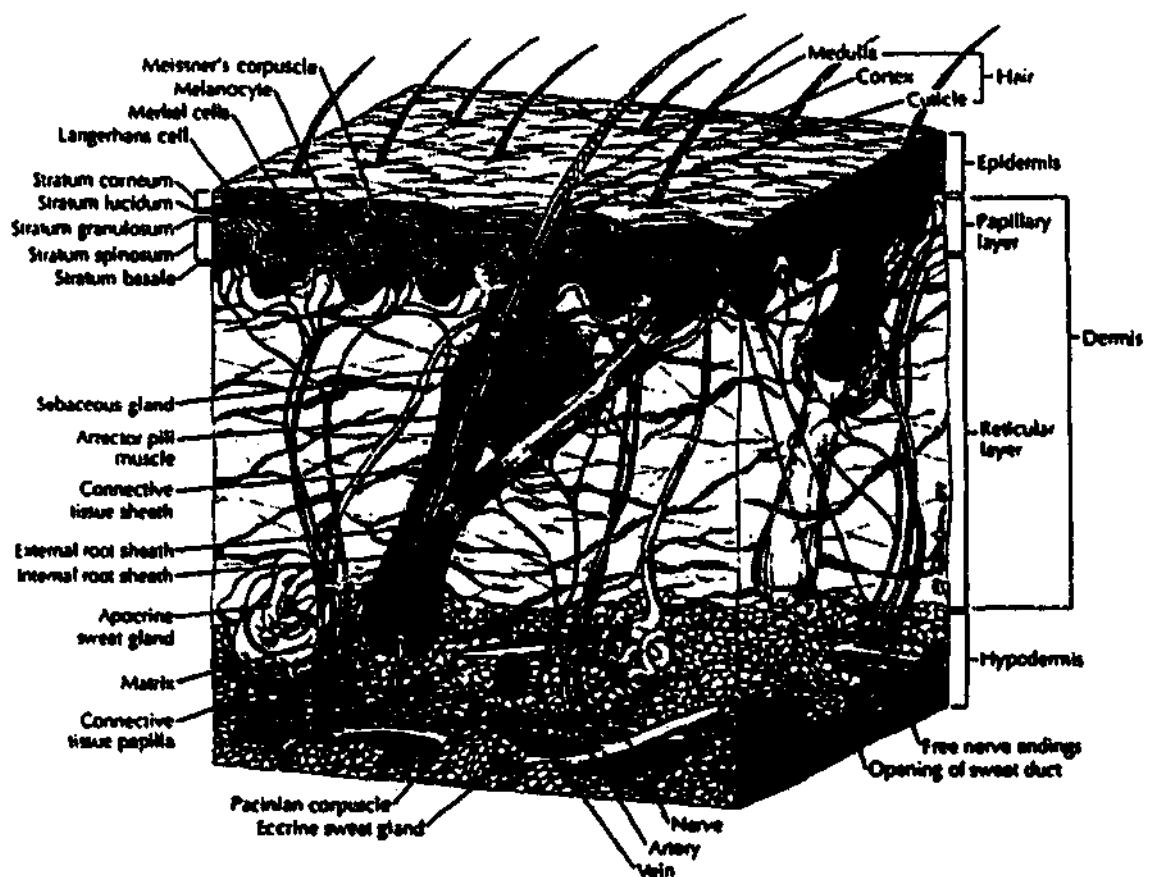


Figure 1.1. Schematic representation of human skin and its appendages(2).

As the skin enables the body to interact most intimately with its environment it is not surprising that the functions of the skin relate to its situation as an interface between the body and the external environment. Accordingly, an important function of the skin is to maintain homeostasis of the body by limiting the loss of water, electrolytes and other

body constituents whilst maintaining a barrier to the ingress of foreign substances from the environment (3). The skin fulfills this role by, for example (4, 5):

- i. helping to maintain a relatively constant internal body temperature in the face of variable external temperatures
- ii. encumbering the penetration of foreign substances, such as chemical, microorganisms and other pathogens
- iii. protecting the body from external radiation, including visible light, ultraviolet (UV) light, and ionizing radiation

The skin also offers physical protection against mechanical stress and external pressure. The presence of water – and possibly other substances – within the stratum corneum render this integument soft and flexible whilst the underlying skin layers (the dermis and hypodermis) provide bulk, cushioning, and mobility (4). Sensory nerves within the skin also aid in the protection of the body by sensing external influences, such as heat, cold, pressure, and pain.

The skin's outermost layer, the stratum corneum, is a heterogeneous structure comprised of 15 to 25 layers of flattened, hexagonal cornified cells (corneocytes) that are embedded in a continuous array of extracellular lipids (1). Although it is reported that the surface area of skin exposed to the environment can exceed 2 m² (6), the true surface area of the stratum corneum is difficult to determine due the presence of macroscopic furrows (or microwrinkles) (7). In fact, it has been estimated that the presence of these furrows can increase the surface area of skin exposed to the environment by up to 30% (8).

Although it serves a principle role in maintaining homeostasis, the stratum corneum is an extremely thin structure, being only 10 to 20 µm in cross-sectional thickness (1). However, the thickness of, and the number of corneocytes within, the stratum corneum can vary considerably among different individuals and among different body sites (9, 10). Despite this large degree of inter- and intra-individual variability, the thickness of the stratum corneum at any given body site remains relatively constant due to the fact that corneocytes are continuously shed from the stratum corneum surface at a rate which balances the formation of new corneocytes. The *de novo* production of corneocytes originates from the viable epidermis, which is the unvascularised skin layer located immediately below the stratum corneum.

The epidermis is a continuous stratified squamous epithelium. Although it is devoid of blood vessels, the epidermis receives all of its nutrients, and disposes of its waste products, by diffusional exchange with the underlying dermis (11). The majority (~90%) of cells within the epidermis are keratinocytes, which undergo progressive stages of maturation and, ultimately, terminal differentiation as they migrate from the basal epidermal layers to the stratum corneum (12). The thickness of the viable epidermis also varies dramatically with anatomical site. Although most of the body has an average epidermal thickness of 40 to 50 μm , it is increased to about 80 μm on the wrists and back of the hand and reaches 400 μm on the front of the fingers (13).

The stratum corneum and epidermis are not continuous structures as they are pierced by hair follicles, pilosebaceous units and sweat gland ducts. The roots of the hair follicles (and associated pilosebaceous units) and the secretory coils of the sweat glands are supported by the dermis. The dermis, which is innervated and highly vascularised, consists essentially of a matrix of connective tissue woven from fibrous proteins that are embedded in an amorphous ground substance of mucopolysaccharide that is sparsely populated with cells. As the dermis is the thickest skin layer (its thickness ranges from 3 to 5 mm (4)) it is responsible for giving the skin its bulkiness. Beneath the dermis is the hypodermis (though it is absent on the eyelids and male genitalia), which consists mainly of adipose tissue. It is also transversed by a system of blood vessels, although this is not as pronounced as in the dermis.

The structure and dynamics of each of these skin layers and the skin appendages will be described in detail in the following sections. As the barrier function of the skin can be mainly attributed to the stratum corneum, the structure and function of this integument is discussed separately in Section 1.2.

1.1.1. The epidermis

The epidermis is comprised of several cell layers that are traditionally identified in terms of their location and appearance: the stratum basale, stratum spinosum and stratum granulosum (Figures 1.1 and 1.2). However, as “the *raison d'être* of the epidermis is to make the stratum corneum” (14) it is important to recognise that the architecture of the epidermis represents the dynamic processes involved in the generation of the stratum corneum (i.e. the different stages of keratinocyte mitosis and differentiation).

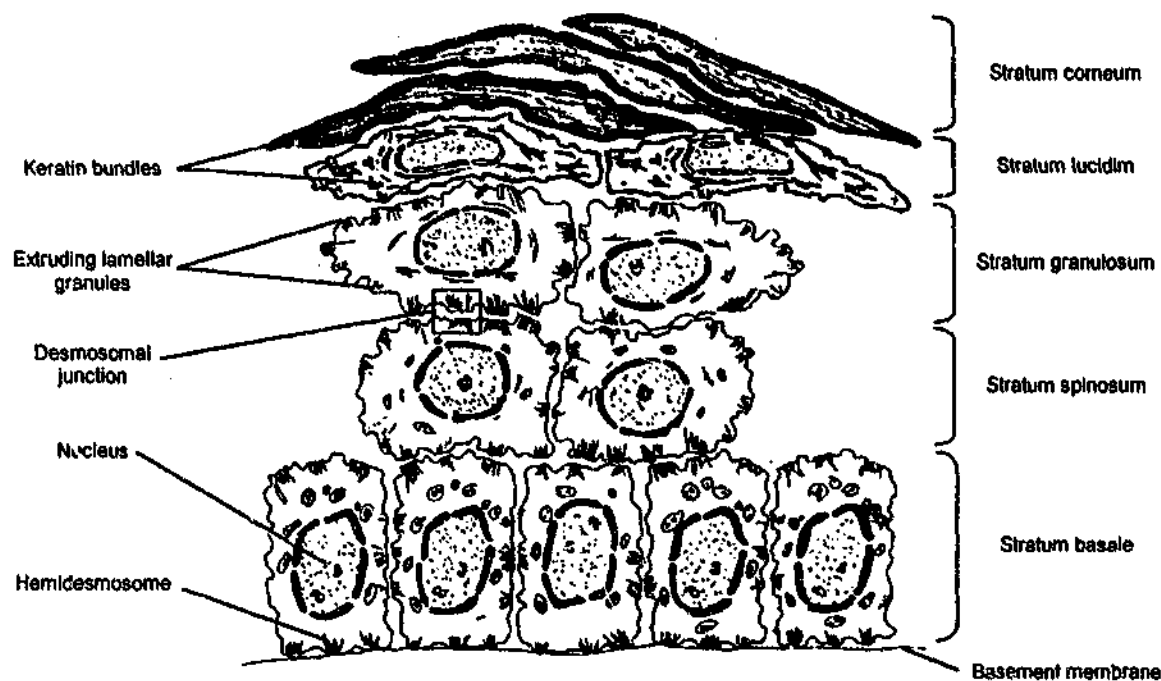


Figure 1.2. Schematic representation of the morphological and structural changes that occur during keratinocyte differentiation. Adapted from Schaefer and Redelmeier (15) and Walters and Roberts (1).

1.1.1.1. *Stratum basale*

The stratum basale is the mitotically active layer of the epidermis where the keratinocytes divide and begin the process of differentiation. Immediately below the stratum basale is the acellular basement membrane, which serves three major functions: dermal-epidermal adherence, mechanical support for the epidermis, and the control of the passage of cells and some large molecules (such as proteins) across the junction (1, 6). The basal keratinocytes, which are arranged in a "fence post" fashion along the basement membrane, are typically elongated in appearance, contain a prominent nucleus and are relatively undifferentiated (6, 16) (Figure 1.2). Two major types of basal cell have been identified, which vary in their function and appearance (16). Serrated basal cells have low mitotic activity and contain well-developed projections that extend into the dermis. Thus, it is thought that their principal function is to anchor the epidermis to the dermis (16). On the other hand, nonserrated basal cells have a smoother border and are believed to function as stem cells which have the capacity to divide and produce new cells (16). The

mitotic division of these basal cells is regulated by various intrinsic and extrinsic factors (17).

Whereas hemidesmosomes are responsible for attaching the basal cells to the basement layer, desmosomes are cell-cell junctions that are responsible for maintaining intercellular cohesion and communication (1). The desmosomal junction contains two types of transmembrane glycoproteins (desmogleins and desmocollins) that essentially provide a link between the keratin intermediate filaments of adjacent keratinocytes (1). The attachment of the basal cells to the basement layer, and to each other, is also maintained by adherens junctions, which are cell-cell junctions that differ from hemidesmosomes and desmosomes in terms of morphological structure, molecular composition and linkage to a basal keratinocyte (they are linked to cytoplasmic microfilaments of actin instead of cytoplasmic keratin intermediate filaments) (1, 18).

Basal keratinocytes synthesise two major keratins, keratin 14 (type I) and keratin 5 (type II) (1, 17, 18). However, as the keratinocytes migrate to the stratum spinosum and the stratum granulosum, the synthesis of these keratins is reduced and replaced by larger keratins, keratin 10 (type I) and keratin 1 (type II). In contrast to the keratin pair expressed by basal keratinocytes, keratins 1 and 10 aggregate to form supramolecular keratin assemblies called macrofibrils, which are important structural components of the epidermis (17). This differentiation-dependent regulation of keratin expression appears to have functional significance within the epidermis, since premature aggregation of the basal keratinocytes could potentially eliminate the stem cell population (17).

1.1.1.2. *Stratum spinosum*

As the keratinocytes move from the stratum basale to the stratum spinosum they become flatter in appearance, their nucleus reduces in size and they contain more keratin filaments (16). Spine-like structures (or “prickles”) also appear on the cell surface, which is one of the first noticeable steps in keratinocyte differentiation (along with the expression of keratins 1 and 10) (16, 17). These spinous projections, which appear to form bridges between the keratinocytes, have been identified as desmosomes (16). The cytoplasm of these keratinocytes also contains a complete complement of organelles (including a nucleus, nucleoli, an endoplasmic reticulum, Golgi apparatus and mitochondria) as well as a few bundles of keratin filaments (16).

Within the upper cell layers of the stratum spinosum, intracellular membrane coating granules (otherwise known as Odland bodies or lamellar granules) appear in the cytosol, which marks the transition between the stratum spinosum and the stratum granulosum (1).

1.1.1.3. Stratum granulosm

As keratinocyte differentiation continues into the stratum granulosm, the keratinocytes become noticeably flatter in appearance. The most prominent feature of these keratinocytes is the presence of keratohyalin granules within the cytoplasm (16). The keratohyalin granules contain profilaggrin, which is a histadine-rich, neutral phosphoprotein (17). As the keratinocytes migrate from the stratum granulosm to the stratum corneum profilaggrin is converted to filaggrin, which aids in the assembly of the keratin filaments in the extracellular space (4, 17). Membrane coating granules are also present within the cytoplasm of these keratinocytes (in the endoplasmic reticulum and Golgi apparatus) (1). Although they are also present within the stratum spinosum, the prevalence of membrane coating granules increases in the stratum granulosm (12, 16).

The membrane coating granules are ovoid bodies that are comprised of a lipid membrane that surrounds one or more stacks of lamellar disks, which are aligned parallel to each other (11). These lamellar disks are believed to be the precursors of the intercellular lipid lamellae of the stratum corneum (19). Hydrolytic enzymes are also present within the membrane coating granules (1). The most notable enzyme, stratum corneum chromatryptic enzyme (SCCE), is able to locate at the desmosomal junctions and has thus been implicated in the process of desquamation (1) (Section 1.2.4.).

1.1.1.4. Final stages of keratinocyte differentiation

As the keratinocytes migrate from the uppermost layers of the stratum granulosm to the stratum corneum, the membrane coating granules migrate to the apical side of the keratinocytes, where they fuse with the basement membrane and eventually secrete their contents into the intercellular space (16). The polar lipid precursors derived from the lamellar bodies are enzymatically converted in part into neutral lipids, which are subsequently modified and rearranged edge-to-edge (20). They eventually fuse to form

broad, multiple intercellular lipid lamellae that are orientated approximately parallel to the surface of the cells (19).

Concomitantly, the nucleus and all other cellular organelles are destroyed by proteases, DNase, RNase, acid hydrolysase and plasminogen activator and as a result the keratinocytes become flattened and compacted (17). This region of intense enzymatic activity and cellular remodelling is often referred to as the stratum lucidum and appears to form the first layer of the stratum corneum (6, 17).

Evidently, the entire process of epidermal differentiation is aimed toward the generation of the specific morphology of the stratum corneum, which is described in Section 1.2.2.

1.1.1.5. Other cells in the epidermis

Other cells that are present in the epidermis are Langerhans cells, Merkel cells, and melanocytes. Langerhans cells are dendritic cells that migrate from the bone marrow (6). In recent years, it has been recognised that these cells are involved in the immune response of the skin: they appear to bind contact allergens in the skin and transport them to the lymph nodes, where they present these antigens to T lymphocytes (1).

Merkel cells are closely associated with nerve endings present on the dermal side of the basement membrane, which may indicate that they are involved in the sensation of touch (1, 4). Although there has been no direct evidence to support this function, most researchers believe that Merkel cells play a role in the mechanosensory system, the trophic action on peripheral nerve fibres, the stimulation and maintenance of keratinocyte proliferation, and the release of bioactive agents to the sub-epidermal structures (1, 4).

Melanocytes are also present within the stratum basale, in a ratio of about 1:36 with basal cells (6). Their main function is to produce melanin, which is synthesised in membrane-bound organelles (the melanosomes), and to distribute it to the keratinocytes (1). Melanin is responsible for pigmentation of the skin and hair. The main function of melanin within the skin is to provide protection against the harmful effects of UV radiation (4, 5).

1.1.2. The dermis

The dermis is subdivided into two layers, the papillary dermis and the reticular dermis. The papillary dermis is located immediately below the basement membrane, where the dermal papillae (which appear as upward-facing pegs) interdigitate with the rete ridges (or downward-facing pegs) of the epidermis (Figure 1.1) (5). This structural arrangement enables the epidermis to receive its nutritive, immune and other support systems via the dermal papillae, which are highly vascularised (5). The reticular dermis, which constitutes the bulk of the dermis, extends from the base of the papillary dermis to the hypodermis.

The dermis contains collagen (~75%), reticulin (a very fine collagen) (0.4%) and elastin fibers (4%) (4). Whilst the collagenous fibers provide a scaffold of support and cushioning, elastin fibers are responsible for the elasticity of the skin (1). The dermal fibres are embedded in an amorphous ground substance, which is essentially comprised of mucopolysaccharides (or proteoglycans) formed by hyaluronic acid, chondroitin sulphate, dermatan sulphate, and heparan sulphate (6). Proteoglycans are capable of absorbing copious amounts of water and thus form an aqueous, gel-like substance. It is likely that proteoglycans function to maintain an appropriate level of hydration (to meet metabolic needs) and an ion balance (for the exclusion of large macromolecules) (6). They also serve to support the dermal components and may also play a role in cell migration and differentiation (6). Fibronectin is an adhesive glycoprotein that is also present within the dermis (6). Its functions include the promotion of cell adhesion (particularly the attachment of cells to collagen), spreading, migration, chemotaxis, phagocytosis, matrix and basement membrane organisation, and growth factor secretion (6).

The dermis is sparsely populated with cells. Fibroblasts are the most abundant cell type in the dermis and are responsible for the production of connective tissue components, such as collagen and fibronectin (4). Mast cells, macrophages, lymphocytes, and melanocytes are also present in the dermal tissue (6).

1.1.3. The hypodermis

The hypodermis is essentially comprised of loose connective tissue and a network

of adipocytes, which are arranged in lobules and linked to the dermis by interconnecting collagen and elastin fibres. Other cells that are present within the hypodermis include fibroblasts and macrophages (1). The major functions of the hypodermis are heat insulation, shock absorption and energy storage. It also anchors the skin to the underlying muscles and supports the skin's vascular and neural systems (1).

1.1.4. Vascular, lymphatic and neural systems within the skin

An extensive vascular system transverses the hypodermis and, in particular, the dermis and is responsible for maintaining the viability of the skin (providing for cutaneous nutrition, repair and immune responses and maintaining tissue homeostasis) and contributes to the skin's function as a protective barrier between the body and its external environment (playing a role in immune response and thermoregulation) (1).

The vascular surface that is available for the exchange of materials between the blood and local tissue is approximately equivalent to the surface area of the skin, with the average rate of blood flow through the skin being about 0.05 ml/min/cm^2 (21). The significance of this abundant blood supply to percutaneous drug absorption is discussed in Section 1.3.

The cutaneous blood supply arises from arterial branches that penetrate the hypodermis and underlying muscles, which give rise to two important plexuses in the dermis: a lower horizontal plexus located at the interface between the dermis and hypodermis and a superficial horizontal plexus in the papillary dermis (22). The lower plexus, which is formed by the vessels from the underlying hypodermis and muscles, give rise to arterioles and venules that ascend vertically to interconnect with the upper horizontal plexus. It also forms numerous lateral tributaries that supply the appendages (e.g. hair follicles and sweat glands).

The superficial horizontal plexus supplies capillary loops found in the dermal papillae. These papillary loops are responsible for providing the papillary dermis and epidermis with nutritive support (6). Post capillary venules form as the papillary loop descends into the superficial horizontal plexus and these venules are the site where inflammatory cells migrate from the vascular space to the surrounding tissue (22).

Although the cutaneous vasculature provides critical nutritive and inflammatory functions, the majority (~85%) of total blood flow through the skin effects

thermoregulatory homeostasis (23). The distribution of blood flow through the skin is mainly regulated by two components of the microvascular system: arteriovenous anastomoses and pre-capillary sphincters (24). The arteriovenous anastomoses are located between the capillaries and are most prominent in acral skin, such as the fingertips and toe pads (25). During vasodilatation, they are capable of shunting blood directly from the arterial to the venous side, bypassing the capillaries, and thus increasing overall blood flow and heat dissipation (24, 26). In the papillary dermis, the pre-capillary sphincters control blood flow to the capillaries of the dermal papillae (22). Both arteriovenous anastomoses and pre-capillary sphincters are responsive to systemic stimuli (such as core temperature changes, cardiovascular homeostasis and emotional stress) and local stimuli (such as pain, inflammation, pressure and local temperature changes) (24).

The lymphatic system of the skin is also organised into upper and lower horizontal plexuses (27). However, the lymphatic vessels are located slightly deeper in the papillary dermis and are not contained within the hypodermis (28, 29). The lymphatic system is responsible for the continual removal of excess fluid, waste products and macromolecules (such as proteins) from the extravascular compartment of the dermis (28). The lymphatic vessels also direct antigen-presenting cells to the lymph nodes and are thus vital for the development of cellular immunity (28).

A complex network of somatic sensory and autonomic nerves is also present in the skin (5). There are at least five known types of somatosensory receptors: Meissner's corpuscles, Merkel's corpuscles, Krause's end bulbs, Ruffini terminals and Pacinian corpuscles (6). With the exception of the Merkel's corpuscles (which may be located in the epidermis), all of these receptors are located in the dermis (6). They are responsible for cutaneous sensation, such as pain, pressure, itch, hot and cold. The somatosensory and autonomic nerves of the skin form flat networks in the papillary dermis and they innervate the blood vessels and skin appendages (the hair papillae, the arrector pili attached to the hair follicle and the eccrine glands) (5).

1.1.5. Skin appendages

1.1.5.1. Hair

Hair forms a protective coating over the entire body, except the lips, soles of the

feet, palms of the hand, nipples and glabrous skin. It is mainly comprised of hard keratin, which, unlike the soft keratin found in the stratum corneum, has a high sulphur content (4). Hair is synthesised in the hair follicles, which are invaginations of the epidermis and stratum corneum that slant into the dermis and may extend to the hypodermis (Figure 1.1). The base of the hair follicle (the hair bulb) encloses a stud of the dermis (connective tissue papilla), which contains blood vessels that provide nutrients to the growing hair matrix. A smooth muscle, the arrector pili, is also attached to the hair follicle. With exposure to cold, or when stimulated by the sympathetic nervous system, this muscle contracts, causing the hair to stand erect and/or a skin bulge to form in front of the follicle (resulting in “goose bumps”).

1.1.5.2. Sebaceous glands

Sebaceous glands originate from the epidermis and are primarily located in the dermis, where they are usually found in association with hair follicles (thus forming a pilosebaceous unit) (Figure 1.1). They are under hormonal control and are most abundant in the scalp, forehead and upper back. The sebaceous glands, which are connected to the hair follicles via ducts, deposit their secretions (a mixture of squalene, cholesterol, cholesterol esters, wax esters, and triglycerides) into the upper third of the follicular canal (30, 31). The sebum is subsequently distributed to the skin surface, where it has an acidic pH between 4.8 and 6.4 (6) and also contains free fatty acids and small amounts of mono- and diglycerides due to the bacterial hydrolysis of some of the triglycerides (30). As the sebaceous glands secrete sebum by a holocrine mechanism, the phospholipids of the cell membranes are not present within sebum, but their fatty acids may be secreted and re-esterified into sebum lipids (30). Sebum lubricates the skin and the short chain free fatty acids found within this secretion are bacteriostatic and fungistatic (4).

1.1.5.3. Sweat glands

Sweat glands are divided into two subtypes: eccrine and apocrine glands. Eccrine glands, which are epidermal in origin, are the most abundant type of glandular structure and constitute two-thirds of all sweat glands (1). Eccrine sweat is a watery, hypotonic fluid (containing sodium, chloride, potassium, urea, and lactate) derived from plasma,

which has a slightly acidic pH (4). The sweat is manufactured in a secretory coil embedded in the lower dermis or hypodermis and travels, via a duct that leads through the dermis, to the skin surface. The principle function of sweat is to cool the body in response to high external temperature and physical exertion: after the eccrine sweat glands pour out their secretion over the skin surface, the water evaporates and removal of the heat of vaporisation cools the body (4). As the autonomic nervous system innervates the glands, emotional stress can also cause sweating.

Apocrine glands develop as part of the pilosebaceous unit and tend to be larger than eccrine sweat glands (4). They are mainly located at the axillae, perianal and genital regions, and the mammary areola. The bulk of the gland forms a tubule, which lies in the hypodermis, and a secreting duct that opens into the neck of the hair follicle, above the sebaceous gland. Few ducts exist onto the skin surface. The apocrine gland secretes a milky fluid that contains lipids, proteins, lipoproteins and saccharides (4). This odourless fluid can develop a characteristic odour upon metabolism by surface bacteria (32). The secretion of apocrine sweat is regulated by the autonomic nervous system, thus emotional stress may provoke discharge. Although they play no part in thermoregulation, apocrine glands are considered to be vestigial secondary sex organs that have no apparent function (4).

1.1.5.4. Nails

The nail apparatus essentially consists of the nail folds, nail matrix, nail bed and hyponychium, all of which form the nail plate (33). The nail plate is a hard and mechanically rigid structure that is held in place by lateral nail folds and the nail bed. It is made up of ~25 stacked layers of terminally differentiated, keratinised cells that are held together by globular, cysteine-rich proteins, which form disulphide links that act as 'glue' (33). The nail plate is mostly comprised of keratin: most (~80%) of which is hard keratin, whilst the remainder is soft keratin (34, 35). The nail plate has a water content in the order of 10 to 30%, which is important for nail elasticity and flexibility (33).

1.2. STRUCTURE, DYNAMICS AND BARRIER FUNCTION OF THE STRATUM CORNEUM

1.2.1. Assignment of the stratum corneum as the rate-limiting barrier layer of the skin

The low permeability of human skin to various substances has been known for some time and as early as 1853 it was recognised that the various skin layers were not equally permeable (21). However, it was not until water permeability experiments were conducted on isolated skin samples that it was realised that the stratum corneum was the primary rate-limiting barrier (16). This observation was verified by Blank, who used adhesive cellophane tape to progressively remove layers of the stratum corneum (36). These experiments revealed that the permeability of water through excised, full-thickness skin increased when the lowest layers of the stratum corneum were removed. Accordingly, it was concluded that the rate-limiting barrier was located in the lowest regions of the stratum corneum. However, after this data was reinterpreted by Schleuplein it was ascertained that the bulk of the stratum corneum is a uniformly good diffusion barrier (21).

The ability of the stratum corneum to control both the loss of water and the influx of exogenous materials can be related in part to its high density (up to 1.4 g/cm^3 in its dry state), low level of hydration (of 15 to 20% compared with the average 70% for the body), and the low surface area that is available for solute diffusion (as discussed in forthcoming sections, it appears that substances entering the body do so via the very narrow intercellular regions of the stratum corneum) (1). The barrier function of the stratum corneum is further facilitated by the inconspicuous shedding of individual cells or aggregates of cells from the stratum corneum (desquamation), where the total turnover time of the stratum corneum is of the order of 2 to 4 weeks (37).

All of these characteristics are afforded by the unique chemical and physical morphology of the stratum corneum, which, as mentioned in Section 1.1.1, results from the terminal differentiation of the basal keratinocytes of the epidermis.

1.2.2. Components of the stratum corneum

The stratum corneum is a unique, heterogeneous integument essentially composed of 15 to 25 layers of stacked, terminally differentiated keratinocytes that are embedded in a continuous array of extracellular lipids. This structural arrangement has given birth to the analogy of the stratum corneum as a brick wall in which the corneocytes are the “bricks” and the intercellular lipids are the “mortar” (16).

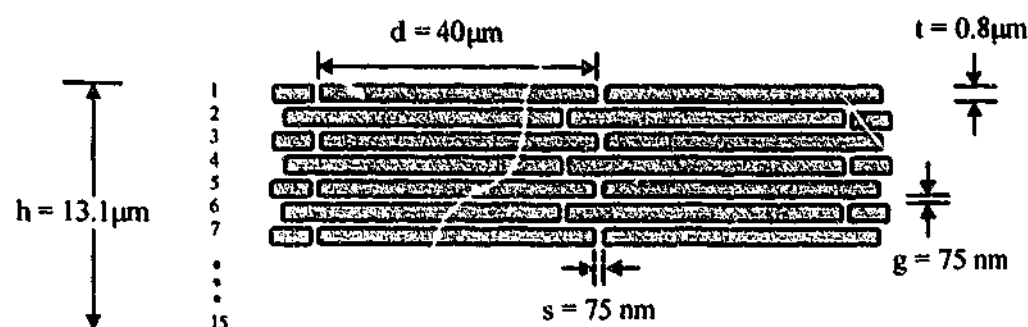


Figure 1.3. A schematic representation of the “brick and mortar” model of human stratum corneum (adapted from Johnson et al (38)). The dimensions shown are the corneocyte diameter (d), corneocyte thickness (t) and the vertical and lateral thickness of the intercellular space (g and s , respectively). According to this particular model, the thickness of the stratum corneum (h) is $13.1\mu\text{m}$, which corresponds to 15 stacked layers of corneocytes.

It is evident from the “brick and mortar” model shown in Figure 1.3 that the corneocytes occupy the most space within the stratum corneum whereas the intercellular lipid lamellae are located in the very narrow regions between the corneocytes. Accordingly, the stratum corneum is mostly comprised of intra-corneocyte protein (75 to 80%w/w on a dry basis) whereas the intercellular lipids account for 5 to 15 %w/w of the total dry weight (39). Though not included in the model, the cornified cell envelope accounts for ~7%w/w of dry weight (40).

1.2.2.1. Corneocytes

During the final stages of differentiation, the keratinocytes of the stratum granulosum are transformed into the flat, hexagonal, keratin-filled corneocytes of the

stratum corneum. The corneocytes are aligned parallel to the stratum corneum surface and each corneocyte measures approximately 0.5 to 1.5 μm thick, with a diameter ranging from 34 to 46 μm (41). However, these dimensions can vary according to age, anatomical location and conditions that influence epidermal proliferation, such as UV radiation (42).

As the nucleus and other cellular organelles of the keratinocyte are completely destroyed during the transition from the stratum granulosum to the stratum corneum, the cell becomes filled with keratin intermediate filaments (predominantly keratins 1 and 10) and other associated matrix proteins, such as those involved in the cornified cell envelope (11, 16). Consequently, the interior of the corneocytes is essentially comprised of an insoluble matrix of protein that consists primarily of soft keratin, which is mostly in the α -helical conformation (43).

As alluded to in Section 1.1.1.1, keratins 1 and 10 aggregate to form dense keratin fibrils (macrofibrils) within the corneocyte. During the terminal stages of epidermal differentiation, profilaggrin (which is synthesised in the keratohyalin granules of the keratinocytes of the stratum granulosum) is processed by dephosphorylation and proteolysis to form filaggrin, which binds to the keratin intermediate filaments and facilitates their aggregation into macrofibril bundles (44). The keratin intermediate filaments are stabilised by intra- and inter-molecular disulphide bonds and it is thought that that filaggrin organises the keratin filaments such that appropriate disulphide bonds can be formed (17). After its formation from profilaggrin, filaggrin is processed into free amino acids that are osmotically-active (44). These amino acids, along with various other proteins, form an amorphous, sulphur-rich matrix of proteins that surrounds the keratin fibers (20, 45, 46).

The macrofibrils that are formed from the aggregation of the keratin intermediate filaments are orientated approximately parallel to the long dimension of the corneocyte (47). Due to their orientation within the corneocyte, these fibrils confer structural rigidity on the corneocyte (47).

1.2.2.2. Cornified cell envelope

The cornified cell envelope consists of two components: a thick layer (~15 nm) adjacent to the cytoplasm of the corneocyte which is composed of various structural

proteins, and a thin layer (~4 nm) composed of lipids (11, 40). The assembly of the cornified cell envelope is believed to occur via three principal stages and begins in the upper layers of the stratum spinosum (48):

1. *Initiation:* A monolayer of proteins forms along the entire inner surface of the keratinocyte membrane, including over the desmosomes, forming a scaffold. These proteins (including envoplakin, periplakin and involucrin and other cellular proteins such as the desmosomes) are cross-linked by N^{ϵ} -(γ -glutamyl)lysine isopeptide bonds.
2. *Formation of the lipid envelope:* Hydroxyceramide molecules, which contain long ω -hydroxyacyl chains comprised of 30 to 34 carbons, form a lipid monolayer over the entire corneocyte surface and are covalently bound to the glutamine residues of scaffold proteins such as involucrin via ester linkages (20). It is thought half of the lipid molecules are covalently bound to the scaffold proteins by the ω -hydroxy terminus and the other half by the sphingosine head-group (11) (Figure 1.4). This arrangement allows for the unbound portion of the hydroxyceramides to interdigitate into the lipid bilayers of the intercellular space (16).
3. *Reinforcement:* Loricrin, complexed with small proline-rich proteins, and small amounts of other proteins (such as cystatin A) are cross-linked with the pre-existing protein layer. In addition to the N^{ϵ} -(γ -glutamyl)lysine isopeptide bonds formed by the action of transglutaminase enzymes, other protein cross-links are also formed within the protein scaffold, such as N^1, N^8 -bis-(γ -glutamyl)spermidine and disulphide bonds (42). This extensive network of cross linking contributes to the overall integrity and the insolubility of this structure. The keratin intermediate filament-filaggrin complex also becomes cross-linked to the protein scaffold (42).

Although the cornified cell envelope itself does not possess intrinsic water barrier properties, it is thought to play an important role in the organisation of the intercellular lipid lamellae, inter-corneocyte cohesion, the semi-permeable properties of the stratum corneum and/or the unusual resistance of the stratum corneum to proteolytic enzymes (16, 49).

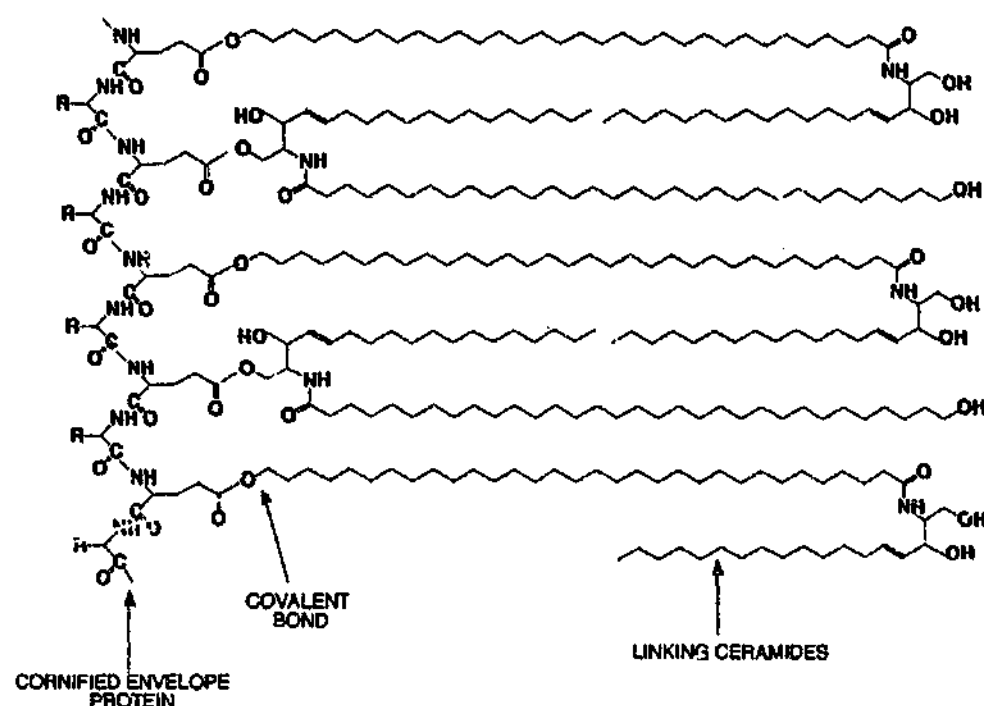


Figure 1.4. A representation of the cornified cell envelope. Adapted from Lazo et al (50).

1.2.2.3. Corneodesmosomes

During the final stages of epidermal differentiation the structure of epidermal desmosomes is also modified such that an electron-dense plug referred to as a corneodesmosome is formed (51). Analogous to the functions of the desmosomal structures in the epidermis, the corneodesmosomes provide a link between the keratin intermediate filaments of adjacent corneocytes, “riveting” the cells together (47). Corneodesmosomes are composed of the same transmembrane glycoproteins found in desmosomes (desmogleins and desmocollins) as well as additional specialised proteins such as corneodesmosin, which plays a critical role in cohesion within the corneodesmosomal structure (51).

1.2.2.4. Intercellular lipids

The intercellular lipids of the stratum corneum form a continuous phase of broad lipid lamellae that are orientated approximately parallel to the stratum corneum surface (52, 53). As previously mentioned, the membrane coating granules contain lamellar disks,

which are precursors of the intercellular stratum corneum lipids. These lipid precursors include phospholipids, free sterols, and glucosylceramides (54). During the transition from the stratum granulosum to the stratum corneum, the membrane coating granules fuse with the plasma membrane of the granular cell and discharge their contents into the intercellular space (refer to Section 1.1.4). Following the extrusion of the lamellar disks, the polar lipid precursors are enzymatically cleaved to form nonpolar lipids that are eventually assembled into lamellar structures (which will be described in forthcoming sections). In particular, acid hydrolases break down the phospholipids into free fatty acids and glucosylceramides to ceramides (53).

As a result of these biochemical transformations, there are distinct variations in the distribution of lipid classes during the course of epidermal differentiation (1). In particular, phospholipids – which dominate in the stratum basale – are absent in the stratum corneum. Consequently, the intercellular space of the stratum corneum contains an unusual lipid composition consisting of a roughly equimolar mixture of ceramides, cholesterol and free fatty acids (1, 16, 55) (Table 1.1).

Concurrent with the changes in lipid composition that occur following the extrusion of the lamellar granule contents, the stacks of lamellar disks extruded from the membrane coating granules are rearranged edge-to-edge and then fuse to form the continuous intercellular lamellae (11). It is thought that the lamellar disks are formed by the flattening of membrane-bound vesicles (liposomes), which results in intercellular lamellar sheets comprised of double lipid bilayers (11).

During the formation of the lipid lamellae at the interface between the stratum granulosum and stratum corneum, the lamellae orientate parallel to the corneocytes and the lipid monolayer of the cornified cell envelope acts as a template during this process (i.e. it acts as a substrate to which the unbound lipids may adhere and adopt their lateral organisation) (52). Interestingly, however, isolated lipid mixtures of ceramides and cholesterol reveal a similar phase behaviour to that found in intact stratum corneum (56). Thus, it is thought that the cornified lipid envelope may not be important for the formation of the lamellar phases, but is very important for the orientation of the lipid lamellae in the stratum corneum (52).

Table 1.1. General composition of stratum corneum lipids (expressed as percentage of the total weight (%w/w) or total mole fraction (mol %) of extracted stratum corneum lipids). Adapted from Wertz and Downing (16) and Walters and Roberts (1).

Lipid	% w/w	mol %
Cholesterol esters	10.0	7.5
Cholesterol	26.9	33.4
Cholesterol sulphate	1.9	2.0
Total cholesterol	38.8	42.9
Ceramide 1	3.2	1.6
Ceramide 2	8.9	6.6
Ceramide 3	4.9	3.5
Ceramide 4	6.1	4.2
Ceramide 5	5.7	5.0
Ceramide 6	12.3	8.6
Total ceramides	41.1	29.5
Fatty acids	9.1	17.0
Others	11.1	10.6

As previously mentioned, the major lipid classes found within the intercellular space of the stratum corneum are ceramides, cholesterol and free fatty acids. At present, eight different classes of ceramides have been isolated from human stratum corneum, where the classification is arbitrarily based on polarity, with ceramide 1 being the least polar (1) (Figure 1.5). The ceramides consist of a sphingosine or phytosphingosine base to which a non-hydroxy or α -hydroxy fatty acid is chemical linked. Within the stratum corneum, the fatty acid acyl chains are predominantly comprised of 24 and 26 carbons (57, 58).

Due to their amphiphilic structure and long-chain constituent acyl fatty acids, ceramides are thought to play a critical role in the barrier function of the stratum corneum (1, 16, 58-60). However, despite the fact that numerous studies have demonstrated that ceramides are required for the normal barrier function of the stratum corneum (49, 61, 62), the exact functions of the individual ceramide types are still not fully understood (1). However, due to their hydrogen-bonding capabilities it is likely that the ceramides form inter-lipid hydrogen bonds between their head-group moieties and that these bonds play a critical role in the formation of very rigid sublattices (52).

Ceramide 1, which possess a unique molecular structure consisting of a linoleic acid chemically bound to a 30 to 34 carbon ω -hydroxy fatty acid, has been found to play a critical role in the organisation of the intercellular lipid lamellae. It is postulated that the long ω -hydroxyacyl chain of ceramide 1 completely spans one lipid bilayer whilst its ester-linked linoleate inserts into an adjacent bilayer (16). This arrangement enables ceramide 1 to act as a "molecular rivet" that links two adjacent bilayers together, thus allowing for a tightly-packed structure (16, 63).

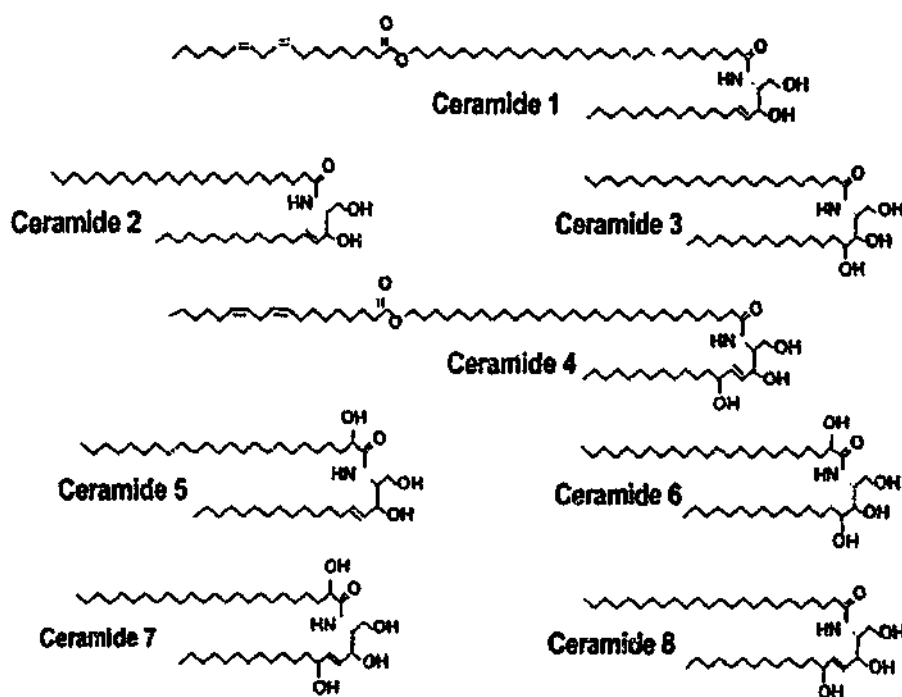


Figure 1.5. Molecular structures of the ceramides found within the intercellular space of human stratum corneum. From Bouwstra et al (19).

In most biological membranes cholesterol acts as a stabiliser and reduces the mobility of the lipid alkyl chains. It is likely that cholesterol serves a similar function in the intercellular lipid lamellae of the stratum corneum as it appears to loosen the chain packing of the ceramide alkyl chains (64). Although the exact role of cholesterol esters within the lipid lamellae is quite elusive, it is possible that these lipids span adjacent lipid bilayers and act as additional stabilising agents (1).

The role of cholesterol sulphate appears to be somewhat varied. It has been demonstrated that cholesterol sulphate is required for the formation of proper lipid phase

behaviour over a wide temperature range as it stabilises the lipid lamellar phases. This function may be due, or partly due, to the electrostatic interactions induced by the negatively charged sulphate group and/or the ability of cholesterol sulphate to dissolve cholesterol in the lamellar phases (19). As mentioned in Section 1.2.4, cholesterol sulphate also plays a role in the desquamation process.

The free fatty acids of the stratum corneum intercellular space are composed of saturated long-chain acids in which the majority are lignoceric acid (comprised of a 24-carbon chain) and hexacosanoic acid (comprised of a 26-carbon chain) (1). Saturated and unsaturated fatty acids with shorter chains are also found within the upper layers of the stratum corneum, however these are components of the sebaceous lipids. Although the exact roles of the free fatty acids are unclear, free fatty acids increase the solubility of cholesterol in lipid mixtures which may be essential for the barrier function of the stratum corneum (63).

1.2.3. Relationship between stratum corneum microstructure and barrier function

It was not until the 1950's and 1960's that experiments were performed which demonstrated that removal of the stratum corneum lipids by solvent extraction dramatically increased water permeability, indicating that the intercellular lipids play a critical role in the barrier function of the stratum corneum (53). The contribution of the lipid bilayers to the ability of the stratum corneum to act as a barrier that limits the permeation of various substances and water loss through the skin can be attributed to their highly ordered arrangement (47).

As the carbon chains of the free fatty acids and most ceramides found within the intercellular space are non-branched and saturated, they can attract each other through van der Waal's attraction as the lipids aggregate to form bilayers structures. This high degree of attraction results in a tight, closely-packed and well-organised crystalline structure (47) (Figure 1.6). As mentioned in Section 1.2.2.4, the association between the adjacent ceramide molecules is also stabilised by hydrogen bonding interactions between the polar head groups.

From this highly ordered arrangement it may be inferred that the lipid lamellae exist as a very stable, crystalline phase. However, as the stratum corneum is a somewhat semi-permeable membrane (rather than an *impermeable* membrane) it is apparent that the

intercellular lipid lamellae do not entirely exist in a crystalline state (21, 47). Consequently, various models have been developed – based on the results of various biophysical studies on the stratum corneum – in order to define the physical state of the lipid lamellae.

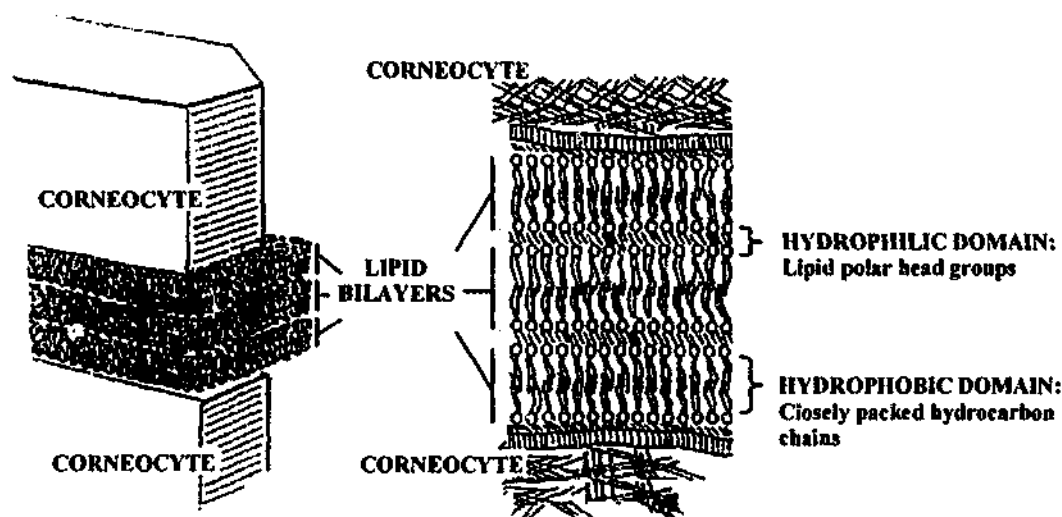


Figure 1.6. A schematic representation of the highly ordered arrangement of the intercellular lipid bilayers within human stratum corneum. Adapted from Lindberg and Forslind (47).

For instance, the “domain mosaic model” proposed by Forslind and colleagues suggests that large crystalline domains are separated by thin liquid crystalline channels and that any water present in the intercellular space associates with the liquid crystalline phase (47). On the other hand, Bouwstra and co-workers have proposed a “sandwich model” in which a narrow fluid domain is sandwiched between two broad crystalline lipid layers (59). More recently it has been revealed that although lipid packing is predominantly orthohombic (crystalline phase) there may be some lipids that have a looser, hexagonal packing (gel phase) in the upper layers of the stratum corneum (65).

Although the exact physical state of the lipid lamellae has not yet been elucidated, it is evident from the diverse range of biophysical investigations that have been conducted over recent decades that the intercellular lipid bilayers show an exceptional degree of conformational order (66) and therefore impose a high degree of diffusional

resistance to solute permeation. For instance, it is well established that the stratum corneum intercellular lipid bilayers undergo phase transitions (in which the alkyl chains of the lipid bilayers change from a closely-packed, crystalline state or a gel-like state to a liquid-crystalline state) at ~35, 70 and 80 °C, with the latter being associated with the corneocyte lipid envelope (67). Thus, at normal physiological skin temperatures (~32°C) the stratum corneum would function as a coherent barrier towards solute transport (47). It has been demonstrated, however, that water vapour permeability increases as a function of increasing temperature and that this effect is most likely to be related to a decrease in the conformational order of the lipid alkyl chains (68, 69). Furthermore, at temperatures above 70°C water vapour permeability is characterised by an activation energy similar to that of free diffusion, suggesting that the stratum corneum lipid bilayers offer little diffusional resistance under these conditions (68).

1.2.4. Desquamation

In order to maintain a constant stratum corneum thickness at any given body site the superficial parts of this integument must be continuously shed, or desquamated, at a rate which balances the formation of new corneocytes. Although the exact mechanisms involved in desquamation are not fully understood, it would appear that corneodesmosomes are responsible for inter-corneocyte cohesion and thus their proteolytic degradation plays a critical role during this process (51). An event that has been implicated in this process is the activation of stratum corneum chymotryptic enzyme (SCEE) and stratum corneum tryptic enzyme (SCTE) (1). Other proteins that may play a role in desquamation include cathepsin D, desquamin and stratum corneum gelatinase (1). It has also been suggested that corneodesmosin, which is associated with the extracellular part of the corneodesmosome, is continuously degraded in the stratum corneum (1).

One change in lipid composition that has been found to accompany desquamation is a decrease in the amount of cholesterol sulphate (16). As cholesterol sulphate may have an inhibitory effect on desquamation (51), it is possible that its degradation plays an important role in the exfoliative process.

1.2.5. Repair of barrier function following perturbation

Damage to the stratum corneum may result from physical insult (such as tape-stripping) or exposure of the skin to various chemicals (such as those used to enhance drug permeation through the skin – dimethyl sulphoxide, surfactants and Azone® are some examples (Section 1.4.3.2)) (70). Once the stratum corneum is perturbed a variety of signalling responses are initiated to stimulate a metabolic response within the underlying epidermis, which is ultimately aimed towards normalising the stratum corneum barrier function. The restoration of barrier function appears to follow a biphasic process (42, 71). During the initial rapid phase of barrier recovery there is a temporary increase in the secretion of lamellar bodies from the granular cells of the epidermis, an increase in cholesterol and fatty acid synthesis and accelerated production and secretion of new lamellar bodies into the intercellular space (71). During the subsequent, slower phase there is an increase in ceramide synthesis and an increase in deoxyribonucleic acid synthesis, which leads to epidermal hyperplasia (71). Repeated or severe barrier disruption may also stimulate an inflammatory response, which involves the deeper skin layers (42).

1.3. PRINCIPLES OF PERCUTANEOUS DRUG ABSORPTION

1.3.1. Drug absorption through the skin

Substances that come into contact with the skin surface, either deliberately or accidentally, can penetrate the stratum corneum, permeate the skin strata and eventually diffuse into the underlying tissues or become absorbed into the dermal blood supply and hence the systemic circulation (Figure 1.7). From a pharmaceutical standpoint, this process can be exploited and/or manipulated in order to deliver substances (1, 72-74):

- i. to the skin surface (e.g. cosmetics, sunscreens, insect repellents)
- ii. to targeted skin layers (e.g. corticosteroids to treat localised skin disorders)
- iii. to underlying tissues (e.g. non steroidal anti-inflammatory agents to treat muscular inflammation)

- iv. into the systemic circulation (e.g. oestradiol to treat symptoms of menopause, nicotine to aid smoking cessation, glyceryl trinitrate for the treatment of angina pectoris and fentanyl for the treatment of chronic cancer-related pain)

As evidenced by the latter examples, the skin has become a popular site for systemic drug administration, which can mainly be attributed to the fact that transdermal drug delivery (TDD) presents numerous advantages over conventional routes of drug administration, which are discussed in Section 1.5.1. However, TDD also has limitations, which are mainly related to the biological, physicochemical and pharmacokinetic aspects of percutaneous absorption (75, 76). For instance, due to the efficient barrier properties of the stratum corneum there will be a characteristic lag time prior to the accumulation of adequate plasma drug concentrations and the onset of therapeutic action. Thus, TDD is not suitable for acute conditions where a rapid therapeutic effect is desired.

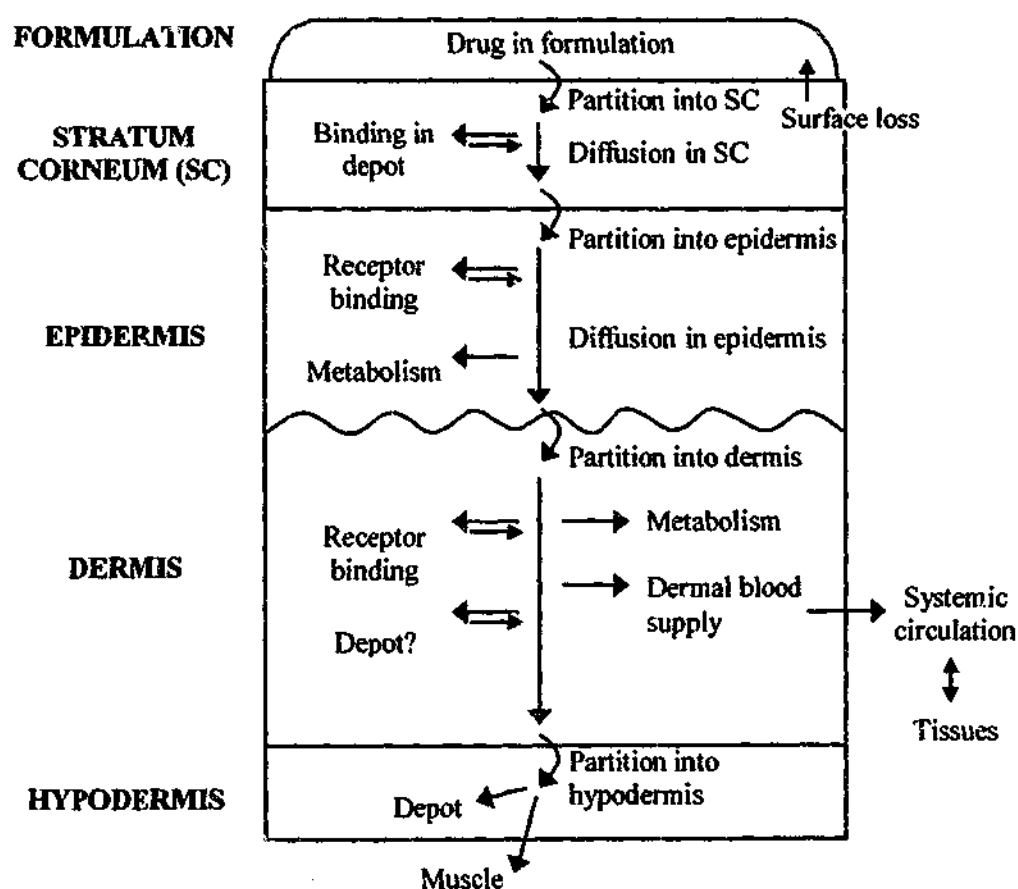


Figure 1.7. Diagrammatic representation of some of the processes involved in the absorption of substances through the skin. Modified from Barry (77) and Walters and Roberts (1).

The initial point of contact for a topically applied drug is the skin surface, which is covered by sebum, sweat and surface bacteria. It is thought that this superficial layer has a negligible impact on percutaneous absorption as it permits the penetration of both polar and non-polar compounds (75). It is possible, however, that some drugs are degraded by surface bacteria (75). It has also been proposed that desquamation can reduce the percutaneous absorption of lipophilic chemicals or chemicals with high molecular weights (78).

As the stratum corneum is the main rate-limiting barrier of the skin, the partitioning of a drug into the stratum corneum and its subsequent diffusion through this integument are critical determinants of percutaneous drug absorption. As discussed in forthcoming sections, the rate and extent of either of these processes are influenced by the physicochemical properties of the drug and of the applied formulation. Provided that the stratum corneum does not act as a significant depot for the drug, the drug will then partition into the underlying epidermis.

As discussed in forthcoming sections, the stratum corneum and the epidermis are quite distinct structures in that the stratum corneum essentially provides a lipophilic milieu for drug diffusion whereas the epidermis provides a more hydrophilic domain. As the epidermis does not contain a local blood supply, it essentially serves as an unstirred aqueous boundary layer for any substance with high lipid solubility and low aqueous solubility (71) (refer to Section 1.3.3.2.3). As the epidermis also contains a variety of enzymes, a significant amount of the drug may not reach the underlying skin strata if the drug is susceptible to enzymatic degradation (75).

Although the dermis represents another hydrophilic domain within the skin it is thought that the diffusional resistance offered by this layer is unlikely to have a significant effect on the percutaneous absorption of lipophilic substances as they will be cleared by the local blood supply (79). It has been shown, however, that lymphatic flow may limit the clearance of larger solutes (80). The dermis is also a potential site in which substances may bind to proteins, such as receptor ligands (and thus exert a physiologic effect) and it is a further site for metabolic degradation (81). Partitioning into the hypodermis and underlying muscles can occur if the drug bypasses the dermal blood supply (73). As the hypodermis is predominantly composed of adipose tissue, it is possible that lipophilic drugs may accumulate within this layer if they are not cleared by the dermal blood supply (81).

At the simplest level, percutaneous drug absorption might be regarded as a series of steps involving partitioning and diffusion through a multilaminated structure. As each skin layer can be regarded as an isotropic medium that contributes a diffusional resistance to the overall resistance of the structure, it is evident that the layer that imposes the greatest resistance to the transport of most drugs through the skin is the stratum corneum (21).

1.3.2 Transport pathways through the stratum corneum

Given that the stratum corneum is not continuous, but pierced by hair follicles and sweat glands, there are three potential routes of drug transport across the stratum corneum: transappendageal, transcellular or intercellular (73, 82) (Figure 1.8).

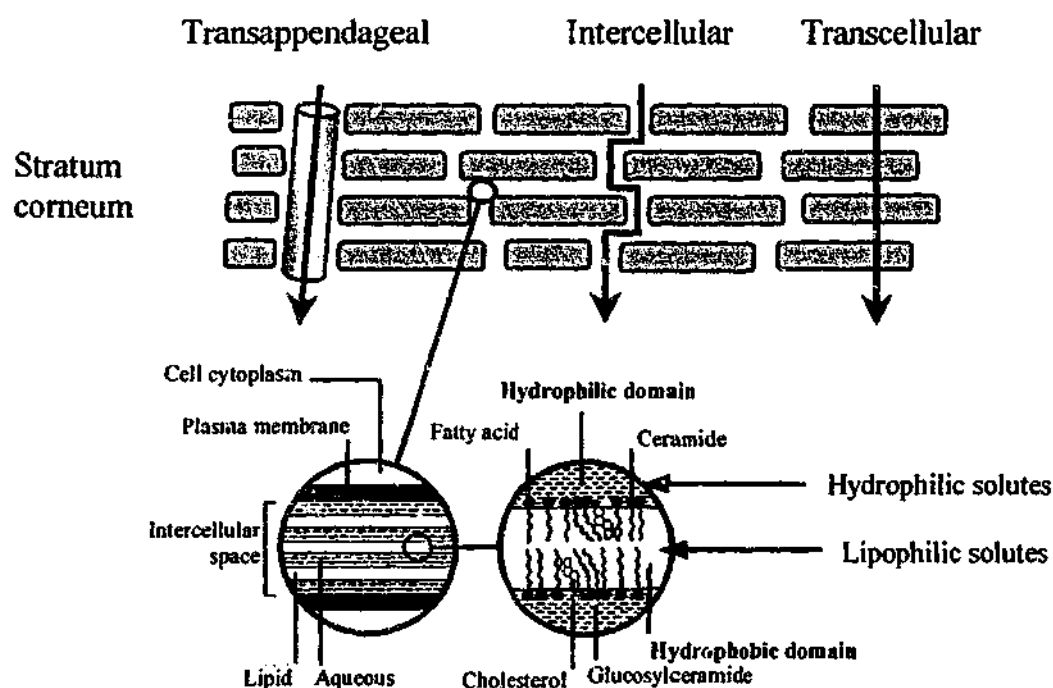


Figure 1.8. Potential transport pathways through the stratum corneum. Adapted from Barry (82) and Roberts (73).

The contribution of the skin appendages (the transappendageal pathway) to transdermal transport remains controversial. As the hair follicles only occupy 0.1% of the total skin area and drug diffusion along the sweat pores would be against an outward aqueous flow, it is thought that this route may only be of minor significance (83). On the

other hand, Scheuplein has suggested that the transappendageal pathway dominates transport during the early stages of drug permeation whereas bulk diffusion through the stratum corneum predominates during the latter stages (84). Although it is possible that the transappendageal route offers an alternative pathway for a permeating molecule, it is generally accepted that diffusion through the bulk of the stratum corneum dominates during the latter stages of skin transport (75).

Drug diffusion through the transcellular pathway involves an alternate passage through the predominately aqueous corneocytes and the narrow intercellular lipid domain between the corneocytes. On the other hand, the intercellular route involves drug permeation solely via the intercellular lipid matrix. The question as to which route dominates drug transport through the stratum corneum has been subject to much conjecture. It has been suggested that for a penetrating drug the relative importance of these two routes will depend on its solubility, its partition coefficients for the proteinaceous (aqueous) and lipid domains and its diffusivities within these phases (82). In agreement with this theory, it has been proposed that the uptake of relatively hydrophilic solutes (with a log octanol/water partition coefficient ($\log K_{OCT/W}$) < 3) is governed by the intra-corneocyte protein domain while more lipophilic solutes ($\log K_{OCT/W} > 3$) reside preferentially in the intercellular lipid domain (85). It must be borne in mind, however, that in order for a drug to penetrate the corneocytes, it must associate with the cornified cell envelope (the lipid monolayer is significantly more hydrophobic than the intercellular lipid lamellae (83) and the scaffold of proteins are highly insoluble) as well as the tightly-packed intra-corneocyte keratin intermediate filaments. As these components are likely to make the corneocytes very dense and almost impermeable to solute transport (39), it is thought that the corneocytes act as mechanical barriers that increase the diffusional path-length of solutes (83).

In light of these factors, it is probably not surprising that there is accumulating evidence to suggest that the intercellular route dominates the transport of both hydrophilic and lipophilic drugs (75, 86-88). As diffusional and morphometric data supports the presence of lipid and polar pathways through the intercellular lipid domain (75, 89), Roberts et al have proposed a bicontinuous intercellular transport pathway in which lipophilic solutes associate with the hydrophobic domain (the closely-packed hydrocarbon chains) of the lipid bilayers whilst relatively hydrophilic solutes traverse the intercellular domain via the lipid polar head group region (75) (Figure 1.8).

Although it is likely that the intercellular route dominates drug permeation, the structure of the stratum corneum dictates that a penetrating molecule must diffuse through the intercellular lipids regardless of which transport pathway predominates. Thus, it is generally accepted that the diffusional resistance offered by the intercellular stratum corneum lipids plays a critical role in skin permeation (39).

1.3.3. Factors affecting percutaneous drug absorption

1.3.3.1. Biological factors

1.3.3.1.1. Anatomical site

Percutaneous drug absorption can vary depending on the area of the body to which the drug of interest is applied (90, 91). Although site-to-site variations in skin permeability may not follow the same pattern for all compounds, it is generally agreed that some body sites (such as the head and genital region) are usually more permeable than others (such as the extremities) (90). For instance, the skin penetration of benzoic acid, caffeine and acetyl salicylic acid has been found to decrease in the order of forehead > postauricular > abdomen > arm (92).

Although the thickness of and the number of corneocytes within the stratum corneum can vary among different anatomical sites (9, 10), it has been demonstrated that these differences are insufficient to account for regional variations in percutaneous drug absorption (93). Rather, it would appear that site-to-site variations in skin permeability are related to differences in the content and composition of the stratum corneum lipids (93-96).

1.3.3.1.2. Age, sex and race

At present, the relationship between age or sex and skin permeability has been not been extensively investigated. Most of the evidence reported to date seems to indicate that percutaneous drug absorption is not significantly different between men and women (90, 97-99). However, there are conflicting reports as to whether age-related differences affect percutaneous drug absorption in humans. Although some researchers have reported that the skin of the newborn infants, children and/or the elderly are more permeable than

that of adults (71, 77, 90, 100), several studies have failed to show any age-related differences in skin permeability (71, 77, 90, 97, 98, 100). It is possible, however, that the physicochemical properties of the drug of interest may be an important consideration when assessing age-related variations in percutaneous absorption (101). Although further research needs to be conducted, it is possible that various morphological and physiological determinants could be responsible for age-related differences in percutaneous drug absorption such as a reduced level of skin hydration, reduced epidermal turnover, decreased microvascular blood flow, and an increase in the size of the corneocytes (90).

Differences have been found in both the permeability and structure of skin of different racial descent. For instance, Caucasian skin has been found to be more permeable, have fewer stratum corneum cell layers and a lower lipid content than black skin (90). Different hyperaemic responses have also been detected between black and white skin (90). The permeability of compounds such as methyl nicotinate has been found to vary among Caucasians, Hispanics, Blacks, and Asians (102). It has been reported that although the corneocytes of Caucasian, Hispanic, Black, and Asian stratum corneum are of a similar size there are differences in spontaneous desquamation (90). Inter-racial variations in stratum corneum ceramide content have also been reported (103).

1.3.3.1.3. Dermal blood supply

As alluded to in previous sections, the dermal blood flow usually functions as a "sink" for diffusing substances that reach this skin layer. As this "sink" ensures that dermal drug concentrations remain near zero and that the concentration gradient across the epidermis remains maximal, it is possible that an increase in dermal blood flow could reduce drug residence time in the dermis and increase the concentration gradient across the epidermis (i.e. increase the rate and extent of percutaneous drug absorption) (71). As the stratum corneum is the rate-limiting barrier towards the permeation of most drugs, the dermal blood supply may have a greater effect on percutaneous absorption when the barrier function of the stratum corneum is compromised or when dermal blood flow is drastically reduced (71, 77).

1.3.3.1.4. Exercise, humidity and temperature

It has been demonstrated that exercise, an increase in skin or body temperature and/or an increase in humidity can enhance percutaneous drug absorption (104-108). Although it is possible that exercise and elevated skin and body temperature can enhance percutaneous drug absorption by increasing the rate of dermal blood flow (106-108), changes in skin temperature can also have a profound effect on the phase behaviour of the stratum corneum intercellular lipid lamellae, as previously discussed in Section 1.2.3.

1.3.3.1.5. Skin condition

Several factors can impair the barrier function of the stratum corneum. For instance, various skin disorders (such as ichthyosis, psoriasis and atopic, irritant-contact and allergy-contact dermatitis) have been shown to impair skin barrier function (as assessed by an increase in transepidermal water loss) (71). Various solvents, drugs and vehicles can also alter the barrier properties of the skin. For instance, some solvents (such as methanol, ethanol, acetone, dimethylsulphoxide, ethyl ether, chloroform and carbon tetrachloride) have been found to extract lipids from the stratum corneum (109). On the other hand, it has been proposed that keratolytic agents, such as salicylic acid, resorcinol and urea impair the barrier properties of the stratum corneum via protein denaturation (109). It has also been suggested that polar solvents, such as water and propylene glycol, may alter the integrity of the stratum corneum by osmotic- or hygroscopic-related effects (109). As discussed in Section 1.4.3.2, chemical penetration enhancers may also reduce the barrier function of the stratum corneum.

1.3.3.1.6. Cutaneous metabolism

It has been recognised for some time that the skin contains a variety of enzymes that are capable of metabolising both endogenous chemicals (such as hormones and steroids) and foreign substances that come into contact with it (110, 111). Many of the drug metabolising enzymes that have been identified in the skin are similar to those found in the liver, although quantitative and qualitative differences in enzymatic activity have been observed (90). In general, the specific activities of cutaneous metabolising enzymes appear to be lower than their hepatic counterparts (90). However, certain enzymes (such

as N-acetyltransferases and reductases) have demonstrated fairly high activity (90). Some of the enzymes found within the skin include enzymes involved in both Phase 1 "functionalisation" reactions (such as oxidation enzymes that belong to the cytochrome P-450 system, reductases and esterases) and Phase 2 "conjugation" reactions (such as glutathione transferases, glucuronosyltransferases, sulfotransferases and acetyltransferases) (111). Studies into the localisation of various enzymes in the skin indicate that in most instances the epidermis, sebaceous glands and upper portion of the hair follicles are the major locations of xenobiotic enzymes and that the enzymatic activity of the epidermis is generally greater than that of the dermis (111).

As the metabolism of foreign substances involves detoxification and elimination processes, which result in the formation of molecules that are more hydrophilic and easily excreted, it is evident that cutaneous metabolism can contribute to the clearance of xenobiotics from the skin, which in turn can reduce the extent of percutaneous drug absorption and hence the pharmacological effect of the substance (110). Thus, a major potential outcome of cutaneous metabolism is the "skin first-pass effect" in which a significant amount of a topically-applied substance is metabolised on route to its site of action in regions of the skin or into the systemic circulation (75).

1.3.3.1.7. Species differences

It is well established that inter-species variations in percutaneous drug absorption exist. Many different animal models have been used to study *in vitro* and *in vivo* percutaneous drug absorption including mice, rats, rabbits, monkeys, and pigs (75, 90). Several differences have been reported in the structure and barrier function of the skin from different animals and – not surprisingly – the permeability of various substances. For instance, the skin of small laboratory animals (such as mice and rats) usually has a higher number of hair follicles than that of human skin and is generally more permeable to various solutes (90). Species-related differences in percutaneous drug absorption have also been related to differences in the enzymatic activity of the skin (112) as well as differences in stratum corneum thickness, corneocyte adhesion, surface lipid content and intercellular lipid content and/or composition (90, 113). In general, species-related differences in skin permeability are usually less than 5-fold and the permeability of pig and rhesus monkey skin has been found to be similar to that of human skin (90).

1.3.3.2. Physicochemical determinants

As active transport processes across the skin have not been observed, the usual laws of thermodynamics that pertain to passive diffusion processes can be applied to skin permeation phenomena (21). At the simplest and most ideal level the stratum corneum can be regarded as an homogenous slab of inert material that has a finite and uniform thickness ¹. Consequently, the penetration of most drugs across the stratum corneum is generally regarded as a passive diffusion process that, at the simplest level, can be described by Fick's first law of diffusion ² (114).

The mathematical theory of Fick's first law of diffusion is based on the hypothesis that the rate of transfer (or flux (J)) of a diffusing substance at any point in a system and at any instant is proportional to the concentration gradient (114, 115):

$$J = \frac{DC}{RT} \left[-\frac{d\mu}{dx} \right] \quad 1.1$$

$$= -DC \frac{d \ln a}{dx} \quad (\mu = \mu^\circ + RT \ln a) \quad 1.2$$

$$= -DC \left[\frac{D \ln C}{dx} + \frac{D \ln \gamma}{dx} \right] \quad (a = \gamma C) \quad 1.3$$

$$= -D \left[\frac{dC}{dx} + \frac{C d \ln \gamma}{dx} \right] \quad 1.4$$

$$= -\frac{DdC}{dx} \quad (\text{for a constant } \gamma) \quad 1.5$$

where D is the diffusion coefficient of the drug in the barrier, R is the gas constant, T is the absolute temperature, $d\mu/dx$ is the chemical potential gradient across the membrane, a is the thermodynamic activity of the drug, which is the product of concentration, C ,

¹ Although the stratum corneum is a heterogeneous structure that is biochemically active, this is a theoretical model that permits convenient mathematical solutions to skin diffusion phenomena.

² Fick's second law of diffusion, which relates the rate of change in concentration with time at a given point in a system to the rate of change in the concentration gradient at that point, is also used to derive mathematical solutions to non-steady state boundary conditions, where the principle of conservation of matter must be considered when describing drug transport across the stratum corneum (refer to Chapters 2 and 4).

and the activity coefficient, γ .

Equation 1.5 shows that the concentration of drug across the membrane decreases linearly as a function of increasing distance from the outermost surface of the membrane in contact with the vehicle to the innermost surface of the membrane (i.e. it describes a steady-state concentration-distance profile) and that the rate of transfer of the diffusing drug is the same across all sections of the membrane. Although Equation 1.5 implies that the concentration gradient becomes the driving force for drug transport, it should be noted (as highlighted by Equations 1.2 to 1.4) that the origin of drug transport across the skin is a gradient in the chemical potential or activity, where the skin provides the resistance or proportionality factor between the flux and the activity gradient (116). The rate of transfer across the membrane, dQ/dt , is given by (115):

$$\frac{dQ}{dt} = \frac{D(C_0 - C_h)}{h} \quad 1.6$$

where h is the thickness of the membrane, Q is the amount of drug penetrated per unit area of the membrane, C_0 is the concentration of drug at the outermost surface of the membrane in contact with the vehicle and C_h is the concentration of drug at the innermost surface of the membrane. The concentration of drug at the outermost surface of the membrane is related to the concentration of the drug in the vehicle (C_v) by the stratum corneum-vehicle partition coefficient, K_{scv} :

$$K_{scv} = \frac{C_0}{C_v} \quad 1.7$$

Thus, if a high, fixed concentration of drug is maintained at the outermost surface of the membrane and the concentration of the drug at the innermost surface of the membrane is maintained at zero (i.e. "sink" conditions), the rate of drug transfer (or drug flux) across the membrane can be given by (115):

$$J_{ss} = \frac{DK_{scv}C_v}{h} \quad 1.8$$

where J_{ss} is the steady-state drug flux across the membrane. It is evident from this simplified form of Fick's first law of diffusion that the major physicochemical

determinants of solute flux are C_v , $K_{sc/v}$ and D . As highlighted in forthcoming sections, these parameters can be affected by various drug-vehicle, vehicle-skin, and drug-skin interactions. There are numerous drug-vehicle, vehicle-skin, and drug-skin interactions that may affect percutaneous drug absorption (75, 117), however only those that are relevant to the work described in this thesis are described.

1.3.3.2.1. Drug-vehicle Interactions

It would appear from Equation 1.8 that drug flux across the skin is proportional to the concentration of drug in the applied vehicle. It is pertinent to bear in mind, however, that the driving force for diffusive transport across the stratum corneum is a gradient in the chemical potential or activity of the drug (Equation 1.2). Thus, Equation 1.8 can be re-written as (118):

$$J_{ss} = \frac{a_v D}{\gamma_{sc} h} \quad 1.9$$

where a_v is the thermodynamic activity of the drug in the vehicle and γ_{sc} is its activity coefficient in the stratum corneum. The thermodynamic activity of the drug in the vehicle can be regarded as the tendency of the drug to partition out of the vehicle and into the stratum corneum (in other words, the "escaping tendency" of the drug from the vehicle) (118, 119). It is evident from this definition that an increase in the thermodynamic activity of the drug in the vehicle will increase its partitioning into the uppermost layers of the stratum corneum, which in turn will increase the activity gradient across the stratum corneum (119).

As drug flux across the stratum corneum is proportional to the concentration of the drug in the applied vehicle, the ratio of drug concentration to its solubility in the vehicle (i.e. the degree of saturation, C_v/S_v) may be used as an indication of the drug's "escaping tendency" from the vehicle (119). In a saturated solution, excess solid drug exhibits maximum thermodynamic activity, as the solid state is the pure form of the drug. Hence, the thermodynamic activity of dissolved drug, which is available for partitioning into the skin, will also be maximal as it is equal to that of the solid drug with which it is in equilibrium (118). Thus, a major deduction from these concepts is that drug flux across the skin will be maximal when the thermodynamic activity of the applied drug is

maximal. This will occur when C_v exceeds its solubility limit in the vehicle (i.e. when the applied vehicle is a saturated solution). Otherwise, when the applied vehicle is a sub-saturated solution, drug flux across the skin will be proportional to the degree of saturation, provided the vehicle does not interact with the stratum corneum (118, 120).

1.3.3.2.2. Vehicle-skin interactions

A major assumption relevant to the use of Fick's first law of diffusion is that components of the applied formulation do not interact with the stratum corneum. It is known, however, that vehicles can penetrate the stratum corneum and in most instances alter the barrier properties of the stratum corneum. Water, for example, is a common vehicle used in topical and transdermal formulations. It is known that upon contact with liquid water, the stratum corneum can absorb up to five times its dry weight of this substance, which would obviously increase the level of hydration of the stratum corneum (121). It has been demonstrated on numerous occasions that an increase in stratum corneum hydration can influence its permeability to various substances (121, 122). The possible mechanisms by which water disrupts the barrier properties of the stratum corneum are described in Chapter 4 (Section 4.4.1). It is also known that viscous vehicles (such as white soft paraffin, lanolin) and occlusive transdermal delivery systems (patches) can increase the level of hydration of the stratum corneum, whereas other vehicles (particularly humectants such as glycerol) can "withdraw" water from the skin (77). On the other hand, some vehicle components (such as chemical penetration enhancers) can reduce the barrier function of the stratum corneum by extracting or perturbing the organisation of the intercellular lipid bilayers (refer to Section 1.4.3.2).

1.3.3.2.3. Drug-skin interactions

Various models have been proposed in order to define structure-activity relationships in skin permeability, most of which pertain to relationships between K_{SC} and/or D (or D/h) and the physicochemical properties of the applied drug (75, 83).

As topically-applied drugs must penetrate both the intercellular lipid domain of the stratum corneum and the more hydrophilic milieu of the epidermis before reaching the systemic circulation, they must possess balanced lipid and water solubilities. Drugs that

are too hydrophilic are unlikely to partition from the vehicle into the stratum corneum whereas drugs that are too lipid soluble will have a high affinity for the stratum corneum and are thus unlikely to partition (or readily partition) into the epidermis. Thus, the rate-limiting factor in the percutaneous absorption of a highly lipophilic compound will be its partitioning at the stratum corneum-epidermal interface (123). Consequently, a parabolic relationship is often observed between the percutaneous absorption of a series of homologous compounds and their $\log K_{oc/w}$ values (75), where optimal values of $\log K_{oc/w}$ for percutaneous absorption are generally between 1 to 3 (124). A parabolic relationship has also been observed between the percutaneous absorption of a series of homologous compounds and their solubility parameters, where optimal absorption is observed for compounds that have a solubility parameter close to that of the stratum corneum lipids (refer to Chapter 4).

A negative linear correlation between solute flux and melting point has been observed for various drugs (123), which highlights the fact that the solubility and diffusivity of a solute in the intercellular stratum corneum lipid domain is also determined by its melting point and crystallinity (83). High-melting, hard crystalline drugs with low enthalpies of fusion are generally less soluble than soft, low-melting crystals (125).

The diffusivity of a solute within the intercellular lipid lamellae will also depend on its molecular size and hydrogen bonding abilities (75). It has been found that the stratum corneum is predominantly a hydrogen-bond donor and that the diffusion coefficient of a drug within the stratum corneum (expressed as $\log D$) decreases as the number of hydrogen bonding groups on the molecule increases, reaching a limiting minimum value for molecules with about four hydrogen-bonding groups (75). It has been proposed that the hydrogen bonding ability of a diffusing molecule will dictate its diffusion within or across the lipid and polar domains of the stratum corneum lipid bilayers (83). In particular, weak hydrogen-bonding molecules will not bind to the polar head group region and will therefore diffuse freely through the lipophilic core of the lipid bilayers whereas strong hydrogen-bonding molecules will be attracted to the rigid polar walls of the lamellae and will diffuse more slowly through this domain (83).

The diffusion coefficient of a drug within the stratum corneum lipid domain is also related to its molecular weight and molecular volume (83). Although it is likely that molecular weight has little effect on the diffusivity of small drugs moieties ($MW < 600$ Da), the diffusion of larger molecules ($MW > 1000$ Da) such as proteins is likely to be

hindered in part by their bulk and also because they usually contain multiple hydrogen bonding groups (125).

In addition to the above-mentioned physicochemical parameters, drug-skin interactions also include those in which the solute binds to binding sites (such as proteins) in the skin (in terms of showing resistance to being washed off or removed from the skin, this is known as 'substantivity') or those in which the solute may alter the barrier properties of the skin (75).

1.4. PASSIVE ENHANCEMENT STRATEGIES IN PERCUTANEOUS DRUG ABSORPTION

It is evident from previous sections that the stratum corneum is a formidable barrier to most topically-applied substances and as such the rate of drug transfer across this membrane is often the major rate-limiting step in percutaneous drug absorption. Thus, in terms of TDD, it is often difficult to deliver therapeutically relevant amounts of drug to the systemic circulation following its topical application to a convenient area of skin. This is confounded by the fact that there is often a lag-time associated with TDD. Although these difficulties can be alleviated in part by selecting suitable drug candidates (Section 1.5.2.1) it is often necessary to employ various enhancement strategies.

It is apparent from the simplified forms of Fick's first law of diffusion presented in Section 1.3.4.2 that the important physicochemical determinants of drug flux across the skin are the thermodynamic activity of the drug in the applied vehicle, the partition coefficient of the drug between the stratum corneum and the vehicle ($K_{sc/v}$) and the diffusion coefficient of the drug within the stratum corneum (D). Thus, enhancement strategies that are often employed to enhance percutaneous drug absorption are fundamentally aimed at optimising one or more of these parameters.

1.4.1. Strategies that influence thermodynamic activity

As the degree of saturation (C_v/S_v) provides a measure of the thermodynamic activity of a drug in an applied formulation, this parameter can be modified in order to optimise percutaneous drug absorption. Increasing the concentration of a drug in a given

vehicle will increase drug flux across the skin (126), however this strategy is limited by the fact that a drug will have a finite solubility within a given formulation. Thermodynamic optimisation of a formulation can also be achieved by reducing the solubility of the drug in the vehicle. Vehicles or other formulation components that are good solvents for the drug will "retain" the drug by reducing its thermodynamic activity whereas those that are poor solvents will increase its thermodynamic activity (119). However, as a topically-applied drug must be in molecular form in order to permeate the skin, this approach needs to be tailored such that the drug "is sufficiently soluble...but not so soluble" (126) in the vehicle in order to maintain a favourable stratum corneum-vehicle partition coefficient.

1.4.1.1. Supersaturation

Supersaturated systems are those in which the drug exhibits unusually high (i.e. greater than unity) thermodynamic activity. This high level of thermodynamic activity will most likely be accompanied by a similar rise in the thermodynamic activity of the drug in the outermost layer of the stratum corneum (127). Accordingly, the chemical potential gradient formed across the stratum corneum will be substantially greater than that formed from a saturated solution. Thus, "maximal" drug flux across the skin (i.e. flux achieved with a saturated solution) can be enhanced many-fold. For instance, Megrab et al demonstrated that compared with the *in vitro* flux obtained from a saturated solution, oestradiol flux across human epidermis was enhanced up to 12-fold following the application of solutions that were up to 12-fold supersaturated (128).

Supersaturated states can be attained using volatile vehicles (129, 130), mixed cosolvent systems (131, 132), temperature changes (132) or the uptake of water into the formulation from the skin (132). In most supersaturated systems crystallisation can occur and impart instability to the system (131). In such instances, anti-nucleant polymers may be incorporated into the formulation.

As alluded to previously, a topically-applied drug must be in solution in order to penetrate the skin. Therefore, drug precipitation or crystallisation may impose a dissolution-rate limiting effect on percutaneous drug absorption and may thus counteract the enhancing effects of supersaturation. This has been demonstrated when small volumes of volatile or volatile:non-volatile vehicle systems have been used in order to

achieve supersaturated states. Although supersaturation caused by the evaporation of the volatile vehicle component has been shown to increase drug flux, it has also been found that increasing the concentration of drug or the volatile component in the vehicle may lead to drug precipitation and to a subsequent decrease in drug flux (129, 130).

1.4.2. Strategies that improve drug solubility in the stratum corneum

Vehicles and/or formulation excipients can modify the solubility of a drug within the stratum corneum, thus increasing the partitioning of the drug from the vehicle into the stratum corneum. As discussed in Chapter 4, solubility parameters provide a measure of how materials will interact with each other: materials that have similar solubility parameters are likely to have a high affinity for each other (133). Thus, a vehicle or formulation excipient that permeates the skin can increase the solubility of a drug within the stratum corneum (and hence $K_{sc/v}$) by shifting the solubility parameter of the stratum corneum lipids ($\delta \sim 20 \text{ MPa}^{1/2}$ (134)) in the direction of the drug (135). For instance, propylene glycol ($\delta \sim 29 \text{ MPa}^{1/2}$ (136)) has been found to increase the skin permeability of metronidazole ($\delta \sim 28 \text{ MPa}^{1/2}$) (135). Similarly, Transcutol® – which is also thought to alter the solubility parameter of the stratum corneum lipids – has been found to increase the permeation of some drugs through the skin by increasing their stratum corneum-vehicle partition coefficients (137, 138). Other solvents, such as ethanol and N-methyl pyrrolidone, may also alter the solubility parameter of the stratum corneum lipids (135).

1.4.2.1. Strategies that reduce the barrier function of the stratum corneum

1.4.2.1.1. Occlusion

It is well established that occlusion of the skin enhances the percutaneous absorption of most drugs (with the exception of many highly lipophilic drugs) and that this effect is related in part to an increase in the humidity under the occlusive system and hence an increase in the level of hydration of the stratum corneum (121). With regard to transdermal drug delivery, the best example of an occlusive delivery system is a transdermal patch.

1.4.2.1.2. Chemical penetration enhancers

By definition, chemical penetration enhancers (CPEs) (or accelerants, absorption promoters or adjuvants) are substances that are incorporated into transdermal formulations in order to promote the penetration of topically applied substances (139, 140). Hundreds of substances have been investigated for their ability to enhance drug penetration through the skin. These substances include sulphoxides, alcohols, fatty acids, polyols, amines, amides, surfactants, alkanes, terpenes and Azone® and Azone® analogues (140). However, in order to be acceptable, safe and effective, a CPE must possess the properties outlined in Table 1.2.

Table 1.2. Desirable properties of a chemical penetration enhancer (141).

-
- Pharmacologically inert
 - Non-irritating, non-allergenic, non-toxic
 - Non damaging to viable cells
 - Rapid onset of effect with a predictable duration of activity
 - Effects are completely and rapidly reversible upon removal
 - Effects do not cause the loss of endogenous materials from the body
 - Physically and chemically compatible with drugs and excipients in the dosage form
 - Cosmetically acceptable when applied to the skin
 - Odorless, inexpensive, tasteless, colourless
-

In light of the previous considerations outlined in this introduction it is evident that in order to promote the skin penetration of a topically applied substance, a CPE must partition into the stratum corneum and interact with its constituents in a manner that ultimately reduces the resistance of the skin to drug diffusion (39). In an attempt to identify the potential modes of action of CPEs, the Lipid-Protein-Partitioning (LPP) theory has been developed, which essentially describes three mechanisms that may dominate accelerant action (142, 143):

- i. disruption of the intercellular lipid bilayers
- ii. interaction within intracellular proteins

- iii. improvement of partitioning of a drug, co-enhancer or cosolvent into the stratum corneum

The LPP theory has subsequently been extended to include (75):

- iv. disruption of the cornified cell envelope
- v. effect on intercellular junctions, such as desmosomes
- vi. alteration of drug partitioning between stratum corneum components and the intercellular lipids

It has been suggested that the effectiveness of a CPE resides in its ability to alter the principal transport pathways associated with drug penetration across the stratum corneum (39). Although it is generally thought that the intercellular lipid route dominates solute transport, it should be kept in mind that a penetrating molecule would diffuse through the intercellular lipids regardless of which transport pathway dominates. Substances that perturb the highly ordered arrangement of the intercellular lipid bilayers are therefore likely to reduce the diffusional resistance of the stratum corneum to most solutes (39, 144-147).

Like the ceramide molecules that are thought to play a critical role in stabilising the lamellar structure, many CPEs have a polar head group and a long alkyl chain, which enables them to insert between the lipid bilayers and disrupt the packing of the ceramide molecules (148, 149). Thus, depending on their structure and physicochemical properties, many CPEs can disrupt the organisation of the intercellular lipid bilayers by interacting with the polar head groups and/or the hydrophobic tails of the lipid bilayers (Figure 1.9) (39, 75, 132, 142, 143).

Interactions with the polar head groups can modify hydrogen bonding and ionic forces, which may disturb the hydration spheres of the lipid bilayers and subsequently disturb lipid packing within this plane (39, 142). This perturbation may make the domain more fluid – and may possibly increase the water volume between the bilayers – which may therefore promote the diffusion of (polar/hydrophilic) solutes within this region. Disruption to the polar head group region would also alter the packing of the lipid alkyl chains, which may also reduce the resistance of this region to the diffusion of (non-polar/lipophilic) solutes.

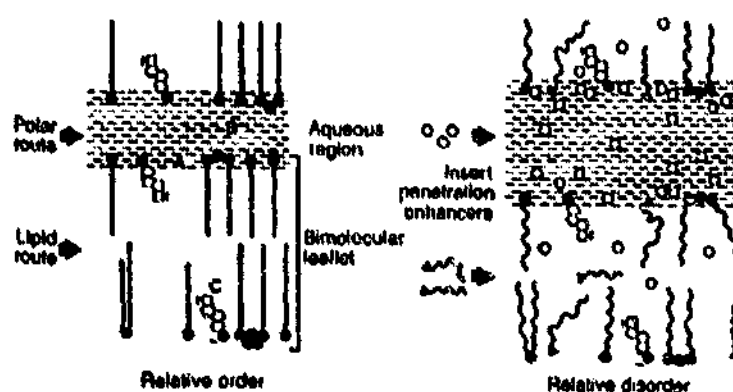


Figure 1.9. The possible sites at which a chemical penetration enhancer can interact with the stratum corneum intercellular lipid bilayers: at or near the polar groups (A and B) and/or between the hydrophobic alkyl chains (142).

For instance, one of the most researched CPEs is Azone[®], which has been found to be effective in enhancing the transdermal fluxes of a variety of compounds (39). Due to its structure, Azone[®] adopts a "soup spoon" configuration as it inserts between the lipid bilayers, which causes its lactam functionality to lie in the plane of the polar head group region (39). Experimental data has shown that Azone[®] fluidises the stratum corneum lipids (39, 150-152), which has been related to its ability to reduce the packing of the lipid alkyl chains and its ability to modify inter-lipid hydrogen bonding between the polar head groups of adjacent ceramide molecules (152, 153).

Due to their structure, many CPEs can insert between the hydrocarbon chains of the lipid bilayers, thus disturbing their packing, increasing their fluidity and ultimately reducing their diffusional resistance (142). In some instances, alterations in the hydrophobic region of the bilayers may also alter the packing of the polar head groups, which may ultimately facilitate solute diffusion through this region (142). The ability of CPEs to disturb the packing of the lipid alkyl chains appears to be related to structural features such as the length (10 to 14 carbons appears optimal (154)) and degree of saturation of their hydrocarbon chains. For instance, the enhancing ability of *cis*-monounsaturated fatty acids (such as oleic acid) has been related to the "kink" in their alkenyl chains, which may disrupt the tight packing of the lipid bilayers (146, 155, 156).

At high loadings, some CPEs (such as oleic acid and terpenes) may reduce the diffusional resistance of the stratum corneum lipids by forming separate fluid phases within or between the lipid lamellae (157-159). For oleic acid, it has been suggested that

this solid-fluid phase separation enhances drug transport through the stratum corneum through the formation of permeable defects in the lamellae (159). The ability of oleic acid to become heterogeneously dispersed in the lipid lamellae has also been related to the *cis* double bond in its alkenyl chain (132).

CPEs may reduce the barrier function of the stratum corneum by a number of other mechanisms. For instance, various solvents and micellar solutions have been found to extract lipids from the stratum corneum (160). It has also been proposed that CPEs such as propylene glycol, ethanol and dimethylsulphoxide alter the conformation of intracellular keratin filaments by replacing bound water molecules (39). Various caustic solvents such as acids and phenols may also disrupt intracellular keratin organisation and may destroy desmosomal junctions (75).

As discussed in Section 1.2.5, any disruption to the barrier function of the stratum corneum will elicit a biological repair response. For this reason, and various other reasons, many existing CPEs can cause skin damage, irritation or allergenicity, which potentially renders them clinically unacceptable (124). However, newly synthesised CPEs are subject to lengthy regulatory approval procedures that are equivalent to those for any new chemical entity, which could impede their development (124). Therefore, considerable effort is presently directed at identifying common, generally regarded as safe (GRAS) substances that possess permeation-modulating properties.

The efforts of our research group have primarily focused on the potential of certain sunscreen agents to enhance TDD (161). Of these agents, octisalate (OS) and padimate O (PO) have gained the most attention. The major attraction of these compounds is that they have GRAS status and over many years of use as topical sunscreens they have shown a low incidence of local skin reactions (161).

Although OS and PO have both been found to enhance the *in vitro* and/or *in vivo* percutaneous absorption of a variety of drugs (162-169), there is currently little insight into their possible mechanism(s) of action. Based on their chemical structures (Figure 1.10) and physicochemical properties (Table 1.3), OS and PO would be expected to have a high affinity for the stratum corneum lipids as they are highly lipophilic, have low water solubility, their solubility parameters are close to that of the stratum corneum lipids, they are liquids at room temperature and they are amphiphilic structures.

Although OS and PO have been found to lower the transition temperature of model stratum corneum lipid mixtures (170), it is evident from the many possible modes of

action that have been proposed for various CPEs that any number of mechanisms may be responsible for the enhancing effects of OS and PO. As the effectiveness of a CPE resides in its ability to alter the transport pathways associated with drug penetration across the stratum corneum (39), a knowledge of the mechanisms of action of OS and PO would assist in their rational use as CPEs. Consequently, further mechanistic studies are required in order to elucidate the possible mechanism(s) of action of OS and PO.

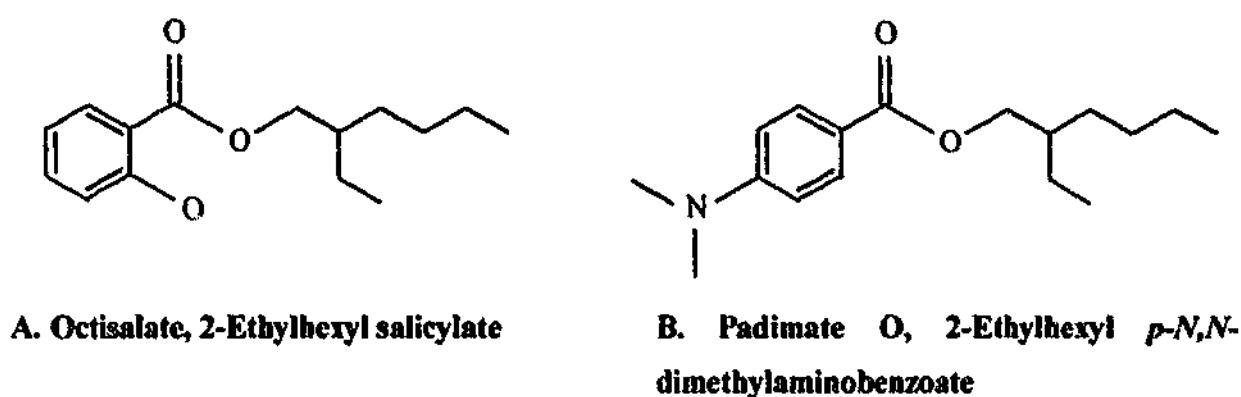


Figure 1.10. The chemical structures of octisalate and padimate O

Table 1.3. Some physicochemical properties of octisalate and padimate O

	Octisalate	Padimate O
Physical form ^a	Non-volatile, colourless to pale yellow liquid, characteristically bland odour	Non-volatile, pale yellow mobile liquid, characteristically mild odour
MW (Da) ^a	250.34	277.40
LogK _{oct/w} ^b	5.97	5.77
Octanol solubility (mg/ml) ^c	709.14	205.77
Water solubility (µg/ml) ^b	0.717	0.198
δ (MPa ^{1/2}) ^d	21.74	18.4

^a Martindale The Complete Drug Reference, 32nd Edn, Pharmaceutical Press, London UK, 1999

^b Estimated using EPI Suite (v.3.11) computer software package (U.S. Environmental Protection Agency)

^c Experimentally determined at 32°C, refer to Chapter 4 (Section 4.3.5.2)

^d Estimated using Thermo Chemical Properties Estimation Software: Solubility Parameter Estimation from Fedor's Cohesive Energy (obtained from <http://www.pirika.com/chem/TCPEE/TCPE.htm>)

1.5. TRANSDERMAL DELIVERY OF OPIOID ANALGESICS

1.5.1. Rationale

Although opioid pharmacotherapy is the mainstay treatment for chronic, nociceptive cancer pain (171), there are several disadvantages associated with conventional forms of drug administration, which limits the clinical versatility and utility of most opioid analgesics. For instance (172-174):

- i. most opioids have limited oral bioavailability due to extensive first-pass metabolism in the gastrointestinal tract (GIT) and liver
- ii. fluctuating periods of side effects or toxicity and inadequate pain relief may result from peak and trough opioid serum levels associated with conventional dosage regimens, such as periodic oral, intravenous (IV) bolus or intramuscular (IM) administration
- iii. IV, IM or subcutaneous opioid administration is not only invasive, but requires specialised training and is most appropriate in an inpatient setting with non-ambulant patients.

Thus, the impetus for utilising novel routes of opioid administration comes from the goal to maximise analgesia, minimise side effects and provide a convenient dosage schedule for cancer patients who require parenteral opioid administration (175). In this context, TDD may confer a "real benefit" over conventional routes of opioid administration as it (76, 161, 173, 176):

- i. bypasses the GIT, thus transdermally administered drugs are not effected by the variables that influence gastrointestinal absorption, such as chemical degradation. Parenteral forms of drug delivery may also be desirable for patients who are unable to swallow or tolerate oral medications due to head or neck cancer or opioid-induced side effects
- ii. avoids first-pass metabolism in the GIT and liver
- iii. is non-invasive

- iv. produces relatively constant serum drug levels. This attribute is particularly advantageous for the systemic delivery of opioids with a narrow therapeutic window as fluctuations in serum levels (associated with inadequate pain relief or toxicity) are eliminated
- v. provides sustained drug delivery. This allows for the implementation of simplified, convenient (e.g. once-daily) dosage regimens over a long-term basis. This feature of TDD also expands clinical role of opioids that have been limited by unacceptably short half-lives
- vi. allows for the relatively facile termination of systemic drug input by removal of the transdermal delivery system from the skin (provided that significant levels of the drug do not accumulate within the skin)

However, as highlighted throughout this introduction, the use of the skin to deliver therapeutically relevant drug concentrations into the systemic circulation is often associated with various difficulties, including (1):

- i. the efficient rate-limiting barrier properties of the stratum corneum
- ii. the skin's "first-pass" metabolic effect
- iii. the potential for a transdermal delivery system to cause skin irritation
- iv. identifying an appropriate enhancement strategy to facilitate percutaneous drug absorption
- v. an incomplete understanding of the mechanisms involved with some permeation enhancement strategies. This has been particularly evident with CPEs.

1.5.2. Technical feasibility

In light of the above-mentioned problems associated with TDD, the following considerations would assist in the design, development and optimisation of a transdermal delivery system that has the potential to be a useful addition to the armamentarium against cancer pain:

- i. Select an opioid analgesic that has the physicochemical, pharmacokinetic and pharmacodynamic properties that are amenable to TDD
- ii. Select a delivery system that incorporates the necessary enhancement strategies to facilitate percutaneous drug absorption and reduces the potential for skin irritation
- iii. Understand the mechanism(s) involved in skin permeation enhancement.

As the latter consideration is fundamental to the objectives of this thesis, the following sections describe how the former aspects of TDD were considered during the initial stages of this research.

1.5.2.1. Drug candidate selection

Some of the physicochemical, pharmacokinetic and pharmacodynamic properties of an ideal drug candidate for TDD are listed in Table 1.4. The properties of some opioid analgesics that were evaluated for their technical feasibility are listed in Appendix I. In addition to these properties, it was also necessary to consider the clinical role of different opioids in cancer pain management.

For instance, partial agonists may precipitate withdrawal symptoms in opioid-dependent patients and may also be incapable of relieving severe cancer pain as a ceiling to their analgesic effect may occur at high doses (177). Thus, although buprenorphine appears to be a good candidate for TDD (178) (refer to Appendix I), its role in cancer pain management may be somewhat limited.

Mixed agonist-antagonists (such as pentazocine, nalbuphine and butorphanol) may also be of limited use in cancer pain management as they may precipitate withdrawal symptoms in opioid-dependent patients and can cause psychotomimetic side effects (174).

In light of these problems, the selection of a feasible candidate for TDD was limited to pure opioid receptor agonists. Based on their chemical structures, most opioid agonists may be classified as phenanthrene, phenylpiperidine, or diphenylheptane derivatives (179).

Table 1.4. Some physicochemical, pharmacokinetic and pharmacodynamic properties of a feasible drug candidate for transdermal drug delivery (123-125, 134, 161).

Property	Feasible drug candidate
Daily dose	< 50mg/day ^a
MW	< 1000 Da, preferably < 500 to 600 Da
MP	Preferably < 200°C
LogK _{oct/w}	Between 1 to 3
δ	~ 20 MPa ^{1/2}
Hydrogen bonding groups	< 3
Elimination half life (t _{1/2})	A couple to few hours
Oral bioavailability	Negligible

^a For practical, cosmetic and economic reasons, the size of a transdermal delivery system should not exceed ~ 50 cm². Due to the barrier properties of the stratum corneum, it may not be possible to deliver more than 50 mg of drug per day (123). For the same reasons, therapeutic plasma concentrations of the drug should be of the order of ng/ml.

Phenanthrene derivatives include codeine, hydromorphone, levorphanol, morphine, oxycodone and oxymorphone. In general, these compounds were not considered feasible candidates for TDD as they are not very potent, have relatively high melting points and their lipid and water solubilities are unsuitably balanced (in most instances, log K_{oct/w} < 1). In further support of this notion was the research conducted by Roy and Flynn who, based on their data, concluded that the low *in vitro* skin permeability of codeine, morphine and hydromorphone coupled with their low potencies make these drug poor transdermal candidates: the estimated patch sizes for these compounds were ridiculously large (ranging from 2,631 cm² for hydromorphone to 62,500 cm² for morphine) (180).

Methadone (a diphenylheptane derivative) is another opioid that has been proposed as a drug for cancer pain management (175). However, it has good oral bioavailability (~ 85%) and a long plasma half life (17 to 24 h, with reports of up to 50 h in some cancer patients) (175) and is therefore an unsuitable candidate for TDD.

Phenylpiperidine derivatives include pethidine (meperidine), fentanyl, sufentanil, lofentanil and alfentanil. Although pethidine has a solubility parameter that is close to what may be the optimum for stratum corneum permeation ($\delta = 19.6 \text{ MPa}^{1/2}$) and a very

low melting point (180), it is relatively hydrophilic ($\log K_{OCT/W} \approx 1.6$) and not very potent (required daily doses may be of the order of 150 to 600 mg IV/IM (refer to Appendix II)).

Based on their physicochemical, pharmacokinetic and pharmacodynamic properties, all of the remaining phenylpiperidine derivatives have the potential to be suitable candidates for TDD (refer to Appendix I), however i) alfentanil is not as potent as fentanyl (181), ii) due to its high potency, large doses of naloxone cannot displace lofentanil receptor binding and therefore there may be issues regarding its safety (182, 183) and iii) while sufentanil appears to be an ideal candidate for TDD, there were problems with its availability at the time this research was initiated. Thus, fentanyl was chosen as a model opioid analgesic during this research because:

- i. its role in cancer pain management has been established
- ii. it has suitable physicochemical properties
- iii. low doses are required to produce analgesia
- iv. it undergoes extensive first-pass metabolism (184)
- v. it has a high safety therapeutic safety index (LD_{50}/ED_{50}) (185).

The chemical structure and some physicochemical, pharmacokinetic, and pharmacodynamic properties of fentanyl are shown in Figure 1.11 and Table 1.4, respectively. In addition to the above-mentioned attributes, previous studies with skin homogenates indicate that the percutaneous absorption of fentanyl is unlikely to be significantly affected by cutaneous metabolism (186).

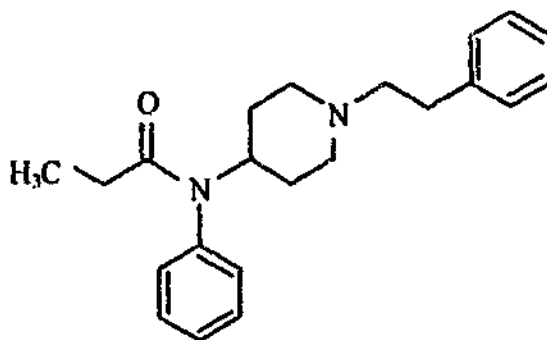


Figure 1.11. The chemical structure of fentanyl

Table 1.4. Some physicochemical, pharmacokinetic, and pharmacodynamic properties of fentanyl

Daily dose	100 – 600 µg (IV) ^a
Therapeutic levels	0.2 – 2 ng/ml ^a
MW	336.48 Da ^b
MP	83 – 84 °C ^c
pK _a	8.9 ^d
LogK _{ow}	2.86 ^e
δ	20.0 MPa ^{1/2} ^e
Hydrogen bonding groups	1
t _{1/2p}	3.7 h ^e
Oral bioavailability (LD ₅₀ /ED ₅₀)	Negligible ^f 2727 ^e

^a From Muijsers and Wagstaff (187)^b Martindale The Complete Drug Reference, 32nd Edn, Pharmaceutical Press, London UK, 1999^c From Roy and Flynn (180)^d From Roy and Flynn (188)^e From Willens et al (185)^f From Scholz (184)

The feasibility of using the transdermal route to deliver therapeutically relevant amounts of fentanyl into the systemic circulation has been previously established (176, 178, 180, 189-191). Like most other compounds, it has been found that the unionised form of fentanyl permeates the skin more readily than its ionised counterpart (97). As it is a weak base, the transdermal delivery of fentanyl by iontophoresis has received a great deal of attention (178). Although the research conducted to date indicates that therapeutic plasma concentrations can be achieved within a relatively short period of time, the feasibility of the iontophoretic transdermal delivery of fentanyl appears to be limited to acute or breakthrough pain (178).

Given that the transdermal delivery rate (TDR) required to maintain steady-state therapeutic plasma concentrations of a drug can be estimated as (192):

$$\text{TDR} = \text{Therapeutic concentration at steady state (C}_{\text{ss}}) \times \text{total body clearance (CL)}$$

then the TDR required for fentanyl ($C_{\text{ss}} = 0.2 - 2 \text{ ng/ml}$ and $\text{CL} = 53 \text{ L/h}$ (187)) will be approximately 10 to 100 µg/h, which amounts to a required delivery rate of 0.24 to 2.4 mg/day. Evidently, a TDR within this range is achievable with delivery systems that are

less than 50 cm²: the Durogesic[®] patch, which is the only fentanyl-containing transdermal therapeutic system (TTS) that is commercially available at present, is available in sizes of up to 40 cm² and delivers fentanyl at a rate of 25 µg/h per 10 cm² patch size (193). The effectiveness of this TTS has also been demonstrated in chronic cancer pain management: it has been reported that after an initial lag time most cancer patients experience adequate analgesia following the topical application of the Durogesic[®] patch and in most instances analgesia was superior to the preceding treatment (178, 187). However, as mentioned in Chapter 3, a major problem associated with occlusive transdermal therapeutic systems, such as Durogesic[®], is their potential to cause skin irritation

1.5.2.2. Transdermal delivery system

In an attempt to utilise a delivery system that reduces the potential for skin irritation and incorporates the necessary enhancement strategies to facilitate the percutaneous absorption of fentanyl, a non-occlusive delivery system was utilised during this research. As mentioned in Chapter 3, the key feature of this delivery system is the application of a small dose (a “finite” dose) of a volatile:non-volatile vehicle system in which OS or PO are the non-volatile components and ethanol is the volatile component of the system. Due to the fact that a “finite dose” of the formulation is applied to the skin, the percutaneous absorption of fentanyl from a delivery system of this nature may be affected by a number of variables including the changing thermodynamic properties of the formulation due to the evaporation of ethanol and the potential for OS and PO to reduce the barrier function of the stratum corneum.

1.6. OBJECTIVES OF THIS THESIS

The primary objective of this thesis was to investigate the possible mechanism(s) by which OS and PO facilitate the percutaneous absorption of fentanyl *in vitro* under the “finite dose” conditions that would prevail if the non-occlusive transdermal delivery system of interest was applied to humans *in vivo* (i.e. predicted conditions of use).

In order to achieve this objective, it was first necessary to identify a suitable a model for studying the percutaneous absorption of fentanyl *in vitro* and the effects of OS and PO. The objectives of subsequent research were to first establish the feasibility of

using OS and PO to enhance the transdermal delivery of fentanyl under predicted *in vivo* conditions of use and then to determine some of the possible mechanism(s) by which OS and PO enhance the transdermal delivery of fentanyl under simulated *in vivo* conditions of use. Due to the nature of the delivery system, it was hypothesised that OS and PO would facilitate the skin penetration of fentanyl by altering its thermodynamic activity in the applied vehicle. However, it was also hypothesised that OS and PO would penetrate and subsequently interact with components of the stratum corneum in a manner that increases the partitioning of fentanyl into the stratum corneum and/or increases the diffusivity of fentanyl within the stratum corneum. In order to investigate these hypotheses, the following objectives were established:

- i. To investigate the whether OS and PO increase the partitioning of fentanyl into the stratum corneum and if so, to elucidate whether OS and PO enhance fentanyl partitioning into the stratum corneum by increasing its affinity for the stratum corneum lipids
- ii. To determine whether OS and PO modify the distribution of fentanyl across the stratum corneum
- iii. To investigate the whether OS and PO increase the diffusion of fentanyl through the stratum corneum and if so, to investigate whether OS and PO perturb the barrier properties of the stratum corneum by extracting and/or reducing the conformational order of the intercellular lipid bilayers.

As the ultimate aim of further research (beyond this research) is to develop a formulation that, when applied to the skin surface, will deliver sufficient quantities of fentanyl to the systemic circulation in order to achieve and maintain chronic cancer pain control over an acceptable period of time in humans *in vivo*, another objective of this research was:

- iv. To determine the distribution profiles of OS and PO across human stratum corneum *in vitro* and *in vivo* in order to gain further insight into their possible mechanism(s) of action *in vitro* and to elucidate whether this *in vitro* data was predictive for their distribution across human stratum corneum (and perhaps some of their mechanism(s) of action) *in vivo*.

1.7. REFERENCES

1. Walters KA, Roberts MS. 2002. The Structure and Function of Skin. In Walters KA, ed. Dermatological and Transdermal Formulations. New York: Marcel Dekker, Inc., pp 1-39.
2. Monteiro-Riviere NA. 1991. Comparative Anatomy, Physiology, and Biochemistry of Mammalian Skin. In Hobson DW, ed. Dermal and Ocular Toxicology - Fundamentals and Methods. Boca Raton, Florida: CRC Press, Inc., pp 3-71.
3. Rougier A, Lotte C, Maibach HI. 1999. *In Vivo* Relationship Between Percutaneous Absorption and Transepidermal Water Loss. In Bronaugh RL, Maibach HI, ed. Percutaneous Absorption Drugs, Cosmetics, Mechanisms, Methodology. New York: Marcel Dekker, Inc., pp 117-132.
4. Barry BW. 1983. Dermatological Formulations. Percutaneous Absorption. New York: Marcel Dekker, Inc. pp 1-48.
5. Nasemann T, Saverbrey W, Burgdorf WHC. 1983. Fundamentals of Dermatology. Berlin: Springer-Verlag. pp 1-14.
6. Wysocki AB. 1985. A Review of the Skin and Its Appendages. *Adv Wound Care* 8:53-70.
7. Schaefer H, Zesch A, Stüttgen G. 1982. Skin Permeability. Berlin: Springer-Verlag. pp 545-550.
8. Kligman AM, Zheng P, Lavker RM. 1985. The Anatomy and Pathogenesis of Wrinkles. *Br J Dermatol* 113:37-42.
9. Anderson RL, Cassidy JM. 1973. Variation in Physical Dimensions and Chemical Composition of Human Stratum Corneum. *J Invest Dermatol* 61:30-32.
10. Holbrook KA, Odland GF. 1974. Regional Differences in the Thickness (Cell Layers) of the Human Stratum Corneum: An Ultrastructural Analysis. *J Invest Dermatol* 62:415-422.
11. Downing DT. 1992. Lipid and Protein Structures in the Permeability Barrier of Mammalian Epidermis. *J Lipid Res* 33:301-313.
12. Piérard GE, Goffin V, Hermanns-Le T, Piérard-Franchimont C. 2000. Corneocyte Desquamation (Review). *Int J Mol Med* 6:217-221.
13. Whitton JT, Everall JD. 1973. The Thickness of the Epidermis. *Br J Dermatol* 89:467-476.
14. Kligman AM. 1964. The Biology of the Stratum Corneum. In Montagna W, Lobitz Jnr WC, ed. The Epidermis. New York: Academic Press, pp 387-433.
15. Schaefer H, Redelmeier TE. 1996. Skin Barrier: Principles of Percutaneous Absorption. Basel: Karger. p 45.
16. Wertz PW, Downing DT. 1989. Stratum Corneum: Biological and Biochemical Considerations. In Hadgraft J, Guy RH, ed. Transdermal Drug Delivery Developmental Issues and Research Initiatives. New York: Marcel Dekker, Inc., pp 1-22.
17. Eckert RL. 1989. Structure, Function, and Differentiation of the Keratinocyte. *Physiol Rev* 69:1316-1346.
18. Ishiko A, Matsunaga Y, Matsunaga T, Aiso S, Nishikawa T, Shimizu H. 2003. Immunomolecular Mapping of Adherens Junction and Desmosomal Components in Normal Human Epidermis. *Exp Dermatol* 12:747-754.

19. Bouwstra JA, Honeywell-Nguyen PL, Gooris GS, Ponc M. 2003. Structure of the Skin Barrier and its Modulation by Vesicular Formulations. *Prog Lipid Res* 42:1-36.
20. Downing DT, Stewart ME. 2000. Epidermal Composition. In Lodén M, Maibach HI, ed. *Dry Skin and Moisturizers Chemistry and Function*. Boca Raton, Florida: CRC Press, pp 13-26.
21. Scheuplein RJ, Blank IH. 1971. Permeability of the Skin. *Physiol Rev* 51:702-747.
22. Braverman IM. 2000. The Cutaneous Microcirculation. *J Invest Dermatol Symp Proc* 5:3-9.
23. Hern S, Mortimer PS. 1999. Visualization of Dermal Blood Vessels - Capillaroscopy. *Clin Exp Dermatol* 24:473-478.
24. Schechner J. 2002. Red Skin Re-Read. *J Invest Dermatol* 119:781-782.
25. Rendell MS, Milliken BK, Finnegan MF, Finnery DA, Healy JC. 1997. The Skin Blood Flow Response in Wound Healing. *Microvasc Res* 53:222-234.
26. Netten PM, Wollersheim H, Thien T, Lutterman JA. 1996. Skin Microcirculation of the Foot in Diabetic Neuropathy. *Clin Science* 91:559-565.
27. Ryan TJ. 1978. The Lymphatics of the Skin. In Jarret A, ed. *The Physiology and Pathophysiology of the Skin*. London: Academic Press, pp 1755-1780.
28. Skobe M, Detmar M. 2000. Structure, Function, and Molecular Control of the Skin Lymphatic System. *J Invest Dermatol Symp Proc* 5:14-19.
29. Braverman IM, Keh-Yen A. 1981. Ultrastructure of the Human Dermal Microcirculation III. The Vessels in the Mid- and Lower Dermis and Subcutaneous Fat. *J Invest Dermatol* 77:
30. Stewart ME. 1992. Sebaceous Gland Lipids. *Semin Dermatol* 11:100-105.
31. Motwani MR, Rhein LD, Zatz JL. 2002. Influence of Vehicles on the Phase Transition of Model Sebum. *J Soc Cosmet Chem* 53:35-42.
32. Kligman AM, Shehadeh N. 1964. Pubic Apocrine Glands and Odor. *Arch Dermatol* 89:461-463.
33. Murdan S. 2002. Drug Delivery to the Nail Following Topical Application. *Int J Pharm* 236:1-26.
34. Baden HP, Goldsmith LA, Fleming B. 1973. A Comparative Study of the Physicochemical Properties of Human Keratinised Tissues. *Biochim Biophys Acta* 322:269-272.
35. Forslind B. 1970. Biophysical Studies of the Normal Nail. *Acta Derm Venereol* 50:161-168.
36. Blank IH. 1965. Cutaneous Barriers. *J Invest Dermatol* 45:249-256.
37. Egelrud T. 2000. Desquamation in the Stratum Corneum. *Acta Derm Venereol Suppl (Stockh)* 208:44-45.
38. Johnson ME, Blankschtein D, Langer R. 1997. Evaluation of Solute Permeation Through the Stratum Corneum: Lateral Bilayer Diffusion as the Primary Transport Mechanism. *J Pharm Sci* 86:1162-1172.
39. Suhonen TM, Bouwstra JA, Urtti A. 1999. Chemical Penetration Enhancement of Percutaneous Absorption in Relation to Stratum Corneum Structural Alterations. *J Control Release* 59:149-161.
40. Kalinin AE, Kajava AV, Steinert PM. 2002. Epithelial Barrier Function: Assembly and Structural Features of the Cornified Cell Envelope. *BioEssays* 24:789-800.
41. Plewig G, Marples RR. 1970. Regional Differences of Cell Sizes in the Human Stratum Corneum. *J Invest Dermatol* 54:13-18.

42. Harding CR. 2004. The Stratum Corneum: Structure and Function in Health and Disease. *Dermatol Therap* 17:6-15.
43. Park AC, Baddiel CB. 1972. Rheology of Stratum Corneum-I: A Molecular Interpretation of the Stress-Strain Curve. *J Soc Cosmet Chem* 23:3-12.
44. Pearton DJ, Dale BA, Presland RB. 2002. Functional Analysis of the Profilaggrin N-Terminal Peptide: Identification of Domains that Regulate Nuclear and Cytoplasmic Distribution. *J Invest Dermatol* 119:661-669.
45. Maltoltsy AG. 1975. Desmosomes, Filaments and Keratohyaline Granules: Their Role in the Stabilization and Keratinization of the Epidermis. *J Invest Dermatol* 65:127-142.
46. Maltoltsy AG. 1976. Keratinization. *J Invest Dermatol* 67:20-25.
47. Lindberg M, Forslind B. 2000. The Skin as a Barrier. In Lodén M, Maibach HI, ed. *Dry Skin and Moisturizers Chemistry and Function*. Boca Raton, Florida: CRC Press, pp 27-37.
48. Kalinin A, Marekov LN, Steinert PM. 2001. Assembly of the Epidermal Cornified Cell Envelope. *J Cell Science* 114:
49. Behne M, Uchida Y, Seki T, de Montellano PO, Elias PM, Holleran WM. 2000. Omega-Hydroxyceramides are Required for Corneocyte Lipid Envelope (CLE) Formation and Normal Epidermal Permeability Barrier Function. *J Invest Dermatol* 114:185-192.
50. Lazo ND, Meine JG, Downing DI. 1995. Lipids are Covalently Attached to Rigid Corneocyte Protein Envelopes Existing Predominantly as β -Sheets: A Solid-State Nuclear Magnetic Resonance Study. *J Invest Dermatol* 105:296-300.
51. Egelrud T. 2000. Desquamation. In Lodén M, Maibach HI, ed. *Dry Skin and Moisturizers Chemistry and Function*. Boca Raton, Florida: CRC Press, pp 109-117.
52. Bouwstra JA. 1997. The Skin Barrier, A Well-Organized Membrane. *Colloid Surf A-Physicochem Eng Asp* 123-124:403-413.
53. Madison KC. 2003. Barrier Function of the Skin: "La Raison d'Être" of the Epidermis. *J Invest Dermatol* 121:231-241.
54. Freinkel RK, Traczyk TN. 1985. Lipid Composition and Acid Hydrolase Content of Lamellar Granules of Fetal Rat Epidermis. *J Invest Dermatol* 85:295-298.
55. Norlén L. 2003. Skin Barrier Structure, Function and Formation - Learning from Cryo-Electron Microscopy of Vitreous, Fully Hydrated Native Human Epidermis. *Int J Cosmet Sci* 25:209-226.
56. Bouwstra JA, Gooris GS, Cheng K, Weerheim A, Bras W, Ponc M. 1996. Phase Behaviour of Isolated Skin Lipids. *J Lipid Res* 37:999-1011.
57. Bouwstra JA, Pilgram GS, Gooris GS, Koerten HK, Ponc M. 2001. New Aspects of the Skin Barrier Organization. *Skin Pharmacol Appl Skin Physiol* 14:52-62.
58. Bouwstra JA, Dubbelaar FE, Gooris GS, Weerheim AM, Ponc M. 1999. The Role of Ceramide Composition in the Lipid Organisation of the Skin Barrier. *Biochim Biophys Acta* 1419:127-136.
59. Bouwstra JA, Gooris GS, Dubbelaar FE, Ponc M. 2001. Phase Behavior of Lipid Mixtures Based on Human Ceramides: Coexistence of Crystalline and Liquid Phases. *J Lipid Res* 42:1759-1770.

60. Glombitza B, Müller-Goymann CC. 2002. Influence of Different Ceramides on the Structure of *In Vitro* Model Lipid Systems of the Stratum Corneum Lipid Matrix. *Chem Phys Lipids* 117:29-44.
61. Motta S, Monti M, Sesana S, Caputo R, Carelli S, Ghidoni R. 1993. Ceramide Composition of the Psoriatic Scale. *Biochim Biophys Acta* 1182:147-151.
62. Imokawa G, Kuno H, Kawai M. 1991. Stratum Corneum Lipids Serve as a Bound-Water Modulator. *J Invest Dermatol* 96:845-851.
63. Bouwstra JA, Gooris GS, Dubbelaar FE, Weerheim AM, Ijzerman AP, Ponc M. 1998. Role of Ceramide 1 in the Molecular Organization of the Stratum Corneum Lipids. *J Lipid Res* 39:186-196.
64. Chen H, Mendelsohn R, Rerek ME, Moore DJ. 2001. Effect of Cholesterol on Miscibility and Phase Behavior in Binary Mixtures with Synthetic Ceramide 2 and Octadecanoic Acid. *Infrared Studies. Biochim Biophys Acta* 1512:345-356.
65. Pilgram GS, Engelsma-van Pelt AM, Bouwstra JA, Koerten HK. 1999. Electron Diffraction Provides New Information on Human Stratum Corneum Lipid Organization Studied in Relation to Depth and Temperature. *J Invest Dermatol* 113:403-409.
66. Moore DJ, Rerek ME. 2000. Insights into the Molecular Organization of Lipids in the Skin Barrier from Infrared Spectroscopy Studies of Stratum Corneum Lipid Models. *Acta Derm Venereol Suppl (Stockh)* 208:16-22.
67. Naik A, Guy RH. 1997. Infrared Spectroscopic and Differential Scanning Calorimetric Investigations of the Stratum Corneum Barrier Function. In Potts RO, Guy RH, ed. *Mechanisms of Transdermal Drug Delivery*. New York: Marcel Dekker, Inc., pp 87-162.
68. Golden GM, Guzek DB, Kennedy AH, McKie JE, Potts RO. 1987. Stratum Corneum Lipid Phase Transitions and Water Barrier Properties. *Biochemistry* 26:2382-2388.
69. Potts RO, Francoeur ML. 1990. Lipid Biophysics of Water Loss Through the Skin. *Proc Natl Acad Sci USA* 87:3871-3873.
70. Haberkamp MB. 1994. Skin Permeation Enhancement Reversibility. In Hsieh DS, ed. *Drug Permeation Enhancement*. New York: Marcel Dekker, Inc., pp 43-58.
71. Roberts MS, Walters KA. 1998. The Relationship Between Structure and Barrier Function of Skin. In Roberts MS, Walters KA, ed. *Dermal Absorption and Toxicity Assessment*. New York: Marcel Dekker, Inc., pp 1-42.
72. Ridout G, Santus GC, Guy RH. 1988. Pharmacokinetic Considerations in the Use of Newer Transdermal Formulations. *Clin Pharmacokinet* 15:114-131.
73. Roberts MS. 1997. Targeted Drug Delivery to the Skin and Deeper Tissues: Role of Physiology, Solute Structure and Disease. *Clin Exp Pharm Physiol* 24:874-879.
74. Guy RH. 1987. Transdermal Drug Delivery: A Perspective. *J Control Release* 4:237-251.
75. Roberts MS, Cross SE, Pellett MA. 2002. Skin Transport. In Walters KA, ed. *Dermal and Transdermal Formulations*. New York: Marcel Dekker, Inc., pp 89-195.
76. Benson H, Prankerd RJ. 1997. Optimisation of Drug Delivery 4. Transdermal Drug Delivery. *Aust J Hosp Pharm* 27:441-448.

77. Barry BW. 1983. Dermatological Formulations. Percutaneous Absorption. New York: Marcel Dekker, Inc. pp 127-233.
78. Reddy MB, Guy RH, Bunge AL. 2000. Does Epidermal Turnover Reduce Percutaneous Penetration? *Pharm Res* 17:1414-1419.
79. Cross SE, Magnusson BM, Winckle G, Anissimov YG, Roberts MS. 2003. Determination of the Effect of Lipophilicity on the *In Vitro* Permeability and Tissue Reservoir Characteristics of Topically Applied Solutes in Human Skin Layers. *J Invest Dermatol* 120:759-764.
80. Cross SE, Roberts MS. 1993. Subcutaneous Absorption Kinetics of Interferon and Other Solutes. *J Pharm Pharmacol* 45:606-609.
81. Schaefer H, Zesch A, Stüttgen G. 1982. Skin Permeability. Berlin: Springer-Verlag. pp 590-624.
82. Barry BW. 1987. Mode of Action of Chemical Penetration Enhancers in Human Skin. *J Control Release* 1987:85-97.
83. Pugh WJ, Hadgraft J, Roberts MS. 1998. Physicochemical Determinants of Stratum Corneum Permeation. In Roberts MS, Walters KA, ed. *Dermal Absorption and Toxicity Assessment*. New York: Marcel Dekker, Inc., pp 245-268.
84. Scheuplein RJ. 1972. Properties of the Skin as a Membrane. *Adv Biol Skin* 22:125-152.
85. Raykar PV, Fung MC, Anderson BD. 1988. The Role of Protein and Lipid Domains in the Uptake of Solutes by Human Stratum Corneum. *Pharm Res* 5:140-150.
86. Boddé HE, Kruithof MAM, Brussee J, Koerten HK. 1989. Visualization of Normal and Enhanced $HgCl_2$ Transport Through Human Skin *In Vitro*. *Int J Pharm* 253:13-24.
87. Albery WJ, Hadgraft J. 1979. Percutaneous Absorption: *In Vivo* Experiments. *J Pharm Pharmacol* 31:140-147.
88. Juninger HE, Boddé HE, de Haan FHN. 1994. Visualization of Drug Transport Across Human Skin and the Influence of Penetration Enhancers. In Hsieh DS, ed. *Drug Permeation Enhancement*. New York: Marcel Dekker, Inc., pp 59-89.
89. Sznitowska M, Berner B. 1995. Polar Pathway for Percutaneous Absorption. *Curr Probl Dermatol* 22:164-170.
90. Brain K, Walters KA, Watkinson AC. 2002. Methods for Studying Percutaneous Absorption. In Walters KA, ed. *Dermal and Transdermal Formulations*. New York: Marcel Dekker Inc., pp 197-269.
91. Wester RC, Maibach HI. 1999. Regional Variation in Percutaneous Absorption. In Bronaugh RL, Maibach HI, ed. *Percutaneous Absorption: Drugs, Cosmetics, Mechanisms, Methodology*. New York: Marcel Dekker, Inc., pp 107-116.
92. Rougier A, Lotte C, Dupius D. 1987. An Original Predictive Method for *In Vivo* Percutaneous Absorption Studies. *J Soc Cosmet Chem* 28:397-417.
93. Elias PM, Cooper ER, Korr A, Brown BE. 1981. Percutaneous Transport in Relation to Stratum Corneum Structure and Lipid Composition. *J Invest Dermatol* 76:297-301.

94. Norlén L, Nicander I, Rozell BL, Oilmar S, Forslind B. 1999. Inter- and Intra-Individual Differences in Human Stratum Corneum Lipid Content Related to Physical parameters of Skin Barrier Function *In Vivo*. *J Invest Dermatol* 112:72-77.
95. Lampe MA, Burlingame AL, Whitney J, Williams ML, Brown BE, Roitman E, Elias PM. 1983. Human Stratum Corneum Lipids: Characterization and Regional Variations. *J Lipid Res* 24:120-130.
96. Grubauer G, Feingold K, Harris RM, Elias PM. 1989. Lipid Content and Lipid Type as Determinants of the Epidermal Permeability Barrier. *J Lipid Res* 30:89-96.
97. Roy SD, Flynn GL. 1990. Transdermal Delivery of Narcotic Analgesics: pH, Anatomical, and Subject Influences on Cutaneous Permeability of Fentanyl and Sufentanil. *Pharm Res* 7:842-847.
98. Houle JM, Strong A. 2002. Clinical Pharmacokinetics of Verteporfin. *J Clin Pharmacol* 42:547-557.
99. Schwartz JB. 2003. The Influence of Sex on Pharmacokinetics. *Clin Pharmacokinet* 42:107-121.
100. Roskos KV, Maibach HI. 1992. Percutaneous Absorption and Age. Implications for Therapy. *Drug Aging* 2:432-449.
101. Roskos KV, Maibach HI, Guy RH. 1989. The Effect of Aging on Percutaneous Absorption in Man. *J Pharmacokinet Biopharm* 17:617-630.
102. Leopold CS, Maibach HI. 1996. Effect of Lipophilic Vehicles on *In Vivo* Skin Penetration of Methyl Nicotinate in Different Races. *Int J Pharm* 139:161-167.
103. Richards GM, Oresajo CO, Halder RM. 2003. Structure and Function of Ethnic Skin and Hair. *Dermatol Clin* 21:595-600.
104. Klemsoal TO, Gjesdal K, Zahlse K. 1995. Physical Exercise Increases Plasma Concentrations of Nicotine During Treatment with a Nicotine Patch. *Br J Clin Pharmacol* 39:677-679.
105. Gupta SK, Southam M, Gale R, Hwang SS. 1992. System Functionality and Physicochemical Model of Fentanyl Transdermal System. *J Pain Symptom Manage* 7:S17-26.
106. Akomeah F, Nazir T, Martin GP, Brown MP. 2004. Effect of Heat on the Percutaneous Absorption and Skin Retention of Three Model Penetrants. *Eur J Pharm Sci* 21:337-345.
107. Danon A, Ben-Shimon S, Ben-Zvi Z. 1986. Effect of Exercise and Heat Exposure in Percutaneous Absorption of Methyl Salicylate. *Eur J Clin Pharmacol* 31:49-52.
108. Vanakoski J, Seppälä T, Sievi E, Lunell E. 1996. Exposure to High Ambient Temperature Increases Absorption and Plasma Concentration of Transdermal Nicotine. *Clin Pharmacol Ther* 60:308-315.
109. Menon GK, Lee SH, Roberts MS. 1998. Ultrastructural Effects of Some Solvents and Vehicles on the Stratum Corneum and Other Skin Components: Evidence for an "Extended Mosaic-Partitioning Model of the Skin Barrier". In Roberts MS, Walters KA, ed. *Dermal Absorption and Toxicity Assessment*. New York: Marcel Dekker, Inc., pp 727-751.
110. Bashir SJ, Maibach HI. 1999. Cutaneous Metabolism of Xenobiotics. In Bronaugh RL, Maibach HI, ed. *Percutaneous Absorption: Drugs, Cosmetics, Mechanisms, Methodology*. New York: Marcel Dekker, Inc., pp 65-80.
111. Iotchkiss SA. 1998. Dermal Metabolism. In Roberts MS, Walters KA, ed. *Dermal Absorption and Toxicity Assessment*. New York: Marcel Dekker, Inc., pp 43-101.

112. Rittirod T, Hatanaka T, Uraki A, Hino K, Katayama K, Koizumi T. 1999. Species Difference in Simultaneous Transport and Metabolism of Ethyl Nicotinate in Skin. *Int J Pharm* 178:161-169.
113. Sato K, Sugibayashi K, Morimoto Y. 1991. Species Differences in Percutaneous Absorption of Nicorandil. *J Pharm Sci* 80:104-107.
114. Watkinson AC, Brain KR. 2002. Basic Mathematical Principles in Skin Permeation. In Walters KA, ed. *Dermatological and Transdermal Formulations*. New York: Marcel Dekker, Inc., pp 61-88.
115. Ostrenga J, Steinmetz C, Poulsen B. 1971. Significance of Vehicle Composition. I. Relationship Between Topical Vehicle Composition, Skin Penetrability, and Clinical Efficacy. *J Pharm Sci* 60:1175-1179.
116. Cooper ER, Berner B. 1985. Skin Permeability. In Skerrow D, Skerrow CJ, ed. *Methods in Skin Research*. Chichester: Wiley-International, pp 417-419.
117. Idson B. 1975. Percutaneous Absorption. *J Pharm Sci* 64:901-924.
118. Barry BW. 1985. Optimizing Percutaneous Absorption. In Bronaugh RL, Maibach HI, ed. *Percutaneous Absorption Mechanisms, Methodology, Drug Delivery*. New York: Marcel Dekker, Inc., pp 489-511.
119. Zatz JL, Sarpotdar PP. 1987. Influence of Vehicles on Skin Penetration. In Kydonieus AF, Berner B, ed. *Transdermal Delivery of Drugs*. Boca Raton, Florida: CRC Press Inc., pp 87-91.
120. Lalor CB, Flynn GL, Weiner N. 1995. Formulation Factors Affecting Release of Drug From Topical Vehicles. II. Effect of Solubility On *In Vitro* Delivery of a Series of n-Alkyl p-Aminobenzoates. *J Pharm Sci* 84:673-676.
121. Wester RC, Maibach HI. 1995. Penetration Enhancement by Skin Hydration. In Smith EW, Maibach HI, ed. *Percutaneous Penetration Enhancers*. Boca Raton, Florida: CRC Press, pp 21-28.
122. Roberts MS, Walker M. 1993. Water: The Most Natural Penetration Enhancer. In Walters KA, Hadgraft J, ed. *Pharmaceutical Skin Penetration Enhancement*. New York: Marcel Dekker, Inc., pp 1-30.
123. Guy RH, Hadgraft J. 1989. Selection of Drug Candidates for Transdermal Drug Delivery. In Hadgraft J, Guy RH, ed. *Transdermal Drug Delivery: Developmental Issues and Research Initiatives*. New York: Marcel Dekker Inc., pp 59-81.
124. Guy RH. 1996. Current Status and Future Prospects of Transdermal Drug Delivery. *Pharm Res* 13:1765-1769.
125. Flynn GL, Stewart B. 1988. Percutaneous Drug Penetration: Choosing Candidates for Transdermal Development. *Drug Dev Res* 13:169-185.
126. Gummer CL. 1985. Vehicles as Penetration Enhancers. In Bronaugh RL, Maibach HI, ed. *Percutaneous Absorption Mechanisms, Methodology, Drug Delivery*. New York: Marcel Dekker, Inc., pp 561-570.
127. Pellett MA, Roberts MS, Hadgraft J. 1997. Supersaturated Solutions Evaluated with an *In Vitro* Stratum Corneum Tape Stripping Technique. *Int J Pharm* 151:91-98.
128. Megrab NA, Williams AC, Barry BW. 1995. Oestradiol Permeation Through Human Skin and Silastic Membrane: Effects of Propylene Glycol and Supersaturation. *J Control Release* 36:277-294.

129. Chiang CM, Flynn GL, Weiner ND, Szpunar GJ. 1989. Bioavailability Assessment of Topical Delivery Systems: Effect of Vehicle Evaporation Upon *In Vitro* Delivery of Minoxidil From Solution Formulations. *Int J Pharm* 55:229-236.
130. Coldman MF, Poulsen BJ, Higuchi T. 1969. Enhancement of Percutaneous Absorption by the Use of Volatile: Nonvolatile Systems as Vehicles. *J Pharm Sci* 58:1098-1102.
131. Davis AF, Hadgraft J. 1993. Supersaturated Systems as Topical Drug Delivery Systems. In Walters KA, Hadgraft J, ed. *Pharmaceutical Skin Penetration Enhancement*. New York: Marcel Dekker, Inc., pp 243-267.
132. Hadgraft J. 2001. Skin, the Final Frontier. *Int J Pharm* 224:1-18.
133. Hansen CM. 2000. *Hansen Solubility Parameters: A User's Handbook*. Boca Raton, Florida: CRC Press, Inc. pp 1-24.
134. Liron Z, Cohen S. 1984. Percutaneous Absorption of Alkanoic Acids II: Application of Regular Solution Theory. *J Pharm Sci* 73:538-542.
135. Hadgraft J. 1999. Passive Enhancement Strategies in Topical and Transdermal Drug Delivery. *Int J Pharm* 184:1-6.
136. Vaughan CD. 1985. Using Solubility Parameters in Cosmetics Formulations. *J Soc Cosmet Chem* 36:319-333.
137. Harrison JE, Watkinson AC, Green DM, Hadgraft J, Brain K. 1996. The Relative Effect of Azone® and Transcutol® on Permeant Diffusivity and Solubility in Human Stratum Corneum. *Pharm Res* 13:542-546.
138. Puglia C, Bonina F, Trapani G, Franco M, Ricci M. 2001. Evaluation of *In Vitro* Percutaneous Absorption of Lorazepam and Clonazepam from Hydro-Alcoholic Gel Formulations. *Int J Pharm* 228:79-87.
139. Shah VP. 1994. Skin Penetration Enhancers: Scientific Perspectives. In Hsieh DS, ed. *Drug Permeation Enhancement*. New York: Marcel Dekker, Inc., pp 19-23.
140. Chattaraj SC, Walker RB. 1995. Penetration Enhancer Classification. In Smith EW, Maibach HI, ed. *Percutaneous Penetration Enhancers*. Boca Raton, Florida: CRC Press, pp 5-19.
141. Williams AC, Barry BW. 1998. Chemical Penetration Enhancement: Possibilities and Problems. In Roberts MS, Walters KA, ed. *Dermal Absorption and Toxicity Assessments*. New York: Marcel Dekker, Inc., pp 297-312.
142. Barry BW. 1988. Action of Skin Penetration Enhancers - Lipid Protein Partitioning Theory. *Int J Cosmet Sci* 10:281-293.
143. Barry BW. 1991. Lipid-Protein-Partitioning Theory of Skin Penetration Enhancement. *J Control Release* 15:237-248.
144. Ribaud C, Garson JC, Doucet J, Leveque JL. 1994. Organization of Stratum Corneum Lipids in Relation to Permeability: Influence of Sodium Lauryl Sulfate and Preheating. *Pharm Res* 11:1414-1418.
145. Ogiso T, Iwaki M, Bechako K, Tsutsumi Y. 1976. Enhancement of Percutaneous Absorption by Laurocapram. *J Pharm Sci* 65:762-767.

146. Golden GM, McKie JE, Potts RO. 1987. Role of Stratum Corneum Lipid Fluidity in Transdermal Drug Flux. *J Pharm Sci* 76:25-28.
147. Yamane MA, Barry BW. 1995. Effects of Terpenes and Oleic Acid as Skin Penetration Enhancers Towards 5-Fluorouracil As Assessed With Time; Permeation, Partitioning and Differential Scanning Calorimetry. *Int J Pharm* 116:237-251.
148. Brain KR, Walters KA. 1993. Molecular Modeling of Skin Permeation Enhancement by Chemical Agents. In Walters KA, Hadgraft J, ed. *Pharmaceutical Skin Penetration Enhancement*. New York: Marcel Dekker, Inc., pp 389-416.
149. Vávrová K, Hrabálek A, Doležal P, Šámalová L, Palát K, Zbytovská J, Holas T, Klimentová J. 2003. Synthetic Ceramide Analogues as Skin Permeation Enhancers: Structure-Activity Relationships. *Bio Med Chem* 11:5381-5390.
150. Allan G. 1995. Azone®. In Smith EW, Maibach HI, ed. *Percutaneous Penetration Enhancers*. Boca Raton, Florida: CRC Press, pp 129-136.
151. Lee G. 1995. Interaction of Azone® with Model Lipid Systems. In Smith EW, Maibach HI, ed. *Percutaneous Penetration Enhancers*. Boca Raton, Florida: CRC Press, Inc., pp 195-210.
152. Lambert WJ, Higuchi WI, Knutson K, Krill SL. 1989. Dose-Dependent Enhancement Effects of Azone on Skin Permeability. *Pharm Res* 6:798-803.
153. Hadgraft J, Peck J, Williams DG, Pugh WJ, Allan G. 1996. Mechanisms of Action of Skin Penetration Enhancers/Retarders: Azone and Analogues. *Int J Pharm* 141:17-25.
154. Bouwstra JA, Peschier LJC, Brussee J, Boddé HE. 1989. Effect of N-alkyl-azocycloheptan-2-ones Including Azone on the Thermal Behavior of Human Stratum Corneum. *Int J Pharm* 52:47-54.
155. Francoeur ML, Golden GM, Potts RO. 1990. Oleic Acid: Its Effects on Stratum Corneum in Relation to (Trans)Dermal Drug Delivery. *Pharm Res* 7:621-627.
156. Goodman M, Barry BW. 1988. Action of Penetration Enhancers on Human Skin as Assessed by the Permeation of Model Drugs 5-Fluorouracil and Estradiol. I. Infinite Dose Technique. *J Invest Dermatol* 91:323-327.
157. Cornwell PA, Barry BW, Stoddart CP, Bouwstra JA. 1994. Wide-Angle X-Ray Diffraction of Human Stratum Corneum: Effect of Hydration and Terpene Enhancer Treatment. *J Pharm Pharmacol* 46:938-950.
158. Walker M, Hadgraft J. 1991. Oleic Acid- A Membrane 'Fluidiser' or Fluid Within the Membrane? *Int J Pharm* 71:R1-R4.
159. Ongpipattanakul B, Burnette RR, Potts RO, Francoeur ML. 1991. Evidence that Oleic Acid Exists in a Separate Phase Within Stratum Corneum Lipids. *Pharm Res* 8:350-354.
160. Barry BW. 2001. Novel Mechanisms and Devices to Enable Successful Transdermal Drug Delivery. *Eur J Pharm Sci* 14:101-114.
161. Finnin BC, Morgan TM. 1999. Transdermal Penetration Enhancers: Applications, Limitations, and Potential. *J Pharm Sci* 88:955-958.
162. Morgan TM, Parr RA, Reed BL, Finnin BC. 1998. Enhanced Transdermal Delivery of Sex Hormones in Swine with a Novel Topical Aerosol. *J Pharm Sci* 87:1219-1225.

163. Bakalova MV, Morgan TM, Reed BL, Finnin BC. 1997. The Effect of Pretreatment With New 'Safe' Penetration Enhancers on the Diffusion of NSAIDs Across Shed Snake Skin. In Brain KR, James VJ, Walters KA, ed. Perspectives in Percutaneous Penetration. Cardiff, UK: STS, p 78.
164. Finnin BC, Morgan TM, Klose K, Bakalova MV, Taylor D, Reed BL. 1997. Enhancement of Epidermal Penetration of NSAIDs by Padimate O, Octyl Salicylate and Octyl Methoxycinnamate. AAPS Annual Meeting. Pharm Res 14:S304.
165. Klose K, Taylor D, Reed BL, Finnin BC. 1997. Enhanced Percutaneous Penetration of Ibuprofen Determined by Microdialysis in Conscious Rats. In Brain KR, James VJ, Walters KA, ed. Perspectives in Percutaneous Penetration. Cardiff, UK: STS, p 77.
166. Klose K. 1999. Development of Methods to Evaluate Enhanced Percutaneous Penetration (PhD Thesis). Melbourne: Monash University.
167. Morgan TM, Reed BL, Finnin BC. 1998. Enhanced Skin Permeation of Sex Hormones With Novel Topical Spray Vehicles. J Pharm Sci 87:1213-1218.
168. Morgan TM, O'Sullivan HMM, Reed BL, Finnin BC. 1998. Transdermal Delivery of Estradiol in Postmenopausal Women with a Novel Topical Aerosol. J Pharm Sci 87:1226-1228.
169. Nicolazzo JA. 2000. Strategies for the Enhancement of Testosterone Transdermal Delivery (Honours Thesis). Melbourne: Monash University.
170. White EL, Reed BL, Finnin BC. 1997. Effect of Padimate O, Octyl Salicylate and Laurocapram on the Thermal Profile of a Model Stratum Corneum Lipid Mixture. Proceedings of the Australian Pharmaceutical Science Association Conference, Sydney, Australia, P45.
171. Cherny NJ, Chang V, Frager G, Ingham JM, Tiseo PJ, Popp B, Portenoy RK, Foley KM. 1995. Opioid Pharmacotherapy in the Management of Cancer Pain: A Survey of Strategies Used by Pain Physicians for the Selection of Analgesic Drugs and Routes of Administration. Cancer 76:1283-1293.
172. Slattery PJ, Boas RA. 1987. New Methods of Delivery of Opiates for Relief of Pain. Curr Therap 223-249.
173. Caplan RA, Southam M. 1990. Transdermal Drug Delivery and Its Application to Pain Control. In Benedetti C, Chapman CR, Giron G, ed. Advances in Pain Research and Therapy. New York: Raven Press Ltd., pp 233-240.
174. American Pain Society. 1990. Principles of Analgesic Use in the Treatment of Acute Pain and Chronic Cancer Pain, 2nd Edition. Clin Pharm 9:601-612.
175. Foley KM. 1995. Misconceptions and Controversies Regarding the Use of Opioids in Cancer Pain. Anticancer Drugs 6 Suppl 3:4-13.
176. Varvel JR, Shafer SL, Hwang SS, Coen PA, Stanski DR. 1989. Absorption Characteristics of Transdermally Administered Fentanyl. Anesthesiology 70:928-934.
177. McQuay HJ. 1991. Opioid Clinical Pharmacology and Routes of Administration. Br Med Bull 47:703-717.
178. Grond S, Radbruch L, Lehmann KA. 2000. Clinical Pharmacokinetics of Transdermal Opioids: Focus on Transdermal Fentanyl. Clin Pharmacokinet 38:59-89.

179. American Society of Hospital Pharmacists. 2000. AHFS Drug Information. Bethesda, MD: Board of Directors of the American Society of Hospital Pharmacists. p 1886.
180. Roy SD, Flynn GL. 1989. Transdermal Delivery of Narcotic Analgesics: Comparative Permeabilities of Narcotic Analgesics Through Human Cadaver Skin. *Pharm Res* 6:825-832.
181. Clotz MA, Nahata MC. 1991. Clinical Uses of Fentanyl, Sufentanil, and Alfentanil. *Clin Pharm* 10:581-593.
182. Maguire P, Tsai N, Kamal J, Cometta-Morini C, Upton C, Loew G. 1992. Pharmacological Profiles of Fentanyl Analogs at Mu, Delta and Kappa Opiate Receptors. *Eur J Pharmacol* 213:219-225.
183. Davis PJ, Cook DR. 1986. Clinical Pharmacokinetics of the Newer Intravenous Anaesthetic Agents. *Clin Pharmacokinet* 11:18-35.
184. Scholz J, Steinfath M, Schulz M. 1996. Clinical Pharmacokinetics of Alfentanil, Fentanyl and Sufentanil. An Update. *Clin Pharmacokinet* 31:275-292.
185. Willens JS, Myslinski NR. 1993. Pharmacodynamics, Pharmacokinetics, and Clinical Uses of Fentanyl, Sufentanil, and Alfentanil. *Heart Lung* 22:239-251.
186. Roy SD, Hou SY, Witham SL, Flynn GL. 1994. Transdermal Delivery of Narcotic Analgesics: Comparative Metabolism and Permeability of Human Cadaver Skin and Hairless Mouse Skin. *J Pharm Sci* 83:1723-1728.
187. Muijsers RBR, Wagstaff AJ. 2001. Transdermal Fentanyl. An Updated Review of its Pharmacological Properties and Therapeutic Efficacy in Chronic Cancer Pain Control. *Drugs* 61:2289-2307.
188. Roy SD, Flynn GL. 1989. Solubility Behavior of Narcotic Analgesics in Aqueous Media: Solubilities and Dissociation Constants of Morphine, Fentanyl, and Sufentanil. *Pharm Res* 6:147-151.
189. Michaels AS, Chandrasekaran SK, Shaw JE. 1975. Drug Permeation Through Human Skin: Theory and *In Vitro* Experimental Measurement. *AIChEJ* 21:985-996.
190. Roy SD, Gutierrez M, Flynn GL, Cleary GW. 1996. Controlled Transdermal Delivery of Fentanyl: Characterizations of Pressure-Sensitive Adhesives for Matrix Patch Design. *J Pharm Sci* 85:491-495.
191. Sebel PS, Barrett CW, Kirk CJ, Heykants J. 1987. Transdermal Absorption of Fentanyl and Sufentanil in Man. *Eur J Clin Pharmacol* 32:529-531.
192. Berner B, John VA. 1994. Pharmacokinetic Characterisation of Transdermal Delivery Systems. *Clin Pharmacokinet* 26:121-134.
193. Lehmann KA, Zech D. 1992. Transdermal Fentanyl: Clinical Pharmacology. *J Pain Symptom Manage* 7 Suppl 3:8-16.

CHAPTER 2

DEVELOPMENT OF A SUITABLE MODEL FOR STUDYING *IN VITRO* FENTANYL PERCUTANEOUS ABSORPTION

2.1. INTRODUCTION

The most common methods for evaluating *in vitro* percutaneous drug absorption involve the use of “diffusion cells” (1). The diffusion cell technique is a popular approach for investigating the kinetics and mechanisms of transdermal drug delivery (2), can serve as a tool for the rapid screening of vehicle effects during the initial stages of formulation development (3, 4), offers advantages associated with cost, time, and practicality and provides opportunities to reduce, refine, and replace *in vivo* animal studies (1, 4, 5).

Although many variations of the diffusion cell exist, the two systems that are commonly used are static and flow-through diffusion cells (1, 3). Both types of diffusion cell are acceptable methods to predict *in vivo* percutaneous drug absorption (4, 6), and it has been reported that both systems produce equivalent results (7). In either cell design, the skin membrane is mounted between a donor chamber and a receptor chamber, and the amount of compound permeating through the skin (from the applied formulation (the donor side) to receptor solution (the receptor side)) is determined as a function of time. While the static diffusion cell is useful for the evaluation of large drug volumes, a flow-through design (which was employed for the diffusion studies described in this thesis) allows for automatic sampling and continuous flow of solution through the receiver chamber to maintain sink conditions (8).

Over recent decades, considerable emphasis has been placed on the need for relevant *in vitro* data produced in a reliable and reproducible manner. Several protocols have been written in an attempt to aid the development and standardization of *in vitro* testing procedures (6). These guidelines address a number of issues that are pertinent to the accurate *in vitro* evaluation of transdermal drug delivery. They also highlight that an important issue to be considered prior to conducting an *in vitro* percutaneous drug absorption study is the selection of an appropriate receptor solution.

The primary objective of a receptor solution is, essentially, to mimic the sink conditions that prevail during percutaneous drug absorption *in vivo*. Therefore, in an effort to obtain reliable *in vitro* data that is predictive of *in vivo* percutaneous absorption, the concentration of the permeating compound within the receptor solution must remain consistently low during an *in vitro* experiment. It is now generally accepted that, in order to maintain an adequate diffusion gradient across the skin, the thermodynamic activity of

the compound within the receptor solution must not exceed 10% of its activity within the donor solution (4, 9)

A commonly used receptor phase is isotonic phosphate buffer pH 7.4. However, the use of an entirely aqueous receptor solution is not recommended for compounds with limited aqueous solubility (i.e. less than $\sim 10\mu\text{g/ml}$ or $\log K_{\text{OCT/W}} \sim 3$) (9, 10), as diffusion of the compound across the aqueous receptor layer may become rate-limiting (11). Consequently, under these conditions, *in vitro* permeation data can grossly underestimate the rate of percutaneous drug absorption *in vivo* (10, 12). Franz (13) addressed this problem as early as 1975, when he excluded highly water-insoluble compounds as it was felt that their *in vitro* permeability might be “artificially limited due to their insolubility in the dermal bathing solution”. This issue was subsequently investigated by a number of workers, who generally observed that the *in vitro* skin permeation of lipophilic compounds could be improved by replacing aqueous receptor fluids with solutions containing solubilising agents (10, 14, 15).

Examples of solubilising agents added to receptor solutions include bovine serum albumin (BSA), nonionic surfactants (such as polyethylene glycol oleyl ether (Volpo 20), polyethylene-polypropylene glycol (Poloxamer 188), octoxynol 9 (Triton-X 100), polysorbate 80 (Tween 80)), and organic solvents (such as ethanol or methanol) (1, 10, 16, 17). However, the presence of BSA or nonionic surfactants in the receptor solution can complicate sample analysis (1). Therefore, receptor solutions containing organic solvents are particularly useful as they provide reasonable sink conditions for many permeating compounds, are simple to prepare, and eliminate the need for anti-microbial agents (which may also interfere with permeant analysis). For instance, ethanol:water systems (at concentrations of up to 50%v/v ethanol) have been used for studying the percutaneous absorption of a variety of lipophilic compounds (1, 17).

Kasting et al (12) utilised either isotonic phosphate buffer pH 7.4 or a 1:1 ethanol:water system as receptor solutions for studying the *in vitro* skin permeation of highly lipophilic compounds. Whilst it was found that use of the phosphate buffer led to under-predicted percutaneous absorption *in vivo*, it was also evident that use of the ethanol:water system led to an over-prediction of drug absorption. It is likely that this latter error was incurred by the back-diffusion of ethanol into the skin, which could have led to alterations in the physical and chemical properties of the stratum corneum.

Therefore, care must be exercised when using a solubilising agent, such as ethanol, as the receptor solution itself must not adversely effect the barrier properties of the skin or the physicochemical properties of the permeating compound (4).

2.2. OBJECTIVES

The overall objective of these studies was to select a receptor solution that would maintain sink conditions during the *in vitro* investigation of fentanyl absorption without deleteriously affecting the barrier properties of the skin.

It was necessary to explore this concept as fentanyl has a relatively high octanol-water partition coefficient ($\log K_{OCT/W} = 2.86$ at 37°C) and its solubility in citrate-phosphate buffer (pH 7.4) had been reported to be $51\text{ }\mu\text{g/ml}$ at 37°C (18). Isotonic phosphate buffer pH 7.4 preserved with 0.1%w/v sodium azide (IPB pH 7.4 (NaN_3)) is often used as a receptor solution when conducting *in vitro* skin diffusion studies in our research group and by an affiliated pharmaceutical company, Acrux Ltd. (19). However, when studying the *in vitro* percutaneous absorption of lipophilic compounds, dilute aqueous solutions of ethanol (containing 10 to 30%v/v ethanol) have often been employed by these groups (19). Therefore, the percutaneous absorption of fentanyl *in vitro* was investigated using either IPB pH 7.4 (NaN_3) or 20%v/v aqueous ethanol as the receptor solution.

In light of previous research, it was hypothesised that 20%v/v aqueous ethanol could potentially alter the barrier properties of the skin. Therefore, a secondary objective of this research was to investigate the possible mechanism(s) by which the ethanolic receptor solution may alter fentanyl absorption. Consequently, the effect of the ethanolic receptor on the partition coefficient of fentanyl between human stratum corneum (SC) and water were compared to that of IPB pH 7.4 (NaN_3).

It will become evident in Chapter 3 that the ultimate intention of these *in vitro* percutaneous absorption studies was to determine whether octisalate (OS) and padimate O (PO) enhance the percutaneous absorption of fentanyl. Therefore, another objective of the work presented in this chapter was to determine whether the ethanolic receptor solution modified the mechanism(s) by which OS enhanced the *in vitro* percutaneous absorption of fentanyl. It was hypothesised that the ethanolic receptor solution could alter

skin penetration, and hence the mechanism(s) of action, of OS as it is a highly lipophilic compound ($\log K_{OCT/W} = 5.77^1$) that is sparingly soluble in IPB pH 7.4 ($< 1 \mu\text{g/ml}$ (20)).

2.3. MATERIALS AND METHODS

2.3.1. Materials

Fentanyl was manufactured by Macfarlan Smith Ltd. (Edinburgh, UK). OS was supplied by Bronson and Jacobs (Australia). HPLC grade acetonitrile was supplied by Merck (Australia). Purified water was obtained from a Milli-Q™ water purification system (Millipore, Bedford, MA, USA). All other chemicals were of analytical grade.

2.3.2. Fentanyl saturated solubility studies

Fentanyl was added in excess to IPB pH 7.4 (NaN_3), 20%v/v aqueous ethanol, or water. The suspensions were vortexed for 30 sec, then placed in a shaking water bath at $32 \pm 1^\circ\text{C}$ (SS40-D, Grant Instruments (Cambridge) Ltd., England) where they were agitated at 15 strokes/min for 72 h. At the end of this equilibration period, the samples were centrifuged at 3500 rpm for 20 min at 32°C in a Beckman GS-CR centrifuge (Beckman Instruments Inc., Palo Alto, CA, USA). The pH of the supernatant was determined using a Metrohm 632 pH meter (Metrohm Herisau, Switzerland). A 1000 μl aliquot was diluted with an appropriate volume of either IPB pH 7.4 (NaN_3) or 20%v/v aqueous ethanol. The concentration of fentanyl within each sample was then determined using the HPLC/UV assay detailed in Section 2.3.5. The saturated solubility of fentanyl in each of the fluids was determined in triplicate.

2.3.3. In vitro skin diffusion studies

2.3.3.1. Skin preparation

Human female abdominal epidermis was separated from abdominal tissue obtained from two individual donors following abdominoplasty. Full-thickness skin samples were

¹ Estimated using EPISuite (Version 3.11) computer software package (U.S. Environmental Protection Agency)

prepared by removing subcutaneous tissue and fat from the underside of the dermal membrane using a stainless steel surgical blade. Epidermal membranes were prepared by a heat-separation technique (21). After the full-thickness skin samples were immersed in water (maintained at 60°C) for 45 sec, the epidermis was removed by gently peeling it away from the dermis. The epidermal membranes were floated (SC-side up) over purified water whilst being transferred onto filter paper. The samples were dried overnight under ambient conditions and stored in aluminum foil at -20°C for not more than 12 months (22). The samples were defrosted under ambient conditions for approximately 2 to 4 h prior to use.

2.3.3.2. *In vitro* diffusion studies

In vitro skin diffusion studies were performed using modified stainless steel flow-through diffusion cells. The donor chamber of each cell consisted of a well that could hold a maximum of 4000 µl of donor solution, and the skin placed between the donor and receptor chambers had a diffusion area of 0.79 cm².

Parallel diffusion studies were conducted, where the receptor solution comprised either IPB pH 7.4 (NaN₃) or 20%v/v aqueous ethanol. To avoid the formation of air bubbles beneath the skin, the receptor solution was heated to 40°C, then degassed by spraying it in fine droplets under vacuum with continuous stirring. The solution was degassed three times before each diffusion study.

For each diffusion experiment, thawed epidermal membranes were cut into square pieces, each with an area of approximately 1 cm², and were mounted over the receptor well. The donor and receptor chambers were then bolted tightly together. Before transferring the skin to the diffusion cell, the receptor compartment was filled with approximately 100 µl of receptor solution and a wire mesh was placed over the receptor well. The wire mesh encourages turbulent flow of receptor solution through the receptor well, which mitigates the formation of unstirred, limiting boundary layers and thus helps maintain sink conditions (3, 23). It also prevents air bubbles from forming beneath the skin.

The diffusion cells were mounted onto a hollow stainless steel bar, through which thermostated water was pumped to maintain the temperature of the cells at 32 ± 0.5°C. To ensure sink conditions were maintained throughout a diffusion study, the receptor

solution was pumped through the receptor compartment at a flow rate of 1 ml/h by means of a peristaltic pump (Watson Marlow Microcassette Pump, UK). As the receptor chamber had a volume capacity in the order of 50 μ l, the total volume of receptor solution was replaced approximately 20 times per hour at this flow rate. The diffusion experiments were conducted over a 24 h period, whereby diffusion samples were collected every hour for the first four hours, then every two hours for the remaining 24 h, using an automated fraction collector (ISCO Retriever II, NE).

The skin was initially equilibrated with the receptor fluid for 1 h before the commencement of each study. For all diffusion experiments, the donor solution was a saturated aqueous solution of fentanyl. The donor solution was prepared by dispersing excess fentanyl (3 mg/ml) in purified water. The solution was vortexed for 1 min and placed in water bath maintained at $32 \pm 1^\circ\text{C}$, where it was continuously shaken at 15 strokes/min for 72 h. The donor solution was vortexed for 30 sec immediately before application to the skin to ensure uniform dispersion of the solid fentanyl crystals. It was applied to the skin at a dose of 2000 μ l.

In order to investigate the effect of the receptor solution on the absorption of fentanyl, the equilibration period between the skin and the receptor solution was extended for a further 2 or 12 h period prior to the application of the donor solution ($4 < n < 12$).

To investigate the effect of the receptor solution on the enhancement of fentanyl percutaneous absorption by OS, the skin was either left untreated (control) or was pretreated with a finite dose ($5 \mu\text{l}/\text{cm}^2$) of 5%w/v OS in 95%v/v ethanol for a period of either 2 or 12 h ($4 < n < 12$). The skin was then rinsed three times with 500 μ l of purified water and gently blotted dry with low-lint, absorbent tissue (Kimwipes®, Kimberly-Clark Australia). The donor solution was then applied to the skin.

2.3.4. Stratum corneum-water partitioning studies

2.3.4.1. Isolation of human stratum corneum

SC sheets were isolated from freshly separated epidermis (which were prepared according to the method described in Section 2.3.3.1) using the method described by Cornwell et al (24). The SC was obtained by floating the epidermis (SC-side up) over an aqueous solution of 0.0001%w/v trypsin (bovine, type III (Sigma-Aldrich, St Louis, MO,

USA)) and 0.5%w/v sodium bicarbonate for 12 h (24). After this time, the SC was removed from the trypsin solution and sandwiched between filter paper. To ensure complete removal of digested epidermal material, the underside of the SC was blotted dry with cotton balls, rinsed several times with purified water and then floated (epidermal-side down) over purified water for several hours. The SC was then transferred onto wire mesh (SC-side up) and dried under ambient conditions for 12 h. The dried SC sheets were stored over silica gel, under vacuum, for a maximum of 2 weeks.

2.3.4.2. *Stratum corneum-water partitioning studies*

Desiccated SC was die-punched into 5 cm² circular pieces and the individual discs were weighed on a Mettler Toledo balance (Mettler Toledo, AT261, Switzerland). The discs were laid flat, epidermal-side down, over filter paper and, using wire mesh for support, they were floated over the receptor solution (either IPB pH 7.4 (NaN₃) or 20%v/v aqueous ethanol (n=5)). In order to mimic the experimental conditions described in Section 2.3.3.2, the SC discs were equilibrated with the receptor solution for 1 h. At the end of this initial equilibration period, the discs were left in contact with the receptor solution for an additional 2 or 12 h period. Thereafter, the SC discs were removed from the receptor solution, separated from the wire mesh and filter paper, and immersed in 3000 µl of an aqueous solution sub-saturated with fentanyl. The solution was prepared by adding 60 µg/ml of fentanyl to purified water. After equilibrating the solution at 32 ± 1°C for 72 hours, it was filtered through a 0.20 µm filter before use to ensure the complete removal of excess solid.

After the SC was added to the solution, the samples were vortexed for 30 sec, and then placed in a shaking water bath maintained at 32 ± 1°C. The samples were stored in the water bath, where they were continuously shaken at a rate of 15 strokes/min, for 24 h. At the end of the 24 h period, the SC discs were removed from the bathing solution. Excess solution that had adsorbed onto the SC surface was removed by sandwiching the discs between filter paper for 30 sec. The discs were then re-weighed.

Fentanyl uptake into the SC was determined by a depletion method (25). The concentration of fentanyl within the bathing solution was determined before and after 24 h immersion of the SC discs using the HPLC/UV assay described in Section 2.3.5.

2.3.5. Analytical methods

Fentanyl concentrations within the permeation, partitioning or saturated solubility samples were determined using reverse phase HPLC in conjunction with UV detection. The HPLC system consisted of a Waters 610 pump, Waters 600E system controller, Waters 712 WISP autosampler, and Waters 486 UV absorbance detector. The data was analysed on a Shimadzu C-R6A integrator (Shimadzu Corp., Japan).

Fentanyl quantification was performed using a Waters Symmetry C₁₈ column (5µm particle size, 3.9 x 150 mm) and a RP-8 Newguard cartridge guard column (Aquapore 7 µm, 3 x 15 mm, Alltech/Perkin Elmer, CA, USA). The injection volume was 150 µl. The mobile phase (32%v/v acetonitrile, 68%v/v water, 0.068%v/v perchloric acid (70%v/v), and 10 mM heptane sulphonic acid) was pumped through the column at a flow rate of 1ml/min. UV detection was performed at 210 nm. The retention time for fentanyl under these conditions was ~12.1 min.

Calibration curves for each assay (i.e. fentanyl in IPB pH 7.4 (NaN₃) or 20%v/v aqueous ethanol) were constructed using standard solutions at concentrations within the range of 0.05 to 10 µg/ml. A linear relationship between peak area and concentration was confirmed by the correlation coefficient generated by linear regression (using the least squares method) of the calibration curve, which was weighted by a factor of 1/x. The linearity of each assay was excellent ($r^2 > 0.995$).

Intra-day precision and accuracy were determined from standard solutions (n=5) at three different concentrations (0.05, 1 and 10 µg/ml). Intra-day precision and accuracy were highly satisfactory, as %CV was less than 3.5% and less than 9.0% and accuracy ranged from 99.3 to 104.4% and from 96.5 to 101.6% for fentanyl in either IPB pH 7.4 (NaN₃) or 20%v/v aqueous ethanol, respectively.

Inter-day precision of each assay was determined over three different days, using standard solutions freshly prepared on each day of analysis. Each assay was highly reproducible, with precision (%CV) being less than 5.3% or 3.6% for fentanyl in either IPB pH 7.4 (NaN₃) or 20%v/v aqueous ethanol, respectively.

2.3.6. Mathematical analysis

2.3.6.1. Fentanyl diffusional parameters

Fentanyl permeation profiles were fitted to the following solution of Fick's second law of diffusion (refer to Chapter 4) (26):

$$Q_t = AK_{SC/V}hC_v \left[D \frac{t}{h^2} - \frac{1}{6} - \frac{2}{\pi^2} \sum_{n=1}^{\infty} \frac{(-1)^n}{n^2} \exp\left(-\frac{D^2 n^2 \pi^2 t}{h^2}\right) \right] \quad 2.1$$

Where Q_t is the amount of fentanyl that permeates the epidermis into the receptor solution at time, t . A is the skin surface diffusion area, $K_{SC/V}$ is the partition coefficient of fentanyl between the SC and the vehicle (water), h is the thickness of the SC (which was assumed to be 13 μm (27)), D is the diffusion coefficient of fentanyl within the SC, and C_v is the concentration of fentanyl within the donor solution. As the donor solution was saturated with fentanyl and was applied to the skin at a sufficiently large dose, it was assumed that the concentration of fentanyl within the donor solution did not significantly deplete over the duration of the experiment. Hence, C_v was replaced by the saturated solubility of fentanyl in water (91.47 $\mu\text{g/ml}$ at 32°C).

The parameters $K_{SC/V}h$ and D/h^2 in Equation 2.1 were replaced by the terms a and b , respectively. The parameters a and b were derived by fitting the permeation data to the theoretical equation, using a computer software package (SigmaPlot®, Version 8.01, SPSS Inc., USA). A non-linear least squares method was used to fit the data. The permeability coefficient, K_p , was then calculated by multiplying the parameters a and b , which is therefore equivalent to the expression:

$$K_p = \frac{K_{SC/V}D}{h} \quad 2.2$$

Fentanyl flux (J) across the skin was calculated from the permeability coefficient, where:

$$J = K_p \times C_v \quad 2.3$$

2.3.6.2. Stratum corneum-water partition coefficient

The partition coefficient of fentanyl between isolated human SC and water ($K_{SC/W}$) was calculated according to the following equation (28):

$$K_{SC/W} = \frac{K^*}{\rho_D} \times \frac{W_D}{V_H} \quad 2.4$$

Where:

$$K^* = \frac{\text{Mass } (\mu\text{g}) \text{ of fentanyl} / \text{Mass (mg) of desiccated SC}}{\text{Mass } (\mu\text{g}) \text{ of fentanyl} / \text{Mass (mg) of donor solution}}$$

ρ_D = Density of the donor solution (g/cm^3)

W_D = Mass (g) of desiccated SC (i.e. SC weight prior to immersion in the donor solution)

V_H = Volume (cm^3) of hydrated SC, which is determined from the weight of the SC after 24 h immersion in the sub-saturated fentanyl solution, assuming that the SC has a density of $1 \text{ g}/\text{cm}^3$ (29))

2.3.6.3. Enhancement ratios generated by octisalate pretreatment

The enhancement of the various diffusional parameters (J , K_p , $K_{SC/W}$ or D) derived from Equations 2.1 and 2.3 and of the partition coefficient of fentanyl between isolated SC and water ($K_{SC/W}$) (calculated from Equation 2.4) following pretreatment with OS was defined in terms of an enhancement ratio (ER), where:

$$ER = \frac{\text{Parameter derived from epidermis or SC pretreated with OS}}{\text{Parameter derived from untreated epidermis or SC}} \quad 2.5$$

2.3.7. Statistical analysis

Statistical significance was determined between the sample means of the treatment groups using the Student's t-test (two-tailed). A probability of $p < 0.05$ was considered statistically significant. All results are presented as the mean \pm SEM.

2.4. RESULTS AND DISCUSSION

2.4.1. Fentanyl solubility and sink conditions

The saturated solubility of fentanyl in water (the donor vehicle) and in each of the receptor solutions, the solution pH, and the predicted percentage of fentanyl ionisation are shown in Table 2.1. Firstly, it should be noted that the solubility of fentanyl in IPB pH 7.4 (NaN_3) at 32°C was markedly higher than that previously reported in citrate-phosphate buffer pH 7.4 at 25°C (18) (~448 $\mu\text{g/ml}$ versus ~51 $\mu\text{g/ml}$). It is also important to note that the saturated solubility of fentanyl in IPB pH 7.4 (NaN_3) was higher than its solubility in 20%v/v aqueous ethanol ($p=0.0199$). This difference is likely to be related to the degree by which fentanyl is ionised in either receptor solution. Due to its buffer capacity, the addition of excess fentanyl to IPB pH 7.4 (NaN_3) resulted in a suspension with pH ~ 7.66. As fentanyl is weak base ($\text{pK}_a \sim 8.99$ (30)), it was assumed that approximately 96% of fentanyl within the solution existed in its ionised form. Hence, it is probable that the overall solubility of fentanyl in IPB pH 7.4 (NaN_3) is due to appreciable ionisation of the compound within this fluid. On the other hand, fentanyl was likely to be approximately 65% ionised within the ethanolic receptor solution (pH ~ 8.73).

Table 2.1. The saturated solubility and predicted percentage of ionisation of fentanyl in water, isotonic phosphate buffer pH 7.4, 0.1%w/v sodium azide (IPB pH7.4 (NaN_3)) or 20%v/v aqueous ethanol (20% aq. EtOH).

Solvent	Fentanyl saturated solubility ($\mu\text{g/ml}$)	Solution pH	Predicted % fentanyl ionised ^a
Water	91.47 \pm 1.14	9.22 \pm 0.04	~37
IPB pH 7.4 (NaN_3)	447.59 \pm 10.00 ^b	7.66 \pm 0.02	~96
20% aq. EtOH	417.34 \pm 2.97	8.73 \pm 0.14	~65

^a Based on the finding that fentanyl has a pK_a value of 8.99 (30).

^b Statistically significant difference compared with the saturated solubility of fentanyl in 20% aqueous ethanol ($p<0.05$).

As the solubility of fentanyl in 20%v/v aqueous ethanol was still relatively high, it does not appear that the presence of the free base limited fentanyl solubility. It is therefore likely both the unionised and ionised forms of fentanyl were solubilised in the ethanolic receptor solution.

It is generally assumed that sink conditions are maintained during a diffusion experiment when the final concentration of the permeant within the receptor solution does not exceed 10 to 20% of its concentration at saturation (31, 32). Therefore, to ensure that sink conditions were maintained during the diffusion studies, the concentration of fentanyl found within either receptor solution at the completion of a diffusion experiment (after a 2 or 12 h equilibration period between the skin and receptor solution) are expressed as the percentage of the saturated solubility of fentanyl in water (the donor solution) and in the receptor solution in Table 2.2.

It is evident from the percentages shown in Table 2.2 that fentanyl concentrations found within either receptor solution were extremely low (less than 3%), relative to its saturated solubility within the donor or receptor solutions, at the completion of the diffusion experiments. Based on this finding it is reasonable to assume that fentanyl has adequate solubility in either IPB pH 7.4 (NaN_3) or 20%v/v aqueous ethanol to maintain sink conditions during a diffusion experiment.

Table 2.2. Fentanyl concentrations found within isotonic phosphate buffer pH 7.4, 0.1%w/v sodium azide (IPB pH 7.4 (NaN_3)) or 20%v/v aqueous ethanol (20% aq. EtOH) at the completion of a 24 h diffusion experiment (following a 2 or 12 h equilibration period between the skin and receptor solution) ($4 < n < 12$).

Receptor solution	2 h equilibration period			12 h equilibration period		
	Fentanyl conc. ($\mu\text{g/ml}$)	% SS DS ^a	% SS RS ^a	Fentanyl conc. ($\mu\text{g/ml}$)	% SS DS ^a	% SS RS ^a
IPB pH 7.4 (NaN_3)	1.24 ± 0.09	1.36 ± 0.10	0.28 ± 0.02	1.40 ± 0.07	1.53 ± 0.08	0.31 ± 0.02
20% aq. EtOH	1.26 ± 0.10	1.38 ± 0.11	0.30 ± 0.02	2.74 ± 0.20	3.00 ± 0.22	0.66 ± 0.05

^a Concentrations expressed as a percentage of the saturated solubility of fentanyl in water (the donor solution) (% SS DS) and the receptor solution (% SS RS).

However, this finding alone may not totally discount the use of the ethanol: water system, particularly as the overall solubility of fentanyl in IPB pH 7.4 (NaN_3) is possibly due to appreciable ionisation of the compound within this fluid. It has been previously established that the free-base form is almost entirely responsible for fentanyl permeation through skin (33, 34). Therefore, when selecting a receptor solution, it is judicious to perform *in vitro* skin diffusion studies in conjunction with saturated solubility studies to ensure that percutaneous drug absorption is not detrimentally effected by alterations to the barrier properties of the skin and the physicochemical properties of the permeating compound.

2.4.2. Effect of an ethanolic receptor solution on fentanyl percutaneous absorption

The profiles generated for fentanyl permeation through the epidermis into IPB pH 7.4 (NaN_3) or 20%v/v aqueous ethanol (following a 2 or 12 h equilibration period between the skin and receptor solution) are shown in Figures 2.1 and 2.2, respectively. As seen in Figure 2.1, the mean cumulative amount of fentanyl that permeated the epidermis previously equilibrated with IPB pH 7.4 (NaN_3) for either 2 or 12 h was not significantly different ($43.42 \pm 2.03 \mu\text{g}/\text{cm}^2$ versus $40.29 \pm 1.41 \mu\text{g}/\text{cm}^2$ at 24 h, respectively).

On the other hand, fentanyl permeation was significantly affected when aqueous ethanol was used as the receptor solution. As demonstrated in Figure 2.2, the mean cumulative amount of fentanyl permeating the epidermis equilibrated with 20%v/v aqueous ethanol for 2 h was $45.19 \pm 1.63 \mu\text{g}/\text{cm}^2$ at 24 h. As this amount is comparable to that attained when the skin was equilibrated with IPB pH 7.4 (NaN_3) for 2 h, it would appear from these initial observations that, after relatively short equilibration periods, the presence of 20%v/v ethanol in the receptor solution did not adversely effect the barrier function of the skin. However, when the skin was equilibrated with the ethanolic receptor solution for a 12 h period, the mean cumulative amount of fentanyl that permeated the epidermis at 24 h dramatically increased to $74.98 \pm 4.51 \mu\text{g}/\text{cm}^2$ ($p < 0.0001$ compared with epidermis equilibrated with either 20%v/v aqueous ethanol for 2 h or with IPB pH 7.4 for 12 h). Consequently, it would appear that after longer equilibration periods, the presence of ethanol in the receptor solution altered the barrier properties of the epidermis.

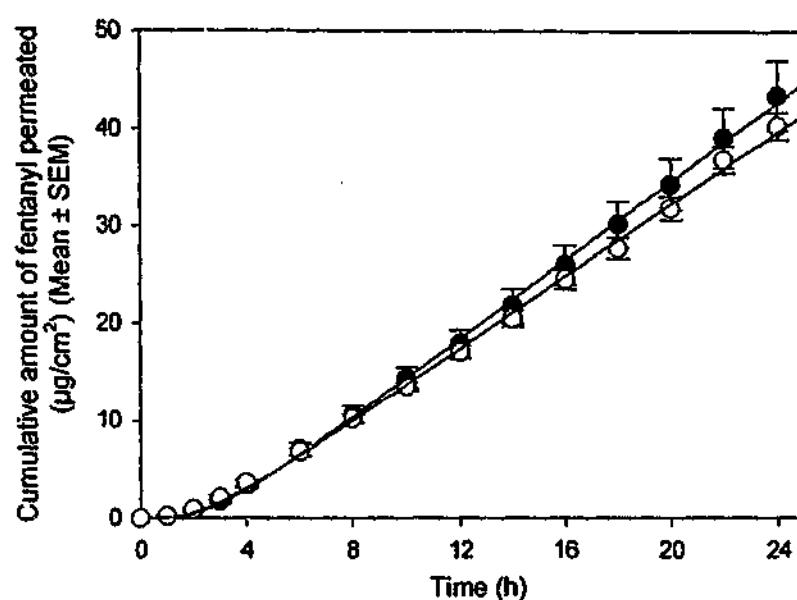


Figure 2.1. Permeation profiles for fentanyl permeating human epidermis, following a 2 h (●) or 12 h (○) equilibration period with isotonic phosphate buffer pH 7.4, 0.1%w/v sodium azide. The solid lines represent a non-linear regression of the data to Equation 2.1 ($r^2=0.999$ and 1.000 for the 2 h and 12 h profiles, respectively).

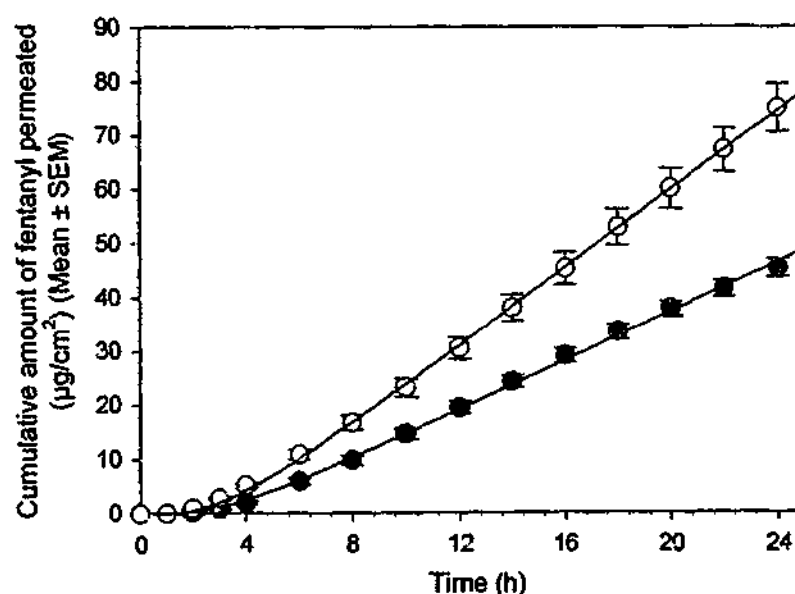


Figure 2.2. Permeation profiles for fentanyl permeating human epidermis, following a 2 h (●) or 12 h (○) equilibration period with 20%v/v aqueous ethanol. The solid lines represent a non-linear regression of the data to Equation 2.1 ($r^2=0.999$ and 1.000 for the 2 and 12 h profiles, respectively).

The diffusional parameters associated with the fentanyl permeation profiles are presented in Tables 2.3 and 2.4. In the first instance, none of the diffusional parameters were effected when the equilibration time between the epidermis and IPB pH 7.4 (NaN_3) was extended from 2 to 12 h (Table 2.3). Furthermore, the permeability coefficient (K_p) and flux (J) were in the order of ~ 0.02 cm/h and ~ 2 $\mu\text{g}/\text{cm}^2/\text{h}$, respectively, which are in agreement with previous research (33-35).

The permeability coefficient of fentanyl through epidermis in contact with IPB pH 7.4 (NaN_3) ($K_p = 0.022 \pm 0.001$ cm/h) was comparable to that through skin in contact with 20%v/v aqueous ethanol ($K_p = 0.025 \pm 0.002$ cm/h) after a 2 h equilibration. As the permeability coefficient is an overall manifestation of the driving force for drug diffusion across the skin (36-38), it is therefore probable that the concentration gradient of fentanyl formed across the skin was similar in the presence of either IPB pH 7.4 (NaN_3) or 20%v/v aqueous ethanol. This finding is in agreement with the results generated from the saturated solubility studies, where the final concentration of fentanyl found within either receptor solution was found to be less than 10% of its maximum solubility in the donor solution (Table 2.2).

Despite this similarity in overall permeability, it is also apparent from the data presented in Tables 2.3 and 2.4 that the mechanisms involved in fentanyl permeation were different in the presence of either receptor solution, following a 2 or 12 h equilibration period. In particular, compared with skin that had been equilibrated with IPB pH 7.4 (NaN_3), it appears that the partitioning of fentanyl into the SC was significantly enhanced whilst its diffusivity in the SC was reduced in the presence of the ethanolic receptor solution.

It is also evident from the data presented in Table 2.4 that prolonged contact between the skin and the ethanolic receptor solution altered fentanyl permeation, as the permeability coefficient of fentanyl significantly increased from 0.025 ± 0.002 cm/h to 0.040 ± 0.002 cm/h as the equilibration time was extended from 2 to 12 h ($p < 0.0001$). Furthermore, it appeared that this effect was predominantly due to enhancement of fentanyl partitioning into the SC ($p < 0.0001$), as the diffusion coefficient of fentanyl within the SC remained relatively unchanged.

Table 2.3. Diffusional parameters derived from fentanyl permeation of human epidermis equilibrated with isotonic phosphate buffer pH 7.4, 0.1%w/v sodium azide.

Equilibration period (h)	J ($\mu\text{g}/\text{cm}^2/\text{h}$)	K_p (cm/h)	D (cm/h $\times 10^{-8}$)	K_{scv}
2	2.01 ± 0.09	0.022 ± 0.001	9.65 ± 0.52	299.69 ± 19.85
12	1.83 ± 0.18	0.020 ± 0.002	10.71 ± 0.79	247.31 ± 21.69

Table 2.4. Diffusional parameters derived from fentanyl permeation of human epidermis equilibrated with 20%v/v aqueous ethanol.

Equilibration period (h)	J ($\mu\text{g}/\text{cm}^2/\text{h}$)	K_p (cm/h)	D (cm/h $\times 10^{-8}$)	K_{scv}
2	2.29 ± 0.18	0.025 ± 0.002	7.82 ± 0.45^a	414.85 ± 29.92^a
12	$3.65 \pm 0.18^{a,b}$	$0.040 \pm 0.002^{a,b}$	8.11 ± 0.27^a	$639.08 \pm 26.08^{a,b}$

^a Statistically significant difference compared with isotonic phosphate buffer pH 7.4, 0.1%w/v NaN_3 ($p < 0.05$).

^b Statistically significant difference between 2 and 12 h equilibration periods ($p < 0.05$).

It has been proposed that dilute ethanol ($\leq 25\%v/v$) may increase SC lipid fluidity, and thus solute diffusivity, via interactions at the polar head group region of the lipid bilayers (39). However, the collective findings from several other studies (including differential scanning calorimetric and Fourier transform infrared techniques) have demonstrated that ethanol does not significantly alter the degree of SC lipid inter-alkyl chain interactions (40, 41). On the contrary, the results from Fourier transform infrared spectroscopic studies indicate that ethanol may cause a slight ordering, rather than disordering, of the SC lipid acyl chains (42). It has been proposed that a possible explanation for this "ordering" effect is that ethanol promotes the interdigitation of the hydrocarbon chains by displacement of bound water molecules at the polar head-

group/membrane interface (40, 42, 43). It appears that the finding that fentanyl diffusivity in SC equilibrated with 20%v/v aqueous ethanol was significantly lower than its diffusivity in SC equilibrated with IPB pH 7.4 (NaN_3) is consistent with these previous findings.

In addition to these effects on SC lipids, it has also been suggested that ethanol may cause swelling and secondary conformational changes within keratinised protein fibrils, which may possibly increase the diffusional volume within the SC protein domain (44). At high concentrations, ethanol has also been found to extract lipids from the SC, which has been suggested to lead to localized regions of greater free volume within the lipid alkyl chain regions and "pore" formation (45-47).

Despite these observed effects on SC lipid and protein domains, results from several studies strongly suggest that enhancement of solute partitioning into the SC is the primary mechanism of action of dilute ethanol (48-51). Thus, the finding that the ethanolic receptor solution enhanced fentanyl partitioning into the SC is concordant with this earlier research. Given that the principal role of ethanol as a "penetration enhancer" is to solubilise compounds (51), and that fentanyl is freely soluble in ethanol (Table 3.1, Section 3.4.1), the finding that the ethanol: water system enhanced fentanyl partitioning into the SC can most likely be attributed to an increase in drug solubility within the SC. Due to the excellent correlation between the SC-water partitioning studies and the skin permeation studies, and previous research which has demonstrated that the main rate-limiting barrier for fentanyl permeation resides in the SC (33), it is likely that the solubilising effect of ethanol is mostly significant within the SC itself, rather than in the underlying epidermis. As discussed in Section 2.4.3, the results from the SC-water partitioning studies support this hypothesis.

2.4.3. Effect of an ethanolic receptor solution on fentanyl partitioning between isolated human stratum corneum and water

The partition coefficients of fentanyl between human SC (equilibrated with either receptor solution for 2 or 12 h) and water are represented in Table 2.5. The partition coefficients of fentanyl between SC, equilibrated with IPB pH 7.4 (NaN_3) for 2 or 12 h, and water were 252.82 ± 21.79 and 240.93 ± 17.90 , respectively.

Table 2.5. The partition coefficients of fentanyl between human stratum corneum (equilibrated with either isotonic phosphate buffer pH 7.4, 0.1%w/v sodium azide (IPB pH 7.4 (NaN₃) or 20%v/v aqueous ethanol (20% aq. EtOH) for 2 h (K_{Eq,2h}) or 12 h (K_{Eq,12h})) and water.

Receptor solution	K _{Eq,2h}	K _{Eq,12h}	K _{Eq,12h} / K _{Eq,2h} ^a	K' _{Eq,12h} / K' _{Eq,2h} ^b
IPB pH 7.4 (NaN ₃)	252.82 ± 21.79	240.93 ± 17.90	0.95 ± 0.14	0.83 ± 0.07
20% aq. EtOH	476.53 ± 53.26 ^c	798.55 ± 45.39 ^{c,d}	1.68 ± 0.19	1.54 ± 0.06

^a Ratio between the partition coefficient of fentanyl between isolated human stratum corneum and water generated after a 12 and 2 h equilibration period with receptor solution.

^b Ratio between the partition coefficient of fentanyl between the stratum corneum and water generated after a 12 and 2 h equilibration period with receptor solution, derived from the *in vitro* skin diffusion studies

^c Statistically significant difference compared with the partition coefficient of fentanyl between stratum corneum (equilibrated with isotonic phosphate buffer pH 7.4, 0.1%w/v NaN₃ for the equivalent period of time) and water (p<0.05).

^d Statistically significant difference compared with K_{Eq,2h} (p<0.05).

Not only are these partition coefficients very similar (K_{Eq,12h} / K_{Eq,2h} = 0.95 ± 0.14), but they are also in very good agreement with those generated from the *in vitro* diffusion studies (Table 2.3). Consequently, the results from these studies support the finding that that IPB pH 7.4 (NaN₃) does not modify fentanyl partitioning into the SC when it is in contact with the skin for a prolonged period.

The partition coefficients of fentanyl between SC, equilibrated with 20%v/v aqueous ethanol for 2 or 12 h, and water were 476.53 ± 53.26 and 798.55 ± 45.39, respectively. Firstly, these partition coefficients were significantly higher than the corresponding partition coefficients derived from SC equilibrated with IPB pH 7.4 (NaN₃) for the same length of time (p=0.0046 and p<0.001 for 2 and 12 h equilibration periods, respectively). It is also important to note that fentanyl partitioning into SC equilibrated with 20%v/v aqueous ethanol significantly increased as the contact time between the skin and the ethanolic receptor solution was extended from 2 h to 12 h (p=0.0018). This is also consistent the findings from the *in vitro* diffusion studies (shown in Table 2.4). In addition, the ratio by which fentanyl partitioning into the SC was enhanced as the equilibration period was extended from 2 to 12 h (K_{Eq,12h} / K_{Eq,2h} = 1.68 ± 0.19) was also similar to that obtained from the diffusion studies (K_{Eq,12h} / K_{Eq,2h} = 1.54 ± 0.06). Therefore, the findings from these independent SC-water partitioning studies

support the notion that the presence of ethanol within the receptor solution modifies fentanyl partitioning into the skin, and that this effect is mostly confined to the SC.

2.4.4. Effect of an ethanolic receptor solution on the mechanism(s) by which octisalate enhances fentanyl percutaneous absorption

The profiles generated from fentanyl permeation of skin that had either been left untreated, or pretreated with OS are shown in Figures 2.3 and 2.4. The enhancement ratios that were determined from the diffusional parameters derived from these profiles are shown in Tables 2.6 and 2.7. It is evident from Figures 2.3 and 2.4 that pretreatment of the skin with 5%w/v OS significantly enhanced fentanyl permeation, regardless of the type of receptor medium used. When IPB pH 7.4 (NaN_3) was used as the receptor solution (Figure 2.3), the mean cumulative amount of fentanyl permeating the skin that had either been left untreated or pretreated with OS for 2 h was $43.42 \pm 2.03 \mu\text{g}/\text{cm}^2$ and $72.95 \pm 2.82 \mu\text{g}/\text{cm}^2$ at 24 h, respectively ($p < 0.0001$). These values are comparable to those obtained at 12 h, whereby the cumulative amount of fentanyl permeating untreated skin or skin pretreated with OS was $40.29 \pm 1.41 \mu\text{g}/\text{cm}^2$ and $75.22 \pm 5.40 \mu\text{g}/\text{cm}^2$ at 24 h, respectively ($p < 0.0001$). It is therefore not surprising that similar enhancement ratios were generated for the permeability coefficient of fentanyl through skin pretreated with OS for either 2 or 12 hours ($\text{ER}(K_p) = 1.65 \pm 0.12$ and 1.76 ± 0.20 at 2 and 12 h, respectively (Table 2.6)).

As mentioned in Section 2.4.2, fentanyl permeation through untreated skin equilibrated with 20%v/v aqueous ethanol significantly increased as the equilibration time was extended from 2 to 12 h. In particular, and as illustrated by Figure 2.4, the mean cumulative amount of fentanyl permeating untreated skin, in contact with the ethanolic receptor solution, for 2 or 12 h was $45.19 \pm 1.63 \mu\text{g}/\text{cm}^2$ and $74.98 \pm 4.18 \mu\text{g}/\text{cm}^2$ at 24 h, respectively. This corresponds to an increase in fentanyl permeation by a factor of 1.66. However, it is evident from Figure 2.4 that fentanyl permeation through skin pretreated with OS (and in contact with 20%v/v aqueous ethanol) also increased as the exposure time was lengthened from 2 to 12 h. The mean cumulative amount of fentanyl permeating skin that had been pretreated with OS for 2 or 12 h was $78.92 \pm 1.80 \mu\text{g}/\text{cm}^2$ and $118.31 \pm 7.04 \mu\text{g}/\text{cm}^2$ at 24 h, respectively. This difference corresponds to an increase in fentanyl permeation by a factor of 1.50.

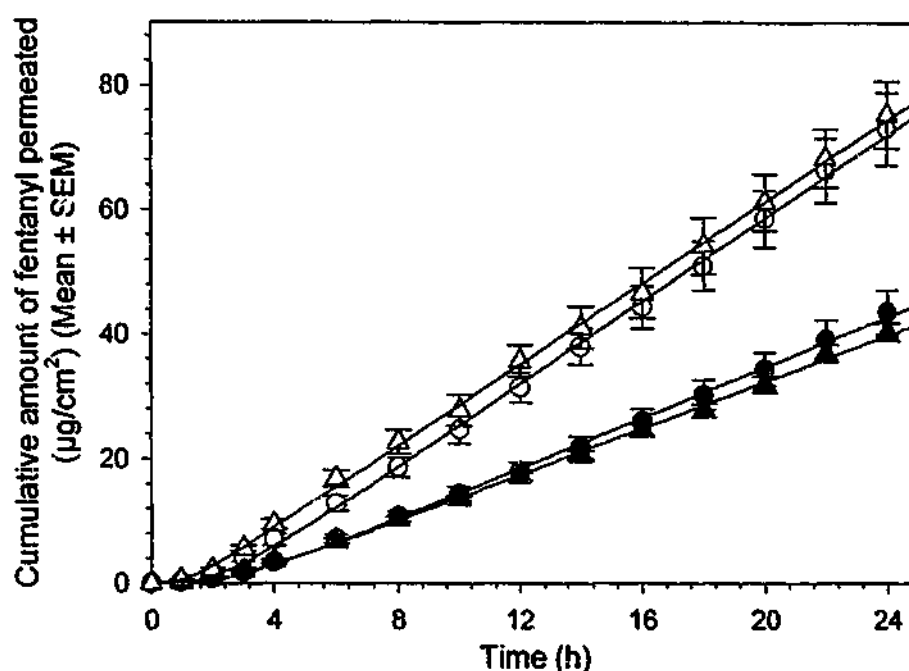


Figure 2.3. Permeation profiles for fentanyl permeating human epidermis either left untreated (closed symbols) or pretreated with 5%w/v OS (open symbols), when isotonic phosphate buffer pH 7.4, 0.1%w/v sodium azide was used as the receptor solution. Circles represent 2 h exposure time, whilst triangles represent 12 h exposure time. The solid lines represent a non-linear regression of the data to Equation 2.1 ($r^2=0.999$ for all profiles).

Table 2.6. Enhancement ratios for the diffusional parameters derived from fentanyl permeation through human epidermis pretreated with 5%w/v OS, using isotonic phosphate buffer pH 7.4, 0.1%w/v sodium azide as the receptor solution.

Pretreatment time (h)	ER (K_p)	ER (D)	ER ($K_{sc/v}$)
2	$1.65 \pm 0.12^*$	1.21 ± 0.08	$1.36 \pm 0.11^*$
12	$1.76 \pm 0.20^*$	$2.10 \pm 0.23^*$	0.84 ± 0.10

* Statistically significant difference compared with untreated skin ($p<0.05$).

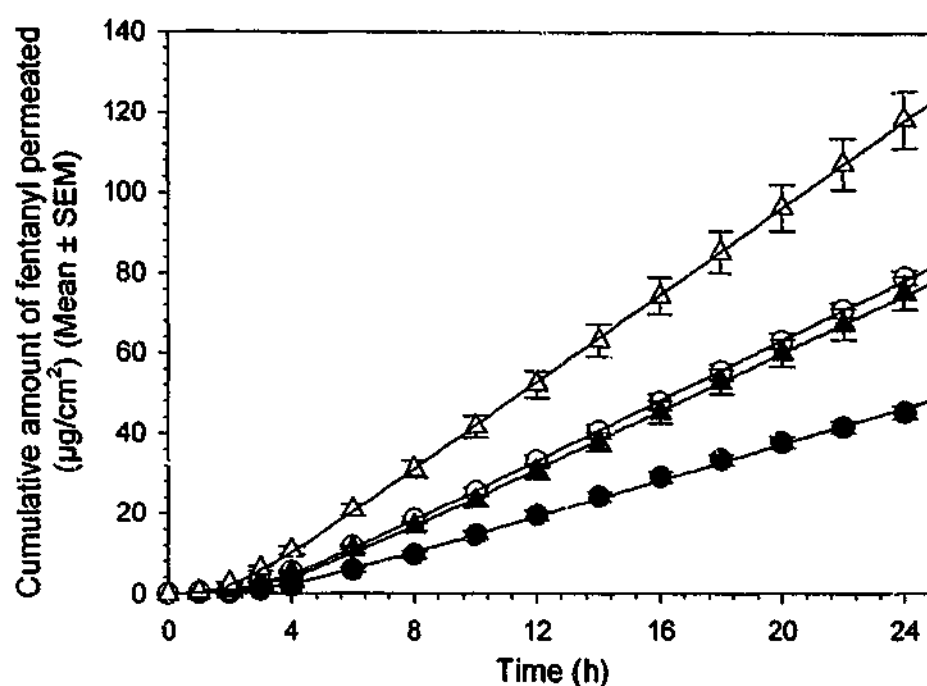


Figure 2.4. Permeation profiles for fentanyl permeating human epidermis either left untreated (closed symbols) or pretreated with 5%w/v OS (open symbols), when 20%v/v aqueous ethanol was used as the receptor solution. Circles represent 2 h exposure time, whilst triangles represent 12 h exposure time. The solid lines represent a non-linear regression of the data to Equation 2.1 ($r^2=0.999$ and 1.000 for profiles of 2 and 12 h untreated skin, respectively, and $r^2=1.000$ for profiles of skin pretreated for 2 and 12 h).

Table 2.7. Enhancement ratios for the diffusional parameters derived from fentanyl permeation through human epidermis pretreated with 5%w/v OS, using 20%v/v aqueous ethanol as the receptor solution.

Pretreatment time (h)	ER (K_p)	ER (D)	ER (K_{scv})
2	$1.65 \pm 0.04^*$	1.12 ± 0.03	$1.47 \pm 0.04^*$
12	$1.50 \pm 0.03^*$	$1.53 \pm 0.03^*$	0.98 ± 0.02

* Statistically significant difference compared with untreated skin ($p < 0.05$).

It would therefore appear that prolonged contact between the skin and the ethanolic receptor solution increased fentanyl permeation to a similar degree, regardless of whether the skin was left untreated or pretreated with OS. Consequently, the enhancement ratio generated for the permeability coefficient of fentanyl through skin pretreated with OS for 2 h was comparable to that obtained following 12 h pretreatment with OS ($ER(K_p) = 1.65 \pm 0.04$ and 1.50 ± 0.03 at 2 and 12 h, respectively (Table 2.7)).

It is of interest to note that the enhancement ratios for the permeability coefficients of fentanyl ($ER(K_p)$) through skin pretreated with OS were of similar magnitudes, regardless of the pretreatment time, or the type of receptor solution used. Furthermore, the apparent mechanism(s) by which OS enhanced fentanyl permeability appeared to be unaffected by the type of receptor solution used. After pretreating the skin for 2 h with OS, enhancement of fentanyl partitioning into the SC appeared to be the predominant mechanism responsible for fentanyl permeation enhancement. However, as the pretreatment time was extended to 12 h, it appeared that enhancement of fentanyl permeability by OS was predominantly due to enhancement of fentanyl diffusivity within the SC. The enhancement ratios generated for fentanyl partitioning and diffusion coefficients at these pretreatment times not only followed similar trends, but were also of similar magnitudes when either IPB pH 7.4 (NaN_3) or 20%v/v aqueous ethanol was used as the receptor solution. These findings may suggest that the concentration (and hence the solubility) of OS within the SC is unaffected by the presence of ethanol in the receptor solution.

Given that OS is a highly lipophilic compound, the apparent "ineffectiveness" of the ethanol: water receptor solution is not surprising. The reduced effectiveness of various chemical penetration enhancers has been previously reported for highly lipophilic compounds (52-54). It has therefore been proposed that the co-administration of a solvent that increases the solubility of a hydrophobic compound in the largely aqueous epidermal layer may aid percutaneous absorption (55). As the epidermis is likely to act as the rate-limiting barrier towards the mass transfer of OS across the skin, this enhancement strategy may be applicable to OS permeation. Furthermore, the ethanolic receptor solution is in continual contact with the epidermis, rather than the SC. Therefore, it would be reasonable to speculate that any effect ethanol may have on OS solubility within the epidermis would be discernible, as the SC would not act as the rate-limiting barrier towards ethanol permeation under these circumstances. However, as the receptor

solution contained only 20%v/v ethanol, it is possible that the concentration(s) of ethanol attained within the epidermis were not high enough to improve the solubility of OS within this aqueous layer. Therefore, it would appear that OS might be retained within the SC even in the presence of a dilute ethanolic receptor solution. Consequently, it would seem that an ethanolic receptor solution (at concentrations of up to 20%v/v ethanol) provides no added benefit over IPB pH 7.4 (NaN_3) in an investigation of the effect of a lipophilic chemical penetration enhancer on the percutaneous absorption of fentanyl.

2.5. CONCLUSIONS

Although fentanyl is a relatively lipophilic compound, it has adequate solubility in either IPB pH 7.4 (NaN_3) or 20%v/v aqueous ethanol to maintain sink conditions during a 24 h *in vitro* skin diffusion experiment. Although the use of ethanol:water systems is recommended for lipophilic compounds, it became evident from the present studies that the presence of ethanol in the receptor solution significantly altered the mechanisms that were involved in fentanyl permeation of the skin. In particular, fentanyl partitioning into the SC was significantly enhanced in the presence of the ethanolic receptor solution. Consequently, it may be concluded from these studies that the presence of ethanol in the receptor medium modifies the barrier properties of the SC towards fentanyl permeation.

It has also been demonstrated that the apparent mechanisms by which OS enhanced fentanyl permeation through the skin were the same, regardless of whether IPB pH 7.4 (NaN_3) or 20%v/v aqueous ethanol was used as the receptor solution. Furthermore, the magnitudes by which OS enhanced fentanyl partitioning into, and its diffusivity within, the SC appeared to be unaffected by the composition of the receptor medium. These findings would suggest that the use of an ethanolic receptor solution (at concentrations up to 20%v/v ethanol) does not offer any advantages over IPB pH 7.4 (NaN_3) when investigating the effects of a lipophilic chemical penetration enhancer on the percutaneous absorption of fentanyl.

In conclusion, IPB pH 7.4 (NaN_3) appears to be the preferred receptor solution to use when studying the *in vitro* percutaneous absorption of fentanyl as it provides an adequate sink for fentanyl permeation without altering the barrier properties of the skin.

2.6. REFERENCES

1. Brain KR, Walters KA, Watkinson AC. 1998. Investigation of Skin Permeation *In Vitro*. In Roberts MS, Walters KA, ed. *Dermal Absorption and Toxicity Assessment*. New York: Marcel Dekker, Inc., pp 161-187.
2. Flynn GL, Smith WM, Hagen TA. 1987. *In Vitro* Transport. In Kydonieus AF, Berner B, ed. *Transdermal Delivery of Drugs*. Boca Raton, Florida: CRC Press Inc., pp 45-59.
3. Gummer CL. 1989. The *In Vitro* Evaluation of Transdermal Delivery. In Hadgraft J, Guy RH, ed. *Transdermal Drug Delivery: Developmental Issues and Research Initiatives*. New York: Marcel Dekker Inc., pp 177-194.
4. Howes D, Guy R, Hadgraft J, Heylin J, Hoeck U, Kemper F, Maibach H, Marty J, Merk H, Parra J, Rekkas D, Rondelli I, Schaefer H, Tauber U, Verbiere N. 1996. Methods for Assessing Percutaneous Absorption. Report and Recommendations of ECVAM Workshop 13. *ATLA* 24:81-106.
5. Behl CR. 1994. *In Vivo* and *In Vitro* Skin Uptake and Permeation Studies: Critical Considerations and Factors Which Affect Them. In Shah VP, Maibach HI, ed. *Topical Drug Bioavailability, Bioequivalence, and Penetration*. New York: Plenum Press, pp 225-259.
6. Bronaugh RL. 1998. Current Issues in the *In Vitro* Measurement of Percutaneous Absorption. In Roberts MS, Walters KA, ed. *Dermal Absorption and Toxicity Assessment*. New York: Marcel Dekker, Inc., pp 155-159.
7. Addicks WJ, Flynn GL, Weiner N. 1987. Validation of a Flow-Through Diffusion Cell for Use in Transdermal Research. *Pharm Res* 4:337-341.
8. Bronaugh RL, Collier SW. 1991. Protocol for *In Vitro* Percutaneous Absorption Studies. In Bronaugh RL, Maibach HI, ed. *In Vitro* Percutaneous Absorption: Principles, Fundamentals, and Applications. Boca Raton, Florida: CRC Press, Inc, pp 237-242.
9. Skelly JP, Shah VP, Maibach HI, Guy RH, Wester RC, Flynn G, Yacobi A. 1987. FDA and AAPS Report of the Workshop on Principles and Practices of *In Vitro* Percutaneous Penetration Studies: Relevance to Bioavailability and Bioequivalence. *Pharm Res* 4:265-267.
10. Bronaugh RL, Stewart RF. 1984. Methods for *In Vitro* Percutaneous Absorption Studies III: Hydrophobic Compounds. *J Pharm Sci* 73:1255-1258.
11. Diez-Sales O, Copovi A, Casabó VG, Herráez M. 1991. A Modelistic Approach Showing the Importance of the Stagnant Aqueous Layers in *In Vitro* Diffusion Studies, and *In vitro - In Vivo* Correlations. *Int J Pharm* 77:1-11.
12. Kasting GB, Francis WR, Bowman LA, Kinnott GO. 1997. Percutaneous Absorption of Vanilloids: *In Vivo* and *In Vitro* Studies. *J Pharm Sci* 86:142-146.
13. Franz TJ. 1975. Percutaneous Absorption. On the Relevance of *In Vitro* Data. *J Invest Dermatol* 64:190-195.
14. Hoelgaard A, Møllgaard B. 1982. Permeation of Linoleic Acid Through Skin *In Vitro*. *J Pharm Pharmacol* 34:610-611.

15. Brown DW, Ulsamer AG. 1975. Percutaneous Penetration of Hexachlorophene as Related to Receptor Solutions. *Food Cosmet Toxicol* 13:81-86.
16. Cross SE, Anissimov YG, Magnusson BM, Roberts MS. 2003. Bovine-Serum-Albumin-Containing Receptor Phase Better Predicts Transdermal Absorption Parameters for Lipophilic Compounds. *J Invest Dermatol* 120:589-591.
17. Jones SP, Greenway MJ, Orr NA. 1989. The Influence of Receptor Fluid on *In Vitro* Percutaneous Absorption. *Int J Pharm* 53:43-46.
18. Roy SD, Flynn GL. 1989. Transdermal Delivery of Narcotic Analgesics: Comparative Permeabilities of Narcotic Analgesics Through Human Cadaver Skin. *Pharm Res* 6:825-832.
19. Klose, K. 2000. Standard Operating Procedure: *In Vitro* Diffusion (No. 009/1). Melbourne, Australia, Acrux Ltd. pp. 1-4.
20. Walters KA, Brain KR, Hewes D, James VJ, Kraus AL, Tectsel NM, Toulon M, Watkinson AC, Gettings SD. 1997. Percutaneous Penetration of Octyl Salicylate from Representative Sunscreen Formulations Through Human Skin *In Vitro*. *Food Chem Toxicol* 35:1219-1225.
21. Bronaugh RL, Congdon ER, Scheuplein RJ. 1981. The Effect of Cosmetic Vehicles on the Penetration of N-Nitrosodiethanolamine Through Excised Human Skin. *J Invest Dermatol* 76:94-96.
22. Harrison SM, Barry BW, Dugard PH. 1984. Effects of Freezing on Human Skin Permeability. *J Pharm Pharmacol* 36:261-262.
23. Stehle RG, Higuchi WI. 1983. *In Vitro* Model for Transport of Solutes in Three-Phase System. II. Experimental Considerations. *J Pharm Sci* 61:1931-1935.
24. Cornwell PA, Barry BW, Bouwstra JA, Gooris GS. 1996. Modes of Action of Terpene Penetration Enhancers in Human Skin: Differential Scanning Calorimetry, Small-Angle X-Ray Diffraction and Enhancer Uptake Studies. *Int J Pharm* 127:9-26.
25. Raykar PV, Fung MC, Anderson BD. 1988. The Role of Protein and Lipid Domains in the Uptake of Solutes by Human Stratum Corneum. *Pharm Res* 5:140-150.
26. Díez-Sales O, Watkinson AC, Herráez-Domínguez M, Javaloyes C, Hadgraft J. 1996. A Mechanistic Investigation of the *In Vitro* Human Skin Permeation Enhancing Effect of Azone®. *Int J Pharm* 129:33-40.
27. Johnson ME, Blankachtein D, Langer R. 1997. Evaluation of Solute Permeation Through the Stratum Corneum: Lateral Bilayer Diffusion as the Primary Transport Mechanism. *J Pharm Sci* 86:1162-1172.
28. Parry GE, Bunge AL, Silcox GD, Pershing LK, Pershing DW. 1990. Percutaneous Absorption of Benzoic Acid Across Human Skin. I. *In Vitro* Experiments and Mathematical Modeling. *Pharm Res* 7:230-236.
29. Anderson BD, Cassidy JM. 1973. Variation in Physical Dimensions and Chemical Composition of Human Stratum Corneum. *J Invest Dermatol* 61:30-32.
30. Roy SD, Flynn GL. 1989. Solubility Behavior of Narcotic Analgesics in Aqueous Media: Solubilities and Dissociation Constants of Morphine, Fentanyl, and Sufentanil. *Pharm Res* 6:147-151.

31. Hanson WA. 1982. Theoretical Concepts. In Hanson WA, ed. Handbook of Dissolution Testing. Oregon: Pharmaceutical Technology Publications, p 4.
32. Guy RH, Hadgraft J. 1989. Selection of Drug Candidates for Transdermal Drug Delivery. In Hadgraft J, Guy RH, ed. Transdermal Drug Delivery: Developmental Issues and Research Initiatives. New York: Marcel Dekker Inc., pp 59-81.
33. Roy SD, Flynn GL. 1990. Transdermal Delivery of Narcotic Analgesics: pH, Anatomical, and Subject Influences on Cutaneous Permeability of Fentanyl and Sufentanil. *Pharm Res* 7:842-847.
34. Roy SD, Hou SY, Witham SL, Flynn GL. 1994. Transdermal Delivery of Narcotic Analgesics: Comparative Metabolism and Permeability of Human Cadaver Skin and Hairless Mouse Skin. *J Pharm Sci* 83:1723-1728.
35. Michaels AS, Chandrasekaran SK, Shaw JE. 1975. Drug Permeation Through Human Skin: Theory and *In Vitro* Experimental Measurement. *AIChEJ* 21:985-996.
36. Ostrenga J, Steinmetz C, Poulsen B. 1971. Significance of Vehicle Composition. I. Relationship Between Topical Vehicle Composition, Skin Penetrability, and Clinical Efficacy. *J Pharm Sci* 60:1175-1179.
37. Ostrenga J, Steinmetz C, Poulsen B, Yett S. 1971. Significance of Vehicle Composition. II. Prediction of Optimal Vehicle Composition. *J Pharm Sci* 60:1180-1183.
38. Cooper ER, Berner B. 1985. Skin Permeability. In Skerrow D, Skerrow CJ, ed. Methods in Skin Research. Chichester: Wiley-International, pp 417-419.
39. Ghanem AH, Mahmoud H, Higuchi WI, Liu P, Good WR. 1992. The Effects of Ethanol on the Transport of Lipophilic and Polar Permeants Across Hairless Mouse Skin: Methods/Validation of a Novel Approach. *Int J Pharm* 78:137-156.
40. Krill SL, Knutson K, Higuchi WI. 1992. Ethanol Effects on the Stratum Corneum Lipid Phase Behavior. *Biochim Biophys Acta* 1112:273-280.
41. Golden GM, McKie JE, Potts RO. 1987. Role of Stratum Corneum Lipid Fluidity in Transdermal Drug Flux. *J Pharm Sci* 76:25-28.
42. Bommannan D, Potts RO, Guy RH. 1991. Examination of the Effect of Ethanol on Human Stratum Corneum *In Vivo* Using Infrared Spectroscopy. *J Control Release* 16:299-304.
43. Knutson K, Krill SL, Zhang J. 1990. Solvent-Mediated Alterations of the Stratum Corneum. *J Control Release* 11:93-103.
44. Kurihara-Bergstrom T, Knutson K, De Noble LJ, Goates CY. 1990. Percutaneous Absorption Enhancement of an Ionic Molecule by Ethanol-Water Systems in Human Skin. *Pharm Res* 7:762-766.
45. Ghanem AH, Mahmoud H, Higuchi WI, Rohr UD, Borsadia S, Liu P, Fox JL, Good WR. 1987. The Effects of Ethanol on Transport of β -Estradiol and Other Permeants in Hairless Mouse Skin. *J Control Release* 6:75-83.
46. Inamori T, Ghanem AH, Higuchi WI, Srinivasan V. 1994. Macromolecular Transport In and Effective Pore Size of Ethanol Pretreated Human Epidermal Membrane. *Int J Pharm* 105:113-123.

47. Peck KD, Ghanem AH, Higuchi WI. 1994. Hindered Diffusion of Polar Molecules Through and Effective Pore Radii Estimates of Intact and Ethanol Treated Human Epidermal Membrane. *Pharm Res* 11:1306-1314.
48. Pershing LK, Lambert LD, Knuston K. 1990. Mechanism of Ethanol-Enhanced Estradiol Permeation Across Human Skin *In Vivo*. *Pharm Res* 7:170-175.
49. Berner B, Mazzenga GC, Otte JH, Steffens RJ, Juang RH, Ebert CD. 1989. Ethanol: Water Mutually Enhanced Transdermal Therapeutic System II: Skin Permeation of Ethanol and Nitroglycerin. *J Pharm Sci* 78:402-407.
50. Seki T, Sugibayashi K, Morimoto Y. 1987. Effect of Solvents on the Permeation of Nicardipine Hydrochloride Through the Hairless Rat Skin. *Chem Pharm Bull* 35:3054-3057.
51. Yum S, Lee E, Taskovich L, Theeuwes F. 1994. Permeation Enhancement with Ethanol: Mechanism of Action Through Skin. In Hsieh DS, ed. *Drug Permeation Enhancement*. New York: Marcel Dekker, Inc., pp 143-170.
52. Phillips CA, Michniak BB. 1995. Transdermal Delivery of Drugs with Differing Lipophilicities Using Azone Analogs as Dermal Penetration Enhancers. *J Pharm Sci* 84:1427-1433.
53. Baker EJ, Hadgraft J. 1995. *In Vitro* Percutaneous Absorption of Arildone, a Highly Lipophilic Drug, and the Apparent No-Effect of the Penetration Enhancer Azone in Excised Human Skin. *Pharm Res* 12:993-997.
54. Williams AC, Barry BW. 1991. The Enhancement Index Concept Applied to Terpene Penetration Enhancers for Human Skin and Model Lipophilic (Oestradiol) and Hydrophilic (5-Fluorouracil) Drugs. *Int J Pharm* 74:157-168.
55. Hadgraft J. 1999. Passive Enhancement Strategies in Topical and Transdermal Drug Delivery. *Int J Pharm* 184:1-6.

CHAPTER 3

THE EFFECTS OF OCTISALATE AND PADIMATE O ON FENTANYL PERMEATION FROM A "FINITE DOSE"

3.1. INTRODUCTION

Crude methods of transdermal drug delivery (TDD) include the use of semi-solid formulations, such as ointments, creams, gels (1, 2), or plasters (3). However, a major problem associated with such systems is that the covered area of skin (and hence the amount of drug applied to the skin) is often poorly controlled. The poor control over TDD is also confounded by inter- and intra- individual variations in skin permeability, which have been reported to be as high as 46 to 66% (%CV) and 20 to 40%, respectively (4). Therefore, in an effort to alleviate these and other problems, the design and development of transdermal delivery systems (TDSs), particularly transdermal patch delivery systems, has focused on controlling the rate and duration of drug release into the systemic circulation (5). The contribution of a TDS to controlling drug delivery across the skin may be obtained from the following relationship (6):

$$J_{NET} = \left[(J_{SKIN})^{-1} + (J_{TDS})^{-1} \right]^{-1}$$

Thus, if the rate of drug release from the TDS (J_{TDS}) is much smaller in magnitude than drug flux across the skin (J_{SKIN}), then net drug flux from the TDS into the systemic circulation (J_{NET}) will be essentially the same as J_{TDS} . Under such circumstances, the rate of drug delivery is controlled by the TDS and inter-individual variations in skin permeability may thus be reduced. This concept of system-controlled TDD forms the basis for the design of the Durogesic® patch (7, 8), which is the only commercially-available form of transdermal fentanyl at present. It has been reported that the incorporation of a rate-controlling membrane within the Durogesic® patch reduces variation in fentanyl skin permeation by approximately 50% (9).

Unfortunately, however, a major problem associated with many marketed transdermal patch delivery systems, such as Durogesic®, is their potential to cause skin irritation (6, 7, 10-14). The irritation caused by such systems appears to be related to their occlusive nature; condensed moisture from transepidermal water loss and sweat may accumulate underneath the patch which can lead to skin maceration, proliferation of skin microflora, and an increase in the pH of the microenvironment (12, 15). Furthermore, increased humidity under the occlusive system can ultimately render the stratum corneum (SC) more permeable to solute transport (16-21) and less tolerant to the irritant effects of some formulation excipients (6, 22).

In order to sustain the driving force for fentanyl diffusion across the skin during a 72 h application time, the Durogesic[®] patch is comprised of a reservoir that contains 2.5 mg of fentanyl per 10cm² of patch size (23). However, it has been demonstrated that substantial amounts (i.e. 28 to 85%) of the original fentanyl content remain within the system upon its removal from the skin (24-26). Therefore, in addition to the abovementioned problems associated with occlusive TDSs, another problem that is somewhat unique to the Durogesic[®] patch is the potential for unabsorbed fentanyl remaining within the system to be subject to illicit use (27).

In order to circumvent some of the problems associated with transdermal patch delivery systems, Morgan et al have utilised the concept of a metered-dose transdermal spray (MDTS) (28-30). The results from this research demonstrated the feasibility of using rapid-drying, non-occlusive topical spray vehicles, which contain octisalate (OS) and padimate O (PO) to enhance the transdermal delivery of various sex hormones. As alluded to Chapter 1 (Section 1.5.5.2), this method of TDD involves the finite-dose (i.e. 5µl of solution per cm² of skin) application of ethanolic solutions containing either OS or PO and the drug of interest. In addition to minimising some of the problems associated with occlusive TDSs, the use of volatile solvents (under non-occluded conditions) has also been shown to enhance percutaneous drug absorption when compared with occluded systems (31).

Fundamental to this non-occlusive form of TDD is the concept that ethanol rapidly evaporates into the atmosphere which, theoretically, would favour partitioning of drug and OS or PO into the upper layers of the SC (32). As the SC can act as a reservoir for many topically applied substances (33, 34), a depot of drug and OS or PO may eventually form within the SC. Assuming that the drug possess suitably balanced aqueous and lipid solubilities (i.e. log $K_{oct/w}$ between 1 and 3) (35, 36) it will continue to partition into, and diffuse through, the deeper skin layers – and be absorbed into the systemic circulation – until the SC eventually becomes depleted of drug.

In light of this background research and theory, the primary aim of the work presented in this chapter was to investigate whether OS and PO enhance the transdermal delivery of fentanyl under the conditions studied. As mentioned in Chapter 2, *in vitro* skin diffusion studies are often used to investigate the kinetics and mechanisms involved in TDD, and serve as a tool for rapid screening of vehicle effects during the initial stages of formulation development. Hence, the diffusion cell technique was utilised to predict

the effect(s) of OS and PO on the percutaneous absorption of fentanyl *in vivo*. However, whilst there is good evidence to suggest that *in vitro* skin diffusion data is predictive for *in vivo* percutaneous absorption in animals and humans (37-39), a major potential variant in the design of a diffusion cell experiment is the nature of the skin membrane. Although it is preferable to use excised human skin during an *in vitro* skin diffusion study (40), limitations associated with its cost, availability and variable permeability have prompted the wide use of animal skins as substitutes for human skin (41).

Although animal skin is an acceptable model for human skin (40, 42, 43), it is well established that inter-species variations in percutaneous drug absorption exist (as discussed in Chapter 1, Section 1.3.3.1.7). However, in formulation development the rank order of drug release from various vehicles is often more significant than the rates themselves (44). In this instance, animal skin has a theoretical advantage over human skin in that diffusion experiments can be completed in a shorter period of time. Consequently, initial investigations into the effect(s) of OS and PO on fentanyl percutaneous absorption involved the use of shed snake skin as the skin membrane.

Shed snake skin was used as a model membrane during initial investigations as it is easy to obtain and prepare and is essentially representative of human SC (but is devoid of any appendages). Previous studies have also shown that the permeability of several compounds for shed snake skin is similar to, but often slightly less than, human skin (45-48). Furthermore, the mature snake naturally sheds its skin every ~2 to 3 months and thus the animal doesn't have to be sacrificed in order to obtain its skin, the membranes may be stored at room temperature without significant deterioration and, as interfering substances do not leach from the membrane, it usually permits the facile UV analysis of skin permeation samples (45).

3.2. OBJECTIVES

The purpose of the work presented in this chapter was firstly to determine whether OS and PO enhanced the *in vitro* percutaneous absorption of fentanyl under simulated *in vivo* conditions of use. This objective was fundamental to the entire research project as it would help determine the feasibility of using OS or PO to enhance the transdermal delivery of fentanyl. Shed snake skin was initially used as the model membrane to

investigate the effect(s) of OS and PO during the initial stages of formulation development. Of course, the use of excised human skin is preferred for *in vitro* diffusion experiments that are intended to mimic *in vivo* percutaneous drug absorption. Therefore, subsequent diffusion experiments were conducted with human epidermis as the model membrane.

The second objective of these studies was to identify the possible mechanism(s) by which OS and PO enhanced the percutaneous absorption of fentanyl through human epidermis under predicted conditions of use *in vivo*. This latter objective was intended to aid the development of further investigations into the mechanism(s) of action of OS and PO.

3.3. MATERIALS AND METHODS

3.3.1. Materials

Fentanyl was manufactured by Macfarlan Smith Ltd. (Edinburgh, UK). OS and PO were supplied by Bronson and Jacobs (Australia). Acetonitrile (supplied by Merck Pty. Ltd. (Australia)) was of HPLC grade. Water was purified by a Milli-Q™ water purification system (Millipore, Bedford, MA, USA). All other chemicals were of analytical grade.

3.3.2. Saturated solubility studies

Approximately 200 mg of fentanyl was added to 500 μ l of 95%v/v ethanol, OS or PO ($n=3$). The samples were vortexed for 30 sec and placed in a shaking water bath at $32 \pm 1^\circ\text{C}$, where they were continuously shaken at 15 strokes/min for 72 h. To ensure that the solutions remained saturated they were inspected periodically for solid particulate matter during this time. At the end of the equilibration period, the samples were centrifuged at 3500 rpm for 20 min at 32°C in a Beckman GS-CR centrifuge (Beckman Instruments Inc., Palo Alto, CA, USA). Using a glass HPLC syringe (SGE, Australia), a 100 μ l sample of the supernatant was removed and diluted to 100 ml with absolute ethanol. A 100 μ l aliquot of this solution was further diluted to 10 ml with 20%v/v

aqueous ethanol. The concentration of fentanyl following the second dilution was then determined using the HPLC/UV assay described in Section 2.3.5.

3.3.3. Initial screening of the effect(s) of octisalate and padimate O on fentanyl permeation: *In vitro* finite-dose skin diffusion studies using shed snake skin as the model membrane

3.3.3.1. Skin preparation

The skin shed from Children's Python snake (*Liasis childreni*) was used as the model for human SC. Each skin specimen had been gently rinsed with an aqueous solution of 0.1%w/v sodium azide to remove foreign debris. The dorsal portion of the skin was laid flat on glass microscope slides (n=12, on average) and cut into individual pieces with dissecting scissors. The skin pieces were then wrapped in aluminium foil and stored at -20°C for up to twelve months prior to use. Immediately after shedding, the skin had been stored at 4°C for up to seven days before it was prepared and frozen. The skin samples were defrosted under ambient conditions for approximately 2 to 4 h before use.

3.3.3.2. *In vitro* skin diffusion studies

In vitro skin diffusion studies were performed using stainless steel flow-through diffusion cells with a skin surface area available for drug diffusion of 0.79 cm². The maximum capacity of the donor chamber was approximately 500 µl, whilst the receptor compartment held ~50 µl of receptor solution. Isotonic phosphate buffer pH 7.4 (preserved with 0.1%w/v sodium azide) was used as the receptor solution. To avoid air bubbles forming underneath the skin during a diffusion experiment, the receptor solution was heated to 40°C, and degassed by spraying it into fine droplets under vacuum with continuous stirring. The solution was degassed three times before each diffusion study.

The diffusion cells were prepared by firstly over-filling the receptor compartment with approximately 100 µl of receptor solution. A wire mesh was then placed over the receptor well. As mentioned in Section 2.3.3.2, the wire mesh was to encourage turbulent flow of the receptor solution through the receptor compartment, to prevent the formation of air bubbles and help maintain sink conditions.

The defrosted skin samples were cut into circular pieces, each with an area of 2 cm², using a circular die-punch. The individual pieces of skin were placed between low-lint, absorbent tissues (Kinwipes[®], Kimberly-Clark Australia) that were pre-moistened with purified water. This prevented the skin from drying and "curling", which makes it difficult to mount the skin flatly over the receptor well. The skin was then placed over the receptor well and the donor and receptor chambers bolted tightly together.

The diffusion cells were mounted onto a hollow stainless steel bar, through which water (heated to 37°C) was pumped to maintain the temperature of the cells at 32 ± 0.5°C. To ensure sink conditions were maintained during a diffusion study, the receptor solution was pumped through the receptor compartment at a flow rate of 1 ml/h with a peristaltic pump (Watson Marlow Microcasette Pump, UK). At this flow rate, the receptor solution residing within the receptor compartment was replaced approximately 20 times/h. The skin was equilibrated with the receptor solution for a period of 1 h before the donor solution was applied to the skin surface. During this time (approximately 45 min after the skin was equilibrated with receptor solution), the transepidermal water loss (TEWL) from each piece of skin was measured, using an EPI evaporimeter (Servo Med, Stockholm, Sweden), in order to assess skin integrity. TEWL measurements were made by placing the measuring probe over the donor compartment. In order to minimise interference from atmospheric moisture, a rubber O-ring was placed between the surface of the donor compartment and the probe, and the probe was placed over the donor compartment with gentle pressure until a constant TEWL value was established. Only skin samples that produced TEWL measurements between 1.0 to 6.0 g/m²/h were used during the diffusion studies (49).

In order to mimic predicted *in vivo* conditions of use the donor solution was applied as a finite dose (5 µl/cm²) to the skin surface. The donor solution was applied to the center of each piece of skin using a glass HPLC syringe and the diffusion cells were left uncovered to allow the vehicle to evaporate from the skin surface. The donor solutions consisted of 5%w/v fentanyl in 95%v/v ethanol (control), or 5%w/v fentanyl and 2.5, 5 or 7.5%w/v of OS or PO in 95%v/v ethanol (4 < n < 12). Test and control experiments were conducted simultaneously. The diffusion samples were collected every 1 to 4 h over a 24 h period using an automated fraction collector (ISCO Retriever II, NE).

3.3.4. *In vitro* finite-dose skin diffusion studies using human epidermis as the model membrane

3.3.4.1. *Skin preparation*

Human epidermis was separated from abdominal tissue obtained from at least two individual female donors following abdominoplasty. After removing subcutaneous tissue and fat from the underside of the dermal membrane by means of a stainless steel surgical blade, the full-thickness skin samples were immersed in water (maintained at 60°C) for 45 sec (50). The skin samples were then laid flat (SC-side up) and the epidermal layer was detached from the skin by gently peeling it away from the dermis. The epidermal membranes were then floated (SC-side up) over purified water whilst being transferred onto filter paper. The samples were dried overnight under ambient conditions and were then stored in aluminum foil at -20°C for up to 12 months (51). The samples were defrosted under ambient conditions for approximately 2 to 4 h before use.

3.3.4.2. *In vitro* skin diffusion studies

Details of the *in vitro* diffusion experiments are described in Section 3.3.3.2. After preparing the diffusion cells, sections of defrosted epidermal membranes (pre-cut into approximately 1cm² square pieces) were placed between the donor and receptor chambers. As the skin was supported by filter paper, it did not require continual moistening to prevent it from "curling". For all diffusion studies, the skin was equilibrated with the receptor solution for a period of 1 h before application of the donor solution. TEWL measurements were performed ~ 45 min after the skin was equilibrated with receptor solution.

After equilibrating the skin with receptor solution, solutions containing 5%w/v fentanyl and 1, 2.5, 5, 7.5 or 10%w/v of OS or PO in 95%v/v ethanol were applied to the skin surface at a finite dose of 5 µl/cm² (4<n<8). Control experiments were conducted simultaneously, whereby 5%w/v fentanyl in 95%v/v ethanol was applied to the skin surface (4<n<8). The diffusion cells were left unoccluded to allow the physicochemical properties of the applied formulation to change as they would under *in vivo* conditions of use. Diffusion samples were collected every 1 to 4 h over a 24 h period.

3.3.5. Analytical methods

The saturated solubility and skin diffusion samples were analysed using the reverse phase HPLC/UV methods described in Chapter 2 (Section 2.3.5).

3.3.6. Mathematical analysis

3.3.6.1. Shed snake skin as the model membrane

Several mathematical models have been used to describe the percutaneous absorption kinetics of a solute from a donor solution of finite volume (52-57). However, these finite dose diffusion experiments were intended to be a "proof of principle study" (i.e. to determine the feasibility of using OS and PO to enhance fentanyl permeation through the skin). Consequently, mathematical modelling of the finite-dose permeation profiles was not used to derive the diffusional parameters (such as the permeability coefficient and/or solute flux) that are often used to describe percutaneous drug absorption.

Instead, the data was expressed as the amount of fentanyl permeating the skin at time t (Q_t), and the corresponding percentage of the applied dose, both of which are commonly accepted measures of percutaneous absorption under finite-dosing conditions (40, 58-60).

3.3.6.2. Human epidermis as the model membrane

In addition to the details discussed in Section 3.3.6.1, it will become evident from the profiles generated from fentanyl permeation of human epidermis that the percutaneous absorption kinetics of fentanyl did always not follow the general trend expected of a solvent-deposited solute within a 24 h period (i.e. apparent "pseudo steady-state" percutaneous absorption sometimes prevailed, rather than solute depletion). Typical boundary conditions for a finite-dose mathematical diffusion model were therefore not always applicable.

Analogous to the finite dose diffusion studies involving shed snake skin, the permeation data was expressed as the amount of fentanyl permeating the skin at time t (Q_t), and the corresponding percentage of the applied dose.

The cumulative amount of fentanyl permeating the skin at the completion of a diffusion study (i.e. Q_{24h}) was used to determine the enhancement of fentanyl percutaneous absorption by OS or PO. Enhancement was expressed in terms of an enhancement ratio ($ER(Q_{24h})$), where:

$$ER(Q_{24h}) = \frac{Q_{24h} \text{ following application of fentanyl with OS or PO}}{Q_{24h} \text{ following application of fentanyl alone}} \quad 3.1$$

In an effort to understand some of the possible mechanisms by which OS and PO affect the kinetics of fentanyl permeation through the epidermis under finite dosing conditions the data was also expressed as the flux ($\mu\text{g}/\text{cm}^2\text{h}$) (J_{FIN}) of fentanyl across the skin as function of time.

3.3.7. Statistical analysis

Statistical significance was determined using one-way analysis of variance (ANOVA). Post-hoc all pairwise multiple comparison of the means within different groups was performed using the Student-Newman-Keuls (SNK) test. A probability of $p < 0.05$ was considered statistically significant. All results are presented as mean \pm SEM, unless otherwise stated.

3.4. RESULTS AND DISCUSSION

3.4.1. Fentanyl solubility in ethanol, octisalate, or padimate O

The saturated solubility of fentanyl in 95%v/v ethanol, OS or PO is shown in Table 3.1. In order to conserve fentanyl, the solubility study was stopped when it appeared that 200 mg had freely dissolved in 500 μl of ethanol. Consequently, it would seem that the solubility of fentanyl in ethanol surpasses 400 mg/ml . The solubility of fentanyl in neat PO was approximately 26% higher than its solubility in neat OS ($165.08 \pm 1.93 \text{ mg}/\text{ml}$ versus $130.77 \pm 1.47 \text{ mg}/\text{ml}$).

Table 3.1. The saturated solubility of fentanyl in 95%v/v ethanol, OS, or PO at 32°C (n=3).

Solvent	Saturated solubility (mg/ml)
95%v/v ethanol	> 400
OS	130.77 ± 1.47
PO	165.08 ± 1.93

3.4.2. Initial screening for the effect(s) of octisalate and padimate O: Percutaneous absorption of fentanyl through shed snake skin

The profiles representing fentanyl permeation of shed Children's Python snake skin, following the finite-dose application of ethanolic solutions containing 5%w/v fentanyl, with or without 2.5, 5 or 7.5%w/v OS or PO, are shown in Figures 3.1 and 3.2. It is evident from Figure 3.1 that all concentrations of OS significantly enhanced fentanyl permeation of shed snake skin ($p < 0.05$ compared with ethanol alone as the vehicle) (Figure 3.1). In particular, the cumulative amount of fentanyl permeating shed snake skin at 24 h (Q_{24h}) was $16.03 \pm 1.89 \mu\text{g}/\text{cm}^2$ when fentanyl was applied to the skin in ethanol alone. When 2.5%w/v OS was added to the solution, the Q_{24h} significantly increased to $89.63 \pm 11.19 \mu\text{g}/\text{cm}^2$, which corresponds to a 5.59-fold enhancement in fentanyl permeation. This magnitude of enhancement further increased as the concentration of OS increased, whereby the Q_{24h} was $97.23 \pm 10.75 \mu\text{g}/\text{cm}^2$ (6.07-fold enhancement compared with fentanyl applied alone) and $125.56 \pm 13.72 \mu\text{g}/\text{cm}^2$ (7.83-fold enhancement) in the presence of 5% and 7.5%w/v OS, respectively.

On the other hand, PO significantly enhanced fentanyl permeation through shed snake skin only at the highest concentrations investigated (i.e. 5%v/w and 7.5%w/v) ($p < 0.05$ compared with fentanyl applied alone) (Figure 3.2). When PO was added at a concentration of 2.5%w/v, the Q_{24h} slightly (not though significantly) increased by a factor of 1.27 (i.e. from $20.41 \pm 1.96 \mu\text{g}/\text{cm}^2$ when fentanyl was applied alone to $25.99 \pm 2.46 \mu\text{g}/\text{cm}^2$ in the presence of 2.5%w/v PO ($p = 0.1884$)).

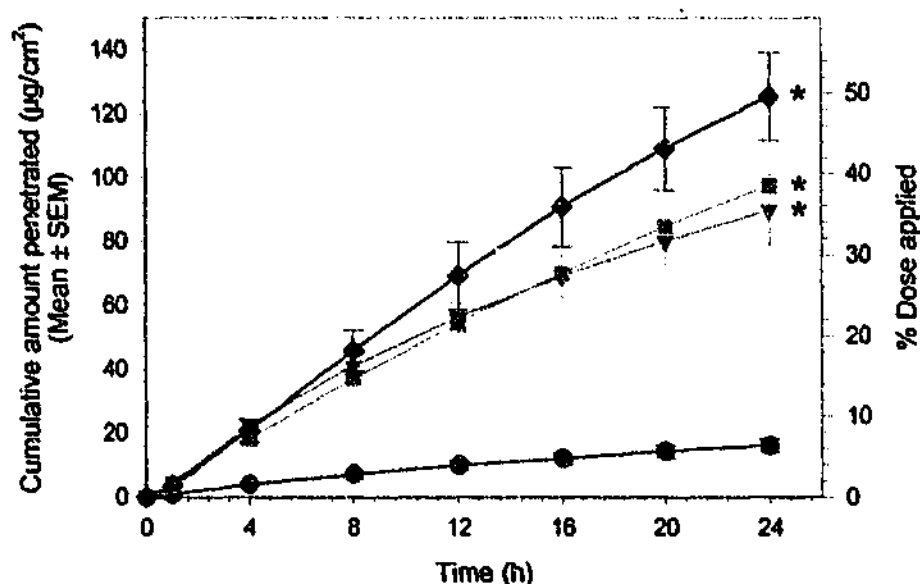


Figure 3.1. Profiles representing fentanyl permeation through shed snake skin, following finite-dose application to the skin. The symbols represent fentanyl permeation following the application of ethanolic solutions containing 5%w/v fentanyl alone (●) (n=20), or with 2.5%w/v OS (▼) (n=8), 5%w/v OS (■) (n=8), or 7.5%w/v OS (◆) (n=6). * denotes statistically significant difference compared with control (5%w/v fentanyl alone) ($p < 0.05$).

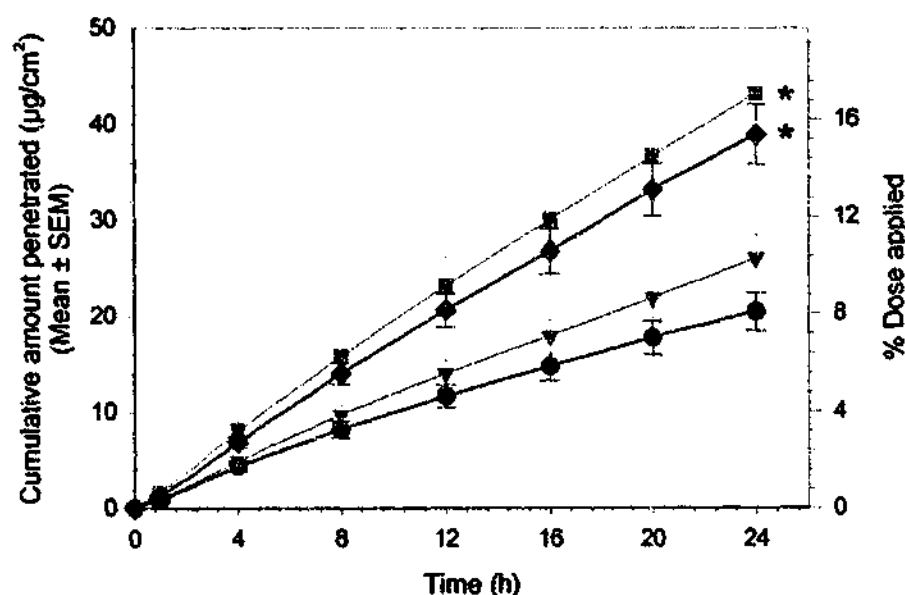


Figure 3.2. Profiles representing fentanyl permeation through shed snake skin, following finite-dose application to the skin. The symbols represent fentanyl permeation following the application of ethanolic solutions containing 5%w/v fentanyl alone (●) (n=24), or with 2.5%w/v PO (▼) (n=6), 5%w/v PO (■) (n=7), or 7.5%w/v PO (◆) (n=8). * denotes statistically significant difference compared with control (5%w/v fentanyl alone) ($p < 0.05$).

The magnitude of this enhancement was further augmented as the PO concentration was increased to 5%w/v, whereby the Q_{24h} was $43.12 \pm 5.42 \mu\text{g}/\text{cm}^2$, which corresponds to a 2.11-fold enhancement. It is interesting to note, however, that increasing the PO concentration to 7.5%w/v did not result in a further increase in the Q_{24h} . In fact, the Q_{24h} observed in the presence of 7.5%w/v PO was $38.91 \pm 3.14 \mu\text{g}/\text{cm}^2$, which is slightly lower than that observed for 5%w/v PO ($p=0.4997$).

Based on these initial findings, it would appear feasible to use either OS or PO to enhance the transdermal delivery of fentanyl. Furthermore, it is apparent that OS possesses superior enhancing capabilities compared with PO. However, in order to draw any conclusions on the relevance of this data to predict fentanyl percutaneous absorption under *in vivo* conditions, the permeation of fentanyl through excised human epidermis must also be considered.

3.4.2.1. Use of shed snake skin as a model membrane for predicting fentanyl permeation through human epidermis, and the effects of octisalate and padimate O, under "finite dosing" conditions

The cumulative amounts of fentanyl permeating human epidermis at 24 h (Q_{24h}) following the finite dose application of fentanyl in ethanol (alone or with 2.5% to 7.5%w/v OS or PO) are compared to those observed for shed snake skin in Tables 3.2 and 3.3. The corresponding enhancement ratios ($ER(Q_{24h})$) are also displayed. It should be noted that fentanyl permeation through human epidermis was markedly (i.e. ~4 to ~6-fold) lower than that observed when shed snake skin was used as the model membrane.

When fentanyl was applied in ethanol alone to the epidermal surface, the Q_{24h} was $4.04 \pm 0.17 \mu\text{g}/\text{cm}^2$ (OS control experiments) and $3.26 \pm 0.18 \mu\text{g}/\text{cm}^2$ (PO control experiments), which corresponds to 1.60% and 1.29% of the total dose applied, respectively. On the other hand, when fentanyl (in ethanol alone) was applied to shed snake skin, the Q_{24h} value was approximately 6.34% to 8.07% of the applied dose.

As the permeability of several compounds through shed snake skin was reported to be similar to, but often slightly less than, that through human epidermis (45-48), it is generally considered that diffusion studies utilising shed snake skin provide conservative estimates for human skin permeation.

Table 3.2. The cumulative amounts of fentanyl permeating human epidermis and shed snake skin at 24 hours (Q_{24h}), following the finite dose application of fentanyl in ethanol (alone (0%w/v OS) or with OS).

OS concentration (%w/v)	Human epidermis		Shed snake skin	
	Q_{24h} ($\mu\text{g}/\text{cm}^2$)	ER(Q_{24h})	Q_{24h} ($\mu\text{g}/\text{cm}^2$)	ER(Q_{24h})
0	4.04 ± 0.15	-	16.03 ± 1.89	-
2.5	$7.07 \pm 0.32^*$	$1.75 \pm 0.08^*$	$89.63 \pm 11.19^*$	$5.59 \pm 0.70^*$
5	$8.14 \pm 0.23^*$	$2.01 \pm 0.04^*$	$97.23 \pm 10.75^*$	$6.07 \pm 0.67^*$
7.5	$8.50 \pm 0.20^*$	$2.10 \pm 0.03^*$	$125.56 \pm 13.72^*$	$7.83 \pm 0.86^*$

* Statistically significant difference compared with fentanyl applied alone (without OS) ($p < 0.05$)

Table 3.3. The cumulative amounts of fentanyl permeating human epidermis and shed snake skin at 24 hours (Q_{24h}), following the finite dose application of fentanyl in ethanol (alone (0%w/v PO) or with PO).

PO concentration (%w/v)	Human epidermis		Shed snake skin	
	Q_{24h} ($\mu\text{g}/\text{cm}^2$)	ER(Q_{24h})	Q_{24h} ($\mu\text{g}/\text{cm}^2$)	ER(Q_{24h})
0	3.26 ± 0.18	-	20.41 ± 1.96	-
2.5	$4.24 \pm 0.28^*$	$1.30 \pm 0.09^*$	25.99 ± 2.46	1.27 ± 0.21
5	$5.19 \pm 0.31^*$	$1.59 \pm 0.08^*$	$43.12 \pm 5.42^*$	$2.11 \pm 0.27^*$
7.5	$4.09 \pm 0.11^*$	$1.25 \pm 0.03^*$	$38.91 \pm 3.14^*$	$1.91 \pm 0.15^*$

* Statistically significant difference compared with fentanyl applied alone (without OS) ($p < 0.05$)

However, it has also been demonstrated that the permeability characteristics of shed snake skin may vary depending on the species of snake from which the skin was obtained and whether dorsal or ventral skin is used (61). Whilst comparing the permeability of progesterone through skin shed from three different species of snake, Haigh et al observed that python skin was the most permeable membrane, with dorsal skin being skin being significantly more permeable than ventral skin (61). As the dorsal section of skin

shed from Children's Python snake was utilised for the diffusion studies presented in this chapter, it is likely that both of these factors may have contributed the relatively high degree of fentanyl permeation through this membrane. It has been proposed that the greater permeability of compounds through dorsal skin of the python may be a result of a number of anatomical factors (61):

- i. as dorsal skin is generally thinner than ventral skin, it may be a less robust membrane
- ii. scales on dorsal skin are often smaller than the scales on ventral skin, thus there is a greater hinge:scale ratio for dorsal skin. This may effectively increase the surface area available for drug diffusion if solute permeation occurs mainly through the hinge region of the skin. The cross-sectional thickness of the hinge region is also considerably thinner than that of the scale region.
- iii. in addition to the previous point, the scales of shed python snake skin are smaller than those of skin shed from other snake species.

The low permeability of fentanyl through human epidermis (compared with shed snake skin) may also be confounded by the fact that i) although the SC is the main rate-limiting barrier for fentanyl permeation, the underlying aqueous epidermal layer may also impose some degree of diffusional resistance (as discussed in Chapter 4, Section 4.4.1) and/or ii) abdominal skin was used for these diffusion studies, which has been shown to be one of the least permeable anatomical sites in the body (62-64).

In relation to fentanyl permeation enhancement, it was found that fentanyl permeation of human epidermis was enhanced 1.75- to 2.10-fold when OS was incorporated into the ethanolic solution at concentrations of between 2.5% to 7.5%w/v. This degree of enhancement is approximately three times lower than that observed for fentanyl permeation enhancement for shed snake skin.

It is also pertinent to note, however, that OS appeared to enhance fentanyl permeation through both membranes in a concentration-dependent manner. Similarly, a somewhat parabolic relationship was observed between PO concentration and fentanyl permeation enhancement for both shed snake skin and human epidermis. However, the capacity by which PO enhanced fentanyl permeation through human epidermis was

comparable to that through shed snake skin. At concentrations between 2.5% to 7.5%w/v, PO enhanced fentanyl permeation through human epidermis and shed snake skin by 1.25- to 1.59-fold and 1.27- to 2.11-fold, respectively.

It is also pertinent to note, however, that OS appeared to enhance fentanyl permeation through both membranes in a concentration-dependent manner. Similarly, a somewhat parabolic relationship was observed between PO concentration and fentanyl permeation enhancement for both shed snake skin and human epidermis. However, the capacity by which PO enhanced fentanyl permeation through human epidermis was comparable to that through shed snake skin. At concentrations between 2.5% to 7.5%w/v, PO enhanced fentanyl permeation through human epidermis and shed snake skin by 1.25- to 1.59-fold and 1.27- to 2.11-fold, respectively.

The utility of shed snake skin as a model membrane for studying the effects of various chemical penetration enhancers on percutaneous drug absorption has been previously investigated (45, 65-74). One such investigation demonstrated that use of shed snake skin either underestimated or overestimated the effects of Azone® and oleic acid on the permeation of 5-fluorouracil through human epidermis, depending on the pretreatment method (45). Although the investigators did not provide a possible explanation as to why the use of shed snake overestimated the effects of these enhancers compared with human skin, they did propose that the squamate membranes underestimated the effects of Azone® and oleic acid (formulated in propylene glycol) because of structural differences between shed snake skin and human SC. Unlike human SC, which is essentially comprised of corneocytes (filled with alpha keratin) imbedded in an array of intercellular lipids (75), shed snake skin consists of three distinct layers; a beta-keratin-rich outermost layer, a lipid-rich intermediate mesos layer, and an alpha-keratin-rich innermost layer (76-79). It was proposed that the presence of the upper beta-keratin layer in shed snake skin imposes an additional barrier towards the permeation of the lipophilic enhancers and thus hinders their ability to reach, and therefore interact with, the lipids present within the mesos layer. Consequently, the enhancers may fail to modify the packing of the lipids present within shed snake skin to the same extent as they would in human SC. Although the membrane lipophilicity and total lipid content may be similar between shed snake skin and human SC (47, 48), this notion may be further supported by the fact that shed snake skin is not only comprised of C16-18 fatty acids, which are also predominant in human SC, but also phospholipids (instead of

sphingolipids that are present in mammalian SC) (76-80). It is therefore possible that the phospholipids present with squamate membranes and the sphingolipids present within human SC interact with lipophilic chemical penetration enhancers via different mechanism(s) and/or to different degree(s).

In light of these reports, it would appear that if the beta-keratin layer was able to impede the transport of OS or PO to the lipid-rich mesos layer, it did not cause the results from the shed snake skin diffusion studies to significantly underestimate the effect(s) of OS and PO on fentanyl permeation through human epidermis. On the contrary, it is possible the interactions between OS and skin lipids are more pronounced within shed snake skin compared with human SC. On the other hand, it would appear that the interactions between PO and shed snake skin lipids are similar to those between PO and human SC lipids. This could imply that OS and PO interact with skin lipids via different mechanisms. However, in order to draw any definitive conclusions from these studies, further detailed investigations that compare the effect(s) of OS and PO on the structure and composition of shed snake skin and human SC lipids are also required. Although this is beyond the objectives of the present studies, it is a proposed avenue for future research.

Given that OS and PO possess similar physicochemical properties, and that the free energies of transfer of various functional groups are similar between shed snake skin and human skin (48), it is perhaps unlikely that the different magnitudes of enhancement caused by OS and PO were due to physicochemical variables involved in percutaneous drug absorption. It is also unlikely that the integrity of shed snake skin was significantly compromised during the diffusion studies. Firstly, when the integrity of shed snake skin was challenged in a previous study by an eight-day hydration study or by a four-minute pretreatment with acetone, the skin did not show any detectable signs of deterioration, nor was the permeability of the model permeant, 5-fluorouracil, significantly increased (45). Secondly, only skin pieces that exhibited TEWL measurements within accepted limits (i.e. between 1.0 to 6.0g/m²h) were used during the diffusion studies presented in this chapter.

In summary, the use of shed snake skin seemed to over-predict fentanyl permeation of female abdominal human epidermis and the enhancing effects of OS. Consequently, the utility of shed skin snake as a model membrane appears to be limited to predicting the rank order by which OS and PO enhance fentanyl permeation of human SC. Therefore, the execution of further diffusion studies, using human epidermis as the

diffusional membrane, was deemed necessary in order to predict the effect(s) of OS and PO on fentanyl percutaneous absorption of human skin *in vivo*.

3.4.3. The effects of octisalate and padimate O on the *in vitro* percutaneous absorption of fentanyl through human epidermis under "finite dosing" conditions

3.4.3.1. Fentanyl permeation through human epidermis under "finite dosing" conditions

The profiles representing fentanyl permeation through excised human epidermis under finite-dosing conditions are shown in Figures 3.3 and 3.4. It should be noted that the concentration range of OS or PO that was investigated during these studies was extended to include concentrations of 1%w/v and 10%w/v. This was done in an attempt to identify any trends that may be apparent between fentanyl permeation enhancement and OS or PO concentration.

It is evident from the profiles shown in Figures 3.3 and 3.4 that fentanyl has relatively low permeability for the epidermis. In particular, when fentanyl was applied to the skin in ethanol alone, only $1.29 \pm 0.07\%$ (PO control) and $1.60 \pm 0.07\%$ (OS control) of the total dose applied permeated into the receptor solution at 24 h. It is also apparent that the presence of 1% to 10%w/v OS or 2.5% to 7.5%w/v PO significantly enhanced the cumulative amount of fentanyl permeating the epidermis at 24 h ($p < 0.05$ compared with control). However, even when maximum enhancement was attained, which was in the presence of 10%w/v OS or 5%w/v PO, the topical bioavailability of fentanyl remained relatively low, with $3.58 \pm 0.24\%$ or $2.05 \pm 0.12\%$ of the total dose applied permeating the skin at 24 h, respectively.

In a previous study, it was demonstrated that fentanyl possessed relatively moderate permeability (i.e. 0.8 to 3.8 $\mu\text{g}/\text{cm}^2\text{h}$) across excised human epidermis compared with various ionogenic and nonionogenic substances (81). Roy and Flynn have also investigated the relationships between the *in vitro* permeation rates of various narcotic analgesics through human skin and their physicochemical properties (82). The collective findings from these studies revealed that fentanyl permeation of human epidermis was up to 3-fold higher than that of morphine, hydromorphone, and codeine – all of which are opioid alkaloids that have aqueous solubilities higher than that of fentanyl.

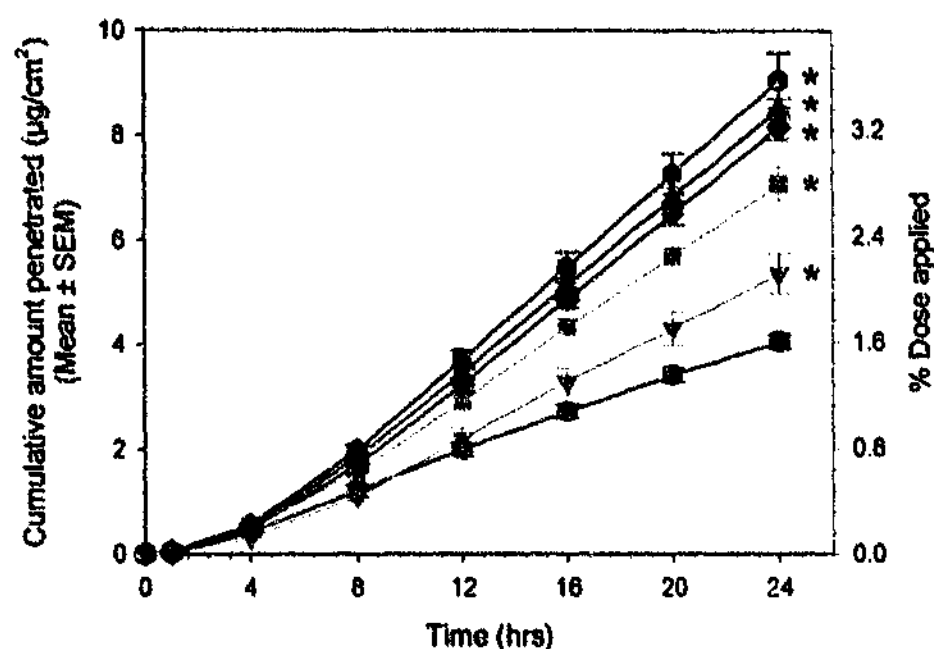


Figure 3.3. Profiles representing fentanyl permeation of human epidermis, following finite-dose application to the skin. The symbols represent fentanyl permeation after the application of ethanolic solutions containing 5%w/v fentanyl alone (control) (●) (n=32), or with 1%w/v OS (▼) (n=7), 2.5%w/v OS (■) (n=5), 5%w/v OS (◆) (n=6), 7.5%w/v OS (▲) (n=7), or 10%w/v OS (●) (n=8). * denotes statistically significant difference compared with 5%w/v fentanyl applied alone ($p < 0.05$).

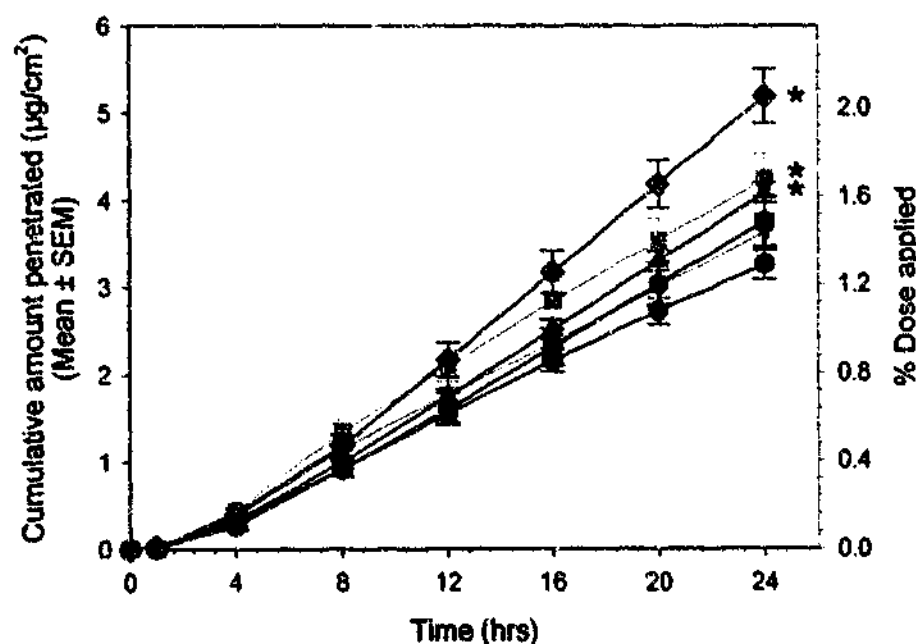


Figure 3.4. Profiles representing fentanyl permeation of human epidermis, following finite-dose application to the skin. The symbols represent fentanyl permeation after the application of ethanolic solutions containing 5%w/v fentanyl alone (control) (●) (n=30), or with 1%w/v PO (▼) (n=8), 2.5%w/v PO (■) (n=8), 5%w/v PO (◆) (n=8), 7.5%w/v PO (▲) (n=8), or 10%w/v PO (●) (n=8). * denotes statistically significant difference compared with 5%w/v fentanyl applied alone ($p < 0.05$).

Based on the comparisons these authors made between the permeability coefficients of the narcotic analgesics through human epidermis and their various physicochemical properties, the relatively facile permeability of fentanyl through human epidermis, and particularly through the SC, was largely attributed to its:

- i. moderate lipophilicity ($K_{oct/w} = 717$ at pH 7.4 (the intrinsic K_{ow} of fentanyl free base was calculated as 23,390 at pH 7.4)
- ii. low melting point (84°C), which may be reflective of its relatively low intracrystalline cohesiveness and moderate hydrophobicity (35, 83).
- iii. solubility parameter of $20.04 \text{ MPa}^{1/2}$, which is close to what may be the optimum for human SC (19.83 to $20.44 \text{ MPa}^{1/2}$) (84). As the compatibility of a solute-solvent mixture may increase as their respective solubility parameters approach similar values (84, 85), this finding could indicate that fentanyl is soluble in the lipoidal phases of the SC (refer to Chapter 4).

In light of these previous findings, it may be somewhat surprising that the finite-dose diffusion studies presented in this chapter demonstrate that fentanyl possesses relatively low permeability through human skin and that there appeared to be a parabolic relationship between fentanyl permeation enhancement and the concentration of PO in the applied vehicle.

However, it is important to note that previous investigators utilised an infinite dose technique, whereby an aqueous donor solution, saturated with fentanyl, was applied to the skin. The use of such a technique would lead to optimised conditions for drug transport through the skin. As the penetration of a drug through the skin is dependent upon its chemical potential within the applied vehicle, fentanyl flux across the skin would be optimal (44, 86-88). Furthermore, the infinite dose technique involves the application of a sufficient amount of permeant to the skin such that significant depletion of the permeant reservoir does not occur over the course of a diffusion experiment. Finally, it cannot be ignored that the skin is continuously bathed in an aqueous receptor solution and an aqueous donor vehicle, which could potentially increase the hydration state of the SC – an effect which may alter the barrier properties of the SC and hence increase drug permeability through the skin (89, 90).

On the other hand, a finite-dose diffusion study often involves the application of a solvent-deposited depot of the permeant to the skin surface. Consequently, the diffusable source of permeant that resides at the skin surface eventually depletes over the course of time and, for the bulk of the experiment, the skin surface is essentially exposed to a relatively "dry" environment.

To further illustrate these points, a previous *in vivo* study was conducted by Sebel et al (91), whereby fentanyl was applied as a finite dose to the forearms of human subjects and urine samples were collected over 12 h intervals for a period of 96 h. Although an aqueous solution was used to deliver fentanyl to the skin, it was allowed to evaporate into the atmosphere before a protective cover was applied to the application site. Under these conditions, the amount of fentanyl excreted in the subject's urine at 24 h corresponded to only ~4.5% of the dose absorbed.

It should also be pointed out that fentanyl has been shown to undergo negligible metabolic degradation in fresh human cadaver skin homogenates (92). Consequently, the low permeability of fentanyl observed during the studies presented in this chapter is unlikely to be a result of appreciable cutaneous metabolism.

3.4.3.2. Kinetics of fentanyl permeation through human epidermis under finite-dosing conditions and the effect(s) of octisalate and padimate O

The ERs generated for the mean cumulative amount of fentanyl permeating the epidermis at 24 h ($ER(Q_{24h})$), following the finite-dose application of 5%w/v fentanyl in ethanol, either alone or with 1 to 10%w/v OS or PO, are presented in Figure 3.5.

As evidenced from these profiles, OS significantly enhanced fentanyl permeation at all concentrations investigated ($p < 0.05$ compared with fentanyl applied in ethanol alone). At a concentration of 1%w/v, OS enhanced fentanyl permeation by a ratio of 1.32 ± 0.10 . The magnitude of this enhancement was elevated to $ER(Q_{24h}) = 1.78 \pm 0.09$ as the OS concentration was increased to 2.5%w/v ($p < 0.05$ compared with the $ER(Q_{24h})$ generated at 1%w/v OS). Fentanyl permeation enhancement was further augmented as the concentration of OS was gradually increased, such that a maximum $ER(Q_{24h})$ of 2.24 ± 0.27 was eventually attained at 10%w/v OS. However, it should be noted that incremental changes to the $ER(Q_{24h})$ became less conspicuous as the OS concentration was increased from 5 to 10%w/v.

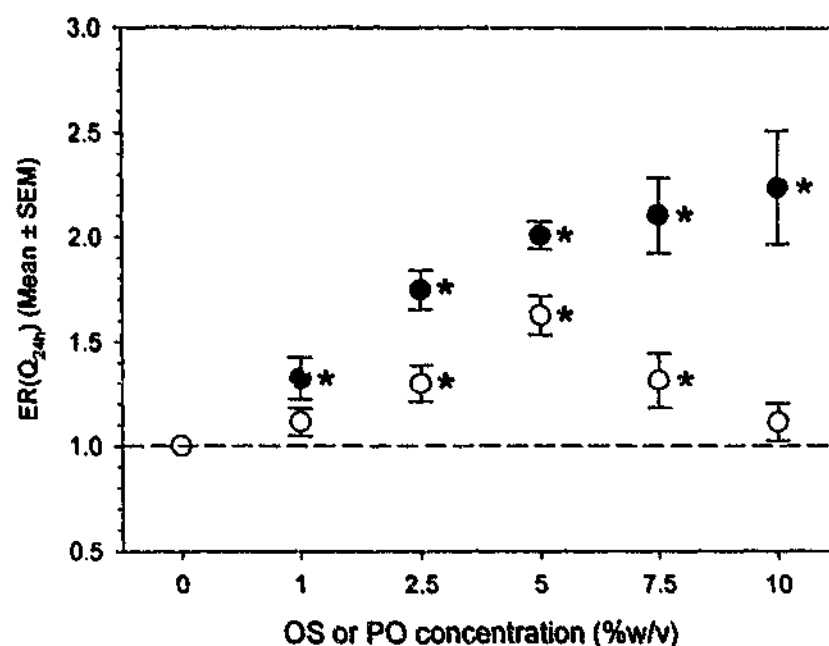


Figure 3.5. Enhancement ratios for the mean cumulative amount of fentanyl permeating human epidermis at $t = 24$ h ($ER(Q_{24h})$) after it is applied to the skin with 1 to 10%w/v OS (●) or PO (○) at a finite dose. $ER(Q_{24h}) = 1$ is equivalent to no enhancement (shown as a dotted line). * corresponds to an ER where the Q_{24h} generated in the presence of OS or PO is significantly different compared with the Q_{24h} generated when fentanyl was applied alone (control) ($p < 0.05$) ($5 < n < 32$).

When fentanyl was applied with PO, a somewhat parabolic relationship seemed to exist between the degree of fentanyl permeation enhancement and PO concentration, with significant enhancement only apparent at concentrations between 2.5 to 7.5%w/v. Because of this relationship, PO appeared to exert an optimal effect on fentanyl permeation at a concentration of 5%w/v ($ER(Q_{24h}) = 1.63 \pm 0.09$). Although enhancement of fentanyl permeation was still evident at 7.5%w/v PO, it is important to note that the $ER(Q_{24h})$ generated at this concentration was in fact significantly lower compared to that observed at 5%w/v. The $ER(Q_{24h})$ was further reduced as the PO concentration was increased to 10%w/v. Consequently, at this highest concentration investigated, PO appeared to have a marginal effect on fentanyl permeation.

It is also obvious from these profiles that fentanyl permeation enhancement was consistently higher in the presence of OS, rather than PO. In fact, at concentrations above

1%w/v, the ERs that were produced for OS were significantly higher compared to the corresponding ratios generated for the equivalent concentrations of PO.

Therefore, in order to gain a better understanding of i) the inherently low permeability of fentanyl through the epidermis under these finite dosing conditions, ii) the likely mechanism(s) involved in fentanyl permeation through the epidermis, and iii) the concentration-dependent effect(s) of OS and PO of fentanyl permeation under finite-dosing conditions, fentanyl flux across the epidermis (J_{FIN}) is presented as a function of time in Figures 3.6 and 3.7.

It is obvious from the profiles that the trends in fentanyl flux across the skin vary depending on whether it is applied alone or with different concentrations of OS or PO. This observation is, on one level, somewhat unusual when one considers the kinetics of percutaneous drug absorption under finite- and infinite-dosing conditions (52-54, 56, 57, 93-95). Under infinite dosing conditions, the time course of drug absorption can be divided into three distinct phases (94) (Figure 3.8.A.):

- i. A lag phase, whereby the drug partitions into, and diffuses through the skin, yet does not appear in the receptor solution
- ii. A nonlinear phase, during which the rate of drug appearance within the receptor solution eventually begins to increase
- iii. A linear phase, where the drug flux across the skin remains constant and steady-state percutaneous drug absorption prevails.

On the contrary, the finite-dose application of a drug to the skin surface typically results in an initial lag phase, after which time drug flux rises to a maximum (Figure 3.8.B.). However, as drug absorption through the skin continues, the effective drug concentration residing at the skin surface starts to deplete so that, eventually, the rate of drug absorption through the skin can no longer be sustained. During this time, drug flux across the skin starts to decline and continues to do so until the diffusable source of drug residing at the skin surface becomes exhausted. Consequently, steady-state conditions do not usually transpire during a finite-dose diffusion experiment.

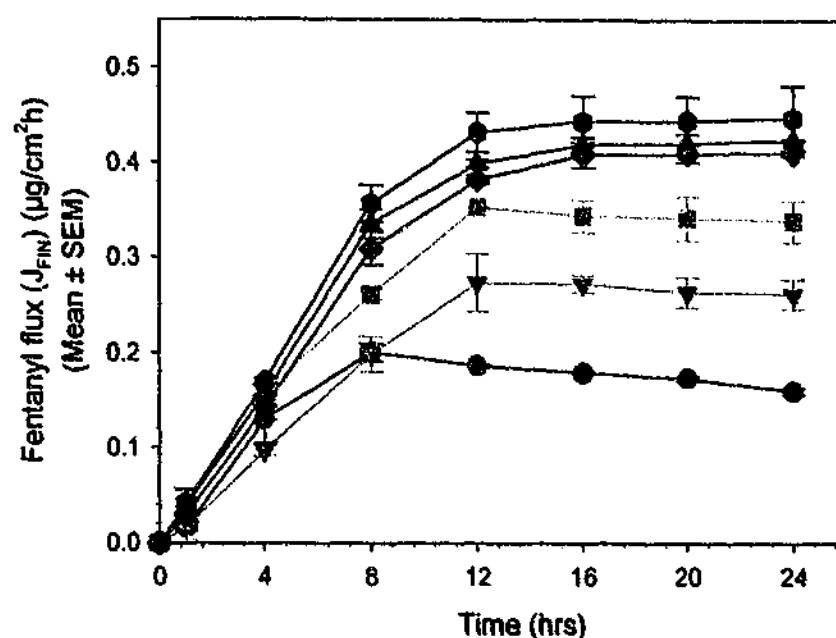


Figure 3.6. Profiles representing fentanyl flux across human epidermis, following finite dose application to the skin (J_{FIN}). The symbols represent fentanyl permeation after the application of ethanolic solutions containing 5%w/v fentanyl alone (control) (●) ($n=32$), or with 1%w/v OS (▼) ($n=7$), 2.5%w/v OS (■) ($n=5$), 5%w/v OS (◆) ($n=6$), 7.5%w/v OS (▲) ($n=7$), or 10%w/v OS (●) ($n=8$). * denotes statistically significant difference compared with 5%w/v fentanyl applied alone ($p<0.05$).

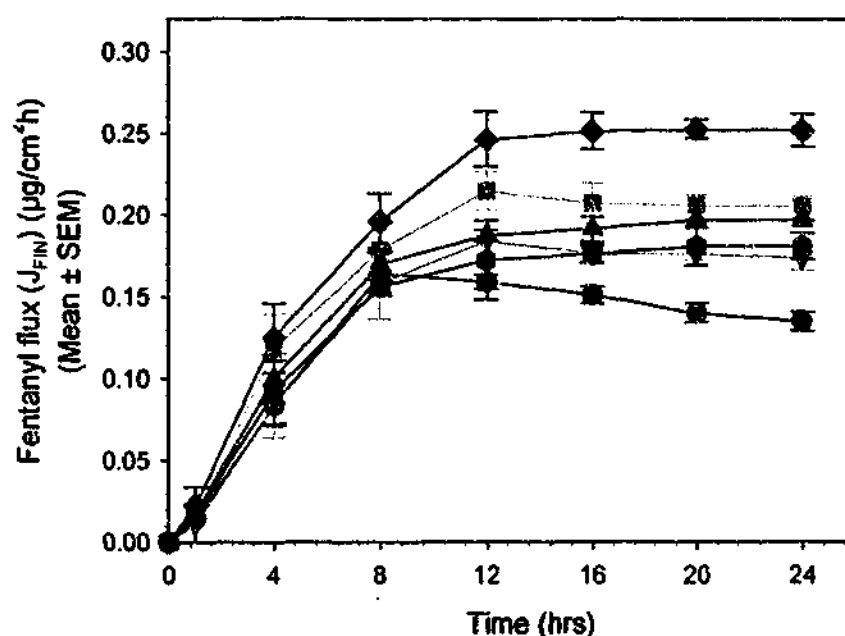


Figure 3.7. Profiles representing fentanyl flux across human epidermis, following finite dose application to the skin (J_{FIN}). The symbols represent fentanyl permeation after the application of ethanolic solutions containing 5%w/v fentanyl alone (control) (●) ($n=30$), or with 1%w/v PO (▼) ($n=8$), 2.5%w/v PO (■) ($n=8$), 5%w/v PO (◆) ($n=8$), 7.5%w/v PO (▲) ($n=8$), or 10%w/v PO (●) ($n=8$). * denotes statistically significant difference compared with 5%w/v fentanyl applied alone ($p<0.05$).

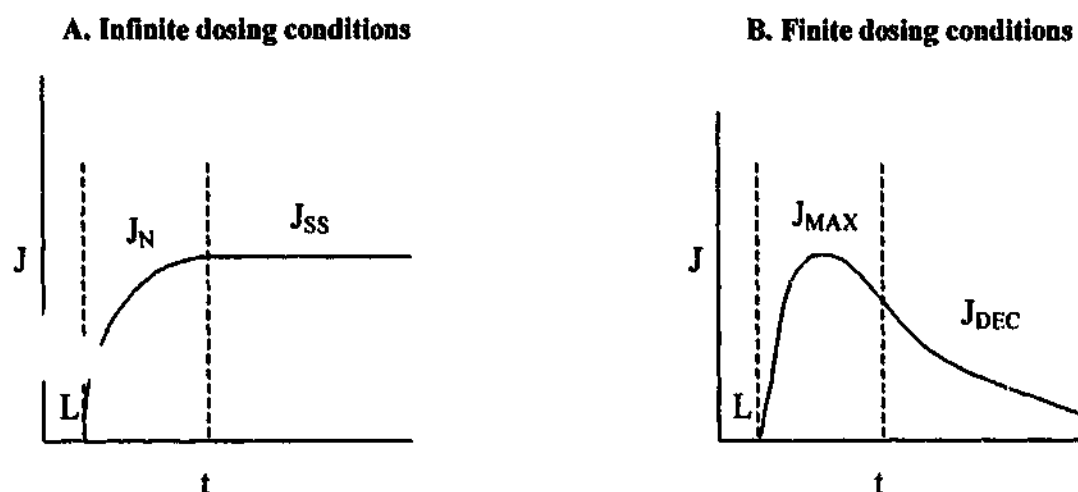


Figure 3.8. Schematic diagrams representing typical profiles of drug flux across the skin (J) as a function of time (t) under infinite (A) and finite (B) dosing conditions. The significance of a lag phase (L), a nonlinear phase (J_N), steady-state drug flux (J_{SS}), maximum drug flux (J_{MAX}), and period of time where drug flux declines (J_{DEC}) is discussed in the text. These diagrams typify the collective findings from various percutaneous drug absorption studies (52-54, 56, 57, 93-95).

Therefore, it is evident that when fentanyl was applied to the skin surface in ethanol alone, or in ethanolic solutions containing low concentrations of either OS or PO, the kinetics of fentanyl permeation through the skin are typical of what might be expected under finite-dosing conditions. However, in the presence of high OS or PO concentrations (i.e. 5% to 10%w/v), fentanyl permeation kinetics appear to follow a trend that is somewhat similar to that under infinite-dosing conditions. A possible explanation for these phenomena is provided in the proceeding paragraphs.

It is well recognised that the SC acts as a rate-limiting barrier to the ingress of topically-applied drugs. Consequently, the factors that influence drug partitioning into, and diffusivity within, the SC may play an important role in total percutaneous drug absorption (96). Therefore, the results presented in Figures 3.6 and 3.7 are likely to reflect the influence of ethanol, OS and PO on fentanyl partitioning into the uppermost layers of the SC and its subsequent diffusion through this boundary layer. In the first instance, the rate of fentanyl penetration across the skin will be dependent on its chemical potential within the vehicle. As fentanyl partitions from the vehicle and into the skin, the concentration gradient that forms across the skin will be influenced by drug-vehicle-skin interactions (97). The primary interactions relevant to fentanyl and the vehicle will be

governed by the solubility of fentanyl and its diffusivity within the vehicle (97-99). Hence, the thermodynamic activity of fentanyl in the vehicle is a major factor determining fentanyl partitioning into and permeation through the skin. As fentanyl was applied in ethanol alone during the control experiments, the impact of a purely ethanolic vehicle towards fentanyl permeation will first be considered.

As ethanol is a volatile liquid, it will rapidly evaporate into the atmosphere under finite-dosing conditions. Hence, during these initial stages, the concentration of fentanyl within the remaining vehicle will dramatically increase. Consequently, it is evident from Figures 3.6 and 3.7 that when fentanyl was applied in ethanol alone, fentanyl flux across the skin gradually increases from zero to 8 h after its application to the skin. As this event is devoid of any compensatory increase in solubility, it is likely that fentanyl will attain a transient state of high thermodynamic activity within the vehicle, during which time its partitioning into the SC will be optimal (fentanyl flux appeared to climax at approximately 8 h, where $J_{(FIN)} = 0.20 \pm 0.01$ and $0.16 \pm 0.01 \mu\text{g}/\text{cm}^2\text{h}$ for OS and PO controls, respectively).

However, the fact that i) the rate of fentanyl permeation of the skin gradually declined during the terminal phase of the diffusion experiment (i.e. after peak fentanyl flux was attained at 8 h) and ii) only a small percentage of the applied dose permeated the skin at 24 h may indicate that a significant amount of fentanyl residing on the skin surface may have been "unavailable" for partitioning into and subsequent diffusion through the skin¹. It is probable that this is in part due to the complete ethanol evaporation from the skin surface: as the concentration of fentanyl within the remaining vehicle quickly exceeds that achievable at saturation, drug precipitation is likely to occur and thus drug partitioning into the SC may be impaired.

It is also apparent from Figures 3.6 and 3.7 that the presence of OS or PO markedly changed the kinetics of fentanyl permeation through the skin and the manner in which they do so is dependent upon their applied concentration. In the first instance, the different kinetics of fentanyl permeation through the skin may be attributed to the fact that the addition of OS or PO to the formulation results in a volatile:non volatile vehicle system.

¹ It could also indicate that a significant amount of fentanyl that penetrates the skin binds to proteins within the skin and hence becomes "unavailable" for subsequent partitioning into the receptor solution. This possibility was not investigated during this research.

Thus, as ethanol completely evaporates into the atmosphere, a film of OS or PO will be deposited on the skin surface. As this film contains high concentrations of fentanyl, the partitioning of fentanyl into the SC will remain thermodynamically favoured following ethanol evaporation. Due to the high solubility of fentanyl within OS or PO (Table 3.1), it is also likely that the deposition of this 'enhancer film' may reduce the tendency for drug precipitation.

Consequently, at low concentrations (i.e. 1% and 2.5%w/v), the presence of OS or PO appeared to prolong the time at which maximum fentanyl flux across the skin was attained (from 8 to 12 h) and significantly increased the magnitude of the maximum fentanyl flux across the skin ($p < 0.05$) compared with that attained when fentanyl was applied with ethanol alone; $J_{(FIN)} = 0.27 \pm 0.03 \mu\text{g}/\text{cm}^2\text{h}$ and $0.34 \pm 0.00 \mu\text{g}/\text{cm}^2\text{h}$ in the presence of 1% and 2.5%w/v OS, respectively; and $J_{(FIN)} = 0.18 \pm 0.00 \mu\text{g}/\text{cm}^2\text{h}$ and $0.21 \pm 0.02 \mu\text{g}/\text{cm}^2\text{h}$ in the presence of 1% and 2.5%w/v PO, respectively. However, even in the presence of 1% and 2.5%w/v OS or PO, the rate of fentanyl permeation appears to gradually decline immediately after peak fentanyl flux is attained. This trend may be apparent because, at low OS or PO concentrations, it is probable that a significant proportion of the OS or PO dose applied to the skin also partitions into the SC. The consequences of this effect may be two-fold: the partitioning of OS or PO into the SC may favour fentanyl partitioning into and/or diffusivity within SC, however as the OS or PO concentration residing at the skin surface gradually becomes depleted, fentanyl may eventually precipitate out of the deposited 'enhancer film'.

When the concentration of OS or PO was increased from 5% to 10%w/v, the kinetics of fentanyl permeation through the skin appeared to change again. From 0 to ~12 h, fentanyl flux across the skin gradually increased over time, then during the later stages of the diffusion experiment (i.e. from 12 or 16 h onwards) it appeared to plateau. As this trend is similar to that expected under infinite-dose conditions, it is likely that, in the presence of high OS or PO concentrations, the amount of fentanyl available for partitioning into, and subsequent diffusion through the skin does not significantly decrease over time and, consequently, apparent "steady-state" permeation across the skin eventually ensues. It is possible that, at concentrations of 5%w/v and above, the amount of OS or PO applied to the skin surface surpasses the maximum amount that can be absorbed by the SC. Consequently, a portion of the applied OS or PO dose may remain at

the skin surface during the latter stages of a diffusion experiment, which may maintain a diffusable (or solubilised) source of fentanyl that is available for partitioning into the SC.

It is interesting to note that increasing the OS concentration from 5% to 7.5% and 10%w/v enhanced apparent "steady-state" fentanyl flux across the skin (appJ_{ss}) (from $0.40 \pm 0.01 \mu\text{g}/\text{cm}^2\text{h}$ to $0.42 \pm 0.01 \mu\text{g}/\text{cm}^2\text{h}$ and $0.44 \pm 0.00 \mu\text{g}/\text{cm}^2\text{h}$, respectively). It is also notable that the appJ_{ss} values achieved in the presence of high PO concentrations were generally inferior to those attained in the presence of OS. Furthermore, when the concentration of PO was increased from 5% to 7.5% and 10%w/v, appJ_{ss} appeared to decline (from $0.25 \pm 0.00 \mu\text{g}/\text{cm}^2\text{h}$ to $0.19 \pm 0.00 \mu\text{g}/\text{cm}^2\text{h}$ and $0.18 \pm 0.00 \mu\text{g}/\text{cm}^2\text{h}$, respectively). At this point, it should be noted that a major factor that will govern the thermodynamic activity of fentanyl within the 'enhancer film' (and hence its rate of transfer into the SC) will be its solubility in OS or PO themselves.

As indicated by the data presented in Table 3.1, the saturated solubility of fentanyl in PO is higher than its solubility in OS by approximately 26%. It is therefore probable that, compared with OS, the inferior appJ_{ss} values (and $\text{ER}(\text{Q}_{24\text{h}}$ values)) generated for PO may be due to the lower thermodynamic activity of fentanyl within the PO film deposited at the skin surface. However, if the activity of fentanyl within the 'enhancer film' was the only predominating factor responsible for the rate of percutaneous absorption, then increases in both OS and PO concentration might be expected to attenuate fentanyl permeation across the skin.

As this trend was only observed at high PO concentrations, one also has to consider the interactions that may occur within the rate-limiting barrier (i.e. the SC itself). As discussed in Chapter 1, it would be reasonable to speculate – based on their physicochemical properties, and particularly their high lipophilicity – that OS and PO would have a high affinity for, and could possibly interact with, the intercellular SC lipids. For instance, SC lipid perturbation has been demonstrated following pretreatment of the SC with the putative chemical penetration enhancers, oleic acid ($\text{LogK}_{\text{OCT/W}} = 7.73^2$) and Azone[®] ($\text{LogK}_{\text{OCT/W}} = 6.21$ (100)) (101-105). Like oleic acid and Azone[®], OS and PO would partition preferentially into the lipid regions of the SC due to their high lipid solubility ($\text{LogK}_{\text{OCT/W}} = 5.97$ and 5.77^1 , respectively). Furthermore, the solubility

² Estimated using EPISuite (Version 3.11) computer software package (U.S. Environmental Protection Agency)

parameters of OS and PO are 21.74 and 18.34 MPa^{1/2},³, respectively, which are similar to the expected solubility parameter of the SC lipids (19.83 to 20.44 MPa^{1/2}) (84).

However, the question as to whether OS and PO interact with SC lipids in a manner that ultimately perturbs the barrier properties of the SC cannot be determined from the work presented in this chapter. This can mainly be attributed to the fact that interpretation of the effects of OS and PO on fentanyl partitioning and/or diffusion from the data generated from these finite dose diffusion studies is confounded by the compositional changes that occur within the applied formulation.

3.5. CONCLUSIONS

Although previous investigators have claimed that shed snake skin provides a permeability barrier similar to that of human SC, the work presented in this chapter has illustrated that the dorsal skin of Children's Python snake is four to six times more permeable than human female abdominal epidermis. However, in terms of rank order of enhancement, OS and PO exert similar effects on fentanyl permeation through both shed snake skin and excised human epidermis. Consequently, the results from these initial investigations demonstrate that both OS and PO enhance the *in vitro* percutaneous absorption of fentanyl under predicted *in vivo* conditions and have thus established the feasibility of using OS or PO to enhance the transdermal delivery of fentanyl.

Analysis of fentanyl flux across excised human epidermis also depicted how the presence of OS or PO modified the rate of fentanyl delivery across the skin, presumably by altering the physicochemical properties of the applied formulation. The general pattern in fentanyl skin permeation from solutions containing low concentrations (i.e. 1% and 2.5%w/v) of OS or PO closely resembled that from solutions containing fentanyl alone.

However, as the initial rate of fentanyl delivery across the skin was significantly enhanced in the presence of low OS or PO concentrations, it would appear that a key function of OS or PO (under finite dosing conditions) is to enhance fentanyl partitioning into the skin by preventing significant drug precipitation following the rapid evaporation of ethanol from the skin surface. Moreover, it would appear that this effect may be

³ Estimated using Thermo Chemical Properties Estimation Software (Solubility Parameter Estimation from Fedor's Cohesive Energy Density) obtained from <http://www.pirika.com/chem/TCPEE/TCPE.htm>

sustained for a longer period of time in the presence of high (i.e. 5%w/v and above) concentrations of OS or PO such that pseudo-steady-state percutaneous absorption of fentanyl eventually prevails.

During the course of these experiments, obvious differences between OS and PO also became apparent. In particular:

- i) Shed snake skin appeared to be more sensitive to the effects of OS than human epidermis, whereas PO enhanced fentanyl permeation through both membranes to a similar degree
- ii) At concentrations between 1% to 10%w/v, OS significantly enhanced fentanyl permeation through human epidermis in a somewhat concentration-dependent manner. On the other hand, a parabolic relationship existed between PO concentration and fentanyl permeation enhancement such that significant enhancement was only observed at PO concentrations between 2.5% to 7.5%w/v, with maximum enhancement attained at 5%w/v PO.
- iii) Under finite-dosing conditions, the enhancing capabilities of OS generally appeared to be superior to that of PO.

The latter finding can largely be accounted for by the fact that the solubility of fentanyl in OS is lower than its solubility in PO and hence fentanyl is likely to exhibit a higher thermodynamic activity within the deposited OS 'enhancer film'. The other discrepancies, however, cannot be entirely explained in terms of the differing physicochemical properties of the 'enhancer films' deposited on the skin surface. These findings therefore beg the question as to whether, in addition to their effects on the physicochemical attributes of the applied formulation, OS and PO interact with SC lipids via different mechanisms and/or to different degrees. Hence, the effects of OS and PO on fentanyl partitioning into, and diffusivity within, the SC will be specifically investigated in subsequent chapters.

3.6. REFERENCES

1. Walters KA, Brain KR. 2002. Dermatological Formulation and Transdermal Systems. In Walters KA, ed. *Dermatological and Transdermal Formulations*. New York: Marcel Dekker, Inc., pp 319-399.
2. Barry BW. 1983. *Dermatological Formulations: Percutaneous Absorption*. New York: Marcel Dekker, Inc., pp 296-350.
3. Chien YW. 1987. Advances in Transdermal Systemic Medication. In Chien YW, ed. *Transdermal Controlled Systemic Medications*. New York: Marcel Dekker, Inc., pp 1-22.
4. Southwell D, Barry BW, Woodford R. 1984. Variations in Permeability of Human Skin Within and Between Specimens. *Int J Pharm* 18:299-309.
5. Ridout G, Santos GC, Guy RH. 1988. Pharmacokinetic Considerations in the Use of Newer Transdermal Formulations. *Clin Pharmacokinet* 15:114-131.
6. Berner B, John VA. 1994. Pharmacokinetic Characterisation of Transdermal Delivery Systems. *Clin Pharmacokinet* 26:121-134.
7. Grond S, Radbruch L, Lehmann KA. 2000. Clinical Pharmacokinetics of Transdermal Opioids: Focus on Transdermal Fentanyl. *Clin Pharmacokinet* 38:59-89.
8. Lehmann KA, Zech D. 1992. Transdermal Fentanyl: Clinical Pharmacology. *J Pain Symptom Manage* 7 Suppl 3:8-16.
9. Hwang SS, Nichols KC, Southam M. 1991. Transdermal Permeation: Physiological and Physicochemical Aspects. In Lehmann KA, Zech D, ed. *Transdermal Fentanyl: A New Approach To Prolonged Pain Control*. Berlin: Springer-Verlag, pp 1-7.
10. Donner B, Zenz M, Strumpf M, Raber M. 1998. Long-Term Treatment of Cancer Pain With Transdermal Fentanyl. *J Pain Symptom Manage* 15:168-175.
11. Hogan DJ, Maibach HI. 1990. Adverse Dermatologic Reactions to Transdermal Drug Delivery Systems. *J Am Acad Dermatol* 22:811-814.
12. Hurkmans JFGM, Bodde HE, Van Driel LMJ, Van Doorne H, Junginger HE. 1985. Skin Irritation Caused By Transdermal Drug Delivery Systems During Long Term (5 Days) Application. *Br J Dermatol* 112:461-467.
13. Schmidt RJ. 1989. Cutaneous Side Effects in Transdermal Drug Delivery: Avoidance Strategies. In Hadgraft J, Guy RH, ed. *Transdermal Drug Delivery: Developmental Issues and Research Initiatives*. New York: Marcel Dekker, Inc., pp 83-98.
14. Southam MA. 1995. Transdermal Fentanyl Therapy: System Design, Pharmacokinetics and Efficacy. *Anticancer Drugs* 6 Suppl 3:29-34.
15. Aly R, Shirley C, Cunico B, Maibach HI. 1978. Effect of Prolonged Occlusion on the Microbial Flora, pH, Carbon Dioxide and Transepidermal Water Loss on Human Skin. *J Invest Dermatol* 71:378-381.

16. Qiao GL, Riviere JE. 1995. Significant Effects of Application Site and Occlusion on the Pharmacokinetics of Cutaneous Penetration and Biotransformation of Parathion *In Vivo* in Swine. *J Pharm Sci* 84:425-432.
17. Tata S, Flynn GL, Weiner ND. 1995. Penetration of Minoxidil from Ethanol/Propylene Glycol Solutions: Effect of Application Volume and Occlusion. *J Pharm Sci* 84:
18. Hotchkiss SA, Miller JM, Caldwell J. 1992. Percutaneous Absorption of Benzyl Acetate Through Rat Skin *In Vitro*. 2. Effect of Vehicle and Occlusion. *Food Chem Toxicol* 30:
19. Piotrowski J. 1967. Further Investigations on the Evaluation of Exposure to Nitrobenzene. *Br J Ind Med* 24:60-65.
20. Feldmann RJ, Maibach HI. 1965. Penetration of ^{14}C Hydrocortisone Through Normal Skin. *Arch Dermatol* 91:661-666.
21. McKenzie AW, Stoughton RB. 1962. Method For Comparing Percutaneous Absorption of Steroids. *Arch Dermatol* 86:88-90.
22. Walters KA. 1989. Penetration Enhancers and Their Use in Transdermal Therapeutic Systems. In Hadgraft J, Guy RH, ed. *Transdermal Drug Delivery: Developmental Issues and Research Initiatives*. New York: Marcel Dekker, Inc., pp 197-246.
23. Anonymous. 2004. Durogesic Transdermal System. In Thomas J, ed. *Australian Prescription Products Guide*. Melbourne: Australian Pharmaceutical Company Limited, pp 1308-1311.
24. Marquardt KA, Tharratt RS, Musallam NA. 1995. Fentanyl Remaining in a Transdermal System Following Three Days of Continuous Use. *Ann Pharmacother* 29:
25. Portenoy RK, Southam MA, Gupta SK, Lapin J, Layman M, Inturrisi CE, Foley KM. 1993. Transdermal Fentanyl for Cancer Pain. Repeated Dose Pharmacokinetics. *Anesthesiology* 78:36-43.
26. Varvel JR, Shafer SL, Hwang SS, Coen PA, Stanski DR. 1989. Absorption Characteristics of Transdermally Administered Fentanyl. *Anesthesiology* 70:928-934.
27. Reeves MD, Giniher CJ. 2002. Fatal Intravenous Misuse of Transdermal Fentanyl. *Med J Aust* 177:526.
28. Morgan TM, O'Sullivan HMM, Reed BL, Finnin BC. 1998. Transdermal Delivery of Estradiol in Postmenopausal Women with a Novel Topical Aerosol. *J Pharm Sci* 87:1226-1228.
29. Morgan TM, Reed BL, Finnin BC. 1998. Enhanced Skin Permeation of Sex Hormones With Novel Topical Spray Vehicles. *J Pharm Sci* 87:1213-1218.
30. Morgan TM, Parr RA, Reed BL, Finnin BC. 1998. Enhanced Transdermal Delivery of Sex Hormones in Swine with a Novel Topical Aerosol. *J Pharm Sci* 87:1219-1225.
31. Taylor LJ, Lee RS, Long M, Rawlings AV, Tubek J, Whitehead L, Moss GP. 2002. Effect of Occlusion on the Percutaneous Penetration of Linoleic Acid and Glycerol. *Int J Pharm* 249:157-164.
32. Morgan TM. 1998. *Transdermal Drug Delivery with Topical Aerosols (PhD Thesis)*. Melbourne: Monash University.

33. Miselnicky SR, Lichtin JL, Sakr A. 1988. The Influence of Solubility, Protein Binding, and Percutaneous Absorption on Reservoir Formation in Skin. *J Soc Cosmet Chem* 39:169-177.
34. Clarys P, Gabard B, Barel AO. 1999. A Qualitative Estimate of the Influence of Halcinonide Concentration and Urea on the Reservoir Formation in the Stratum Corneum. *Skin Pharmacol Appl Skin Physiol* 12:85-89.
35. Guy RH, Hadgraft J. 1989. Selection of Drug Candidates for Transdermal Drug Delivery. In Hadgraft J, Guy RH, ed. *Transdermal Drug Delivery: Developmental Issues and Research Initiatives*. New York: Marcel Dekker Inc., pp 59-81.
36. Guy RH. 1996. Current Status and Future Prospects of Transdermal Drug Delivery. *Pharm Res* 13:1765-1769.
37. Franz TJ. 1975. *In Vitro* vs *In Vivo* Percutaneous Absorption: On the Relevance of *In Vitro* Data. *J Invest Dermatol* 64:190-195.
38. Bronaugh RL, Maibach HI. 1985. Percutaneous Absorption of Nitroaromatic Compounds: *In Vivo* and *In Vitro* Studies in Human and Monkey Skin. *J Invest Dermatol* 84:180-183.
39. Hadgraft J, Woldd HM. 1998. *In Vitro/In Vivo* Correlations in Transdermal Drug Delivery. In Roberts MS, Walters KA, ed. *Dermal Absorption and Toxicity Assessment*. New York: Marcel Dekker, Inc., pp 269-279.
40. Howes D, Guy R, Hadgraft J, Heylings J, Hceck U, Kemper F, Maibach H, Marty J, Merk H, Parra J, Rekkas D, Rondelli I, Schaefer H, Tauber U, Verbieke N. 1996. Methods for Assessing Percutaneous Absorption. Report and Recommendations of ECVAM Workshop 13. *ATLA* 24:81-106.
41. Wester RC, Maibach HI. 1993. Animal Models for Percutaneous Absorption. In Shah VP, Maibach HI, ed. *Topical Drug Bioavailability, Bioequivalence and Penetration*. New York: Plenum Press, pp 333-347.
42. Bronaugh RL, Collier SW. 1991. Protocol for *In Vitro* Percutaneous Absorption Studies. In Bronaugh RL, Maibach HI, ed. *In Vitro* Percutaneous Absorption: Principles, Fundamentals, and Applications. Boca Raton, Florida: CRC Press, Inc, pp 237-242.
43. Brain KR, Walters KA, Watkinson AC. 1998. Investigation of Skin Permeation *In Vitro*. In Roberts MS, Walters KA, ed. *Dermal Absorption and Toxicity Assessment*. New York: Marcel Dekker, Inc., pp 161-187.
44. Zatz JL. 1991. Assessment of Vehicle Factors Influencing Percutaneous Absorption. In Bronaugh RL, Maibach HI, ed. *In Vitro* Percutaneous Absorption: Principles, Fundamentals, and Applications. Boca Raton, Florida: CRC Press, Inc., pp 51-66.
45. Rigg PC, Barry BW. 1990. Shed Snake Skin and Hairless Mouse Skin as Model Membranes for Human Skin During Permeation Studies. *J Invest Dermatol* 94:235-240.
46. Takahashi K, Tamagawa S, Katagi T, Rytting JH, Nishihata T, Mizuno N. 1993. Percutaneous Permeation of Basic Compounds Through Shed Snake Skin as a Model Membrane. *J Pharm Pharmacol* 45:882-886.

47. Itoh T, Magavi R, Casady RL, Nishihata T, Rytting H. 1990. A Method to Predict the Percutaneous Permeability of Various Compounds: Shed Snake Skin as a Model Membrane. *Pharm Res* 7:1302-1306.
48. Itoh T, Xia J, Magavi R, Nishihata T, Rytting H. 1990. Use of Shed Snake Skin as a Model Membrane for *in Vitro* Percutaneous Penetration Studies : Comparison with Human Skin. *Pharm Res* 7:1042-1047.
49. Nangia A, Berner B, Maibach HI. 1999. Transepidermal Water Loss Measurements for Assessing Skin Barrier Functions During *In Vitro* Percutaneous Absorption Studies. In Bronaugh RL, Maibach HI, ed. *Percutaneous Absorption: Drugs, Cosmetics, Mechanisms, Methodology*. New York: Marcel Dekker, Inc., pp 587-594.
50. Bronaugh RL, Congdon ER, Scheuplein RJ. 1981. The Effect of Cosmetic Vehicles on the Penetration of N-Nitrosodiethanolamine Through Excised Human Skin. *J Invest Dermatol* 76:94-96.
51. Harrison SM, Barry BW, Dugard PH. 1984. Effects of Freezing on Human Skin Permeability. *J Pharm Pharmacol* 36:261-262.
52. Kasting GB. 2001. Kinetics of Finite Dose Absorption Through Skin 1. Vanillylnonanamide. *J Pharm Sci* 90:202-212.
53. Kubota K, Yamada T. 1990. Finite Dose Percutaneous Drug Absorption: Theory and its Application to *In Vitro* Timolol Permeation. *J Pharm Sci* 79:1015-1019.
54. Kubota K, Maibach HI. 1991. Estimation of the Permeability Coefficient From a Finite-Dose *In Vitro* Percutaneous Drug Permeation Study. *J Pharm Sci* 80:1001-1002.
55. Cooper ER, Berner B. 1985. Finite Dose Pharmacokinetics of Skin Penetration. *J Pharm Sci* 74:1100-1102.
56. Anissimov YG, Roberts MS. 1999. Diffusion Modeling of Percutaneous Absorption Kinetics. 2. Finite Vehicle Volume and Solvent Deposited Solids. *J Pharm Sci* 90:504-520.
57. Bhatt PP, Hanna MS, Szeptycki P, Higuchi T. 1989. Finite Dose Transport of Drugs in Liquid Formulation Through Stratum Corneum: Analytical Solution to a Diffusion Model. *Int J Pharm* 50:197-203.
58. Skelly JP, Shah VP, Maibach HI, Guy RH, Wester RC, Flynn G, Yacobi A. 1987. FDA and AAPS Report of the Workshop on Principles and Practices of *In Vitro* Percutaneous Penetration Studies: Relevance to Bioavailability and Bioequivalence. *Pharm Res* 4:265-267.
59. Bronaugh RL, Hood HL, Kraeling MEK, Yourick JJ. 1999. Determination of Percutaneous Absorption by *In Vitro* Techniques. In Bronaugh RL, Maibach HI, ed. *Percutaneous Absorption Cosmetics, Mechanisms, Methodology*. New York: Marcel Dekker, Inc., pp 229-233.
60. Bronaugh RL. 1998. Current Issues in the *In Vitro* Measurement of Percutaneous Absorption. In Roberts MS, Walters KA, ed. *Dermal Absorption and Toxicity Assessments*. New York: Marcel Dekker, Inc., pp 155-159.
61. Haigh JM, Beyssac E, Chanet L, Aiache J-M. 1998. *In Vitro* Permeation of Progesterone from a Gel Through the Shed Skin of Three Different Snake Species. *Int J Pharm* 170:151-156.

62. Scheuplein RJ, Blank IH. 1971. Permeability of the Skin. *Physiol Rev* 51:702-747.
63. Wester RC, Maibach HI. 1999. Regional Variation in Percutaneous Absorption. In Bronaugh RL, Maibach HI, ed. *Percutaneous Absorption: Drugs, Cosmetics, Mechanisms, Methodology*. New York: Marcel Dekker, Inc., pp 107-116.
64. Rougier A, Lotte C, Maibach HI. 1987. *In Vivo* Percutaneous Penetration of Some Organic Compounds Related to Anatomic Site in Humans: Predictive Assessment by the Stripping Method. *J Pharm Sci* 76:451-454.
65. Bhatt PP, Rytting JH, Topp EM. 1991. Influence of Azone and Lauryl Alcohol on the Transport of Acetaminophen and Ibuprofen Through Shed Snake Skin. *J Pharm Sci* 72:219-226.
66. Barry BW. 1990. Some Problems in Predicting Human Percutaneous Absorption via *In Vitro* Animal Models. In Scott RC, Guy RH, Hadgraft J, ed. *Prediction of Percutaneous Penetration Methods Measurements Modeling*. London: IBC Technical Services Ltd., pp 204-212.
67. Bhattachar SN, Rytting JH, Itoh T, Nishihata T. 1992. The Effects of Complexation with Hydrogenated Phospholipid on the Transport of Salicylic Acid, Diclofenac and Indomethacin Across Snake Stratum Corneum. *Int J Pharm* 79:263-271.
68. Büyüktimkin S, Büyüktimkin N, Rytting JH. 1993. Synthesis and Enhancing effect of 2-(*N,N*-dimethylamino)propionate on the Transepidermal Delivery of Indomethacin, Clonidine and Hydrocortisone. *Int J Pharm* 10:1632-1637.
69. Fleeker C, Wong O, Rytting JH. 1989. Facilitated Transport of Basic and Acidic Drugs in Solutions Through Snake Skin by a New Enhancer- Dodecyl *N,N*-dimethylamino acetate. *Pharm Res* 6:443-448.
70. Fu Lu M, Lee D, Subba Rao G. 1992. Percutaneous Absorption Enhancement of Leuprolide. *Pharm Res* 9:1575-1579.
71. Hirvonen J, Rytting JH, Paronen P, Urtti A. 1991. Dodecyl *N,N*-Dimethylamino Acetate and Azone Enhance Drug Penetration Across Human, Snake and Rabbit Skin. *Pharm Res* 8:933-937.
72. Suh H, Jun HW. 1996. Effectiveness and Mode of Action of Isopropyl Myristate as a Permeation Enhancer for Naproxen Through Shed Snake Skin. *J Pharm Pharmacol* 48:812-816.
73. Turunen TM, Büyüktimkin S, Büyüktimkin N, Urtti A, Paronen P, Rytting JH. 1993. Enhanced Delivery of 5-Fluorouracil Through Shed Snake Skin by Two New Transdermal Penetration Enhancers. *Int J Pharm* 92:89-95.
74. Kuramoto M, Tanaka T, Makita H, Nakamura Y, Yata N. 1996. Characteristics of Shed Snake Skin Permeability to Indomethacin and Fatty Alcohols. *J Pharm Pharmacol* 48:680-684.
75. Roberts MS, Walters KA. 1998. The Relationship Between Structure and Barrier Function of Skin. In Roberts MS, Walters KA, ed. *Dermal Absorption and Toxicity Assessment*. New York: Marcel Dekker, Inc., pp 1-42.
76. Roth SI, Jones WA. 1970. The Ultrastructure of Epidermal Maturation in the Skin of the Boa Constrictor (*Constrictor Constrictor*). *J Ultrastruct Res* 32:69-93.
77. Landmann L. 1979. Keratin Formation and Barrier Mechanisms in the Epidermis of Natrix Natrix (Reptilia:Serpentes): An Ultrastructural Study. *J Morphol* 162:93-126.

78. Landmann L. 1980. Lamellar Granules in Mammalian, Avian, and Reptilian Epidermis. *J Ultrastruct Res* 72:245-263.
79. Landmann L, Stolinski C, Martin B. 1981. The Permeability Barrier in the Epidermis of the Grass Snake During the Resting Stage of the Sloughing Cycle. *Cell Tissue Res* 215:369-382.
80. Roberts JB, Lillywhite HB. 1983. Lipids and the Permeability of Epidermis from Snakes. *J Exp Zool* 228:1-9.
81. Michaels AS, Chandrasekaran SK, Shaw JE. 1975. Drug Permeation Through Human Skin: Theory and *In Vitro* Experimental Measurement. *AIChEJ* 21:985-996.
82. Roy SD, Flynn GL. 1989. Transdermal Delivery of Narcotic Analgesics: Comparative Permeabilities of Narcotic Analgesics Through Human Cadaver Skin. *Pharm Res* 6:825-832.
83. Flynn GL, Stewart B. 1988. Percutaneous Drug Penetration: Choosing Candidates for Transdermal Development. *Drug Dev Res* 13:169-185.
84. Liron Z, Cohen S. 1984. Percutaneous Absorption of Alkanoic Acids II: Application of Regular Solution Theory. *J Pharm Sci* 73:538-542.
85. Vaughan CD. 1985. Using Solubility Parameters in Cosmetics Formulations. *J Soc Cosmet Chem* 36:319-333.
86. Cooper ER, Berner B. 1985. Skin Permeability. In Skerrow D, Skerrow CJ, ed. *Methods in Skin Research*. Chichester: Wiley-International, pp 417-419.
87. Ostrenga J, Steinmetz C, Poulsen B. 1971. Significance of Vehicle Composition. I. Relationship Between Topical Vehicle Composition, Skin Penetrability, and Clinical Efficacy. *J Pharm Sci* 60:1175-1179.
88. Ostrenga J, Steinmetz C, Poulsen B, Yett S. 1971. Significance of Vehicle Composition. II. Prediction of Optimal Vehicle Composition. *J Pharm Sci* 60:1180-1183.
89. Roberts MS, Walker M. 1993. Water: The Most Natural Penetration Enhancer. In Walters KA, Hadgraft J, ed. *Pharmaceutical Skin Penetration Enhancement*. New York: Marcel Dekker, Inc., pp 1-30.
90. Wester RC, Maibach HI. 1995. Penetration Enhancement by Skin Hydration. In Smith EW, Maibach HI, ed. *Percutaneous Penetration Enhancers*. Boca Raton, Florida: CRC Press, pp 21-28.
91. Sebel PS, Barrett CW, Kirk CJ, Heykants J. 1987. Transdermal Absorption of Fentanyl and Sufentanil in Man. *Eur J Clin Pharmacol* 32:529-531.
92. Roy SD, Hou SY, Witham SL, Flynn GL. 1994. Transdermal Delivery of Narcotic Analgesics: Comparative Metabolism and Permeability of Human Cadaver Skin and Hairless Mouse Skin. *J Pharm Sci* 83:1723-1728.
93. Borsadia S, Ghanem AH, Seta Y, Higuchi WI, Flynn GL, Behl CR, Shah VP. 1992. Factors to Be Considered in the Evaluation of Bioavailability and Bioequivalence of Topical Formulations. *Skin Pharmacol* 5:129-145.
94. Franz TJ. 1978. The Finite Dose Technique as a Valid *In Vitro* Model for the Study of Percutaneous Absorption in Man. *Curr Probl Dermatol* 7:58-68.

95. Franz TJ, Lehman PA, Franz SF, North-Root H, Demetrulias JL, Kelling CK, Moloney SJ, Gettings SD. 1993. Percutaneous Penetration of *N*-Nitrosodiethanolamine Through Human Skin (*In Vitro*): Comparison of Finite and Infinite Dose Applications from Cosmetic Vehicles. *Fundam Appl Toxicol* 21:213-221.
96. Zatz JL. 1983. Fundamentals of Transdermal Controlled Drug Administration: Physicochemical Considerations. *Drug Dev Res* 9:561-577.
97. Hilton J, Woollen BH, Scott RC, Auton TR, Trebilcock KL, Wilks MF. 1994. Vehicle Effects on *In Vitro* Percutaneous Absorption through Rat and Human Skin. *Pharm Res* 11:1396-1400.
98. Lalor CB, Flynn GL, Weiner N. 1995. Formulation Factors Affecting Release of Drug From Topical Vehicles. II. Effect of Solubility On *In Vitro* Delivery of a Series of *n*-Alkyl *p*-Aminobenzoates. *J Pharm Sci* 84:673-676.
99. Chiang CM, Flynn GL, Weiner ND, Szpunar GJ. 1989. Bioavailability Assessment of Topical Delivery Systems: Effect of Vehicle Evaporation Upon *In Vitro* Delivery of Minoxidil From Solution Formulations. *Int J Pharm* 55:229-236.
100. Allan G. 1995. Azone®. In Smith EW, Maibach HI, ed. *Percutaneous Penetration Enhancers*. Boca Raton, Florida: CRC Press, pp 129-136.
101. Pilgram GS, van der Meulen J, Gooris GS, Koerten HK, Bouwstra JA. 2001. The Influence of Two Azones and Sebaceous Lipids on the Lateral Organization of Lipids Isolated from Human Stratum Corneum. *Biochim Biophys Acta* 1511:244-254.
102. Lambert WJ, Higuchi WI, Knutson K, Krill SL. 1989. Dose-Dependent Enhancement Effects of Azone on Skin Permeability. *Pharm Res* 6:798-803.
103. Francoeur ML, Golden GM, Potts RO. 1990. Oleic Acid: Its Effects on Stratum Corneum in Relation to (Trans)Dermal Drug Delivery. *Pharm Res* 7:621-627.
104. Naik A, Pechtold LARM, Potts RO, Guy RH. 1995. Mechanism of Oleic Acid-Induced Skin Penetration Enhancement *In Vivo* in Humans. *J Control Release* 37:299-306.
105. Golden GM, McKie JE, Potts RO. 1987. Role of Stratum Corneum Lipid Fluidity in Transdermal Drug Flux. *J Pharm Sci* 76:25-28.

CHAPTER 4

THE EFFECTS OF OCTISALATE AND PADIMATE O ON FENTANYL PERMEATION, PARTITIONING, AND DIFFUSION

4.1. INTRODUCTION

It was demonstrated in Chapter 3 that octisalate (OS) and padimate O (PO) enhance the percutaneous absorption of fentanyl *in vitro* under finite-dosing conditions. Although this effect appears to be related to the influence that OS and PO exert on the physicochemical properties of the applied formulation, other mechanisms that might be responsible for enhanced fentanyl permeation were not elucidated from the data. In particular, the effects of OS and PO on fentanyl partitioning and diffusivity were not investigated in Chapter 3 as the interpretation of these parameters from finite dose skin diffusion data can be confounded by the fact that it is impossible to separate noninteractive¹ from interactive² contributions to solute flux (1, 3). Therefore, in order to determine the effect(s) of OS and PO on fentanyl partitioning and diffusion (i.e. the interactive effects of OS and PO) in an uncomplicated manner, the noninteractive mechanisms that might contribute to enhanced fentanyl permeation must be controlled.

This can be accomplished, using the diffusion cell model, by pretreating the skin with the vehicle(s) of interest for a specified time and then applying the solute to the skin via a simple solution (i.e. a donor solution) (1, 3). In order to ensure that the donor solution does not become significantly depleted of solute (i.e. that an "infinite dose" of solute is applied to the skin), a "large" volume of a saturated solution may be utilised during studies of this nature. By definition, the activity of excess solid drug (and the dissolved form of the drug with which it is in equilibrium with) is assigned a value of unity and thus the activity of the solution may be estimated as C_v/S_v (as discussed in Chapter 1). This confers the notion that saturated solutions (which contain solvents that don't significantly interact with the SC) should have the same noninteractive contribution to solute flux, despite differences in solute concentration (5).

¹ Noninteractive mechanisms that contribute to enhanced solute flux across the skin often pertain to the thermodynamic activity of the solute within the applied vehicle. This effect does not involve any interactions between the vehicle and the stratum corneum (SC) (1).

² Interactive mechanisms pertain to interactions between the vehicle and the SC that lead to a change in the barrier properties of the SC (e.g. extraction or perturbation of the SC lipids or a change in the solubility characteristics of the SC) (1)

The mathematical boundary conditions that usually apply to an "infinite dose" diffusion experiment are as follows (6-9):

- i. The solute is fixed at a high thermodynamic activity on one side (i.e. the donor side) of the SC
- ii. At time $t = 0$ the SC is completely devoid of solute
- iii. The solute equilibrates instantaneously at the skin-vehicle interface
- iv. Solute diffusion begins at the donor side of the SC and continues toward the receptor side of the SC
- v. The solute diffuses into a receptor sink throughout the diffusion experiment

It is also assumed that:

- vi. The SC is an inert, homogenous membrane that acts as the principle barrier towards solute diffusion
- vii. The diffusion coefficient of the solute within the SC remains constant
- vii. The solute does not bind to nor is it metabolised within the SC

Therefore, increases in the cumulative amount (Q) of solute that permeates the skin at time, t can be described by the following solution to Fick's second law of diffusion³ (10):

$$Q = AK_{SC/V}C_v h \left[D \frac{t}{h^2} - \frac{1}{6} - \frac{2}{\pi^2} \sum_{n=1}^{\infty} \frac{(-1)^n}{n^2} \exp\left(\frac{-D^2 n^2 \pi^2 t}{h^2}\right) \right] \quad 4.1$$

Where A is the skin surface diffusion area, $K_{SC/V}$ is the apparent partition coefficient of the solute between the SC and the vehicle, h is the diffusional pathlength of the SC and D is the apparent diffusion coefficient of the solute within the SC. As t in Equation 4.1 approaches infinity, Equation 4.1 approaches the straight line:

³ In the original form of Equation 4.1, the term C_0 (the concentration of solute in the outer layer of the SC) is used instead of $K_{SC/V}C_v$. As the value for C_0 is extremely difficult to measure, it is replaced with the term $K_{SC/V}C_v$ as it assumed that the outer layers of the SC rapidly equilibrate with the vehicle (9).

$$Q = \frac{DK_{SC/V}C_V}{h} \left[t - \frac{h^2}{6D} \right] \quad 4.2$$

Graphic representations of Equations 4.1 and 4.2 are depicted in Figure 4.1. If Equation 4.2 is extrapolated to the time axis, the intercept obtained at $Q=0$ yields a value known as the lag time (t_{lag}), which is directly related to the diffusional pathlength and inversely related to the diffusion coefficient:

$$t_{lag} = \frac{h^2}{6D} \quad 4.3$$

Although it is commonplace to derive diffusion coefficients using this extrapolation method (otherwise known as the "lag time method") (9), the reliability of this approach has recently been criticised as it relies heavily on the attainment of steady-state drug diffusion (11). Furthermore, it is difficult to accurately measure the diffusional pathlength of the SC. Not only does this difficulty arise from experimental complications, it is still a matter of controversy as to whether this value should reflect the actual thickness of the SC or the tortuous intercellular SC lipid pathway (12-16). In addition, small errors in determining the cumulative amount of solute permeating the skin at longer time points can lead to large errors in the lag times derived from linear extrapolation of steady-state diffusion data (17). Consequently, negative lag times are occasionally calculated and/or lag time values are susceptible to significant variability. In order to circumvent this latter problem, many investigators now use computer software packages to fit "infinite" dose skin diffusion data to Equation 4.1 (18-24). Using this approach, apparent partition and diffusion coefficients can be derived using diffusion data generated at all time points, rather than the data only contained within the steady-state region.

The results generated from the "infinite" dose diffusion studies presented in the initial sections of this chapter indicate that OS and PO enhance fentanyl permeation of human skin by increasing its apparent SC-vehicle partition coefficient. As independent SC-water partitioning studies (presented in this chapter) confirmed this finding, subsequent experiments that are described in Chapter 4 focus on elucidating the possible mechanism(s) by which OS and PO alter this parameter.

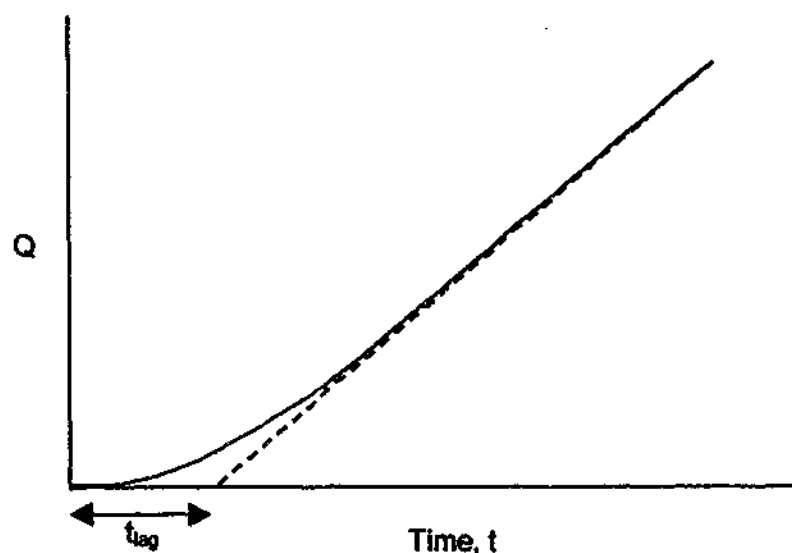


Figure 4.1. Profiles representing the time course for diffusion of a solute across a membrane (i.e. the SC) obtained by plotting the cumulative amount of solute that permeates the membrane (Q) as a function of time, t (8, 9). The solid line represents the profile described by Equation 4.1. Steady-state solute flux across the membrane is achieved when the profile becomes linear. Extrapolation of the linear portion of this profile to the t intercept that corresponds to $Q=0$ yields the lag time, t_{lag} . The dashed line represents the profile described by Equation 4.2.

As the partition coefficient of a solute between the SC and a vehicle can be approximated by the ratio of its solubility in the SC (S_{SC}) and the vehicle (S_V) (Equation 4.4) (25, 26), chemical penetration enhancers (CPEs) may enhance the partitioning of a solute into the SC by improving the solute's solubility in this environment:

$$K_{SC/V} = \frac{S_{SC}}{S_V} \quad 4.4$$

In order to investigate whether this mechanism of action was relevant to the enhancing effects of OS and PO, octanol (OCT) and isopropyl myristate (IPM) were used to simulate the chemical environment of SC lipids (9, 27-36) as:

- i. OCT is the most popular organic solvent that has been used to estimate SC-water partition coefficients (8, 9) and the polarity of OCT has been shown to be similar to that of the SC lipids (28, 36).

- ii. IPM has also been recommended for work relating to skin diffusion as its blend of polar and non-polar properties is thought to mimic the complex lipid/polar nature of the SC (9). In addition, there is accumulating evidence to suggest that the overall partitioning character of solutes into the SC lipid domain can be approximated by that into IPM (27, 30, 33).

4.2. OBJECTIVES

The primary objective of the work presented in this chapter was to determine whether OS and PO enhance fentanyl permeation of human skin by increasing its partitioning into and/or diffusivity within the SC. As the "infinite dose" diffusion cell technique is commonly used to derive these diffusional parameters, this methodology was initially employed to determine the effects of OS and PO on fentanyl permeation, partitioning and diffusivity.

It will become apparent, however, that a number of possible limitations may be associated with this experimental design. Consequently, a secondary objective of the work presented in this chapter was to confirm and further investigate the effects of OS and PO on fentanyl partitioning into the SC. In addition to conducting partitioning experiments between isolated human SC and water, it was necessary to elucidate whether OS and PO influence fentanyl partitioning into the SC by improving its affinity for the SC lipids.

In order to probe this mechanism of action, the saturated solubility of fentanyl in OS and PO was compared to that in the model organic phases, OCT and IPM. As the solubility of a solute in a particular solvent can be characterised by its respective solubility parameters, another objective of this work was to identify – using partial solubility parameters – the possible intermolecular forces of attraction that may be important in fentanyl solubilisation.

In order to determine whether the apparent trends in fentanyl solubility were indicative of its partitioning characteristics, the partition coefficient of fentanyl between either OS or PO and water was compared to that between either OCT or IPM and water, and the concentration-dependent effects of OS and PO on the partition coefficient of fentanyl between IPM and water were investigated.

4.3. MATERIALS AND METHODS

4.3.1. Materials

Fentanyl was manufactured by Macfarlan Smith (Edinburgh, UK). OS and PO were supplied by Bronson and Jacobs (Australia). IPM, OCT, oleic acid and diethylene glycol monoethyl ether (Transcutol®) were obtained from Sigma-Aldrich Corporation (St. Louis, MO, USA). 1-dodecyl azacycloheptan-2-one (Azone®) was manufactured by Yick-Vic Pharmaceuticals, China. HPLC grade acetonitrile and methanol were supplied by Merck (Australia). Water was purified by a Milli-Q™ water purification system (Millipore, Bedford, MA, USA). All other chemicals were of analytical grade.

4.3.2. "Infinite dose" *in vitro* skin diffusion studies

4.3.2.1. Skin preparation

Human abdominal epidermis was separated from tissue obtained from at least two individual female donors following abdominoplasty, according to the method described in Chapter 3 (Section 3.3.4.1).

4.3.2.2. "Infinite dose" skin diffusion studies

Details of the *in vitro* diffusion experiments are described in Chapter 3 (Sections 3.3.3.2 and 3.3.4.2). As previously described, the skin was equilibrated with receptor solution (isotonic phosphate buffer pH 7.4, 0.1 %w/v sodium azide) for a period of 1 h. TEWL measurements were performed approximately 45 min after the skin was equilibrated with receptor solution and only skin pieces that yielded TEWL values between 1.0 to 6.0 g/m²h (37) were used during the studies.

After the 1 h equilibration period with receptor solution, the skin was either left untreated or was pretreated with a finite dose (5 µl/cm²) of 95%v/v ethanol alone or 95%v/v ethanol containing 1, 2.5, 5, 7.5 or 10%w/v of OS or PO (4 < n < 10) for a period of 2 h. In the instance where the diffusion model was challenged with putative CPEs, the skin was either left untreated (control) or was pretreated with 95%v/v ethanol containing 5%w/v Azone®, 5 or 10%w/v oleic acid, or 5 or 20%w/v Transcutol® for 2 h.

After pretreating the skin with any enhancer, the skin surface was rinsed three times with 500 μ l of purified water and gently blotted dry with low-lint, absorbent tissue (Kimwipes[®], Kimberly-Clark Australia). A saturated aqueous solution containing fentanyl was then applied to the skin surface. The solution was pre-prepared by dispersing excess fentanyl (3 mg/ml) in purified water. The solution was vortexed for 1 min, then placed in a water bath (SS40-D, Grant Instruments (Cambridge) Ltd., England) maintained at $32 \pm 1^\circ\text{C}$, where it was continuously shaken at 15 strokes/min for 72 h. The donor solution was vortexed for 30 sec immediately before application to the skin to ensure uniform dispersion of the solid fentanyl crystals. It was applied to the skin at a dose of 2000 μ l. The diffusion studies were conducted over 24 h, whereby samples were collected every hour for the first 4 h then every 2 h thereafter using an automated fraction collector (ISCO Retriever II, NE).

4.3.3. Stratum corneum-water partitioning studies

4.3.3.1. Isolation of human stratum corneum

SC sheets were isolated from freshly-separated epidermis according to the method described in Chapter 2 (Section 2.3.4.1).

4.3.3.2. Stratum corneum-water partitioning studies

Desiccated SC was die-punched into 5 cm² circular pieces and the individual discs were weighed on a Mettler Toledo balance (AT261, Mettler, Switzerland). The discs were then laid flat, epidermal-side down, over filter paper and, using wire mesh for support, they were floated over receptor solution (isotonic phosphate buffer pH 7.4, 0.1%w/v sodium azide).

After an 1 h equilibration period with the receptor solution, the SC was either left untreated (control) or was pretreated with a finite dose (5 μ l/cm²) of 95%v/v ethanol alone or 95%v/v ethanol containing 1, 2.5, 5, 7.5 or 10%w/v of either OS or PO for 2 h (n=5). In order to ensure that the pretreatment solution was uniformly spread across the entire SC surface, it was applied in the following manner:

- i. Small aliquots of the solution were initially "dotted" over the SC surface

- ii. The aliquots were then immediately smeared together using the tip of the same pipette tip that was used during step i.
- iii. Step ii. was performed until a uniform film of solution covered the entire SC surface

In order to mimic the experimental conditions that prevailed during the infinite dose diffusion studies (Section 4.3.2.2), the SC discs were left in contact with the receptor solution during the 2 h pretreatment. At the completion of the 2 h pretreatment time, the SC discs were removed from the receptor solution and excess solution residing at the SC surface was removed using the surface wipe procedure described in Section 4.3.3.3. To ensure that control samples were treated in the same manner, the surface wipe procedure was also performed on untreated SC samples. Following the surface wipe procedure, the SC discs were immersed in 3000 μ l of an aqueous solution that had been sub-saturated with fentanyl. The solution had been previously prepared by adding 60 μ g/ml of fentanyl to purified water. After the solution was equilibrated at $32 \pm 1^\circ\text{C}$ for 72 h, it was filtered through a 0.22 μ m filter (Millex[®] PTFE fluoropore Syringe Driven Filter Unit, Millipore Corporation, Bedford, MA, USA) immediately prior to use in order to ensure complete removal of excess solid.

After the SC was added to the solution, the samples were vortexed for 30 sec, and then placed in a water bath maintained at $32 \pm 1^\circ\text{C}$, where they were continuously shaken at 15 strokes/min for 24 h. At the end of the 24 h period, the SC discs were removed from the aqueous bathing solution. Excess solution that had adsorbed onto the SC surface was removed by sandwiching the discs between filter paper for 30 sec. The discs were then re-weighed. The pH of the bathing solution was determined (using a Metrohm 632 pH meter (Metrohm Herisau, Switzerland)) after it had been centrifuged at 3500 rpm at 32°C for 15 min (Beckman GS-CR centrifuge, Beckman Instruments Inc., Palo Alto, CA, USA).

Fentanyl uptake into the SC was determined by a depletion method (28), whereby the concentration of fentanyl within the bathing solution was determined before and after the 24 h immersion period. A 1,000 μ l aliquot of the solution was diluted with 5 ml isotonic phosphate buffer pH 7.4, 0.1%w/v sodium azide and the concentration of fentanyl within the diluted sample was analysed using the HPLC/UV method described in Chapter 2 (Section 2.3.5).

4.3.3.3. Surface wipe procedure

4.3.3.3.1. Surface wipe procedure

At the end of the 2 h pretreatment time, each SC disc was laid flat (SC-side up) over a glass microscope slide. In order to remove excess OS or PO remaining at the SC surface, three $\sim 10\text{ cm}^2$ circular pieces of filter paper were applied to the surface. A glass microscope slide was placed over the filter paper and gentle pressure was applied for 30 sec. This procedure was performed twice. In order to remove any OS or PO residing within the SC furrows, cotton buds (Johnson and Johnson, Australia) were then rolled over the SC surface in the following manner:

- i. Starting from the upper apex of the SC disc and working down, the surface was wiped in a unidirectional manner (left to right, then right to left) until the entire area was swabbed.
- ii. Starting from the left apex of the SC disc, and working across, the surface was wiped in a unidirectional manner (up and down) until the entire area was swabbed.
- iii. Steps i. and ii. were performed twice, using a fresh cotton bud each time.

4.3.3.3.2. Validation of the surface wipe procedure

4.3.3.3.2.1. Surface wipe samples

Human SC was isolated from freshly-separated epidermis according to the method described in Chapter 2 (Section 2.3.4.1). Desiccated SC was die-punched into 5 cm^2 circular pieces and the individual discs were placed over filter paper (SC-side up) and, using wire mesh for support, they were floated over isotonic phosphate buffer pH 7.4, 0.1 %w/v sodium azide for a period of 1 h. Solutions containing 0.1, 1, 5, or 10%w/v OS or PO in 95%v/v ethanol were then applied as a "finite dose" ($5\text{ }\mu\text{l}/\text{cm}^2 = 25\text{ }\mu\text{l}$) to the SC surface such that 25, 250, 1250 or 2500 μg of OS or PO was left deposited at the SC surface ($n = 5$). As it was possible that OS and PO would rapidly partition into the SC following their application to the SC surface, the solutions were left in contact with the SC for a period of 20 sec. The surface wipe procedure described in Section 4.3.3.3.1 was

then performed. The filter paper and cotton buds that were used during the surface wipe were placed in a glass vial and a 10 ml aliquot of 100% methanol was added. After the samples were vortexed for 30 sec, they were gently shaken on a horizontal mixer (Ratek Instruments Pty. Ltd., Victoria, Australia) for 16 h at ambient temperature (Stage 1). Following this initial extraction period, the sample was vortexed for 30 sec and the filter paper and cotton buds were transferred to a fresh glass vial and 5ml of methanol was added. The sample was vortexed for 30 sec and placed on the horizontal mixer for 8 h at ambient temperature (Stage 2). At the end of the 8 h period, the extract retained from Stage 1 was added to the contents of the glass vial. After vortexing the sample for 1 min, a 5ml aliquot was removed and centrifuged at 3500 rpm for 15 min at 25°C. An aliquot of the supernatant was diluted to an appropriate volume in order to yield a concentration that was within the limits of the HPLC/UV assay. Samples containing OS were diluted with 85%v/v acetonitrile, 15%v/v purified water containing 0.27%v/v trifluoroacetic acid and samples containing PO were diluted with 82%v/v acetonitrile, 18%v/v purified water containing 0.22%v/v trifluoroacetic acid. The concentration of OS or PO within the sample was determined using the HPLC/UV assay described in Section 4.3.6.2.

4.3.3.3.2.2. Surface wipe standards

SC samples ($n = 25$) were prepared using the method described in Section 4.3.3.3.2.2. After the SC discs were equilibrated with receptor solution for 1 hour, 95%v/v ethanol was applied as a "finite dose" ($5 \mu\text{l}/\text{cm}^2 = 25\mu\text{l}$) to the SC surface and it was left in contact with the SC for 20 sec. The surface wipe procedure described in Section 4.3.3.3.1 was then performed in order to obtain blank surface wipe samples. The filter paper and cotton buds were then transferred to glass vials and a 25 μl aliquot of 0, 0.1, 1, 5, or 10%w/v OS or PO in 95 %v/v ethanol was added to the vial. The ethanol was evaporated under a gentle stream of nitrogen for 20 sec such that 0, 25, 250, 1250 or 2500 μg of OS or PO was left deposited in the vial and the extraction procedure described in Section 4.3.3.3.2.1 was performed. The concentration of OS or PO within the standard solutions was determined using the HPLC/UV assays described in Section 4.3.6.2.

4.3.3.3.2.3. Recovery, accuracy and precision

Recovery, intra- and inter-day precision and accuracy for the surface wipe procedure are presented in Table 4.1. Recovery was determined by comparing the peak areas of OS or PO extracted from the surface wipe samples to those generated from the surface wipe standards. Intra-day precision and accuracy were determined from the surface wipe samples prepared at the four different concentrations (i.e. 25, 250, 1250 or 2500 µg per 5 cm² SC surface area). Inter-day precision was determined by repeating the surface wipe procedure at these different concentrations on three different days.

It is evident from the results shown in Table 4.1 that the recovery of OS and PO from the SC surface was excellent (above 90%) at all concentrations investigated. The surface wipe procedure was very reproducible as intra- and inter-day precision (%CV) was within accepted limits (<15%) at all concentrations.

Table 4.1. Recovery, intra- and inter-day precision, and accuracy for the OS and PO surface wipe procedure.

	Amount (µg)	Spiked amount (µg) (Mean ± SD)	% Recovery (Mean ± SD)	Inter-day precision (%CV)	Intra-day precision (%CV)	Accuracy (%)
OS	25	24.7 ± 1.0	99.2 ± 4.6	8.2	8.7	98.7
	250	247.0 ± 6.3	96.2 ± 2.3	5.3	5.7	98.8
	1250	1231.5 ± 34.0	96.4 ± 3.5	3.9	6.2	98.5
	2500	2468.9 ± 36.8	96.3 ± 4.9	2.8	3.3	98.8
PO	25	25.4 ± 1.3	91.6 ± 7.1	8.2	11.4	101.7
	250	241.7 ± 4.2	90.3 ± 4.6	6.3	3.8	96.7
	1250	1304.7 ± 43.0	93.4 ± 2.9	4.8	7.4	104.4
	2500	2575.9 ± 50.9	96.4 ± 4.7	3.5	4.4	103.0

4.3.4. Fentanyl partitioning between liquid organic phases and water

To obtain an equilibrium distribution of fentanyl between IPM and water, the recommendations of Leo et al (34) were followed. Fentanyl (5 mg) was dissolved in 125 μ l of OS, PO, OCT, IPM, or IPM containing 1, 2.5, 5, 7.5 or 10%w/v OS or PO ($n = 4$). Purified water (5000 μ l) was then added to the organic phase. After inverting the mixture 100 times over 5 min, the immiscible phases were separated by centrifugation at 3500 rpm for 20 min at 32°C. The samples were then left to stand at 32°C for 24 h. Following this equilibration period, a 2,000 μ l aliquot of the aqueous phase was removed from the sample and centrifuged twice at 3500 rpm for 20 min (at 32°C). In the instance where water was mixed with PO, OCT or IPM (alone or containing OS or PO), the organic phase formed a "top layer" over the aqueous phase. Therefore, the "top-layer" of organic phase and a ~1000 μ l portion of aqueous phase residing at the aqueous-organic phase interface was removed with a glass pasteur pipette before the aliquot of aqueous phase was removed for centrifugation. After centrifugation, a ~1000 μ l aliquot of aqueous phase was removed from the upper portion of the sample and discarded. The pH of the remaining aqueous phase was then determined using a Metrohm 632 pH meter. After the pH measurements were performed, a 1,000 μ l aliquot of the aqueous phase was removed and diluted with 5 ml isotonic phosphate buffer pH 7.4, 0.1%w/v sodium azide for HPLC/UV analysis (the details of which are given Chapter 2 (Section 2.3.5)).

4.3.5. Saturated solubility studies

4.3.5.1. Saturated solubility of fentanyl in isopropyl myristate and octanol

Approximately 100 mg of fentanyl was added to 500 μ l of IPM or OCT ($n = 3$). The samples were vortexed for 30 sec and placed in a shaking water bath, where they were continuously shaken at 15 strokes/min at $32 \pm 1^\circ\text{C}$ for 72 h. The samples were inspected periodically to ensure that they remained saturated during this time. Following the 72 h equilibration period, the samples were centrifuged at 3500 rpm for 20 min at 32°C. Using a HPLC glass syringe (SGE, Australia), a 100 μ l aliquot of the supernatant was removed from the sample and diluted to 100 ml with absolute ethanol. A 100 μ l aliquot of this solution was further diluted to 10 ml with 20%v/v aqueous ethanol and the

concentration of fentanyl within this solution was determined using the HPLC/UV assay described in Chapter 2 (Section 2.3.5).

4.3.5.2. Saturated solubility of octisalate and padimate O in octanol

Approximately 1000 μ l of OS or PO was added to 1000 μ l of IPM or OCT ($n=3$) and the same procedure described in Section 4.3.5.1 was conducted. After the samples were centrifuged, a 100 μ l aliquot of the supernatant was removed from the sample (using a HPLC glass syringe) and diluted to 100 ml with 100% methanol. A 100 μ l aliquot of this solution was further diluted to 100 ml with either 85%v/v acetonitrile, 15%v/v purified water (containing 0.27%v/v trifluoroacetic acid) (OS-containing samples) or 82%v/v acetonitrile, 18%v/v purified water (containing 0.22%v/v trifluoroacetic acid) (PO-containing samples). The concentration of OS or PO within the samples was determined using the HPLC/UV assays described in Section 4.3.6.2.

4.3.6. Analytical methods

4.3.6.1. Chromatographic assays for fentanyl quantification in permeation, partitioning, and saturated solubility samples

Fentanyl concentrations within the permeation, partitioning (aqueous phase), and saturated solubility samples were determined using the reverse phase HPLC/UV methods described in Chapter 2 (Section 2.3.5).

4.3.6.2. Chromatographic assays for octisalate and padimate O quantification in surface wipe extracts, and saturated solubility samples

The concentration of OS or PO within the surface wipe extracts and the saturated solubility samples was determined using reverse phase HPLC in conjunction with UV detection. The HPLC system consisted of a Waters 610 pump, Waters 600E system controller, Waters 712 WISP autosampler, and Waters 486 UV absorbance detector. The data was analysed on a Shimadzu C-R6A integrator (Shimadzu Corp., Japan).

Quantification of OS or PO was performed using a Waters Symmetry C₈ cartridge column (5 μ m particle size, 3.9 x 150 mm) and a RP-8 Newguard cartridge guard column

(Aquapore 7 μm , 3 x 15 mm, Alltech/Perkin Elmer, CA, USA). Further details of the individual HPLC/UV assay conditions are given in Table 4.2.

Stock solutions were prepared by dissolving OS or PO in 95%v/v ethanol to yield a concentration of 50 $\mu\text{g/ml}$. Standard solutions were prepared by diluting aliquots of stock solution to appropriate volumes with mobile phase in order to yield concentrations within the range of 0.1 to 10 $\mu\text{g/ml}$. Calibration curves for each assay were constructed by plotting peak area against concentration. The linearity of each calibration curve (weighted by a factor of $1/x$) was confirmed by the correlation coefficient generated by linear regression (using a least squares method). The linearity of each assay was excellent as the gradient of each calibration curve was always statistically different from 0 ($p < 0.01$) and the correlation coefficients were always greater than 0.995.

Intra-day precision and accuracy were determined from standard solutions prepared at three different concentrations (0.1, 1 and 10 $\mu\text{g/ml}$) ($n = 5$). Intra-day precision and accuracy were highly satisfactory as precision (%CV) ranged from 3.3 to 9.0% (OS HPLC/UV assay) and 1.6 to 7.5% (PO HPLC/UV assay) and accuracy ranged from 102.0 to 107.2% (OS HPLC/UV assay) and 95.0 to 103.0% (PO HPLC/UV assay).

Inter-day precision was determined by analysing standard solutions ($n = 5$) prepared at 0.1, 1 and 10 $\mu\text{g/ml}$ over three different days. The inter-day precision of each assay was excellent as precision (%CV) ranged from 0.69 to 4.8% and 0.8 to 6.9% for the OS and PO HPLC/UV assays, respectively.

Table 4.2. HPLC/UV assay conditions for octisalate and padimate O

Injection volume (μl)		Mobile phase Composition (%v/v)	Flow rate (ml/min)	Detection wavelength (nm)	Retention time (min)
OS	20	85%v/v acetonitrile, 15%v/v water containing 0.27%v/v trifluoroacetic acid	1	240	~5.6
PO	10	82%v/v acetonitrile, 18%v/v water containing 0.22%v/v trifluoroacetic acid	1	310	~5.5

4.3.7. Mathematical analysis

4.3.7.1. Fentanyl diffusional parameters derived from infinite dose skin diffusion studies

Permeation profiles generated from the infinite dose diffusion studies were fitted to the solution of Fick's second law of diffusion described in Equation 4.1. For these studies, the diffusional pathlength of the SC was assumed to be 13 μm (16). As the donor solution was saturated with fentanyl and was applied to the skin at a sufficiently large dose, it was assumed that the concentration of fentanyl within the donor solution (C_v) did not significantly deplete over the duration of the experiment. Hence, C_v was replaced by the saturated solubility of fentanyl in water (91.47 $\mu\text{g/ml}$ at 32°C, (Chapter 2, Section 2.4.1)).

The parameters $K_{SC/V}h$ and D/h^2 in Equation 4.1 were replaced by the terms a and b , respectively⁴. The parameters a and b were derived by fitting the permeation data to the theoretical equation, using a computer software package (SigmaPlot®, Version 8.01, SPSS Inc., USA). A non-linear least squares method was used to fit the data. The permeability coefficient, K_p , was then calculated by multiplying the parameters a and b , which is therefore equivalent to the expression (38):

$$K_p = \frac{K_{SC/V}D}{h} \quad 4.5$$

Fentanyl flux (J) across the skin was calculated from the permeability coefficient, where:

$$J = K_p \times C_v \quad 4.6$$

The magnitudes by which ethanol alone or ethanol containing either OS or PO enhanced the fentanyl diffusional parameters (i.e. J , K_p , $K_{SC/V}$ or D) were defined in terms of enhancement ratios (ERs), where:

⁴ As the same donors were used for all diffusion experiments, it was assumed that the thickness of the SC did not significantly differ.

$$ER = \frac{\text{Parameter derived from skin pretreated with ethanol alone or ethanol containing OS or PO}}{\text{Parameter derived from untreated skin}} \quad 4.7$$

In order to challenge the mathematical model, ERs for the various diffusional parameters were also determined following pretreatment of the skin with ethanolic solutions containing putative chemical penetration enhancers (oleic acid, Transcutol® or Azone®).

4.3.8.3. Partition coefficient of fentanyl between human stratum corneum and water

The apparent partition coefficient of fentanyl between isolated human SC and water ($K_{SC/W}$) was calculated according to the following equation (17):

$$K_{SC/W} = \frac{K^*}{\rho_D} \times \frac{W_D}{V_H} \quad 4.8$$

Where:

$$K^* = \frac{\text{Mass } (\mu\text{g}) \text{ of fentanyl} / \text{Mass (mg) of dessicated SC}}{\text{Mass } (\mu\text{g}) \text{ of fentanyl} / \text{Mass (mg) of donor solution}}$$

$$\rho_D = \text{Density of the aqueous fentanyl solution (g/cm}^3\text{)}$$

$$W_D = \text{Mass (g) of desiccated SC}$$

$$V_H = \text{Volume (cm}^3\text{) of hydrated SC, which is determined from the weight of the SC after 24 h immersion in the donor solution (assuming that the SC has a density of 1 g/cm}^3\text{ (39) and that the density of the donor solution did not significantly alter the density of the SC).}$$

In order to correct for the effects of fentanyl ionisation, the intrinsic partition coefficient of fentanyl free base between the SC and water ($K_{SC/W (INT)}$) was calculated using the following equation (26, 40):

$$K_{SC/W (INT)} = K_{SC/W} [10^{(pK_a - pH)} + 1] \quad 4.9$$

where the pH term in Equation 4.9 refers to the pH of the aqueous phase. Based on

previous research, it was assumed that fentanyl has a pK_a value of 8.99 (41).

The ERs generated for the apparent and intrinsic partition coefficients of fentanyl between the SC and water were calculated according to Equation 4.7.

4.3.8.4. Partition coefficients of fentanyl between liquid organic phases and water

The apparent partition coefficients of fentanyl between the organic phases (OS, PO, OCT or IPM (alone or with OS or PO added)) and water ($K_{ORG/W}$) were calculated using the following equation (42):

$$K_{ORG/W} = \frac{A_{ORG}}{V_{ORG}} \times \frac{V_W}{A_W} \quad 4.10$$

Where A_{ORG} and A_W is the amount (μg) of fentanyl in the organic phase or water at 24 h, respectively. V_{ORG} and V_W is the volume (ml) of organic phase and water. It should be noted that A_{ORG} was calculated by the difference in the amount of fentanyl initially dissolved in the organic phase and the amount of fentanyl present within the water phase at 24 hours (A_W).

In order to correct for the effects of fentanyl ionisation, the intrinsic partition coefficient of fentanyl free base between the organic phase and water ($K_{ORG/W (INT)}$) was calculated using Equation 4.9. Enhancement of the apparent and intrinsic partition coefficients of fentanyl between IPM and water by OS and PO was defined in terms of an ER, where:

$$ER = \frac{K_{IPM/W} \text{ or } K_{IPM/W (INT)} \text{ in the presence of OS or PO}}{K_{IPM/W} \text{ or } K_{IPM/W (INT)} \text{ in the absence of OS or PO}} \quad 4.11$$

4.3.8. Statistical analysis

Statistical significance was determined using one-way analysis of variance (ANOVA). Post-hoc all pairwise multiple comparison of the means within different groups was performed using the Student-Newman-Keuls (SNK) test. A probability of

$p < 0.05$ was considered statistically significant. All results are presented as the mean \pm SEM, unless otherwise stated.

4.6. RESULTS AND DISCUSSION

4.4.1. Diffusional parameters derived from "infinite dose" skin diffusion studies.

The profiles representing fentanyl permeation of human epidermis, left untreated or pretreated with ethanol alone or ethanolic solutions containing 1 to 10%w/v OS or PO are presented in Figures 4.2 and 4.3. As discussed in Section 4.3.8.1, the permeation profiles were fitted to Equation 4.1 in order to derive the parameters K_p , J , $K_{sc/v}$ and D . These individual parameters, and the ERs for these parameters, are presented in Tables 4.3 and 4.4 and Figures 4.4 and 4.5, respectively. It should be noted that the permeability coefficient of fentanyl through untreated skin and its flux across untreated skin were 0.020 ± 0.001 cm/h and 1.80 ± 0.07 $\mu\text{g}/\text{cm}^2\text{h}$, respectively, which are in good agreement with previous research (40, 43-45).

Fentanyl permeability through skin pretreated with ethanol alone was slightly, though not significantly, higher compared to that through untreated skin. Despite this minimal effect on overall permeability, the apparent mechanisms involved in permeation through the skin were dramatically different following pretreatment with ethanol alone. In particular, the degree of fentanyl partitioning into the SC was significantly greater compared with untreated skin ($\text{ER}(K_{sc/v}) = 1.49 \pm 0.13$), whilst its diffusivity within the SC was slightly reduced ($\text{ER}(D) = 0.75 \pm 0.07$).

When the skin was pretreated with ethanolic solutions containing 1 to 10%w/v OS, fentanyl permeability was significantly enhanced ($p < 0.05$ compared with untreated skin). Furthermore, a strong correlation was observed between enhancement of fentanyl permeability and OS concentration ($r^2 = 0.986$). At the lowest concentration investigated (1%w/v), it appeared that enhancement of fentanyl permeability was mainly a consequence of improved fentanyl diffusion through the SC ($\text{ER}(D) = 1.43 \pm 0.14$, $p < 0.05$ compared with untreated and ethanol-pretreated skin).

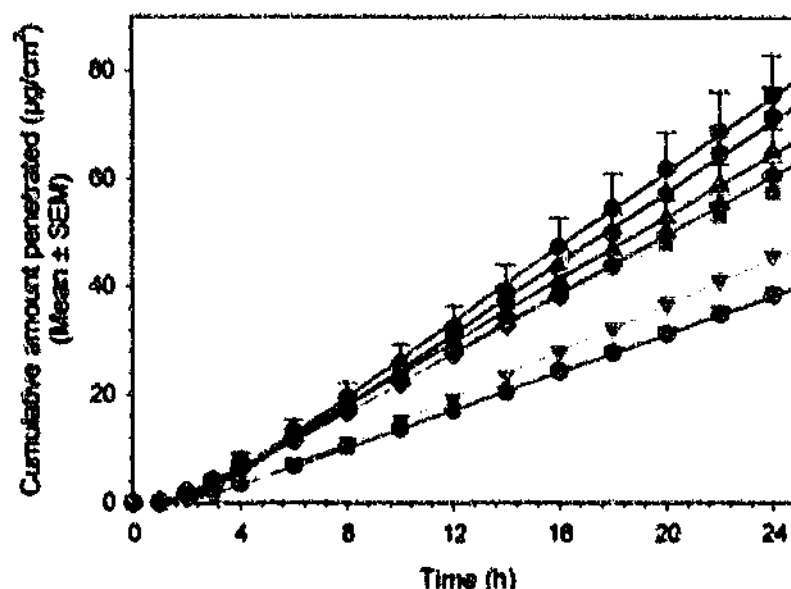


Figure 4.2. Profiles representing fentanyl permeation of human epidermis under "infinite dose" conditions. The symbols represent fentanyl permeation through untreated epidermis (●) ($n=64$) or epidermis pretreated for 2 h with ethanol alone (▼) ($n=5$) or ethanolic solutions containing 1%w/v OS (⊠) ($n=5$), 2.5%w/v OS (◆) ($n=6$), 5%w/v OS (▲) ($n=6$), 7.5%w/v OS (●) ($n=6$), or 10%w/v OS (●) ($n=5$). The solid lines represent a non-linear regression of the data to Equation 4.1 ($r^2 > 0.999$, standard error of the estimate (SEE) < 0.80 and $p < 0.0001$ for all profiles).

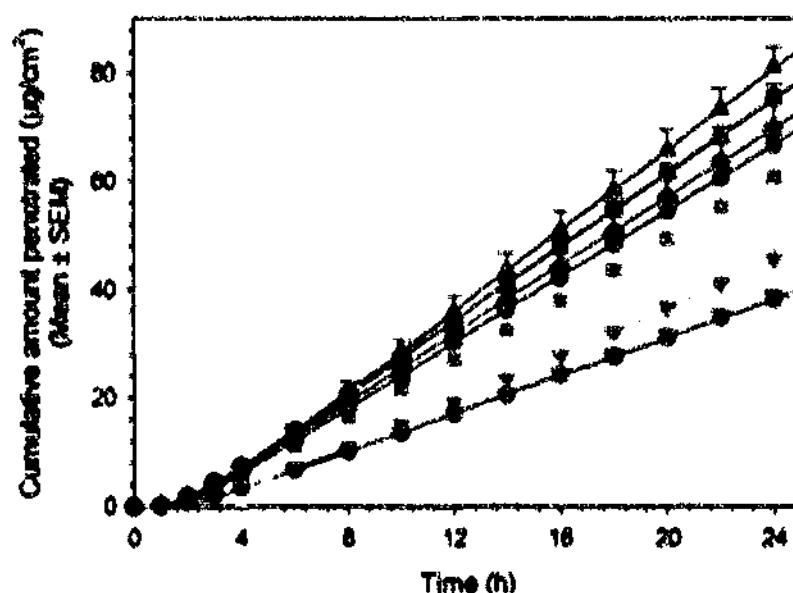


Figure 4.3. Profiles representing fentanyl permeation of human epidermis under "infinite dose" conditions. The symbols represent fentanyl permeation through untreated epidermis (●) ($n=64$) or epidermis pretreated for 2 h with ethanol alone (▼) ($n=5$) or ethanolic solutions containing 1%w/v PO (⊠) ($n=7$), 2.5%w/v PO (◆) ($n=6$), 5%w/v PO (▲) ($n=5$), 7.5%w/v PO (●) ($n=6$), or 10%w/v PO (●) ($n=6$). The solid lines represent a non-linear regression of the data to Equation 4.1 ($r^2 > 0.999$, standard error of the estimate (SEE) < 0.33 and $p < 0.0001$ for all profiles).

Table 4.3. Diffusional parameters derived from fentanyl permeation of human epidermis that had been left untreated or pretreated with ethanol alone (0%w/v OS) or ethanolic solutions containing 1 to 10%w/v OS ($4 < n < 64$).

OS concentration (%w/v)	K _p (cm/h)	Flux ($\mu\text{g}/\text{cm}^2\text{h}$)	K _{ACV}	D ($\text{cm}^2/\text{h} \times 10^{-7}$)
Untreated	0.020 ± 0.001	1.80 ± 0.07	234 ± 16	1.10 ± 0.08
0	0.022 ± 0.001	2.00 ± 0.08	$348 \pm 31^*$	0.82 ± 0.07
1	$0.029 \pm 0.001^*$	$2.65 \pm 0.11^*$	240 ± 23	$1.57 \pm 0.07^*$
2.5	$0.031 \pm 0.002^*$	$2.81 \pm 0.15^*$	310 ± 24	1.29 ± 0.13
5	$0.034 \pm 0.002^*$	$3.14 \pm 0.20^*$	$372 \pm 24^*$	1.20 ± 0.02
7.5	$0.038 \pm 0.003^*$	$3.50 \pm 0.33^*$	$428 \pm 34^*$	1.16 ± 0.24
10	$0.040 \pm 0.003^*$	$3.69 \pm 0.30^*$	$453 \pm 42^*$	1.16 ± 0.06

* Statistically significant difference compared with control (untreated epidermis) ($p < 0.05$)

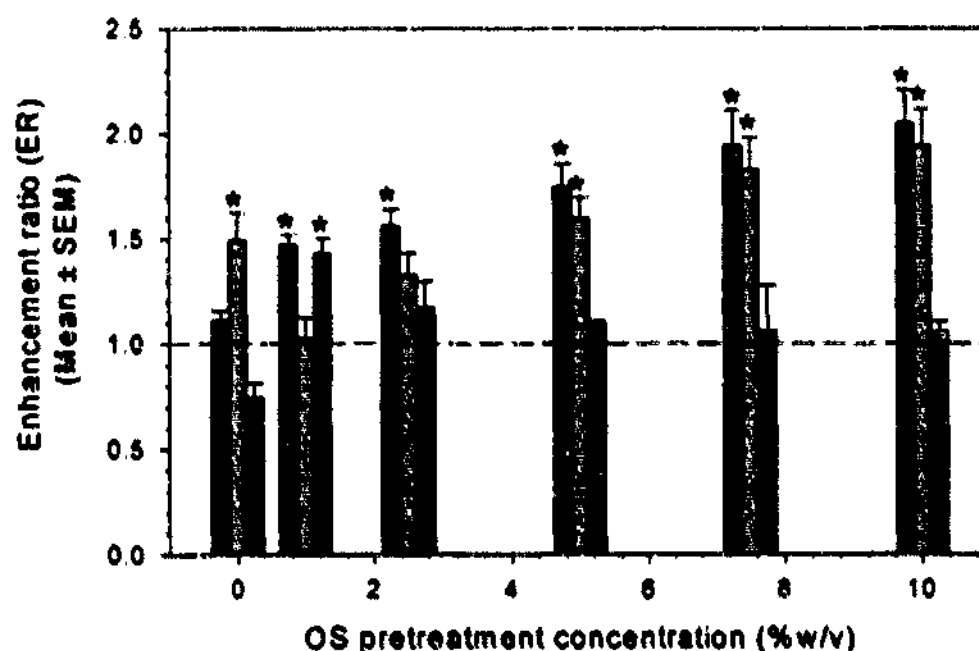


Figure 4.4. Enhancement ratios (ERs) for the diffusional parameters (K_p or J (□), K_{ACV} (▨) and D (■)) derived from fentanyl permeation of human epidermis pretreated with 95%v/v ethanol alone (0%w/v OS) or ethanolic solutions containing 1 to 10%w/v OS. ER=1 is equivalent to no enhancement (shown by the dotted line). * corresponds to an ER where the parameter generated from skin pretreated with OS was significantly different compared with that generated from untreated skin (control) ($p < 0.05$) ($4 < n < 32$).

Table 4.4. Diffusional parameters derived from fentanyl permeation of human epidermis that had been left untreated or pretreated with ethanol alone (0%w/v PO) or ethanolic solutions containing 1 to 10%w/v PO (4<n<64).

PO concentration (%w/v)	K _p (cm/h)	Flux (µg/cm ² h)	K _{scv}	D (cm ² /h x 10 ⁻⁷)
Untreated	0.020 ± 0.001	1.80 ± 0.07	234 ± 16	1.10 ± 0.08
0	0.022 ± 0.001	2.00 ± 0.08	348 ± 31*	0.82 ± 0.07
1	0.026 ± 0.002*	2.09 ± 0.26*	309 ± 30	1.08 ± 0.11
2.5	0.033 ± 0.002*	3.01 ± 0.20*	373 ± 30*	1.16 ± 0.15
5	0.041 ± 0.003*	3.91 ± 0.21*	460 ± 30*	1.17 ± 0.12
7.5	0.037 ± 0.002*	3.50 ± 0.15*	386 ± 28*	1.26 ± 0.06
10	0.034 ± 0.001*	3.33 ± 0.09*	312 ± 18	1.41 ± 0.10

* Statistically significant difference compared with control (untreated epidermis) (p<0.05)

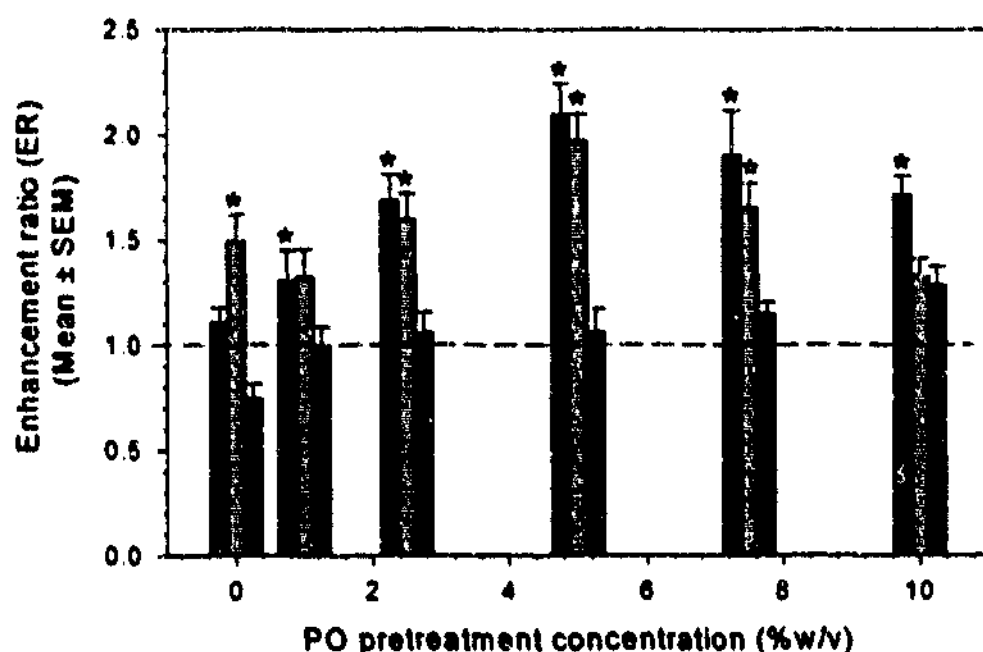


Figure 4.5. Enhancement ratios (ERs) for the diffusional parameters (K_p or J (■), K_{scv} (■) and D (■)) derived from fentanyl permeation of human epidermis pretreated with 95%v/v ethanol alone (i.e. 0%w/v PO) or ethanolic solutions containing 1 to 10%w/v PO. ER=1 is equivalent to no enhancement (shown by the dotted line). * corresponds to an ER where the parameter generated from skin pretreated with PO was significantly different compared with that generated from untreated skin (control) (p<0.05) (4<n<32).

However, as the OS concentration was increased from 1 to 2.5%w/v, it was evident that the effect of OS on fentanyl diffusion within the SC was attenuated, whilst its effect on fentanyl partitioning concomitantly increased. Whilst the effect of OS on fentanyl diffusion within the SC remained relatively unchanged as the OS concentration was further elevated to 5, 7.5 and 10%w/v, fentanyl partitioning into the SC progressively increased. Consequently, a very good correlation seemed to exist between enhancement of fentanyl partitioning and OS concentration ($r^2 = 0.933$ between 1 to 10 %w/v OS concentration).

Compared with untreated skin, PO also significantly enhanced fentanyl permeability through the skin at all concentrations investigated. At concentrations between 1 to 5%w/v, the ratio by which PO enhanced fentanyl permeability appeared to increase with increasing PO concentration, with a maximum $ER(K_p)$ of 2.09 ± 0.13 observed at 5%w/v PO. However, as the PO concentration was further increased to 7.5 and 10%w/v, enhancement of fentanyl permeability declined to $ER(K_p)$ of 1.95 ± 0.09 and 1.74 ± 0.06 , respectively.

A similar relationship was observed between enhancement of fentanyl partitioning and PO concentration, such that maximum enhancement of fentanyl partitioning was observed at 5%w/v ($ER(K_{SC/V}) = 1.91 \pm 0.12$). However, slight reductions in the $ER(K_{SC/V})$ were incurred as the concentration of PO was further increased to 7.5 and 10%w/v. Due to the magnitudes of these reductions, fentanyl partitioning into skin pretreated with 7.5 %w/v PO was still significantly higher compared with untreated skin ($ER(K_{SC/V}) = 1.54 \pm 0.12$), though it was only marginally enhanced following pretreatment with 10 %w/v ($ER(K_{SC/V}) = 1.44 \pm 0.08$).

At these higher concentrations, the effect of PO on fentanyl diffusivity within the SC also appeared to change – though only slightly. At concentrations up to 5 %w/v, PO appeared to exert no effect on fentanyl diffusion through the SC ($ER(D)$ ranged from 0.98 ± 0.1 at 1%w/v to 1.07 ± 0.1 at 5%w/v). However, as the concentration of PO was increased from 5%w/v to 7.5 and 10 %w/v, fentanyl diffusivity through the SC marginally increased, such that the $ER(D)$ was 1.28 ± 0.10 at 10%w/v PO.

In order to confirm the validity of these results, the effects of putative CPEs (Azone®, oleic acid and Transcutol®) were investigated using the infinite dose technique in conjunction with the mathematical model described in Section 4.3.8.1. The ERs generated from these analyses are presented in Figure 4.6. As seen in Figure 4.6, 5%w/v

Azone[®] significantly enhanced fentanyl permeability through human epidermis compared with untreated skin ($ER(K_p)=1.82 \pm 0.13$) and this effect appears mostly due to enhanced partitioning into the SC ($ER(K_{SC/V})=1.47 \pm 0.09$, $p<0.05$ compared with untreated skin). On the other hand, Azone[®] had little effect on fentanyl diffusivity within the SC ($ER(D)=0.94 \pm 0.05$).

Although the exact mechanisms by which Azone[®] enhances solute permeability through the SC are still under investigation, there is strong evidence to suggest that Azone[®] interacts with intercellular SC lipids to increase the degree of fluidity of the hydrophobic regions of the lipid lamellae, which is likely to reduce the diffusional resistance within the SC lipid domain (46-53).

The results of several permeation studies have supported these findings as they generally indicate that the diffusion coefficients of numerous compounds are increased in the presence of Azone[®] (54-56). The effect of Azone[®] on solute diffusivity may also depend on its concentration as it has previously been observed that a somewhat parabolic relationship exists between enhancement of solute diffusivity and the concentration of Azone[®] within the SC, with maximum enhancement observed at a SC loading of ~12%w/w (47). However, even at enhancer loadings of up to ~25%w/w, the diffusivity of the lipophilic compound, diazepam, within Azone[®]-treated skin was still higher compared with the corresponding control. Given that the SC may have been loaded with up to ~19%w/w of Azone[®] during the studies presented in this chapter it was somewhat unexpected that Azone[®] was found to exert no effect on fentanyl diffusivity within the SC.

Using the model hydrophilic compound 4-cyanophenol, Harrison et al (21) also attempted to identify the mechanisms by which Azone[®] enhanced solute permeability by fitting skin diffusion data to Equation 4.1. However, it was found that application of the deconvolution technique to skin diffusion data was unable to detect significant changes in solute diffusivity compared with control. Although these investigators reported that the small enhancement ratio (<2) generated from these studies may have led to an inability to detect changes in solute partitioning and diffusion, other possible explanations will be discussed in forthcoming paragraphs.

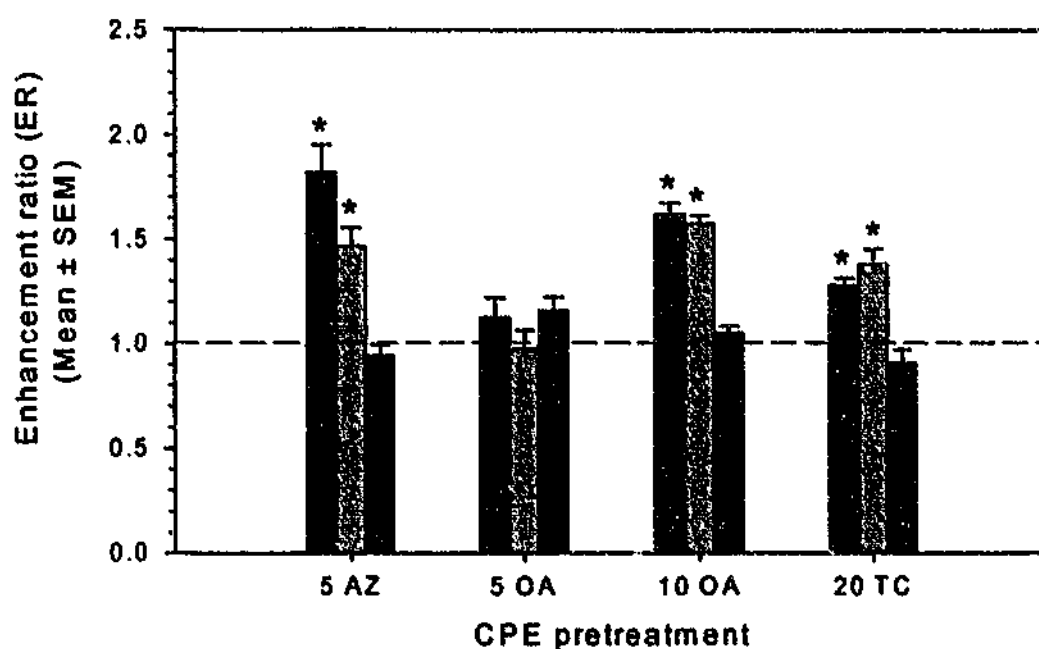


Figure 4.6. Enhancement ratios (ERs) for the diffusional parameters (K_p or J (■), $K_{sc/v}$ (▨) and D (■)) derived from fentanyl permeation through human epidermis pretreated with ethanolic solutions containing 5%w/v Azone® (5 AZ) ($n=4$), 5%w/v oleic acid (5 OA) ($n=5$), 10%w/v oleic acid (10 OA) ($n=5$) or 20%w/v Transcutol® (20 TC) ($n=5$). ER=1 is equivalent to no enhancement (shown by the dotted line). * corresponds to an ER where the parameter generated from skin pretreated with the CPE is significantly different compared with that generated from untreated skin (control) $p<0.05$.

Whilst the majority of research into the mechanism(s) of action of Azone® support the notion that it enhances solute diffusivity within the SC, there is some evidence to suggest that it can also increase solute partitioning into the SC (19, 24, 57). However, this effect may depend on the concentration of Azone® used and the lipophilicity of the solute in question. For instance, it has been reported that at a concentration of 5%w/w Azone®, enhancement of solute partitioning is limited to compounds which possess a $\log K_{OCT/w}$ value of up to ~ 2.7 (19). Given that fentanyl has a $\log K_{OCT/w}$ value of 2.86 (40) and that the solubility parameter of Azone® is close to that of fentanyl ($\delta = 18.53 \text{ MPa}^{1/2}$ for Azone® (50) and $\delta = 19.64 \text{ MPa}^{1/2}$ for fentanyl (4)) it is not surprising that Azone® appeared to increase fentanyl partitioning into the SC.

Analogous to 5%w/v Azone®, 10%w/v oleic acid also appeared to enhance fentanyl permeability through the skin by increasing its skin-vehicle partition coefficient ($ER(K_p)=1.62 \pm 0.05$ and $ER(K_{sc/v})=1.57 \pm 0.04$, $p<0.05$ compared with untreated skin (for both parameters)). However, at a concentration of 5%w/v, oleic acid appeared to

exert little or no effect on fentanyl permeability and partitioning. At both concentrations investigated, oleic acid appeared to exert only a marginal effect on fentanyl diffusivity, with $ER(D) = 1.15 \pm 0.07$ and 1.05 ± 0.03 at 5 and 10%w/v, respectively. As with Azone[®], the mechanisms of action of oleic acid have been widely studied using a variety of *in vitro* techniques (58). Based on the results obtained from early spectrophotometric and calorimetric studies, it has been postulated that oleic acid reduces the diffusional resistance of the intercellular SC lipids by increasing the fluidity of the lipid bilayers (53, 59-61). However, more recent infrared spectroscopic studies have demonstrated that oleic acid does not globally modify the conformational order of the SC lipids, but rather decreases lipid viscosity and/or produces "defects" by forming separate fluid phases within the "solid" lipid domains within the SC (59, 62, 63). Consequently, it is thought that oleic acid may enhance transdermal permeability through a dual mechanism (involving lipid conformational permutations and phase separation) that ultimately perturbs the SC lipid bilayer structure (62). It therefore seems reasonable to question the finding that oleic acid did not significantly enhance fentanyl diffusivity within the SC.

In addition to its effect on SC lipids, oleic acid has also been found to increase solute partitioning into the SC (64-68). Various mechanisms have been proposed for this effect. For instance, fatty acids have been found to increase the permeation rate of the polar solvent, propylene glycol (66, 69). Thus, it has been suggested that fatty acids may enhance solute partitioning by a "solvent-drag" mechanism. Given that the oleic acid was delivered to the skin using the polar solvent, ethanol, and that ethanol was found to have a favourable effect on fentanyl partitioning, it is therefore possible that oleic acid enhances fentanyl partitioning by increasing the partitioning of ethanol into the SC during the pretreatment period. Another proposed mechanism pertains to the notion that cationic compounds can "ion-pair" with oleic acid (67, 70). Due to the formation of an electrically neutral species, this effect may facilitate the transport of the more hydrophilic, ionised form of the solute in question (71). As fentanyl is a weakly basic compound ($pK_a = 8.99$ (41)), it is likely to exist in its unionised and ionised forms within the donor solution (water saturated with fentanyl was found to have a pH value of 9.22 (per Chapter 2, Section 2.4.1)) and within the SC (in which the pH may vary from ~5 to ~7 (72, 73). Consequently, it is possible that enhancement of fentanyl partitioning could be partly due to the pairing of cationic fentanyl species with oleic acid.

Unlike oleic acid and Azone[®], the mechanism(s) by which Transcutol[®] is believed to enhance solute permeability are solely confined to its effect on solute partitioning. In particular, it has been suggested that Transcutol[®] enhances solute flux across the SC by altering the solubility parameter of the SC (21, 56, 74). Hence, the finding that Transcutol[®] enhances fentanyl partitioning and not its diffusivity is consistent with the findings from other investigators.

In summary, the theoretical model proposed in Equation 4.1 seems capable of detecting changes in fentanyl partitioning. However, it is evident from the above-mentioned research conducted into the mechanisms of action of oleic acid and Azone[®] that it may be insensitive to changes in fentanyl diffusivity. The suspected "inability" of the model to detect significant changes in fentanyl diffusivity may be due to a number of factors, for instance:

- i. The ERs generated for the diffusion coefficient of fentanyl were too small and/or the error associated with the fitted values of D were too excessive to detect statistical significance (ER(D) was less than 1.43 and %CV ranged from 1.47 to 20.34)
- ii. The model assumes a constant membrane thickness (h) (which was assumed to be 13 μm)
- iii. The model assumes that the epidermis does not act as a barrier towards fentanyl permeation
- iv. Water present in the donor solution may permeate into the SC, which could possibly "mask" the effects of OS and PO on fentanyl diffusivity.

In relation to membrane thickness, the value of 13 μm assumes that fentanyl permeates the SC via a transcellular pathway. On the other hand, if drug permeation occurs mostly via the intercellular lipid region, then the diffusional pathlength is believed to be of the order of 350 to 880 μm (75, 76). Regardless of which of these values accurately describes the pathlength for drug permeation through the SC, the model described in Section 4.1 fails to recognise the tortuosity of the highly organised SC lipids (13, 16, 77) and the potential for CPEs to alter this parameter. This limitation could be quite significant when studying the mechanisms of action of CPEs that may alter the diffusional resistance of the SC lipids as, under these circumstances, it is unlikely that the

effective diffusional pathlength through SC treated with a CPE will be the same as that through untreated SC.

Although the SC is believed to be a rate-limiting barrier towards the permeation of most substances, the underlying epidermis may also act as an aqueous boundary layer, and therefore assume rate control, during the percutaneous absorption of highly lipophilic compounds (i.e. $\log K_{OC/W} > 2$) (78). Although previous research has demonstrated that the SC is the principle barrier for the transport of fentanyl (44, 45), one particular study has shown that the aqueous strata of human skin may also impose some degree of resistance towards fentanyl permeation (40). Although this aqueous resistance to fentanyl diffusion does not appear to be as significant as the resistance imposed by the SC itself, it is possible that the effects of OS and PO on fentanyl diffusivity in the SC were "under-estimated" because the epidermis also contributes to the total resistance imposed on fentanyl diffusion.

A final point to note is that the SC can imbibe copious amounts of water (upon contact with liquid water) (79-82). As this phenomenon has also been observed after brief exposure times (i.e. 2 to 6 h) (83, 84), it is probable that water present within the donor solution hydrated the SC to hyper-physiological levels during the diffusion experiments presented in this chapter. Due to the low solubility of water in the lipid lamellae (SC lipids may be maximally hydrated at less than one water molecule per lipid molecule (85)) and evidence to suggest that SC hydration does not cause "swelling" or disordering of the intercellular lipid lamellae (86, 87) it has been suggested that most water contained within hydrated SC is either absorbed in the corneocytes or forms separate phases within the intercellular lipid region (85). This notion has been further supported by various electron microscopic experiments, which have revealed that high levels of SC hydration result in water uptake by the corneocytes and the formation of separate water domains in the intercellular space (80, 84, 88, 89). On the other hand, however, there is also evidence to suggest that hyper-physiological levels of water may induce SC lipid disorder (90-94). In light of these previous findings, it is possible that high levels of SC hydration obscured the enhancing effects of OS and PO on fentanyl diffusivity as a result of physical (e.g. the SC lipids may reach a state of maximal "perturbation" due to the formation of separate water domains and/or fluidisation) and/or chemical alterations (e.g. the intercellular space may become a more "polar" environment).

Due to these possible limitations, it is difficult to ascertain whether the data generated from this model provide an accurate depiction of the mechanisms of action of OS and PO or whether the effects of OS and PO on fentanyl diffusivity were confounded by experimental artifacts. Due to this uncertainty, it was necessary to employ other experimental methods to investigate the mechanism(s) of action of OS and PO. Therefore, the remainder of this chapter focuses on other methods for determining the effect of OS and PO on fentanyl partitioning into the SC, whilst the research presented in Chapter 7 was intended to investigate some of the effects of OS and PO on SC lipids.

4.4.2. Fentanyl partitioning between isolated human stratum corneum and water

The apparent and intrinsic partition coefficients generated from fentanyl partitioning between isolated human SC (untreated or pretreated with OS or PO) and water are shown in Tables 4.5 and 4.6⁵. The ERs generated from these values are compared to those generated from the infinite dose skin diffusion studies in Figures 4.7 and 4.8.

It is important to note that the apparent partition coefficients (i.e. the $K_{SC/W}$ values) generated from the partitioning of fentanyl between untreated SC and water are in good agreement with that derived from the "infinite dose" skin diffusion studies ($K_{SC/W} = 210 \pm 7$ (OS control) and $K_{SC/W} = 128 \pm 5$ (PO control) versus $K_{SC/W} = 234 \pm 16$). Furthermore, the $ER(K_{SC/W})$ values produced for OS and PO from the SC-water partitioning studies are very similar to those obtained from the diffusion studies (statistically significant differences among the corresponding ER values were not detected at any of the OS or PO concentrations investigated). It is also evident from the aqueous phase pH values shown in Tables 4.5 and 4.6 that the presence of either OS or PO within the SC did not significantly alter the pH of the aqueous bathing solution. Consequently, similar trends were apparent between either $ER(K_{SC/W})$ or $ER(K_{SC/W (INT)})$ and OS or PO pretreatment concentration (Figures 4.7 and 4.8).

⁵ Differences between the values reported in Tables 4.5 and 4.6 for untreated and ethanol-treated SC samples appear to be largely due to differences between i) the initial concentration of fentanyl in the donor solution (~62 µg/ml for OS experiments versus ~45 µg/ml for PO experiments) and ii) the level of SC hydration (refer to Appendix II)

Table 4.5. Apparent and intrinsic partition coefficients of fentanyl between isolated human SC and water ($K_{SC/W}$ or $K_{SC/W (INT)}$) and aqueous phase pH (measured at $t = 24h$). The SC was either left untreated or pretreated with ethanol alone (0%w/v OS) or ethanolic solutions containing 1 to 10%w/v OS ($n=5$).

OS pretreatment concentration (%w/v)	$K_{SC/W}$	$K_{SC/W (INT)}$	Aqueous phase pH
Untreated	210 ± 7	6390 ± 194	7.52 ± 0.00
0	264 ± 18	7967 ± 445	7.52 ± 0.01
1	211 ± 20	6434 ± 585	7.52 ± 0.00
2.5	235 ± 14	7219 ± 486	7.52 ± 0.01
5	$278 \pm 8^*$	$8657 \pm 235^*$	7.51 ± 0.01
7.5	$318 \pm 11^*$	$10036 \pm 557^*$	7.51 ± 0.01
10	$340 \pm 19^*$	$10838 \pm 675^*$	7.50 ± 0.01

* Statistically significant difference compared with control (untreated SC) ($p < 0.05$)

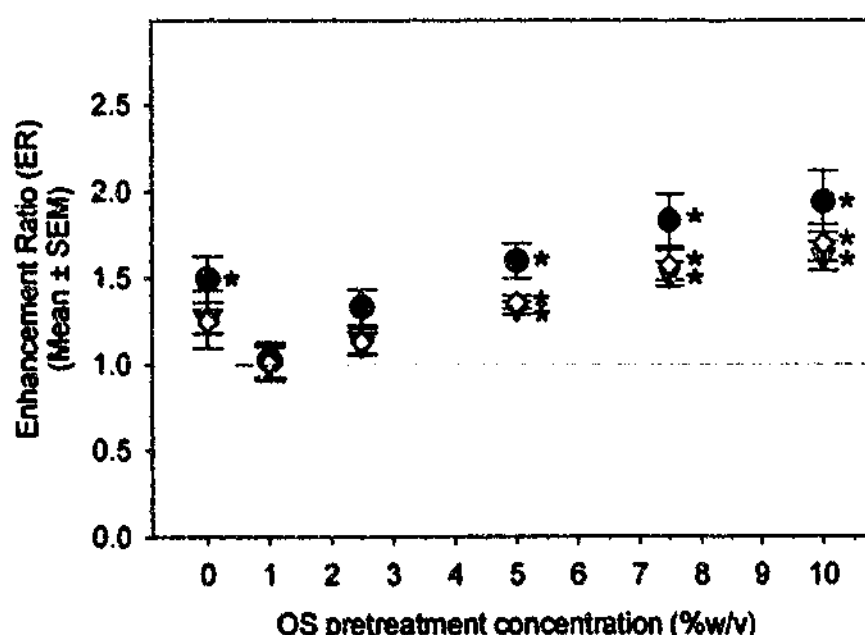


Figure 4.7. Enhancement ratios (ERs) for the apparent partition coefficient of fentanyl between human SC (pretreated with ethanol alone (0%w/v OS) or ethanolic solutions containing 1 to 10%w/v OS) and water derived from infinite dose skin diffusion studies (●) ($4 < n < 32$) or SC-water partitioning studies (▼) ($n=5$). ERs for the intrinsic partition coefficient of fentanyl free base between human SC and water (derived from the SC-water partitioning studies) are also shown (◇). $ER=1$ is equivalent to no enhancement (shown by the dotted line). * corresponds to statistically significant difference compared with control (untreated epidermis or SC) ($p < 0.05$).

Table 4.6. Apparent and intrinsic partition coefficients of fentanyl between isolated human SC and water ($K_{SC/W}$ or $K_{SC/W(INT)}$) and aqueous phase pH (measured at $t = 24h$). The SC was either left untreated or pretreated with ethanol alone (0%w/v PO) or ethanolic solutions containing 1 to 10%w/v PO ($n=5$).

PO pretreatment concentration (%w/v)	$K_{SC/W}$	$K_{SC/W(INT)}$	Aqueous phase pH
Untreated	128 ± 5	5214 ± 181	7.39 ± 0.00
0	144 ± 17	5781 ± 620	7.39 ± 0.01
1	129 ± 12	5382 ± 614	7.38 ± 0.02
2.5	223 ± 24*	8861 ± 808*	7.40 ± 0.02
5	257 ± 35*	10265 ± 820*	7.39 ± 0.03
7.5	225 ± 12*	9397 ± 474*	7.38 ± 0.00
10	171 ± 13	7342 ± 626	7.37 ± 0.01

* Statistically significant difference compared with control (untreated SC) ($p<0.05$)

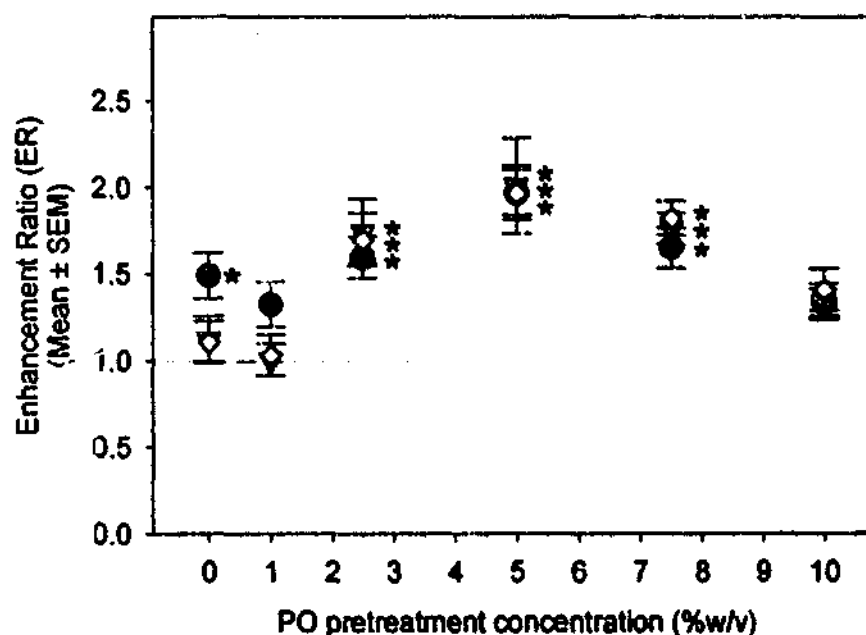


Figure 4.8. Enhancement ratios (ERs) for the apparent partition coefficient of fentanyl between human SC (pretreated with ethanol alone (0%w/v PO) or ethanolic solutions containing 1 to 10%w/v PO) and water derived from infinite dose skin diffusion studies (●) ($4<n<32$) or SC-water partitioning studies (▼) ($n=5$). ERs for the intrinsic partition coefficient of fentanyl free base between human SC and water (derived from the SC-water partitioning studies) are also shown (◇). ER=1 is equivalent to no enhancement (shown by the dotted line). * corresponds to statistically significant difference compared with control (untreated epidermis or SC) ($p<0.05$).

Hence, the ER values obtained from these SC-water partitioning studies confirm that:

- i. OS enhances fentanyl partitioning into the SC in a concentration-dependent manner ($r^2=0.989$ and 0.990 for $ER(K_{SC/W})$ and $ER(K_{SC/W(INT)})$, respectively) and that fentanyl partitioning is significantly enhanced at OS concentrations at and above 5%w/v ($p<0.05$ compared with untreated SC)
- ii. A somewhat parabolic relationship exists between the concentration of PO applied to the SC and enhancement of fentanyl partitioning. Due to this parabolic trend, PO appears to exert a significant enhancing effect on fentanyl partitioning only at concentrations between 2.5 to 7.5%w/v ($p<0.05$ compared with untreated SC).

Due to the possible limitations associated with the diffusion model described in Equation 4.1 (Section 4.4.1), it is important to note that the correlation observed here validates the use of the model to elucidate the effects of OS and PO on fentanyl partitioning into the SC.

4.4.3. Fentanyl solubility in liquid organic phases

The saturated solubility of fentanyl in IPM, OCT, OS and PO, and the solubility parameters of these organic phases, are shown in Table 4.7. In the first instance, it is evident that the solubility of fentanyl in OS or PO is greater than its solubility in either IPM (by a factor of ~2.3 and ~2.8, respectively) or OCT (by a factor of ~1.7 and ~2.1, respectively). The significance of these findings to fentanyl partitioning becomes apparent when one considers that the partition coefficient of a solute between the SC and a vehicle can be defined by the ratio of its activity (or "effective" concentration) in the SC (a_{SC}) and the vehicle (a_V) (25):

$$K_{SC/V} = \frac{a_{SC}}{a_V} \quad 4.12$$

Table 4.7. Solubility parameters of fentanyl, ceramide 6 (CER-6), isopropyl myristate (IPM), octanol (OCT), octisalate (OS) and padimate O (PO)

Organic phase (Solvent)	Molar volume of solvent ^a (cm ³ /mole)	Fentanyl saturated solubility		Mole fraction solubility (x10 ⁻²)	Solubility Parameters					
					Hildebrand		Hansen ^f			
					δ of solvent (δ_1) (MPa ^{1/2})	$(\delta_1 - \delta_2)^{1/2}$ ^c	δ of solvent (δ_{T2}) (MPa ^{1/2})	$(\delta_{D1} - \delta_{D2})^2$	$(\delta_{P1} - \delta_{P2})^2$	$(\delta_{H1} - \delta_{H2})^2$
CER-6	-	-	-	-	-	-	20.07	16.69	2.62	10.84
IPM	308.42	57.23 ± 1.16	0.17	4.98	17.39	5.05	16.03	22.70	3.88	16.86
OCT	154.66	77.52 ± 2.05	0.23	3.44	21.07 ^e	2.05	21.04	6.94	2.08	15.62
OS	247.22	130.77 ± 1.47 ^b	0.39	8.76	21.74 ^e	4.42	21.27	8.53	10.13	5.84
PO	285.00	165.08 ± 1.93 ^b	0.49	12.27	18.35 ^d	1.04	19.26	8.04	2.78	3.59

^a Calculated using Molecular Modeling Pro software package (Version 5.1.7), ChemSW[®] Inc, where MV=density/molecular weight

^b Per Chapter 3 (Section 3.4.1)

^c Obtained from Sloan et al (2)

^d Estimated using Thermo Chemical Properties Estimation Software: Solubility Parameter Estimation from Fedor's Cohesive Energy (obtained from <http://www.pirika.com/chem/TCPEE/TCPE.htm>) where $\delta=(E/V)^{1/2}$, where E=cohesive energy (cal/mole) and V=molar volume (cm³/mole). The obtained values were divided by 2.0455 to convert from (cal/cm³)^{1/2} to MPa^{1/2}

^e The Hildebrand solubility parameter of fentanyl (δ_1) was assumed to be 19.64 MPa^{1/2} (4)

^f The total (Hildebrand) (δ_1), dispersion (δ_D), polar (δ_P) and hydrogen bonding (δ_H) solubility parameters were estimated using an empirically-based method (Molecular Modeling Pro Software Package (Version 5.1.7)). The Hansen solubility parameters of fentanyl and the solvent are designated by subscripts 1 and 2, respectively. For fentanyl the estimated parameters were $\delta_T = 21.97$ MPa^{1/2}, $\delta_D = 20.29$ MPa^{1/2}, $\delta_P = 4.67$ MPa^{1/2}, $\delta_H = 7.02$ MPa^{1/2}.

As $K_{SC/V}$ can be approximated by the relative solubility of the solute within each of these phases it would be reasonable to speculate that, at an elementary level, OS and PO enhance fentanyl partitioning into the SC by improving its relative affinity for the SC lipids (assuming that the solubility of fentanyl in either IPM or OCT approximates that in the SC lipids). In order to understand the possible mechanism(s) by which OS and PO enhance the solubility of fentanyl within these model organic phases, it is necessary to consider that the activity of a solute in solution is defined as (95):

$$a = X\gamma \quad 4.13$$

where the terms X and γ are the mole fraction and the activity coefficient of the solute in the solution, respectively.

In an ideal solution, the activity coefficient is assigned a value of unity (i.e. $\gamma = 1$) and therefore $a=X$. Thus, the activity of the solute in its standard state (i.e. the pure solid) (S) can be expressed in terms of its ideal solubility (X^0) (25, 42, 95):

$$\ln S = \ln X^0 \cong \frac{-\Delta H_f}{RT} \left[\frac{1}{T} - \frac{1}{T_m} \right] \quad 4.14$$

where ΔH_f is the molar heat of fusion, T_m is the melting point of the solute, R is the gas constant and T is absolute temperature. In a non-ideal solution, however, $\gamma < 1$ due to solute-solvent interactions and therefore the mole fraction solubility of the solute (X) becomes:

$$\ln X = \ln X^0 - \ln \gamma \cong \frac{-\Delta H_f}{RT} \left[\frac{1}{T} - \frac{1}{T_m} \right] - \ln \gamma \quad 4.15$$

The term $\ln \gamma$ in Equation 4.15 is essentially defined by the intermolecular forces of attraction that must be overcome in order to remove a molecule from the solute phase and deposit it in the solvent. These intermolecular interactions may be characterised as (25, 26, 95, 96):

- i. London dispersion forces
- ii. Dipole-dipole or induced dipole-dipole interactions
- iii. Hydrogen bonding, or electron exchange, forces

In the commonly-used Hildebrand solubility parameter approach, which was developed to predict how materials will interact with each other, $\ln \gamma$ is defined as (2):

$$\ln \gamma = [\delta_i - \delta_v]^2 \frac{V_i(\phi_v)^2}{RT} \quad 4.16$$

where δ_i and δ_v are the solubility parameters⁶ of the solute and the solvent, respectively, V_i is the molar volume of the solute and ϕ_v is the volume fraction of the solvent. By substituting Equation 4.16 into Equation 4.15 it is evident that a solute will have a high affinity for a solvent with a similar solubility parameter (i.e. the term $[\delta_i - \delta_v]^2$ is minimised).

As $K_{SC/V}$ can be defined in terms of Equation 4.16, this concept may also be relevant to the enhancing effect(s) of vehicles or CPEs on the partitioning of a solute into the SC (2):

$$\ln K_{SC/V} = \ln \gamma_v - \ln \gamma_{SC} = [\delta_i - \delta_v]^2 \frac{V_i \phi_v^2}{RT} - [\delta_i - \delta_{SC}]^2 \frac{V_i \phi_{SC}^2}{RT} \quad 4.17$$

Thus a CPE can increase the partition coefficient of a solute by shifting the solubility parameter of the SC closer to that of the solute (thus reducing the value for $[\delta_i - \delta_{SC}]^2$).

However, a major shortcoming of the Hildebrand solubility parameter approach is that it assumes that molecules predominantly interact through London dispersion forces and it therefore cannot be applied to systems that are capable of forming hydrogen and/or dipole-dipole bonds (95, 97). This limitation is somewhat apparent from the data presented in Table 4.7 as the rank order by which $[\delta_i - \delta_v]^2$ decreases is not consistent with

⁶ The Hildebrand solubility parameter, δ , is defined as $\delta = (E/V)^{1/2}$, where E is the energy of vaporisation and V is the molar volume of the solvent or solute in question.

the rank order by which fentanyl solubility increases. The observation that the saturated solubility (mg/ml) of fentanyl is approximately 1.7 times higher in OS than it is in OCT, although the solubility parameter of OCT is closer to that of fentanyl ($[\delta_{\text{FEN}} - \delta_{\text{OCT}}]^2 = 2.1$) than is the solubility parameter of OS ($[\delta_{\text{FEN}} - \delta_{\text{OS}}]^2 = 4.4$) highlights this incongruity. Furthermore, if the solubility parameter of the SC is in the order of 19.8 to 20.2 MPa^{1/2} (98), $[\delta_{\text{FEN}} - \delta_{\text{SC}}]^2$ will be approximately 0.03 to 0.31 (assuming that the solubility parameter of fentanyl is 19.64 MPa^{1/2} (4)). As these values are lower in magnitude than either $[\delta_{\text{FEN}} - \delta_{\text{OS}}]^2$ or $[\delta_{\text{FEN}} - \delta_{\text{PO}}]^2$ it would seem unlikely that OS and PO favourably alter the solubility parameter of the SC.

In an attempt to circumvent this particular limitation of the Hildebrand solubility parameter approach, multicomponent (or "partial") solubility parameters have been developed in order to predict solute solubility and to define the type and strength of the intermolecular forces that govern the 'compatibility' of a solute-solvent system (25, 99). For instance, the so-called Hansen solubility parameter approach defines the total (or Hildebrand) solubility parameter (δ_T) as (96):

$$\delta_T^2 = \delta_D^2 + \delta_P^2 + \delta_H^2 \quad 4.18$$

where δ_D , δ_P and δ_H describe the contributions of London dispersion forces, Keesom dipolar interactions and hydrogen bonding, respectively. This concept has been further developed by Skaarup in order to define the 'distance' (R_a) between a solvent and solute based on their respective partial solubility parameters (designated by subscripts 1 and 2, respectively) (96):

$$(R_a)^2 = 4(\delta_{D2} - \delta_{D1})^2 + (\delta_{P2} - \delta_{P1})^2 + (\delta_{H2} - \delta_{H1})^2 \quad 4.19$$

Equation 4.19 highlights the notion that materials that have similar Hansen solubility parameters will exhibit a high affinity for each other and the extent of the similarity in a given situation will determine the extent of their interaction.

As shown in Table 4.7, these concepts have been utilised in order to gain further insight into the possible mechanisms by which OS and PO interact with fentanyl. As ceramides are considered to play a key role in the lipid lamellae organisation, resistance

to environmental change and physical and chemical stress (100), the partial solubility parameters of ceramide 6 (CER-6) (which is believed to be the most powerful hydrogen bonding lipid (101)) have also been included in Table 4.7.

In terms of the parameter $[\delta_{D2}-\delta_{D1}]^2$, it is evident that the contribution of London dispersion forces towards the compatibility of fentanyl with OS and PO is comparable to that with OCT. On the other hand, the $[\delta_{D2}-\delta_{D1}]^2$ value derived between fentanyl and either IPM or CER-6 exceeds that of OS and PO. This discrepancy is most likely due to the presence of the longer alkyl chain within the structures of IPM and CER-6. Hence, if the δ_D of IPM more closely resembles that of the SC lipids (as exemplified by CER-6) than does the δ_D of OCT, it would be reasonable to speculate that the higher solubility of fentanyl in OS and PO (compared with IPM and presumably the SC lipids) may be partly due to this parameter. With regard to the $[\delta_{P2}-\delta_{P1}]^2$ parameter, it is evident that the difference between fentanyl and PO is similar to that between fentanyl and OCT, IPM or CER-6. On the other hand, the relatively large difference between the δ_P of fentanyl and the δ_P of OS may be related to presence of the phenolic hydroxyl and the carbonyl functional groups as both of these moieties are highly polarized. However, as the saturated solubility of fentanyl in OS is relatively high it would appear that the large variation in this parameter is not entirely reflective of the interaction capability of OS with fentanyl. On the other hand, the higher solubility of fentanyl in OS and PO (compared with OCT and IPM) is consistent with the lower $[\delta_{H2}-\delta_{H1}]^2$ values associated with these solvents. This observation could possibly suggest that the hydrogen bonding parameter is more significant than the dispersion or polar parameters in differentiating the solubility of fentanyl within each of these phases. As the $[\delta_{H2}-\delta_{H1}]^2$ values associated with OS and PO are also lower than the $[\delta_{H2}-\delta_{H1}]^2$ value calculated for CER-6, these findings may also indicate that hydrogen bonding (or electron-exchange) interactions between fentanyl and OS or PO play a key role in increasing the affinity of fentanyl for the SC lipid domain. However, the validity and significance of this hypothesis – particularly in relation to the possible effects of OS and PO on the solubility and partitioning of fentanyl in the SC lipid domain – will require further investigation. Unfortunately, such investigations are beyond the scope of the work presented in this thesis.

4.4.4. Fentanyl partitioning between liquid organic phases and water

The apparent and intrinsic partition coefficients of fentanyl between IPM or OCT and water are shown in Tables 4.8 and 4.9, respectively. As OCT-water partition coefficients are widely used to approximate SC-water partition coefficients, it is noteworthy that the values for the apparent and intrinsic partition coefficients of fentanyl between OCT and water obtained from these studies are in good agreement with those generated from previous research (where the experimentally-determined value of $K_{OCT/W}$ was 717 and the calculated value of $K_{OCT/W (INT)}$ was 23390 (40).

However, it would also appear that the apparent and intrinsic $K_{OCT/W}$ and $K_{IPM/W}$ values overestimate the apparent and intrinsic partition coefficients for fentanyl between untreated isolated human SC and water (the $K_{SC/W}$ and $K_{SC/W (INT)}$ values derived from all of the untreated SC-water partitioning studies were 171.21 ± 14.36 and 5879.76 ± 247.69 , respectively ($n=10$)). An obvious discrepancy between the OCT- or IPM-water and the SC-water partitioning studies is that the latter method utilises a biological membrane which, upon incubation with water for prolonged periods, may become excessively hydrated (79-82). As mentioned in Section 4.4.1, water contained within SC hydrated to hyper-physiological levels may either be absorbed by the corneocytes or form separate phases within the intercellular lipid region (80, 84, 88, 89). Furthermore, it is evident from Appendix II that the weight of the desiccated SC discs used during the SC-water partitioning studies increased by 50 to 100%w/w at the completion of these experiments. At this high level of hydration, it is probable that water present within the SC possesses similar properties to that of bulk water (91). Thus, the presence of "unbound" water may transform the SC into a more "polar" environment, which could effectively retard the partitioning of fentanyl free base. On the other hand, the water solubility of OCT is relatively low (2.3M) and water-saturated IPM essentially contains no solubilised water (33). Thus, the partitioning of fentanyl into these organic phases would be unaffected by the presence of excess water. Hence, it may be reasonable to assume that the partitioning of fentanyl into IPM or OCT represents its partitioning into an unadulterated lipidic environment, rather than a lipid domain "contaminated" with water.

Table 4.8. The apparent partition coefficients of fentanyl between various organic phases (octanol (OCT), isopropyl myristate (IPM), octisalate (OS) or padimate O (PO)) and water ($K_{ORG/W}$) and the concentration of fentanyl within each of these phases at $t=24h$ ($n=4$).

Organic phase	$K_{ORG/W}$	Fentanyl concentration	
		Organic phase (mg/ml)	Aqueous phase (μ g/ml)
IPM	604 ± 9	38.72 ± 0.03	64.13 ± 0.89
OCT	826 ± 4	39.04 ± 0.03	47.29 ± 0.22
OS	1700 ± 32^a	39.57 ± 0.05	23.32 ± 0.59
PO	350 ± 3^b	37.85 ± 0.03	108.01 ± 0.90

^a Statistically significant difference compared with $K_{IPM/W}$, $K_{OCT/W}$ and $K_{PO/W}$ ($p<0.05$)

^b Statistically significant difference compared with $K_{IPM/W}$, $K_{OCT/W}$ and $K_{OS/W}$ ($p<0.05$)

Table 4.9. The intrinsic partition coefficients of fentanyl free base between various organic phases (octanol (OCT), isopropyl myristate (IPM), octisalate (OS) or padimate O (PO)) and water ($K_{ORG/W (INT)}$) and aqueous phase pH values at $t=24h$ ($n=4$).

Organic phase	$K_{ORG/W (INT)}$	Aqueous phase pH
IPM	12248 ± 120	7.71 ± 0.01
OCT	20421 ± 467	7.62 ± 0.01
OS	37873 ± 972^a	7.66 ± 0.01
PO	49577 ± 509^b	6.84 ± 0.00

^a Statistically significant difference compared with $K_{IPM/W (INT)}$, $K_{OCT/W (INT)}$ and $K_{PO/W (INT)}$ ($p<0.05$)

^b Statistically significant difference compared with $K_{IPM/W (INT)}$, $K_{OCT/W (INT)}$ and $K_{OS/W (INT)}$ ($p<0.05$)

In addition, it is evident from Appendix I that the weight of the dessicated SC discs used during the SC-water partitioning studies increased by $76.0 \pm 4.1\%w/w$ at the completion of these experiments. At this high level of hydration, it is probable that water present within the SC possesses similar properties to that of bulk water (91). Thus, the presence of "unbound" water may transform the SC into a more "polar" environment, which could effectively retard the partitioning of fentanyl free base. On the other hand, the water solubility of OCT is relatively low (2.3M) and water-saturated IPM essentially contains no solubilised water (33). Thus, the partitioning of fentanyl into these organic phases would be unaffected by the presence of excess water. Hence, it may be reasonable to assume that the partitioning of fentanyl into IPM or OCT represents its partitioning into an unadulterated lipidic environment, rather than a lipid domain "contaminated" with water.

The apparent and intrinsic partition coefficients of fentanyl between OS or PO and water are also shown in Tables 4.8 and 4.9. It would appear from the apparent partition coefficients that, relative to water, OS is a considerably more favourable environment for fentanyl partitioning compared with either IPM or OCT ($p < 0.05$). On the other hand, the apparent partition coefficient for fentanyl between PO and water is markedly lower than that between either IPM or OCT and water ($p < 0.05$). Given that the saturated solubility of fentanyl in PO is higher than that in either IPM or OCT (Table 4.7), this finding was somewhat unexpected.

Considering that OS and PO are better solvents for fentanyl than are IPM and PO, it was also surprising that differences between the apparent partition coefficients could be attributed to differences between the aqueous phase concentrations of fentanyl and not the organic phase concentrations (Table 4.8). However, as fentanyl is a weak base ($pK_a = 8.99$ (41)), it is likely that the degree to which it is ionised in the aqueous phase governs its partitioning behaviour.

As shown in Table 4.9, the pH values for aqueous phase in contact with OS, IPM or OCT were quite comparable and thus it is likely that fentanyl was ionised to a similar extent within each of these aqueous phases (approximately 95.5, 95.0 or 95.9% of fentanyl may have been ionised in the presence of OS, IPM and OCT, respectively). On the other hand, aqueous phase in contact with PO was slightly more acidic than that in contact with the other organic phases and hence it is likely that the degree of fentanyl ionisation was higher within this medium (approximately 99.3% of fentanyl may have

been ionised in the presence of PO). As it has been demonstrated that the neutral form of a solute often has a greater affinity for SC lipids (and other organic liquids) than its ionised counterpart(s) (33, 38, 102, 103), it is therefore not surprising to find that if the apparent partition coefficients were corrected for fentanyl ionisation, then – relative to water – both OS and PO appeared to be significantly more favourable environments for the partitioning of the unionised form of fentanyl compared with either OCT or IPM ($p < 0.05$) (Table 4.9).

It should also be highlighted that if the organic phases were ranked in order of decreasing $K_{ORG/W(INT)}$ values, then: $PO > OS > OCT > IPM$, as this is the same as the rank order by which the saturated solubility of fentanyl within each of the organic phases decreased (Table 4.7). Thus, not only would it seem that the tendency for fentanyl free base to partition into these organic phases may be related to its saturated solubility, it would also be reasonable to speculate that OS and PO may enhance the partitioning of fentanyl free base into the SC by improving its solubility within the SC lipid domain. In order to further investigate this phenomenon, the concentration-dependent effects of OS and PO on fentanyl partitioning between IPM and water were investigated.

4.4.5. The effects of octisalate and padimate O on fentanyl partitioning between isopropyl myristate and water.

The apparent and intrinsic partition coefficients of fentanyl free base between IPM (alone (0%w/v) or containing 1 to 10%w/v of either OS or PO) and water are shown in Tables 4.10 and 4.11, respectively. The enhancement ratios that correspond to these values are presented in Figures 4.9 and 4.10.

With respect to the apparent partition coefficients (Table 4.10 and Figure 4.9), it is evident that OS did not enhance fentanyl partitioning into IPM at any concentration investigated. However, it is also apparent that the addition of OS to IPM reduced the pH of the aqueous phase in a concentration-dependent manner ($r^2 = 0.990$). Consequently, when the effects of fentanyl ionisation were accounted for, OS appeared to enhance the intrinsic partition coefficient of fentanyl free base in a manner that was linearly dependent on its concentration in IPM ($r^2 = 0.996$ when $ER(K_{OS \text{ in IPM/W}}(INT))$ was defined as a function of OS concentration in IPM) (Figure 4.10).

Table 4.10. The apparent partition coefficients of fentanyl between IPM (alone (0%) or containing 1-10%w/v of either OS or PO) and water ($K_{(OS \text{ or } PO \text{ in IPM/W})}$) ($n=4$).

OS or PO concentration in IPM (%w/v)	$K_{(OS \text{ in IPM/W})}$		$K_{(PO \text{ in IPM/W})}$	
	$K_{(OS \text{ in IPM/W})}$	Aqueous phase pH	$K_{(PO \text{ in IPM/W})}$	Aqueous phase pH
0	643 ± 15	7.73 ± 0.00	643 ± 15	7.73 ± 0.00
1	668 ± 23	7.72 ± 0.00	619 ± 12	7.64 ± 0.01
2.5	668 ± 9	7.71 ± 0.00	600 ± 12	7.58 ± 0.00
5	661 ± 16	7.68 ± 0.00	588 ± 23	7.51 ± 0.00
7.5	676 ± 11	7.67 ± 0.00	573 ± 28	7.44 ± 0.01
10	666 ± 8	7.64 ± 0.00	547 ± 22*	7.34 ± 0.01

* Statistically significant difference compared with the apparent partition coefficient derived from IPM alone ($p < 0.05$).

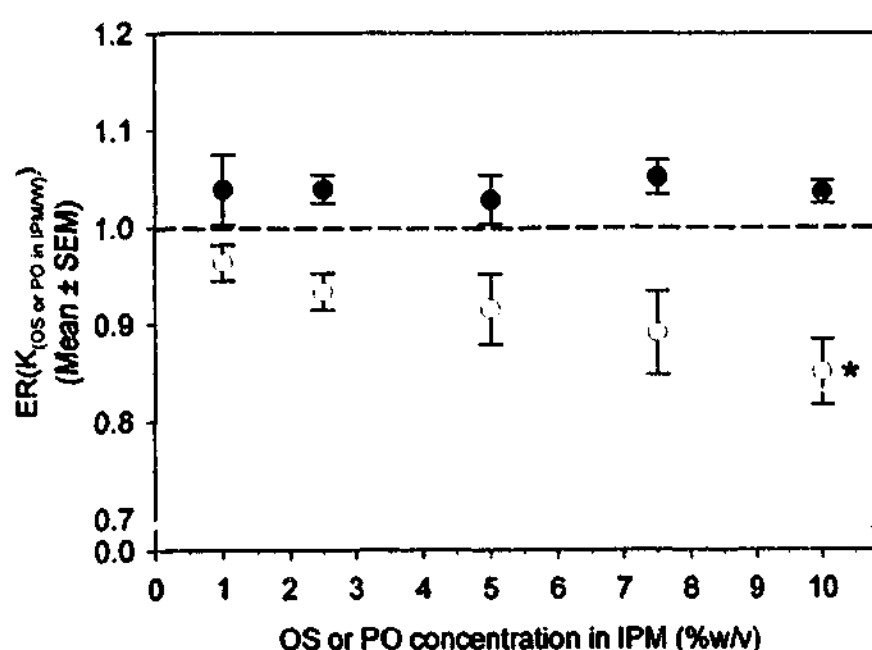


Figure 4.9. Enhancement ratios (ERs) generated for the apparent partition coefficients of fentanyl between IPM (alone (0%) or containing 1-10%w/v of either OS (●) or PO (○)) and water ($K_{(OS \text{ or } PO \text{ in IPM/W})}$). ER=1 is equivalent to no enhancement (shown by the dotted line). * corresponds to a statistically significant difference compared with the apparent partition coefficient derived from IPM alone ($p < 0.05$).

Table 4.11. The intrinsic partition coefficients of fentanyl free base between IPM (alone (0%) or containing 1-10%w/v of either OS or PO) and water ($K_{(OS \text{ or } PO \text{ in IPM/W}) (INT)}$) ($n=4$).

OS or PO concentration in IPM (%w/v)	$K_{(OS \text{ in IPM/W}) (INT)}$	$K_{(PO \text{ in IPM/W}) (INT)}$
0	12344 ± 287	12344 ± 287
1	13163 ± 367	13323 ± 133
2.5	13478 ± 276*	13948 ± 149*
5	14241 ± 389*	15015 ± 469*
7.5	14959 ± 167*	16148 ± 633*
10	15500 ± 250*	17632 ± 667*

* Statistically significant difference compared with the intrinsic partition coefficient derived from IPM alone ($p<0.05$).

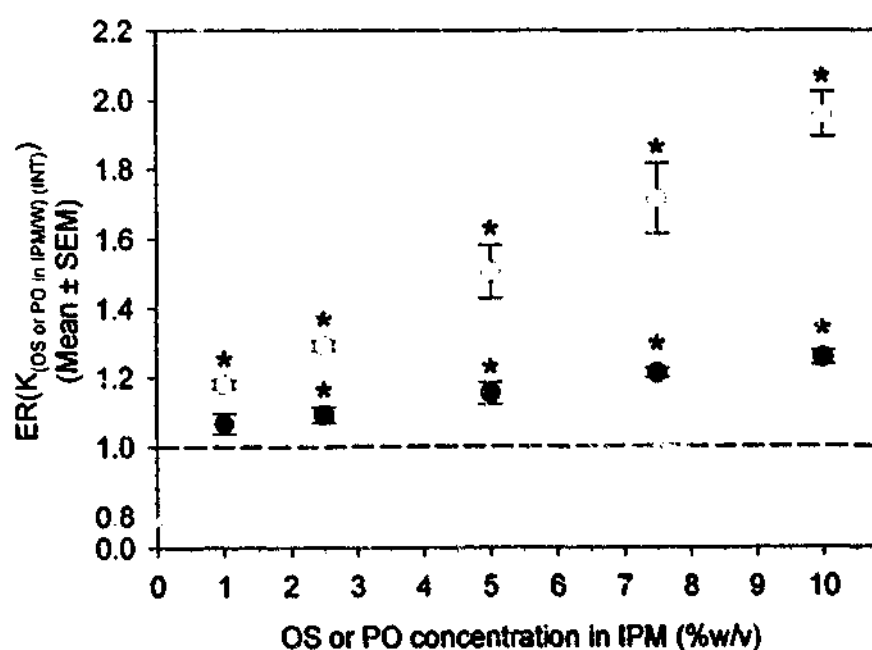


Figure 4.10. Enhancement ratios for the intrinsic partition coefficients of fentanyl free base between IPM (alone (0%) or containing 1-10%w/v of either OS (●) or PO (○)) and water ($K_{(OS \text{ or } PO \text{ in IPM/W}) (INT)}$). $ER=1$ is equivalent to no enhancement (shown by the dotted line). * corresponds to a statistically significant difference compared with the intrinsic partition coefficient derived from IPM alone ($p<0.05$).

Furthermore, the partitioning of fentanyl free base was significantly enhanced when OS was added to IPM at concentrations at or above 2.5%w/v (Table 4.11).

A similar phenomenon was observed when the effects of PO were investigated. Firstly, PO appeared to decrease the apparent partition coefficient of fentanyl into IPM in a somewhat concentration-dependent manner ($r^2=0.978$) such that fentanyl partitioning into IPM was significantly reduced at the highest concentration investigated (10%w/v) ($p<0.05$ compared with the $K_{(IPM/W)}$). However, as with OS, PO also appeared to reduce the pH of the aqueous phase in a concentration-dependent manner ($r^2=0.998$). As expected (from the aqueous phase pH values shown in Table 4.9), PO seemed to exert a greater influence over aqueous phase pH than did OS. Hence, after the apparent partition coefficients were corrected for fentanyl ionisation it was found that PO actually enhanced fentanyl partitioning into IPM in a concentration-dependent fashion ($r^2 = 0.998$ for $ER(K_{(1$ to 10%w/v PO in IPM/W) (INT)) versus PO concentration in IPM) (Figure 4.9). It is also evident that the ER ($K_{(PO$ in IPM/W) (INT)) values generated at a given concentration of PO were superior to the ER($K_{(OS$ in IPM/W) (INT)) values produced at the same concentration of OS. This is consistent with the finding that fentanyl has higher solubility in PO than it does in OS (Table 4.7).

4.4.6. Factors governing the partitioning of fentanyl into human stratum corneum

The following findings would indicate that OS and PO enhance fentanyl partitioning into SC lipids by improving its solubility within this environment:

- i. Based on the "distance" between their partial solubility parameters, fentanyl appeared to be more "compatible" with OS and PO than with OCT, IPM or CER-6
- ii. The saturated solubility of fentanyl in either OS or PO was greater than that in either IPM or OCT
- iii. The partitioning of fentanyl free base from water into OS or PO was greater than that from water into IPM or OCT
- iv. OS and PO enhanced the intrinsic partition coefficient of fentanyl free base between IPM and water in a manner that was linearly dependent on their concentration in IPM.

However, although the linear relationship between $ER(K_{OS \text{ in IPM/W}}(INT))$ and OS (in IPM) concentration is consistent with that observed between $ER(K_{SC/W})$ and OS pretreatment concentration, the linear trend between $ER(K_{PO \text{ in IPM/W}}(INT))$ and PO (in IPM) concentration is discordant with the parabolic relationship between $ER(K_{SC/W})$ and PO pretreatment concentration (Sections 4.4.2 and 4.4.5). In contrast to the pH-dependent effects that were observed during the IPM-water partitioning studies, pretreating the SC with either OS or PO did not result in alterations to aqueous phase pH during the SC-water partitioning studies. Therefore, it seems that the mechanism(s) by which PO enhances fentanyl partitioning into the SC were confounded by different degrees of fentanyl ionisation. Thus, it is possible that the discrepancy between the SC-water and IPM-water partitioning studies was a consequence of one or more of the following contingencies:

- i. The physical and chemical limitations imposed by the SC
- ii. OS and PO could interact with the SC via different mechanism(s)
- iii. Other mechanism(s) (in addition to increased fentanyl solubility) may also be responsible for the enhancing effects of OS and PO on fentanyl partitioning into the SC

4.4.6.1. Physical and chemical constraints within the stratum corneum

Due to the physical limitations imposed by the SC it is likely that the concentrations of OS or PO that were added to IPM did not accurately reflect the concentrations of OS or PO that permeated into the SC lipid domain after the SC was pretreated during the infinite dose diffusion studies (Section 4.4.1) and the SC-water partitioning studies (Section 4.4.2). A concentration range of 1 to 10%w/v of OS or PO in IPM was used in order to investigate concentration-dependent effects on fentanyl partitioning between IPM and water. However, the application of ethanolic solutions containing 1 to 10%w/v of OS or PO would have deposited 50 to 500 $\mu\text{g}/\text{cm}^2$ of enhancer at the SC surface (Table 4.12). If approximately 10 to 20% (per Chapter 6) of this deposited amount permeated the SC at $t = 2 \text{ h}$ and if the fractional volume of SC lipids is of the order of $\sim 10\%w/w$ (16), then – assuming that OS and PO were entirely distributed within the intercellular space at all SC concentrations – the concentrations of OS or PO

found within the SC lipids after pretreatment could have been of the order of ~40 to ~800 mg/cm³ (i.e. ~4 to ~80%w/v) (Table 4.12). Clearly the upper range of these predicted SC lipid concentrations exceeds the highest IPM concentrations of OS or PO that were investigated during the IPM-water partitioning studies. However, as the intrinsic partitioning and the saturated solubility of fentanyl in OS and PO were both greater than that in IPM it is likely that increasing the IPM concentrations of OS or PO up to 80%w/v would have further augmented the partitioning of fentanyl free base into IPM.

Furthermore, it is uncertain as to whether OS and PO would entirely associate with the intercellular lipid domain when they are present within the SC at relatively high concentrations. Using the method described in Section 4.3.5.2, it was found that the saturated solubility of OS and PO in OCT was 709.14 ± 93.93 mg/ml and 205.77 ± 21.72 mg/ml at 32°C, respectively. If the solubility of OS and PO in OCT approximates that in the SC lipids it is possible that – within the concentration range investigated – pretreating the SC with OS may result in SC lipid concentrations that were below its saturated solubility within this environment.

Table 4.12. Predicted SC lipid concentrations of OS and PO resulting from 2h pretreatment of the SC with ethanolic solutions containing 1 to 10%w/v of OS or PO.

OS or PO pretreatment concentration (%w/v)	Amount deposited at skin surface (mg/cm ²)	Predicted SC lipid concentration after 2h pretreatment (approx.) ^a	
		mg/cm ³	%w/v
1	50	40 - 80	4 - 8
2.5	125	100 - 200	10 - 20
5	250	200 - 400	20 - 40
7.5	375	300 - 600	30 - 60
10	500	400 - 800	40 - 80

^a Assuming that; i. 10 to 20% of the total applied dose permeates the SC at t=2h (per Chapter 7), ii. the length of the SC is 13µm (16), iii. the density of the SC is 1g/cm³ (39), iii. SC lipids occupy 10%w/w of the total weight of the SC (16) and iii. solute permeation occurs via the intercellular lipid region (75, 76, 104-107).

Thus, it would be reasonable to assume that most – if not all – of the OS permeating the SC after a 2 h pretreatment would have been associated with the intercellular lipid region. On the other hand, pretreating the SC with higher concentrations of PO (i.e. above 5%w/v) may have resulted in SC lipid concentrations that exceeded saturation. Consequently, the correlation between the IPM-water partitioning data and the data derived from experiments involving human skin pretreated with PO may be confounded by the possibility that:

- i. The partitioning of PO into the SC lipid domain may have become solubility-limited at higher pretreatment concentrations and/or
- ii. When high concentrations (i.e. those exceeding saturation within the SC lipids) of PO were present within the SC, other effects (perhaps not directly associated with the SC lipids) may have come into action and counteracted the mechanism(s) by which PO enhanced fentanyl partitioning. This possibility is discussed in further detail in Section 4.4.6.2.

4.4.6.2. Possible differences between interaction: with octisalate or padimate O and human stratum corneum

Another explanation as to why OS and PO appear to exert different concentration-dependent enhancing effects on fentanyl permeation and partitioning into the SC pertains to the possibility that they interact differently with the components of the SC. It is evident from their chemical structures (Chapter 1, Figure 1.10) that OS contains an *ortho*-substituted hydroxyl functional group on the 2-ethylhexyl phenyl ring whilst PO contains a *para*-substituted dimethylamino moiety.

Although this is the only difference between the chemical structures of OS and PO, it is probable that the polar head group of a CPE influences the way in which the enhancer interacts with the SC. For instance, it has been demonstrated that *ortho*-substitution on the phenyl ring of dimethyl sulphoxide derivatives (iminosulfuranes) yielded compounds with greater enhancer activity compared with those produced by substitution on the *para*-position (108). Hence, *para*- (versus *ortho*-) substitution on the PO phenyl ring may reduce the potential for PO to interact auspiciously with SC in order to enhance fentanyl partitioning. To further elaborate on this phenomenon, Warner et al

(31, 32) used a series of partitioning experiments between either OCT or hexane and phosphate-buffered saline to support the notion that the contribution of a polar head group to the activity of a penetration enhancer results from its ability to partition favourably into the polar (or semipolar) regions of the SC lipid bilayers and not via any specific interaction of the polar head group with the lipid bilayers. Thus, the potency of an enhancer may be related to the ability of the polar head group to assist in the translocation of the enhancer to a site of action. Based on the findings of this research it is possible that OS and PO are located in (and therefore interact with) different regions of the SC lipid bilayers.

In light of previous research demonstrating the importance of hydrogen bonding interactions in stabilising lipid bilayers and influencing solute penetration through the SC, Hadgraft et al (109) have suggested that modification of hydrogen bonding within SC lipids is also a possible mode of action of penetration "modifiers". As it is likely that the presence of the phenyl hydroxyl group within the structure of OS imparts stronger hydrogen bonding donor and acceptor characteristics than the dimethylamino group would impart for PO⁷, it is therefore possible that OS forms stronger hydrogen bonds with adjacent lipid molecules than would PO. Thus, it may be reasonable to infer that OS has a greater tendency to displace lipid molecules (hence creating "fluidised" regions) within the lamellae. This hypothesis is further supported by the data presented in Chapter 7, where attenuated total reflectance Fourier transform infrared (ATR-FTIR) analyses revealed that pretreating full-thickness human skin samples with OS resulted in shifts of the CH₂ symmetric and asymmetric stretching frequencies (originating from the hydrocarbon chains of the lipid bilayers) to higher wavenumbers in a manner that was linearly dependent on the applied concentration of OS. On the other hand, PO did not appear to exert an effect on these frequencies at any concentration investigated.

Based on all of the possibilities mentioned thus far, it would be reasonable to expect that the enhancing capability of PO would be inferior to that of OS. However, it should be kept in mind that PO might improve the affinity of fentanyl for the SC lipid domain. Thus, it is possible that at low SC lipid concentrations, a predominant mechanism by which PO enhances fentanyl permeation is by increasing its solubility

⁷ Using Molecular Modeling Pro software package (Version 5.1.7) (ChemSW[®] Inc), the hydrogen bond donor (α) and acceptor (β) values for OS and PO were estimated to be $\alpha = 0.48$ and $\beta = 0.12$ units for OS and $\alpha = 0.37$ and $\beta = 0.02$ for PO.

within the SC lipid domain. However, in addition to the factors mentioned in Section 4.4.6.1 it is also possible that at higher SC lipid concentrations of PO:

- i. The contribution of specific interactions between either PO and the SC lipid bilayers becomes significant and/or
- ii. Other forces come into play that also influence fentanyl permeation

An example of the latter possibility relates to the effect of Azone® on SC water content. Numerous studies have revealed that there is a parabolic concentration-dependence on the ability of Azone® to enhance solute permeation through the skin (50). For instance, Díez-Sales et al discovered that compared with relatively low concentrations (1 or 5%w/v), higher concentrations of Azone® (10%w/v) reduced or even eliminated its enhancing effect on the skin permeation of compounds with moderate to high lipophilicity (19). As previous research had demonstrated that, in addition to its fluidising effect on SC lipids, Azone® increases the water content of human SC (110), Díez-Sales et al proposed that high concentrations of Azone® reduced the partitioning of these lipophilic compounds by increasing the hydration state of the SC. This notion is in agreement with studies on extended bilayer structures, where it was found that increasing the bilayer concentration of Azone® resulted in an increased ability of the fluid bilayers to imbibe water (52). Although the effect of PO on SC water content has not been investigated in this thesis, this example highlights the possibility that other factors may alter the partitioning of a solute into the SC.

4.4.6.3. Other mechanisms by which octisalate and padimate O may enhance fentanyl partitioning into human stratum corneum

It is inferred from the discussions in Sections 4.4.6.1 and 4.4.6.2 that a major limitation with using model organic liquids (instead of SC lipids in their endogenous environment) is that the physical and biological characteristics that are germane to the barrier properties of the SC cannot be reproduced. As discussed in Chapter 1, the SC lipids show an exceptional degree of organisation and form lamellae that are orientated approximately parallel to the corneocyte surface (111-113). Furthermore, the lateral packing of these lipids is mainly crystalline and hexagonal (114). Thus, due to their

highly ordered arrangement, the SC lipid bilayers would impose a high diffusional resistance towards solute permeation. This has been demonstrated on numerous occasions, whereby intercellular lipid disorganization has resulted in the increased permeability of various solutes (60, 115-117). It has also been demonstrated that the quality of the SC barrier is not only dependent on SC lipid bilayer organisation but also on SC lipid content and composition. For instance, Elias et al have shown that solute permeability is inversely correlated with SC lipid weight (107), whilst other studies have revealed the importance of variations in the content of specific lipid fractions (118). It is also important to note that SC lipid extraction has often led to enhanced solute partitioning into the SC (30, 119-121) and it has been proposed that perturbation of the SC lipid bilayers may improve solute partitioning within this domain, thus increasing overall solute penetration through the SC (54, 122). In light of the possibility that OS and PO may extract and/or fluidise the SC lipids, the effects of OS and PO on SC lipids have been investigated *in vitro* using ATR-FTIR (Chapter 7).

4.6. CONCLUSIONS

Both OS and PO significantly enhanced fentanyl permeation across human epidermis under "infinite dose" conditions. The ability of OS to enhance the permeability and partition coefficients of fentanyl was linearly dependent upon its pretreatment concentration (1 to 10%w/v) with a parabolic relationship between PO pretreatment concentration and fentanyl permeation and partitioning enhancement being evident (maximum enhancement was achieved at 5%w/v PO and further increases in pretreatment concentration (to 7.5 and 10%w/v) resulted in an attenuation of its enhancing capability). As similar trends were observed between the enhancement of fentanyl permeability and partitioning, it would therefore appear from the data derived from the "infinite dose" diffusion studies and the SC-water partitioning studies that a major mechanism by which OS and PO enhance fentanyl permeation through human skin is by increasing its partition coefficient between the SC and the vehicle.

However, due to limitations associated with the "infinite dose" diffusion studies, it is difficult to determine whether OS and PO alter fentanyl diffusivity within the SC lipid domain (OS only appeared to exert a significant effect on fentanyl diffusion at a pretreatment concentration of 1%w/v, whilst PO did not seem to alter this parameter) or

whether the effects of OS and PO on fentanyl diffusivity were confounded by experimental artifacts. Therefore, other techniques have been employed in subsequent chapters in order to investigate the effects of OS and PO on the SC lipids (Chapter 7).

Most of the data presented in this chapter focused on elucidating whether OS and PO enhanced fentanyl partitioning by improving its affinity for the SC lipid domain. Using OCT and IPM to simulate the chemical environment of the SC lipids, it was found that:

- i. The saturated solubility of fentanyl in OS and PO was greater than that in either OCT or IPM. The rank order by which fentanyl solubility decreased was $PO > OS > OCT > IPM$.
- ii. Based on differences between partial solubility parameters, it would appear that higher solubility of fentanyl in OS and PO (compared with OCT and IPM) can be attributed to London dispersion and/or hydrogen bonding interactions. Although the contribution of these interactions towards an understanding of the mechanism(s) by which OS and PO enhance fentanyl partitioning into the SC requires further investigation, it is interesting to note that the differences between the London dispersion and hydrogen bonding solubility parameters were lower between fentanyl and OS or PO than those between fentanyl and CER-6.
- iii. The intrinsic partition coefficient of fentanyl free base between either OS or PO and water was greater than that between either OCT or IPM and water. The rank order by which the intrinsic partition coefficient decreased was the same as that for the saturated solubility of fentanyl within each of these organic phases. This similarity would infer that the tendency for fentanyl free base to partition between each of these organic phases and water is related to its affinity for the organic phase.
- iv. Both OS and PO enhanced the intrinsic partition coefficient of fentanyl free base between IPM and water in a manner that was linearly dependent on their concentration in IPM. As the partitioning behaviour of fentanyl free base appears to be related to its solubility in the organic phase, it would be reasonable to assume that OS and PO enhanced the partitioning of fentanyl into IPM by improving its solubility in this organic phase.

Based on all of these findings, it would appear that OS and PO improve fentanyl partitioning into the SC by – or partly by – increasing its affinity for the SC lipid domain. However, the fact that a linear trend was not observed between PO pretreatment concentration and the enhancement of fentanyl partitioning into human SC raises the question as to whether other determinants influence the ability of PO to enhance fentanyl partitioning into the SC at higher pretreatment concentrations. The following factors may be responsible for this phenomenon:

- i. As the saturated solubility of PO in OCT was found to be ~3.4 times lower than that of OS in OCT, the partitioning of PO in the SC lipid domain may become solubility-limited at relatively high pretreatment concentrations and/or
- ii. OS and PO may interact differently with the SC. For example, OS and PO may be located (and/or interact with) different regions of the SC lipid bilayers or OS may form stronger hydrogen bonds with adjacent lipid molecules. The contribution of these specific interactions may only become significant at higher pretreatment concentrations.
- iii. Other events may occur within the SC, which exert a negative effect on fentanyl partitioning. For instance, as with Azone[®] the enhancing effects of PO could be reduced at higher pretreatment concentrations as a result of increased SC water content.

Although not all of these factors have been investigated in this thesis, they must certainly be considered when future investigations into the mechanism(s) of action of OS and PO are conducted.

It is also pertinent to note that other mechanisms (in addition to increased fentanyl solubility within the SC lipid domain) may also be responsible for the enhancing effects of OS and PO on fentanyl permeation and partitioning. In particular, as SC lipid extraction and/or fluidisation are also possible mechanism(s) by which CPEs can enhance solute permeation and partitioning, it is likely that the enhancing effects of OS and PO can also be attributed to their effects on SC lipids. These effects have been investigated in Chapter 7.

4.7. REFERENCES

1. Zatz JL. 1991. Assessment of Vehicle Factors Influencing Percutaneous Absorption. In Bronaugh RL, Maibach HI, ed. *In Vitro* Percutaneous Absorption: Principles, Fundamentals, and Applications. Boca Raton, Florida: CRC Press, Inc., pp 51-66.
2. Sloan KB, Koch SA, Siver KG, Flowers FP. 1986. Use of Solubility Parameters of Drug and Vehicle to Predict Flux Through Skin. *J Invest Dermatol* 87:244-252.
3. Zatz JL, Sarpotdar PP. 1987. Influence of Vehicles on Skin Penetration. In Kydonieus AF, Berner B, ed. *Transdermal Delivery of Drugs*. Boca Raton, Florida: CRC Press Inc., pp 87-91.
4. Roy SD, Flynn GL. 1988. Solubility and Related Physicochemical Properties of Narcotic Analgesics. *Pharm Res* 5:580-586.
5. Higuchi T. 1960. Physical Chemical Analysis of Percutaneous Absorption Process From Creams and Ointments. *J Soc Cosmet Chem* XI:85-97.
6. Daynes HA. 1920. The Process of Diffusion Through A Rubber Membrane. *Proc R Soc Lond A* 97:286-307.
7. Barrer RM. 1939. Permeation, Diffusion and Solution of Gases. *Trans Faraday Soc* 35:628-643.
8. Watkinson AC, Brain KR. 2002. Basic Mathematical Principles in Skin Permeation. In Walters KA, ed. *Dermatological and Transdermal Formulations*. New York: Marcel Dekker, Inc., pp 61-88.
9. Barry BW. 1983. *Dermatological Formulations. Percutaneous Absorption*. New York: Marcel Dekker, Inc. pp 49-94.
10. Crank J. 1975. *The Mathematics of Diffusion*. London: Oxford University Press. pp 44-68.
11. Potts RO, Guy RH. 1994. Drug Transport Across the Stratum Corneum and the Attainment of Steady-State Flux. *Proceedings of the 21st International Symposium on Controlled Release of Bioactive Materials (Nice)*, Deerfield, USA, 162-163.
12. Peck KD, Higuchi WI. 1997. Characterization of the Passive Transdermal Diffusional Route of Polar/Ionic Permeants. In Potts RO, Guy RH, ed. *Mechanisms of Transdermal Drug Delivery*. New York: Marcel Dekker, Inc., pp 267-290.
13. Talreja P, Kleene NK, Pickens WL, Wang TF, Kasting GB. 2001. Visualization of the Lipid Barrier and Measurement of Lipid Pathlength in Human Stratum Corneum. *AAPS PharmSci* 3:1-9.
14. Bunge AL, Guy RH, Hadgraft J. 1999. The Determination of a Diffusional Pathlength Through the Stratum Corneum. *Int J Pharm* 188:121-124.
15. Pellett MA, Watkinson AC, Hadgraft J, Brain KR. 1997. Comparison of Permeability Data from Traditional Diffusion Cells and ATR-FTIR Spectroscopy. Part II. Determination of Diffusional Pathlengths in Synthetic Membranes and Human Stratum Corneum. *Int J Pharm* 154:217-227.
16. Johnson ME, Blankschtein D, Langer R. 1997. Evaluation of Solute Permeation Through the Stratum Corneum: Lateral Bilayer Diffusion as the Primary Transport Mechanism. *J Pharm Sci* 86:1162-1172.

17. Parry GE, Bunge AL, Silcox GD, Pershing LK, Pershing DW. 1990. Percutaneous Absorption of Benzoic Acid Across Human Skin. I. *In Vitro* Experiments and Mathematical Modeling. *Pharm Res* 7:230-236.
18. Tang H, Blankschtein D, Langer R. 2002. Prediction of Steady-State Skin Permeabilities of Polar and Nonpolar Permeants Across Excised Pig Skin Based on Measurements of Transient Diffusion: Characterization of Hydration Effects on the Skin Porous Pathway. *J Pharm Sci* 91:1891-1907.
19. Díez-Sales O, Watkinson AC, Herréiz-Domínguez M, Javaloyes C, Hadgraft J. 1996. A Mechanistic Investigation of the *In Vitro* Human Skin Permeation Enhancing Effect of Azone®. *Int J Pharm* 129:33-40.
20. Dias M, Farinha A, Faustino E, Hadgraft J, Pais J, Toscano C. 1999. Topical Delivery of Caffeine from Some Commercial Formulations. *Int J Pharm* 182:41-47.
21. Harrison JE, Watkinson AC, Green DM, Hadgraft J, Brain K. 1996. The Relative Effect of Azone® and Transcutol® on Permeant Diffusivity and Solubility in Human Stratum Corneum. *Pharm Res* 13:542-546.
22. Pellett MA, Watkinson AC, Hadgraft J, Brain KR. 1997. Comparison of Permeability Data from Traditional Diffusion Cells and ATR-FTIR Spectroscopy. Part I. Synthetic Membranes. *Int J Pharm* 154:205-215.
23. Watkinson AC, Joubin H, Green DM, Brain KR, Hadgraft J. 1995. The Influence of Vehicle on Permeation from Saturated Solutions. *Int J Pharm* 121:27-36.
24. Okamoto H, Hashida M, Sezaki H. 1988. Structure-Activity Relationship of 1-Alkyl- or 1-Alkenylazacycloalkanone Derivatives as Percutaneous Penetration Enhancers. *J Pharm Sci* 77:418-424.
25. Roberts MS, Cross SE, Pellett MA. 2002. Skin Transport. In Walters KA, ed. *Dermal and Transdermal Formulations*. New York: Marcel Dekker, Inc., pp 89-195.
26. Florence AT, Attwood D. 1988. *Physicochemical Properties of Pharmacy*. London: Macmillan Press Ltd. pp 131-171.
27. Roberts MS, Sloan KB. 2000. Prediction of Transdermal Flux of Prodrugs of 5-Fluorouracil, Theophylline, and 6-Mercaptopurine with a Series/Parallel Model. *J Pharm Sci* 89:1415-1431.
28. Raykar PV, Fung MC, Anderson BD. 1988. The Role of Protein and Lipid Domains in the Uptake of Solutes by Human Stratum Corneum. *Pharm Res* 5:140-150.
29. Roberts MS, Anderson RA, Swarbrick J. 1977. Permeability of Human Epidermis to Phenolic Compounds. *J Pharm Pharmacol* 29:677-683.
30. Surber C, Wilhelm KP, Maibach HI, Guy RH. 1990. Partitioning of Chemicals into Human Stratum Corneum: Implications for Risk Assessment Following Dermal Exposure. *Fundam Appl Toxicol* 15:99-107.
31. Warner KS, Li SK, He N, Suhonen TM, Chantéart D, Bolikal D, Higuchi WI. 2003. Structure-Activity Relationship for Chemical Skin Permeation Enhancers: Probing the Chemical Microenvironment of the Site of Action. *J Pharm Sci* 92:1305-1322.

32. Warner KS, Li SK, Higuchi WI. 2001. Influences of Alkyl Group Chain Length and Polar Head Group on Chemical Skin Permeation Enhancement. *J Pharm Sci* 90:1143-1153.
33. Oakley DM, Swarbrick J. 1987. Effects of Ionization on the Percutaneous Absorption of Drugs: Partitioning of Nicotine Into Organic Liquids and Hydrated Stratum Corneum. *J Pharm Sci* 76:866-871.
34. Leo A, Hansch C, Elkins D. 1971. Partition Coefficients and Their Uses. *Chem Reviews* 71:525-616.
35. Flynn GL. 1971. Structural Approach to Partitioning: Estimation of Steroid Partition Coefficients Based Upon Molecular Constitution. *J Pharm Sci* 60:345-353.
36. Anderson BD, Higuchi WI, Raykar PV. 1988. Heterogeneity Effects on Permeability-Partition Coefficient Relationships in Human Stratum Corneum. *Pharm Res* 5:566-573.
37. Nangia A, Berner B, Maibach HI. 1999. Transepidermal Water Loss Measurements for Assessing Skin Barrier Functions During *In Vitro* Percutaneous Absorption Studies. In Bronough RL, Maibach HI, ed. *Percutaneous Absorption: Drugs, Cosmetics, Mechanisms, Methodology*. New York: Marcel Dekker, Inc., pp 587-594.
38. Scheuplein RJ, Blank IH. 1971. Permeability of the Skin. *Physiol Rev* 51:702-747.
39. Anderson BD, Cassidy JM. 1973. Variation in Physical Dimensions and Chemical Composition of Human Stratum Corneum. *J Invest Dermatol* 61:30-32.
40. Roy SD, Flynn GL. 1989. Transdermal Delivery of Narcotic Analgesics: Comparative Permeabilities of Narcotic Analgesics Through Human Cadaver Skin. *Pharm Res* 6:825-832.
41. Roy SD, Flynn GL. 1989. Solubility Behavior of Narcotic Analgesics in Aqueous Media: Solubilities and Dissociation Constants of Morphine, Fentanyl, and Sufentanil. *Pharm Res* 6:147-151.
42. Martin A. 1993. *Physical Pharmacy*. 4th Edn. Baltimore, USA: Williams & Wilkins. pp 212-250.
43. Michaels AS, Chandrasekaran SK, Shaw JE. 1975. Drug Permeation Through Human Skin: Theory and *In Vitro* Experimental Measurement. *AIChEJ* 21:985-996.
44. Roy SD, Hou SY, Witham SL, Flynn GL. 1994. Transdermal Delivery of Narcotic Analgesics: Comparative Metabolism and Permeability of Human Cadaver Skin and Hairless Mouse Skin. *J Pharm Sci* 83:1723-1728.
45. Roy SD, Flynn GL. 1990. Transdermal Delivery of Narcotic Analgesics: pH, Anatomical, and Subject Influences on Cutaneous Permeability of Fentanyl and Sufentanil. *Pharm Res* 7:842-847.
46. Lambert WJ, Higuchi WI, Knutson K, Krill SL. 1989. Dose-Dependent Enhancement Effects of Azone on Skin Permeability. *Pharm Res* 6:798-803.
47. Schückler F, Lee G. 1992. Relating the Concentration-Dependent Action of Azone and Dodecyl-L-Pyroglytamate on the Structure of Excised Human Stratum Corneum to Changes in Drug Diffusivity, Partition Coefficient and Flux. *Int J Pharm* 80:81-89.
48. Pilgram GS, van der Meulen J, Gooris GS, Koerten HK, Bouwstra JA. 2001. The Influence of Two Azones and Sebaceous Lipids on the Lateral Organization of Lipids Isolated from Human Stratum Corneum. *Biochim Biophys Acta* 1511:244-254.

49. Rolland A, Brzokewicz A, Shroot B, Jamouille J. 1991. Effect of Penetration Enhancers on the Phase Transition of Multilamellar Liposomes of Dipalmitoylphosphatidylcholine. A Study by Differential Scanning Calorimetry. *Int J Pharm* 76:217-224.
50. Hadgraft J, Williams DG, Allan G. 1993. Azone. Mechanisms of Action and Clinical Effect. In Walters KA, Hadgraft J, ed. *Pharmaceutical Skin Penetration Enhancement*. New York: Marcel Dekker, Inc., pp 175-197.
51. Bouwstra JA, Boddé HE. 1995. Human SC Barrier Impairment by N-Alkyl-Azacycloheptanones: A Mechanistic Study of Drug Flux Enhancement, Azone® Mobility, and Protein and Lipid Perturbation. In Smith EW, Maibach HI, ed. *Percutaneous Penetration Enhancers*. Boca Raton, Florida: CRC Press, Inc., pp 137-158.
52. Lee G. 1995. Interaction of Azone® with Model Lipid Systems. In Smith EW, Maibach HI, ed. *Percutaneous Penetration Enhancers*. Boca Raton, Florida: CRC Press, Inc., pp 195-210.
53. Goodman M, Barry BW. 1986. Action of Skin Permeation Enhancers Azone, Oleic Acid and Decylmethyl Sulphoxide: Permeation and DSC Studies. *J Pharm Pharmacol* 38S:71.
54. Ogiso T, Iwaki M, Paku T. 1995. Effect of Various Enhancers on Transdermal Penetration of Indomethacin and Urea, and Relationship Between Penetration Parameters and Enhancement Factors. *J Pharm Sci* 84:482-488.
55. Chow DS, Kaka I, Wang TI. 1984. Concentration-Dependent Enhancement of 1-Dodecylazacycloheptan-2-one on the Percutaneous Penetration Kinetics of Triamcinolone Acetonide. *J Pharm Sci* 73:1794-1799.
56. Puglia C, Bonina F, Trapani G, Franco M, Ricci M. 2001. Evaluation of *In Vitro* Percutaneous Absorption of Lorazepam and Clonazepam from Hydro-Alcoholic Gel Formulations. *Int J Pharm* 228:79-87.
57. Okamoto H, Hashida M, Sezaki H. 1991. Effect of 1-Alkyl- or 1-Alkenylazacycloalkanone Derivatives on the Penetration of Drugs with Different Lipophilicities Through Guinea Pig Skin. *J Pharm Sci* 80:39-45.
58. Aungst BJ. 1995. Fatty Acids as Skin Permeation Enhancers. In Smith EW, Maibach HI, ed. *Percutaneous Penetration Enhancers*. Boca Raton, Florida: CRC Press, Inc., pp 277-287.
59. Walker M, Hadgraft J. 1991. Oleic Acid- A Membrane 'Fluidiser' or Fluid Within the Membrane? *Int J Pharm* 71:R1-R4.
60. Golden GM, McKie JE, Potts RO. 1987. Role of Stratum Corneum Lipid Fluidity in Transdermal Drug Flux. *J Pharm Sci* 76:25-28.
61. Francoeur ML, Golden GM, Potts RO. 1990. Oleic Acid: Its Effects on Stratum Corneum in Relation to (Trans)Dermal Drug Delivery. *Pharm Res* 7:621-627.
62. Naik A, Pechtold LARM, Potts RO, Guy RH. 1995. Mechanism of Oleic Acid-Induced Skin Penetration Enhancement *In Vivo* in Humans. *J Control Release* 37:299-306.
63. Ongpipattanakul B, Burnette RR, Potts RO, Francoeur ML. 1991. Evidence that Oleic Acid Exists in a Separate Phase Within Stratum Corneum Lipids. *Pharm Res* 8:350-354.

64. Aungst BJ, Blake JA, Hussain MA. 1990. Contributions of Drug Solubilization, Partitioning, Barrier Disruption, and Solvent Permeation to the Enhancement of Skin Permeation of Various Compounds with Fatty Acids and Amines. *Pharm Res* 7:712-718.
65. Nomura H, Kaiho F, Sugimoto Y, Miyashita Y, Dohi M, Kato Y. 1990. Percutaneous Absorption of Indomethacin From Mixtures of Fatty Alcohol and Propylene Glycol (FAPG Bases) Through Rat Skin: Effects of Oleic Acid Added to FAPG Base. *Chem Pharm Bull* 38:1421-1424.
66. Yamada M, Uda Y, Tanigawara Y. 1987. Mechanism of Enhancement of Percutaneous Absorption of Molsidomine by Oleic Acid. *Chem Pharm Bull* 35:3399-3406.
67. Green PG, Guy RH, Hadgraft J. 1988. *In Vitro* and *In Vivo* Enhancement of Skin Permeation with Oleic and Lauric Acids. *Int J Pharm* 48:103-111.
68. Green PG, Hadgraft J, Ridout G. 1989. Enhanced *In Vitro* Permeation of Cationic Drugs. *Pharm Res* 6:628-632.
69. Mahjour M, Mauser BE, Fawzi MB. 1989. Skin Permeation Enhancement Effects of Linoleic Acid and Azone® on Narcotic Analgesics. *Int J Pharm* 56:1-11.
70. Green PG, Hadgraft J. 1987. Facilitated Transfer of Cationic Drugs Across a Lipoidal Membrane by Oleic Acid and Lauric Acid. *Int J Pharm* 37:251-255.
71. Matschiner S, Neubert R, Wohlrab W. 1995. The Use of Ion Pairing to Facilitate Percutaneous Absorption of Drugs. In Smith EW, Maibach HI, ed. *Percutaneous Penetration Enhancers*. Boca Raton, Florida: CRC Press, Inc., pp 407-417.
72. Ohman H, Vahlquist A. 1994. *In Vivo* Studies Concerning a pH Gradient in Human Stratum Corneum and Upper Epidermis. *Acta Derm Venereol Suppl (Stockh)* 74:375-379.
73. Wagner H, Kostka KH, Lehr CM, Schaefer UF. 2003. pH Profiles in Human Skin: Influence of Two *In Vitro* Test Systems for Drug Delivery Testing. *Eur J Pharm Biopharm* 55:57-65.
74. Hadgraft J. 1999. Passive Enhancement Strategies in Topical and Transdermal Drug Delivery. *Int J Pharm* 184:1-6.
75. Albery WJ, Hadgraft J. 1979. Percutaneous Absorption: *In Vivo* Experiments. *J Pharm Pharmacol* 31:140-147.
76. Potts RO, Francoeur ML. 1991. The Influence of Stratum Corneum Morphology on Water Permeability. *J Invest Dermatol* 96:495-499.
77. Cussler EL, Hughes SE, Ward WJ, Aris R. 1988. Barrier Membranes. *J Membr Sci* 38:161-174.
78. Guy RH, Hadgraft J. 1989. Selection of Drug Candidates for Transdermal Drug Delivery. In Hadgraft J, Guy RH, ed. *Transdermal Drug Delivery: Developmental Issues and Research Initiatives*. New York: Marcel Dekker Inc., pp 59-81.
79. Idson B. 1978. Hydration and Percutaneous Absorption. *Curr Probl Dermatol* 7:132-141.
80. Bouwstra JA, De Graaff A, Gooris GS, Nijssse J, Wiechers JW, van Aelst AC. 2003. Water Distribution and Related Morphology in Human Stratum Corneum at Different Hydration Levels. *J Invest Dermatol* 120:750-758.

81. Roberts MS, Walker M. 1993. Water: The Most Natural Penetration Enhancer. In Walters KA, Hadgraft J, ed. *Pharmaceutical Skin Penetration Enhancement*. New York: Marcel Dekker, Inc., pp 1-30.
82. Wester RC, Maibach HI. 1995. Penetration Enhancement by Skin Hydration. In Smith EW, Maibach HI, ed. *Percutaneous Penetration Enhancers*. Boca Raton, Florida: CRC Press, pp 21-28.
83. Warner RR, Boissy YL, Lilly NA, Spears MJ, McKillop L, Marshall JL, Stone KJ. 1999. Water Disrupts Stratum Corneum Lipid Lamellae: Damage is Similar to Surfactants. *J Invest Dermatol* 113:960-966.
84. Warner RR, Stone KJ, Boissy YL. 2003. Hydration Disrupts Human Stratum Corneum Ultrastructure. *J Invest Dermatol* 120:275-284.
85. Mak VH, Potts RO, Guy RH. 1991. Does Hydration Affect Intercellular Lipid Organization in the Stratum Corneum? *Pharm Res* 8:1064-1065.
86. Hou SY, Mitra AK, White SH, Menon GK, Ghadially MR, Elias PM. 1991. Membrane Structures in Normal and Essential Fatty Acid-Deficient Stratum Corneum: Characterization of Ruthenium Tetroxide Staining and X-Ray Diffraction. *J Invest Dermatol* 96:215-223.
87. Bouwstra JA, de Vries MA, Bras W, Brussee J, Gooris GS. 1990. The Influence of C_n Azones on the Structure and Thermal Behaviour of Human Stratum Corneum. *Proc Int Symp Control Rel Bioact Mater* 17:33-34.
88. van Hal DA, Jeremiasse E, Juninger HE, Spies F, Bouwstra JA. 1996. Structure of Fully Hydrated Human Stratum Corneum: A Freeze-Fracture Electron Microscopy Study. *J Invest Dermatol* 106:89-95.
89. Suhonen TM, Bouwstra JA, Urtti A. 1999. Chemical Penetration Enhancement of Percutaneous Absorption in Relation to Stratum Corneum Structural Alterations. *J Control Release* 59:149-161.
90. Alonso A, Meirelles NC, Tabak M. 1995. Effect of Hydration Upon the Fluidity of Intercellular Membranes of Stratum Corneum: An EPR Study. *Biochim Biophys Acta* 1237:6-15.
91. Alonso A, Meirelles NC, Yushmanov VE, Tabak M. 1996. Water Increases the Fluidity of Intercellular Membranes of Stratum Corneum: Correlation with Water Permeability, Elastic, and Electrical Resistance Properties. *J Invest Dermatol* 106:1058-1063.
92. Golden GM, Guzek DB, Harris RR, McKie JE, Potts RO. 1986. Lipid Thermotropic Transitions in Human Stratum Corneum. *J Invest Dermatol* 86:255-259.
93. Knuston K, Potts RO, Guzek DB, Golden GM, McKie JE, Lambert WJ, Higuchi WI. 1985. Macro- and Molecular Physical-Chemical Considerations in Understanding Drug Transport in the Stratum Corneum. *J Control Release* 2:67-87.
94. Van Duzee BF. 1975. Thermal Analysis of Human Stratum Corneum. *J Invest Dermatol* 65:404-408.
95. Hagen TA, Flynn GL. 1983. Solubility of Hydrocortisone in Organic and Aqueous Media: Evidence for Regular Solution Behavior in Apolar Solvents. *J Pharm Sci* 72:409-414.
96. Hansen CM. 2000. *Hansen Solubility Parameters: A User's Handbook*. Boca Raton, Florida: CRC Press, Inc. pp 1-24.

97. Greenlaugh DJ, Williams AC, Timmins P, York P. 1999. Solubility Parameters as Predictors of Miscibility in Solid Dispersions. *J Pharm Sci* 88:1182-1190.
98. Liron Z, Cohen S. 1984. Percutaneous Absorption of Alkanoic Acids II: Application of Regular Solution Theory. *J Pharm Sci* 73:538-542.
99. Hancock BC, York P, Rowe RC. 1997. Use of Solubility Parameters in Pharmaceutical Dosage Design. *Int J Pharm* 148:1-21.
100. Elias PM. 1983. Epidermal Lipids, Barrier Function and Desquamation. *J Invest Dermatol* 80:44-49.
101. Wertz PW. 1992. Epidermal Lipids. *Semin Dermatol* 11:106-113.
102. Smith E, Surber E. 2000. The Absolute Fundamentals of Transdermal Permeation. In Gabard B, al e, ed. *Dermatopharmacology of Topical Drugs*. Germany: Springer, pp 23-35.
103. Inoue K, Ogawa K, Suzuki Y, Okada J, Kusai A, Ikeda M, Nishimura K. 2000. The Skin Permeation Mechanism of Ketotifen: Evaluation of Permeation Pathways and Barrier Components in the Stratum Corneum. *Drug Dev Ind Pharm* 26:45-53.
104. Abraham MH, Chadha HS, Mitchell RC. 1995. The Factors That Influence Skin Penetration of Solutes. *J Pharm Pharmacol* 47:8-16.
105. Albery WJ, Hadgraft J. 1979. Percutaneous Absorption: Theoretical Description. *J Pharm Pharmacol* 31:129-139.
106. Boddé HE, van den Brink I, Koerten HK, De Haan FH. 1991. Visualization of *In Vitro* Percutaneous Penetration of Mercuric Chloride; Transport Through Intercellular Space Versus Cellular Uptake Through Desmosomes. *J Control Release* 15:227-236.
107. Elias PM, Cooper ER, Korc A, Brown BE. 1981. Percutaneous Transport in Relation to Stratum Corneum Structure and Lipid Composition. *J Invest Dermatol* 76:297-301.
108. Kim N, El-Khalili M, Henary MM, Strekowski L, Michniak BB. 1999. Percutaneous Penetration Enhancement Activity of Aromatic *S,S*-Dimethyliminosulfuranes. *Int J Pharm* 187:219-229.
109. Hadgraft J, Peck J, Williams DG, Pugh WJ, Allan G. 1996. Mechanisms of Action of Skin Penetration Enhancers/Retarders: Azone and Analogues. *Int J Pharm* 141:17-25.
110. Sugibayashi K, Nakayama S, Seki T, Hosoya K, Morimoto Y. 1992. Mechanism of Skin Penetration-Enhancing Effect by Laurocapram. *J Pharm Sci* 81:58-64.
111. Swartzendruber DC, Wertz PW, Kitko DJ, Madison KC, Downing DT. 1989. Molecular Models of the Intercellular Lipid Lamellae in Mammalian Stratum Corneum. *J Invest Dermatol* 92:251-257.
112. Breathnach AS, Goodman T, Stolinski C, Gross M. 1973. Freeze-Fracture Replication of Cells of Stratum Corneum of Human Epidermis. *J Anat* 114:65-81.
113. Holman BP, Spies F, Bodde HE. 1990. An Optimized Freeze-Fracture Replication Procedure for Human Skin. *J Invest Dermatol* 94:332-335.
114. Bouwstra JA, Dubbelaar FE, Gooris GS, Weerheim AM, Ponc M. 1999. The Role of Ceramide Composition in the Lipid Organisation of the Skin Barrier. *Biochim Biophys Acta* 1419:127-136.

115. Krill SL, Knutson K, Higuchi WI. 1992. The Stratum Corneum Lipid Thermotropic Phase Behaviour. *Biochim Biophys Acta* 1112:281-286.
116. Naik A, Guy RH. 1997. Infrared Spectroscopic and Differential Scanning Calorimetric Investigations of the Stratum Corneum Barrier Function. In Potts RO, Guy RH, ed. *Mechanisms of Transdermal Drug Delivery*. New York: Marcel Dekker, Inc., pp 87-162.
117. Ribaud C, Garson JC, Doucet J, Leveque JL. 1994. Organization of Stratum Corneum Lipids in Relation to Permeability: Influence of Sodium Lauryl Sulfate and Preheating. *Pharm Res* 11:1414-1418.
118. Lampe MA, Burlingame AL, Whitney J, Williams ML, Brown BE, Roitman E, Elias PM. 1983. Human Stratum Corneum Lipids: Characterization and Regional Variations. *J Lipid Res* 24:120-130.
119. Surber C, Wilhelm KP, Hori M, Maibach HI, Guy RH. 1990. Optimization of Topical Therapy: Partitioning of Drugs into Stratum Corneum. *Pharm Res* 7:1320-1324.
120. Walter K, Kurz H. 1988. Binding of Drugs to Human Skin: Influencing Factors and the Role of Tissue Lipids. *J Pharm Pharmacol* 40:689-693.
121. Kurz H, Fichtl B. 1983. Binding of Drugs to Tissues. *Drug Metab Rev* 14:467-510.
122. Phillips CA, Michniak BB. 1995. Transdermal Delivery of Drugs with Differing Lipophilicities Using Azone Analogs as Dermal Penetration Enhancers. *J Pharm Sci* 84:1427-1433.

CHAPTER 5

THE EFFECTS OF OCTISALATE AND PADIMATE O ON FENTANYL DISTRIBUTION ACROSS HUMAN STRATUM CORNEUM

5.1. INTRODUCTION

It is well-recognised that the stratum corneum (SC) acts as a barrier to percutaneous drug absorption (1, 2), and may serve as a reservoir for many topically applied substances (3, 4). Furthermore, the interactions between and the physicochemical properties of drug, vehicle, and SC influence drug partitioning into and diffusion across the SC (i.e. the early processes involved in percutaneous absorption) and may therefore play an important role in total percutaneous drug absorption (5).

Considering these factors, it is reasonable to infer that drug concentrations within the SC will be predictive of drug concentrations that will be available for absorption into the underlying tissues and systemic circulation (6). Rougier and coworkers substantiated this hypothesis, using several compounds belonging to various chemical classes and with different physicochemical properties (7). They found that a strong correlation existed between the total amount of compound penetrating the skin within 96 h and the amount of compound found within the SC after a 30 min exposure time ($r^2=0.96$, $p<0.001$). This correlation was independent of the contact time, dose applied, vehicle used, anatomical site, and animal species.

The "tape stripping technique", such as the one employed by Rougier et al, is an increasingly popular method used to investigate the localization and distribution of substances within the SC (8). In essence, this technique involves the application of a chemical (within a vehicle) to the SC surface for a predetermined exposure time. After the non-volatile components of the formulation are wiped from the SC surface, adhesive tape is applied to and removed from the SC surface. Layers of the SC (and drug contained within them) are sequentially removed by repeating the tape strip procedure. The drug is extracted from the sequential tape strips and drug concentrations within the extracts are determined using a suitable analytical method (9).

The mass of SC removed by tape stripping is influenced by a number of experimental factors, such as the adhesive properties of the tape (10), the composition of the applied formulation (11), and the hydration state of the SC (12). Therefore, the number of tape strips reported to remove most, or all, of the SC varies from 10 to 100 tape strips (13, 14).

The "tape stripping technique" offers numerous advantages over alternative methods used to measure drug concentrations within the SC and total percutaneous drug

absorption. Skin surface biopsies or SC scraping techniques can also be used for the direct determination of drug concentrations within the SC (15-19). Given that these procedures involve removal of the SC by cyanoacrylate glue (skin surface biopsies) or scraping with a dermal steel curette (SC scraping) they are generally more invasive than the "tape stripping technique". Furthermore, these methods do not remove SC layers in a controlled, sequential manner and reliable determination of drug content within the SC can be obscured by the presence of sebum, sweat, or hair follicles. In terms of determining percutaneous drug absorption *in vivo*, plasma and/or excreta concentrations of topically applied substances are frequently low due to the excellent barrier properties of the SC. Therefore, to circumvent problems associated with inadequate analytical assay sensitivity, radioactively labeled compounds are often used during *in vivo* experimentation (20). Hence, from a practical and ethical standpoint, the "tape stripping technique" is not only less invasive and less time consuming, but can also eliminate the need for radiolabeled substances.

Due to the advantages of the "tape stripping technique", it is not surprising that it has been used to investigate the efficacy, bioavailability and bioequivalence of topical dosage forms (21-26), SC barrier function (9, 27-29), reservoir capacity (9, 30, 31), and changes to the physicochemical and physiological properties of the SC as a function of increasing SC depth (32-35). The application of this technique to probe the mechanisms involved in transdermal drug delivery is of particular relevance to the work presented in this chapter.

The amount of drug and the thickness of the SC removed by each tape strip can be quantified in order to determine drug distribution across the SC (i.e. concentration-depth profiles). The data generated from these studies can be used to analyse the effects of different vehicles and/or chemical penetration enhancers on drug permeation through the skin (6, 36-39).

It has also become common practice to fit drug distribution profiles to the following non-steady-state solution to Fick's Second Law of Diffusion (40-43):

$$C_x = K_{SC/V} C_V \left\{ 1 - \frac{x}{L} - \frac{2}{\pi} \sum_{n=1}^{\infty} \frac{1}{n} \sin\left(n\pi \frac{x}{L}\right) \exp\left(-\frac{D}{L^2} n^2 \pi^2 t\right) \right\} \quad 5.1$$

where C_x represents the drug concentration within the SC as a function of SC position, x , for a given exposure time, t . $K_{SC/V}$ is the partition coefficient of the drug between the SC and the vehicle, while C_v is the concentration of drug within the vehicle. L is the diffusional pathlength of the drug across the SC, and D is the diffusion coefficient of the drug within the SC. The transport parameters derived from this model ($K_{SC/V}$ and D/L^2) can then be used to calculate the permeability coefficient of the drug through the SC, and estimate drug flux and cumulative transport across the SC. However, this solution for the concentration profile of a drug as a function of relative SC position is only relevant for the boundary conditions depicted in Figure 5.1.

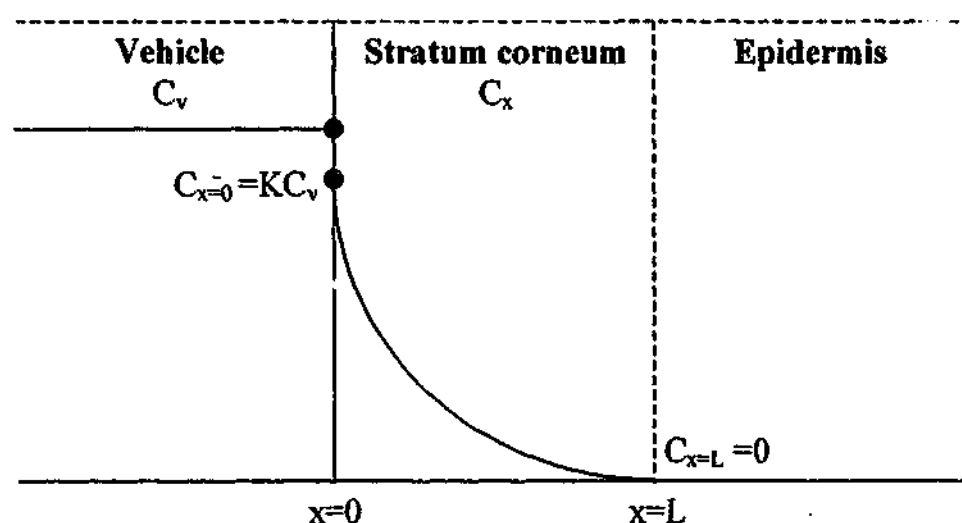


Figure 5.1. Non-steady-state drug concentration profile (C_x) as a function of position (x) within the SC. The drug concentration at the SC surface (C_0) is a product of the drug's skin-vehicle partition coefficient ($K_{SC/V}$) and the concentration of the drug within the applied vehicle (C_v). C_v remains constant over the exposure time. The epidermis acts as a sink for drug diffusion such that there is a negligible concentration of drug present at the base of the SC (i.e. $C_{x=L}=0$).

5.2. OBJECTIVES

The primary objectives of the work presented in this chapter were to determine:

- i. The distribution of fentanyl across human SC at various exposure times
- ii. Whether octisalate (OS) and padimate O (PO) modify fentanyl distribution across the SC, and if so,
- iii. From the distribution data, the likely possible mechanism(s) by which OS and PO modify the passage of fentanyl across the SC.

The secondary objective of these studies was to determine the amount of fentanyl, OS and PO recovered at the SC surface and within the SC, in relation to applied dose and various exposure times.

5.3. MATERIALS AND METHODS

5.3.1. Materials

Fentanyl was manufactured by Macfarlan Smith Ltd (Edinburgh, UK). OS and PO were supplied by Bronson and Jacobs (Australia). Acetonitrile and methanol (Merck Pty Ltd, Australia) were HPLC grade. Water was purified by a Milli-Q™ water purification system (Millipore, Bedford, MA, USA). All other reagents were of analytical grade.

5.3.2. Skin preparation

Human female abdominal tissue was obtained following abdominoplasty from two individual donors. Full-thickness skin samples were prepared by removing subcutaneous tissue and fat from the underside of the dermal membrane using a stainless steel surgical blade. Excess fat residue was removed from the skin surface by gentle blotting with low-lint, absorbent tissue (Kimwipes®, Kimberly-Clark Australia). The skin was stored in aluminium foil at -20°C for up to 12 months prior to use (44). Before the commencement of each study, the skin was defrosted under ambient conditions for approximately 2 to 4

h. The SC surface was rinsed with Milli-Q™ water and gently wiped with Kimwipes® four times, in order to remove any surface contamination.

The skin was then laid flat, SC side up, on a teflon board and dissected into 1 x 5 cm (width x length) sections ($n = 5$) using a stainless steel surgical blade. Each section was laid flat, dermal side up, and quick-dry super glue (Selleys® Fix'n'Go Supa Glue, Selleys, Australia) was blotted onto the ventral surface of the dermis. The skin sections were immediately mounted, SC side up, on to 1 x 7 cm pieces of cardboard (the excess 2 cm in length was to enable handling of the samples). Gentle pressure was then applied to the skin for approximately 10 sec to ensure contact with the cardboard. The SC surface of each sample was quickly (<20 sec) wiped with a Kimwipe® (pre-moistened with ethanol) to ensure complete removal of sebaceous lipids and the skin samples were then left untouched for 5 min to allow the glue to dry.

5.3.3. Tape stripping procedure

To ensure that the skin samples remain *in situ* during the experiment, they were adhered, cardboard side down, onto a 1.5 x 1.5 x 100 cm (height x width x length) rectangular steel rod using double-sided adhesive tape (Scotch® Permanent Double Stick Tape, 3M, Australia).

The formulations were prepared by dissolving 5%w/v fentanyl, alone or with 5%w/v OS or PO, in 95%v/v ethanol. The formulations were applied as a finite dose ($5 \mu\text{l}/\text{cm}^2$) to the SC surface of each skin sample. After a pre-determined exposure time (5 min (0.08 h), 0.5, 2, 6, or 16 h), excess formulation was removed from the SC surface using the procedure described in Section 5.3.4.1. Fentanyl, OS or PO were extracted from the surface wipes using the procedure outlined in Section 5.3.4.2.

After the surface wipe was performed, the SC was progressively removed by sequential adhesive tape stripping. Sections of 1.2 x 5 cm pieces of polyester adhesive tape (3M, product # 8440) were equilibrated under ambient conditions for at least 2 h prior to use. The tape sections were applied to the SC surface and a constant pressure of $240 \text{ g}/\text{cm}^2$ was applied to the tape for 5 sec. The following measures were incorporated into the experimental design to ensure uniform pressure was applied to the tape, and hence uniform contact between the skin and the tape:

- i. Solid stainless steel slabs (total weight 1200 g), with flush surfaces, were used to applied pressure to the tape.
- ii. A steel rod was used to elevate the samples above the bench surface to ensure that the slabs were not in contact with any other matter whilst they were applied to the skin.
- iii. Fat and subcutaneous tissue was carefully removed from the dermis in a manner that produced smooth skin samples.
- iv. Each piece of tape was folded onto itself to produce an ~1 cm overhang at each end. This was done to ensure easy handling of the tape such that even pressure was applied to the tape upon its application and removal from the SC (and to avoid possible contamination of the tape).

After the tape was applied, it was removed from the SC surface. The tape stripping procedure was repeated 20 times in order to remove most of the SC (45). Fentanyl, OS and PO were extracted from the tape strips using the method detailed in Section 5.3.5.1.

The mass of SC removed (M_{sc}) was determined by weighing each tape strip before (i.e. after the equilibration period) and after the tape stripping procedure (Sartorius MC5 microbalance). Assuming a constant SC density (D_{sc}) of 1g/cm^3 (46) and that the SC was uniformly distributed on each tape strip, the length of SC removed (L) was determined from the following equation:

$$L = \frac{M_{sc} D_{sc}}{A_{exp}} \quad 5.2$$

where A_{exp} is the area of skin exposed (5 cm^2).

5.3.4. Surface wipe procedure and extraction

5.3.4.1. Surface wipe procedure

Excess fentanyl, OS or PO were removed from the SC surface by swabbing the surface with cotton buds (Johnson and Johnson, Australia). The cotton buds were rolled over the SC surface in the following manner:

- i. The perimeter of the exposure area was swabbed once
- ii. Starting from the top left hand corner of the exposure area and working down, the SC surface was wiped in a unidirectional manner (left to right, then right to left) until the entire area was swabbed.
- iii. Steps i. and ii. were repeated four times, using a fresh cotton bud each time.

5.3.4.2. Extraction of fentanyl, octisalate, and padimate O from surface wipes

The cotton buds were placed in a glass vial and a 10 ml aliquot of 100% methanol was added. The contents were sealed with a teflon-lined lid, vortexed for 30 sec, and then placed on a horizontal roller mixer (Ratek Instruments Pty Ltd, Victoria, Australia) for gentle mixing over 16 h at ambient temperature (Stage 1). At the end of the 16 h extraction period, the sample was vortexed for 30 sec, the cotton buds were then transferred to an empty glass vial and 5 ml of methanol was added. The sample was vortexed for 30 sec, then placed on the horizontal roller mixer for 8 h at ambient temperature (Stage 2). At the end of the 8 h period, the methanol extract retained from Stage 1 was added to the sample. The sample was then vortexed for 1 min and 5 ml of the extract was centrifuged at 3500 rpm for 15 min at 25°C. A 1 ml aliquot of the supernatant was diluted to 10 ml with methanol for HPLC/UV analysis.

5.3.4.3. Validation of the surface wipe procedure

5.3.4.3.1. Surface wipe samples

A solution containing 0.5%, 2.5%, or 5%w/v of fentanyl, OS or PO in 95% ethanol was applied as a "finite dose" ($5 \mu\text{l}/\text{cm}^2 = 25 \mu\text{l}$) to $1 \times 5 \text{ cm}$ sections of skin ($n = 5$) such that the amount of fentanyl, OS or PO deposited at the SC surface was 125, 625, or 1250 μg , respectively.

In order to minimise chemical loss from the SC surface due to rapid partitioning into the SC, the solutions were in contact with the skin for only 20 sec. It was recognised that ethanol would not have completely evaporated from the SC surface within this exposure time and that its presence could enhance the efficiency of the surface wipe procedure. Therefore, in order to mimic actual experimental conditions as closely as

possible, ethanol was evaporated from the SC surface under a gentle stream of nitrogen during the 20 sec exposure time.

Following the surface wipe procedure outlined in Section 5.3.4.1, fentanyl, OS and PO were extracted from the surface wipes as described in Section 5.3.4.2.

5.3.4.3.2. Surface wipe standards

A "finite dose" ($5 \mu\text{l}/\text{cm}^2$) of 95%v/v ethanol alone was applied to the SC surface of $1 \times 5 \text{ cm}$ sections of skin for 20 sec. As described above, ethanol was evaporated from the skin surface under a gentle stream of nitrogen during this exposure time. The surface wipe procedure (Section 5.3.4.1) was then performed in order to obtain blank surface wipe samples.

Blank cotton buds were placed in a glass vial, and a 25 μl aliquot of 0.5%, 2.5%, or 5%v/v of fentanyl, OS or PO in 95%v/v ethanol was added to the vial. The ethanol was evaporated under nitrogen for 20 sec such that 125, 625, or 1250 μg of analyte was deposited in the vial. The extraction procedure outlined in Section 5.3.4.2 was performed.

5.3.4.3.3. Recovery, accuracy, and precision

The HPLC/UV assay methods used for the detection of fentanyl, OS, and PO are detailed in Section 5.3.6. Recovery was determined by comparing the peak areas of fentanyl, OS or PO extracted from the surface wipe samples to the peak areas generated from surface wipe standards (i.e. blank surface wipes spiked with analyte). Intra-day precision and accuracy of the procedure were determined from the surface wipe samples ($n=5$) at the three different concentrations (125, 625, or 1250 μg per 5 cm^2 skin surface area). Inter-day precision was determined by repeating the surface wipe procedure for these different concentrations on three different days.

The recovery, accuracy and precision of the surface wipe procedure for fentanyl, OS and PO are presented in Table 5.1.

5.3.5.2. Validation of fentanyl, octisalate, and padimate O extraction from tape strips

5.3.5.2.1. Tape strip samples

A “finite dose” ($5 \mu\text{l}/\text{cm}^2$) of 95%v/v ethanol alone was applied to the SC surface of 1×5 cm sections of skin for 20 sec ($n = 3$). Ethanol was evaporated from the skin surface under a gentle stream of nitrogen during this exposure time. After the surface wipe was performed (Section 5.3.4.1) tape strips were applied to, and removed from the SC surface according to the procedure described in Section 5.3.3 ($n = 5$ tape strips per skin sample).

The tape strips were then laid flat, adhesive side up. Ethanolic solutions containing 4, 40, 400, or 2,000 $\mu\text{g}/\text{ml}$ of fentanyl, OS, or PO were applied to the samples, at a dose of 25 μl , in order to deposit 0.1, 1, 10, or 50 μg of analyte, respectively. The samples were left *in situ*, at ambient conditions, for 2 h. This exposure time was arbitrarily chosen to allow the ethanol to evaporate and also to allow the analyte to partition into the SC removed by the tape. At the end of the 2 h period, fentanyl, OS or PO were extracted from the tape strips (Section 5.3.5.1).

It should be noted that the samples were prepared in this manner, rather than directly dosing the SC with analyte before tape stripping, in order to minimise potential sources of variation. For instance, the presence of furrows in the skin and potential differences between SC weights removed by tape stripping are factors that could potentially confound the results obtained with the latter approach.

5.3.5.2.2. Tape strip standards

The skin was prepared and tape-stripped using the method described above. However, rather than dosing the tape strips with analyte, they were left blank and immediately transferred to 15 ml glass centrifuge vials. 25 μl aliquots of ethanolic solutions containing 4, 40, 400, or 2,000 $\mu\text{g}/\text{ml}$ of fentanyl, OS or PO were also added to the vials. Ethanol was evaporated under nitrogen for 20 sec such that 0.1, 1, 10, or 50 μg of analyte was deposited in the vials, respectively. The extraction procedure described in Section 5.3.5.1 was then performed.

5.3.5.2.3. Recovery, accuracy, and precision

The HPLC/UV assay methods that were used for the quantification of fentanyl, OS and PO in the tape strip extracts are detailed in Section 5.3.6.

Recovery was determined by comparing the peak areas of fentanyl, OS or PO extracted from the tape strip samples to the peak areas of blank tape strips to which fentanyl, OS or PO were added. Intra-day precision and accuracy of the procedure were determined from the tape strip standards ($n = 5$) prepared at the different concentrations (0.1, 1, 10, or 50 μg per 5 cm^2 skin surface area). The tape strip extracts containing analyte at these known concentrations were prepared on three different days in order to determine inter-day precision. The recovery, accuracy and precision of the assay procedures for fentanyl, OS and PO extracts from the tape strips are presented in Table 5.2.

Table 5.2. Recovery, intra- and inter-day precision, and accuracy of fentanyl, OS and PO extraction from SC tape strips.

	Amount (μg)	% Recovery (Mean \pm SD)	Inter-day precision (%CV)	Intra-day precision (%CV)	Accuracy (%)
Fentanyl	0.1	101.2 \pm 11.5	7.8	8.8	107.9
	1	103.1 \pm 5.0	4.9	5.4	105.6
	10	98.0 \pm 2.1	3.8	2.4	99.1
	50	99.5 \pm 3.8	2.6	4.6	100.6
OS	0.1	92.6 \pm 6.4	8.1	8.2	104.7
	1	100.3 \pm 9.0	3.0	7.2	106.8
	10	96.2 \pm 5.1	3.9	6.3	100.3
	50	102.0 \pm 5.7	2.5	4.9	98.3
PO	0.1	97.3 \pm 4.9	9.6	11.8	104.8
	1	101.2 \pm 5.6	5.3	8.9	97.4
	10	98.5 \pm 4.7	4.7	1.3	96.6
	50	93.9 \pm 8.2	3.1	2.0	109.0

5.3.6. Analytical methods

Concentrations of fentanyl, OS or PO within the surface wipe and tape strip extracts were determined using RP- HPLC/UV. The HPLC system consisted of a Waters 610 pump, Waters 600E system controller, Waters 712 WISP autosampler, and Waters 486 UV absorbance detector. The data was analysed on a Shimadzu C-R6A integrator (Shimadzu Corp., Japan).

Fentanyl quantification was performed using a Waters Symmetry C₁₈ column (5µm particle size, 3.9 x 150 mm) and a RP-8 Newguard cartridge guard column (Aquapore 7 µm, 3 x 15mm, Alltech/Perkin Elmer, CA). The injection volume was 30 µl. Mobile phase (35%v/v acetonitrile, 65%v/v water, 0.068%v/v perchloric acid (70%v/v), and 10 mM heptane sulphonic acid) was pumped through the column at a flow rate of 1ml/min. UV detection was performed at 210 nm. The retention time for fentanyl under these conditions was ~6.9 min.

A Waters Symmetry C₈ cartridge column (5µm particle size, 3.9x150mm) and RP-8 Newguard cartridge guard column was used for the quantification of OS and PO. Further details of the individual HPLC/UV assay conditions are provided in Table 5.3.

Calibration curves for each assay were constructed using standard solutions at concentrations within the range of 0.1 to 10 µg/ml. A stock solution of fentanyl, OS or PO (50 µg/ml in methanol) was diluted with an appropriate volume of methanol to yield the expected standard solution concentration. A linear relationship between peak area and concentration was confirmed by the correlation coefficient generated by linear regression (using the least squares method) of the calibration curve, which, for each assay, was weighted by a factor of 1/x. The linearity of all assays was excellent ($r^2 > 0.995$).

Intra-day precision and accuracy were determined from standard solutions (n=5) of three different concentrations (0.1, 1 and 10 µg/ml). Precision (%CV) was highly satisfactory for all assays (less than 6% for fentanyl, less than 9% for OS and less than 8% for PO). The accuracy of each assay was also satisfactory, ranging from 98.5 to 101.1% for fentanyl, 94.3 to 101.8% for OS and 97.6 to 101.5% for PO.

Inter-day precision of each assay was determined over three different days, using standard solutions prepared on each day of analysis. All assays were highly reproducible, with precision being less than 5% for fentanyl, less than 7% for OS and less than 8% for PO.

Table 5.3. HPLC/UV assay conditions for octisalate and padimate O

	Injection volume (μ l)	Mobile phase Composition (%v/v)	Flow rate (ml/min)	Detection wavelength (nm)	Retention time (min)
OS	40	65% acetonitrile, 15% methanol, 20% water, 0.04% trifluoroacetic acid	0.9	310	~10.0
PO	80	65% acetonitrile, 15% methanol, 20% water, 0.04% trifluoroacetic acid	0.9	345	~8.9

5.3.7. Mathematical analysis

5.3.7.1. Normalisation of stratum corneum depth and fentanyl concentrations within the stratum corneum

Fentanyl concentrations in the SC were determined as a function of position within the SC (x) relative to the total thickness of SC removed by tape stripping (L) (41). The normalised SC depth (x/L) for the n th tape strip was calculated using the following equation:

$$\frac{x}{L} = \frac{\sum_{i=1}^n L_{SCi}}{\sum_{i=1}^N L_{SCi}} \quad 5.3$$

Where L_{SCi} is the length of SC removed for tape strip, i , and N is the total number of tape strips. Due to inter- and intra- subject variations in total SC thickness and differences in the amount of SC removed by each tape strip (47), it was necessary to normalise SC depth in this manner to facilitate data analysis. As discussed in Section 5.4.1, the amount of fentanyl found within the SC was also normalised to the SC weight removed due to similar reasons.

Only the information gathered (i.e. concentrations of fentanyl found within the SC and normalised SC depth) from tape strips 2 to 20 were used to construct the distribution

profiles presented in Section 5.4.2. The amount of fentanyl removed from the first tape strip was considered to represent unabsorbed fentanyl residing at the SC surface (22). Therefore, the amount of fentanyl residing at the SC surface at a given exposure time represents the sum of the amount of fentanyl extracted from tape strip 1 and the amount extracted from the surface wipe.

5.3.7.2. Areas under the fentanyl distribution profiles

The areas under the fentanyl distribution profiles (i.e. areas under the curves (AUCs) were calculated using the trapezoidal method (48):

$$AUC = \frac{C_i + C_{i+1}}{2} \times \left(\frac{x}{L_{i+1}} - \frac{x}{L_i} \right) \quad 5.4$$

where C_i is the SC concentration of fentanyl at a normalised position within the SC (x/L_i) removed by tape strip, i . AUCs were calculated between x/L for tape strip 2 and x/L for tape strip 20 (i.e. the entire SC) ($AUC_{x/L_2 \rightarrow 20}$), between x/L for tape strip 2 and x/L for tape strip 10 (i.e. the upper region of the SC) ($AUC_{x/L_2 \rightarrow 10}$), and between x/L for tape strip 11 and x/L for tape strip 20 (i.e. the lower region of the SC) ($AUC_{x/L_{11} \rightarrow 20}$) (Figure 5.2).

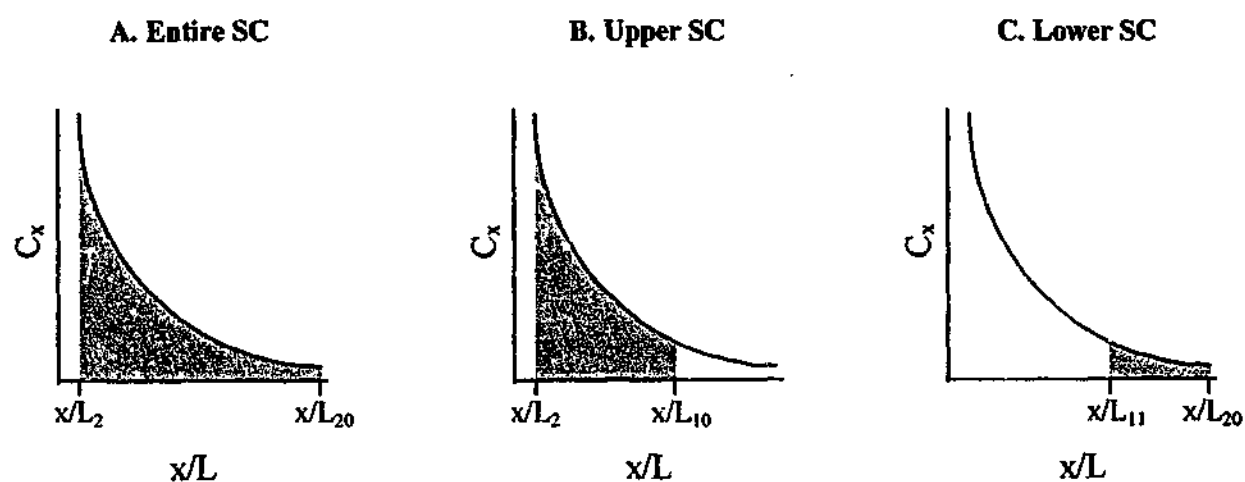


Figure 5.2. Schematic representation showing AUCs calculated for fentanyl distribution profiles (i.e. drug concentration at SC position, x , (C_x) versus normalised SC depth (x/L)) between the limits of A) x/L for tape strip 2 (x/L_2) and tape strip 20 (x/L_{20}) (the entire SC, $AUC_{x/L_2 \rightarrow 20}$), B) x/L for tape strip 2 (x/L_2) and tape strip 10 (x/L_{10}) (the upper region of the SC, $AUC_{x/L_2 \rightarrow 10}$) or C) x/L for tape strip 11 (x/L_{11}) and tape strip 20 (x/L_{20}) (the lower region of the SC, $AUC_{x/L_{11} \rightarrow 20}$)

5.3.7.3. Kinetic modeling of stratum corneum surface clearance

When fentanyl was applied alone, the amount residing at the SC surface appeared to decline bi-exponentially as a function of time. Hence the two compartment model defined in Equation 5.5 was used in order to determine the initial (“distribution”) and subsequent (“elimination”) hybrid rate constants, α and β :

$$A_v = Ae^{-\alpha t} + Be^{-\beta t} \quad 5.5$$

where A and B are pre-exponential constants. When fentanyl (applied with OS or PO), OS or PO were applied to the skin, the decline in the amount of chemical residing at the SC surface (A_v) as a function of time (t) was fitted to the following first-order elimination rate process in order to derive the elimination rate constant (k):

$$A_v = Ae^{-kt} \quad 5.6$$

Semilogarithmic transformations of the amount of chemical residing at the SC surface were determined as a function of time in conjunction with Equations 5.5 and 5.6.

5.3.8. Statistical analysis

Statistical significance was determined using one-way analysis of variance (ANOVA). Post-hoc all pairwise multiple comparison of the means within different groups was performed using the Student-Newman-Keuls (SNK) test. A probability of $p < 0.05$ was considered statistically significant. All results are presented as the mean \pm SEM, unless otherwise indicated.

5.4. RESULTS AND DISCUSSION

5.4.1. Vehicle and time dependent effects on stratum corneum weight removed

The effects of different vehicles on the SC mass removed by tape stripping have been previously documented (11, 37, 49). It has been demonstrated that various solvents

can alter corneocyte cohesion to different degrees (49). Although these studies revealed that ethanol did not significantly increase the cohesiveness of the SC compared with untreated skin, it was found that the subsequent increases in cohesion following exposure to the solvents were related to the amount of lipid extracted from the SC. On the other hand, Higo et al (37) found that the amount of SC removed by tape stripping was significantly greater when the skin was exposed to the penetration enhancer, oleic acid, compared with the corresponding controls. It was postulated that this effect may be due to "loosening" of the corneocytes. In addition, this effect appeared to be dependent on the exposure time, which is consistent with previous research (11).

As discussed in Chapter 7, exposure of the SC to OS or PO may cause lipid extraction from the superficial layers of the SC. Therefore, it would be reasonable to speculate that OS and PO may alter corneocyte cohesion, and thus may influence the mass of SC removed by tape stripping. In light of the findings from Chapter 7 and the previous research mentioned above, it was necessary to investigate whether the presence of OS or PO influenced the mass of SC removed by the tape stripping procedure.

The amount (mg) of SC removed per tape strip and the total amount of SC removed by the entire tape stripping procedure (n=20 tape strips) are shown in Figures 5.3 and 5.4, respectively. As seen in Figure 5.3, the amount of SC removed declines exponentially as a function of tape strip number.

It has frequently been observed, both *in vitro* and *in vivo*, that the mass of SC detached by tape stripping declines exponentially as a function of increasing SC depth (or tape strip number) (45, 50). This relationship is likely to be a consequence of changes to the cohesive properties of the SC with increasing depth.

It has been demonstrated that corneocyte cohesion gradually increases with increasing tape strip number (32, 49). Ultrastructural studies have revealed that initial tape strips (tape strips 1 to 3) removed the upper portion of the stratum disjunctum, in which the corneocytes are "loosely bound" (i.e. minimal inter-corneocyte adhesion) (49). Subsequent tape strips removed the lower portion of the stratum disjunctum (tape strips 4 to 7) and the stratum compactum (tape strips 8 to 10). Consequently, the force required to detach corneocytes gradually increased, reaching a plateau in the stratum compactum. Results from protein content analysis and spectrophotometric methods have supported these findings (51, 52).

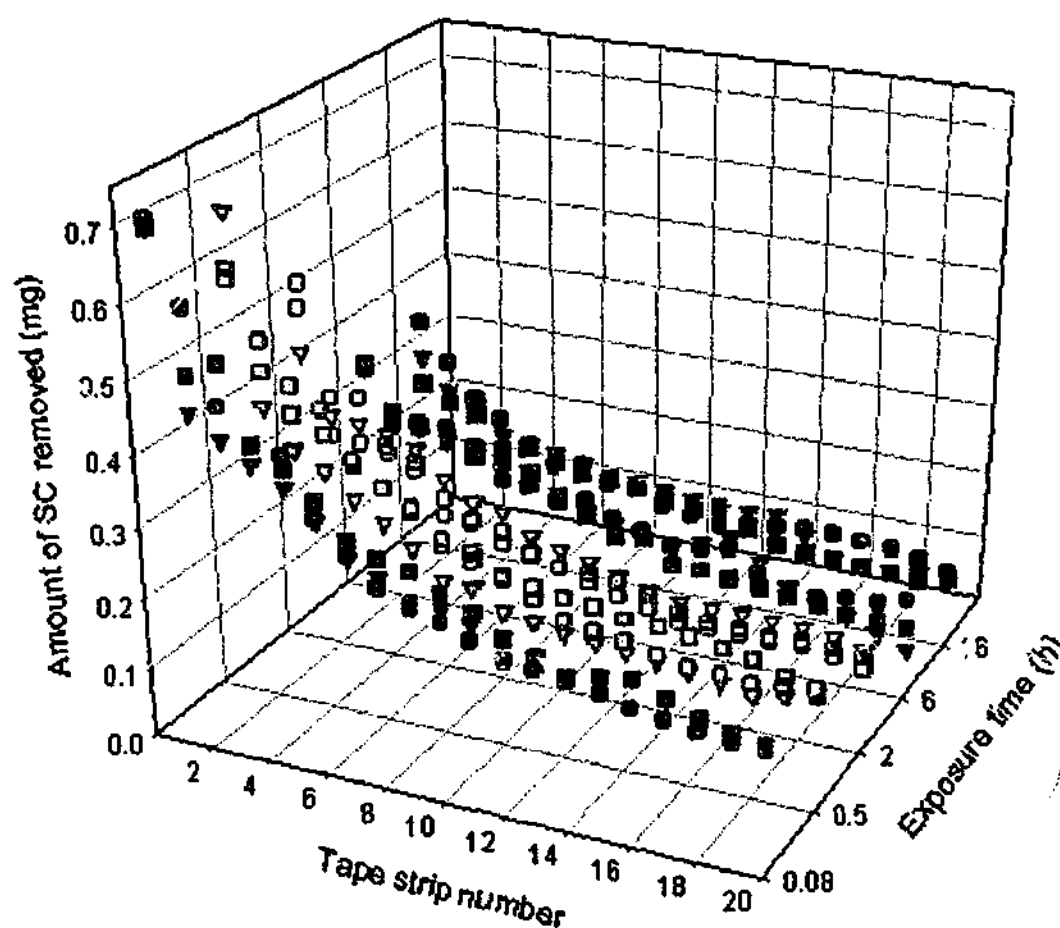


Figure 5.3. Amount of SC removed by tape stripping skin exposed to fentanyl alone (circles), fentanyl with OS (squares), and fentanyl with PO (triangles) at 0.08 h (red), 0.5 h (orange), 2 h (yellow), 6 h (green) and 16 h (blue).

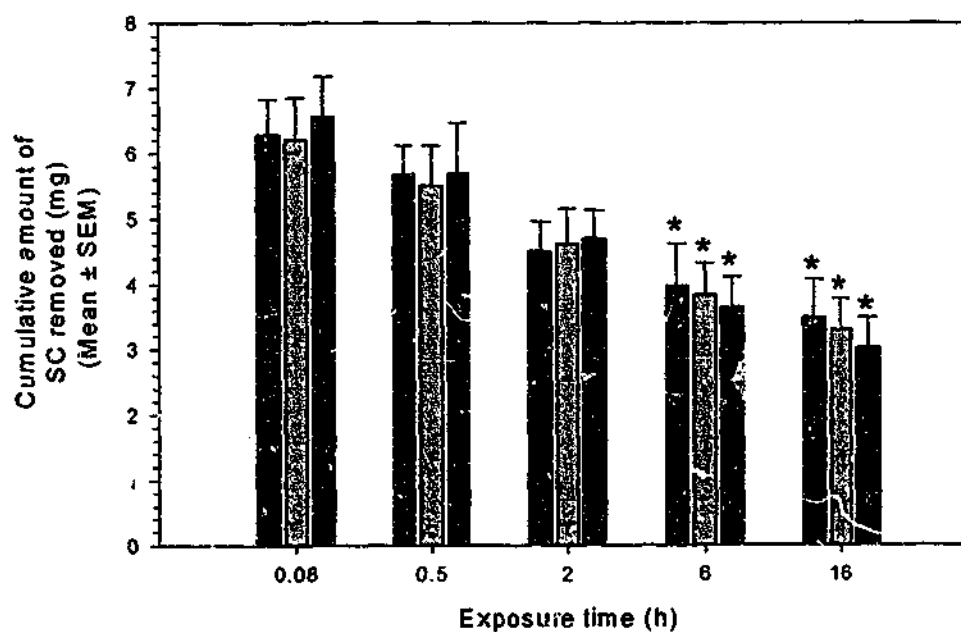


Figure 5.4. Cumulative amount of SC removed by 20 tape strips of skin exposed to fentanyl alone (■), fentanyl with OS (▨), and fentanyl with PO (□). Statistical significance ($p < 0.05$) compared with 0.08h is denoted by *.

Table 5.1. Recovery, intra- and inter-day precision, and accuracy for the fentanyl, OS, and PO surface wipe procedure.

	Amount (μg)	Spiked amount (μg) (Mean \pm SD)	% Recovery (Mean \pm SD)	Inter-day precision (%CV)	Intra-day precision (%CV)	Accuracy (%)
Fentanyl	125	118.4 \pm 2.8	100.5 \pm 7.3	4.4	7.0	93.9
	625	627.8 \pm 14.0	101.5 \pm 3.5	2.3	5.4	102.9
	1250	1240.8 \pm 21.2	98.82 \pm 2.3	1.7	2.1	100.5
OS	125	122.1 \pm 2.0	105.2 \pm 11.2	5.8	7.5	107.5
	625	630.8 \pm 19.5	96.3 \pm 14.3	1.5	3.1	102.8
	1250	1245.4 \pm 30.0	96.9 \pm 4.6	0.6	3.3	99.5
PO	125	130.6 \pm 5.7	98.9 \pm 2.9	6.0	8	103.9
	625	622.9 \pm 13.8	100.9 \pm 10.3	4.1	2.5	98.6
	1250	1251.2 \pm 25.6	103.6 \pm 6.6	2.1	3.0	97.9

5.3.5. Tape strip extraction

5.3.5.1. Extraction of fentanyl, octisalate, and padimate O from tape strips

The tape strips were placed adhesive side down onto filter paper and the samples were then cut to size and individually placed into 15 ml glass centrifuge vials. Aliquots of HPLC grade methanol 100% were added to the tape strip samples. 10 ml was added to each of the first 10 tape strips, and 5ml was added tape strips 11 to 20. The samples were vortexed for 30 seconds and then placed in a 25°C shaking water bath (SS40-D, Grant Instruments, Cambridge, England), where they were continuously shaken at 15 strokes/min for 24 h.

At the end of the 24 h period, the samples were removed from the water bath and vortexed for 30 sec. The tape strips and filter paper were removed from the vials and discarded. The extracts were then centrifuged at 3500 rpm for 15 min at 25°C in a Beckman GS-CR centrifuge (Beckman Instruments, Palo Alto, CA). After centrifugation, a 1 ml aliquot was taken from each of the extracts of tape strips 1 and 2 and diluted to 10 ml with methanol for HPLC/UV analysis. The extracts from tape strips 3 to 20 were analysed undiluted.

As shown in Figures 5.3 and 5.4, the amount of SC removed by the tape stripping procedure gradually declines as the exposure time increases from 0.08 to 16 h. At 0.08 h, the total amount of SC removed by $n=20$ tape strips was in the order of 6 mg per 5cm^2 , which is consistent with previous findings (53). However, at 6 and 16 h, the total amount of SC removed significantly declined to approximately 3 to 4 mg per 5cm^2 ($p<0.05$). Given that the amount of SC removed was not significantly different when the skin was exposed to fentanyl applied with OS or PO compared with fentanyl applied alone at any exposure time, and that the adhesive properties of the tape were constant, it is reasonable to conclude that:

- i. Compared with fentanyl applied alone, the presence of OS or PO did not alter the amount of SC detached from the skin by the tape stripping procedure at any exposure time and
- ii. The gradual decline in SC mass removed by tape stripping as a function of increasing exposure time is likely to be a result of changes to the hydration state of the SC itself.

The hydration state of the SC has been related to the cohesive properties of SC corneocytes, where an apparent increase in SC hydration corresponded to increases in corneocyte cohesion (32). Given these findings, it is not surprising that changes to the hydration state of the SC have resulted in corresponding variations in the weight of SC removed by tape stripping (12). In order to account for the differences in SC weights removed among the various exposure times, fentanyl concentrations within the SC were normalised to the amount of SC removed per tape strip. As mentioned in Section 6.4.2, normalising the data in this manner also accounts for inter- and intra- subject variation in the SC weights removed within each treatment group.

5.4.2. Fentanyl distribution across human stratum corneum

The distribution profiles of fentanyl across human SC at the various exposure times are shown Figure 5.5. When fentanyl was applied alone to the SC for 0.08 h, concentrations declined exponentially as a function of increasing SC depth (Figure 5.5.A). This non-steady state distribution was also evident upon longer exposure times

(0.5 to 6 h). However, at 16 h, fentanyl concentrations appeared to decline more linearly across the SC ($r^2 = 0.938$), which is indicative of pseudo-steady-state diffusion across the SC. This finding is consistent with the lag time (t_{lag}) generated from finite dose diffusion studies with human epidermis (Chapter 3, Figure 3.4), where linear regression of the control (5%w/v fentanyl in ethanol) permeation profiles yields a x-intercept (t_{lag}) of 2 to 3 h. If steady-state flux across the SC occurs after a period of approximately 3 times the lag time (54), it could be estimated from this data that it occurs after approximately 6 to 9 h.

Fentanyl distribution across the SC followed a similar trend when fentanyl was applied with OS (Figure 5.5.B) or PO (Figure 5.5.C). In general, fentanyl concentrations declined exponentially across the SC with exposure times between 0.08 to 6 h. After 16 h of exposure, concentrations became more linearly distributed across the SC ($r^2 = 0.925$ or 0.902 when fentanyl was applied with OS or PO, respectively).

It is pertinent to note from Figure 5.5 that when fentanyl alone was applied to the skin, concentrations within the SC, and specifically within the upper regions of the SC, generally declined as a function of increasing exposure time. However, when fentanyl was applied with OS or PO, concentrations within the upper layers of the SC remained relatively constant over the various exposure times. As discussed in Section 5.4.1, the presence of the enhancers themselves is unlikely to have biased the distribution data, and therefore the discrepancies between the fentanyl distribution profiles are likely to be "real" differences.

The curvilinear nature of the distribution profiles may possibly be a result of the heterogeneous nature of the SC across varying SC depths. The anatomical differences between the various SC strata are described in Section 5.4.1. The intercellular lipid matrix that surrounds the corneocytes is generally regarded as the major route for drug permeation through the SC, with the corneocytes acting as mechanical barriers that effectively increase the diffusional path length (55).

As shown in Figure 5.6 (56), the corneocytes within the superficial layers of the stratum corneum are loosely attached, whereas corneocytes within the deeper regions of the SC are tightly cohesive. If the corneocytes are mechanical barriers to drug permeation, it appears logical that the looser packing of these mechanical "obstructions" would facilitate the entry of a permeant into the upper regions of the SC.

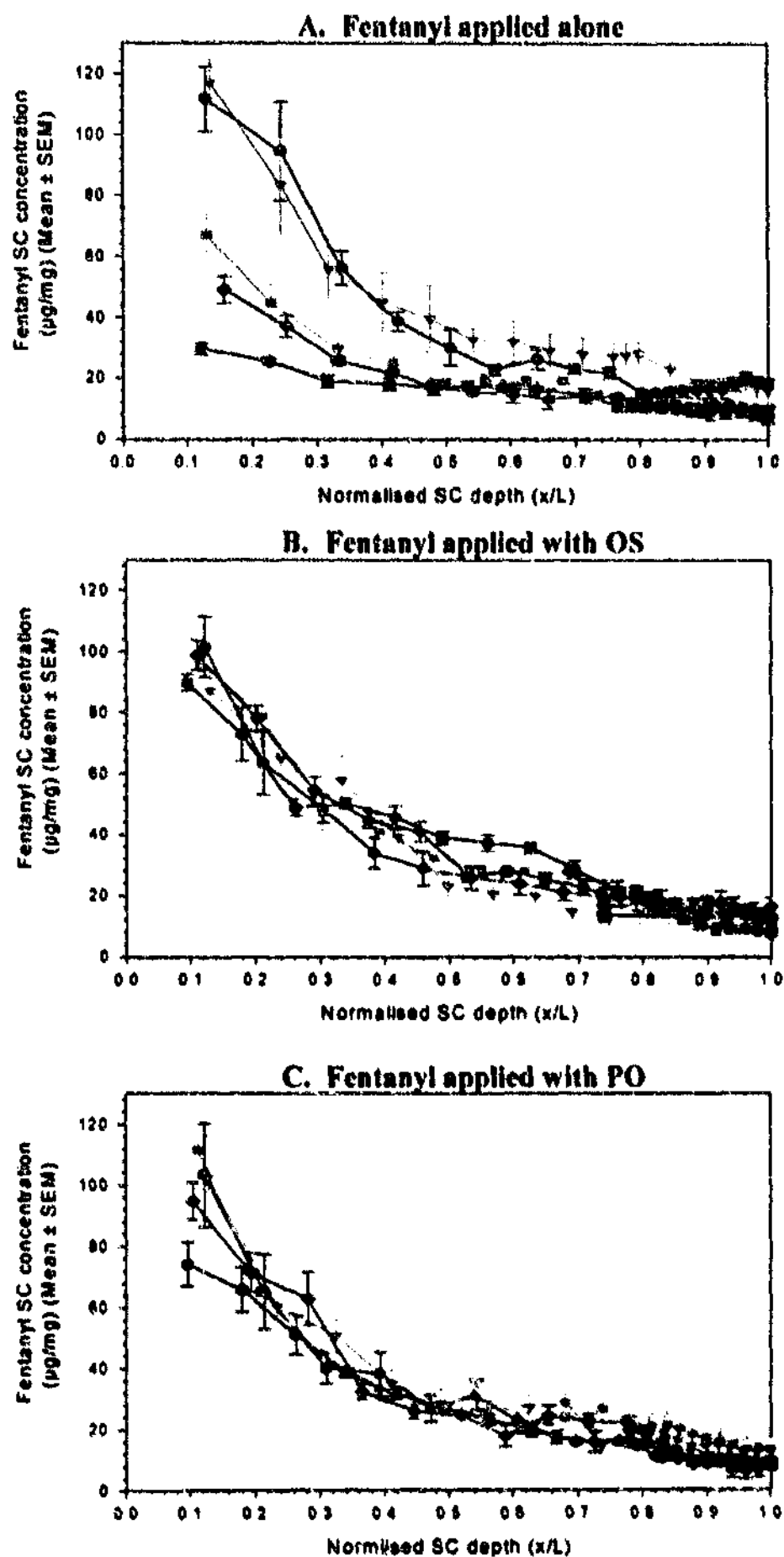


Figure 5.5. Fentanyl distribution profiles across human SC following exposure of fentanyl applied alone (A), with OS (B), or with PO (C) for 0.08 h (●), 0.5 h (▼), 2 h (■), 6 h (◆), and 16 h (●).



Figure 5.6. Transmission electron micrograph of human stratum corneum (x48,750). Intercellular spaces appear empty due to non-staining of the lipid bilayers (56).

Furthermore, the highly ordered organisation of the intercellular lipid lamellar bilayers imposes high diffusional resistance upon drug permeation through the SC (57-60).

Given that:

- i. SC lipid content diminishes and
- ii. lipid chains within the bilayers become more ordered

with increasing SC depth (61), it would appear that there would be

- i. a higher surface area available for drug permeation and
- ii. less resistance towards drug mobility

within the upper regions of the SC. Consequently, the SC is likely to accommodate a greater fraction of chemical within the superficial strata. In addition, lipid content and fluidity decline exponentially as a function of tape strip number, reaching a plateau after the fourth tape strip (61).

5.4.3. Areas under the fentanyl distribution profiles and clearance of fentanyl from the stratum corneum surface

As shown in Figure 5.7.A, optimal fentanyl uptake into the SC occurred shortly after the application of fentanyl alone to the skin, with the AUC for the entire SC rising from 26.83 ± 2.29 at 0.08 h to 30.49 ± 4.91 at 0.5 h. However, it would appear that fentanyl transfer into the SC declined significantly after this time, with $AUC_{x/L2 \rightarrow 20S}$ gradually decreasing to 13.51 ± 0.58 and 12.00 ± 1.29 at 6 and 16 h, respectively ($p < 0.05$ compared with 0.5 h).

As also illustrated by the fentanyl distribution profiles shown in Figure 5.5.A, the significant decline in $AUC_{x/L2 \rightarrow 20}$ can be largely attributed to reductions in the bioavailability of fentanyl within the upper regions of the SC. This trend indicates that fentanyl partitioning from the SC surface to the upper regions of the SC is significantly reduced. Consequently, as permeation into the underlying epidermis and dermis continues, the SC eventually becomes depleted of fentanyl.

The areas under the fentanyl distribution profiles following application of fentanyl with OS or PO are presented in Figures 5.7.B and 5.7.C, respectively. In the presence of OS or PO, initial $AUC_{x/L2 \rightarrow 20S}$ were slightly less than the $AUC_{x/L2 \rightarrow 20}$ attained when fentanyl was applied alone (21.67 ± 1.86 and 23.67 ± 1.05 at 0.08 h in the presence of OS and PO, respectively). However, in contrast to the fluctuating trend observed when fentanyl was applied alone, the $AUC_{x/L2 \rightarrow 20S}$ remained relatively uniform over various exposure times. Consequently, $AUC_{x/L2 \rightarrow 20S}$ achieved at prolonged exposure times were significantly higher in the presence of OS or PO compared to those attained when fentanyl was applied to the skin alone ($p < 0.05$ at 6 and 16 h). Furthermore, as illustrated by the distribution profiles shown in Figure 5.5, this difference appears to be predominantly due to the maintenance of fentanyl concentrations within the upper regions of the SC. The trends in SC concentrations are in agreement with those observed for fentanyl clearance from the SC surface.

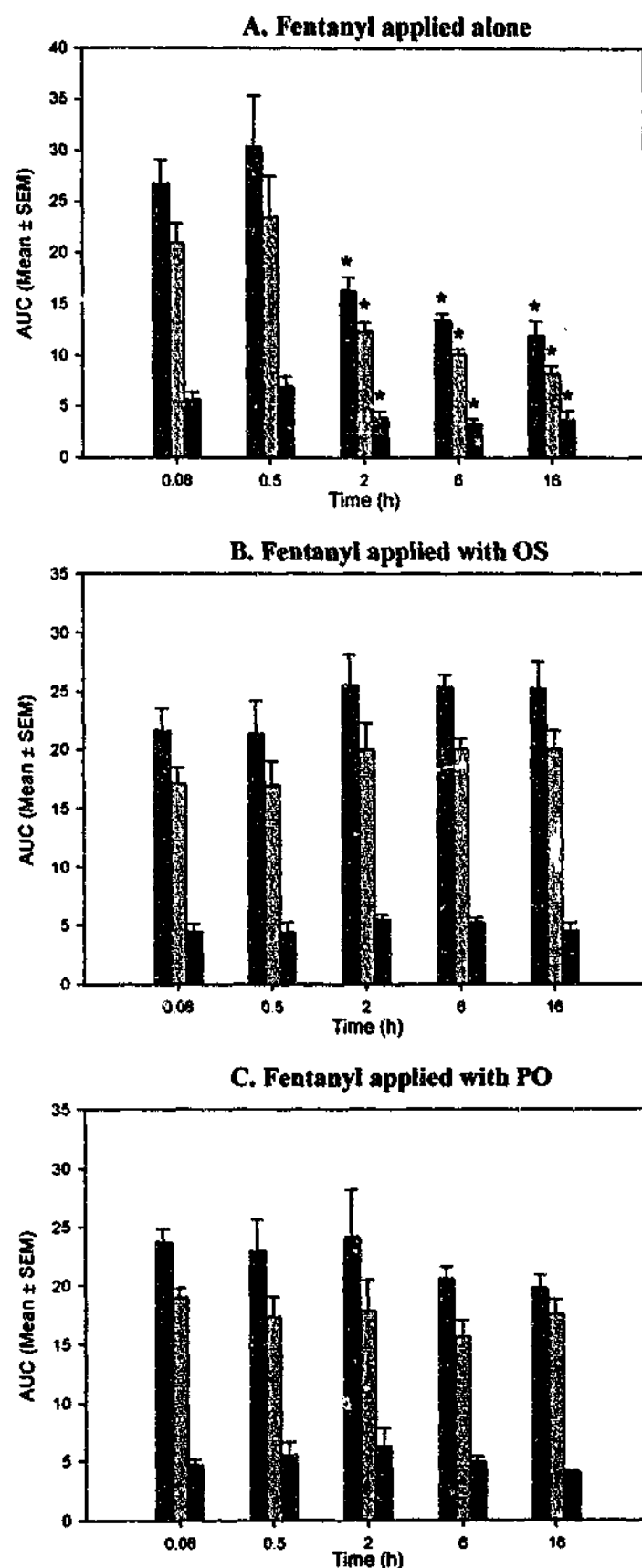


Figure 5.7. Areas under the fentanyl distribution profiles shown in Figure 5.5 (i.e. areas under the curves (AUCs)) following the application of fentanyl alone (A), with OS (B), or with PO (C). AUCs were calculated for the *entire* SC (i.e. SC removed by tape strips 2-20, $AUC_{x/L2 \rightarrow 20}$) (■), the *upper* SC (i.e. SC removed by tape strips 2-10, $AUC_{x/L2 \rightarrow 10}$) (▨) and the *lower* SC (i.e. SC removed by tape strips 11-20, $AUC_{x/L11 \rightarrow 20}$) (■). * Denotes statistically significant difference compared with AUC calculated at the 0.5 h exposure time.

The amount of fentanyl residing at the SC surface at the various exposure times, and the corresponding semilogarithmic transformations, are presented in Figures 5.8 and 5.9. When fentanyl was applied alone, it was apparent that surface concentrations declined by a two compartment process. Upon initial application to the skin, surface concentrations rapidly decreased from $1152.80 \pm 17.14 \mu\text{g}$ at 0.08 h to $1054.62 \pm 21.62 \mu\text{g}$ at 0.5 h ($p < 0.05$), which corresponds to an initial elimination rate constant of -0.0921 h^{-1} . However, after this initial “burst” effect, the rate of fentanyl disappearance from the SC surface dramatically decreased such that surface amounts differed from $1048.11 \pm 25.54 \mu\text{g}$ at 2 h to $1001.84 \pm 20.99 \mu\text{g}$ at 16 h ($k_{0.05-16\text{h}} = -0.00143 \text{ h}^{-1}$). It is likely that this “plateau phase” is indicative of significant retardation of fentanyl uptake into the SC, which corresponds to the reduction in fentanyl SC concentrations that are shown in Figures 5.5.A and 5.7.A.

When fentanyl was applied with OS or PO, the amount residing at the SC surface was $1125.71 \pm 23.44 \mu\text{g}$ and $1121.50 \pm 6.97 \mu\text{g}$, respectively, after 0.08 h of exposure. Given that these initial surface concentrations were similar to that found when fentanyl was applied alone, it would appear that the effect(s) of OS and PO were not instantaneous. However, it is evident from the profiles shown in Figure 6.8 that the overall kinetics of fentanyl SC surface clearance was markedly different in the presence of OS and PO. In particular, the linearity of these profiles suggests that fentanyl was eliminated from the SC surface by a first-order process in the presence of OS or PO. Consequently, fentanyl was continually eliminated from the SC surface and the “plateau phase” observed when fentanyl was applied alone was thus eliminated. Consequently, from 0.08 to 16 h, the amount of fentanyl residing at the SC surface depleted by ~57% and ~40% in the presence of OS and PO, respectively. In comparison, surface concentrations decline by ~13% over the equivalent period of time when fentanyl was applied alone.

The continual steady decline in surface concentrations is consistent with the finding that the bioavailability of fentanyl within the SC (particularly within the upper regions of the SC) remained constant over the various exposure times (Figures 5.7.B and 5.7.C).

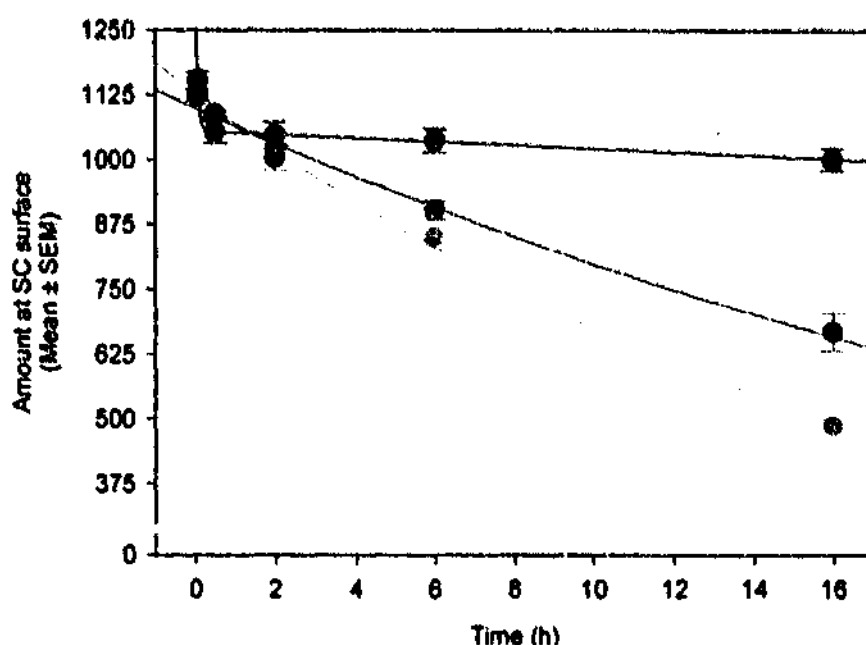


Figure 5.8. The amount of fentanyl residing at the SC surface as a function of exposure time, after the application of fentanyl applied alone (●), with OS (◐), or with PO (◑). The solid lines represent regression of the data to Equations 6.8 (fentanyl alone ($r^2=1.000$)) and 6.9 (fentanyl applied with OS ($r^2=0.999$) or PO ($r^2=0.995$)).

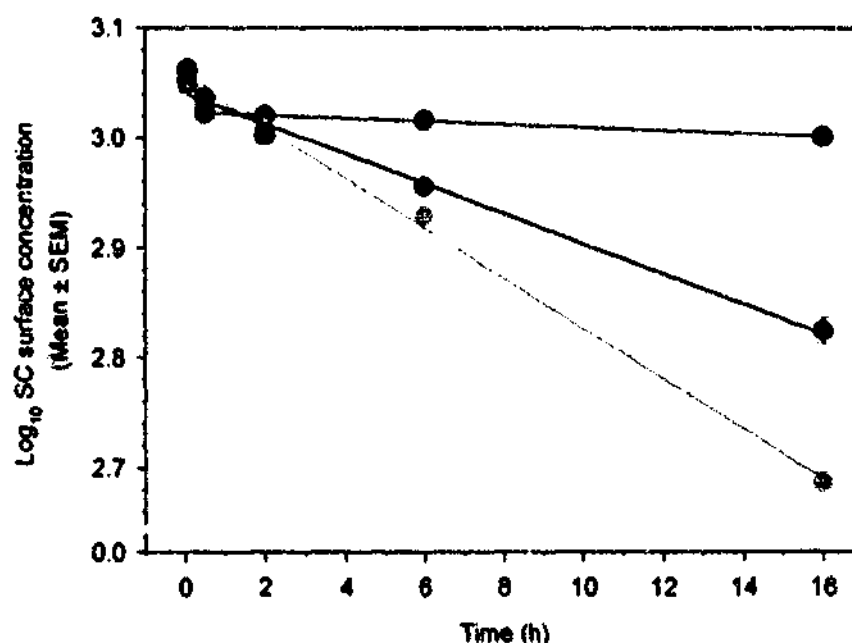


Figure 5.9. Log_{10} transformations of the amount of fentanyl residing at the SC surface as a function of exposure time. The solid lines represent linear regression of the data. Legend:

- Fentanyl applied alone (Slope (0.08 - 0.5 h) = -0.0921 h^{-1} , $r^2 = 1.000$)
(Slope (0.5 - 16 h) = -0.00143 h^{-1} , $r^2 = 0.996$)
- ◑ Fentanyl applied with PO (Slope (0.08 - 16 h) = -0.0137 h^{-1} , $r^2 = 0.999$)
- ◐ Fentanyl applied with OS (Slope (0.08 - 16 h) = -0.0228 h^{-1} , $r^2 = 0.993$)

Semilogarithmic transformations of the amount of fentanyl (applied with OS or PO) residing at the SC surface are compared to those of OS and PO in Figure 5.10. Both OS and PO were eliminated from the SC surface by apparent first-order rate processes. Furthermore, the rate constants generated from each of the fentanyl profiles ($k_{0.08-16h} = -0.0228 \text{ h}^{-1}$ and -0.0137 h^{-1} in the presence of OS and PO, respectively) are almost identical to the rate constants for the surface disappearance of OS and PO ($k_{0.08-16h} = -0.0226 \text{ h}^{-1}$ and -0.0133 h^{-1} for OS and PO, respectively).

The concomitant variations in fentanyl concentrations within the SC and at the SC surface can be explained in terms of the continuous compositional changes of the applied formulations. Upon application of 5%w/v fentanyl alone, ethanol (which constitutes the bulk of the formulation) rapidly evaporates into the atmosphere. The effects of ethanol evaporation are likely to be two-fold. Firstly, as the solubility of fentanyl in the remaining vehicle becomes markedly reduced, it attains a transient state of high thermodynamic activity during which time transport into the skin will be optimal. In addition, ethanol itself is likely to partition into the SC, thus further enhancing fentanyl partitioning into and/or diffusivity within the SC (62, 63). Hence rapid fentanyl clearance from the SC surface and an accompanying increase in SC concentrations were observed from 0.08 to 0.5 h.

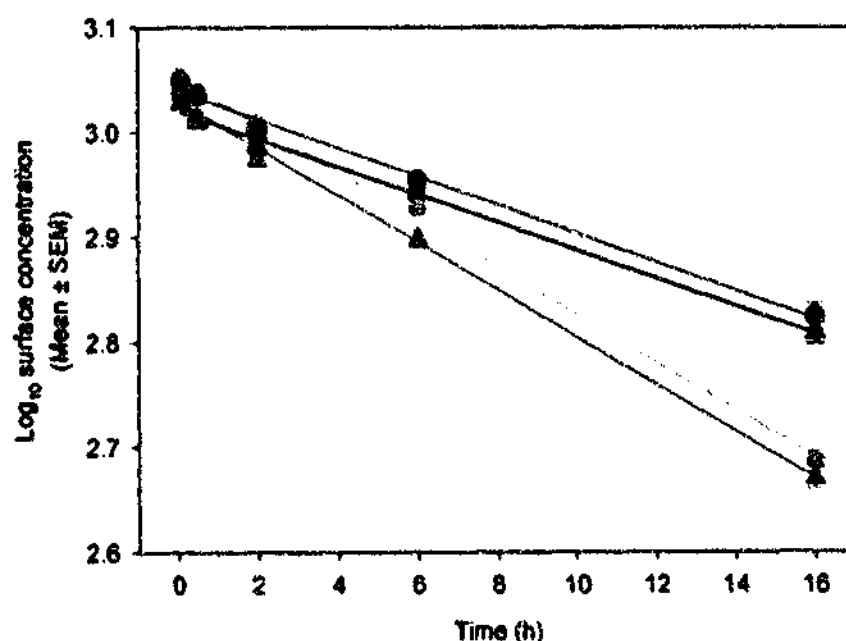


Figure 5.10. Log_{10} transformations of fentanyl (applied with OS or PO), OS and PO SC surface concentrations as a function of exposure time. Legend:

- Fentanyl applied with PO (Slope (0.5-16h) = -0.0137 h^{-1} , $r^2 = 0.999$)
- ▲ PO applied with fentanyl (Slope (0.5-16h) = -0.0133 h^{-1} , $r^2 = 1.000$)
- Fentanyl applied with OS (Slope (0.5-16h) = -0.0228 h^{-1} , $r^2 = 0.993$)
- △ OS applied with fentanyl (Slope (0.5-16h) = -0.0226 h^{-1} , $r^2 = 0.997$)

Theoretically, upon complete evaporation of ethanol, drug precipitation is likely to occur and consequently fentanyl partitioning into the SC is likely to become dissolution-rate limited. However, solid particulate matter was not observed on the SC surface at any exposure time. It could therefore be possible that ethanol evaporation mediates the transformation of fentanyl crystals to polymorphic or amorphous form(s) that possess physicochemical properties less amenable to transport into and across the SC. This is consistent with the finding that the rate of fentanyl clearance from the SC surfaces plateaus after 0.5 h, whilst the subsequent decreases in SC concentrations can be largely attributed to the diminution of fentanyl within the upper regions of the SC.

The incorporation of OS or PO into the formulation results in a volatile:non-volatile vehicle system. Thus, the impact of OS and PO on fentanyl permeation through the SC can be related to both the thermodynamic properties of the applied formulation and the interactions that occur within the SC. In the presence of OS or PO, which are non-volatile liquids, the evaporation of ethanol will result in the formation of a concentrated solution of fentanyl within the film of 'enhancer' remaining at the SC surface. It was established in Chapter 3 that fentanyl has relatively high solubility in both OS ($130.77 \pm 1.47 \mu\text{g/ml}$) and PO ($165.08 \pm 1.93 \mu\text{g/ml}$). The solubilisation of fentanyl by OS and PO would be expected to reduce the escaping tendency of fentanyl from the remaining surface film. This could possibly explain the termination of the "burst" effect observed between 0.08 to 0.5 h when fentanyl was applied in ethanol alone. However, the amount of fentanyl contained within the enhancer films at the SC surface was in excess of its saturated solubility in either enhancer (by factors of ~ 8 and ~6 times the solubility in OS and PO, respectively). Consequently, the SC concentrations of fentanyl applied with OS or PO were not significantly different from those of fentanyl applied alone at short (i.e. less than 2 h) exposure times. Furthermore, the results presented in Chapter 6 and the semilogarithmic transformations of OS and PO SC surface clearance demonstrate that the enhancers themselves permeate into the SC. Thus:

- i. The similarities between the first-order elimination rate constants generated for the surface clearance of fentanyl applied with OS or PO and the enhancers themselves and
- ii. The maintenance of fentanyl concentrations within the upper regions of the SC in the presence the enhancers

could indicate that OS and PO modify fentanyl distribution across the SC by maintaining a diffusable source of fentanyl at the SC surface that they deliver as they themselves partition into the SC. Evidently, this postulated mechanism of action is indicative of enhanced fentanyl partitioning into the SC, which is in agreement with results from the permeation and SC-water partitioning studies presented in Chapters 3 and 4.

It is also of interest to note the magnitudes by which OS and PO enhance fentanyl uptake into the SC. At an exposure time of 16 h, $AUC_{x/L2 \rightarrow 20s}$ for the fentanyl distribution profiles were 12.00 ± 1.29 , 25.32 ± 2.21 and 19.76 ± 1.11 when fentanyl was applied alone or with OS or PO, respectively (Figure 5.7). These figures correspond to enhancement ratios of 2.11 ± 0.15 for OS and 1.65 ± 0.05 for OS and PO, respectively. This is in excellent agreement with the results from the finite dose diffusion presented in Chapter 3, where OS and PO were found to enhance fentanyl permeation through human epidermis by ratios of 2.16 ± 0.10 and 1.66 ± 0.12 at 16 h, respectively and by ratios of 2.01 ± 0.07 and 1.59 ± 0.09 at 24 h, respectively.

5.4.4. Dose accountability

The amount of fentanyl recovered in the SC surface wipes and tape strips at the various exposure times are expressed as a percentage of the initial dose (1250 μg) applied to the skin in Figure 5.11. The data presented in Table 5.4 express the amount of fentanyl at the surface and in the tape strips as a percentage of the total amount of fentanyl recovered. When fentanyl was applied alone to the skin for 0.08 h, total recovery from the SC surface and tape strips was $1312.88 \pm 16.87 \mu\text{g}$ ($104.77 \pm 1.35\%$ of the applied dose) (Figure 5.11.A). A large proportion ($87.81 \pm 1.12\%$) of this recovered amount was distributed at the SC surface, whilst only $160.07 \pm 15.83 \mu\text{g}$ ($12.19 \pm 1.12\%$ of the recovered amount) was retrieved from the tape strips. In fact, at all of the exposure times, the amount of fentanyl residing at the SC surface contributed to the majority (over $\sim 86\%$) of the total amount of fentanyl recovered (Table 5.4).

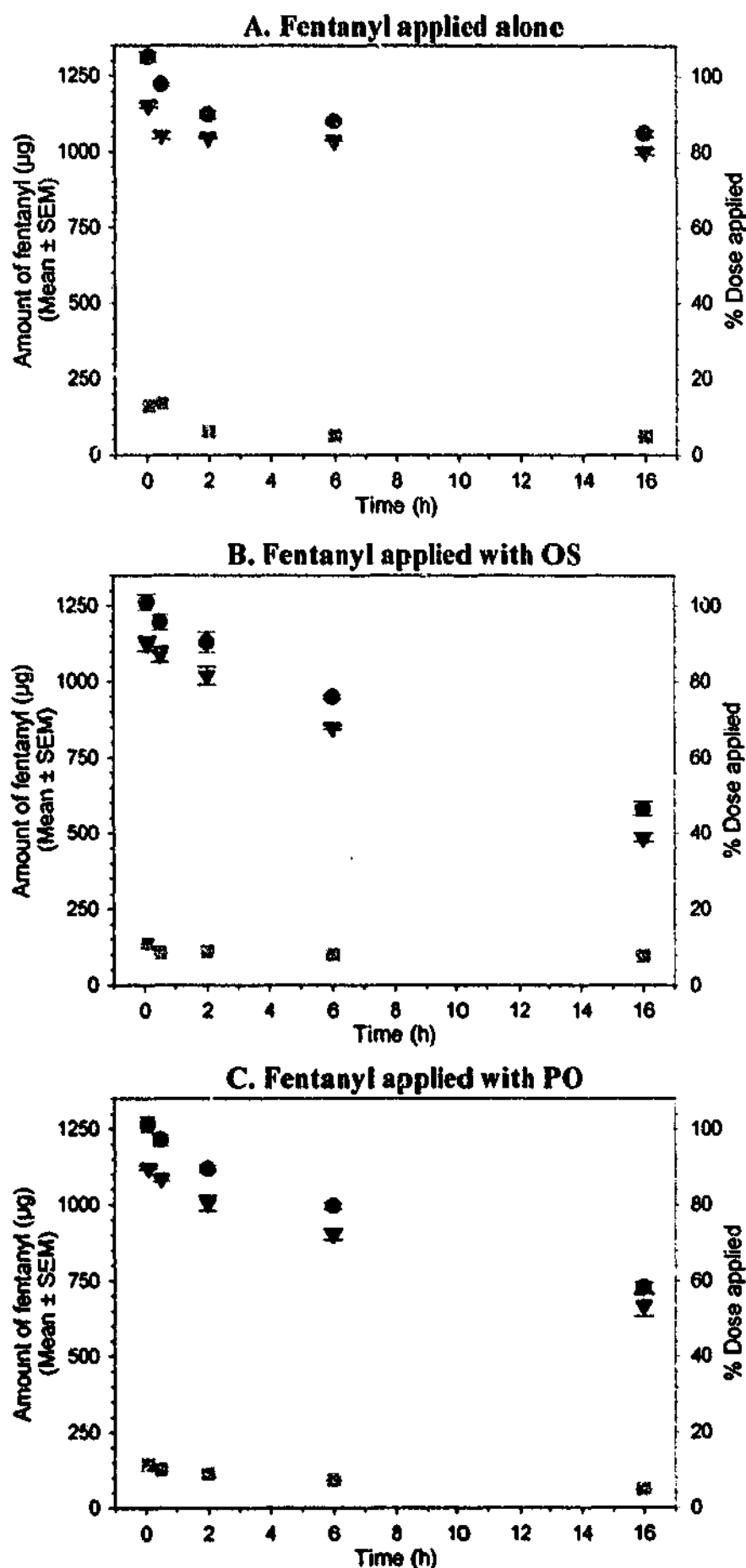


Figure 5.11. Dose accountability (amount (μg) and percentage of applied dose) of fentanyl applied alone (A), with OS (B), or with PO (C). Total recovery (\bullet) represents the total amount recovered in the SC surface wipe and the 20 tape strips. The amount recovered in the SC surface wipe (\blacktriangledown) and the 20 tape strips (\blacksquare) are also displayed.

Table 5.4. Fentanyl disposition across the SC expressed as a percentage of the total amount of fentanyl recovered at each exposure time.

Exposure time (h)	Fentanyl applied Alone		Fentanyl applied with OS		Fentanyl applied with PO	
	Surface	Tape strips	Surface	Tape strips	Surface	Tape strips
0.08	87.78 ± 1.12	12.22 ± 1.12	89.15 ± 1.86	10.84 ± 1.86	88.63 ± 1.35	11.37 ± 1.35
0.5	85.78 ± 0.90	14.22 ± 0.90	91.10 ± 2.04	8.90 ± 2.04	89.43 ± 0.81	10.57 ± 0.81
2	92.5 ± 0.88	7.46 ± 0.88	90.22 ± 2.68	9.78 ± 2.68	89.88 ± 0.78	10.12 ± 0.78
6	93.48 ± 0.71	6.52 ± 0.71	89.48 ± 0.78	10.52 ± 0.78	90.69 ± 0.64	9.31 ± 0.64
16	93.51 ± 0.52	6.49 ± 0.52	83.48 ± 2.46	16.52 ± 2.46	91.77 ± 0.62	8.23 ± 0.62

Only a small percentage (under ~14%) of the initial applied dose was distributed within the SC at all of the exposure times, with maximum fentanyl recovery from the tape strips observed at 0.5 h ($13.47 \pm 0.79\%$ of the initial dose). However, as observed from the normalised data presented in Figure 6.4.A, there was a subsequent decline in the amount of fentanyl present within the tape strips such that only $4.78 \pm 0.35\%$ of the initial dose was recovered at 16 h ($p < 0.05$ compared with 0.08 h).

Given these trends in fentanyl recovery from the SC surface and tape strips, it is not surprising that recovery from the SC surface and total fentanyl recovery appeared to decline by similar bi-exponential processes. Consequently, the total amount of fentanyl recovered at 16 h was $1061.65 \pm 10.87 \mu\text{g}$ ($84.93 \pm 0.87\%$ of the applied dose), which corresponds to a ~19% decrease from the initial point of recovery at 0.08 h ($p < 0.05$).

As seen in Figure 5.11.B, total fentanyl recovery was high ($101.01 \pm 2.04\%$) at 0.08 h when fentanyl was applied to the skin with OS. As noted when fentanyl was applied alone, a substantial fraction (over 83%) of the recovered dose was located at the SC surface at all exposure times (Table 5.4). Although the amount of fentanyl residing at the SC surface significantly declined over time (from $90.06 \pm 1.88\%$ of the applied dose at 0.08 h to $38.86 \pm 1.14\%$ at 16 h ($p < 0.05$)), a compensatory increase in the amount of fentanyl found within the SC tape strips was not evident. In fact, the amount of fentanyl within the SC remained consistently low, with $10.95 \pm 0.59\%$ to $7.69 \pm 0.83\%$ of the applied dose distributed within the SC from 0.08 to 16 h, respectively.

Analogous to the first-order decline in the amount of fentanyl recovered from the SC surface, total fentanyl recovery also appeared to decrease exponentially over time.

Consequently, the amount of fentanyl recovered at the SC surface and within the SC itself only accounted for $46.55 \pm 1.78\%$ of the applied dose at 16 h, which equates to a ~54% loss compared with total recovery at 0.08 h ($p < 0.05$).

Similar observations were evident when fentanyl was applied with PO (Figure 5.11.C and Table 5.4). At 0.08 h, total recovery of the applied dose was high ($101.23 \pm 1.91\%$), with the majority ($88.63 \pm 1.35\%$) of this recovered amount located at the SC surface. However, as the amount of fentanyl residing at the SC surface declined by an apparent first-order rate process, only $53.46 \pm 2.96\%$ of the applied dose was recovered at the surface at 16 h ($p < 0.05$ compared with 0.08 h). The amount of fentanyl retained within the SC also decreased as a function of time (from $11.51 \pm 1.58\%$ of the applied dose at 0.08 h to $4.79 \pm 0.17\%$ at 16 h ($p < 0.05$)). Consequently, total fentanyl recovery significantly declined by ~42% (from $101.23 \pm 1.91\%$ at 0.08 h to $58.25 \pm 1.31\%$ at 16 h ($p < 0.05$)).

The distribution of OS and PO across the SC is discussed in Chapter 6. It is apparent from Figures 5.11 and 5.12 that important similarities exist between the recovery of OS and PO and fentanyl applied with OS and PO. Firstly, at 0.08 h, total recovery was high ($99.39 \pm 2.13\%$ and $97.39 \pm 1.50\%$ of the applied dose of OS and PO, respectively). However, total recovery of the enhancers seemed to decline by first-order rate processes. Consequently, the recovery of OS and PO significantly declined to $43.95 \pm 1.12\%$ and $57.14 \pm 1.11\%$, respectively ($p < 0.05$ compared with 0.08 h). These figures are comparable to the total recovery of fentanyl applied with OS ($46.55 \pm 1.78\%$) and PO ($58.25 \pm 1.31\%$) at 16 h.

It is also evident that the SC only accommodated a small percentage (<11% for OS and <12% for PO) of the applied dose and, therefore, substantial amounts of OS and PO remained at the SC surface at all exposure times. This relationship is similar to that observed when fentanyl was applied alone or with OS or PO. Thus, the net losses in total OS and PO recovery can mainly be attributed to significant declines in the amount of OS and PO residing at the SC surface. From 0.08 to 16 h, surface concentrations declined from $88.41 \pm 1.57\%$ to $37.43 \pm 1.01\%$ and $85.44 \pm 0.73\%$ to $51.54 \pm 1.19\%$ of the applied dose of OS and PO, respectively.

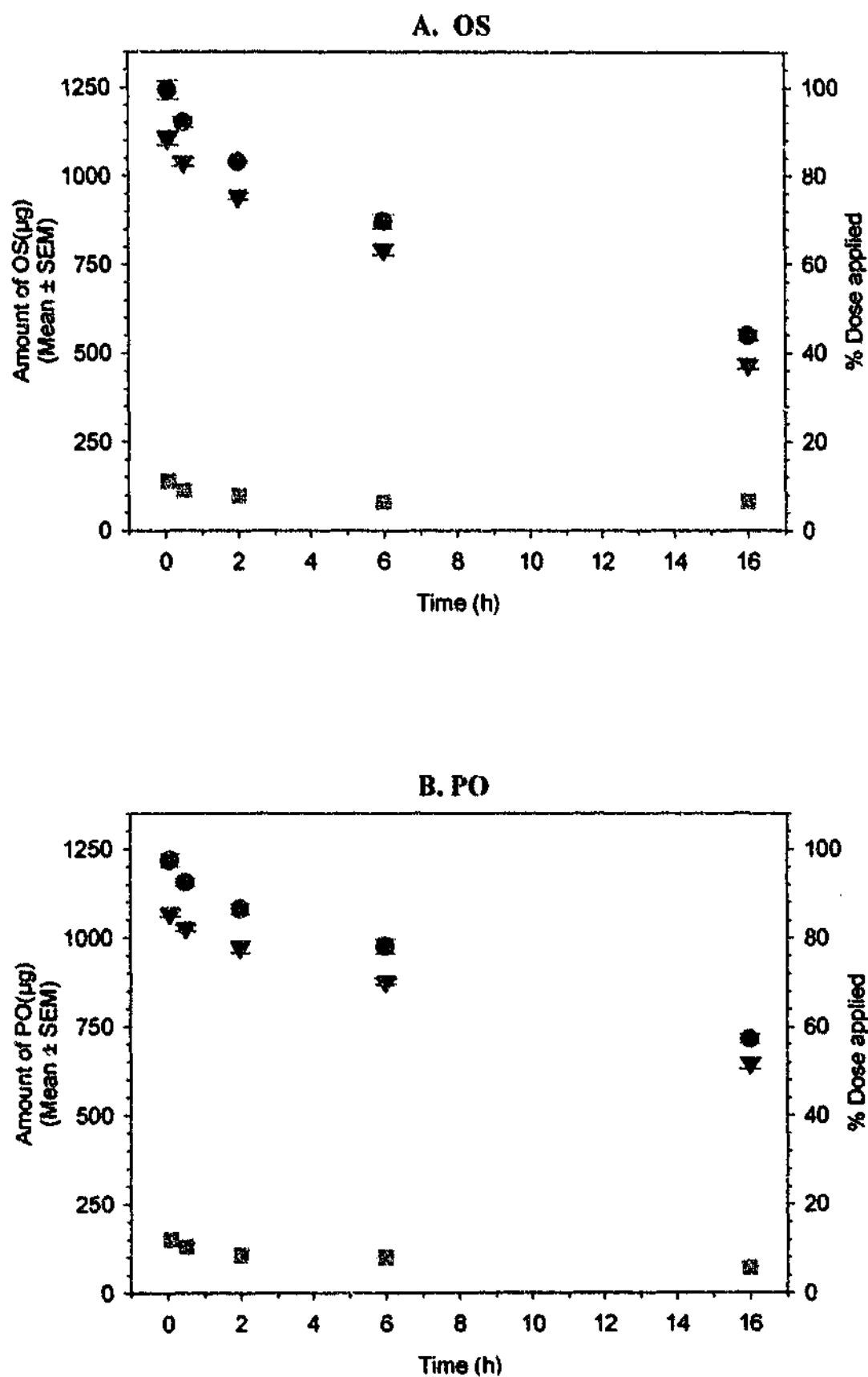


Figure 5.12. Dose accountability (amount (µg) and percentage of applied dose) of OS (A) and PO (B) applied with fentanyl. Total recovery (●) represents the total amount recovered in the SC surface wipe and the 20 tape strips. The amount recovered in the SC surface wipe (▼) and the 20 tape strips (■) are also displayed.

The results of the finite dose diffusion studies presented in Chapter 3 demonstrate that when fentanyl is applied alone or with OS or PO, less than 1%, $2.06 \pm 0.09\%$, or $1.38 \pm 0.10\%$ of the applied dose passes through human epidermis at 16 h, respectively. As OS and PO are highly lipophilic chemicals ($\log K_{\text{OCT/W}} = 5.77$ and 5.97 for OS and PO, respectively), the epidermis is likely to contribute significant resistance towards their mass transfer across the skin. Therefore, significant amounts of OS and PO would not be expected to partition into the epidermis (64).

The low percutaneous absorption of OS and PO has been demonstrated both *in vitro* and *in vivo*, using a variety of different formulations (65). For instance, the *in vitro* permeation of OS from a hydroalcoholic lotion (applied as a finite dose of $5\mu\text{l}/\text{cm}^2$ for 24 h) was found to be less than 1% of the applied dose (66). Hagedorn-Leweke and Lippold (67) have determined the maximum flux of PO across human skin *in vivo* as $0.53\mu\text{g}/\text{cm}^2/\text{h}$, which is also relatively low.

Based on these findings, it could be assumed that reductions in fentanyl, OS or PO recovery that could be attributed to permeation into the underlying epidermal or dermal tissues are in the order of 1 to 2% of the applied dose. However, the magnitudes of these losses are insignificant compared to the net losses in total recovery at 16 h (which vary from 19 to 58% of the applied dose).

Other workers within the field of transdermal drug delivery have also encountered the phenomenon of “unexplained” chemical loss that has resulted in incomplete mass balance. For example, there are several reports of incomplete mass balance following the application of the insecticide, malathion, to skin *in vivo* and *in vitro* (68). The results from these studies indicate that substantial amounts of malathion remain on (and are lost from) the SC surface, whilst small amounts are retained in, and permeate, the skin. Using a non-radioactive assay for the quantification of erythromycin present at the SC surface and within SC tape strips *in vivo*, van Hoogdaem (69) reported a total recovery of ~46% of the applied dose after a 7 h exposure time. The *in vitro* percutaneous absorption studies conducted by Walters et al (66) are of particular relevance to the work currently presented. Under infinite and finite dose conditions, total recovery of OS (applied in a hydroalcoholic vehicle) was ~83% and ~70% at 48 h, respectively. After the application of OS (formulated in an emulsion gel) to human skin *in vitro*, Treffel and Gabard (70) also recovered ~70% of the applied OS dose after a 6 h exposure time. Considering the prevalence of incomplete mass balance, factors that may contribute to significant

chemical loss from the skin must be considered: the most (other than permeation into the deeper skin layers) include cutaneous metabolism, lateral diffusion, evaporation of the chemical into the atmosphere, and desquamation.

There is evidence to suggest that metabolic activity is retained in freshly-excised and frozen, non-viable skin (71-73). Whilst the results of *in vitro* incubation studies with skin homogenates indicate that the cutaneous metabolism of fentanyl is likely to be negligible (74), there is indirect evidence to support the metabolic degradation of OS and PO within the epidermis and dermis. In particular, the esterase hydrolysis of PO has been documented in both viable and nonviable hairless guinea pig and human skin (75). However, based on these studies, the extent of hydrolysis within the skin appears to be low (less than 5% of the absorbed dose). The suspected presence of salicylic acid in the receptor fluid during *in vitro* human skin permeation studies may also imply that OS could be susceptible to cutaneous metabolic degradation (66). However, even when the permeation of, what could have been, salicylic acid was taken into account, total recovery of OS at 48 h was still in the order of 46 to 83% of the applied dose, with the majority of this amount residing at the SC surface. Based on these previous findings, it would seem that the cutaneous metabolism of fentanyl, OS and PO did not significantly contribute to their clearance of from the skin and thus it may not be accountable for the "incomplete" mass balance observed during these present studies.

As discussed in Chapter 6, substantial chemical loss from the skin surface due to lateral diffusion was also unlikely during these tape-stripping experiments as, instead of using a device to expose the defined area of skin, the skin was cut to the defined exposure area (5 cm²).

Topically-applied chemicals can also be lost by desquamation. There is extensive evidence to prove that desquamation can occur *in vitro*. For instance, model systems for the study of desquamation involve the reaggregation of corneocytes obtained from SC that has been isolated from excised skin (76). Intact excised skin has also been used to investigate desquamation (77), with some researchers reporting that the presence of dermal tissue is pivotal to keratinocyte self-renewal *in vitro* (78). However, there is currently no published data on the effects of freezing on SC cell turnover within excised skin. As discussed in Chapter 1 (Section 1.2.4), desquamation is a complex biological process that is regulated by a number of factors, such as various enzymatic processes and the integrity and composition of the intercellular lipids (76, 79, 80). There is evidence to

suggest that enzymatic activity is retained within excised skin that has been stored frozen (71-73), and that freezing does not significantly compromise the integrity and barrier properties of excised skin (44, 81). Furthermore, isolated epidermal keratinocytes from frozen stocks have been subcultured without changes to cell viability, proliferation rate, or morphology (82). These findings may support the notion that desquamation can occur within excised skin that has been stored frozen.

Since chemicals in desquamated SC are not available for diffusion across the skin, it has been suggested that desquamation can significantly reduce the systemic exposure to dermally-absorbed chemicals (83). Reddy et al (84) have described a mathematical model of chemical absorption into the epidermis that examines the effect of exposure time, chemical lipophilicity, and epidermal turnover rate on chemical elimination from the skin by desquamation. It is evident from their model that desquamation exerts a minor effect on the fraction of chemical in the skin that is systemically absorbed for compounds with low to moderate lipophilicity (i.e. $\log K_{OCT/W} < \sim 4$) or $MW < \sim 350-400$ Da, regardless of the exposure time. However, the model also predicts that for chemicals with high lipophilicity ($\log K_{OCT/W} > \sim 4$) or $MW > \sim 350 - 400$ Da, desquamation will significantly reduce systemic absorption. These predictions are consistent with the finding that losses of OS ($\log K_{OCT/W} \sim 5.77$, $MW = 250.34$) and PO ($\log K_{OCT/W} \sim 5.97$, $MW = 277.40$) at the SC surface are far greater than that of fentanyl ($\log K_{OCT/W} \sim 2.91$, $MW = 336.48$) applied alone at prolonged exposure times.

Furthermore, it might also be possible that when fentanyl was applied to the skin with ethanol alone, its subsequent removal from the skin surface by desquamation may have been physically impeded by the deposition of fentanyl crystals at the skin surface following the complete evaporation of ethanol. On the other hand, as previously discussed, it is likely that OS and PO solubilise fentanyl at the SC surface. Therefore, the observation that the SC surface elimination rates of fentanyl (applied with OS or PO) closely resemble those of OS and PO themselves could possibly indicate that fentanyl solubilised in OS or PO may also be effected by desquamation to the same extent as OS or PO themselves.

As complete SC turnover rates are of the order of 14 to 21 days (84), one might expect that the desquamation would not have significantly contributed to the removal of fentanyl, OS or PO from the SC surface during the relatively short (<16 h) exposure times investigated during these studies. However, SC surface clearance (i.e. the transit

time of one cell layer) is reported to be of the order of 6 to 16 h, which equates to 0.16 to 0.06 cell layers per hour (85). Therefore, considering that the majority of the applied dose of fentanyl, OS, or PO resides at the SC surface, it would appear that significant losses due to SC surface clearance could occur within a 16 h exposure time. Furthermore, exogenously-applied chemicals can also enhance desquamation rates by, for example, modulating protease activity or altering lipid fractions within the intercellular spaces of the SC (76, 77). Thus, as OS and PO have been found to reduce the lipid content of the superficial SC layers (Chapter 7), the impact of OS and PO on the rate of cell shedding may also require further consideration.

As fentanyl, OS and PO are all non-volatile substances, one might expect that significant chemical loss from the SC surface due to evaporation would be unlikely. However, it has been shown that the evaporative loss of chemicals with relatively low vapour pressures (of the order of 1.5×10^{-7} to 5.5×10^{-6} mmHg at 20°C) can be significantly affected by the rate of air flow over the skin (86). Thus, although fentanyl, OS, and PO have relatively low vapour pressures (6.52×10^{-8} , 7.13×10^{-6} , and 3.54×10^{-5} mmHg at 25°C, respectively¹), it is possible that a portion of the applied dose may have been lost due to evaporation. Furthermore, as the loss of fentanyl from the SC surface was greater in the presence of OS and PO, it would be reasonable to speculate whether the solubilisation of fentanyl within the solvent-deposited enhancer film affects its rate of evaporation from the SC surface. Therefore, further investigations will be required in order to determine the extent of evaporative loss of fentanyl, OS and PO after their finite dose application to the skin surface and whether the presence of OS and PO affects the evaporative loss of fentanyl from the skin surface.

It should also be noted that, due to the high surface area-to-volume ratios of the tape strip samples, it has been suggested that chemical losses due to evaporation from the tape strip samples can be significant even for chemicals with relatively low volatility (87). To avoid this complication, extraction from the tape strips was commenced immediately after the completion of each experiment. Furthermore, as demonstrated in Chapter 6, an excellent correlation exists between attenuated total reflectance Fourier transform infrared (ATR-FTIR) spectroscopic and HPLC/UV quantification of OS within the tape strips. As ATR-FTIR is used to measure the relative difference in the amount of

¹ Estimated using EPISuite (Version 3.11) computer software package (U.S. Environmental Protection Agency)

OS within the SC before and after each tape strip, whilst HPLC/UV measures the absolute amount of OS within the tape strip samples, the excellent correlation between these two methods would also suggest that chemical losses due to evaporation from the *tape strip samples* (not the skin surface) were insignificant.

5.5. CONCLUSIONS

The results from these studies demonstrate that both OS and PO modify fentanyl distribution across human SC. When fentanyl is applied without OS or PO, its clearance from the SC surface plateaus over prolonged exposure times, whilst fentanyl concentrations within the upper regions of the SC diminish. This trend is indicative of impaired fentanyl partitioning into the SC, which is most likely to be the result of changes to the thermodynamic properties of the applied formulation. On the other hand, it would appear that OS and PO maintain a high fentanyl concentration gradient across the SC by maintaining a diffusable source of fentanyl at the SC surface which they deliver as they themselves partition into the SC. Consequently, it would appear that a mechanism by which OS and PO alter fentanyl distribution across the SC is by enhancement of fentanyl partitioning into the SC.

Although OS and PO appear to enhance fentanyl uptake into the SC, the drastic declines in the amount of fentanyl, OS and PO residing at the SC surface cannot be explained by their permeation into the SC and underlying skin strata. However, it is possible that losses in recovery were due to desquamation and/or evaporative loss. As the loss of fentanyl (applied with OS or PO), OS and PO from the SC surface was quite significant, this phenomenon requires further investigation. However, an important finding from these studies was that OS and PO enhance fentanyl uptake into the SC despite losses from the SC surface.

5.6. REFERENCES

1. Scheuplein RJ, Blank IH. 1971. Permeability of the Skin. *Physiol Rev* 51:702-747.
2. Flynn GL, Durrheim H, Higuchi WI. 1981. Permeation of Hairless Mouse Skin II: Membrane Sectioning Techniques and Influence on Alkanol Permeabilities. *J Pharm Sci* 70:52-56.
3. Miselnicky SR, Lichtin JL, Sakr A. 1988. The Influence of Solubility, Protein Binding, and Percutaneous Absorption on Reservoir Formation in Skin. *J Soc Cosmet Chem* 39:169-177.
4. Clarys P, Gabard B, Barel AO. 1999. A Qualitative Estimate of the Influence of Halcinonide Concentration and Urea on the Reservoir Formation in the Stratum Corneum. *Skin Pharmacol Appl Skin Physiol* 12:85-89.
5. Zatz JL. 1983. Fundamentals of Transdermal Controlled Drug Administration: Physicochemical Considerations. *Drug Dev Res* 9:561-577.
6. Naik A, Kalia YN, Pirot F, Guy RH. 1999. Characterization of Molecular Transport Across Human Stratum Corneum *In Vivo*. In Bronaugh RL, Maibach H, ed. *Percutaneous Absorption: Drugs, Cosmetics, Mechanisms, Methodology*. New York: Marcel Dekker, Inc., pp 149-175.
7. Rougier A, Lotte C, Dupius D. 1987. An Original Predictive Method for *In Vivo* Percutaneous Absorption Studies. *J Soc Cosmet Chem* 28:397-417.
8. Moser K, Kriwet K, Naik A, Kalia YN, Guy RH. 2001. Passive Skin Penetration Enhancement and its Quantification *In Vitro*. *Eur J Pharm Biopharm* 52:103-112.
9. Surber C, Schwarb FP, Smith EW. 1999. Tape-Stripping Technique. In Bronaugh RL, Maibach HI, ed. *Percutaneous Absorption Drugs, Cosmetics, Mechanisms, Methodology*. New York: Marcel Dekker, Inc., pp 395-409.
10. Tsai JC, Weiner ND, Flynn GL, Ferry J. 1991. Properties of Adhesive Tapes Used for Stratum Corneum Stripping. *Int J Pharm* 72:227-231.
11. Tsai J, Cappel MJ, Weiner ND, Flynn GL, Ferry J. 1991. Solvent Effects on the Harvesting of Stratum Corneum From Hairless Mouse Skin Through Adhesive Tape Stripping *In Vitro*. *Int J Pharm* 68:127-133.
12. Weigand DA, Gaylor JR. 1973. Removal of Stratum Corneum *In Vivo*: An Improvement on the Cellophane Tape Stripping Technique. *J Invest Dermatol* 60:84-87.
13. Osamura H, Jimbo Y, Ishihara M. 1984. Skin Penetration of Nicotinic Acid, Methyl Nicotinate, and Butyl Nicotinate in the Guinea Pig-Comparison of *In Vivo* and Excised Skin, and the Effects of Four Dermatologic Conditions. *J Dermatol* 11:471-481.
14. Ohman H, Vahlquist A. 1994. *In Vivo* Studies Concerning a pH Gradient in Human Stratum Corneum and Upper Epidermis. *Acta Derm Venereol Suppl (Stockh)* 74:375-379.
15. Marks R, Dawber RP. 1971. Skin Surface Biopsy: An Improved Technique for the Examination of the Horny Layer. *Br J Dermatol* 84:117-123.
16. Marks R, Dykes P. 1994. Plasma and Cutaneous Drug Levels After Topical Application of Piroxicam Gel: A Study in Healthy Volunteers. *Skin Pharmacol* 7:340-344.

17. Watson WS, Finlay AY. 1988. The Effect of the Vehicle Formulation on the Stratum Corneum Penetration Characteristics of Clobetasol 17-Propionate *In Vivo*. *Br J Dermatol* 118:523-530.
18. Wallace SM, Shah VP, Epstein WL, Greenberg J, Riegelman S. 1977. Topically Applied Antifungal Agents. Percutaneous Penetration and Prophylactic Activity Against Trichophyton Mentagrophytes Infection. *Arch Dermatol* 113:1539-1542.
19. Thielitz A, Helmdach M, Ropke EM, Gollnick H. 2001. Lipid Analysis of Follicular Casts from Cyanoacrylate Strips as a New Method for Studying Therapeutic Effects of Antiacne Agents. *Br J Dermatol* 145:19-27.
20. Franz TJ. 1991. Percutaneous Absorption: In Vivo Methods. *Cosmetics and Toiletries* 106:73-80.
21. Kalia YN, Alberti I, Naik A, Guy RH. 2001. Assessment of Topical Bioavailability *In Vivo*: The Importance of Stratum Corneum Thickness. *Skin Pharmacol Appl Skin Physiol* 14:82-86.
22. Shah VP, Flynn GL, Yacobi A, Maibach HI, Bon C, Fleischer NM, Franz TJ, Kaplan SA, Kawamoto J, Lesko LJ, Marty JP, Pershing LK, Schaefer H, Sequeira JA, Shrivastava SP, Wilkin J, Williams RL. 1998. Bioequivalence of Topical Dermatological Dosage Forms- Methods of Evaluation of Bioequivalence. *Skin Pharmacol Appl Skin Physiol* 11:117-124.
23. Shah VP. 2001. Progress in Methodologies for Evaluating Bioequivalence of Topical Formulations. *Am J Clin Dermatol* 2:275-280.
24. Weigmann H, Lademann J, Schanzer S, Lindemann U, von Pelchrzim R, Schaefer H, Sterry W, Shah V. 2001. Correlation of the Local Distribution of Topically Applied Substances Inside the Stratum Corneum Determined by Tape-Stripping to Differences in Bioavailability. *Skin Pharmacol Appl Skin Physiol* 14:98-102.
25. Pershing LK, Corlett J, Jorgensen C. 1994. *In Vivo* Pharmacokinetics and Pharmacodynamics of Topical Ketoconazole and Miconazole in Human Stratum Corneum. *Antimicrob Agents Chemother* 38:90-95.
26. Pershing LW, Lambert L, Wright ED, Shah VP, Williams RL. 1994. Topical 0.05% Betamethasone Dipropionate. *Arch Dermatol* 130:740-747.
27. Ahn SK, Jiang SJ, Hwang SM, Choi EH, Lee JS, Lee SH. 2001. Functional and Structural Changes of the Epidermal Barrier Induced by Various Types of Insults in Hairless Mice. *Arch Dermatol Res* 293:308-318.
28. Weerheim A, Ponc M. 2001. Determination of Stratum Corneum Lipid Profile by Tape Stripping in Combination with High-Performance Thin-Layer Chromatography. *Arch Dermatol Res* 293:191-199.
29. Stachowitz S, Alessandrini F, Abeck D, Ring J, Behrendt H. 2002. Permeability Barrier Disruption Increases the Level of Serine Palmitoyltransferase in Human Epidermis. *J Invest Dermatol* 119:1048-1052.
30. Cross SE, Magnusson BM, Winckle G, Anissimov YG, Roberts MS. 2003. Determination of the Effect of Lipophilicity on the *In Vitro* Permeability and Tissue Reservoir Characteristics of Topically Applied Solutes in Human Skin Layers. *J Invest Dermatol* 120:759-764.

31. Lindemann U, Teichmann A, Meykadeh N, von Pelchrzim R, Weigmann H, Schaefer H, Sterry W, Lademann J. 2002. Reservoir Function of the Stratum Corneum. Perspective in Percutaneous Penetration, Antibes, France,
32. King CS, Barton SP, Nicholls S, Marks R. 1979. The Change in Properties of the Stratum Corneum as a Function of Depth. *Br J Dermatol* 100:165-172.
33. van der Valk PG, Maibach HI. 1990. A Functional Study of the Skin Barrier to Evaporative Water Loss by Means of Repeated Cellophane-Tape Stripping. *Clin Exp Dermatol* 15:180-182.
34. Wagner H, Kostka KH, Lehr CM, Schaefer UF. 2003. pH Profiles in Human Skin: Influence of Two *In Vitro* Test Systems for Drug Delivery Testing. *Eur J Pharm Biopharm* 55:57-65.
35. Beisson F, Acoubala M, Marull S, Moustakas-Gardies AM, Voultoury R, Verger R, Arondel V. 2001. Use of the Tape Stripping Technique for Directly Quantifying Esterase Activities in Human Stratum Corneum. *Anal Biochem* 290:179-185.
36. Naik A, Pechtold LARM, Potts RO, Guy RH. 1995. Mechanism of Oleic Acid-Induced Skin Penetration Enhancement *In Vivo* in Humans. *J Control Release* 37:299-306.
37. Higo N, Naik A, Bommannan DB, Potts RO, Guy RH. 1993. Validation of Reflectance Infrared Spectroscopy as a Quantitative Method to Measure Percutaneous Absorption *In Vivo*. *Pharm Res* 10:1500-1506.
38. Tsai J, Chuang S, Hsu M, Sheu H. 1999. Distribution of Salicylic Acid in Human Stratum Corneum Following Topical Application *In Vivo*: A Comparison of Six Different Formulations. *Int J Pharm* 188:145-153.
39. Dupius D, Rougier A, Roguet R, Lotte C. 1986. The Measurement of the Stratum Corneum Reservoir: A Simple Method to Predict the Influence of Vehicles on *In Vivo* Percutaneous Absorption. *Br J Dermatol* 115:233-238.
40. Alberti I, Kalia YN, Naik A, Guy RH. 2001. Assessment and Prediction of the Cutaneous Bioavailability of Topical Terbinafine, *In Vivo*, in Man. *Pharm Res* 18:1472-1475.
41. Stinchcomb AL, Pirot F, Touraille GD, Bunge AL, Guy RH. 1999. Chemical Uptake into Human Stratum Corneum *In Vivo* From Volatile and Non-Volatile Solvents. *Pharm Res* 16:1288-1293.
42. Moser K, Kriwet K, Froehlich C, Kalia YN, Guy RH. 2001. Supersaturation: Enhancement of Skin Penetration and Permeation of a Lipophilic Drug. *Pharm Res* 18:1006-1011.
43. Pirot F, Kalia YN, Stinchcomb AL, Keating G, Bunge A, Guy RH. 1997. Characterization of the Permeability Barrier of Human Skin *In Vivo*. *Proc Natl Acad Sci USA* 94:1562-1567.
44. Harrison SM, Barry BW, Dugard PH. 1984. Effects of Freezing on Human Skin Permeability. *J Pharm Pharmacol* 36:261-262.
45. Schaefer H, Stuttgen G, Zesch A, Schalla W, Gazith J. 1978. Quantitative Determination of Percutaneous Absorption of Radiolabeled Drugs *In Vitro* and *In Vivo* by Human Skin. *Curr Probl Dermatol* 7:80-94.
46. Anderson BD, Higuchi WI, Raykar PV. 1988. Heterogeneity Effects on Permeability-Partition Coefficient Relationships in Human Stratum Corneum. *Pharm Res* 5:566-573.

47. Martin E, Neelissen-Subnel MT, De Haan FH, Bodde HE. 1996. A Critical Comparison of Methods to Quantify Stratum Corneum Removed by Tape Stripping. *Skin Pharmacol* 9:69-77.
48. Shargel L, Yu ABC. 1999. *Applied Biopharmaceutics and Pharmacokinetics*. 4th Ed. Stamford, Connecticut, USA: Appleton and Lange. pp 1-28.
49. Chapman SJ, Walsh A, Jackson SM, Friedmann PS. 1991. Lipids, Proteins and Corneocyte Adhesion. *Arch Dermatol Res* 283:167-173.
50. Trebilcock KL, Heylings JR, Wilks MF. 1994. *In Vitro* Tape Stripping as a Model For *In Vivo* Skin Stripping. *Toxicol In Vitro* 8:665-667.
51. Dreher F, Arens A, Mudumba S, Ademola J, Maibach HI. 1998. Colorimetric Method for Quantifying Human Stratum Corneum Removed by Adhesive-Tape-Stripping. *Acta Derm Venereol Suppl (Stockh)* 78:186-189.
52. Weigmann H, Lademann J, Meffert H, Schaefer H, Sterry W. 1999. Determination of the Horny Layer Profile by Tape Stripping in Combination with Optical Spectroscopy in the Visible Range as a Prerequisite to Quantify Percutaneous Absorption. *Skin Pharmacol Appl Skin Physiol* 12:34-45.
53. Pershing LK, Silver BS, Krueger GG, Shah VT, Skelly JP. 1992. Feasibility of Measuring the Bioavailability of Topical Betamethasone Dipropionate in Commercial Formulations using Drug Content in Skin and a Skin Blanching Bioassay. *Pharm Res* 9:45-51.
54. Crank J. 1975. *The Mathematics of Diffusion*. London: Oxford University Press. pp 44-68.
55. Pugh WJ, Hadgraft J, Roberts MS. 1998. Physicochemical Determinants of Stratum Corneum Permeation. In Roberts MS, Walters KA, ed. *Dermal Absorption and Toxicity Assessment*. New York: Marcel Dekker, Inc., pp 245-268.
56. Menon GK, Lee SH, Roberts MS. 1998. Ultrastructural Effects of Some Solvents and Vehicles on the Stratum Corneum and Other Skin Components: Evidence for an "Extended Mosaic-Partitioning Model of the Skin Barrier". In Roberts MS, Walters KA, ed. *Dermal Absorption and Toxicity Assessment*. New York: Marcel Dekker, Inc., pp 727-751.
57. Curatolo W. 1987. The Lipoidal Permeability Barriers of the Skin and Alimentary Tract. *Pharm Res* 4:271-277.
58. Krill SL, Knutson K, Higuchi WI. 1992. The Stratum Corneum Lipid Thermotropic Phase Behaviour. *Biochim Biophys Acta* 1112:281-286.
59. Moore DJ, Rerek ME. 2000. Insights into the Molecular Organization of Lipids in the Skin Barrier from Infrared Spectroscopy Studies of Stratum Corneum Lipid Models. *Acta Derm Venereol Suppl (Stockh)* 208:16-22.
60. Ribaud C, Garson JC, Doucet J, Leveque JL. 1994. Organization of Stratum Corneum Lipids in Relation to Permeability: Influence of Sodium Lauryl Sulfate and Preheating. *Pharm Res* 11:1414-1418.
61. Bommannan D, Potts RO, Guy RH. 1990. Examination of Stratum Corneum Barrier Function *In Vivo* by Infrared Spectroscopy. *J Invest Dermatol* 95:403-408.

62. Bommannan D, Potts RO, Guy RH. 1991. Examination of the Effect of Ethanol on Human Stratum Corneum *In Vivo* Using Infrared Spectroscopy. *J Control Release* 16:299-304.
63. Yum S, Lee E, Taskovich L, Theeuwes F. 1994. Permeation Enhancement with Ethanol: Mechanism of Action Through Skin. In Hsieh DS, ed. *Drug Permeation Enhancement*. New York: Marcel Dekker, Inc., pp 143-170.
64. Jiang R, Roberts MS, Collins DM, Benson HAE. 1999. Absorption of Sunscreens Across Human Skin: An Evaluation of Commercial Products for Children and Adults. *Br J Clin Pharmacol* 48:635-637.
65. Walters KA, Gettings SD, Roberts MS. 1999. Percutaneous Absorption of Sunscreens. In Bronaugh RL, Maibach HI, ed. *Percutaneous Absorption : Drugs, Cosmetics, Mechanisms, Methodology*. New York: Marcel Dekker Inc., pp 861-877.
66. Walters KA, Brain KR, Howes D, James VJ, Kraus AL, Teetsel NM, Toulon M, Watkinson AC, Gettings SD. 1997. Percutaneous Penetration of Octyl Salicylate from Representative Sunscreen Formulations Through Human Skin *In Vitro*. *Food Chem Toxicol* 35:1219-1225.
67. Hagedorn-Leweke U, Lippold BC. 1995. Absorption of Sunscreens and Other Compounds Through Human Skin *In Vivo*: Derivation of a Method to Predict Maximum Fluxes. *Pharm Res* 12:1354-1360.
68. Dary CC, Blancato JN, Saleh MA. 2001. Chemomorphic Analysis of Malathion in Skin Layers of the Rat: Implications for the Use of Dermatopharmacokinetic Tape Stripping in Exposure Assessment to Pesticides. *Regul Toxicol Pharmacol* 34:234-248.
69. van Hoogdalem EJ. 1992. Assay of Erythromycin in Tape Strips of Human Stratum Corneum and Some Preliminary Results in Man. *Skin Pharmacol* 5:124-128.
70. Treffel P, Gabard B. 1996. Skin Penetration and Sun Protection Factor of Ultra-Violet Filters from Two Vehicles. *Pharm Res* 13:770-774.
71. Barrett DA, Rutter N, Davis SS. 1993. An *In Vitro* Study of Diamorphine Permeation Through Premature Human Neonatal Skin. *Pharm Res* 10:583-587.
72. Hewitt PG, Perkins J, Hotchkiss SA. 2000. Metabolism of Fluroxypyr, Fluroxypyr Methyl Ester, and the Herbicide Fluroxypyr Methylheptyl Ester. I: During Percutaneous Absorption Through Fresh Rat and Human Skin *In Vitro*. *Drug Metab Dispos* 128:748-754.
73. Higo N, Hinz RS, Lau DT, Benet LZ, Guy RH. 1993. Cutaneous Metabolism of Nitroglycerin *In Vitro*. II. Effects of Skin Condition and Penetration Enhancement. *Pharm Res* 9:303-306.
74. Roy SD, Hou SY, Witham SL, Flynn GL. 1994. Transdermal Delivery of Narcotic Analgesics: Comparative Metabolism and Permeability of Human Cadaver Skin and Hairless Mouse Skin. *J Pharm Sci* 83:1723-1728.
75. Kenney GE, Sakr A, Lichtin JL, Chou H, Bronaugh RL. 1995. *In Vitro* Skin Absorption and Metabolism of Padimate-O and a Nitrosamine Formed in Padimate-O-Containing Cosmetic Products. *J Soc Cosmet Chem* 46:117-127.
76. Brysk MM, Rajaraman S. 1992. Cohesion and Desquamation of Epidermal Stratum Corneum. *Prog Histochem Cytochem* 25:1-53.

77. Haftel M, Teillon MH, Schmitt D. 1998. Stratum Corneum, Corneodesmosomes and *Ex Vivo* Percutaneous Penetration. *Microsc Res Tech* 43:242-249.
78. Leary T, Jones PL, Appleby M, Blight A, Parkinson K, Stanley M. 1992. Epidermal Keratinocyte Self-Renewal is Dependent upon Dermal Integrity. *J Invest Dermatol* 99:422-430.
79. Egelro J T. 2000. Desquamation in the Stratum Corneum. *Acta Derm Venereol Suppl (Stockh)* 208:44-45.
80. Piérard GE, Goffin V, Hermanns-Le T, Pierard-Franchimont C. 2000. Corneocyte Desquamation (Review). *Int J Mol Med* 6:217-221.
81. Bronaugh RL, Stewart RF, Simon M. 1986. Methods for *In Vitro* Percutaneous Absorption Studies. VII: Use of Excised Human Skin. *J Pharm Sci* 75:1094-1097.
82. Hakkinen L, Koivisto L, Larjava H. 2002. An Improved Method for Culture of Epidermal Keratinocytes from Newborn Mouse Skin. *Methods Cell Sci* 23:189-196.
83. Auton TR, Westhead DR, Woollen BH, Scott RC, Wilks MF. 1994. A Physiological Based Mathematical Model of Dermal Absorption in Man. *Hum Exp Toxicol* 13:51-60.
84. Reddy MB, Guy RH, Bunge AL. 2000. Does Epidermal Turnover Reduce Percutaneous Penetration? *Pharm Res* 17:1414-1419.
85. Kvidera A, Mackenzie IC. 1994. Rates of Clearance of the Epithelial Surfaces of Mouse Oral Mucosa and Skin. *Epithel Cell Biol* 3:175-180.
86. Reifenrath WG, Hawkins GS, Kurtz MS. 1991. Percutaneous Penetration and Skin Retention of Topically Applied Compounds: An *In Vitro* - *In Vivo* Study. *J Pharm Sci* 80:526-532.
87. Reddy MB, Stinchcomb AL, Guy RH, Bunge AL. 2002. Determining Dermal Absorption Parameters *In Vivo* from Tape Strip Data. *Pharm Res* 19:292-298.

CHAPTER 6

DISTRIBUTION OF OCTISALATE AND PADIMATE O ACROSS HUMAN STRATUM CORNEUM

6.1. INTRODUCTION

As discussed in Chapter 5, the “tape stripping technique” has become a popular method for investigating the localisation and distribution of substances within the SC. However, despite the extensive use of this technique to quantify drug concentrations within the SC, little attention has focused on elucidating the distribution of CPEs across the SC. Therefore, in an attempt to gain further insight into the possible mechanism(s) by which OS and PO enhance fentanyl permeation across the SC, the work presented in this chapter focuses on investigating the distribution of these CPEs across human SC.

The impetus for these investigations stemmed from the results presented in Chapters 3, 4 and 5, which suggest that OS and PO may enhance fentanyl partitioning into the SC by altering the thermodynamic properties of the applied formulation (i.e. by maintaining a diffusible source of fentanyl at the SC surface that they co-deliver as they themselves partition into the SC) and by increasing the solubility of fentanyl in the SC lipid domain. Evidently, these findings would imply that OS and PO must permeate the SC in order to exert their effects on fentanyl partitioning. Consequently, this raises the question as to if the mechanisms by which OS and PO enhance fentanyl partitioning into the SC are related to their distribution profiles across the SC.

At present, the question of how the mechanism(s) of action of a CPE relate to its distribution profile across the SC has only been addressed for the putative CPE, oleic acid (OA). Using attenuated total reflectance Fourier transform infrared spectroscopy (ATR-FTIR) in conjunction with the “tape stripping technique”, Naik et al (1) determined the distribution profile of perdeuterated oleic acid ($[^2\text{H}]$ OA) and the conformational order of SC lipids as a function of SC depth. These investigators found that the concentration of $[^2\text{H}]$ OA declined exponentially as a function of increasing mass of SC removed, reaching a limiting value near zero in the deepest layers of the SC probed. It was also determined that the effect of $[^2\text{H}]$ OA on SC lipid disorder was only apparent at the surface and uppermost layers of the SC, where the concentration of $[^2\text{H}]$ OA, and the intrinsic fluidity of the SC lipids, is greatest (2). Mak et al (3) also employed ATR-FTIR to measure OA concentrations within the superficial layers of the SC and the conformational order of SC lipids. These studies showed that treating the SC with 0.5 or 1% OA for 0.5 h produced a concentration-dependent increase in SC lipid disordering. However, further increases in OA concentration from 1% to 10% did not cause any additional lipid disordering effect.

On the other hand, the uptake of OA into human SC was found to increase with an increase in the topically applied concentration of OA from 0.5 to 10%. Consequently, the authors proposed that the maximal lipid perturbing effect of OA was due to a saturation of the effect of OA rather than a solubility limitation (i.e. no more OA could partition into the SC).

An important feature of both of these studies was the use of ATR-FTIR to quantify levels of OA within the SC. As discussed in Chapter 7, infrared (IR) spectroscopy has traditionally been used to investigate the thermotropic phase behaviour of membrane lipids and to study membrane structure and function (4-7). This technique lends itself to such investigations as it measures the molecular vibrations of various constituent groups within an absorbing species, which occur as a result of their interaction with electromagnetic energy (8). One principle of IR spectroscopy, which is germane to the work presented in this chapter, is that the intensity of absorption by a sample is directly proportional to the concentration of the absorbing species (5, 7).

The utility of IR spectroscopy to study the biophysical properties of membranes, such as the SC, and to monitor, measure and characterise drug distribution across the SC has been further extended through the introduction of ATR-FTIR (4). Compared with conventional dispersion infrared spectroscopy, the advantages of the Fourier transform techniques of spectral detection and analysis include higher signal-to-noise ratios, greater accuracy, higher resolution, reduced analysis time and optical throughput (9). The use of an interferometer also allows the simultaneous analysis of all frequencies generated by an absorbing species.

In ATR, an IR-transparent crystal (internal reflection element, IRE) transmits an IR beam from the interferometer to the IR detector. Thus, as the skin is placed (SC-side down) on the IRE it does not transect the IR beam, as it would in dispersive IR spectrometers, but enables spectral acquisition from the material at the crystal-skin interface. That is, when radiation propagates through the IRE (which has a refractive index, n_1) it strikes the interface of the skin (which has a refractive index of n_2) at an angle that is greater than the critical angle, θ_c ($\theta_c = \sin^{-1}(n_2/n_1)$) (Figure 6.1). Under these conditions, the IR beam undergoes total internal reflection within the IRE and as it does, an evanescent wave is established at the skin-crystal interface, which subsequently propagates into the skin. Given that the IRE is IR transparent and the skin generates absorption bands in the energy range of the incident radiation, then each propagation will

cause energy loss due to absorption. This effect is amplified by successive reflections within the skin. As the amplitude of the evanescent wave decays exponentially with increasing distance into the skin its depth of penetration into the skin cannot be defined in absolute terms. Consequently, the “apparent depth of penetration” (D_{app}) is used to approximate the distance at which the incident intensity decreases to 37% of its value at the interface (7, 10):

$$D_{app} = \frac{\lambda}{2\pi n_1 [\sin^2 \theta - (n_2/n_1)^2]^{1/2}} \quad 6.1$$

where λ is the wavelength of interest and θ is the IRE face angle. Thus, as the ATR effect only occurs at close proximity to the IRE, the apparent depth of penetration into a skin sample is usually in the order of 0.3 to 3 μm , depending on the wavelength range of interest, the IRE used, the hydration level of the skin and the entry angle of incident radiation (7). Therefore, the information gathered from an ATR-FTIR scan of human skin pertains only to the uppermost superficial layers of the SC. Information regarding the deeper SC layers can, however, be obtained by using ATR-FTIR in conjunction with the “tape stripping technique”, whereby successive layers of the SC can be removed and subsequently analysed.

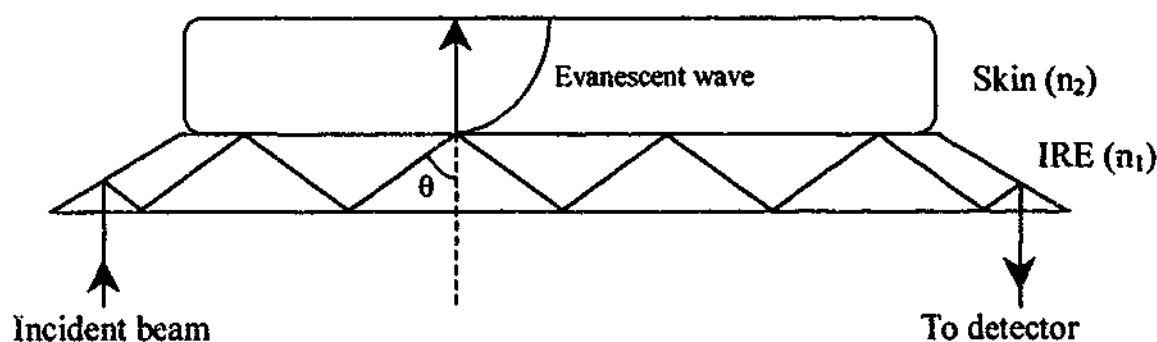


Figure 6.1. Schematic representation of ATR-FTIR. Radiation propagating through an IRE (refractive index, n_1) strikes the interface of the skin (refractive index, n_2), which is placed SC-side down over the crystal, at an angle (θ) that is greater than the critical angle. Consequently, the IR beam is totally internally reflected within the IRE and as such an evanescent wave established at the skin-crystal interface propagates into the skin. Adapted from Naik et al (7).

ATR-FTIR is a convenient method for determining drug distribution across the SC *in vitro* or *in vivo*. It permits a relatively facile analysis of skin samples *in vitro* and *in vivo* as the region of skin under investigation, or an excised skin sample, may be placed directly onto the crystal or a remote fiber-optic probe with an IRE head may be used to transmit the IR beam to the detector. Furthermore, it is a non-destructive and non-invasive method of sample analysis. However, as components of the SC give rise to several IR absorbances, the use of ATR-FTIR to quantify permeant levels within the SC is limited to drugs that generate uniquely identifiable IR absorbances that can be distinguished from those arising from the SC. Furthermore, the difference in the amount of permeant spectrally detected within sequential layers of the SC is used to determine the amount of drug present within a given fraction of SC removed by tape stripping (Figure 6.2). However, it cannot be assumed that the absolute amount of drug removed by any particular tape strip corresponds exactly to the relative measurement acquired. This degree of uncertainty is not applicable to traditional methods of analysis which are used to quantify the amount of drug present in the fraction of SC removed by a tape strip (i.e. the fraction that separates each sequential ATR-FTIR measurement) (Figure 6.2). Consequently, there is a need to establish the correlation between spectroscopic (relative) and absolute measurements of drug concentrations within the SC in order to validate the use of ATR-FTIR as a quantitative tool to assess drug distribution across the SC.

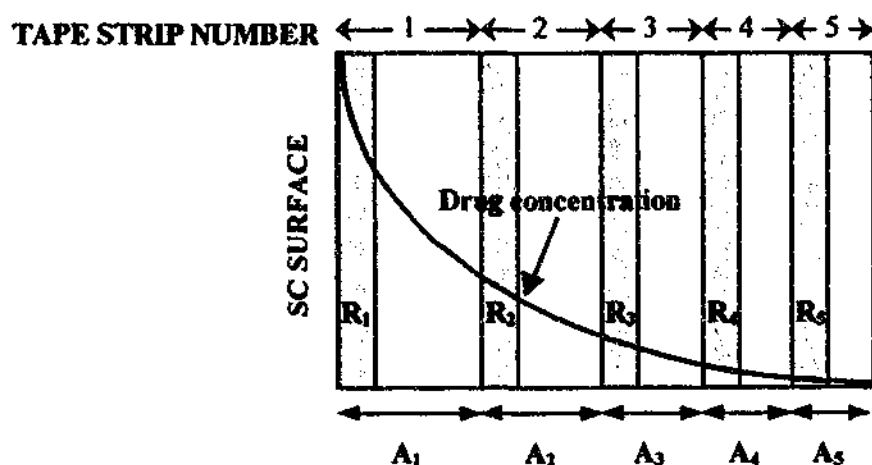


Figure 6.2. Schematic representation of the absolute and spectroscopic determination of drug distribution across the SC. R_n represents the region of the SC analysed by ATR-FTIR, A_n represents the fraction of the SC removed by tape stripping and subjected to a quantitative method of analysis, where n is the tape strip number. Adapted from Higo et al (11).

6.2. OBJECTIVES

The overall objective of the work presented in this chapter was to determine the distribution profiles of OS and PO across human SC in an attempt to gain further insight into the possible mechanism(s) by which they enhance fentanyl permeation. As the time-related effects of OS and PO on fentanyl distribution across human SC *in vitro* were investigated in Chapter 5, an objective of these studies was to investigate the time-related changes in OS and PO distribution profiles across human SC using the same *in vitro* experimental conditions. A second objective of this research was to determine whether this *in vitro* data accurately depicted the time-dependent changes that occur within human SC *in vivo*. Thus, using OS as a model enhancer, distribution profiles were determined across human SC under *in vivo* experimental conditions in order to establish an *in vitro* – *in vivo* correlation.

As ATR-FTIR is becoming an increasingly popular method for measuring permeant levels within the SC, another aim of this research was to determine the validity of this technique as a quantitative tool to assess the distribution of OS and PO across human SC under *in vitro* and *in vivo* experimental conditions.

6.3. MATERIALS AND METHODS

6.3.1. Materials

OS and PO were supplied by Bronson and Jacobs (Australia). HPLC grade acetonitrile and methanol were supplied by Merck (Australia). Water was purified by a Milli-Q™ water purification system (Millipore, Bedford, MA, USA). All other reagents were of analytical grade.

6.3.2. Determination of octisalate and padimate O distribution across human stratum corneum *in vitro*

The distribution of either OS or PO across human SC *in vitro* was determined in conjunction with the experiments described in Chapter 5 (where fentanyl was applied

with either OS or PO). As the details of these experiments are presented in Chapter 5, they have only been summarised in the following sections.

6.3.2.1. Skin preparation

Human female abdominal tissue was obtained following abdominoplasty from two individual donors. The full thickness skin samples were prepared according to the method described in Section 5.3.2. As previously stated, 1 x 5 cm sections of skin were glued onto 1 x 7 cm pieces of cardboard. The SC surface of each sample was quickly (<20 sec) wiped with a Kimwipes® (Kimberly-Clark, Australia) that was pre-moistened with ethanol to ensure complete removal of sebaceous lipids. The skin samples were then left untouched for 5 min to allow the glue to dry.

6.3.2.2. Tape stripping procedure

As described in Section 5.3.3, the skin samples (n=5 for each experiment) were adhered, cardboard side down, onto a 1.5 x 1.5 x 100 cm (height x width x length) rectangular steel rod using double-sided adhesive tape (Scotch® Permanent Double Stick Tape, 3M, Australia).

Formulations containing 5%w/v fentanyl and 5%w/v of either OS or PO in 95%v/v ethanol were then applied as a finite dose ($5 \mu\text{l}/\text{cm}^2$) onto the SC surface of each skin sample. After a pre-determined exposure time (5 min (0.08 h), 0.5, 2, 6, or 16 h), excess formulation was removed from the SC surface using the validated surface wipe procedure described in Section 5.3.4.1.

After the surface wipe was performed, the SC was progressively removed by sequential adhesive tape stripping (Section 5.3.3). The tape stripping procedure was repeated 20 times in order to remove most of the SC (12). In order to determine the distribution profiles of OS or PO across the SC by ATR-FTIR, an ATR-FTIR spectrum of each skin sample was obtained after the surface wipe procedure and after each tape strip. The details of this analytical technique are in Section 6.3.2.3.2. In order to determine the distribution profiles of OS or PO across the SC by HPLC/UV, OS and PO were extracted from the surface wipes and from each tape strip using the validated procedures described in Sections 5.3.4.2. and 5.3.5.1. The amount of OS and PO

extracted from the surface wipe and each tape strip was then quantitated using the validated HPLC/UV assays described in Section 5.3.6.

As described in Section 5.3.3, the mass of SC removed (M_{sc}) was determined by weighing each tape strip before and after the tape stripping procedure on a Sartorius MC5 microbalance. Assuming a constant SC density (D_{sc}) of 1 g/cm³ (13) and that the SC was uniformly distributed on each tape strip, the length of SC removed (L) was determined from the following equation:

$$L = \frac{M_{sc} D_{sc}}{A_{exp}} \quad 6.2$$

where A_{exp} is the area of skin exposed.

6.3.2.3. Analytical methods

6.3.2.3.1. Chromatographic analysis of octisalate and padimate O

The concentrations of OS or PO within the surface wipe and tape strip extracts were determined using the validated HPLC/UV assays that are described in Section 5.3.6.

6.3.2.3.2. Spectroscopic analysis of octisalate and padimate O

6.3.2.3.2.1. Acquisition of ATR-FTIR spectra

Spectral measurements were made using a horizontal ATR Accessory (Pike Technologies, Inc., Madison, WI, USA) fitted into the sample compartment of an Excalibur™ FTS 3500GX spectrometer (Bio-Rad Laboratories, Inc., Cambridge, MA, USA) that was equipped with a liquid nitrogen-cooled mercury-cadmium-telluride detector. The IRE that was supported by the horizontal ATR Accessory was a flat plate, trapezoidal zinc selenide crystal that was 8 cm long, 1 cm wide and 4 cm thick. The entrance and exit faces of the crystal were each cut at a 45° angle. As zinc selenide has a refractive index of 2.4 at 1000 cm⁻¹ and the refractive index of the SC is in the order of ~1.33 to 1.55 (2), then in the spectral range of interest (from 1000 to 1500 cm⁻¹, per

Section 6.1) the apparent depth by which the evanescent IR beam penetrated the SC may have been of the order of ~ 1.5 to ~ 3.5 μm (per Equation 6.1). As the thickness of the keratinocytes within the SC may be in the order of ~ 0.8 μm and the vertical gap between the keratinocytes is of the order of ~ 75 nm (14), then the information gathered from an ATR-FTIR spectrum of this nature pertains only the superficial strata of the SC (the uppermost ~ 1 to ~ 4 cell layers) in contact with the crystal.

In order to obtain an ATR-FTIR spectrum of the skin, each sample was placed SC side down onto the surface of the zinc selenide crystal (Figure 6.3). As the ATR effect only occurs at close proximity to the surface of the crystal, the skin needed have intimate contact with the crystal. This was achieved by placing stainless steel slabs with flush surfaces (total weight 1200 g) on top of the skin. After the skin was placed over the crystal, an ATR-FTIR scan was initiated using a computer software package (Merlin Version 2.97, Bio-Rad Laboratories, Inc.). Each spectrum represented an average of 16 scans, obtained at a resolution of 8 cm^{-1} , over a wavelength range from 750 to 4000 cm^{-1} . A period of 30 sec was required to acquire each spectrum. All measurements were conducted under ambient conditions ($23 \pm 1^\circ\text{C}$; 30 to 40% relative humidity).

6.3.2.3.2.2. Identification of infrared absorbances arising from octisalate and padimate O

Human SC is effectively "IR transparent" at various frequencies within the mid-IR region (Figure 6.5.A). Most notably, these "IR transparent windows" exist between ~ 1800 and $\sim 2800\text{ cm}^{-1}$ and beyond $\sim 3600\text{ cm}^{-1}$. Consequently, the characterisation of molecular transport across human SC by means of ATR-FTIR often relies on the use of model permeants that give rise to a distinct IR absorbance within one of these "IR transparent windows" (4). However, upon inspection of the ATR-FTIR spectra of OS and PO (Figure 6.4), it is evident that both compounds give rise to several distinguishing IR absorbances that are not within the "IR transparent windows" of the SC spectrum.

Both OS and PO give rise to CH_2 and CH_3 symmetric (~ 2857 and $\sim 2875\text{ cm}^{-1}$) and asymmetric (~ 2925 and $\sim 2963\text{ cm}^{-1}$) stretching frequencies. However, these IR absorbances coincide with the CH_2 and CH_3 symmetric and asymmetric stretching frequencies that arise from the SC lipids (Figure 6.5.A).

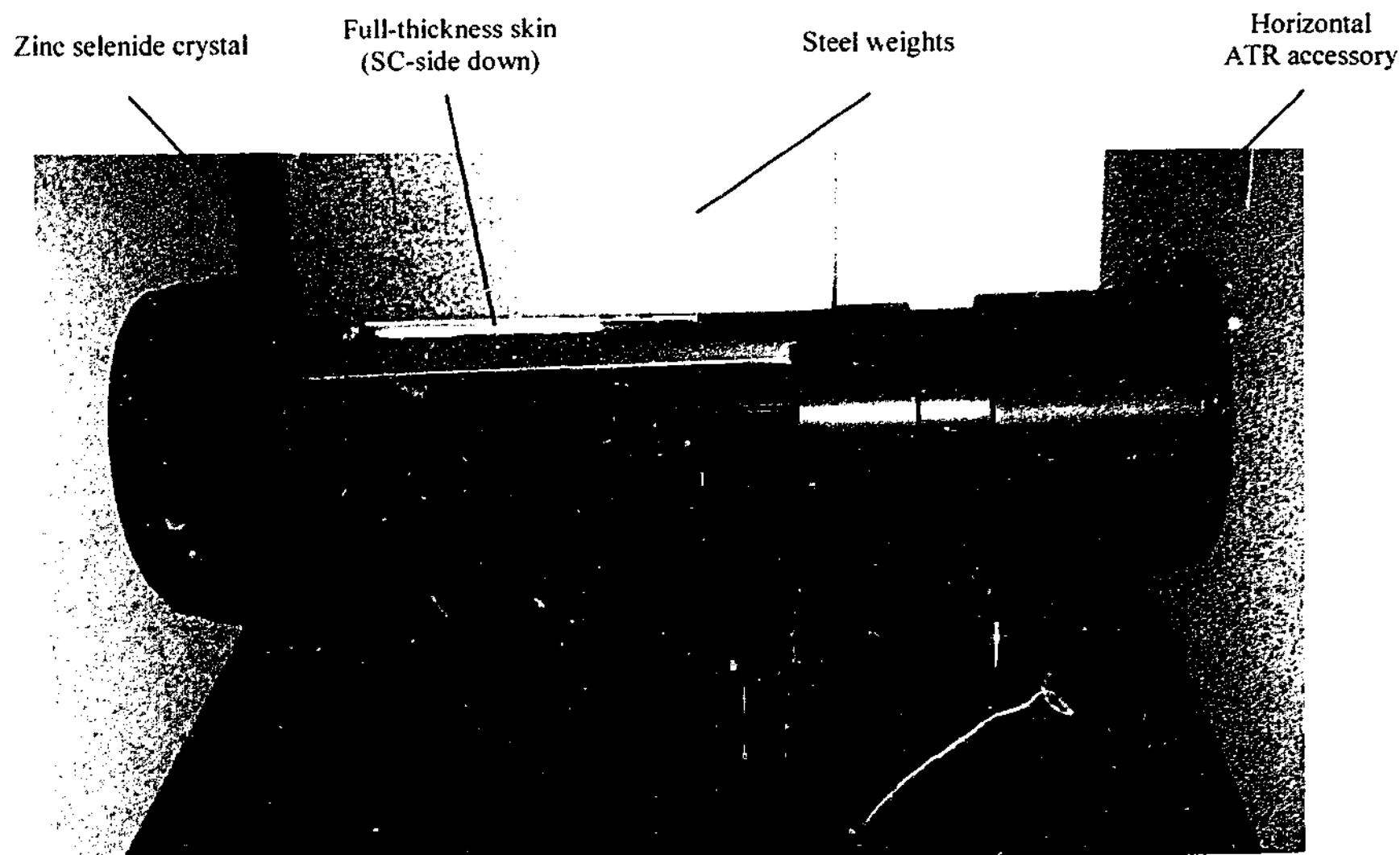


Figure 6.3. A photograph illustrating how an ATR-FTIR spectrum of human SC was acquired from excised full thickness skin.

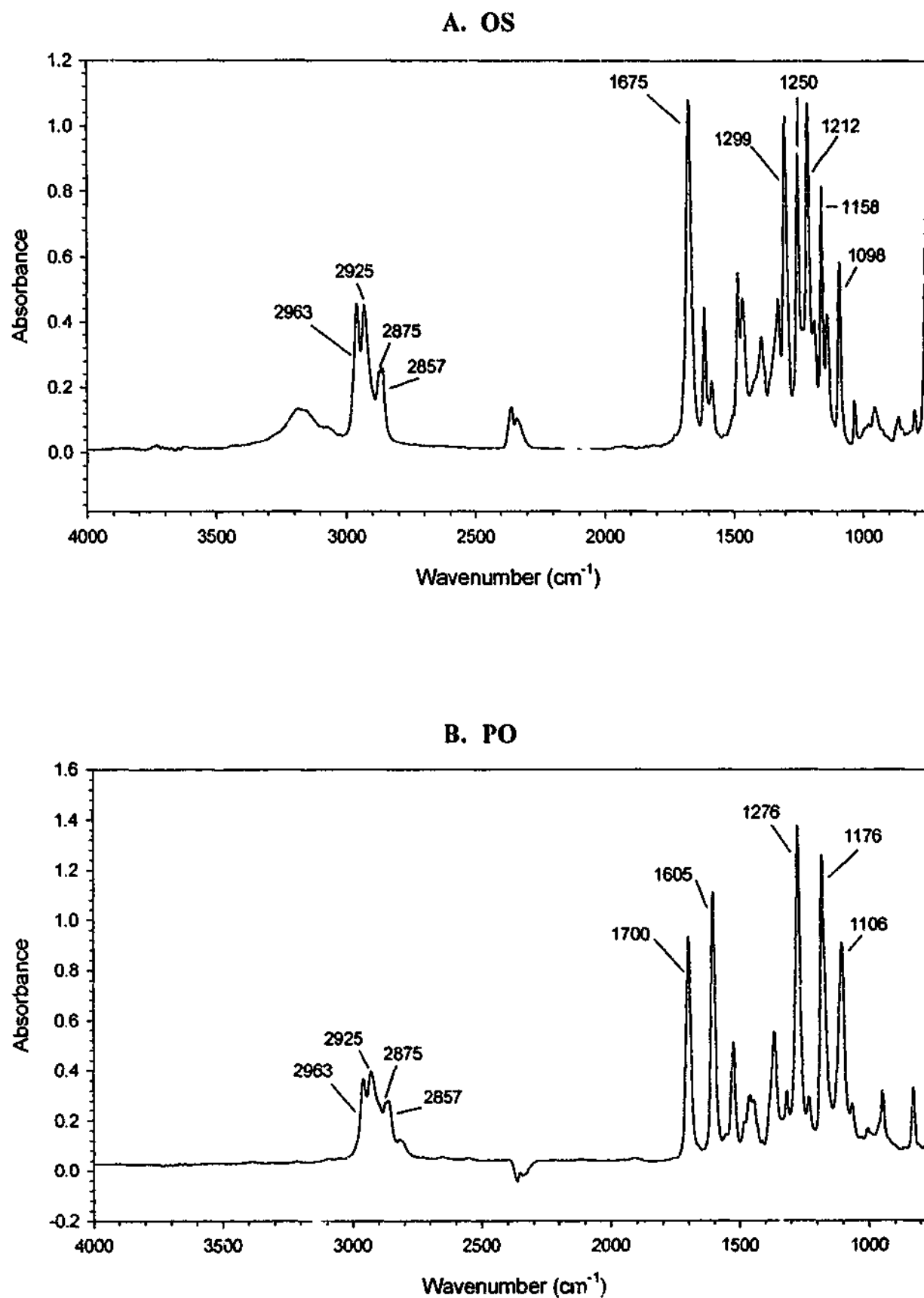
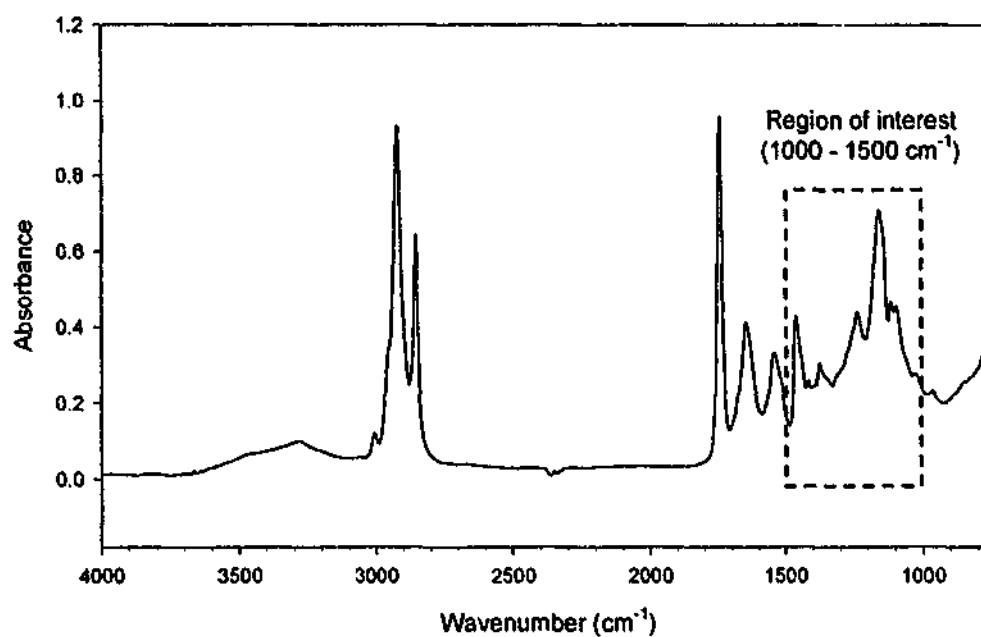


Figure 6.4. ATR-FTIR spectra of 500 µg OS (A) and PO (B) deposited directly onto the surface of a zinc selenide crystal

A. ATR-FTIR spectrum between 750 and 4000 cm^{-1}



B. ATR-FTIR spectrum between 1000 and 1500 cm^{-1}

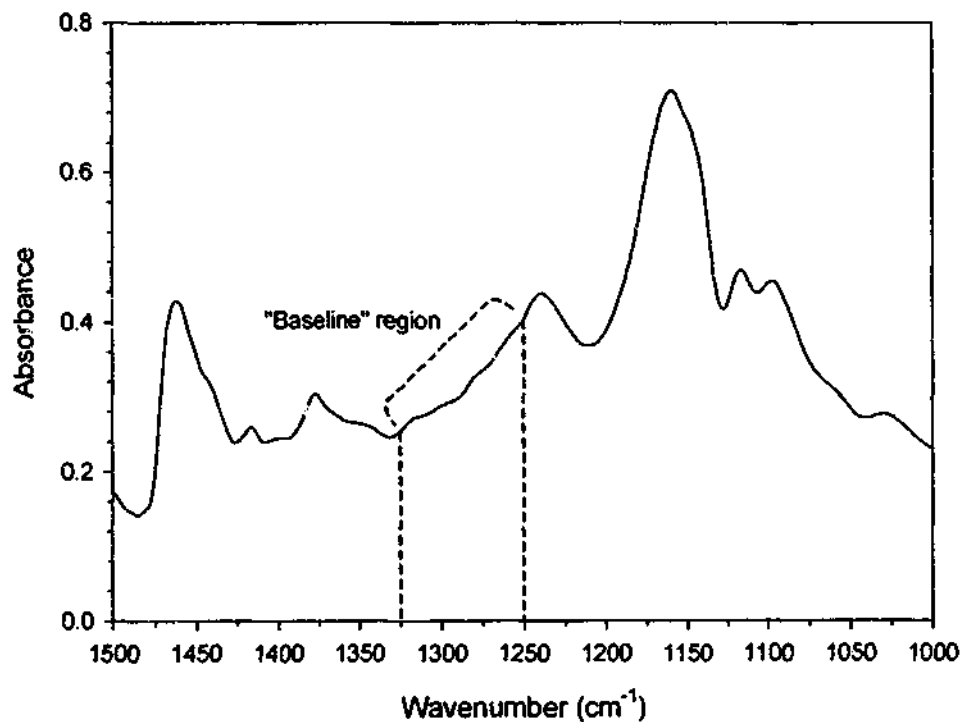


Figure 6.5. Representative ATR-FTIR spectrum of blank (untreated) human abdominal SC from excised full thickness skin within a wavelength range of 750 to 4000 cm^{-1} (A) and the wavelength range of interest (between 1000 and 1500 cm^{-1}) (B).

OS also gives rise to an IR absorbance at 1675 cm^{-1} , whilst PO generates absorbances at 1700 and 1605 cm^{-1} . However, these particular absorbances may be obscured by the carbonyl stretching frequencies that originate from fatty acids (1743 cm^{-1}) within the SC lipid domain or amides within the SC keratinocytes (1656 cm^{-1}). Consequently, the IR absorbances originating from OS and PO that could be used to determine their distribution profiles across human SC were those centered at 1299 , 1250 , 1212 , 1158 or 1098 cm^{-1} for OS and at 1276 , 1176 or 1106 cm^{-1} for PO. Although these IR absorbances are located between ~ 1000 to 1500 cm^{-1} , which corresponds to the “fingerprint” region of an ATR-FTIR spectrum of human SC (Figure 6.5.A), it did not preclude the use of ATR-FTIR to quantify OS and PO concentrations within the SC.

Upon focusing on the spectral range of interest (1000 to 1500 cm^{-1}) within an ATR-FTIR spectrum of human SC (Figure 6.5.B), it becomes evident that a region exists between ~ 1250 and $\sim 1325\text{ cm}^{-1}$ where the IR signal intensities generated from the SC are minimal (i.e. a “baseline” region). Consequently, the IR absorbances that were used to quantify concentrations of OS and PO within the SC were those centered at 1299 and 1276 cm^{-1} , respectively.

6.3.2.3.2.3. Assay validation

The spectroscopic quantification of OS and PO within the SC is based upon the assumption that the intensity or area under the curve of an IR absorbance is directly proportional to the amount of absorbing species. In order to confirm this assumption, calibration curves were constructed on each day of analysis whereby OS or PO was applied to the SC surface of full-thickness skin samples.

Standard solutions at concentrations within the range of 0.4 to 40 mg/ml were prepared by diluting a stock solution of 100 mg/ml of OS or PO in $95\%v/v$ ethanol with an appropriate volume of $95\%v/v$ ethanol. In order to mimic the experimental conditions described in Section 6.3.2.2, $1 \times 5\text{ cm}$ full thickness skin samples were prepared from female abdominal tissue (obtained from three different donors) and glued onto $1 \times 7\text{ cm}$ pieces of cardboard according to the method described in Section 6.3.2.1. After the glue had dried (after $\sim 5\text{ min}$), a $25\text{ }\mu\text{l}$ aliquot of standard solution was applied evenly across the entire SC surface such that the amount of OS or PO deposited onto the SC surface varied from 10 to $1000\text{ }\mu\text{g}$. In order to acquire an ATR-FTIR spectrum of blank SC, a 25

μl aliquot of 95%v/v ethanol was applied to the SC surface of a skin sample ($n=5$ for each calibration curve that was constructed).

Preliminary research indicated that ethanol gave rise to IR absorbances that interfere with those generated from OS and PO. Therefore, immediately after each solution was applied to the SC surface the ethanol was evaporated under a gentle stream of nitrogen for 30 sec. This enabled an ATR-FTIR scan to be obtained before significant amounts of OS or PO had partitioned from the SC surface into the underlying SC layers.

As mentioned previously, stainless steel slabs (total weight 1200 g) were placed over the skin sample whilst an ATR-FTIR scan was performed (Figure 6.3). Each acquired spectrum represented an average of 16 scans, obtained at a resolution of 8 cm^{-1} , over a wavelength range from 750 to 4000 cm^{-1} . A period of 30 sec was required to acquire each spectrum. All measurements were conducted under ambient conditions ($23 \pm 1^\circ\text{C}$; 30 to 40% relative humidity).

The absorbances from OS and PO located at 1299 and 1276 cm^{-1} were integrated between the limits of either ~ 1277 to $\sim 1315\text{ cm}^{-1}$ or ~ 1253 to $\sim 1297\text{ cm}^{-1}$, respectively, in order to obtain the area under the IR absorbance curve. Peak frequency maxima were determined using a center of gravity algorithm, where the location of the peak is determined by the average of the x -values in the region defined by the peak limits weighted by the spectrum height at each x -value:

$$\text{Peak location} = \frac{\sum x_i y_i}{\sum y_i} \quad 6.3$$

where y_i is the height of the spectrum at wavenumber x_i and all x_i are within the defined region.

As signal intensity depends on the degree of contact between the sample and the IRE, it is often necessary to normalise the IR absorbance of interest to relatively constant IR absorbance(s) that arise from the skin, such as the amide I and amide II absorbances originating from the carbonyl stretching and N-H bending vibrational frequencies of the SC keratinocytes (10, 15). This normalization procedure eliminates variability produced by the level of contact between different skin samples and the IRE. However, as revealed in the forthcoming paragraphs, a normalisation procedure was not required for the

quantification of OS and PO within SC *in vitro* as the reproducibility of each ATR-FTIR assay was excellent.

A linear relationship between IR absorbance peak area and the amount of OS or PO deposited on the SC surface was determined by the correlation coefficient generated by linear regression of each calibration curve (using the least squares method). For each assay, the calibration curve was weighted by a factor of $1/x$. Representative calibration curves are shown in Figure 6.6. The linearity of each assay was found to be excellent ($r^2 > 0.995$).

The limit of detection (LOD) and limit of quantification (LOQ) for each assay were calculated as (16):

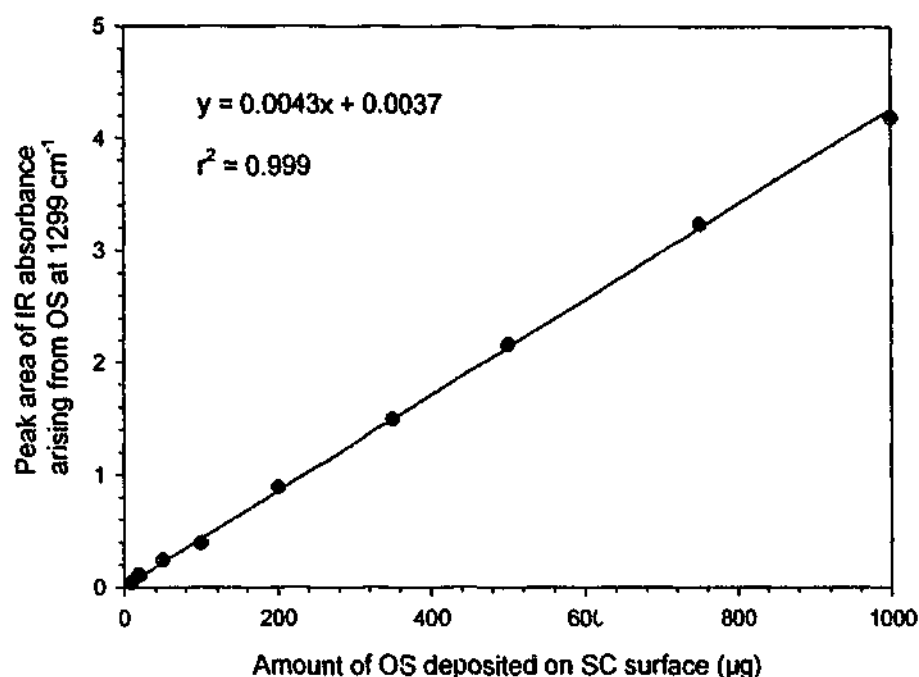
$$\text{LOD} = \frac{3\text{SD}_b}{S} \quad 6.4$$

$$\text{LOQ} = \frac{10\text{SD}_b}{S} \quad 6.5$$

where SD_b is the standard deviation of the peak areas of blank SC integrated between the same limits as the IR absorbances of either OS or PO located at 1299 or 1276 cm^{-1} and S is the slope of the calibration curve. The value 3 in Equation 6.4 is a factor for a 99.9% level of confidence, whilst the factor 10 in Equation 6.5 yields a precision of 10% relative standard deviation (RSD) at the lower limit of quantification (16). Using these equations, the LOD and LOQ for OS were calculated as 2.11 and 7.03 μg , respectively. For PO, $\text{LOD} = 1.07 \text{ }\mu\text{g}$ and $\text{LOQ} = 3.58 \text{ }\mu\text{g}$. The ability of each assay to detect and quantify relatively low amounts of OS and PO within the SC is further exemplified in Figure 6.7 which illustrates that ATR-FTIR spectra of blank SC produced minimal background interference in comparison to various signal intensities of OS and PO at 1299 and 1276 cm^{-1} , respectively.

Intra-day precision and accuracy were determined by applying a 25 μl aliquot of a standard solution (0.4, 4 or 40 mg/ml of OS or PO) to the SC surface of a 1 x 5 cm full thickness skin sample (obtained from a single donor) ($n=5$) such that 10, 100 or 1000 μg of OS or PO was deposited on the SC surface. Inter-day precision was determined by analysing skin samples (obtained from a single donor) ($n=5$) that were treated in the same manner (i.e. 10, 100 or 1000 μg of OS or PO was deposited on the SC surface) on three different days of analysis.

A. Calibration curve for OS quantification



B. Calibration curve for PO quantification

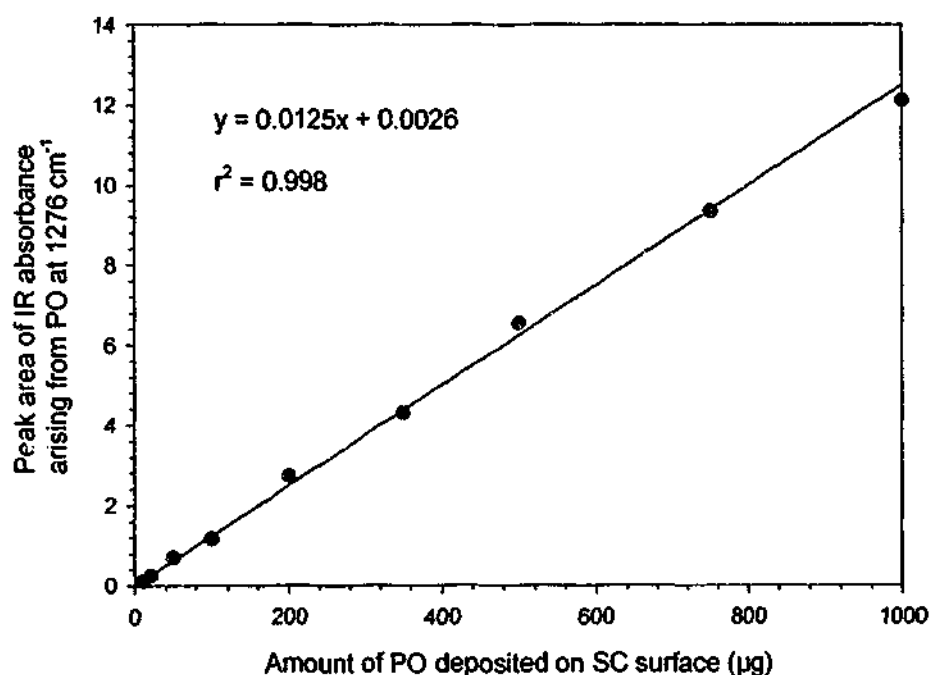
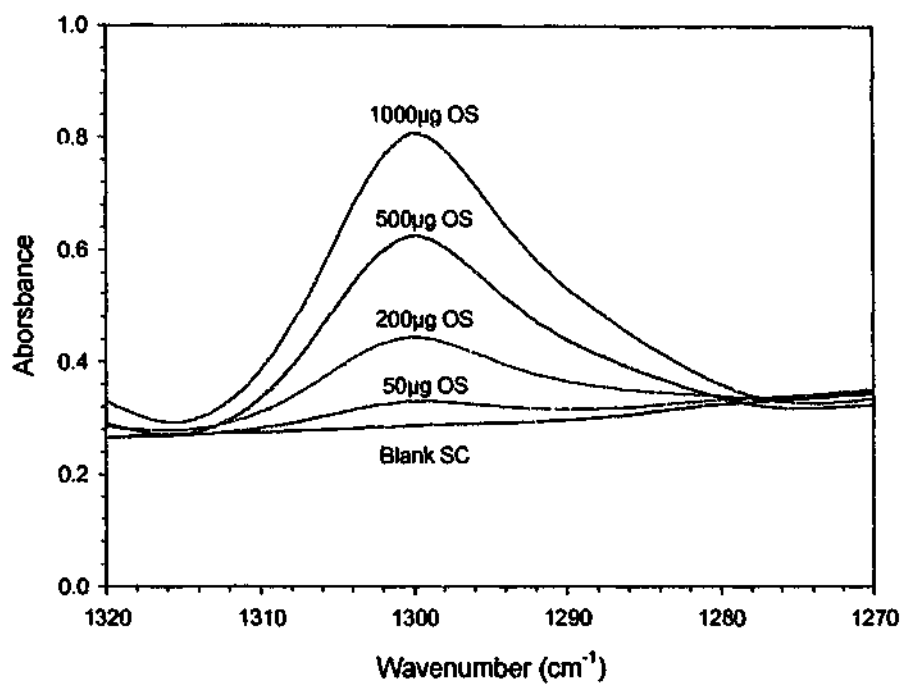


Figure 6.6. Representative calibration curves for the quantification of OS (A) and PO (B) deposited on the surface human abdominal SC (from excised full thickness skin) by ATR-FTIR. The y-axis represents the peak area of the IR absorbance arising from OS or PO at 1299 or 1276 cm⁻¹, respectively. The x-axis is the amount of OS or PO deposited at the SC surface following application of standard solutions at various concentrations.

A. Blank SC versus different amounts of OS



B. Blank SC versus different amounts of PO

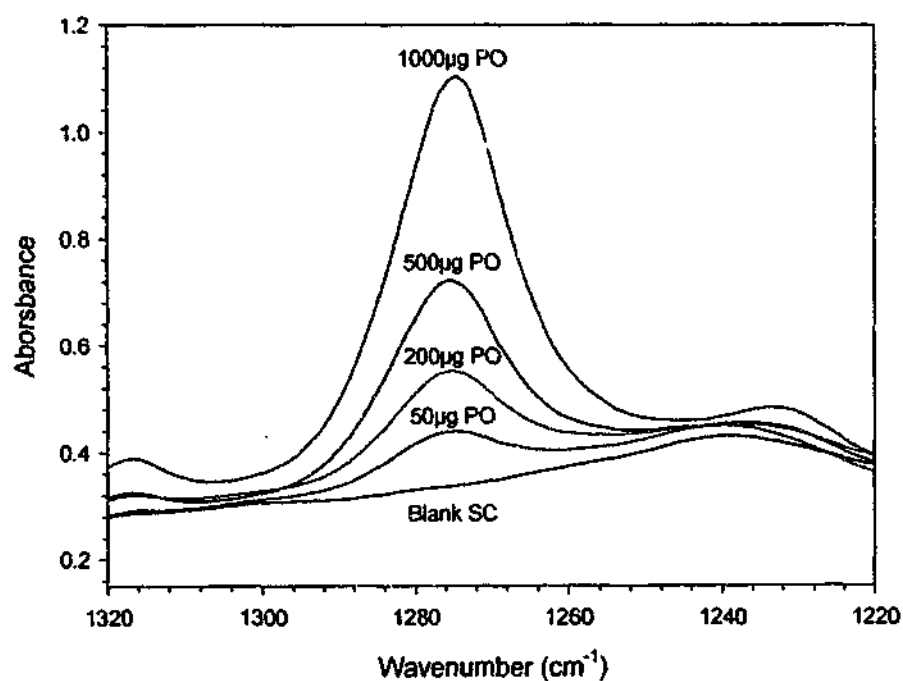


Figure 6.7. ATR-FTIR spectra of blank human abdominal SC from excised full thickness skin and different amounts of OS (A) and PO (B) deposited on the SC surface. Spectra are shown within the wavelength ranges of interest (from 1270 to 1320 cm⁻¹ for OS and from 1220 to 1320 cm⁻¹ for PO).

Each skin sample was prepared and analysed as previously described in this section. Calibration curves, which were produced as previously described, were constructed on each day of analysis using standard solutions that were freshly prepared.

Intra-day reproducibility of each assay was highly satisfactory as precision (%CV) was 2.26, 7.32 and 5.55% at 10, 100 and 1000 µg OS, respectively, and 3.17, 5.67 and 7.61% at 10, 100 and 1000 µg PO, respectively. The accuracy of each assay (expressed as the percentage of the mean observed amount of OS or PO deposited at the SC surface divided by the expected amount of OS or PO deposited at the SC surface) was also satisfactory. Accuracy varied from 102.32 to 107.38% for OS and from 90.24 to 95.79% for PO. Each assay also exhibited excellent inter-day reproducibility as inter-day precision was 8.38, 5.65 and 1.81% at 10, 100 and 1000 µg OS, respectively, and 2.65, 4.39 and 0.17% at 10, 100 and 1000 µg PO, respectively.

In order to determine whether the quantification of OS and PO was reproducible among different donors, inter-subject precision was also determined. As previously described, 10, 100 or 1000 µg of OS or PO was deposited at the SC surface of 1 x 5 cm full thickness skin samples (obtained from three different donors, n = 4 for each donor). Each skin sample was prepared and analysed as previously described in this section. Separate calibration curves were constructed for the quantification of OS or PO deposited at the SC surface of skin obtained from each donor. The quantification of OS or PO within SC obtained from the different donors was highly reproducible as precision (calculated from the mean amount of OS or PO deposited at the SC surface of skin excised from the three different donors and the standard deviation thereof) was 12.29, 7.63 and 3.34% at 10, 100 and 1000 µg OS, respectively, and 9.14, 5.79 and 2.67% at 10, 100 and 1000 µg PO, respectively.

6.3.3. Determination of octisalate distribution across human stratum corneum *in vivo*

6.3.3.1. Participants

Five healthy volunteers (three females, two males) participated in the study, which was approved by *The Standing Committee on Ethics in Research Involving Humans*, Monash University, Victoria, Australia. The participants were aged between 20 and 25

years and had no history of dermatological disease, had not applied any topical medicaments to the skin site under investigation within one month prior to commencement of the study and had not experienced any adverse reactions (including allergic reactions) to sunscreen products or salicylates. Each participant had read a written explanatory statement which outlined the inclusion and exclusion criteria, the experimental procedure and the potential risks involved with the study. The participants, who gave their written consent to participate in their study, were informed that they could withdraw from the study at any time.

One week prior to the commencement of the study, all participants were given the opportunity to have:

- i. A trial tape strip performed on an area of skin in order to verify that they were not allergic to any components of the tape.
- ii. The formulations of interest (95%v/v ethanol alone and 5%w/v OS in 95%v/v ethanol) applied to an area of skin (at a dose of $5 \mu\text{l}/\text{cm}^2$) in order to assess the potential of any adverse reaction(s) occurring during the course of the study.

All of the participants showered using a low-irritant, non-fragranced body wash (QV™ Wash, Ego Pharmaceuticals, Australia) and refrained from applying any medicated or cosmetic topical formulations to the skin site under investigation during the week prior to commencement of the study and whilst the study was being conducted. This was done in order to ensure that the area of skin under investigation was treated in the same manner and to reduce inter-subject variability.

6.3.3.2. Study design

The skin site under investigation was swabbed for approximately 20 sec with a Kimwipes™ saturated with 95%v/v ethanol in order to remove sebaceous lipids from the skin surface. A semi-occlusive polyurethane 10 x 12 cm dressing (Tegaderm™, 3M, St. Paul, MN, USA) was then affixed to the area of interest on the ventral forearm. A 6 x 2 cm area had been cut from the center of the dressing in order to confine the treatment area to 12 cm^2 . The participant extended their left or right forearm over a workbench, such

that the skin site of interest was flat and facing upwards, whilst a 60 μl (i.e. 5 $\mu\text{l}/\text{cm}^2$) aliquot of solution containing 5%w/v OS in 95%v/v ethanol was applied to the exposed area of skin. The participant kept his/her forearm flat and extended over the workbench for a further 60 sec to ensure that most of the ethanol evaporated from the skin surface before he/she resumed any activity.

The solution was left in contact with the skin for a period of 0.08 h (5 min), 0.5, 2, 6, or 16 h. During this time, the participants were allowed to resume their usual daily activities, though they were advised not to participate in any strenuous activity that would cause an elevation in body temperature or excessive sweating.

The solutions were applied to the skin at various times throughout the day (from 9:00 am to 5:00 pm). In order to minimise intra-subject variability, the solutions were applied to randomly-assigned areas of the ventral forearm (17). Solutions were applied to either the right or left forearm on alternate days. In order to reduce the potential for skin irritation and to ensure that all skin sites were treated in the same manner, a designated area of skin was only used once throughout the study.

During all exposure times, the treatment site was left unoccluded. The participants were required to wear T-shirts or rolled-up sleeves during the treatment period in order to eliminate inter-subject variations in loss of OS from the SC surface by rubbing off onto clothing. During the 16 h exposure time, the solution was applied at 5:00 pm in the evening and analysis was performed at 9:00 am the next morning. Therefore, before going to sleep that night each participant affixed a non-occlusive gauze dressing over the treatment area in order to avoid excessive removal of OS from the skin surface by rubbing off onto bedding or clothing. The participants were able to shower or bathe according to their normal routine but were required to keep the entire arm of interest dry by protecting it with a plastic cover or by keeping it away from any body wash or water.

At the end of the treatment period, excess formulation was removed from the SC surface by swabbing the treated area of skin with cotton buds (Johnson and Johnson, Australia) according to the method described in Section 5.3.4.1. For the 16 h exposure time, the gauze dressing was removed from the skin surface immediately prior to the surface wipe. An ATR-FTIR scan of the treated site was then performed (Section 6.3.3.4.2). Following this initial ATR-FTIR scan, the treated area of skin was sequentially tape-stripped in order to progressively remove the SC.

Sections of 2.4 x 6 cm pieces of polyester adhesive tape (3M, Product No. 8440) were applied to the surface of the treated skin site. Each piece of tape was folded onto itself at each end to produce an ~1 cm overhang. This was done to ensure easy handling of the tape such that even pressure was applied to the tape upon its application and removal from the SC and to avoid contamination of the tape. The pieces of tape were equilibrated under ambient laboratory conditions for at least 2 h prior to use. After the tape was applied to the SC surface, solid stainless steel slabs with flush surfaces (weighing 1200 g) were placed over the tape for 5 sec to ensure that uniform pressure was applied to the tape. The tape was then removed from the SC surface. This procedure was repeated 20 times in order to remove most of the SC. An ATR-FTIR spectrum of the treated site was recorded after each tape strip (Section 6.3.3.4.2).

The participant was required to keep his or her forearm extended over a workbench (such that the treated site was flat and facing upwards) whilst the surface wipe and tape stripping were performed. This was done to ensure that even pressure was applied to the skin during these procedures.

The mass of SC removed (M_{sc}) was determined by weighing each tape before (i.e. after the equilibration period) and after the tape stripping procedure on a Sartorius MC5 microbalance. The length of SC removed was determined according to Equation 6.2.

OS was extracted from the surface wipe and from the tape strips according to the methods described in Sections 5.3.4.2 and 5.3.5.1. The amount of OS extracted from the surface wipe performed after the 16 h treatment period was a combination of the amount of OS extracted from the surface wipe and the gauze that was used to cover the treated skin site whilst the participant was sleeping (i.e. the gauze and the cotton buds were added together during the surface wipe extraction). The extracts were analysed by a validated HPLC/UV assay (Section 6.3.3.4.1) in order to determine the absolute amounts of OS removed by the surface wipe and tape strips.

6.3.3.3. Skin irritation

Skin irritation was observed on two separate occasions in two different participants, whereby the treated skin site became erythematous within several hours after the tape stripping procedure. The area was treated with a topical 1%w/w hydrocortisone cream (Dermaid™, Ego Pharmaceuticals Pty. Ltd., Australia) and wound dressing (Solugel™,

Johnson and Johnson Medical Pty. Ltd., Australia). The erythema subsided within several days of using these topical preparations.

6.3.3.4. Analytical methods

6.3.3.4.1. Chromatographic analysis of octisalate

The absolute amounts of OS removed by the surface wipe and tape strips were determined using the validated RP-HPLC/UV assay described in Section 5.3.6.1.

6.3.3.4.2. Spectroscopic analysis of octisalate

6.3.3.4.2.1. Acquisition of ATR-FTIR spectra

Spectral measurements were made using an out of compartment ATR Max II variable angle horizontal ATR accessory (Pike Technologies, Inc., Madison, WI, USA) which was fitted into the sample compartment of the Excalibur™ FTS 3500GX spectrometer. The zinc selenide crystal that was supported by the ATR accessory was 5 cm long, 1 cm wide and 4 cm thick. The entrance and exit faces of the crystal were each cut at a 45° angle. As mentioned in Section 6.3.2.3.2.1, the apparent depth by which the evanescent IR beam penetrated the SC may have been in the order of ~1.5 to ~3.5 μm and therefore the information gathered from an ATR-FTIR spectrum of this nature pertains only the superficial layers of the SC in contact with the crystal. In order to obtain an ATR-FTIR spectrum of the skin, the participant rested his/her forearm over the ATR accessory such that the treated area was directly in contact with the zinc selenide crystal (Figure 6.8). In order to ensure intimate contact between the skin and the crystal, the participant pressed down on their forearm with their “free” hand (Figure 6.8). Each ATR-FTIR spectrum represented an average of 32 scans, obtained at a resolution of 8 cm^{-1} , over a wavelength range from 750 to 4000 cm^{-1} . A period of 60 sec was required to acquire each spectrum. All measurements were conducted under ambient conditions (23 \pm 1°C; 30 to 40% relative humidity).

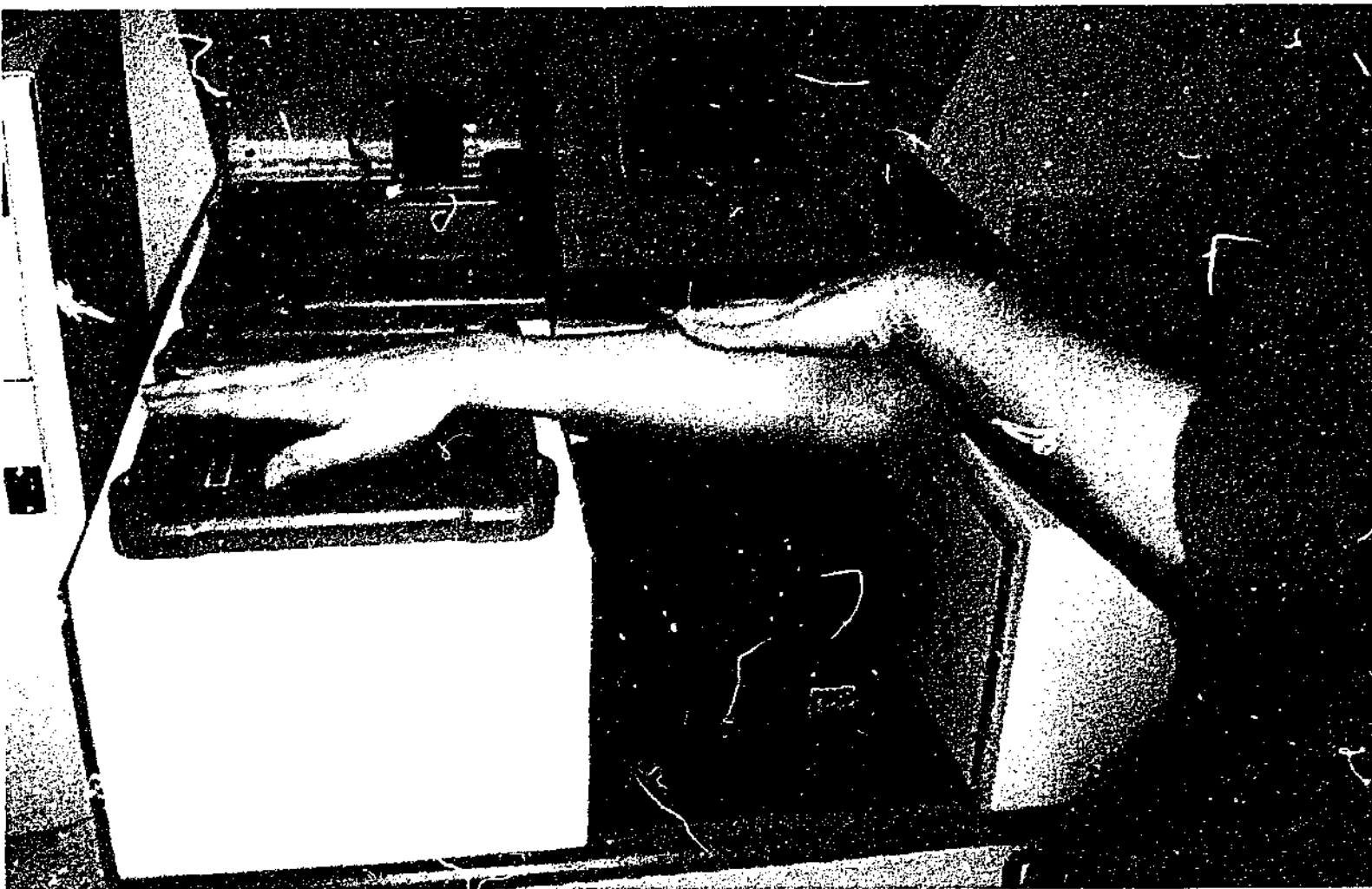


Figure 6.8. A photograph illustrating how an ATR-FTIR spectrum of human SC was acquired from the ventral forearm *in vivo*.

6.3.3.4.2.2. Identification of infrared absorbances arising from octisalate

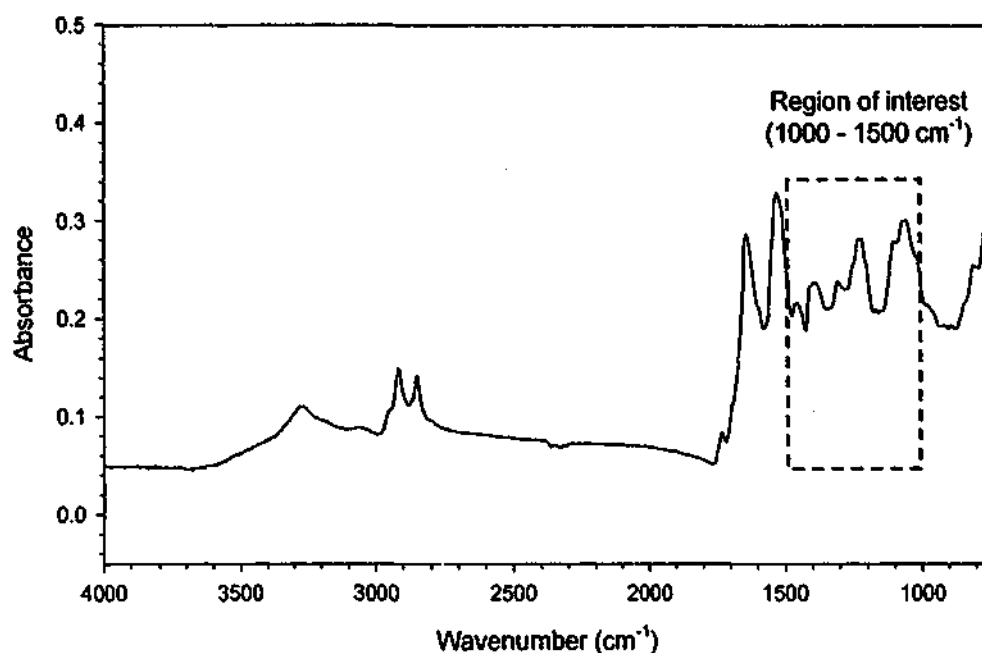
As mentioned in Section 6.3.2.3.2.2, the IR absorbance used to quantify concentrations of OS within the SC *in vitro* was located at 1299cm^{-1} . This IR absorbance was chosen as it corresponded to an area within the ATR-FTIR spectrum of human SC that was free of high intensity IR absorbances arising from the SC itself (i.e. within a wavelength range from 1250 to 1325 cm^{-1}). However, as illustrated in Figure 6.9.A, ATR-FTIR spectra of human forearm SC *in vivo* is somewhat different from that of human SC from excised abdominal full thickness skin. In particular, the IR absorbances arising from human forearm SC *in vivo* are ~10-fold less intense than those generated from SC of excised human abdominal. Furthermore, and of particular relevance to the quantification of OS within the SC, the “fingerprint” region of the ATR-FTIR spectrum (between 1000 and 1500 cm^{-1}) of human forearm SC *in vivo* is characteristically different from that of human SC from excised abdominal skin such that “baseline” regions exist between ~ 1140 to $\sim 1185\text{ cm}^{-1}$ and ~ 1325 to $\sim 1355\text{ cm}^{-1}$ (Figure 6.9.B).

As mentioned in Section 6.3.2.3.2.2, IR absorbances that arise from OS that could potentially be used to determine its distribution across human SC are those located at 1299 , 1250 , 1212 , 1158 or 1098 cm^{-1} . However, the IR absorbance located at 1158 cm^{-1} is the only absorbance that coincides with a “baseline” region within the ATR-FTIR spectrum of human forearm SC *in vivo*. Consequently, this IR absorbance was used to determine the relative amounts of OS present within SC removed by the tape strips *in vivo*.

6.3.3.4.2.3. Assay validation

In order to confirm the assumption that the intensity or area under the curve of an IR absorbance is directly proportional to the amount of absorbing species, calibration curves were constructed whereby OS was applied to the ventral forearm of each participant. Assay validation commenced 3 weeks after the completion of the studies described in Section 6.3.3.2. This washout period was required to ensure that SC barrier function had almost returned to its previous state and that OS applied during the studies did not interfere with assay validation.

A. ATR-FTIR spectrum between 750 and 4000 cm^{-1}



B. ATR-FTIR spectrum between 1000 and 1500 cm^{-1}

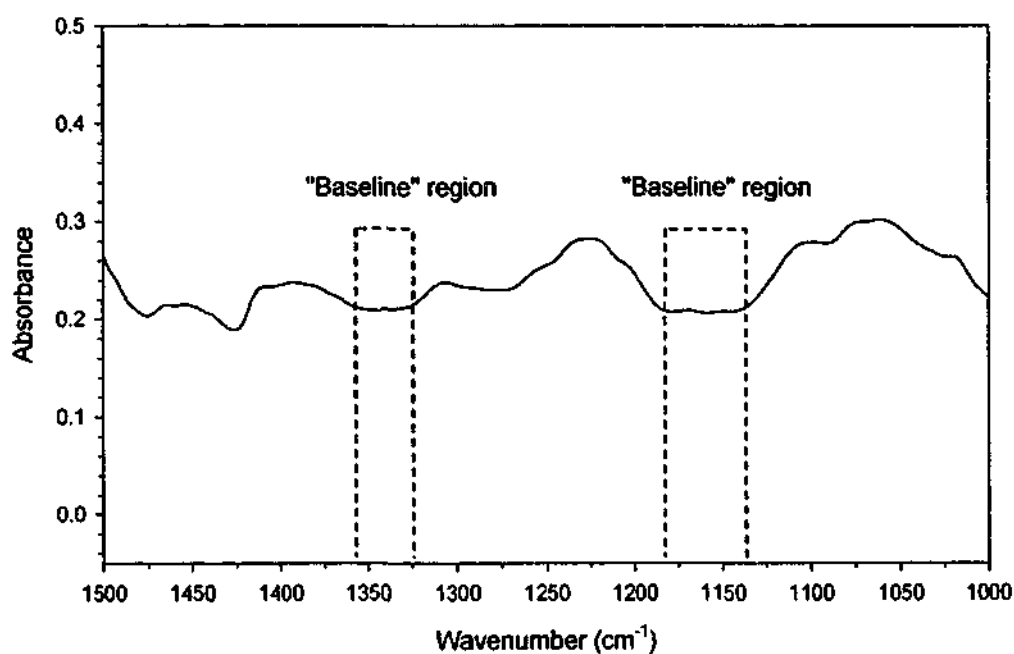


Figure 6.9. Representative ATR-FTIR spectrum of blank ventral forearm human SC *in vivo* within a wavelength range of 750 and 4000 cm^{-1} (A) and the wavelength range of interest (between 1000 and 1500 cm^{-1}) (B).

Standard solutions at concentrations within the range of 0.4 to 20 mg/ml were prepared by diluting a stock solution of 40 mg/ml of OS in 95%v/v ethanol with an appropriate volume of 95%v/v ethanol. In order to mimic the experimental conditions described in Section 6.3.3.2, the area of skin under investigation was swabbed for approximately 20 sec with a Kimwipes™ saturated with 95%v/v ethanol. A semi-occlusive polyurethane 10 x 12 cm Tegaderm™ dressing was then affixed to a randomly-assigned area of skin on the ventral forearm. A 6 x 2 cm area had been cut out from the center of the dressing in order to confine the treatment area to 12 cm². The participant then extended his/her forearm over a workbench such that the skin site of interest was flat and facing upwards. A 50 µl aliquot of standard solution was applied to the exposed area of skin such that the amount of OS deposited at the SC surface varied from 20 to 1000 µg. In order to acquire an ATR-FTIR spectrum immediately after a standard solution was applied to the skin, ethanol deposited onto the SC surface was evaporated under a gentle stream of nitrogen for 30 sec before an ATR-FTIR scan was performed.

In order to acquire ATR-FTIR spectra of blank SC, a 50 µl aliquot of 95%v/v ethanol was applied to the SC surface of a randomly-assigned area of the left and right ventral forearms of each participant (n=5) (n=10 in total). The ethanol was evaporated under a gentle stream of nitrogen for 30 sec before an ATR-FTIR scan was performed.

To acquire an ATR-FTIR spectrum of the skin, the participant rested his/her forearm over the ATR accessory such that the treated area was directly in contact with the zinc selenide crystal (Figure 6.8). In order to ensure intimate contact between the skin and the crystal, the participant pressed down on their forearm with their “free” hand. An ATR scan was initiated using a Merlin computer software package. Each spectrum represented an average of 32 scans, obtained at a resolution of 8 cm⁻¹, over a wavelength range from 750 to 4000 cm⁻¹. A period of 60 sec was required to acquire each spectrum. All measurements were conducted under ambient conditions (23 ± 1°C; 30 to 40% relative humidity).

The IR absorbance from OS centered at ~1156 cm⁻¹ was integrated between the limits of ~1146 and ~1169 cm⁻¹, in order to obtain the area under the IR absorbance curve. As described in Section 6.3.2.3.2.3, peak frequency maxima were determined using a center of gravity algorithm. As mentioned in Section 6.3.2.3.2.3, it is often necessary to normalise the IR absorbance of interest to relatively constant IR absorbance(s) that arise from the skin, such as the amide I and amide II absorbances, in

order to eliminate intra- and inter-subject variability produced by different degrees of contact between the skin and the IRE. Although such a normalisation procedure was not required for the quantification of OS within SC *in vitro*, it was recognised that a reproducible level of contact between the skin and the IRE could not be guaranteed *in vivo*. As the IR absorbance arising from OS at $\sim 1675\text{ cm}^{-1}$ could potentially interfere with the amide I absorbance centered at $\sim 1642\text{ cm}^{-1}$ (Section 6.3.2.3.2.2), the area under the OS absorbance peak centered at $\sim 1156\text{ cm}^{-1}$ was divided by the area under the corresponding amide II absorbance peak centered at $\sim 1526\text{ cm}^{-1}$.

The data points in each calibration curve represented an average of two spectral measurements; one pertaining to OS deposited on an area of the left ventral forearm and the other pertaining to OS deposited on an area of the right ventral forearm.

A linear relationship between the OS absorbance peak area located at $\sim 1156\text{ cm}^{-1}$ (normalised to the amide II absorbance peak area centered at $\sim 1526\text{ cm}^{-1}$) and the amount of OS deposited at the SC surface was determined by the correlation coefficient generated by linear regression of each calibration curve (using the least squares method). Each calibration curve was weighted by a factor of $1/x$. A representative calibration curve for the quantification of OS within SC *in vivo* is shown in Figure 6.10. The linearity of the assay was excellent ($r^2 > 0.995$ for each calibration curve).

As illustrated in Figure 6.11, ATR-FTIR spectra of blank SC *in vivo* produced minimal background interference compared with various signal intensities of OS at 1156 cm^{-1} . The LOD and LOQ for the assay, which were calculated using Equations 6.4 and 6.5 (Section 6.3.2.3.2.3) were relatively low (LOD = $5.73\text{ }\mu\text{g}$ and LOQ = $19.11\text{ }\mu\text{g}$).

Intra-day precision and accuracy were determined by applying three $50\text{ }\mu\text{l}$ aliquots of a standard solution (0.4, 4 or 40 mg/ml of OS or PO) to different areas of the SC surface of the left and right ventral forearm of one participant (i.e. $n = 6$ in total). The treatment site was confined to 12 cm^2 using a Tegaderm™ dressing as previously described in this section. The amount of OS deposited at the SC surface was 20, 100 or $1000\text{ }\mu\text{g}$ following the application of a 0.4, 4 or 40 mg/ml standard solution, respectively. Inter-day precision was determined using the same procedure, but analysis was performed on three different days. Calibration curves, which were constructed as previously described, were generated on each day of analysis using standard solutions that were freshly prepared.

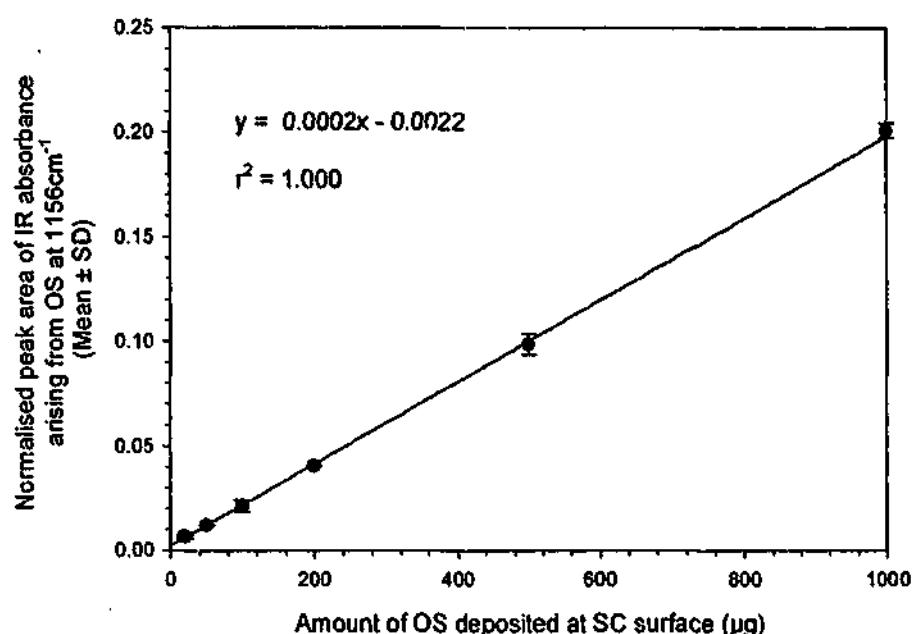


Figure 6.10. A representative calibration curve for the quantification of OS deposited on the surface of human ventral forearm SC *in vivo* by ATR-FTIR. The y-axis represents the peak area of the IR absorbance arising from OS centered at ~1156 cm⁻¹ normalised to the peak area of the amide II IR absorbance (arising from SC keratin) centered at ~1526 cm⁻¹ (n=2 measurements, each pertaining to the right or left forearm). The x-axis represents the amount of OS deposited at the SC surface following the application of standard solutions at various concentrations.

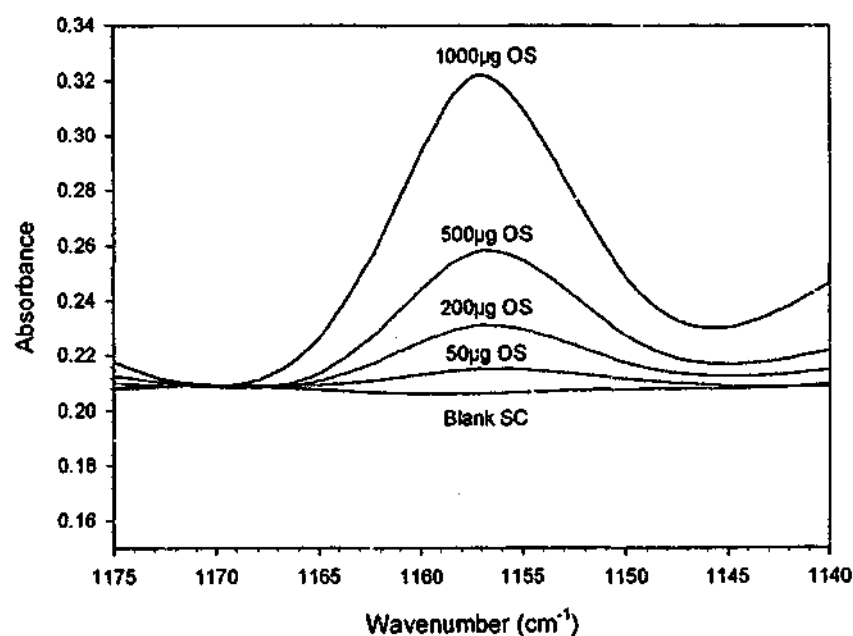


Figure 6.11. ATR-FTIR spectra of blank human ventral forearm SC *in vivo* and different amounts of OS deposited on the SC surface. Spectra are confined to the wavelength range of interest (from 1140 to 1175 cm⁻¹).

Intra-day precision (%CV) and accuracy were satisfactory as precision was 6.68, 5.82 and 4.99% at 20, 100 and 1000 μg OS, respectively, and accuracy ranged from 91.06 to 91.45%. Inter-day precision was also satisfactory as the coefficient of variation about the mean value was 3.54, 2.99 and 9.71% at 20, 100 and 1000 μg OS, respectively.

In order to determine whether the quantification of OS within human SC was reproducible among different subjects *in vivo*, inter-subject precision was determined. All of the participants ($n=5$) involved in the tape-stripping study described in Section 6.3.3.2 also took part in this investigation. As previously described, three 50 μl aliquots of a standard solution (0.4, 4 or 40 mg/ml of OS or PO) were topically applied to different areas (area = 12 cm^2) of the left and right ventral forearm of each participant (i.e. $n = 6$ in total) such that 20, 100 or 1000 μg of OS was deposited at the SC surface. The treatment sites were prepared and analysed as previously described and separate calibration curves were constructed for the quantification of OS within the SC of each participant. The quantification of OS within forearm SC *in vivo* was reproducible among the different participants as precision (calculated from the mean amount of OS detected at the SC surface of the participants' forearms and the standard deviation thereof) was 8.01, 8.77 and 9.02% at 20, 100 and 1000 μg OS, respectively.

6.3.4. Mathematical analysis

6.3.4.1. Normalisation of stratum corneum depth and octisalate and padimate O concentrations within the stratum corneum

As described in Section 5.3.7.1, the amount of OS or PO found within the SC was normalised to the SC weight removed by each tape strip in order to eliminate inter- and intra- subject variations in total SC thickness (18) and differences in the amount of SC removed by each tape strip (19). For similar reasons, the length of SC removed for tape strip, i , was divided by that removed by the total number of tape strips in order to derive the normalised SC depth (x/L) (Section 5.3.7.1).

Only the information gathered (i.e. concentrations of OS or PO found within the SC and normalised SC depth) from tape strips 2 to 26 were used to construct the distribution profiles presented in Section 6.4 as the amount of OS or PO removed from the first tape strip was considered to represent unabsorbed material residing at the SC surface (17).

6.3.4.2. Areas under the octisalate and padimate O distribution profiles

Areas under the OS and PO distribution profiles (areas under the curves (AUCs)) were calculated using the trapezoidal method, as described in Section 5.3.7.2. As previously mentioned, AUCs were calculated for the entire SC ($AUC_{x/L2 \rightarrow 20}$), the upper region of the SC ($AUC_{x/L2 \rightarrow 10}$) and the lower region of the SC ($AUC_{x/L11 \rightarrow 20}$).

6.3.4.3. Kinetic modeling of clearance from the stratum corneum surface

The amount of OS or PO residing at the SC surface at a given exposure time represented the sum of the amount of OS or PO extracted from the first tape strip and the amount extracted from the surface wipe.

The decline in the amount of OS or PO residing at the SC surface (A_v) as a function of time (t) was fitted to the following first order elimination rate process in order to derive the elimination rate constant (k):

$$A_v = Ae^{-kt} \quad 6.6$$

where A is a pre-exponential constant.

6.3.5. Statistical analysis

Statistical significance was determined using one way analysis of variance (ANOVA). Post-hoc all pairwise multiple comparison of the means within different groups was performed using the Student-Newman-Keuls (SNK) test. A probability of $p < 0.05$ was considered statistically significant. All results are presented as the mean \pm SEM, unless otherwise stated.

6.4. RESULTS AND DISCUSSION

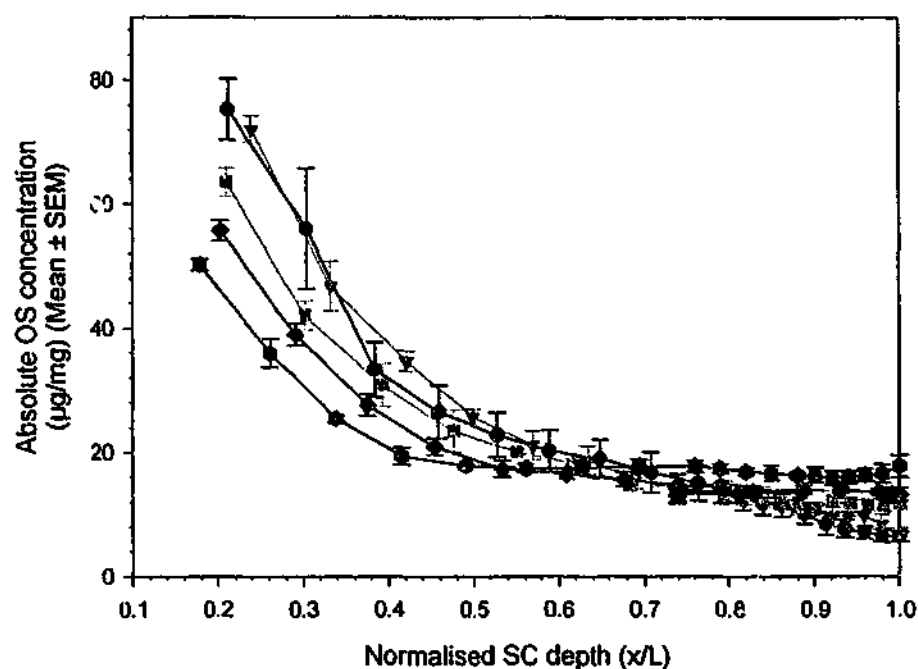
6.4.1. Distribution of octisalate and padimate O across human stratum corneum *in vitro*

The distribution profiles of OS and PO across human SC *in vitro* are shown in Figures 6.12 and 6.13, respectively. At all exposure times, the concentration of either OS or PO declined exponentially as a function of normalised SC depth. At short exposure times (0.08 and 0.5 h), the concentration gradients that had formed across the SC were such that the concentration of OS or PO at a given position within the SC (C_x) gradually declined with increasing SC depth (i.e. as $x \rightarrow L$, $C_x \rightarrow \sim 0$). This type of non-steady-state distribution, where the permeant appears to diffuse into a receptor “sink”, is similar to that observed when fentanyl was applied to the SC surface at exposure times of up to 6 h (Section 5.4.2).

However, it is evident from Figures 6.12 and 6.13 that the concentrations of OS and PO within the deeper regions of the SC ($x/L > \sim 0.8$) gradually increased as the exposure time was extended from 0.5 h to 16 h. This type of diffusion phenomenon – where it would appear that non-steady-state distribution prevails and OS and PO accumulate within the deeper layers of the SC – is discordant with the fentanyl distribution profiles that were apparent at a 16 h exposure time, where fentanyl concentrations declined in a somewhat linear fashion with increasing SC depth (which is indicative of pseudo-steady-state diffusion) and “sink” conditions were maintained (i.e. at $x=L$, $C_x \sim 0$) (Section 5.4.2).

The discrepancy observed between the distribution of the enhancers and the distribution of fentanyl across the SC at relatively long exposure times can be attributed to the fact that these permeants possess different physicochemical properties. As fentanyl is a moderately lipophilic compound ($\log K_{OCT/W} = 2.86$, (20)) that is somewhat soluble in water (Section 2.4.1), the epidermis may impose some degree of resistance towards fentanyl permeation, though it would not be as significant as the resistance imposed by the SC itself. That is, the SC would be the main rate-limiting barrier towards fentanyl permeation and the epidermis would essentially act as a “sink” (as discussed in Section 4.4.1).

A. Distribution profiles determined by HPLC/UV



B. Distribution profiles determined by ATR-FTIR

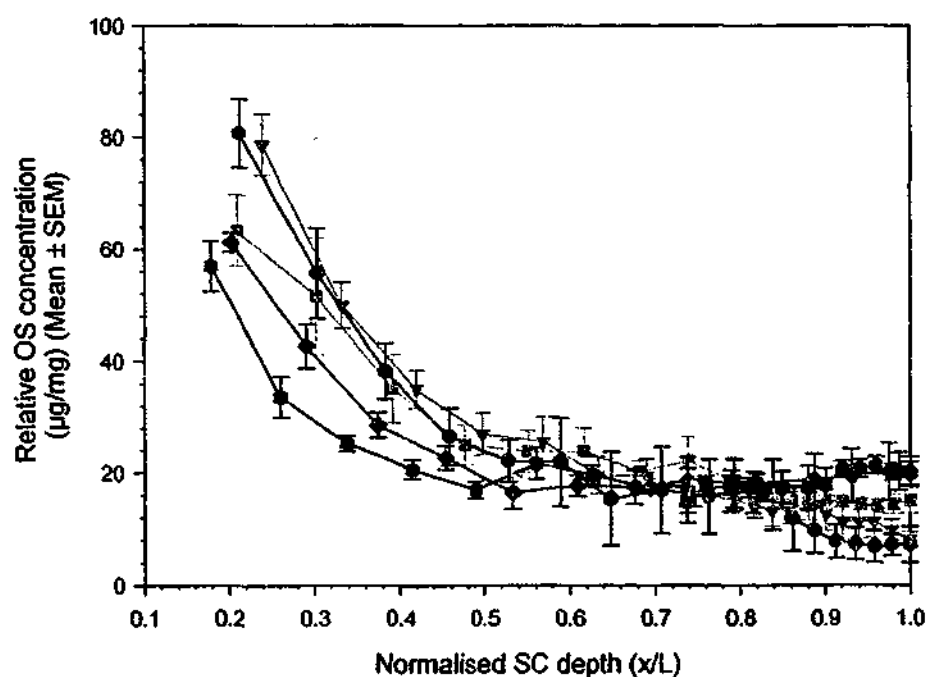
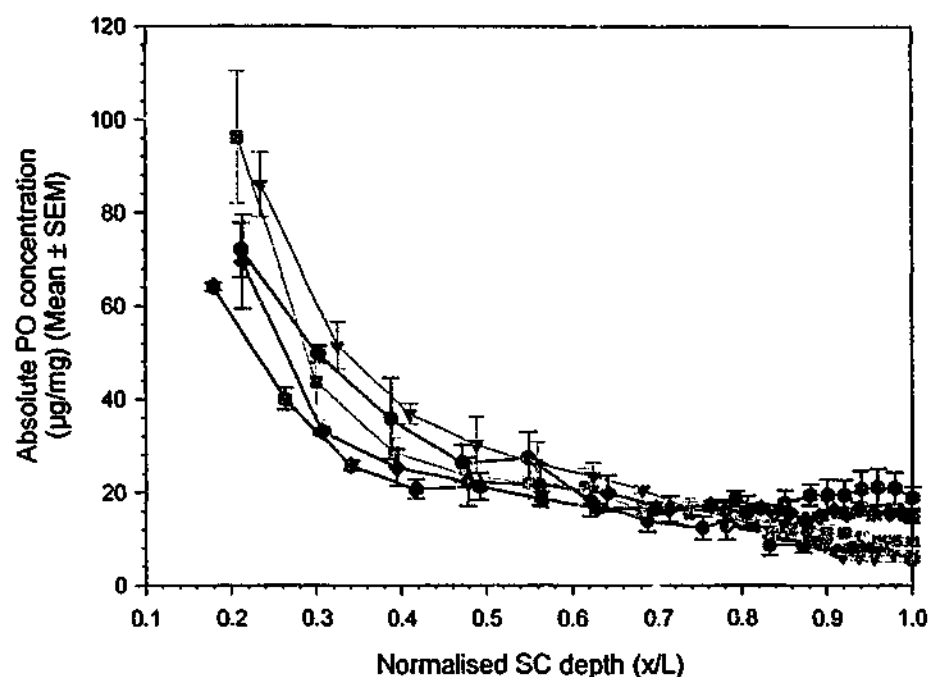


Figure 6.12. Distribution profiles of OS across human SC *in vitro* at 0.08 (●), 0.5 (▼), 2 (■), 6 (◆) or 16h (●) exposure times ($n=5$). The concentration of OS within the SC was determined as a function of normalised SC depth (x/L) by HPLC/UV (absolute concentration) (A) or by ATR-FTIR (relative concentration) (B).

A. Distribution profiles determined by HPLC/UV



B. Distribution profiles determined by ATR-FTIR

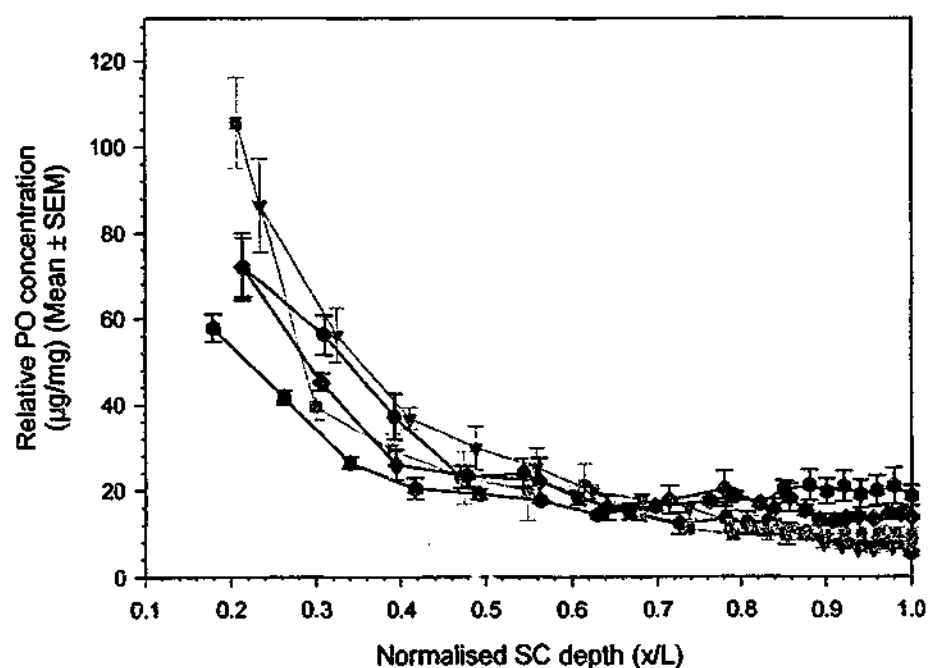


Figure 6.13. Distribution profiles of PO across human SC *in vitro* at 0.08 (●), 0.5 (▼), 2 (■), 6 (◆) or 16h (●) exposure times (n=5). The concentration of PO within the SC was determined as a function of normalised SC depth (x/L) by HPLC/UV (absolute concentration) (A) or by ATR-FTIR (relative concentration) (B).

On the other hand, OS and PO are highly lipophilic ($\log K_{OCT/W} = 5.97$ and 5.77^1 , respectively) and sparingly soluble in water (0.7 and $0.2 \mu\text{g/ml}^1$, respectively). Consequently, the epidermis and dermis would act as aqueous boundary layers during the percutaneous absorption of these compounds (21, 22). Given that the underlying aqueous skin strata are unlikely to act as a “sink” for OS and PO, it is not surprising that they appeared to accumulate within the deeper layers of the SC as the exposure time was increased up to 16 h. The relevance of this finding to the *in vivo* skin penetration of OS and PO is discussed in Section 6.4.3.

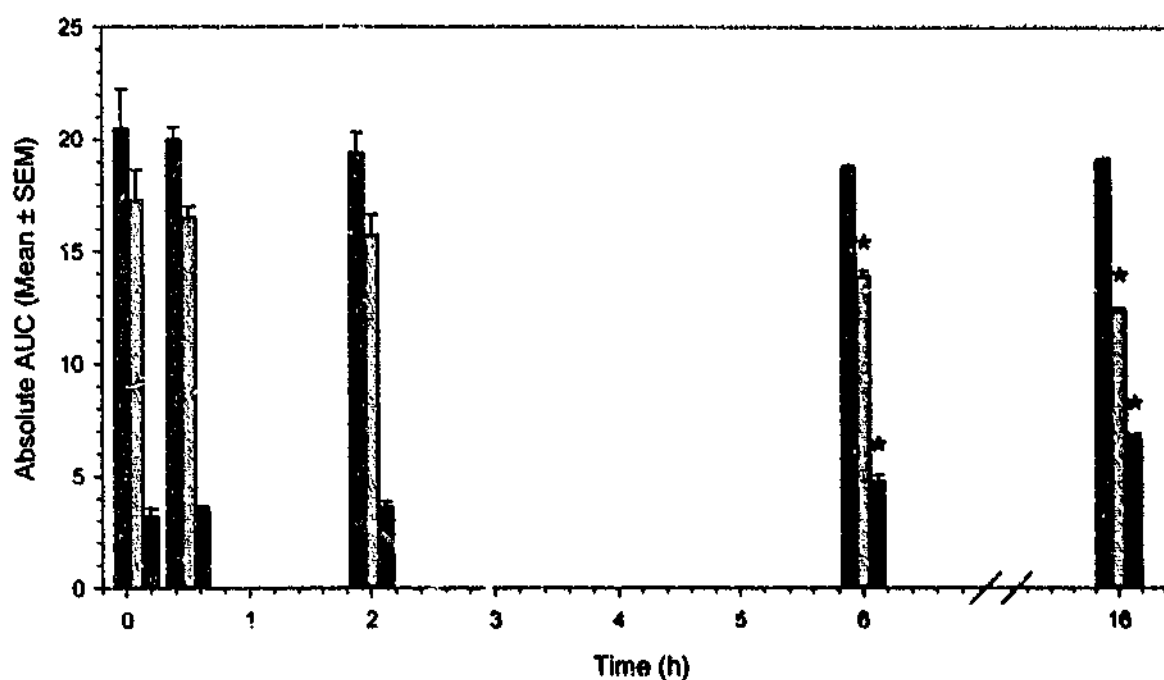
The accumulation of OS and PO within the deeper SC layers is also apparent in Figures 6.14 and 6.15, which show the AUCs for the entire SC ($\text{AUC}_{x/L2 \rightarrow 20}$), the upper region of the SC ($\text{AUC}_{x/L2 \rightarrow 10}$) and the lower region of the SC ($\text{AUC}_{x/L11 \rightarrow 20}$). It is evident that the AUCs of OS and PO for the lower layers of the SC increased as a function of increasing exposure time such that the $\text{AUC}_{x/L11 \rightarrow 20}$ calculated at 6 or 16 h was significantly higher than that determined at 0.08 h ($p < 0.05$). It is also evident from Figures 6.14 and 6.15 that the AUCs of OS and PO for the upper layers of the SC concomitantly declined as a function of increasing exposure time. Consequently, the $\text{AUC}_{x/L2 \rightarrow 10}$ of either OS or PO determined at a 6 or 16 h exposure time was significantly lower than that found at 0.08 h ($p < 0.05$).

The AUCs calculated for the entire SC remained relatively constant at all exposure times ($\text{AUC}_{x/L2 \rightarrow 20}$ s of OS and PO were in the order of ~ 21). Therefore, as it would seem that “mass balance” within the SC was preserved, it would appear that concentrations within the upper and lower layers of the SC tend to approach an “equilibrium concentration” with increasing exposure time (a detailed description of this type of diffusion problem has been provided by Crank (23)).

As mentioned in Section 5.4.3, AUCs of the fentanyl distribution profiles for the entire SC also remained relatively uniform over all exposure times ($\text{AUC}_{x/L2 \rightarrow 20}$ s were ~ 24 and ~ 23 when fentanyl was applied with OS or PO, respectively). However, unlike the distribution phenomena observed with OS and PO, this appeared to be due to the conservation of fentanyl concentrations with the upper and lower layers of the SC.

¹ Estimated using EPISuite (Version 3.11) computer software package (U.S. Environmental Protection Agency)

A. Absolute AUCs



B. Relative AUCs

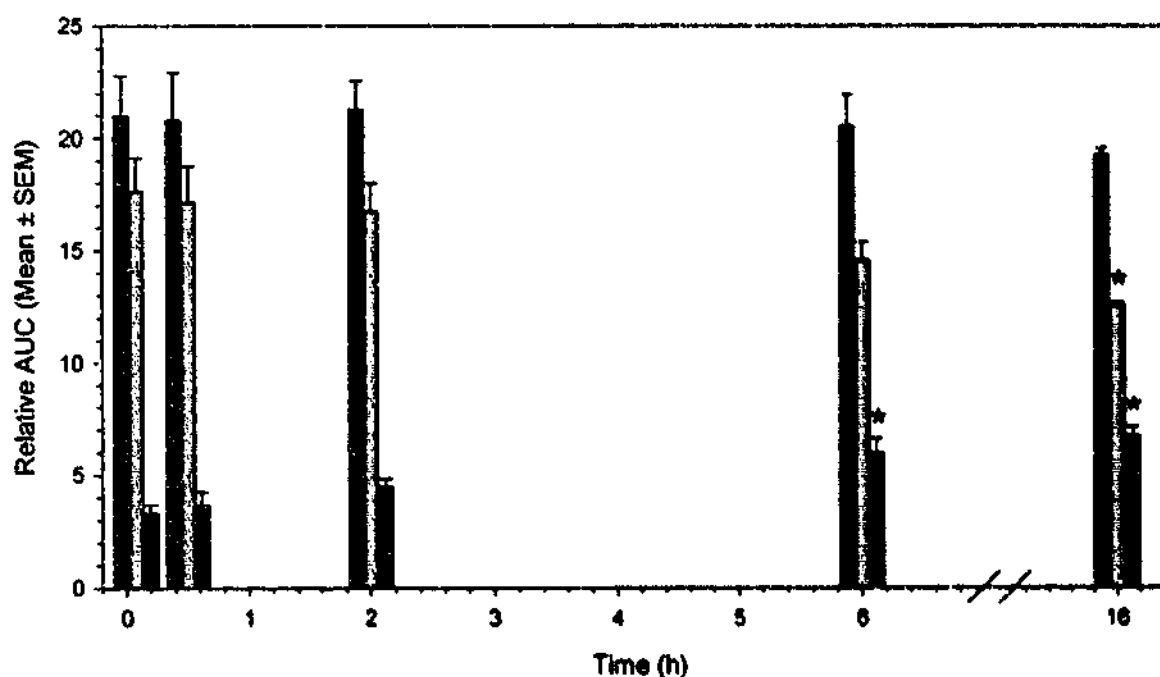
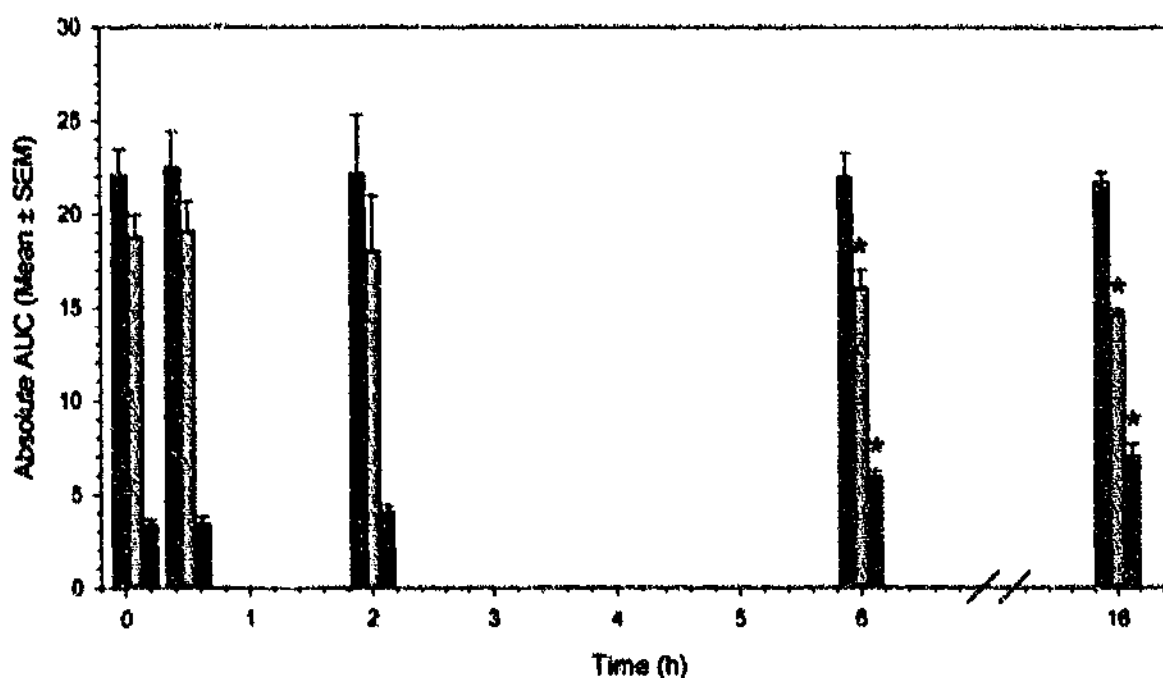


Figure 6.14. AUCs of the OS distribution profiles across human SC *in vitro* (shown in Figure 6.12). AUCs were calculated using the distribution profiles determined either by HPLC/UV (absolute AUC) (A) or by ATR-FTIR (relative AUC) (B). AUCs were determined for the *entire* SC (i.e. SC removed by tape strips 2 to 20, AUC_{0.12-20}) (■), the *upper* SC (i.e. SC removed by tape strips 2 to 10, AUC_{0.12-10}) (▨) and the *lower* SC (i.e. SC removed by tape strips 11 to 20, AUC_{0.11-20}) (□). * Denotes statistically significant difference compared with the AUC calculated at 0.08 h exposure time.

A. Absolute AUCs



B. Relative AUCs

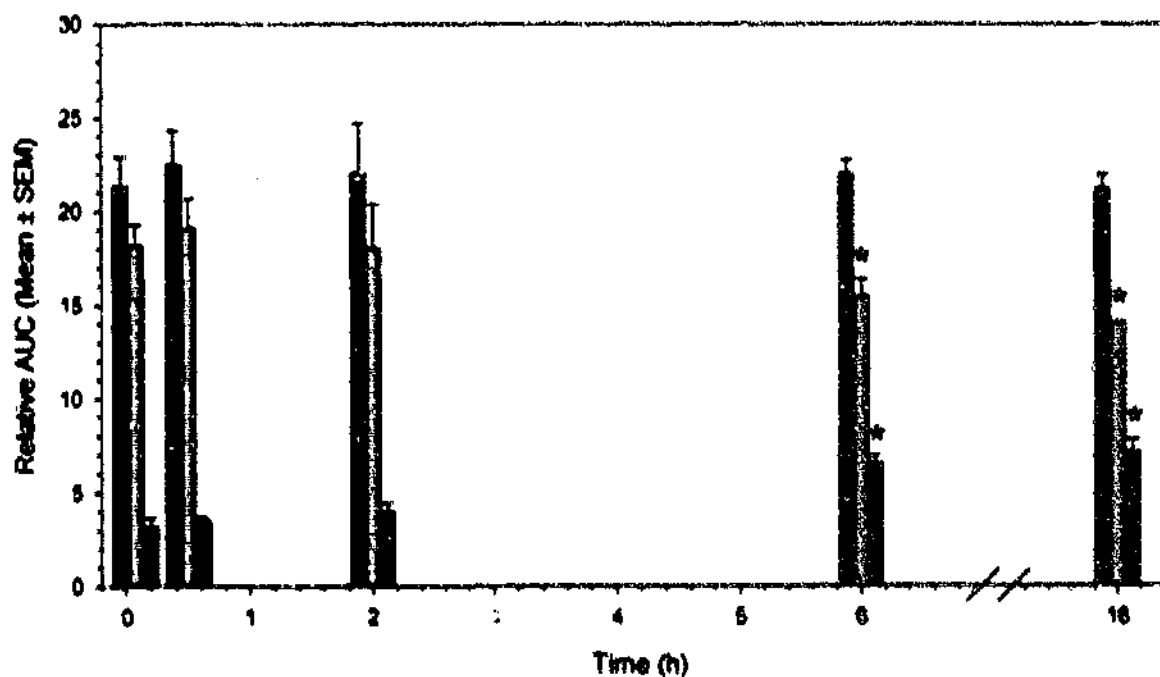


Figure 6.15. AUCs of the PO distribution profiles across human SC *in vitro* (shown in Figure 6.13). AUCs were calculated using the distribution profiles determined either by HPLC/UV (absolute AUC) (A) or by ATR-FTIR (relative AUC) (B). AUCs were determined for the *entire* SC (i.e. SC removed by tape strips 2 to 20, AUC_{0.12-20}) (■), the *upper* SC (i.e. SC removed by tape strips 2 to 10, AUC_{0.12-10}) (▨) and the *lower* SC (i.e. SC removed by tape strips 11 to 20, AUC₁₁₋₂₀) (□). * Denotes statistically significant difference compared with the AUC calculated at 0.08 h exposure time.

The differences between fentanyl distribution across the SC and the distribution of OS and PO across the SC would indicate that the distribution phenomena of OS and PO *within* the SC does not effect that of fentanyl. This is somewhat surprising given that OS and PO were found to increase fentanyl partitioning into the SC by, or partly by, increasing its solubility within the SC lipid domain (Chapter 4). However, it should also be kept in mind that the results presented in Chapter 5 indicate that OS and PO may also alter fentanyl partitioning into the SC by maintaining a diffusable source of fentanyl at the SC surface. Therefore, the observation that, in the presence of OS or PO, the $AUC_{0.12 \rightarrow 10.5}$ of fentanyl remained constant whilst the $AUC_{0.12 \rightarrow 10.5}$ of OS and PO declined may be attributed to the possibility that OS and PO maintain a diffusable source of fentanyl at the SC surface that is available for constant partitioning into the upper layers of the SC (Chapter 5).

The apparent accumulation of OS and PO within the deeper SC layers might also be expected to increase the solubility of fentanyl within the lipids present in this locality and thus augment the rate of fentanyl partitioning at the SC-epidermis interface. As this effect would presumably increase the rate of fentanyl clearance from the deeper layers of the SC, it is probable that this phenomenon would have resulted in decline in fentanyl $AUC_{0.11 \rightarrow 20.5}$ with increasing exposure time. However, this trend was not observed (Section 5.4.3).

Taking into account the discrepancies between the distribution phenomena of fentanyl and the enhancers, and the findings from previous chapters, it is possible that:

- i. As mentioned in Section 4.4.6.3, other mechanism(s) (in addition to increased fentanyl solubility within the SC lipid domain) may also be responsible for the effects of OS and PO on fentanyl partitioning
- ii. The contribution of the effects of OS and PO on fentanyl partitioning from the vehicle to the SC towards fentanyl permeation is more significant than that of their effects on fentanyl partitioning from the SC to the underlying viable tissue.

Whilst the latter possibility is consistent with the results presented in Chapters 3 and 5 and with the notion that the main rate limiting barrier towards fentanyl permeation resides within the SC (24, 25), the former prospect is supported by the results presented

in Chapter 7, which demonstrate that OS and PO may extract lipids from the superficial layers of the SC.

6.4.2. Distribution of octisalate and across human stratum corneum *in vivo*

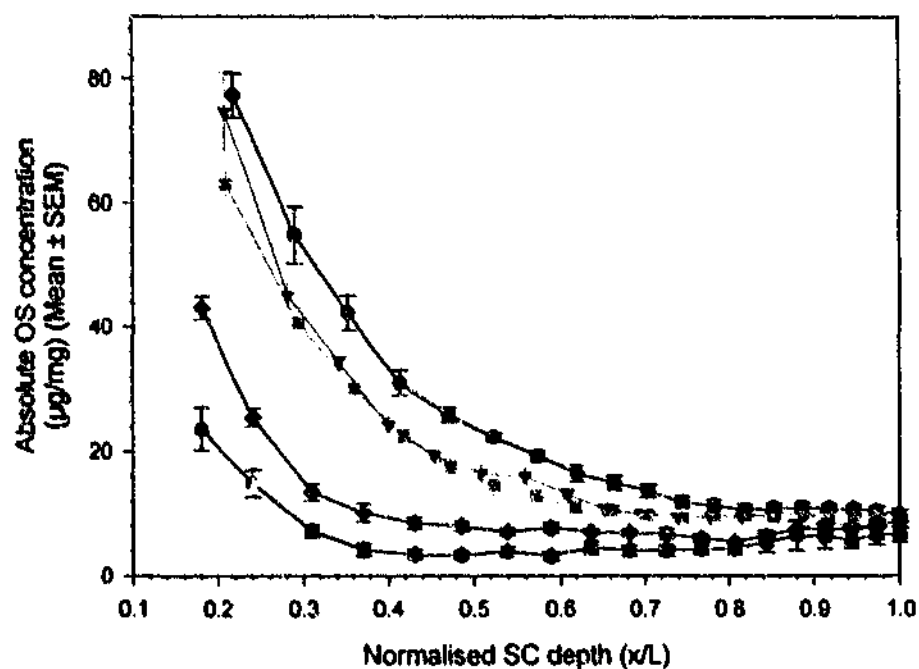
The distribution profiles of OS across human SC *in vivo* are presented in Figure 6.16. It is evident that at all exposure times the concentration of OS within the SC declined exponentially with increasing SC depth. However, it is also apparent that the concentration of OS or PO at any given position in the SC (x/L) decreased with increasing exposure time. This trend is further illustrated in Figure 6.17, where it is evident that the AUCs for the entire SC and for the upper region of the SC significantly declined after a 0.08 h exposure time ($p < 0.05$). It would also appear from Figure 6.17 that similar $AUC_{0.11-208}$ were found at 0.08, 0.5 and 2 h exposure times whilst the $AUC_{0.11-208}$ calculated at the longer exposure times (6 and 16 h) were significantly lower than those determined at 0.08 h ($p < 0.05$). Explanations as to why the topical bioavailability of OS appeared to decrease shortly after (i.e. > 0.08 h) its application to human skin *in vivo* are discussed in Section 6.4.3.

6.4.3. Correlation between the *in vitro* and *in vivo* distribution of octisalate across human stratum corneum

As shown by the data presented in Table 6.1, there was a very good correlation between the AUCs determined from the *in vitro* and *in vivo* distribution profiles at exposure times less than 2 h. However, significant differences between the *in vitro* and *in vivo* AUCs became apparent at the 6 and 16 h exposure times.

These differences can be attributed to the finding that, *in vitro*, the AUC for the entire SC remained relatively uniform, the AUC for the upper region of the SC declined and the AUC for the lower region of the SC concomitantly increased with increasing exposure time. As mentioned in Section 6.4.1, these trends would indicate that OS had accumulated within the lower region of the SC and that OS concentrations in the upper and lower regions of the SC may be approaching an "equilibrium" concentration.

A. Distribution profiles determined by HPLC/UV



B. Distribution profiles determined by ATR-FTIR

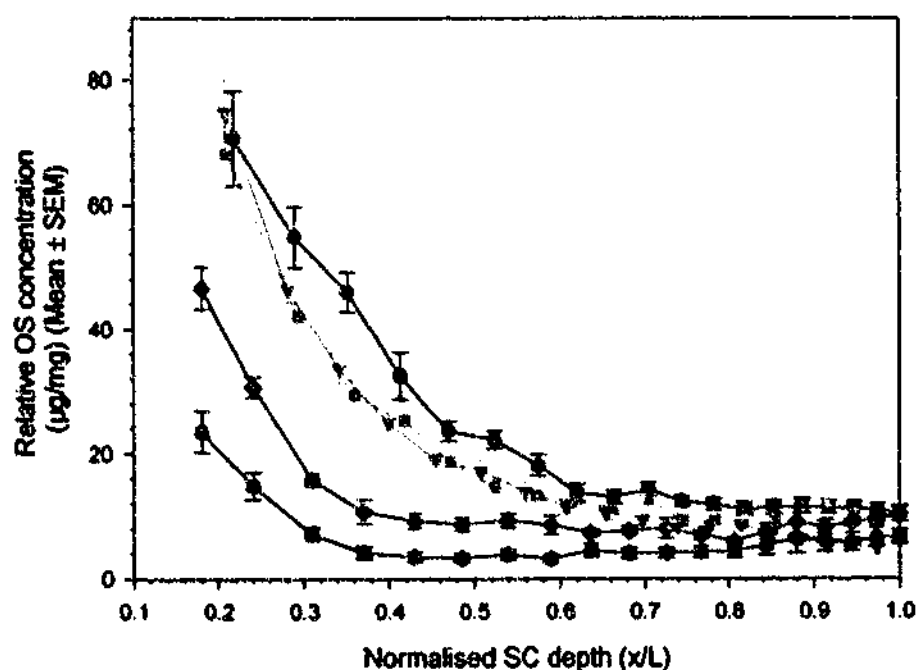
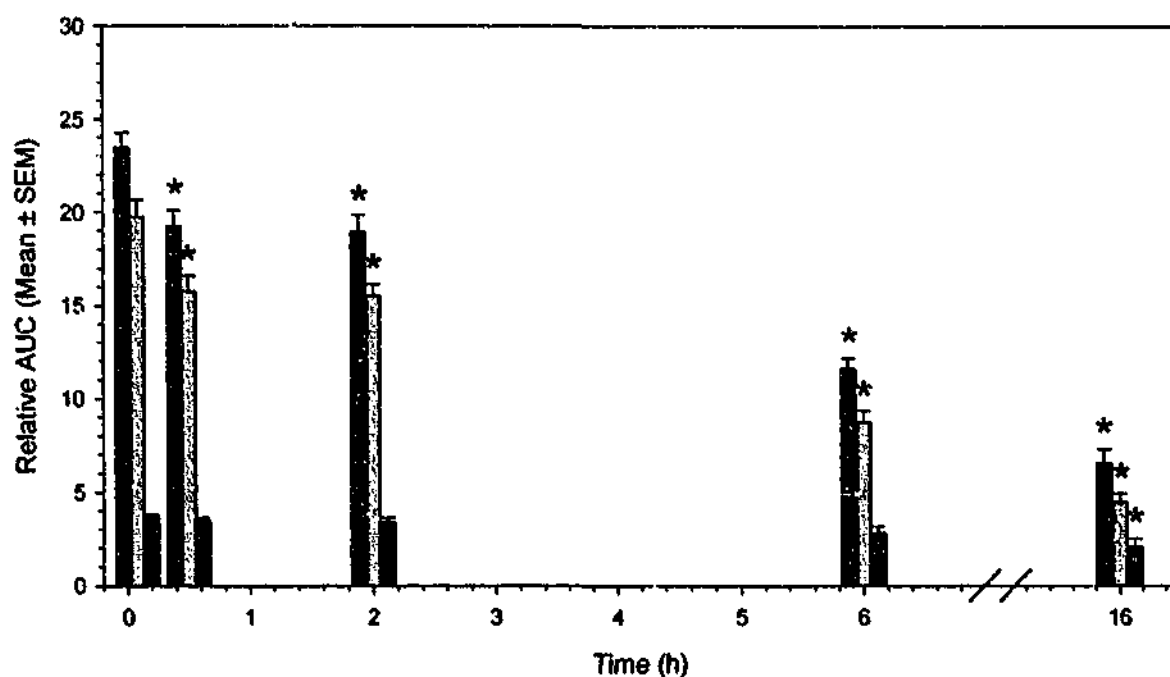


Figure 6.16. Distribution profiles of PO across human SC *in vivo* at 0.08 (●), 0.5 (▼), 2 (■), 6 (◆) or 16h (●) exposure times (n=5). The concentration of PO within the SC was determined as a function of normalised SC depth (x/L) by HPLC/UV (absolute concentration) (A) or by ATR-FTIR (relative concentration) (B).

A. Absolute AUCs



B. Relative AUCs

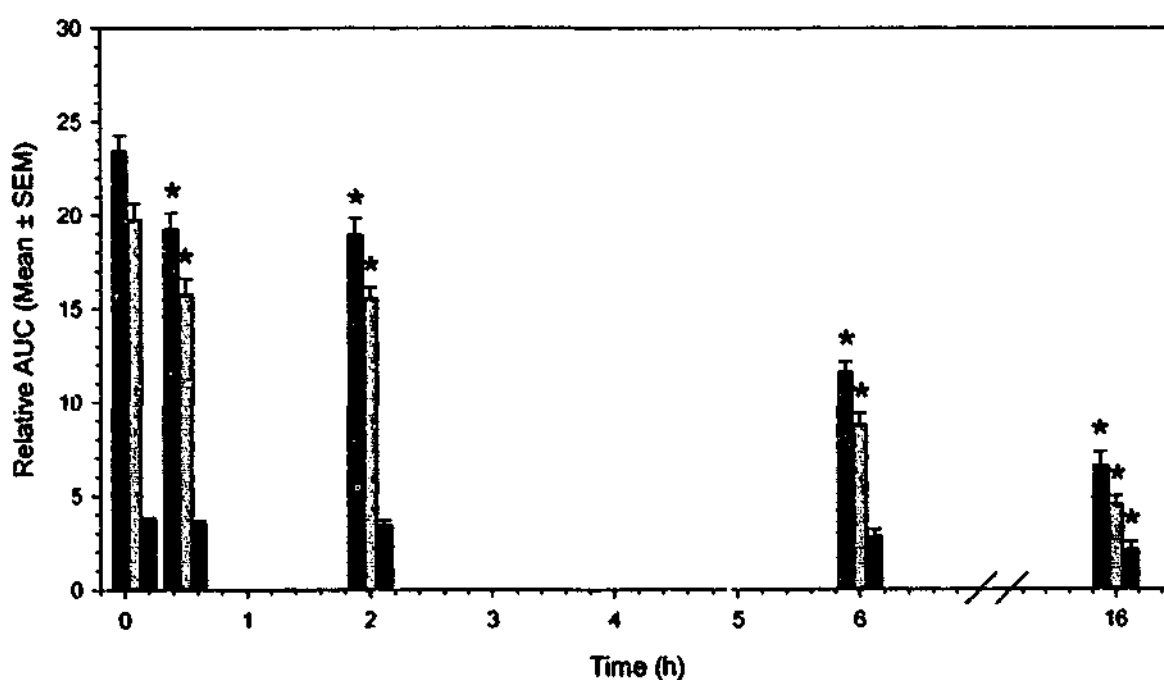


Figure 6.17. AUCs of the OS distribution profiles across human SC *in vivo* (shown in Figure 6.16). AUCs were calculated using the distribution profiles determined either by HPLC/UV (absolute AUC) (A) or by ATR-FTIR (relative AUC) (B). AUCs were determined for the *entire* SC (i.e. SC removed by tape strips 2 to 20, $AUC_{N/L2 \rightarrow 20}$) (■), the *upper* SC (i.e. SC removed by tape strips 2 to 10, $AUC_{N/L2 \rightarrow 10}$) (▨) and the *lower* SC (i.e. SC removed by tape strips 11 to 20, $AUC_{N/L11 \rightarrow 20}$) (□). * Denotes statistically significant difference compared with the AUC calculated at 0.08 h exposure time.

Table 6.1. Absolute AUCs determined from *in vitro* and *in vivo* OS distribution profiles. AUCs for the entire SC ($AUC_{x/L2 \rightarrow 20}$) and the upper ($AUC_{x/L2 \rightarrow 11}$) and lower ($AUC_{x/L11 \rightarrow 20}$) regions of the SC are shown.

Time (h)	$AUC_{x/L2 \rightarrow 20}$		$AUC_{x/L2 \rightarrow 11}$		$AUC_{x/L11 \rightarrow 20}$	
	<i>In vitro</i>	<i>In vivo</i>	<i>In vitro</i>	<i>In vivo</i>	<i>In vitro</i>	<i>In vivo</i>
0.08	20.5 ± 1.7	23.3 ± 0.8	17.3 ± 1.4	19.5 ± 0.7	3.2 ± 0.3	3.8 ± 0.2
0.5	20.0 ± 0.5	19.5 ± 0.4	16.5 ± 0.5	16.2 ± 0.7	3.5 ± 0.2	3.2 ± 0.4
2	19.4 ± 0.9	18.2 ± 0.3	15.7 ± 0.9	15.1 ± 0.3	3.6 ± 0.2	3.1 ± 0.1
6	18.7 ± 0.1*	10.2 ± 0.5*	13.9 ± 0.3*	7.8 ± 0.5*	4.8 ± 0.3*	2.4 ± 0.3*
16	19.0 ± 0.1*	5.8 ± 0.7*	12.4 ± 0.1*	4.0 ± 0.4*	6.6 ± 0.2*	1.8 ± 0.4*

* Statistically significant difference between *in vitro* and *in vivo* AUCs ($p < 0.05$).

On the other hand, the AUC for the entire SC *in vivo* did not remain constant, but rather decreased with increasing exposure time. This was due to a decline in $AUC_{x/L2 \rightarrow 10}$ and, at longer exposure times, $AUC_{x/L11 \rightarrow 20}$ with increasing exposure time. In contrast to what was observed *in vitro*, this trend would imply that OS did not accumulate within the deeper layers of the SC and that the topical bioavailability of OS decreased shortly after its application to the SC surface.

The finding that the distribution phenomenon of OS across human SC *in vitro* does not correlate with that *in vivo* at long exposure times is not surprising. A difference in the *in vitro* and *in vivo* pharmacokinetic behavior of Azone® has been previously observed, with *in vitro* data indicating that its enhancing effect in human full thickness skin may last up to 120 h after a single application (26) whilst *in vivo* distribution studies revealed that reservoir formation does not occur within the SC as little Azone® is present at 20 and 44 h after removal of the applied dose (27). The distribution of the lipophilic compound, flufenamic acid, across human SC was also found to differ under *in vitro* and *in vivo* experimental conditions (28, 29). Compared with profiles generated *in vivo*, the *in vitro* distribution profiles were greater in magnitude at a 3 h exposure time (29). Furthermore, the amount of flufenamic acid present within the SC *in vivo* appeared to decline with increasing incubation time whilst the amount present in the SC *in vitro* increased – or more or less remained constant – with increasing incubation time (28). Evidently, the

different time-related trends in *in vitro* and *in vivo* flufenamic acid distribution similar to those reported for OS in this chapter.

Although the correlation between *in vitro* and *in vivo* skin permeation is, in most cases, reasonably accurate (30) there have also been instances where *in vitro* permeation data did not correspond with *in vivo* percutaneous absorption. For instance, *in vitro* skin permeation data has been found to overestimate the *in vivo* percutaneous absorption of a variety of compounds, such as pesticides (31), phenol analogues (32), boric acid and inorganic borates (33) and vanilloids (34).

Differences in *in vitro* and *in vivo* skin permeation and drug distribution data can be attributed to a number of possible factors. With regard to the studies presented in this chapter, skin samples used during the *in vitro* distribution studies were obtained from the abdominal region of women aged between 25 and 65 (44 ± 9 years, Mean \pm SD) whilst the male and female participants involved in the *in vivo* study were aged between 20 and 25 and forearm skin was investigated. Consequently, differences in the *in vitro* and *in vivo* OS distribution profiles may be partly due to anatomical site age and/or sex-related variations in skin permeability (30, 35-39). However, it is probable that these variations did not significantly confound the correlation between the *in vitro* and *in vivo* OS distribution profiles as the *in vitro* and *in vivo* AUCs were comparable at early exposure times.

It should be kept in mind that different methods were employed to confine the SC surface area under investigation during the *in vitro* and *in vivo* studies. *In vitro*, OS was applied to the entire SC surface of excised skin samples, which eliminated the potential for lateral skin diffusion of OS. On the other hand, a Tegaderm® dressing was used to confine the skin surface area exposed to OS *in vivo*. Although this method may have confined most of the applied OS dose to a defined area of the SC surface, two problems may be envisaged; the dressing adhesive could have been dissolved to some extent by ethanol and/or OS and, after OS had partitioned into the SC, its lateral skin migration could not be prevented. Hence, it is possible that the decline in the *in vivo* AUCs was due, or at least partly due, to the lateral skin distribution of OS from the primary site of application to adjacent skin sites (40-43).

It also cannot be ignored that the physiological processes that govern *in vivo* percutaneous absorption could not have been operational, or fully operational, during the *in vitro* experiments that were employed. As mentioned in Section 5.4.4, it is possible

that frozen, non-viable skin is metabolically active (44-47). However, it has also been demonstrated that the enzymatic activity of excised skin *in vitro* is significantly less than that of skin under *in vivo* conditions (46, 48, 49). As OS may be susceptible to esterase hydrolysis (50), it is therefore possible that *in vitro* concentrations of OS within human SC did not decline partly as a result of reduced metabolic function within the skin.

It was apparent from the results presented in Section 6.4.1 that “sink” conditions may not have prevailed during the *in vitro* skin penetration experiments. This is most likely due to the fact that the dermis, which may act as a stagnant aqueous boundary layer *in vitro*, can impose a significant degree of diffusional resistance towards the permeation of lipophilic compounds (12, 51-53). *In vivo*, however, the resistance offered by the dermis is unlikely to have a significant effect on the permeation of lipophilic solutes as substances reaching this skin layer are continuously cleared by the local blood supply (52, 54, 55). The significance of this discrepancy towards the distribution of a lipophilic compound (hydrocortisone) has previously been investigated (56, 57). As the use of identical experimental conditions permitted a direct comparison of the *in vitro* and *in vivo* distribution profiles, it was revealed from these studies that hydrocortisone had accumulated within the deeper skin layers *in vitro* whilst a steep concentration gradient across the skin was observed *in vivo*. The authors concluded that the different trends in hydrocortisone distribution were due to the absence of a vascular transport system in excised skin *in vitro*. As the *in vitro* and *in vivo* distribution profiles generated for OS followed similar trends, it is possible that lack of dermal clearance *in vitro* also contributed to the poor *in vitro* - *in vivo* correlation observed at longer exposure times.

As observed in Section 5.4.5, the SC only accommodated a small percentage (<11%) of the total OS dose applied to the skin surface *in vitro* and thus substantial amounts of OS remained at the SC surface at all exposure times. As the amount of OS residing at the SC surface and total OS recovery both appeared to decline by first order rate processes, whilst SC concentrations remained relatively constant, it was concluded from the data presented in Section 5.4.5 that significant losses in total OS recovery (from ~99% to ~44% of the dose applied at 0.08 and 16 h, respectively) could be attributed to a decline in the amount of OS residing at the SC surface. In light of the previous discussion regarding dermal blood flow, it is not surprising that *in vitro* concentrations of OS within the SC remained relatively constant at all exposure times despite the decline in SC surface concentrations. However, as implied by the discussion in Section 5.4.4, it was

somewhat unexpected that the amount of OS residing at the SC surface *in vitro* significantly declined as a function of time. It is also evident from Figure 6.18 that the amount of OS residing at the SC surface *in vivo* followed a similar first order decay process to that observed *in vitro*. However, it is also apparent that the rate of OS clearance from the SC surface was higher under *in vivo* conditions than what it was *in vitro* ($k = 0.052$ and 0.163 h^{-1} for *in vitro* and *in vivo* SC surface clearance, respectively). Consequently, the amount of OS residing at the SC surface *in vitro* was significantly higher than that found at the SC surface *in vivo* at longer exposure times longer than 0.5 h (Figure 6.18).

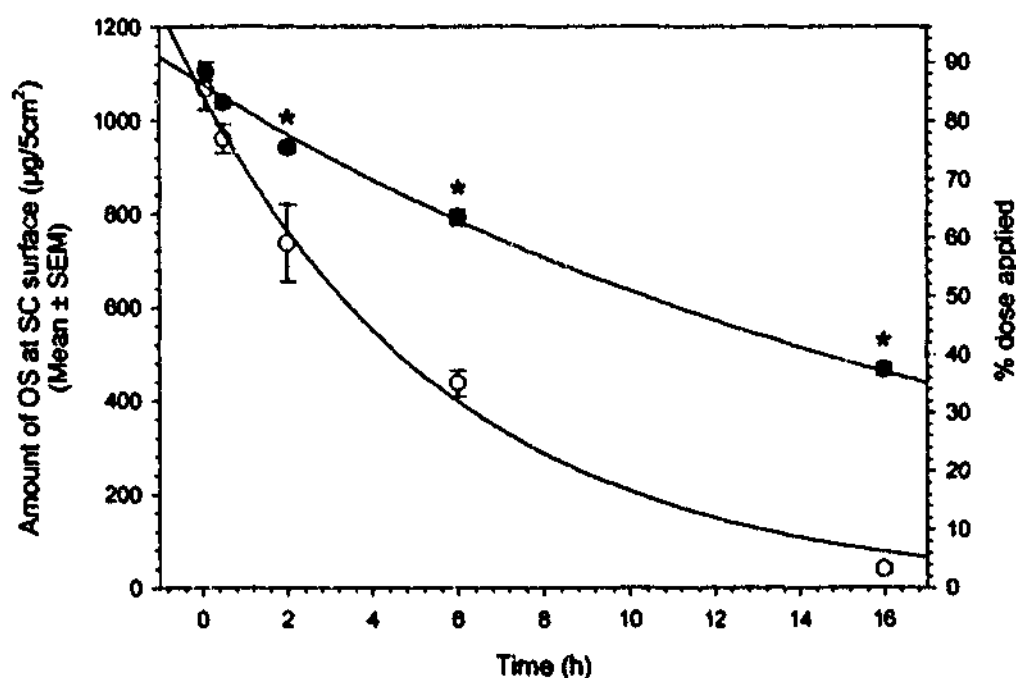


Figure 6.18. The amount of OS residing at the SC surface at various exposure times under *in vitro* (●) and *in vivo* (○) experimental conditions. The solid lines represent regression of the data to Equation 6.6 ($r^2=0.992$ and 0.994 for *in vitro* and *in vivo* data, respectively). * denotes a statistically significant difference between the *in vitro* and *in vivo* amount of OS at the SC surface ($p<0.05$). Note: as the area of skin exposed to OS was 12cm^2 *in vivo* and 5cm^2 *in vitro*, amounts of OS found at the SC surface *in vivo* were divided by a factor of 2.4 (i.e. $12/5 \text{ cm}^2 = 2.4$).

Possible reasons for the disappearance of OS from the SC surface *in vitro* that were mentioned in Section 5.4.4 included loss by evaporation and desquamation. Although the occurrence of desquamation *in vitro* is subject to conjecture, it is likely that the contribution of both of these factors towards OS surface loss was more significant *in vivo* than would what it was under *in vitro* experimental conditions. For instance, Reifenrath et al (58) demonstrated that the evaporative loss of certain compounds from the skin surface may be affected by a change in air flow over the skin and may also effect the extent of percutaneous drug penetration. Furthermore, these investigators had previously shown that the correlation between *in vitro* and *in vivo* measurements is dependent on air flow over the skin (58). Thus, as the participants were free to resume normal everyday activities during the *in vivo* experiments described in this chapter, it is possible that the rate of air flow over the skin *in vivo* was higher than that encountered *in vitro* as the excised skin samples were kept in a stationary position under ambient laboratory conditions. It is also feasible that OS may have been removed from the skin surface *in vivo* by washing or by rubbing off onto clothing or other materials (such as tables or bed linen) (59). Although measures were deployed to minimise these factors (Section 6.3.3.2), this aspect of the experimental design could not have been completely eliminated.

There have also been instances where the difference between *in vitro* and *in vivo* skin permeation data has been attributed to desquamation. For instance, Kasting et al (60) observed that the *in vivo* absorption rates of different lipophilic compounds (vanilloids) gradually declined over a 3 day period whilst *in vitro* absorption rates maintained a steady state. The authors proposed that skin turnover *in vivo* may have accounted for these time-related differences. Work conducted by Franz et al (61) also demonstrated that, for poorly permeating compounds, *in vitro* skin permeation data significantly overestimated *in vivo* percutaneous absorption. The authors rationalised this difference by considering the dynamics of the two systems; *in vivo* there is an average loss, through desquamation, of one cell layer per day which may result in a continuing reduction in the amount of material remaining on the skin whereas *in vitro* most of the material will remain on the skin and continue to serve as a source for absorption.

Although the aforementioned studies were conducted over long periods (from 2 to 5 days) it should be stated that, as mentioned in Section 5.4.4, SC surface clearance (the transit time of one cell layer) may be of the order of 6 to 16 h (62). Thus, in relation to the

work presented in this chapter, it is feasible that significant surface losses due to SC surface clearance can occur within a 16 h exposure time.

Evidently, there are a number of potential factors that could have resulted in the time-related differences that were observed in the *in vitro* and *in vivo* OS distribution profiles across human SC. It is interesting to note from Table 6.2, however, that normalisation of the AUCs for the upper and lower regions of the SC (i.e. expressing $AUC_{v/L2 \rightarrow 10}$ and $AUC_{v/L11 \rightarrow 20}$ as a percentage of $AUC_{v/L2 \rightarrow 20}$) results in an excellent *in vitro-in vivo* correlation at all exposure times. Of particular interest is the observation that normalised *in vitro* and *in vivo* values for $AUC_{v/L2 \rightarrow 10}$ decrease whilst those for $AUC_{v/L11 \rightarrow 20}$ increase with increasing exposure time. Evidently, this trend is consistent with that previously observed with the non-normalised *in vitro* values for $AUC_{v/L2 \rightarrow 10}$ and $AUC_{v/L11 \rightarrow 20}$. Consequently, it would appear that although total SC concentrations of OS appear to decline *in vivo*, the *relative* distribution of OS within the SC follows the same time-related trend as that observed *in vitro*.

Table 6.2. Normalised absolute AUCs determined from *in vitro* and *in vivo* OS distribution profiles, where AUCs for the upper ($AUC_{v/L2 \rightarrow 10}$) and lower regions ($AUC_{v/L11 \rightarrow 20}$) of the SC are expressed as a percentage of the AUC calculated for the entire SC ($AUC_{v/L2 \rightarrow 20}$).

Time (h)	Normalised $AUC_{v/L2 \rightarrow 10}$		Normalised $AUC_{v/L11 \rightarrow 20}$	
	(% of $AUC_{v/L2 \rightarrow 20}$)		(% of $AUC_{v/L2 \rightarrow 20}$)	
	<i>In vitro</i>	<i>In vivo</i>	<i>In vitro</i>	<i>In vivo</i>
0.08	84.2 ± 6.8	83.6 ± 2.9	15.8 ± 1.7	16.4 ± 0.9
0.5	82.6 ± 2.4	83.4 ± 3.6	17.4 ± 0.8	16.6 ± 1.8
2	81.2 ± 4.7	82.9 ± 1.5	18.8 ± 1.2	17.1 ± 0.8
6	74.5 ± 1.4	76.3 ± 3.0	25.5 ± 1.5*	23.7 ± 1.3*
16	65.0 ± 0.8*	68.6 ± 3.9*	35.0 ± 1.3*	31.4 ± 3.1*

* Statistically significant difference compared with AUC at 0.08 h ($p < 0.05$).

Hence, in order to determine whether *in vitro* distribution data for OS can be used to predict *in vivo* distribution at longer exposure times, it may be necessary to repeat these experiments using a study protocol that strictly controls *in vivo* variables (such as air flow over the skin surface and rubbing off onto clothing or other materials), accounts for loss of OS from the SC surface through desquamation and/or evaporation *in vivo* (63, 64), and eliminates variations in skin permeability caused by differences in anatomical region, age and sex.

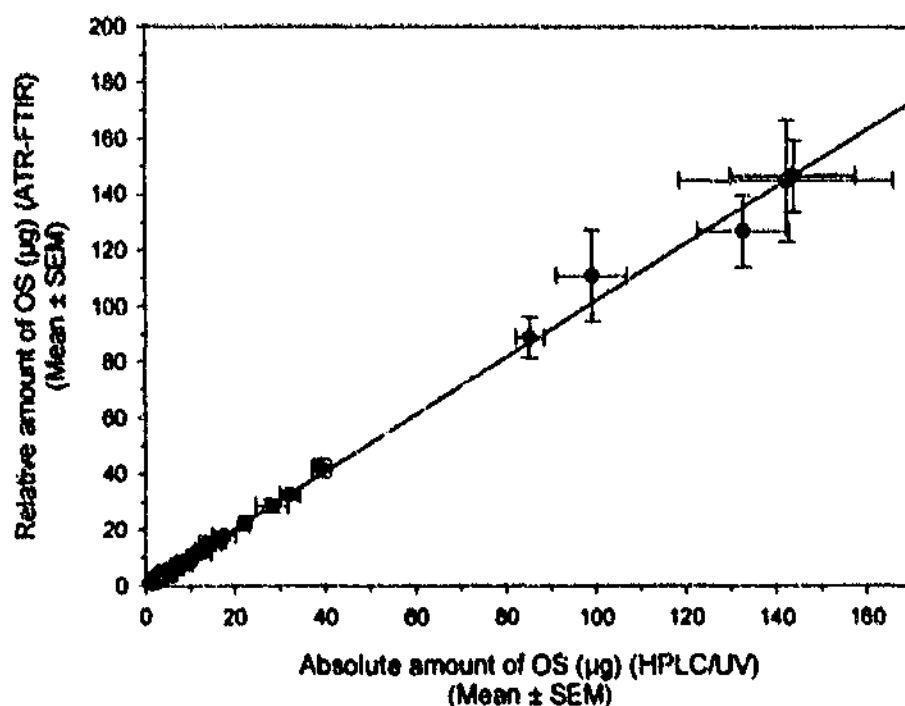
6.4.4. Correlation between the octisalate and padimate O distribution profiles determined by HPLC/UV and ATR-FTIR

In Figure 6.19, the absolute (HPLC/UV) amounts of OS and PO that were found within SC removed by the tape strips *in vitro* are compared with the corresponding relative measurements determined by ATR-FTIR. The same relationship is shown for the *in vivo* measurements of OS in Figure 6.20. It should be noted that the data presented in these figures pertains to the amount of OS or PO removed by each tape strip at all exposure times. As indicated by the *in vitro* and *in vivo* results presented throughout this chapter, there appeared to be an excellent correlation between the data derived from the two different analytical methods ($r^2 = 0.997$ and 0.998 for *in vitro* OS and PO measurements, respectively, and $r^2 = 0.992$ for *in vivo* OS measurements).

As ATR-FTIR is a relatively novel technique for determining drug distribution across the SC, it is worth noting that a very good correlation between ATR-FTIR and other methods of analysis (such as liquid scintillation counting, mass spectrometry and HPLC/UV) has previously been reported (11, 65-67). These findings highlight the potential of ATR-FTIR to accurately determine the distribution of topically-applied drugs within the SC under *in vitro* or *in vivo* experimental conditions.

As ATR-FTIR is a simple and rapid means of determining drug concentrations within the SC, the significance of these findings in relation to future research is evident, particularly if one considers the limitations associated with conventional methods of analysis. For instance, procedures that are employed to extract drug from the tape strip samples are often time-consuming and the use of radiolabeled compounds in humans *in vivo* imposes legal and ethical constraints.

A. Octisalate



B. Padimate O

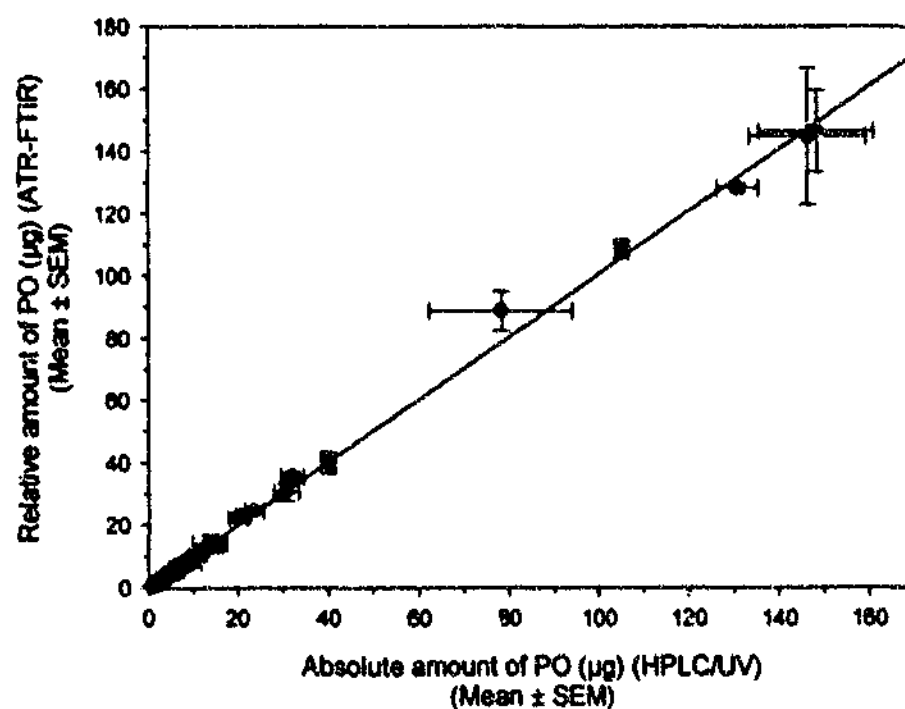


Figure 6.19. Correlation between the absolute (HPLC/UV) amount of OS (A) or PO (B) found within sequential SC layers removed by tape stripping *in vitro* and the corresponding relative measurements determined by ATR-FTIR. The solid line represents linear regression of the data ($y = 1.02x + 0.15$, $r^2 = 0.997$, $p < 0.0001$ for OS and $y = 1.01x - 0.05$, $r^2 = 0.998$, $p < 0.0001$ for PO).

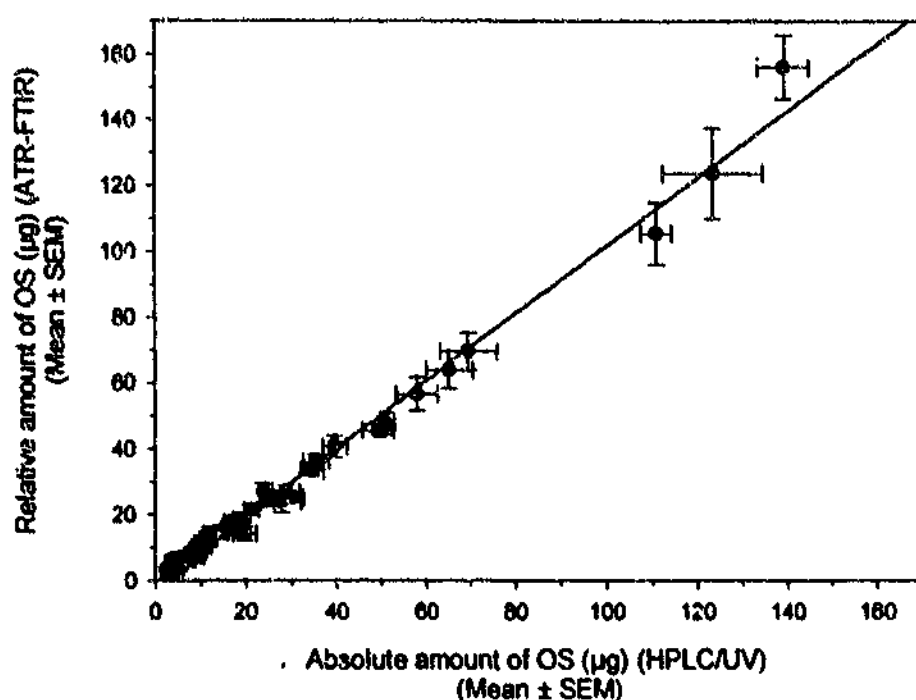


Figure 6.20. Correlation between the absolute (HPLC/UV) amount of OS found within sequential SC layers removed by tape stripping *in vivo* and the corresponding relative measurements determined by ATR-FTIR. The solid line represents linear regression of the data ($y = 1.02x - 0.66$, $r^2 = 0.992$, $p < 0.0001$).

6.5. CONCLUSIONS

It would appear that different time-related trends exist between the distribution of OS and PO and the distribution of fentanyl across human SC *in vitro*. In particular, concentrations of OS or PO within the upper layers of the SC appeared to decline whilst those in the lower regions of the SC increased with time following “finite dose” application to the SC surface. This trend may suggest that, *in vitro*, OS and PO accumulate within the deeper SC layers during prolonged exposure times. On the other hand, when fentanyl was applied (with OS or PO) as a “finite dose” to the SC surface, concentrations within the upper and lower regions remained constant with increasing exposure time and apparent pseudo-steady-state diffusion eventually prevailed (Chapter 5). With regard to the possible mechanism(s) by which OS and PO enhance the permeation of fentanyl across human skin *in vitro*, these different trends appear to suggest that:

- i. in addition to their possible effects on fentanyl solubility within the SC lipid domain, OS and PO may also enhance fentanyl partitioning into the SC via other interactive mechanism(s)
- iii. the contribution of the effects of OS and PO on fentanyl partitioning from the vehicle to the SC towards fentanyl permeation is more significant than that of their effects on fentanyl partitioning from the SC to the underlying skin strata.

However, the differences that were evident between the *in vitro* and *in vivo* OS distribution profiles at longer exposure times highlight that it may be difficult to extrapolate the significance of the mechanism(s) by which OS and PO enhance fentanyl permeation *in vitro* to that of the mechanism(s) that prevail during the percutaneous absorption of fentanyl under *in vivo* conditions. This difficulty arises from the fact that several factors that influence the extent of percutaneous drug absorption *in vivo* would not exist to the same extent, if at all, *in vitro*. For instance, it would appear that factors such as lateral drug diffusion, cutaneous metabolism, desquamation, differences in air flow over the skin and lack of dermal blood supply *in vitro* may have been responsible for the different time-related trends that were evident between the *in vitro* and *in vivo* distribution profiles of OS. Consequently, further research may be required in order to clarify the correlation between the distribution of OS and PO across human SC under *in vitro* and *in vivo* conditions and to investigate the mechanism(s) by which OS and PO enhance the *in vivo* percutaneous absorption of fentanyl.

Due to the excellent correlation that was observed between the ATR-FTIR and HPLC/UV data, another conclusion that can be derived from the work presented in this chapter is that ATR-FTIR can be used to determine the distribution of OS or PO across human SC under *in vitro* or *in vivo* experimental conditions. Although this analytical technique is limited to compounds that generate IR absorbances that can be distinguished from those arising from the SC, it is a relatively facile and efficient means of drug quantification within human SC and may therefore be a valuable quantitative tool for determining topical bioavailability.

6.6. REFERENCES

1. Naik A, Pechtold LARM, Potts RO, Guy RH. 1995. Mechanism of Oleic Acid-Induced Skin Penetration Enhancement *In Vivo* in Humans. *J Control Release* 37:299-306.
2. Bommannan D, Potts RO, Guy RH. 1990. Examination of Stratum Corneum Barrier Function *In Vivo* by Infrared Spectroscopy. *J Invest Dermatol* 95:403-408.
3. Mak VHW, Potts RO, Guy RH. 1990. Oleic Acid Concentration and Effect in Human Stratum Corneum: Non-Invasive Determination by Attenuated Total Reflectance Infrared Spectroscopy *In Vivo*. *J Control Release* 12:67-75.
4. Naik A, Kalia YN, Pirot F, Guy RH. 1999. Characterization of Molecular Transport Across Human Stratum Corneum *In Vivo*. In Bronaugh RL, Maibach H, ed. *Percutaneous Absorption: Drugs, Cosmetics, Mechanisms, Methodology*. New York: Marcel Dekker, Inc., pp 149-175.
5. Potts RO, Francoeur ML. 1992. Physical Methods for Studying Stratum Corneum Lipids. *Semin Dermatol* 11:129-138.
6. Potts RO, Francoeur ML. 1993. Infrared Spectroscopy of Stratum Corneum Lipids. *In Vitro* Results and Their Relevance to Permeability. In Walters KA, Hadgraft J, ed. *Pharmaceutical Skin Penetration Enhancement*. New York: Marcel Dekker, Inc., pp 269-291.
7. Naik A, Guy RH. 1997. Infrared Spectroscopic and Differential Scanning Calorimetric Investigations of the Stratum Corneum Barrier Function. In Potts RO, Guy RH, ed. *Mechanisms of Transdermal Drug Delivery*. New York: Marcel Dekker, Inc., pp 87-162.
8. Hill RR, Rendell DAE. 1975. *The Interpretation of Infrared Spectra*. New York: Heyden & Son Ltd. pp 3-37.
9. Green DW, Reedy GT. 1978. Matrix-Isolation Studies with Fourier Transform Infrared. In Ferraro JR, Basile LJ, ed. *Fourier Transform Infrared Spectroscopy*. New York: Academic Press, Inc., pp 1-59.
10. Pellett MA, Watkinson AC, Hadgraft J, Brain KR. 1997. Comparison of Permeability Data from Traditional Diffusion Cells and ATR-FTIR Spectroscopy. Part II. Determination of Diffusional Pathlengths in Synthetic Membranes and Human Stratum Corneum. *Int J Pharm* 154:217-227.
11. Higo N, Naik A, Bommannan DB, Potts RO, Guy RH. 1993. Validation of Reflectance Infrared Spectroscopy as a Quantitative Method to Measure Percutaneous Absorption *In Vivo*. *Pharm Res* 10:1500-1506.
12. Schaefer H, Stutgen G, Zesch A, Schalla W, Gazith J. 1978. Quantitative Determination of Percutaneous Absorption of Radiolabeled Drugs *In Vitro* and *In Vivo* by Human Skin. *Curr Probl Dermatol* 7:80-94.
13. Anderson BD, Cassidy JM. 1973. Variation in Physical Dimensions and Chemical Composition of Human Stratum Corneum. *J Invest Dermatol* 61:30-32.
14. Johnson ME, Blankschtein D, Langer R. 1997. Evaluation of Solute Permeation Through the Stratum Corneum: Lateral Bilayer Diffusion as the Primary Transport Mechanism. *J Pharm Sci* 86:1162-1172.

15. Mak VHW, Potts RO, Guy RH. 1990. Percutaneous Penetration Enhancement *In Vivo* Measured by Attenuated Total Reflectance Infrared Spectroscopy. *Pharm Res* 7:835-841.
16. Karnes HT, Shiu G, Shah VP. 1991. Validation of Bioanalytical Methods. *Pharm Res* 8:421-426.
17. Shah VP, Flynn GL, Yacobi A, Maibach HI, Bon C, Fleischer NM, Franz TJ, Kaplan SA, Kawamoto J, Lesko LJ, Marty JP, Pershing LK, Schaefer H, Sequeira JA, Shrivastava SP, Wilkin J, Williams RL. 1998. Bioequivalence of Topical Dermatological Dosage Forms- Methods of Evaluation of Bioequivalence. *Skin Pharmacol Appl Skin Physiol* 11:117-124.
18. Marttin E, Neelissen-Subnel MT, De Haan FH, Bodde HE. 1996. A Critical Comparison of Methods to Quantify Stratum Corneum Removed by Tape Stripping. *Skin Pharmacol* 9:69-77.
19. Tsai J, Cappel MJ, Weiner ND, Flynn GL, Ferry J. 1991. Solvent Effects on the Harvesting of Stratum Corneum From Hairless Mouse Skin Through Adhesive Tape Stripping *In Vitro*. *Int J Pharm* 68:127-133.
20. Roy SD, Flynn GL. 1988. Solubility and Related Physicochemical Properties of Narcotic Analgesics. *Pharm Res* 5:580-586.
21. Roberts MS, Walters KA. 1998. The Relationship Between Structure and Barrier Function of Skin. In Roberts MS, Walters KA, ed. *Dermal Absorption and Toxicity Assessment*. New York: Marcel Dekker, Inc., pp 1-42.
22. Guy RH, Hadgraft J. 1989. Selection of Drug Candidates for Transdermal Drug Delivery. In Hadgraft J, Guy RH, ed. *Transdermal Drug Delivery: Developmental Issues and Research Initiatives*. New York: Marcel Dekker Inc., pp 59-81.
23. Crank J. 1975. *The Mathematics of Diffusion*. London: Oxford University Press. pp 44-68.
24. Roy SD, Hou SY, Witham SL, Flynn GL. 1994. Transdermal Delivery of Narcotic Analgesics: Comparative Metabolism and Permeability of Human Cadaver Skin and Hairless Mouse Skin. *J Pharm Sci* 83:1723-1728.
25. Roy SD, Flynn GL. 1990. Transdermal Delivery of Narcotic Analgesics: pH, Anatomical, and Subject Influences on Cutaneous Permeability of Fentanyl and Sufentanil. *Pharm Res* 7:842-847.
26. Wotton PK, Mollgaard B, Hadgraft J, Hoelgaard A. 1985. Vehicle Effect on Topical Drug Delivery. III. Effect of Azone on the Cutaneous Permeation of Metronidazole and Propylene Glycol. *Int J Pharm* 24:19-26.
27. Wiechers JW, Drenth BFH, Jonkman JHG, Zeeuw RA. 1987. Percutaneous Absorption and Elimination of the Penetration Enhancer Azone in Humans. *Pharm Res* 4:519-523.
28. Wagner H, Kostka KH, Lehr CM, Schaefer UF. 2002. Human Skin Penetration of Flufenamic Acid: *In Vivo/In Vitro* Correlation (Deeper Skin Layers) for Skin Samples from the Same Subject. *J Invest Dermatol* 118:540-544.
29. Wagner H, Kostka KH, Lehr CM, Schaefer UF. 2000. Drug Distribution in Human Skin Using Two Different *In Vitro* Test Systems: Comparison with *In Vivo* Data. *Pharm Res* 17:1475-1481.
30. Brain K, Walters KA, Watkinson AC. 2002. Methods for Studying Percutaneous Absorption. In Walters KA, ed. *Dermal and Transdermal Formulations*. New York: Marcel Dekker Inc., pp 197-269.

31. Scott RC, Batten PL, Clowes HM, Jones BK, Ramsey JD. 1992. Further Validation of an *In Vitro* Method to Reduce the Need for *In Vivo* Studies Measuring the Absorption of Chemicals Through the Skin. *Fundam Appl Toxicol* 19:484-492.
32. Surber C, Wilhelm KP, Maibach HI. 1993. *In Vitro* and *In Vivo* Percutaneous Absorption of Structurally Related Phenol and Steroid Analogs. *Eur J Pharm Biopharm* 29:244-248.
33. Wester RC, Hui X, Hartway T, Maibach HI, Bell K, Schell MJ, Northington DJ, Strong P, Culver BD. 1998. *In Vivo* Percutaneous Absorption of Boric Acid, Borax, and Disodium Octaborate Tetrahydrate in Humans Compared to *In Vitro* Absorption in Human Skin from Infinite and Finite Doses. *Toxicol Sci* 45:42-51.
34. Kasting GB. 2001. Kinetics of Finite Dose Absorption Through Skin I. Vanillylnonanamide. *J Pharm Sci* 90:202-212.
35. Feldmann RJ, Maibach HI. 1967. Regional Variation in Percutaneous Penetration of ¹⁴C Cortisol in Man. *J Invest Dermatol* 48:181-183.
36. Maibach HI, Feldmann RJ, Milby TH, Serat WF. 1971. Regional Variation in Percutaneous Penetration in Man. Pesticides. *Arch Environ Health* 23:208-211.
37. Rougier A, Dupuis D, Lotte C, Roguet R, Wester RC, Maibach HI. 1986. Regional Variation in Percutaneous Absorption in Man: Measurement by the Stripping Method. *Arch Dermatol Res* 278:465-469.
38. Tsai JC, Lin CY, Sheu HM, Lo YL, Huang YH. 2003. Noninvasive Characterization of Regional Variation in Drug Transport into Human Stratum Corneum *In Vivo*. *Pharm Res* 20:632-638.
39. Wester RC, Maibach HI. 1999. Regional Variation in Percutaneous Absorption. In Bronaugh RL, Maibach HI, ed. *Percutaneous Absorption: Drugs, Cosmetics, Mechanisms, Methodology*. New York: Marcel Dekker, Inc., pp 107-116.
40. Schicksnus G, Muller-Goymann CC. 2004. Lateral Diffusion of Ibuprofen in Human Skin During Permeation Studies. *Skin Pharmacol Physiol* 17:84-90.
41. Chilcott RP, Dalton CH, Hill I, Davidson CM, Blohm KL, Hamilton MG. 2003. Clinical Manifestations of VX Poisoning Following Percutaneous Exposure in the Domestic White Pig. *Hum Exp Toxicol* 22:255-261.
42. Simonsen L, Petersen MB, Benfeldt E, Serup J. 2002. Development of an *In Vivo* Animal Model for Skin Penetration in Hairless Rats Assessed by Mass Balance. *Skin Pharmacol Appl Skin Physiol* 15:414-424.
43. Weigmann H, Lademann J, v Pelchrizm R, Sterry W, Hagemeister T, R. M, Schaefer M, Lindscheid M, Schaefer H, Shah VP. 1999. Bioavailability of Clobetasol Propionate-Quantification of Drug Concentrations in the Stratum Corneum by Dermatopharmacokinetics Using Tape Stripping. *Skin Pharmacol Appl Skin Physiol* 12:46-53.
44. Barrett DA, Rutter N, Davis SS. 1993. An *In Vitro* Study of Diamorphine Permeation Through Premature Human Neonatal Skin. *Pharm Res* 10:583-587.

45. Hewitt PG, Perkins J, Hotchkiss SA. 2000. Metabolism of Fluroxypyr, Fluroxypyr Methyl Ester, and the Herbicide Fluroxypyr Methylheptyl Ester. I: During Percutaneous Absorption Through Fresh Rat and Human Skin *In Vitro*. *Drug Metab Dispos* 128:748-754.
46. Higo N, Hinz RS, Lau DT, Benet LZ, Guy RH. 1993. Cutaneous Metabolism of Nitroglycerin *In Vitro*. II. Effects of Skin Condition and Penetration Enhancement. *Pharm Res* 9:303-306.
47. Bronaugh RL, Kraeling MEK, Yourick JJ, Hood HL. 1999. Cutaneous Metabolism During *In Vitro* Percutaneous Absorption. In Bronaugh RL, Maibach H, ed. *Percutaneous Absorption: Drugs, Cosmetics, Mechanisms, Methodology*. New York: Marcel Dekker, Inc., pp 57-64.
48. Bando H, Sahashi M, Yamashita F, Takakura Y, Hashida M. 1997. *In Vivo* Evaluation of Acyclovir Prodrug Penetration and Metabolism Through Rat Skin Using a Diffusion/Bioconversion Model. *Pharm Res* 14:56-62.
49. Chang P, Rosenquist MD, Lewis RW, Kealey GP. 1998. A Study of Function Viability and Metabolic Degeneration of Human Skin Stored at 4 Degrees C. *J Burn Care Rehabil* 19:25-28.
50. Walters KA, Brain KR, Howes D, James VJ, Kraus AL, Teetsel NM, Toulon M, Watkinson AC, Gettings SD. 1997. Percutaneous Penetration of Octyl Salicylate from Representative Sunscreen Formulations Through Human Skin *In Vitro*. *Food Chem Toxicol* 35:1219-1225.
51. Cross SE, Magnusson BM, Winckle G, Anissimov YG, Roberts MS. 2003. Determination of the Effect of Lipophilicity on the *In Vitro* Permeability and Tissue Reservoir Characteristics of Topically Applied Solutes in Human Skin Layers. *J Invest Dermatol* 120:759-764.
52. Barry BW. 1983. *Dermatological Formulations. Percutaneous Absorption*. New York: Marcel Dekker, Inc. pp 95-126.
53. Barry BW. 1983. *Dermatological Formulations. Percutaneous Absorption*. New York: Marcel Dekker, Inc. pp 127-233.
54. Schaefer H, Zesch A, Stüttgen G. 1982. *Skin Permeability*. Berlin: Springer-Verlag. pp 607-608.
55. Singh P, Roberts MS. 1997. Local Deep Tissue Penetration of Compounds After Dermal Application: Structure-Tissue Penetration Relationships. *J Pharmacol Exp Ther* 279:908-917.
56. Schaefer H, Zesch A, Stüttgen G. 1982. *Skin Permeability*. Berlin: Springer-Verlag. pp 571-575.
57. Roberts MS, Cross SE, Pellett MA. 2002. Skin Transport. In Walters KA, ed. *Dermal and Transdermal Formulations*. New York: Marcel Dekker, Inc., pp 89-195.
58. Reifenrath WG, Hawkins GS, Kurtz MS. 1991. Percutaneous Penetration and Skin Retention of Topically Applied Compounds: An *In Vitro* - *In Vivo* Study. *J Pharm Sci* 80:526-532.
59. Auton TR, Westhead DR, Woollen BH, Scott RC, Wilks MF. 1994. A Physiological Based Mathematical Model of Dermal Absorption in Man. *Hum Exp Toxicol* 13:51-60.
60. Kasting GB, Francis WR, Bowman LA, Kinnett GO. 1997. Percutaneous Absorption of Vanilloids: *In Vivo* and *In Vitro* Studies. *J Pharm Sci* 86:142-146.
61. Franz TJ. 1978. The Finite Dose Technique as a Valid *In Vitro* Model for the Study of Percutaneous Absorption in Man. *Curr Probl Dermatol* 7:58-68.
62. Kvidera A, Mackenzie IC. 1994. Rates of Clearance of the Epithelial Surfaces of Mouse Oral Mucosa and Skin. *Epithel Cell Biol* 3:175-180.

63. Christensen MS, Nacht S, Kantor SL, Gans EH. 1978. A Method for Measuring Desquamation and Its Use for Assessing the Effects of Some Common Exfoliants. *J Invest Dermatol* 71:289-294.
64. Bucks DA, Maibach HI, Guy RH. 1988. Mass Balance and Dose Accountability in Percutaneous Absorption Studies: Development of a Nonocclusive Application System. *Pharm Res* 5:313-315.
65. Pirot F, Kalia YN, Stinchcomb AL, Keating G, Bunge A, Guy RH. 1997. Characterization of the Permeability Barrier of Human Skin *In Vivo*. *Proc Natl Acad Sci USA* 94:1562-1567.
66. Alberti I, Kalia YN, Naik A, Bonny J, Guy RH. 2001. *In Vivo* Assessment of Enhanced Topical Delivery of Terbinafine to Human Stratum Corneum. *J Control Release* 71:319-327.
67. Alberti I, Kalia YN, Naik A, Bonny J, Guy RH. 2001. Effect of Ethanol and Isopropyl Myristate on the Availability of Topical Terbinafine in Human Stratum Corneum, *In Vivo*. *Int J Pharm* 219:11-19.

CHAPTER 7

THE EFFECTS OF OCTISALATE AND PADIMATE O ON HUMAN STRATUM CORNEUM LIPIDS

7.1. INTRODUCTION

As discussed in Chapter 1, CPEs can alter the barrier function of the SC and subsequently enhance drug penetration through the skin, by reducing the conformational order of the SC intercellular lipid bilayers. Therefore, analytical techniques that have been used to study the structure and barrier function of the SC have also been employed to investigate the mechanism(s) by which CPEs may perturb the organisation of the SC lipids. These techniques include differential scanning calorimetry (DSC) (1-5), electron spin resonance (6-8), X-ray diffraction (5, 9-11), fluorescence, impedance or infrared spectroscopy (12-17) and electron microscopy (18-20). Among this array, infrared spectroscopy – particularly attenuated total reflectance Fourier transform infrared spectroscopy (ATR-FTIR) – has been extensively used to study the barrier function of the SC and to probe the mechanism(s) involved in the effect of CPEs on SC lipid organisation (21-24).

The basic principles of ATR-FTIR, and some of the advantages associated with this technique, were described in Chapter 6. It is also worth noting that ATR-FTIR is a particularly amenable technique for studying the barrier function of the SC and the mechanism(s) of action of CPEs as:

- i. In contrast to DSC, the effects of CPEs on the structural components of the SC can be studied at normal skin or room temperature, rather than at elevated temperatures
- ii. ATR-FTIR is a non-destructive technique and therefore skin samples can be analysed before and after treatment with a CPE. Thus, each skin sample can be used as its own control, which may reduce errors imparted by variations in SC lipid content and fluidity (25-28)
- iii. An ATR-FTIR spectrum provides information on the vibrational modes of the SC components. Thus, this technique can be used to probe the effects of CPEs at a molecular and conformational level.

With regard to the last attribute, the mid-IR range of an ATR-FTIR spectrum of human SC encompasses absorption bands that correspond to fundamental vibrations originating from lipids, proteins and water (Figure 7.1). As the wavenumber of each IR

absorbance is characteristic of underlying molecular motions, an ATR-FTIR spectrum of human SC can provide information about the conformation and immediate environment of atoms within the SC components as well as their participation in chemical bonds (22).

Water present within the SC gives rise to O-H stretching frequencies ($\nu(\text{O-H})$) located at $\sim 3000\text{ cm}^{-1}$ and $\sim 2100\text{ cm}^{-1}$. Although the intensity of the O-H stretching absorbance located at $\sim 2100\text{ cm}^{-1}$ is very weak (it is not evident in Figure 7.1) compared with the broad band located at $\sim 3000\text{ cm}^{-1}$, both IR absorbances have been used to measure water concentrations within the SC (28-30).

The IR absorbances located at ~ 1535 and $\sim 1645\text{ cm}^{-1}$ originate from amide linkages within the SC proteins (31). The amide I band located at $\sim 1645\text{ cm}^{-1}$ corresponds to the carbonyl stretching frequency ($\nu(\text{C=O})$) in the $-\text{CO-NH}$ group. A shift of this IR absorbance to a lower wavenumber may occur if the carbonyl bond is involved in an increased number of hydrogen bonding interactions (i.e. stretching of the C=O bond occurs more easily). On the other hand, the amide II absorbance located at $\sim 1535\text{ cm}^{-1}$ corresponds to an N-H deformation (or bending) frequency ($\delta(\text{N-H})$). Thus, if the amide hydrogen is involved in an increased number of hydrogen bonding interactions the bending mode of the N-H bond becomes more difficult and thus the amide II absorbance may shift to a higher wavenumber.

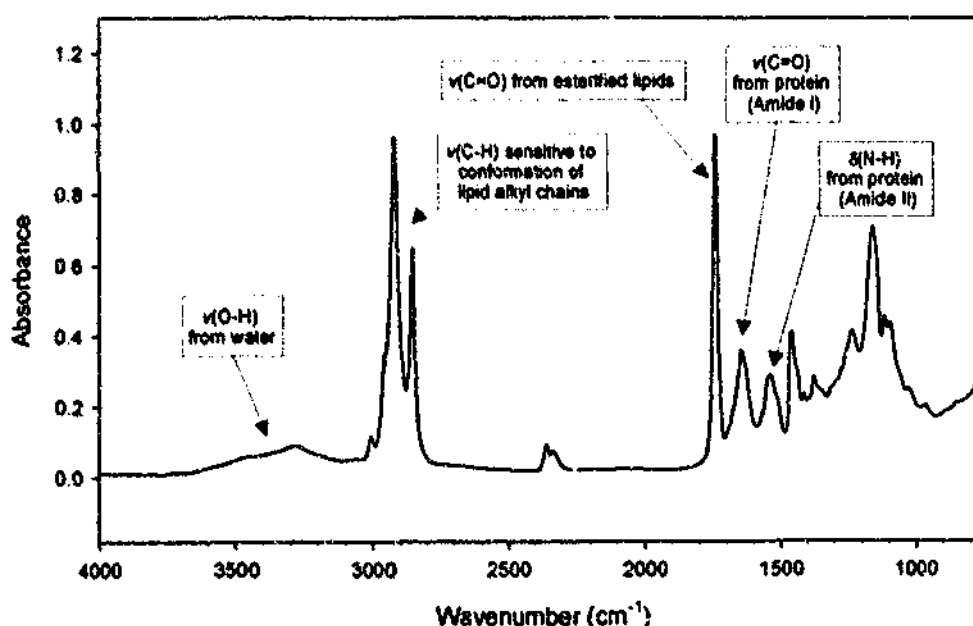


Figure 7.1. A representative ATR-FTIR spectrum of blank human abdominal SC from excised full thickness skin between a wavelength range of 750 to 4000 cm^{-1}

Although the locations of these amide I and amide II absorbances are predominantly influenced by the number of amide linkages involved in hydrogen bonding interactions, analysis of these peak maxima may be confounded by the fact that amide groups are present in both intracellular SC keratin and ceramides contained within the intercellular SC lipid domain (31, 32). However, as extraction of intercellular SC lipids does not appear to affect these amide I and amide II bands, it is believed that the major contribution to these absorbances comes from intracellular keratin (31, 33-35).

The IR absorbances arising from the SC lipids are of particular relevance to the work presented in this chapter. The carbonyl stretching frequency ($\nu(\text{C=O})$) located at $\sim 1740\text{ cm}^{-1}$ is characteristic of ester linkage carbonyls within the polar head-groups of lipids present within the intercellular lipid domain and/or sebaceous lipids residing at the SC surface (28, 36). Analogous to the Amide I $\nu(\text{C=O})$, the position of the lipid-derived $\nu(\text{C=O})$ is sensitive to hydrogen bonding (32, 37). Thus, the lipid-derived $\nu(\text{C=O})$ may provide information on the intra- or inter-molecular hydrogen bonding of the polar head plane of ester lipid bilayers (where a shift of this IR absorbance to a lower wavenumber may occur as a result of increased hydrogen bonding) and/or the structural arrangement of these head-group moieties (32, 37, 38).

The most extensively studied lipid absorbances are those originating from the hydrophobic alkyl chains. In particular, CH_2 symmetric ($\nu_s(\text{CH}_2)$) and asymmetric ($\nu_a(\text{CH}_2)$) stretching frequencies give rise to peak maxima located at ~ 2852 and $\sim 2920\text{ cm}^{-1}$, respectively. Evidence for the assignment of these CH_2 stretching absorbances comes from SC lipid extraction experiments, which demonstrate that removal of the intercellular SC lipids by chloroform-methanol extraction leads to a dramatic decrease ($>95\%$) in the intensity of the CH_2 stretching peaks (39). Further support for the assignment of the ~ 2852 and $\sim 2920\text{ cm}^{-1}$ absorbances to the lipid alkyl chains is provided by temperature-dependent studies (34, 38, 40-42). Upon heating SC samples, the symmetric and asymmetric CH_2 stretching absorbances broaden and shift to higher wavenumbers. In particular, it has been demonstrated that heating the SC from 30 to 115°C results in a sigmoidal relationship between the location of either $\nu_s(\text{CH}_2)$ or $\nu_a(\text{CH}_2)$ and temperature (34, 38, 40-42). At temperatures between 30 and 60°C and above $\sim 80^\circ\text{C}$, there appeared to be only a modest shift to a higher wavenumber. On the other hand, an abrupt increase in to a higher wavenumber was observed at temperatures between ~ 60 and $\sim 80^\circ\text{C}$. Similar trends between $\nu_s(\text{CH}_2)$ or $\nu_a(\text{CH}_2)$ and temperature

have been observed in a variety of lipid systems and have been associated with gel to liquid-crystalline phase transitions, which result in lipid alkyl chain disorder (34, 37, 38).

A brief description of the molecular basis for a shift in the CH₂ stretching frequencies is as follows. In the minimum free-energy state, the lipid alkyl chains adopt an all *trans*-configuration and as such each CH₂ group experiences minimal steric hindrance from neighbouring functional groups (24, 40). However, enhanced mobility of the alkyl chains – as a result of increasing temperature, for example – results in a gel to liquid-crystalline phase transition, forming *gauche* conformers along the alkyl chain. As a result of this configuration, CH₂ stretching is sterically hindered and therefore more energy is required to stretch this bond. Thus, a shift in the CH₂ stretching frequency to a higher wavenumber results when the CH₂ groups along the alkyl chain adopt a *gauche* conformation and the magnitude of this shift is related to the ratio of *gauche* to *trans* conformers (24, 37, 38).

Based on these findings, it is evident that the positions of the CH₂ stretching frequencies are affected by the degree of conformational order and the motional freedom of the lipid alkyl chains (22, 24, 38). Consequently, a shift in a CH₂ stretching frequency to a higher wavenumber (i.e. a blue shift) may be indicative of enhanced mobility, or a decrease in the conformational order, of the lipid alkyl chains.

7.2. OBJECTIVES

As the results presented in Chapters 3, 4 and 5 demonstrated that OS and PO enhance fentanyl permeation through human skin, it was necessary to investigate whether these CPEs reduce the barrier function of the SC by effecting the organisation and/or content of the SC lipids. Thus, the overall objective of the work presented in this chapter was to investigate whether OS and PO reduce the conformational order of the SC lipids and/or extract lipids from the SC using ATR-FTIR.

As the information gathered from an ATR-FTIR spectrum pertains only to the uppermost SC layers that are in contact with the internal reflection element (IRE) (Chapter 6, Section 6.1), the aim of the first set of experiments presented in this chapter was to investigate the concentration- and time-related effects of OS and PO on lipids located within the superficial layers of the SC.

The aim of subsequent experiments presented in this chapter was to use ATR-FTIR in conjunction with the "tape stripping technique" in order to probe the concentration-dependent effects of OS and PO on lipids located within different layers (the upper, middle and lower layers) of the SC.

7.3. MATERIALS AND METHODS

7.3.1. Materials

OS and PO were supplied by Bronson and Jacobs (Australia). All other chemicals were of analytical grade.

7.3.2. Skin preparation

Full-thickness human skin samples were prepared from female abdominal tissue (obtained following abdominoplasty from two individual donors) according to the method described in Section 5.3.2. As mentioned in Section 5.3.2, 1 x 5 cm sections of skin were glued (SC-side up) onto 1 x 7 cm pieces of cardboard. In order to remove sebaceous lipids from the skin surface, the SC surface of each piece of skin was quickly (< 20 sec) wiped with a Kimwipes® (Kimberly-Clark, Australia) that was pre-saturated with 95%v/v ethanol. The skin samples were then left untouched for ~5 min to allow the glue to dry.

7.3.3. Determination of the effects of octisalate and padimate O on lipids located within the superficial layers of the stratum corneum

7.3.3.1. Concentration-dependent studies

Formulations comprised of 95 %v/v ethanol alone (i.e. 0 %w/v OS or PO), or 95 %v/v ethanol containing 1, 2.5, 5, 7.5 or 10 %w/v of OS or PO were applied as a finite dose (5µl/cm²) to the SC surface of 1 x 5 cm sections of human full-thickness skin (n = 5). After a 2 h exposure time, excess formulation was removed from the SC surface using the validated surface wipe procedure described in Section 5.3.4.1. An ATR-FTIR

spectrum of each skin sample was obtained, according to the method described in Section 7.3.5.1, before and after (i.e. after the surface wipe procedure) the formulations were applied to the SC surface.

Experiments were conducted where 1 x 5 cm sections of human full-thickness skin ($n = 5$) were left untreated for a period of 2 h. In order to ensure that untreated skin samples were treated in the same manner as treated skin samples, the surface wipe procedure (described in Section 5.3.4.1) was conducted after the 2 h exposure time. An ATR-FTIR spectrum of each untreated skin sample was obtained, according to the method described in Section 7.3.5.1, before and after (i.e. after the surface wipe procedure) the 2 h exposure time.

7.3.3.2. Time-dependent studies

Formulations comprised of 5 %w/v OS or PO in 95%v/v ethanol were applied as a finite dose ($5\mu\text{l}/\text{cm}^2$) to the SC surface of 1 x 5 cm sections of human full-thickness skin ($n = 5$). The formulations were left in contact with the skin for a period of 0.5, 2, 6, 16 or 24 h. After each pre-determined exposure time, the skin samples were subjected to the validated surface wipe procedure described in Section 5.3.4.1. An ATR-FTIR spectrum of each skin sample was obtained before and after (i.e. after the surface wipe procedure) the designated exposure time, according to the method described in Section 7.3.5.1.

7.3.4. Determination of the concentration-dependent effects of octisalate and padimate O on lipids located within different layers of the stratum corneum

As described in Section 5.3.3, 1 x 5 cm sections of human full-thickness skin were adhered, cardboard-side down, onto a 1.5 x 1.5 x 100 cm (height x width x length) rectangular steel rod using double-sided adhesive tape (Scotch® Permanent Double Stick Tape, 3M, Australia).

The skin samples ($n = 5$) were left untreated or were treated with formulations comprised of 95 %v/v ethanol alone (i.e. 0 %w/v OS or PO), or 95 %v/v ethanol containing 2.5, 5, 7.5 or 10 %w/v of OS or PO. The formulations were applied as a finite dose ($5\mu\text{l}/\text{cm}^2$) to the SC surface and were left in contact with the skin for a 2 h exposure time. Excess formulation was then removed from the SC surface using the validated

surface wipe procedure described in Section 5.3.4.1. The surface wipe procedure was also performed on the untreated skin samples.

Following the surface wipe procedure, layers of the SC were progressively removed by sequential adhesive tape stripping (refer to Section 5.3.3). The tape stripping procedure was repeated 20 times in order to remove most of the SC (43, 44). In order to determine the effects of OS or PO on lipids located within different SC layers, ATR-FTIR spectra were obtained after:

- i. The surface wipe procedure
- ii. Each tape strip, from tape strips 1 to 5
- iii. The 10th, 15th and 20th tape strip

according to the method described in Section 7.3.5.1.

7.3.5. Analytical methods

7.3.5.1. Acquisition of ATR-FTIR spectra

Spectral measurements were made using a horizontal ATR Accessory (Pike Technologies, Inc., Madison, WI, USA) fitted into the sample compartment of an Excalibur™ FTS 3500GX spectrometer (Bio-Rad Laboratories, Inc., Cambridge, MA, USA) that was equipped with a liquid nitrogen-cooled mercury-cadmium-telluride detector. The IRE that was supported by the horizontal ATR Accessory was a flat plate, trapezoidal zinc selenide crystal that was 8 cm long, 1 cm wide and 4 cm thick. The entrance and exit faces of the crystal were each cut at a 45° angle. As mentioned in Section 6.3.2.3.2.1, zinc selenide has a refractive index of 2.4 at 1000 cm⁻¹ and the refractive index of the SC is in the order of ~1.33 to 1.55 (31). Therefore, in the spectral range of interest (from 1000 to 3000 cm⁻¹) the apparent depth by which the evanescent IR beam penetrated the SC may have been in the order of ~1.5 to ~6.9 μm (per Equation 6.1, Chapter 6). As the thickness of the keratinocytes within the SC may be in the order of ~0.8 μm and the vertical gap between the keratinocytes is in the order of ~75 nm (45), the information gathered from an ATR-FTIR spectrum of this nature pertains only to the

superficial SC layers (the uppermost ~1 to ~8 cell layers) that are in contact with the crystal.

In order to obtain an ATR-FTIR spectrum of the skin, each skin sample was placed SC-side down onto the surface of the zinc selenide crystal (refer to Figure 6.3 (Chapter 6)). To achieve intimate and uniform contact between the skin and the crystal, stainless steel weights (total weight 1200 g) were placed on top of the skin whilst an ATR-FTIR scan was conducted. An ATR-FTIR scan was initiated using a computer software package (Merlin Version 2.97, Bio-Rad Laboratories, Inc.). Each spectrum represented an average of 16 scans, obtained at a resolution of 8 cm^{-1} , over a wavelength range from 750 to 4000 cm^{-1} . A period of 30 sec was required to acquire each spectrum. All measurements were conducted under ambient conditions ($23 \pm 1^\circ\text{C}$; 30 to 40% relative humidity).

7.3.5.2. Spectral analysis

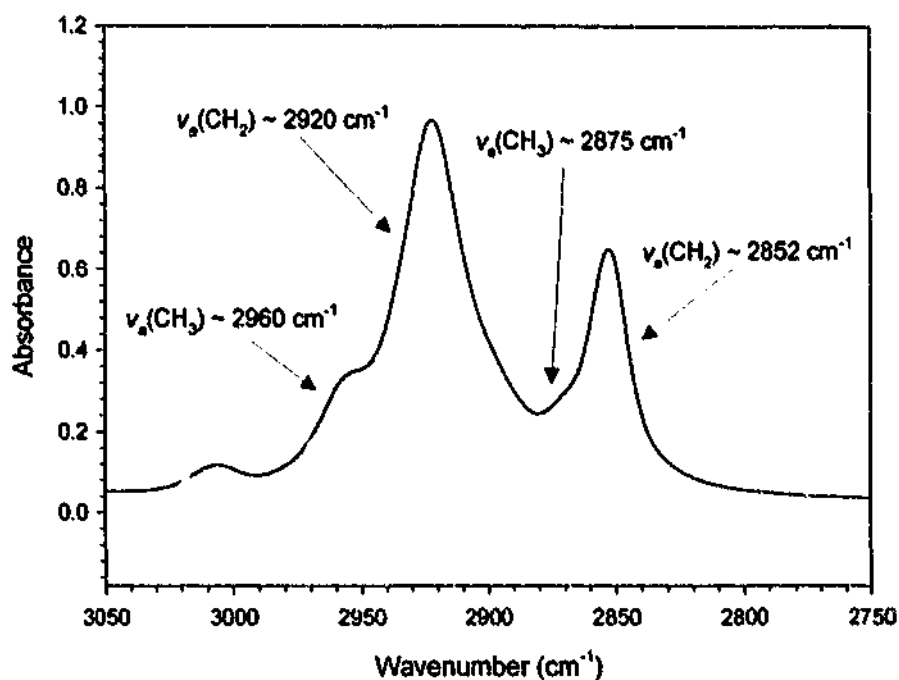
In order to investigate the effects of OS and PO on the SC lipids, attention was focused on the following IR absorbances:

- i. The C=O stretching frequency located at $\sim 1740\text{ cm}^{-1}$
- ii. The CH_2 symmetric and asymmetric stretching frequencies located at ~ 2852 and $\sim 2920\text{ cm}^{-1}$, respectively.

7.3.5.2.1. Deconvolution of the C-H stretching region

As illustrated in Figure 7.2, analysis of $\nu_s(\text{CH}_2)$ and $\nu_a(\text{CH}_2)$ may be confounded by the fact that CH_3 symmetric ($\nu_s(\text{CH}_3)$) and asymmetric ($\nu_a(\text{CH}_3)$) stretching frequencies (which occur at ~ 2875 and $\sim 2960\text{ cm}^{-1}$, respectively) are located on the shoulders of $\nu_s(\text{CH}_2)$ and $\nu_a(\text{CH}_2)$, respectively. Thus, in order to enhance the apparent resolution of the CH_2 and CH_3 stretching frequencies, the region between ~ 2750 and $\sim 3050\text{ cm}^{-1}$ was deconvoluted using a Bessel apodization function with a K-factor of 2, half-bandwidth of 10 and a HW increment of 1. These factors were employed as they appeared to cause minimal spectral distortion during the deconvolution process.

A. ATR-FTIR spectrum between 2750 and 3050 cm^{-1}



B. Deconvoluted ATR-FTIR spectrum between 2750 and 3050 cm^{-1}

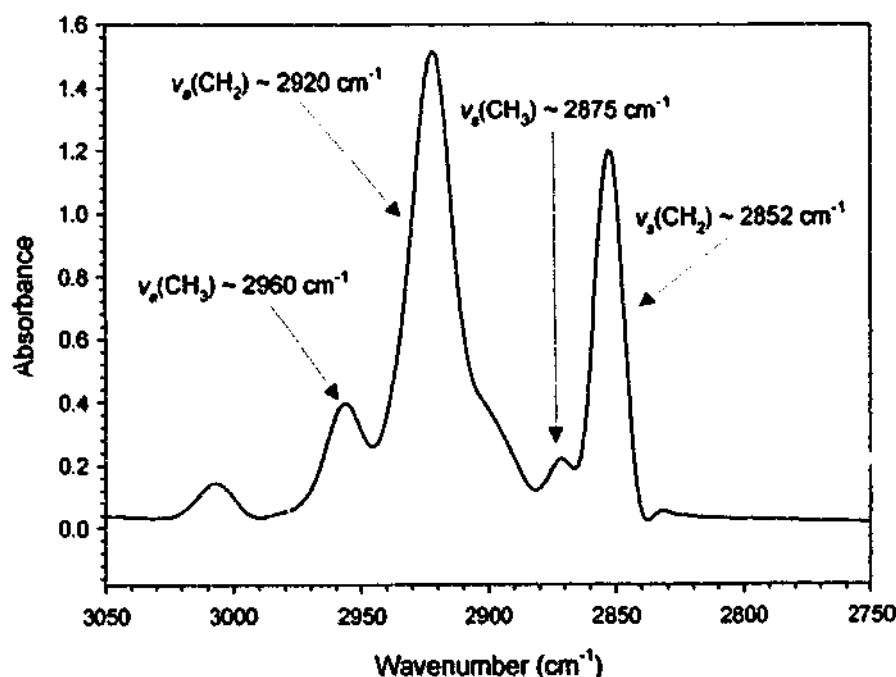


Figure 7.2. Representative ATR-FTIR spectrum of human abdominal SC from excised full-thickness skin within the C-H stretching region, between a wavelength range of 2750 and 3050 cm^{-1} (A). Deconvolution of the spectrum (B) enhances the apparent resolution of the CH_2 and CH_3 symmetric ($\nu_s(\text{CH}_2)$ and $\nu_s(\text{CH}_3)$) and asymmetric ($\nu_a(\text{CH}_2)$ and $\nu_a(\text{CH}_3)$) stretching frequencies.

The spectral parameters (peak frequency maxima (Section 7.3.5.2.2) and peak area or height (Section 7.3.5.2.4)) derived from $\nu_s(\text{CH}_2)$ and $\nu_a(\text{CH}_2)$ pertain to the IR absorbances generated from this deconvolution process.

7.3.5.2.2. Determination of peak frequency maxima

Peak frequency maxima were determined using a center of gravity algorithm, where peak location was determined by the average x-values in the region defined by the peak limits weighted by the spectrum height at each x-value:

$$\text{Peak location} = \frac{\sum x_i y_i}{\sum y_i} \quad 7.1$$

where y_i is the height of the spectrum at wavenumber x_i and all x_i are within the defined region.

7.3.5.2.3. Effects of octisalate and padimate O on the conformational order of stratum corneum lipid bilayers

Phase transitions in SC lipids involving enhanced motional freedom of the hydrocarbon chains (i.e. increased SC lipid fluidity) can be monitored using the bandwidths of the CH_2 stretching absorbances (38, 42, 46, 47), the ratio of the intensities of the CH_2 asymmetric and symmetric absorbances (47) and/or the positions of the CH_2 stretching absorbances (34, 38, 42).

During these studies, the positions of the CH_2 stretching absorbances were used to evaluate the effects of OS and PO on the conformational order of the SC lipid alkyl chains, where it was assumed that a shift of a CH_2 stretching absorbance to a higher wavenumber was due to an increase in the degree of disorder of the lipid alkyl chains (22, 24, 38).

In order to determine the effects of OS and PO on the conformational order of the SC lipid bilayers located within the superficial layers of the SC, peak frequency maxima of $\nu_s(\text{CH}_2)$, $\nu_a(\text{CH}_2)$ and $\nu(\text{C}=\text{O})$ were determined from ATR-FTIR spectra obtained before and after (i.e. after the surface wipe procedure) the SC was left untreated or treated

with OS or PO for a given exposure time. Thus, a shift in the location of an IR absorbance was determined by the difference between the peak frequency maxima calculated before (P_{\max} (before)) and after (P_{\max} (after)) a defined exposure time:

$$\text{Peak shift} = P_{\max}(\text{after}) - P_{\max}(\text{before}) \quad 7.2$$

where P_{\max} (before) and P_{\max} (after) were determined according to the method described in Section 7.3.5.2.2. This approach permitted each piece of skin to act as its own control.

Due to the nature by which ATR-FTIR spectra were acquired during the tape-stripping experiments, it was not possible to use this method of analysis in order to investigate the effects of OS and PO on conformational order of the lipids located in the different layers of the SC (Section 7.3.4). Thus, the effects of OS and PO were evaluated by comparing peak frequency maxima determined from ATR-FTIR spectra of untreated skin (P_{\max} (untreated SC)) to those obtained from spectra of skin treated with OS or PO (P_{\max} (treated SC)):

$$\text{Peak shift} = P_{\max}(\text{treated SC}) - P_{\max}(\text{untreated SC}) \quad 7.3$$

7.3.5.2.4. Effects of octisalate and padimate O on stratum corneum lipid content

Given that:

- i. The intensity of an IR absorbance is directly proportional to the amount of absorbing species (21, 22)
- ii. Changes in the amount of lipids present within the SC have been correlated with the intensity of the CH_2 stretching absorbances (31)
- iii. Removal of SC lipids by chloroform-methanol extraction leads to a decrease in the intensity of the CH_2 stretching absorbances (39, 48)
- iv. Previous researchers have measured changes in the areas and/or heights of CH_2 stretching absorbances in order to evaluate SC lipid extraction caused by solvents or CPEs (13, 49-53)

it was assumed that the integrated intensities of the CH₂ and C=O stretching frequencies would provide a relative measure of the amount of lipid present within the SC. Thus, the areas and heights of these IR absorbances were used to evaluate the effects of OS and PO on SC lipid content.

In order to investigate the effects of OS and PO on the lipid content of the superficial SC layers, the areas and heights of $\nu_s(\text{CH}_2)$, $\nu_a(\text{CH}_2)$ and $\nu(\text{C}=\text{O})$ were determined from ATR-FTIR spectra obtained before and after (i.e. after the surface wipe procedure) the SC was left untreated or treated with OS or PO for a given exposure time. Thus, a decrease (expressed as a percentage (%)) in the area or height of an IR absorbance ($P_{\text{A or Ht decrease}}(\%)$) was determined by the difference between the peak area or height calculated before ($P_{\text{A or Ht}}(\text{before})$) and after ($P_{\text{A or Ht}}(\text{after})$) a defined exposure time:

$$P_{\text{A or Ht decrease}}(\%) = \frac{P_{\text{A or Ht}}(\text{before}) - P_{\text{A or Ht}}(\text{after})}{P_{\text{A or Ht}}(\text{before})} \times 100 \quad 7.4$$

Thus, each piece of skin to acted as its own control. As mentioned in Section 7.3.5.2.3, it was not possible to use this method of analysis in order to investigate the effects of OS and PO on the lipid content of the different SC layers. Thus, $P_{\text{A or Ht decrease}}(\%)$ were calculated by comparing the areas or heights of the IR absorbances arising from ATR-FTIR spectra of untreated skin ($P_{\text{A or Ht}}(\text{untreated SC})$) to those obtained from spectra of skin treated with OS or PO ($P_{\text{A or Ht}}(\text{treated SC})$), where:

$$P_{\text{A or Ht decrease}}(\%) = \frac{P_{\text{A or Ht}}(\text{untreated SC}) - P_{\text{A or Ht}}(\text{treated SC})}{P_{\text{A or Ht}}(\text{untreated SC})} \times 100 \quad 7.5$$

7.3.5.2.5. Uptake of octisalate and padimate O into the superficial layers of the stratum corneum

As discussed in Chapter 6 (Section 6.3.2.3.2), relative amounts of OS or PO within the SC can be quantified using ATR-FTIR. Therefore, in order to determine whether the apparent effects of OS and PO on SC surface lipid content and fluidity were related to the amount of OS or PO taken up into the SC surface layers, the ATR-FTIR spectra

generated from the experiments described in Sections 7.3.3 and 7.3.4 were also used to quantify the amount of OS or PO remaining within the superficial SC layers after a given exposure time (after the surface wipe procedure).

The amounts of OS and PO present within the superficial SC layers after a given exposure time were determined from the peak areas of the IR absorbances located at ~ 1299 and ~ 1276 cm^{-1} (Section 6.3.2.3.2.2), respectively, using the validated ATR-FTIR assays described in Section 6.3.2.3.2.3. Calibration curves were constructed, according to the methods described in Section 6.3.2.3.2.3, on each day of analysis.

As mentioned in Section 6.1, the depth by which the evanescent IR beam penetrates into the SC cannot be defined in absolute terms and consequently an “apparent depth of penetration” is used to approximate the distance at which the incident intensity decreases to 37% of its value at the skin-crystal interface. Furthermore, as mentioned in Section 7.3.5.1, the apparent depth by which the evanescent IR beam penetrated the SC may have been in the order of ~ 1.5 to ~ 6.9 μm during the ATR-FTIR analyses that were performed. Therefore, the amounts of OS and PO that were determined from ATR-FTIR spectra generated from these experiments pertain only to the superficial layers of the SC and are relative (not absolute) measurements.

7.3.6. Statistical analysis

Statistically significant differences between the peak frequency maxima or peak areas and heights obtained before and after a given exposure time were compared using the Student's t-test (two-tailed). Statistical significance between multiple treatment groups (for example, peak shifts obtained following treatment with different concentrations of OS or PO) was determined using one-way analysis of variance (ANOVA), where post-hoc all pairwise multiple comparison of the means within the different groups was performed using the Student-Newman-Keuls (SNK) test.

During all statistical analyses, a probability of $p < 0.05$ was considered statistically significant. All results are presented as the mean \pm SEM, unless otherwise stated.

7.4. RESULTS AND DISCUSSION

7.4.1. The effects of octisalate and padimate O on lipids located within the superficial layers of the stratum corneum

7.4.1.1. Concentration-dependent effects

7.4.1.1.1. Stratum corneum lipid content

The concentration-dependent effects of OS and PO on the peak areas and heights (P_A or H_t) of the CH_2 asymmetric and symmetric stretching frequencies ($\nu_a(CH_2)$ and $\nu_s(CH_2)$) and the $C=O$ stretching frequency ($\nu(C=O)$) are presented in Figures 7.3 and 7.4, respectively. Before commenting on the apparent effects of OS and PO on SC lipid content, it should be noted that:

- i. Leaving the SC untreated for 2 h did not effect the areas and heights of these lipid-derived IR absorbances. This finding was expected as it indicates that exposure of the skin to the atmosphere did not effect SC lipid content. It may also indicate that most, if not all, sebaceous lipids were removed from the SC surface before the experiments were conducted.
- ii. Treating the SC with 95%v/v ethanol (0%w/v OS or PO) resulted in a slight decrease in the areas and heights of $\nu_a(CH_2)$, $\nu_s(CH_2)$ and $\nu(C=O)$ (P_A or H_t decrease (%)) ranged from ~ 3 to $\sim 7\%$. This finding would suggest that ethanol extracts a small amount of lipids from the SC, which is consistent with previous observations (13, 54-56).

The relationship between P_A or H_t decrease (%) and applied OS concentration (%w/v) is presented for the CH_2 and $C=O$ stretching frequencies in Figure 7.3. It is apparent from the graphs presented in Figure 7.3 that there was a linear relationship between P_A or H_t decrease (%) and the concentration of OS that was applied to the SC surface ($r^2 \sim 0.95$, 0.99 and 0.98 for $\nu_a(CH_2)$, $\nu_s(CH_2)$ and $\nu(C=O)$, respectively). This trend would imply that the effect of OS on SC surface lipid content was dependent on its applied concentration.

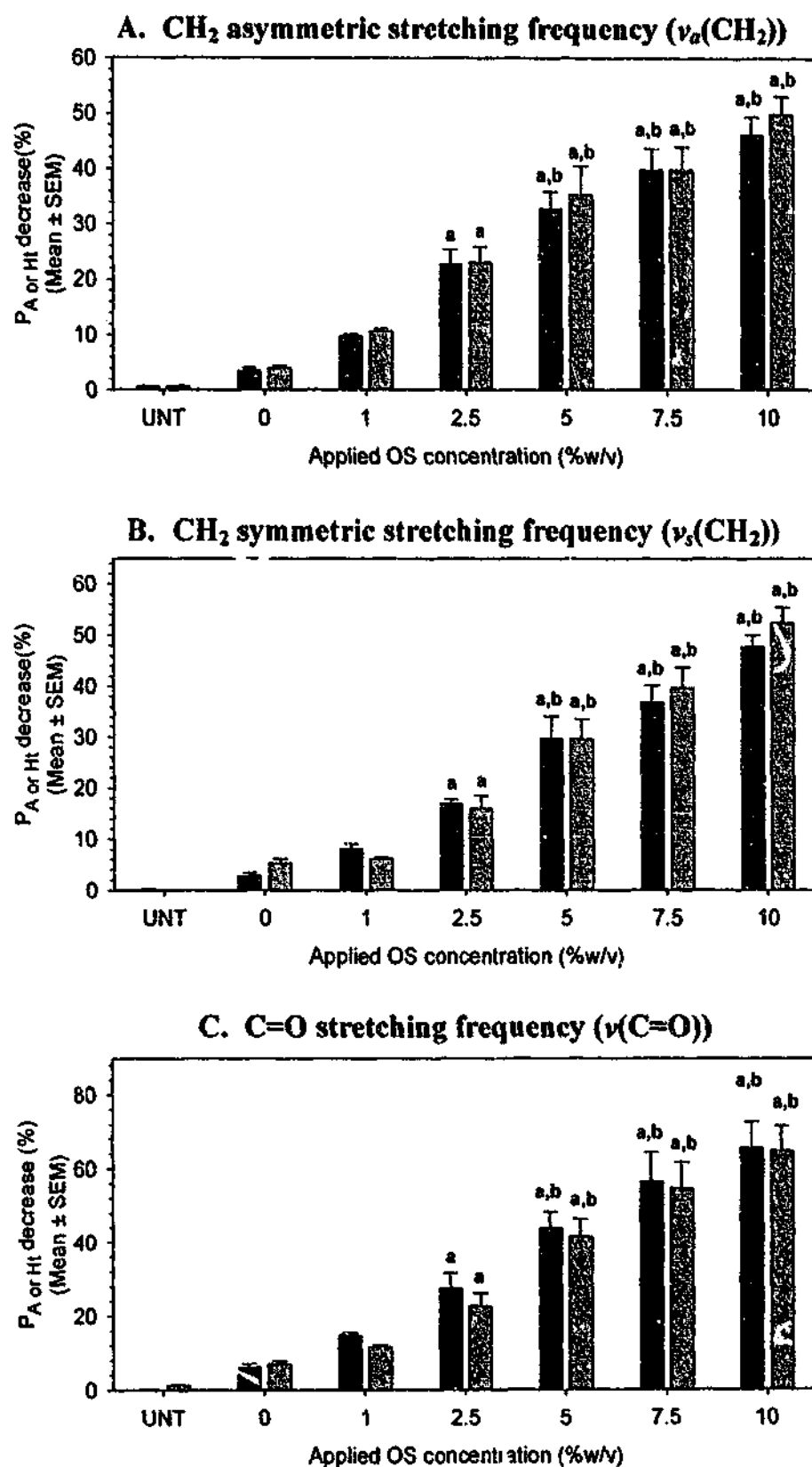


Figure 7.3. The concentration-dependent effects of OS on the peak area (■) and height (▨) of the CH₂ asymmetric stretching frequency (A), the CH₂ symmetric stretching frequency (B) and the C=O stretching frequency (C). The percentage (%) decrease in peak area or height (P_A or H_t decrease (%)) (y-axis) was calculated by comparing the peak areas or heights obtained before and after a 2 h exposure time (Section 7.3.5.2.4). On the x-axis, UNT refers to SC left untreated and 0%w/v OS refers to SC treated with 95%v/v ethanol alone. ^a The % decrease in peak area or height was significantly greater than that obtained after treatment with 95%v/v ethanol alone ($p < 0.05$), ^b Statistically significant difference between the peak areas or heights calculated before and after treatment with OS ($p < 0.05$).

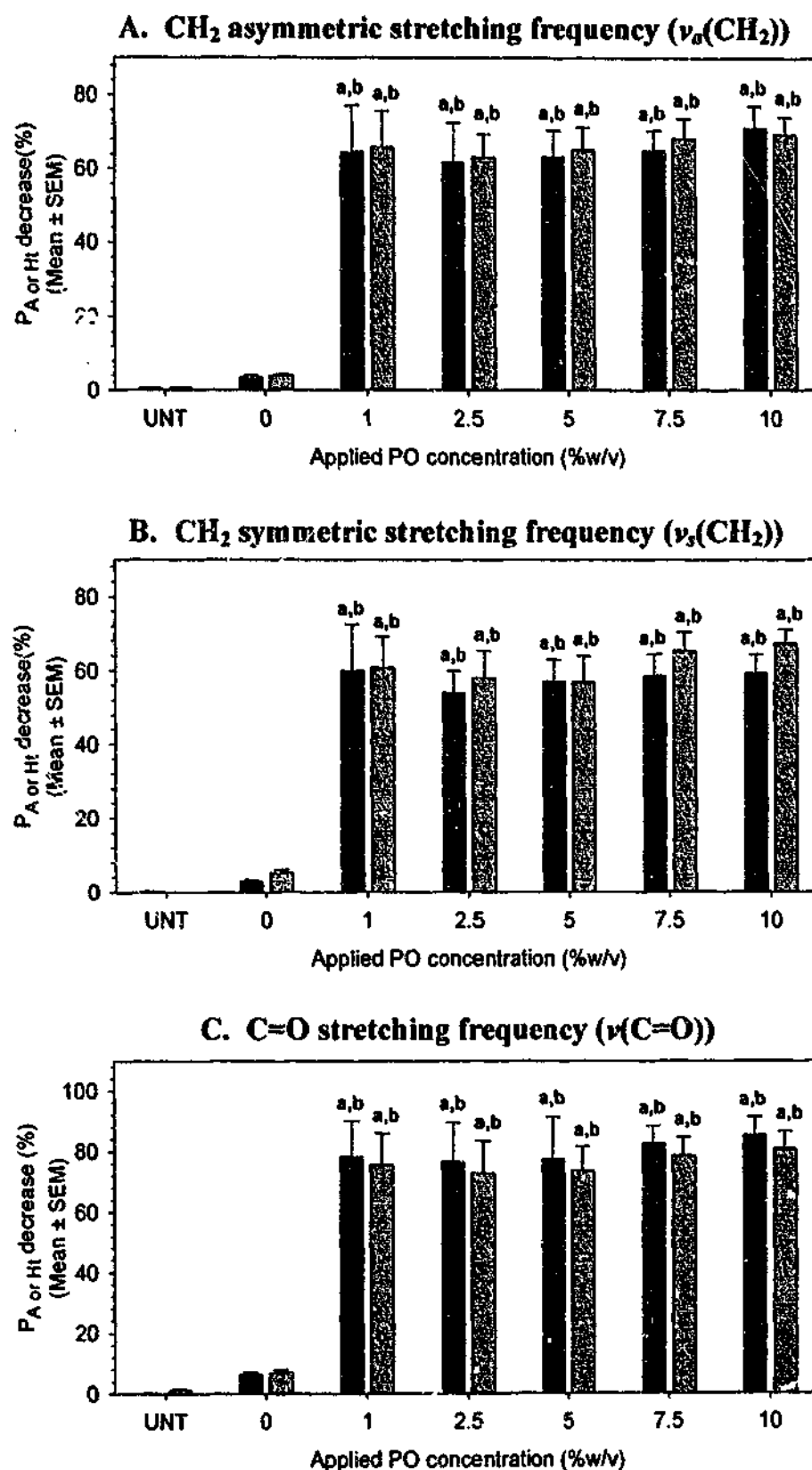


Figure 7.4. The concentration-dependent effects of PO on the peak area (■) and height (▨) of the CH₂ asymmetric stretching frequency (A), the CH₂ symmetric stretching frequency (B) and the C=O stretching frequency (C). The percentage (%) decrease in peak area or height (P_A or H_t decrease (%)) (y-axis) was calculated by comparing the peak areas or heights obtained before and after a 2 h exposure time (Section 7.3.5.2.4). On the x-axis, UNT refers to SC left untreated and 0%w/v PO refers to SC treated with 95%v/v ethanol alone. ^a The % decrease in peak area or height was significantly greater than that obtained after treatment with 95%v/v ethanol alone ($p < 0.05$), ^b Statistically significant difference between the peak areas or heights calculated before and after treatment with PO ($p < 0.05$).

Therefore, it would seem that SC lipid content was only marginally reduced following the topical application of low ($\leq 2.5\%w/v$) OS concentrations (there was not a statistically significant difference between the peak areas or heights determined before and after the SC was treated with 1 or $2.5\%w/v$ OS). However, when the applied concentration of OS was increased from $2.5\%w/v$ to up to $10\%w/v$ there did appear to be a significant reduction in SC lipid content (compared with the areas and heights of the lipid-derived IR absorbances that were determined before OS treatment, peak areas and heights were significantly ($p < 0.05$) lower after the SC was treated for 2 h with 5, 7.5 or $10\%w/v$ OS).

In contrast to the relationship that was observed between $P_{A \text{ or } Ht}$ decrease (%) and applied OS concentration, there did not appear to be a linear correlation between $P_{A \text{ or } Ht}$ decrease (%) and the applied concentration of PO (Figure 7.4). It is also evident from the graphs presented in Figure 7.4 that, compared with peak areas and heights determined before treatment with PO, peak areas and heights were significantly lower after the topical application of 1 to $10\%w/v$ PO ($p < 0.05$). Thus, it would seem that PO significantly reduced SC lipid content and that this effect was saturable within the concentration range investigated.

It is also worth noting that at any given concentration $\nu_s(CH_2)$ and $\nu_a(CH_2)$ $P_{A \text{ or } Ht}$ decreases (%) that were observed after the topical application of PO were significantly greater than the $P_{A \text{ or } Ht}$ decreases (%) that were evident after the topical application of OS ($p < 0.05$). This finding may imply that – within the concentration range investigated – PO reduced SC surface lipid content to a greater extent than did OS. Due to the different concentration-dependent relationships that were apparent, the greater lipid-reducing effect of PO was most obvious when low ($\leq 2.5\%w/v$) concentrations of OS or PO were applied to the skin. For instance, the areas and heights of the CH_2 stretching frequencies decreased by $\sim 10\%$ and $\sim 20\%$ following the topical application of 1% and $2.5\%w/v$ OS, respectively. On the other hand, treatment of the SC with 1 or $2.5\%w/v$ PO resulted in $P_{A \text{ or } Ht}$ decreases that were in the order of $\sim 60\%$. However, even at the highest concentration investigated ($10\%w/v$), whereby OS appeared to exert its greatest effect on SC lipid content, the effect of PO was still superior as ($P_{A \text{ or } Ht}$ decreases were of the order of $\sim 50\%$ and 60 to 70 % following treatment of the SC with $10\%w/v$ OS or 1 to $10\%w/v$ PO, respectively).

A final point to note is that $P_{A \text{ or } H}$ decreases that were observed for either 2.5 to 10%w/v OS or 1 to 10%w/v PO were significantly greater than those observed for 95%v/v ethanol alone ($p < 0.05$). This is quite an important finding as it would imply that the presence of 95%v/v ethanol within the applied formulation did not significantly contribute to the apparent effects of OS (at applied concentrations at or above 2.5%w/v) and PO on SC surface lipid content.

7.4.1.1.2. Conformational order of the stratum corneum lipid bilayers

Shifts in the location of $\nu_a(\text{CH}_2)$, $\nu_s(\text{CH}_2)$ or $\nu(\text{C}=\text{O})$ are plotted as a function of applied OS or PO concentration in Figures 7.5 and 7.6, respectively. Not surprisingly, leaving the skin untreated for 2 h did not effect the location of any of these IR absorbances. However, treating the skin with 95%v/v ethanol resulted in a slight decrease in the locations of $\nu_a(\text{CH}_2)$ and $\nu_s(\text{CH}_2)$ and a significant increase in the location of $\nu(\text{C}=\text{O})$. These observations are in agreement with the results generated from previous FTIR studies, where a slight decrease in the peak frequency of $\nu_a(\text{CH}_2)$ was observed following treatment of the SC with absolute ethanol (13). It was proposed that such a shift was indicative of a slight ordering, rather than a disordering, of the intercellular lipid acyl chains. A plausible explanation for this apparent "ordering" effect is that ethanol promotes the interdigitation of the of the hydrocarbon chains by displacing bound water molecules at the polar head-group/membrane interface (13, 57, 58). The observation that the peak frequency maximum of the C=O stretching absorbance shifted to a higher wavenumber post- ethanol treatment may provide further support for this explanation, as it could indicate that fewer polar head-group carbonyls were involved in hydrogen bonding interactions – an effect which could possibly be due to dehydration of the polar head-group region.

It is evident from Figures 7.5.A and 7.5.B that the CH_2 stretching frequencies shifted to higher wavenumbers following treatment of the SC with OS. Compared with peak frequency maxima determined before treatment, the peak frequency maxima of $\nu_a(\text{CH}_2)$ and $\nu_s(\text{CH}_2)$ were significantly higher following treatment with 1 to 10%w/v OS or 2.5 to 10%w/v OS, respectively ($p < 0.05$).

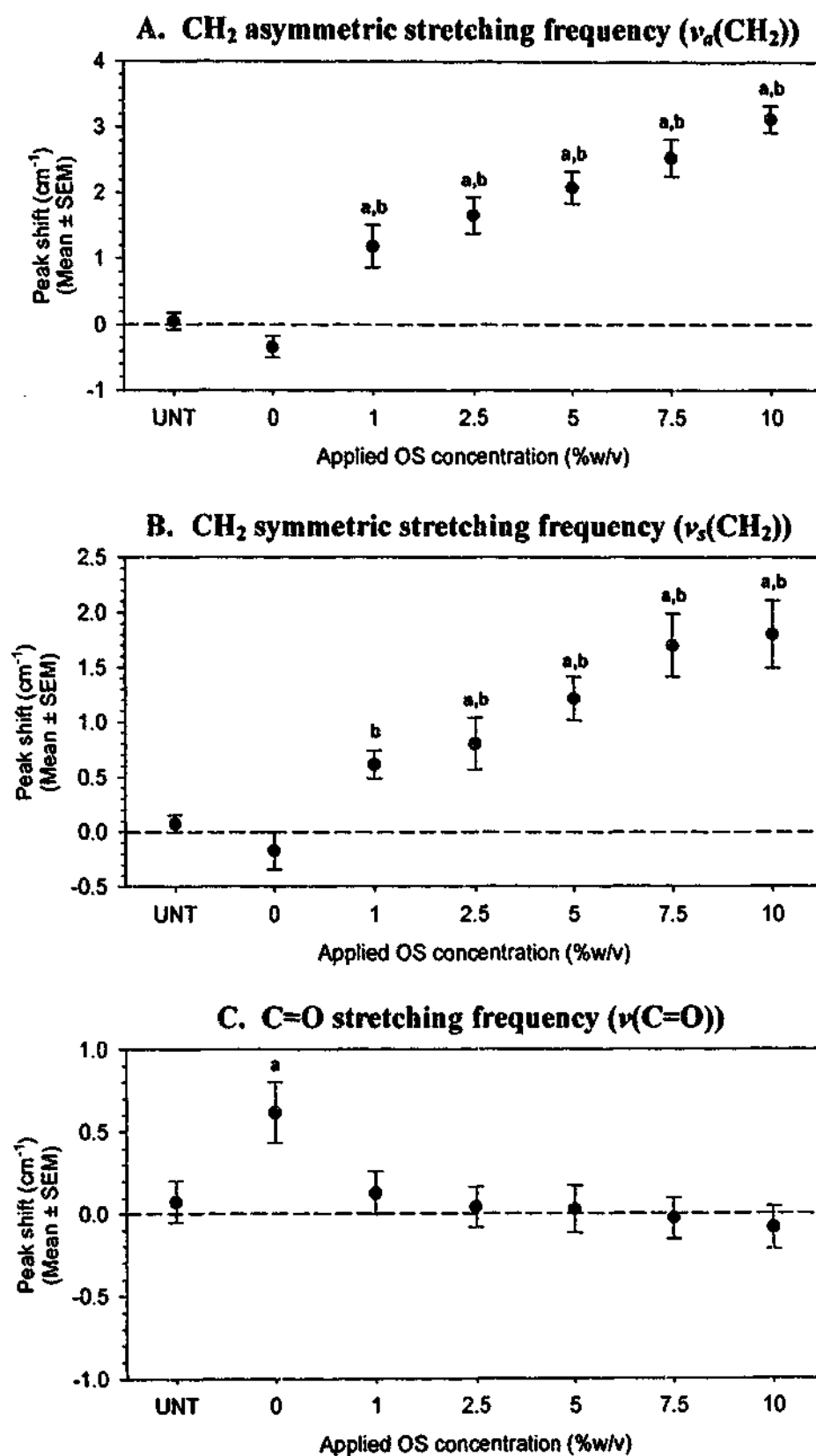


Figure 7.5. The concentration-dependent effects of OS on the location of the CH₂ asymmetric stretching frequency (A), the CH₂ symmetric stretching frequency (B) and the C=O stretching frequency (C). Peak shifts (y-axis) were calculated by comparing peak frequency maxima before and after treatment with OS (Section 7.3.5.2.3). On the x-axis, UNT refers to SC left untreated and 0%w/v OS refers to SC treated with 95%v/v ethanol alone. ^a Statistically significant difference between the peak frequency maximum calculated before and after treatment with OS (or 95%v/v ethanol alone) ($p < 0.05$). ^b The magnitude of the peak shift was significantly greater than that obtained after treatment with 95%v/v ethanol alone ($p < 0.05$).

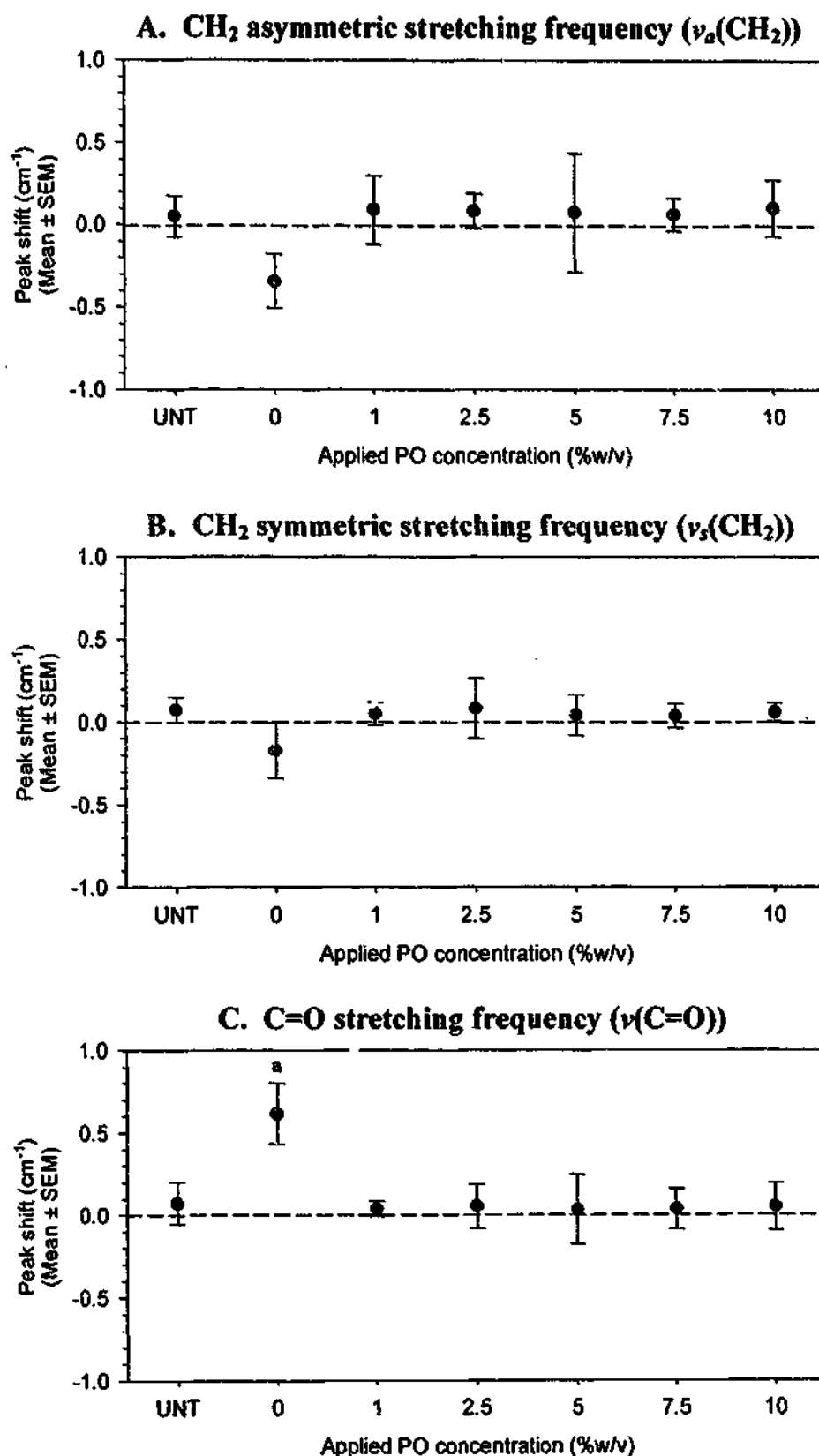


Figure 7.6. The concentration-dependent effects of PO on the location of the CH₂ asymmetric stretching frequency (A), the CH₂ symmetric stretching frequency (B) and the C=O stretching frequency (C). Peak shifts (y-axis) were calculated by comparing peak frequency maxima before and after treatment with PO (Section 7.3.5.2.3). On the x-axis, UNT refers to SC left untreated and 0%w/v PO refers to SC treated with 95%v/v ethanol alone. ^a Statistically significant difference between the peak frequency maximum calculated before and after treatment with PO (or 95%v/v ethanol alone) ($p < 0.05$). ^b The magnitude of the peak shift was significantly greater than that obtained after treatment with 95%v/v ethanol alone ($p < 0.05$).

Furthermore, the magnitudes of these blue shifts appeared to be linearly dependent on the applied concentration of OS ($r^2 = 0.993$ and 0.968 for $\nu_a(\text{CH}_2)$ and $\nu_s(\text{CH}_2)$, respectively). Consequently, maximum peak shifts were observed following the topical application of 10%w/v OS, whereby the locations of $\nu_a(\text{CH}_2)$ and $\nu_s(\text{CH}_2)$ shifted by $+3.13 \pm 0.20 \text{ cm}^{-1}$ and by $+1.80 \pm 0.31 \text{ cm}^{-1}$, respectively. On the other hand, it is evident from Figure 7.5.C that the location of $\nu(\text{C=O})$ was unaffected by treatment of the SC with any concentration of OS.

In contrast to the effects of OS on the peak frequency maxima of $\nu_a(\text{CH}_2)$ and $\nu_s(\text{CH}_2)$, it is evident from Figures 7.6.A and 7.6.B that PO did not exert any effect on the locations of the CH_2 stretching frequencies at any applied concentration investigation. However, a similarity that is apparent between OS and PO is that treatment of the SC with any concentration of PO also did not effect the position of $\nu(\text{C=O})$ (Figure 7.6.C).

It was discussed in Section 7.1 that blue shifts of the CH_2 stretching frequencies may be indicative of enhanced lipid alkyl chain mobility. Therefore, peak shifts of this nature may characterise the transition of the SC lipid lamellae from a gel-like phase to a liquid-crystalline phase. Thus, it would appear from the data presented in Figures 7.5 and 7.6 that OS, but not PO, may reduce the conformational order (or increase the fluidity) of the intercellular lipid bilayers. Furthermore, it would seem that the number of *gauche* conformers in the intercellular lipid alkyl chains may increase as the applied concentration of OS increases.

Given that OS and PO appeared to exert different concentration-dependent effects on fentanyl permeation and partitioning (Chapter 4), it is not surprising to find that they also seem to elicit different effects on the conformational order of the SC lipid bilayers. In fact, one explanation for the different concentration-dependent effects of OS and PO that was offered in Chapter 4 – which appears to be supported by the results presented in Figures 7.5 and 7.6 – was related to the possibility that OS and PO interact differently with the SC components (Section 4.4.6.2). As discussed in greater detail in Section 4.4.6.2, differences between the effects of OS and PO could be related to the possibility that *para*- (versus *ortho*-) substitution on the PO phenyl ring may reduce the potential for PO to interact with the SC lipid bilayers and/or the possibility that OS and PO might be located at different regions within the lipid lamellae.

It was also mentioned in Section 4.4.6.2 that a possible mechanism by which CPEs can alter the conformational order of the SC lipid bilayers is by modification of hydrogen

bonding within the SC lipids. As ceramide 6 is believed to be the most powerful hydrogen bonding lipid (59), it is thought that binding between ceramide 6 molecules represents the strongest intermolecular bonding possible between the SC lipids (60). It has therefore been proposed that in order for a modifier with a long hydrocarbon chain to intercalate between adjacent ceramide molecules it must compete effectively for hydrogen bonding sites in the head-group of the lipid molecule (60). For instance, the CPEs Azone[®] and N-0539 were found to enhance solute permeation through human full-thickness skin and reduce the phase transition temperature of multilamellar dipalmitoyl phosphatidylcholine (DPPC) liposomes (60). These CPEs were estimated to have hydrogen bonding donor (α) and acceptor (β) values of 0 and ~ 0.78 units, respectively. As the strength of ceramide-ceramide bonds was estimated to be ~ 0.18 units (i.e. $\alpha \times \beta$, where $\alpha = 0.33$ and $\beta = 0.56$), it was hypothesised that Azone[®] and N-0539 can bind firmly to a ceramide molecule, displacing the molecule and creating a region of fluidity in the lamellae (i.e. the hydrogen-bond strength of either enhancer to a ceramide alcohol ($0.78 \times 0.33 = 0.26$ units) would be greater than that between two ceramide alcohols (0.18 units)). On the other hand, it was found that the Azone[®] analogue N-0721 exerted a negligible effect on solute permeation and only caused a moderate increase in the phase transition of DPPC liposomes. As it was estimated that N-0721 would have a binding strength of ~ 0.15 units, it was hypothesised that N-0721 would be less efficient at displacing ceramide molecules. As OS and PO appear to possess different hydrogen bonding characteristics, it is possible that a similar phenomenon was responsible for the different effects that OS and PO appear to exert on the conformational order of the SC surface lipids.

The hydrogen bonding strengths of OS and PO are estimated to be $\alpha = 0.29$ and $\beta = 0.63$ units and $\alpha = 0.02$ and $\beta = 0.37$ units, respectively¹. These values would give OS hydrogen bonding strengths of 0.16 and 0.21 units to the secondary alcohols on adjacent ceramide molecules. Thus, it is possible that – like Azone[®] and N-0539 – OS can bind firmly to adjacent ceramide molecules, resulting in displaced or “unbound” lipid molecules within the lamellae, which may effectively increase the overall fluidity of the intercellular lipid domain. On the other hand, the hydrogen bonding strengths of PO to ceramide molecules would be in the order of 0.01 and 0.12 units. It is therefore likely that

¹ Estimated using Molecular Modeling Pro (Version 5.1.7) (ChemSW[®] Inc, Fairfield, CA, USA).

PO behaves more like N-0721 in that is less efficient at binding to (and therefore displacing) ceramide molecules.

Although the above-mentioned hypotheses relate to the binding of OS and PO to secondary alcohols on adjacent ceramide molecules, it would appear from the data presented for the lipid-derived C=O stretching frequency presented in Figures 7.5.C and 7.6.C that neither OS nor PO interact with the carbonyls of the lipid polar head-groups. As the position of the C=O stretching frequency is sensitive to changes in hydrogen bonding, the finding that neither OS nor PO caused this frequency to shift to a lower wavenumber finding may suggest that if OS or PO did exert a restructuring effect on the polar head-group and/or lipid alkyl chain region of the SC lipid bilayers, this effect may not have been due to the formation of strong hydrogen bonds between OS or PO and the carbonyl groups of the lipid polar head region. Given that the carbonyl moieties of the lipid polar head-groups can serve as hydrogen bond acceptors, this finding is consistent with the α and β values calculated for OS and PO as it may indicate that neither OS nor PO act as strong hydrogen bond donors within the SC. However, these conclusions may be confounded by the fact i) in addition to the intercellular lipids, sebum may also contribute to the lipid-derived C=O stretching frequencies detected within the superficial layers of the SC (as mentioned in Section 7.4.2.3) and/or ii) if OS or PO did hydrogen-bond with the carbonyls of the lipid polar head-groups, it is possible that this interaction may not have been reflected by a red shift of the carbonyl stretching frequency due to the presence of ethanol within the SC, which can cause the carbonyl stretching frequency to shift to a higher wavenumber (i.e. the apparent effects of OS or PO may have been offset by the effects of ethanol).

Another potential artifact associated with these ATR-FTIR analyses is related to the possibility that the IR absorbances generated from OS and PO could interfere with the absorbances that arise from the SC lipids. As stated in Section 6.3.2.3.2.2, both OS and PO give rise to CH₂ asymmetric and symmetric stretching absorbances that coincide with those generated by the SC lipid alkyl chains. Furthermore, the CH₂ asymmetric and symmetric stretching frequencies that arise from OS and PO are centered at slightly higher wavenumbers compared with those derived from the SC lipids (refer to Figures 6.4 (Chapter 6) and 7.2). However, given that:

- i. Excess OS or PO was removed from the SC surface (using a validated surface wipe procedure) before the ATR-FTIR scans were acquired
- ii. PO did not cause the CH₂ stretching frequencies to shift to higher wavenumbers although, like OS, it also has potentially interfering IR absorbances

it would appear that any spectral interference caused by OS or PO may not have significantly effected the locations of the CH₂ stretching frequencies derived from the SC lipids. Furthermore, the CH₂ asymmetric and symmetric stretching frequencies that arise from OS are located at ~2925 and ~2857 cm⁻¹, respectively, whilst the peak frequency maxima of the CH₂ asymmetric and symmetric stretching frequencies that arise from the SC lipids are ~2920 and ~2850 cm⁻¹, respectively (Figures 6.4 and 7.2). As there is an equal difference (~5 cm⁻¹) between either of the CH₂ stretching frequencies that arise from OS and the SC lipids, it would be expected that if the presence of OS did artificially shift the SC-derived CH₂ stretching frequencies to higher wavenumbers, the location of the SC-derived $\nu_a(\text{CH}_2)$ would be shifted by approximately the same extent as the SC-derived $\nu_s(\text{CH}_2)$. However, the data presented in Figures 7.5.A and 7.5.B demonstrate that the magnitude by which OS shifted the peak frequency maximum of the lipid-derived $\nu_a(\text{CH}_2)$ was greater than its effect on the location of $\nu_s(\text{CH}_2)$. Since the CH₂ asymmetric stretching frequency is more sensitive to changes in the conformational order of the SC lipid bilayers than the CH₂ symmetric stretching frequency (61, 62), it seems more likely that the elicited peak shifts were due to changes in the conformational order of the SC lipid bilayers rather than interference caused by the IR absorbances derived from OS.

It would also seem that if the presence of OS or PO within the SC significantly contributed to the areas or heights that were determined for the SC-derived CH₂ stretching absorbances (Figures 7.3 and 7.4), then the apparent effects of OS and PO on SC surface lipid content may have been underestimated. However, as significant reductions in SC surface lipid content were apparent, it would appear that the contribution of the OS or PO-derived CH₂ stretching absorbances was relatively inconspicuous.

Although the above-mentioned findings would indicate that the IR absorbances arising from OS or PO did not significantly effect the intensities and locations of the CH₂ stretching frequencies generated from the SC lipids, there is a possibility that the IR data

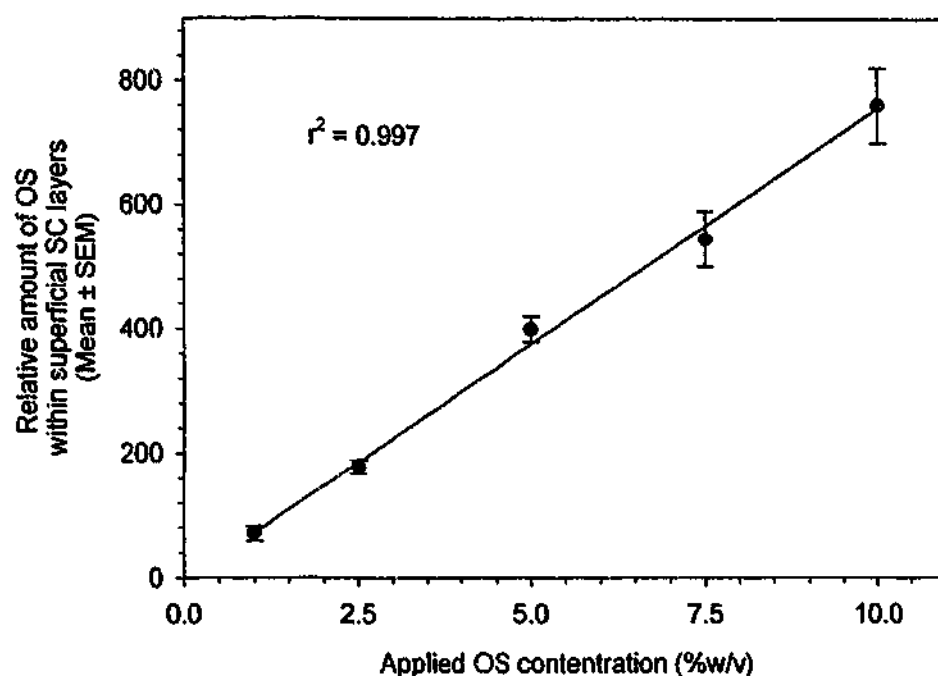
obtained from these studies was confounded by some spectral interference. Thus, in order to confirm the conclusions that were drawn from these analyses, further ATR-FTIR studies will need to be conducted using deuterated OS and PO. The value of using deuterated enhancers during mechanistic ATR-FTIR investigations is based on the fact that the isotopic substitution of deuterium for hydrogen effectively shifts the interfering CH₂ stretching frequencies to lower wavenumbers (into a region of the ATR-FTIR spectrum that is devoid of SC lipid absorbances) (24, 35).

Previous ATR-FTIR investigations into the modes of action of oleic acid and Azone® exemplify how the use of a deuterated enhancer enables the discriminative analysis of SC lipid-derived CH₂ stretching absorbances and the elucidation of the possible mechanism(s) of action of a CPE. For instance, ATR-FTIR investigations into the interactions between perdeuterated oleic acid and SC lipids have provided evidence that oleic acid does not modify the conformational order of the SC lipids, which is in contrast to the results from previous ATR-FTIR investigations into mechanisms of action of non-deuterated oleic acid (16, 63). Rather, perdeuterated oleic acid was found to exist as a separate fluid phase within the “gel phase” of the SC lipid lamellae. On the other hand, ATR-FTIR investigations into the effect(s) of Azone® and its perdeuterated analogue have demonstrated that they both appear to increase the fluidity of the SC lipids (64), which would indicate that, unlike oleic acid, Azone® is homogeneously distributed within the SC lipids (65). It is evident from these previous investigations that future ATR-FTIR studies using deuterated analogues of OS and PO could provide information that contributes towards an understanding of their mechanism(s) of action.

7.4.1.1.3. Uptake of octisalate and padimate O into the superficial layers of the stratum corneum

The relative amounts of OS and PO present within the surface SC layers that were determined from the ATR-FTIR spectra acquired after treatment of the SC with OS or PO are presented in Figure 7.7. As these spectra were acquired after the surface wipe procedure, these measurements reflect the amount of OS or PO taken up *into* the superficial layers of the SC – not the amount of OS or PO remaining *on* the SC surface – after a 2 h exposure time.

A. OS



B. PO

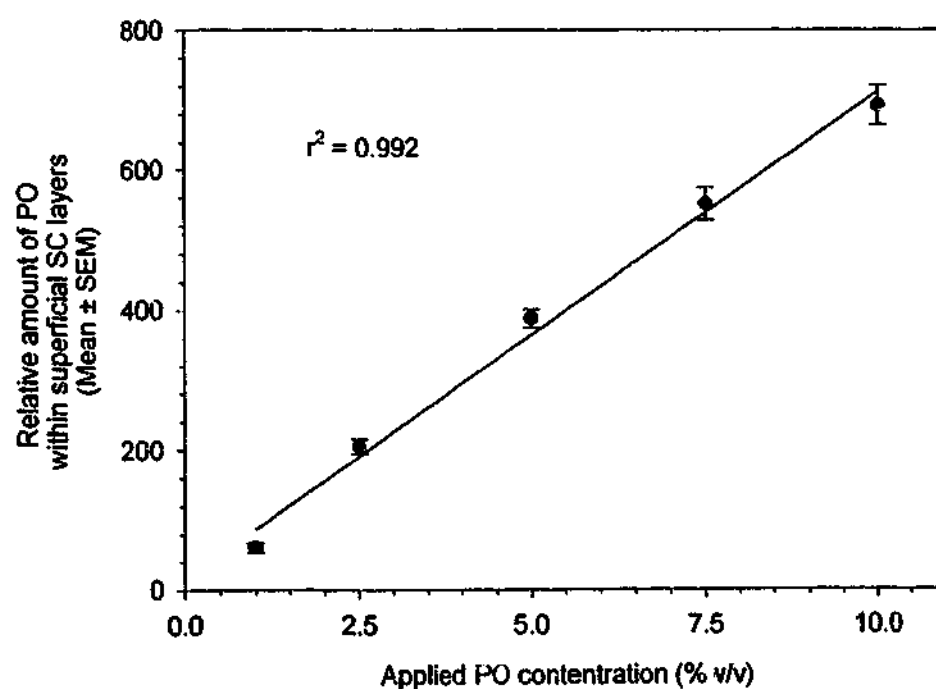


Figure 7.7. The amount of OS (A) or PO (B) taken up into the superficial layers of the SC 2 h after the topical application of formulations containing different concentrations of OS or PO. As the amounts of OS and PO taken up into the superficial SC layers were determined using ATR-FTIR, these amounts are relative measurements. The solid line represents linear regression of the data.

It is evident from Figure 7.7 that the relative amount of either OS or PO that partitioned into the superficial layers of the SC (after a 2 h exposure time) was linearly related to the concentration of OS or PO within the applied formulation ($r^2 = 0.997$ and 0.992 for OS and PO, respectively). As it was ascertained from the data presented Figures 7.3 and 7.5 that the effects of OS on the areas, heights and peak frequency maxima of the CH_2 stretching absorbances were also linearly related to the concentration of OS within the applied formulation, it would seem that apparent effects of OS on SC surface lipid content and fluidity were dependent on the amount of OS taken up into the superficial layers of the SC.

The uptake of PO also appeared to be linearly related to its applied concentration (Figure 7.7.B). However, it was evident from the data presented in Figure 7.4 that degree by which PO reduced the areas and heights of the lipid-derived IR absorbances was unrelated to its applied concentration. Thus, it would seem that the lipid-reducing effect of PO became saturated when it was applied to the SC surface at concentrations between 1 and 10%w/v.

7.4.1.2. Time-related effects

7.4.1.2.1. Stratum corneum lipid content

The time-related effects of OS and PO on the areas and heights of the CH_2 stretching frequencies and the $\text{C}=\text{O}$ stretching frequency are presented in Figures 7.8 and 7.9, respectively. It is evident from Figure 7.8 that exposure of the SC to 5%w/v OS for any period of time between 0.5 and 24 h resulted in a decrease in the areas and heights of $\nu_a(\text{CH}_2)$, $\nu_s(\text{CH}_2)$ and $\nu(\text{C}=\text{O})$ by approximately ~47%, ~52% and ~62%, respectively ($p < 0.05$ compared with the peak areas or heights determined before treatment). As treatment of the SC with OS decreased the peak areas and heights by approximately the same extent at all exposure times, it would appear that significant amounts of lipids were extracted from the superficial layers of the SC shortly (0.5 h) after the topical application of OS and that the magnitude of this effect remained relatively constant within a 24 h exposure time.

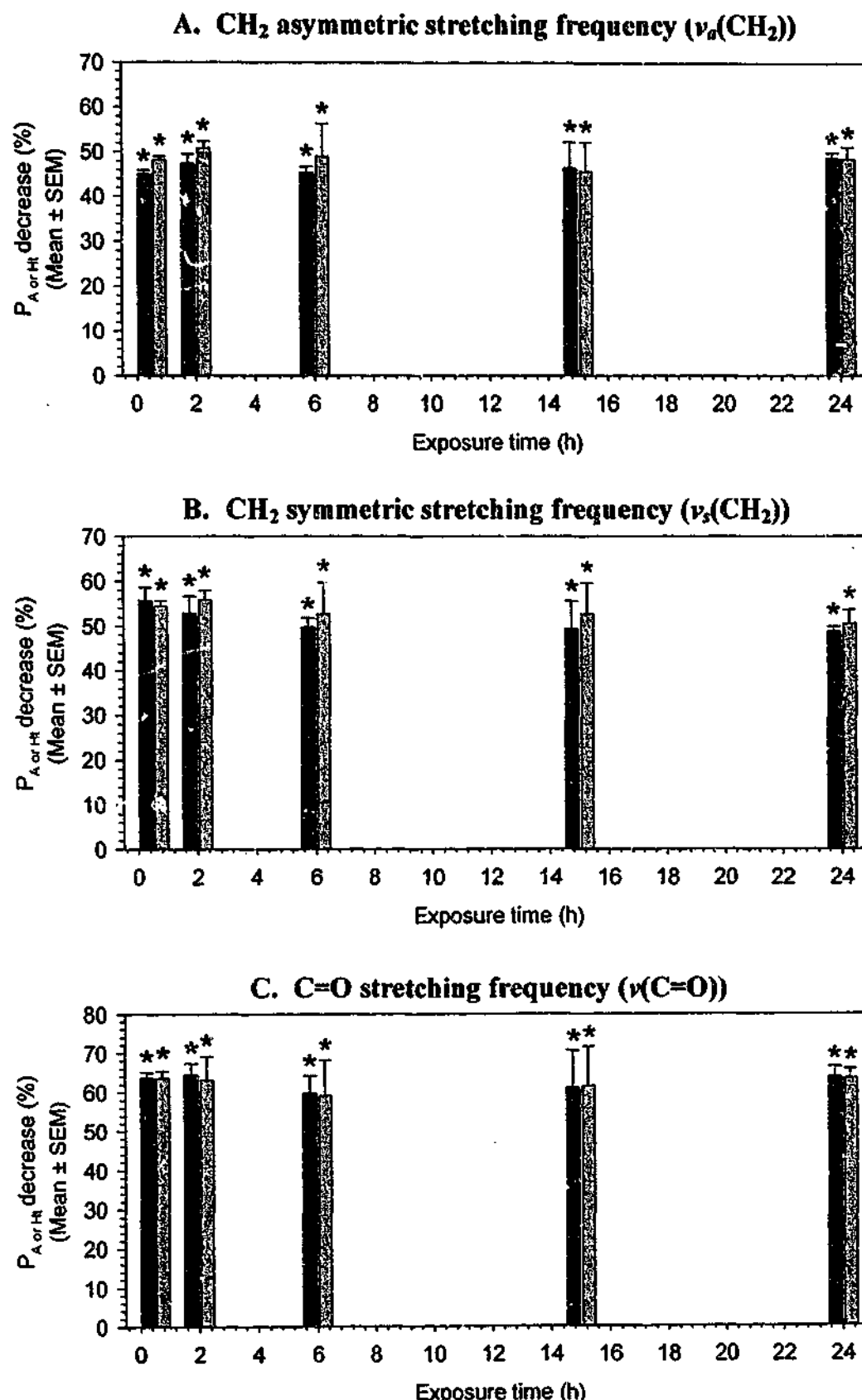


Figure 7.8. The time-related effects of OS on the peak area (■) and height (▨) of the CH₂ asymmetric stretching frequency (A), the CH₂ symmetric stretching frequency (B) and the C=O stretching frequency (C). The percentage (%) decrease in peak area or height (P_A or H_t decrease (%)) (y-axis) was calculated by comparing the peak areas or heights obtained before and after a defined exposure time (x-axis) (Section 7.3.5.2.4). * Statistically significant difference between the peak areas or heights calculated before and after the SC was treated with OS (p<0.05).

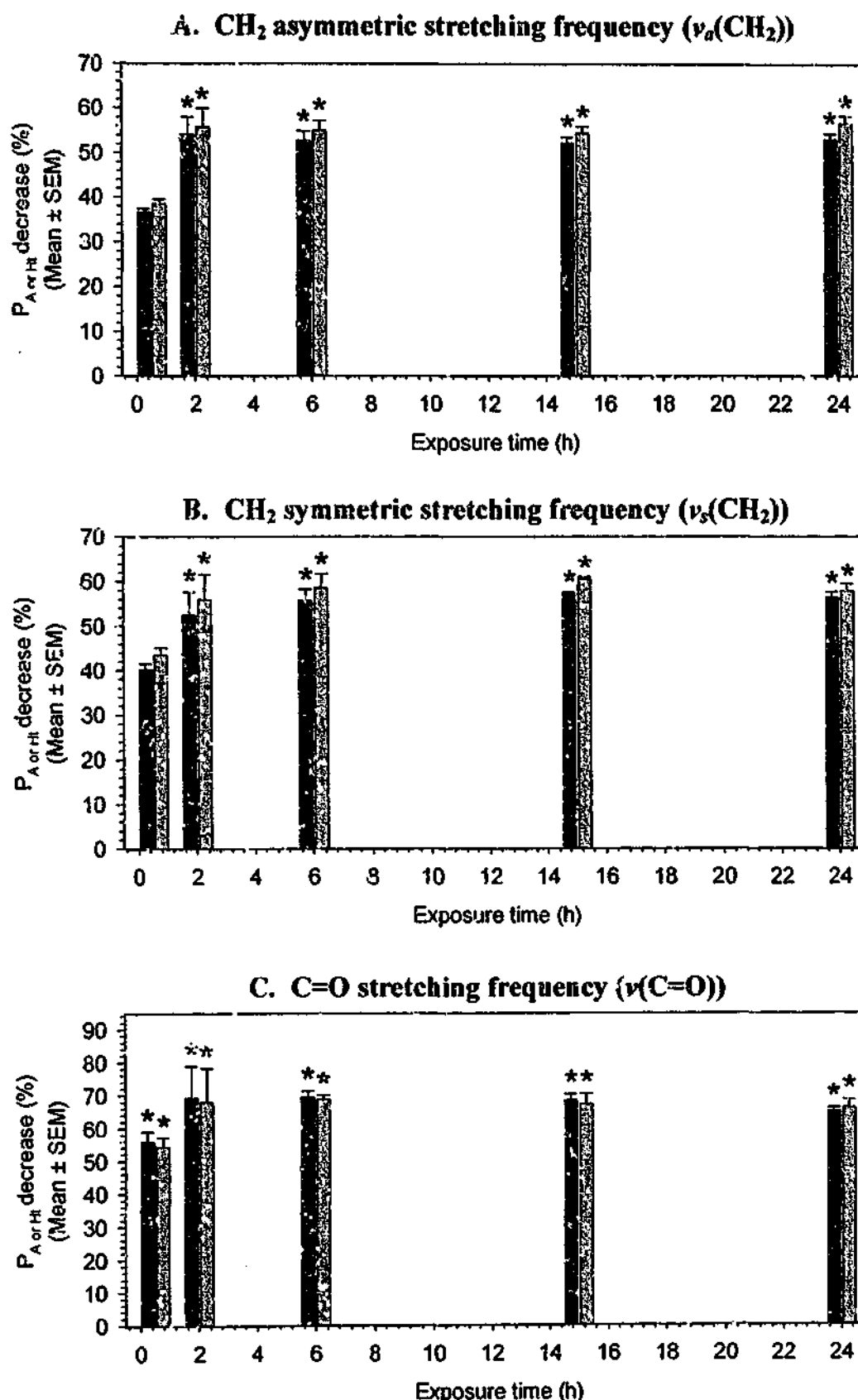


Figure 7.9. The time-related effects of PO on the peak area (■) and height (▨) of the CH₂ asymmetric stretching frequency (A), the CH₂ symmetric stretching frequency (B) and the C=O stretching frequency (C). The percentage (%) decrease in peak area or height (P_{A or H} decrease (%)) (y-axis) was calculated by comparing the peak areas or heights obtained before and after a defined exposure time (x-axis) (Section 7.3.5.2.4). * Statistically significant difference between the peak areas or heights calculated before and after the SC was treated with PO ($p < 0.05$).

On the other hand, it is evident from Figure 7.9 that the maximum effect of PO on the lipid content of the SC surface layers was not apparent until the exposure time was increased beyond 0.5 h. After the SC was treated with 5%w/v PO for 0.5 h, the areas and heights of $\nu_a(\text{CH}_2)$ and $\nu_s(\text{CH}_2)$ were only marginally reduced (P_A or H_I decreases were in the order of ~38% and ~42% for $\nu_a(\text{CH}_2)$ and $\nu_s(\text{CH}_2)$, respectively) whilst the area and height of $\nu(\text{C=O})$ decreased by ~55%. However, the magnitude by which PO reduced the areas and heights of these IR absorbances appeared to increase as the exposure time was extended from 0.5 h to 2 h. After a 2 h exposure time, decreases in the areas and heights of $\nu_a(\text{CH}_2)$, $\nu_s(\text{CH}_2)$ and $\nu(\text{C=O})$ were in the order of ~55%, ~54% and 69% ($p < 0.05$ compared with the peak areas or heights determined before treatment). However, further reductions in peak areas and heights were not apparent at longer exposure times. Instead, the magnitude by which PO appeared to decrease the areas and heights of the lipid-derived IR absorbances remained relatively uniform at exposure times between 2 and 24 h.

Thus, it would appear that, compared with OS, longer exposure times were required for PO to significantly reduce the lipid content of the superficial SC layers (i.e. 2 h versus 0.5 h). However, like OS, it would seem that once PO exerts its maximum effect on SC lipid content the magnitude of this effect remains unchanged over relatively long exposure times.

7.4.1.2.2. Conformational order of the stratum corneum lipid bilayers

Shifts in the location of $\nu_a(\text{CH}_2)$, $\nu_s(\text{CH}_2)$ or $\nu(\text{C=O})$ are plotted as a function of exposure time for either OS or PO in Figures 7.10 and 7.11, respectively. In light of the data presented for the concentration-dependent effects of OS on the locations of $\nu_a(\text{CH}_2)$ and $\nu_s(\text{CH}_2)$ (Figures 7.5.A and 7.5.B), it is not surprising to find that the CH_2 stretching frequencies shifted to higher wavenumbers following treatment of the SC with 5%w/v OS for periods of up to 2 h ($p < 0.05$ compared with peak frequency maxima obtained before treatment with OS) (Figures 7.10.A and 7.10.B). However, it is also evident from Figures 7.10.A and 7.10.B that the magnitude by which OS shifted these peak frequency maxima declined exponentially as a function of increasing exposure time. Consequently, exposure of the SC to OS for 0.5 h resulted in $\nu_a(\text{CH}_2)$ and $\nu_s(\text{CH}_2)$ peak shifts that were significantly greater than those observed after longer exposure times ($p < 0.05$).

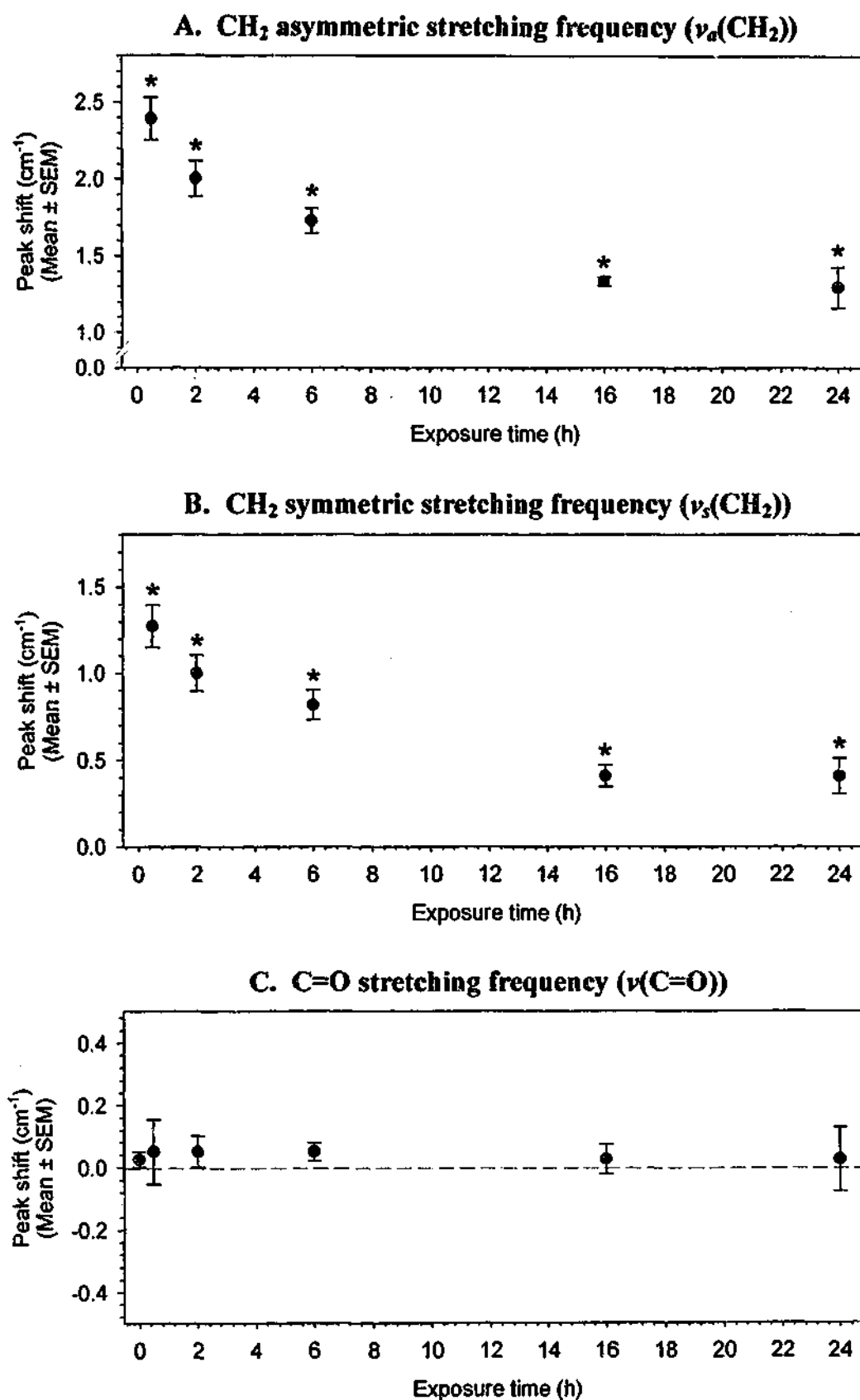


Figure 7.10. The time-related effects of OS on the location of the CH₂ asymmetric stretching absorbance (A), the CH₂ symmetric stretching absorbance (B) and the C=O stretching absorbance (C), where the peak shift is plotted as a function of exposure time. Peak shifts were calculated by comparing peak frequency maxima before and after a given exposure time (Section 7.3.5.2.3). * Statistically significant difference between the peak frequency maxima calculated before and after the SC was treated with OS ($p < 0.05$).

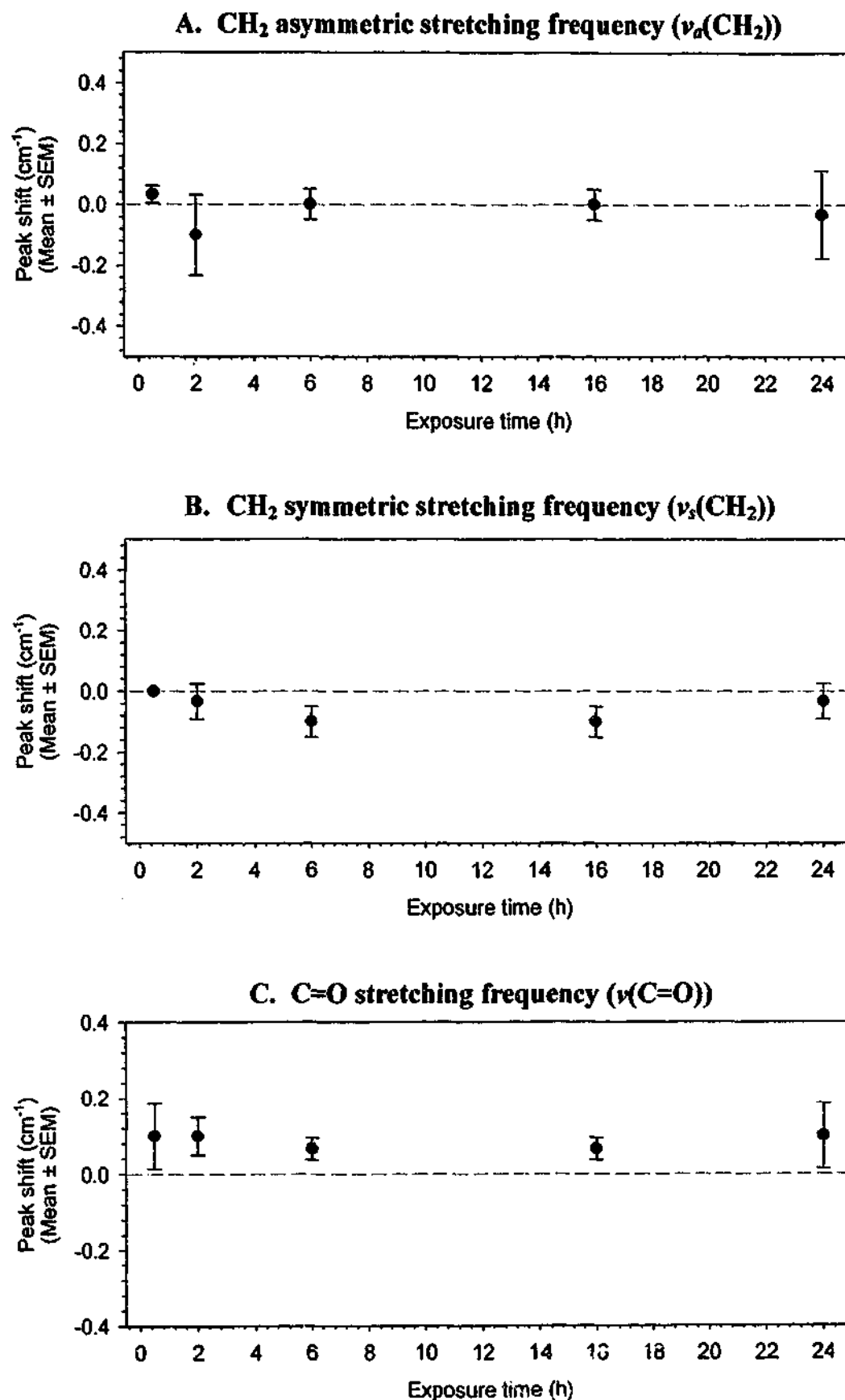


Figure 7.11. The time-related effects of PO on the location of the CH₂ asymmetric stretching absorbance (A), the CH₂ symmetric stretching absorbance (B) and the C=O stretching absorbance (C), where the peak shift is plotted as a function of exposure time. Peak shifts were calculated by comparing peak frequency maxima before and after a given exposure time (Section 7.3.5.2.3). * Statistically significant difference between the peak frequency maxima calculated before and after the SC was treated with PO ($p < 0.05$).

For instance, $\nu_a(\text{CH}_2)$ peak shifts incurred after exposure of the SC to OS for 0.5 and 24 h were $+2.39 \pm 0.14 \text{ cm}^{-1}$ and $+1.29 \pm 0.13 \text{ cm}^{-1}$, respectively. However, even at relatively long exposure times, OS still appeared to exert a significant effect on the conformational order of the lipid bilayers located within the SC surface layer ($\nu_a(\text{CH}_2)$ and $\nu_s(\text{CH}_2)$ peak frequency maxima calculated after treatment of the SC with OS for any period of time between 0.5 and 24 h were significantly higher than those determined before treatment ($p < 0.05$)). On the other hand, treatment of the SC with 5%w/v PO did not effect the location of the CH_2 stretching frequencies at any exposure time investigated (Figures 7.11.A and 7.11.B).

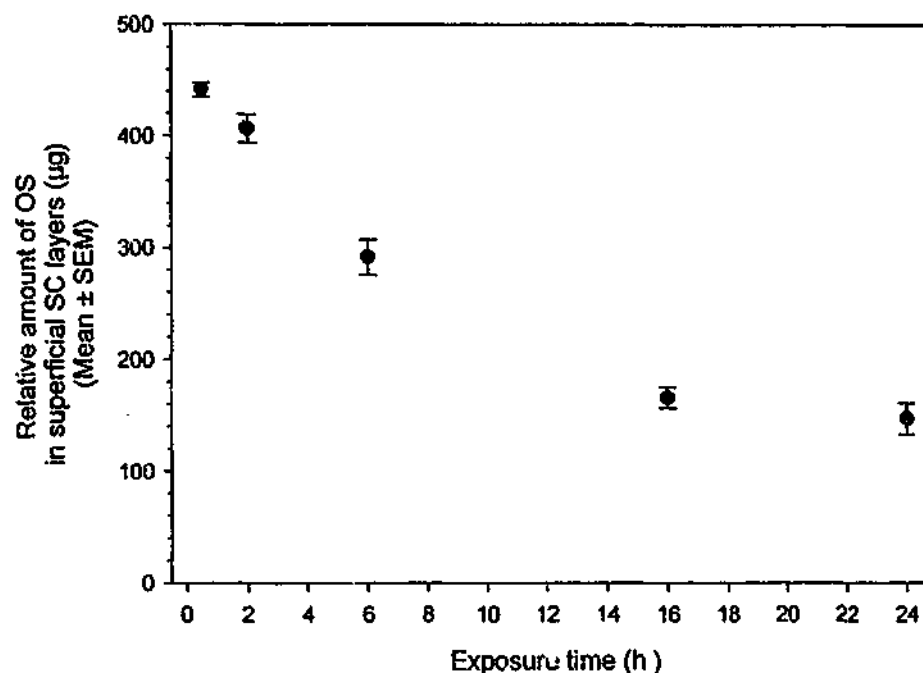
The finding that PO did not appear to effect the conformational order of the SC lipid bilayers after relatively short exposure times (i.e. $< 2 \text{ h}$) is consistent the concentration-dependent results that were presented in Figure 7.6. Furthermore, the results presented in Figures 7.11.A and 7.11.B would suggest that PO exerts a negligible effect on the conformational order of lipid bilayers located within the surface layers of the SC, regardless of how long it is contact with the SC.

Based on the data presented for the concentration-dependent effects of OS and PO on the peak frequency maximum of $\nu(\text{C}=\text{O})$ (Figures 7.5.C and 7.6.C), it is also not surprising to find that neither OS nor PO effected the location of this frequency at any exposure time. As mentioned in Section 7.1, this finding may indicate that neither OS nor PO interacts with carbonyls of the SC lipid polar head-groups.

7.4.1.2.3. Uptake of octisalate and padimate O into the superficial layers of the stratum corneum

Relative amounts of OS or PO present within the uppermost SC layers (determined from the ATR-FTIR spectra obtained after treatment of the SC with either OS or PO) are plotted as a function of exposure time in Figure 7.12. It is evident from Figure 7.12.A that the relative amount of OS present within the superficial SC layers declined exponentially with increasing exposure time. As a similar trend was observed between the effects of OS on the locations of $\nu_a(\text{CH}_2)$ or $\nu_s(\text{CH}_2)$ and exposure time (Figures 7.10.A and 7.10.B), it would appear that the effect of OS on the conformational order of the SC surface lipid bilayers may be dependent on the amount of OS present within this region of the SC.

A. OS



B. PO

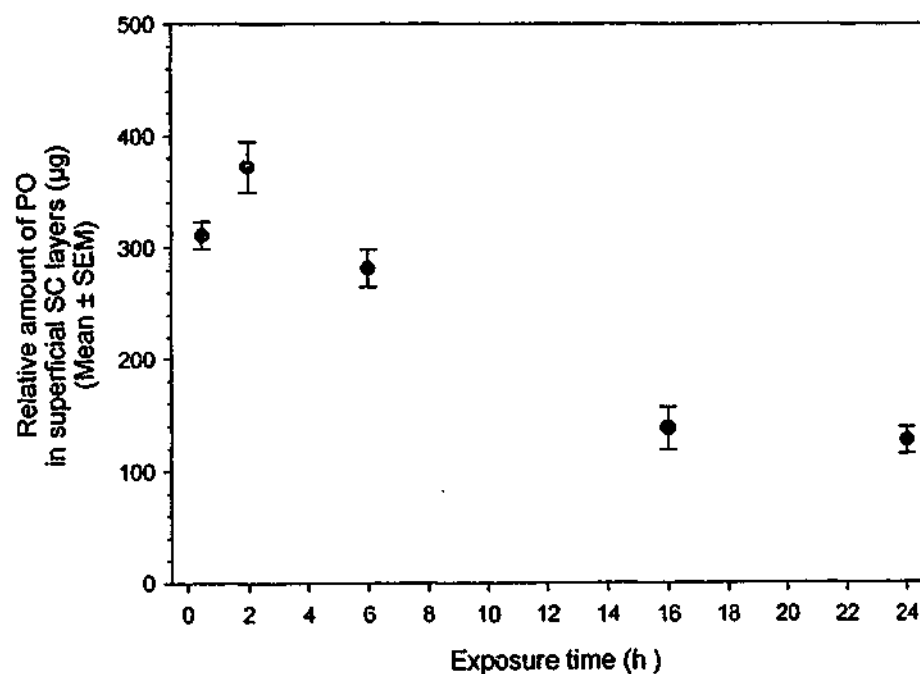


Figure 7.12. The amount of OS (A) or PO (B) present within the superficial layers of the SC following the topical application of 5%w/v OS or PO over various exposure times. As the amounts of OS and PO present within the superficial SC layers were determined using ATR-FTIR, these amounts are relative measurements.

This finding is in agreement with the conclusions derived from the concentration-dependent studies that were conducted (Sections 7.4.1.1.2 and 7.4.1.1.3).

The data derived from the concentration-dependent studies also indicates that the magnitude by which OS reduced SC surface lipid content was also related to the amount of OS taken up into these upper SC layers (Sections 7.4.1.1.1 and 7.4.1.1.3). However, it is apparent from Figures 7.8 and 7.12 that – despite an exponential, time-related decline in the amount of OS within the superficial SC layers – the effect of OS on SC surface lipid content remained relatively constant within exposure times between 0.5 and 24 h.

It is evident from Figure 7.12 that OS rapidly partitions into the upper layers of the SC as maximal levels of OS were present in the superficial SC layers after a 0.5 h exposure time. At this exposure time, treatment of the SC with OS resulted in P_A or H_t decreases that were in the order of ~47%, ~52% and ~62% for $\nu_a(\text{CH}_2)$, $\nu_s(\text{CH}_2)$ and $\nu(\text{C=O})$, respectively. Similar P_A or H_t decreases were also evident at longer exposure times even though it was found that increasing the exposure time from 0.5 h to 24 h resulted in an exponential decline in the amount of OS within the superficial layers of the SC. Thus, it would seem that the degree by which OS reduces the lipid content of the superficial SC layers may actually be related to the *maximum* amount of OS taken up into this upper region of the SC.

The same conclusions can be made regarding the effects of PO on SC surface lipid content. It would appear from Figure 7.12.B that the relative amount of PO that was present within the superficial SC layers increased as the exposure time was extended from 0.5 h to 2 h². Accordingly, the data presented in Figure 7.9 revealed that the magnitude by which PO reduced the areas and heights of the CH_2 and C=O stretching absorbances increased as the exposure time was extended from 0.5 h to 2 h. Although the amount of PO present within the uppermost SC layers subsequently declined when the exposure time was further increased from 2 h to up to 24 h, the degree by which PO decreased the areas and heights of the lipid-derived IR absorbances remained relatively constant within this period of time. Thus, the similarities between the concentration- and time-related effects of OS and PO on SC surface lipid content are evident:

² This finding is consistent with the distribution data presented in Chapter 6 (Section 6.4.1), where it is evident from Figure 6.13 that the concentrations of PO within the uppermost region of the SC increased as the exposure time was extended from 0.08 h to 2 h.

- i. The magnitude by which either OS or PO appear to reduce SC surface lipid content seems to be related to the *maximum* amount of OS or PO taken up into the superficial layers of the SC following their application to the skin surface.
- ii. After OS or PO elicit their “maximum” effect on SC surface lipid content the magnitude of this effect remains relatively constant over longer exposure times, even though the amount of OS or PO present within the surface layers of the SC decreases as a function of increasing exposure time.

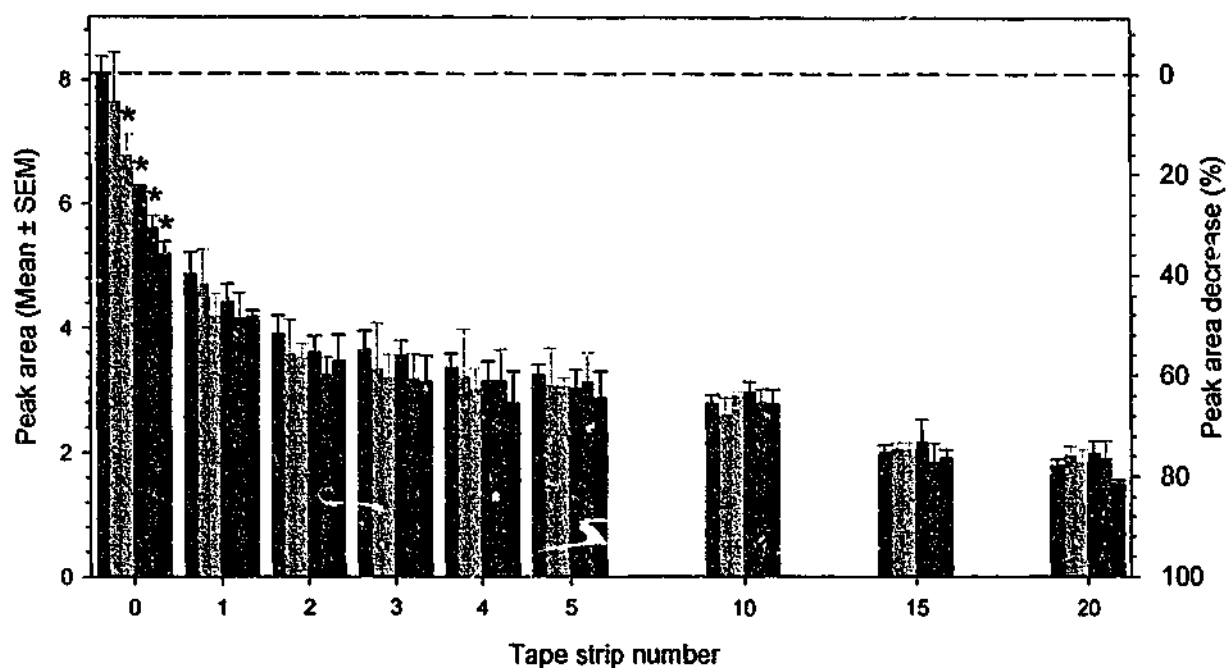
Due to the fact that OS and PO were left in contact with skin for relatively long exposure times, it is difficult to discern whether the latter observation implies that the apparent lipid-reducing effects of OS and PO are not readily reversible *in vitro* once they have been removed from the SC surface. Due to the dynamics of epidermal turnover and the ability of the skin to repair itself, damage to the SC caused by lipid extraction can be reversed by replacement of the damaged tissue (66, 67). Thus, provided that a CPE is not directly toxic to the basal stem cells its effect(s) on SC lipid content should be reversible – after its removal from the skin – within the turnover time of the SC. However, as the repair mechanisms involved in this process are dependent on the metabolic integrity of the skin, it is possible that SC lipid biosynthesis may not be apparent – or readily apparent – *in vitro* (66). Therefore, in order to investigate the reversibility of the effects of OS and PO on SC lipid content further research will need to be conducted, *in vivo*, where SC barrier function is monitored over a period of time after the removal of OS or PO from the SC surface.

7.4.2. The concentration-dependent effects of octisalate and padimate O on lipids located within different layers of the stratum corneum

7.4.2.1. Effects of octisalate and padimate O on stratum corneum lipid content

The area of the CH₂ asymmetric frequencies (obtained from untreated SC, SC treated with 95%w/v ethanol alone and SC treated with either OS or PO) is plotted as a function of tape strip number in Figure 7.13.

A. OS



B. PO

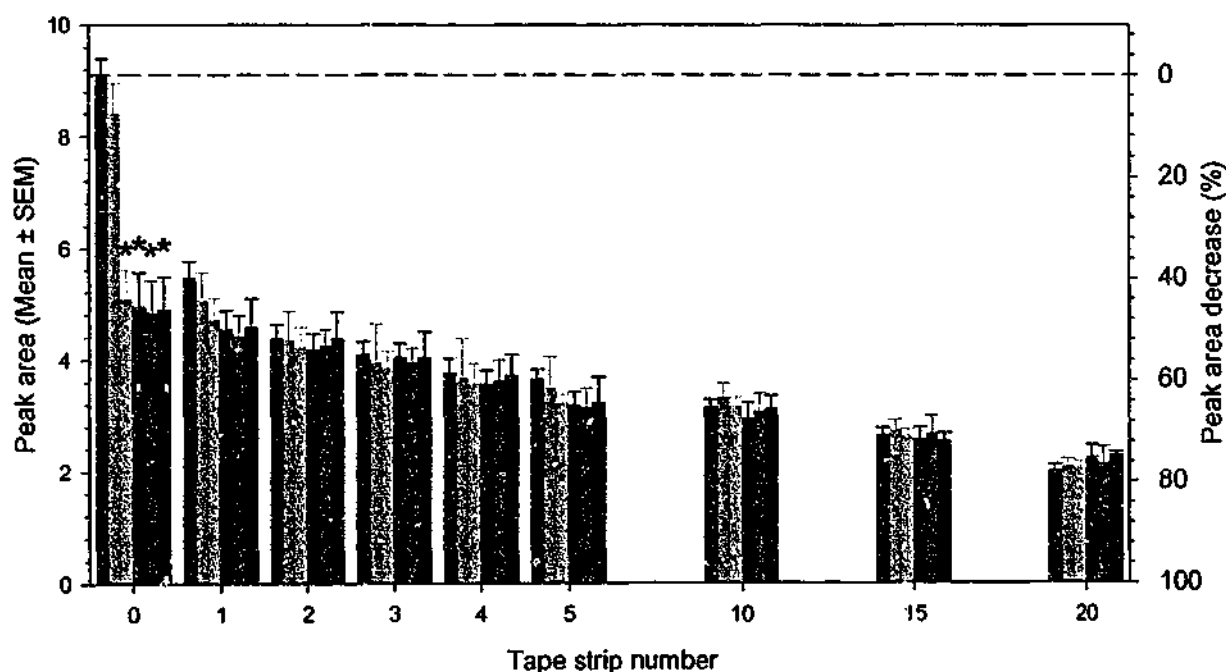


Figure 7.13. Peak area of the CH_2 asymmetric stretching frequency plotted as a function of tape strip number. Peak areas were calculated for untreated SC (■), SC treated with 95%v/v ethanol alone (0%w/v OS or PO) (□) and SC treated with 2.5%w/v (▤), 5%w/v (▥), 7.5%w/v (▧) or 10%w/v (▨) of either OS (A) or PO (B) ($n = 5$). The corresponding peak area decrease (P_A decrease (%)) was determined by comparing the peak areas obtained from treated and untreated SC (Equation 7.5). On the x-axis, a tape strip number of 0 refers to the SC surface (i.e. the peak area obtained after the surface wipe procedure). * Statistically significant difference between the peak areas obtained from treated and untreated SC ($p < 0.05$). The peak areas shown for untreated SC in Figures 7.13.A and 7.13.B are slightly different as different skin samples were used during the control experiments.

It should be noted that similar results were obtained when the areas or heights of the CH₂ asymmetric or symmetric frequencies were plotted as a function of tape strip number. Given that the area of the CH₂ asymmetric stretching absorbance provides a relative measure of SC lipid content (31) and that the tape stripping procedure sequentially removes the SC cell layers (approximately 1 to 2 cell layers are removed by each tape strip (31)), then the graphs presented in Figure 7.13 essentially depict changes in SC lipid content as a function of increasing SC depth. Thus, it would appear that for either untreated or treated skin samples, SC lipid content gradually declined as a function of increasing SC depth.

Compared with the initial peak area obtained after the surface wipe (tape strip 0), the area of the CH₂ stretching absorbance obtained from untreated SC had decreased by approximately 60% after the 5th tape strip was removed from the skin. A less dramatic reduction in the peak area was evident thereafter (peak areas decreases ranged from ~60% after the 5th tape strip to ~85% after the 20th tape strip).

It is evident from Figure 7.13 that there was a similar decline in the peak area of the CH₂ stretching absorbance obtained from SC treated with either 95%v/v ethanol alone or 95%v/v ethanol containing 2.5%w/v to 10%w/v OS or PO with increasing tape strip number (or SC depth). However, significant differences were evident between the peak areas obtained for untreated and treated SC at the SC surface. In accordance with the data previously shown for the concentration-dependent effects of OS or PO on apparent SC surface lipid content (Section 7.4.1.1.1), the data presented in Figure 7.13 indicate that:

- i. Treatment of the SC with 95%v/v ethanol for 2 h resulted in a slight, but not significant, decrease in SC surface lipid content compared with untreated SC (compared with untreated SC, the peak area decreased by approximately 4 to 8% at the SC surface (tape strip 0)).
- ii. Treatment of the SC with 2.5% to 10%w/v of either OS or PO resulted in significant reductions in the area of the CH₂ stretching absorbance detected at the SC surface ($p < 0.05$ compared with untreated SC)
- iii. There was a linear relationship between the peak area detected at the SC surface and applied OS concentration ($r^2 = 0.985$ (between 0 to 10%w/v OS)) (Figure 7.13.A), which would imply that effect of OS on SC surface lipid content was dependent on its applied concentration.

- iv. Similar peak areas were determined at the SC surface of skin samples treated with different concentrations of PO (Figure 7.13.B), which would suggest that the effect of PO on SC surface lipid content became saturated within the applied concentration range investigated.

It is also worth commenting on the magnitudes by which the peak areas obtained at the SC surface decreased after treatment with either OS or PO. As the area of the CH₂ asymmetric stretching absorbance appeared to linearly decline as a function of applied OS concentration, peak area decreases ranged from 16.3 ± 4.1 % at 2.5%w/v OS to 35.9 ± 2.5 % at 10% w/v OS (Figure 7.13.A). On the other hand, the peak areas had decreased by ~45% following the application of 2.5 to 10%w/v PO (Figure 7.13.B). These peak area decreases are slightly lower than those obtained from previous experiments (Section 7.4.1.1.1). As each skin sample could not be used as its own control (i.e. different skin samples were used for the untreated experiments) and because different donors were used during these experiments, it is likely that the different peak area reductions were due to inter- and intra-subject variations in lipid content (25-27). However, it is noteworthy that compared with OS, PO appeared to exert a greater lipid-reducing effect at the SC surface. This finding is in agreement with the data obtained from the concentration-dependent studies that were previously described (Section 7.4.1.1.1).

It should also be highlighted that within the SC layers located below the surface (between tape strips 1 to 20), the areas of the CH₂ stretching absorbance obtained from SC treated with either 95%v/v ethanol alone or 95%v/v ethanol containing either OS or PO were not significantly different to those obtained from untreated SC (Figure 7.13). This finding would suggest that the lipid-reducing effects of OS and PO were mainly confined to the SC surface. A possible explanation for this finding is provided in Section 7.4.2.3.

7.4.2.2. Effects of octisalate on the conformational order of stratum corneum lipids

The peak frequency maxima (P_{MAX}) of the CH₂ asymmetric frequencies obtained from untreated SC, SC treated with 95%w/v ethanol alone or SC treated with either OS or PO are plotted as a function of tape strip number in Figure 7.14.

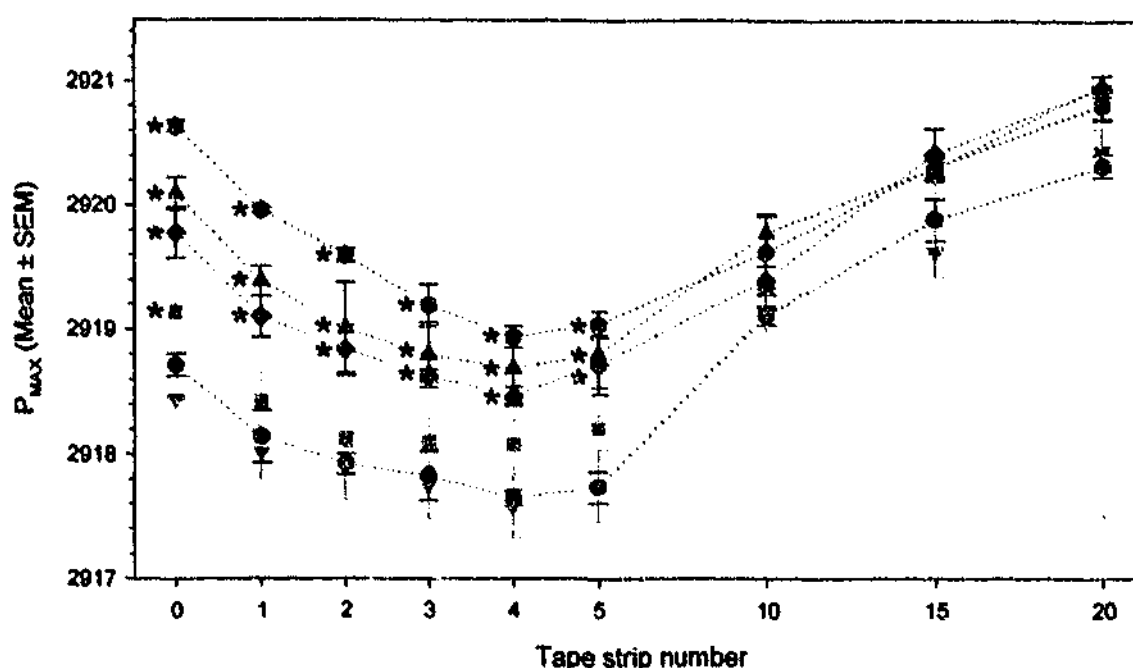


Figure 7.14. Peak frequency maxima (P_{MAX}) of the CH_2 asymmetric stretching frequency plotted as a function of tape strip number. P_{MAX} were calculated for untreated SC (●), SC treated with 95%v/v ethanol alone (i.e. 0%w/v OS) (▼) and SC treated with 2.5%w/v (■), 5%w/v (◆), 7.5%w/v (▲) or 10%w/v (●) of OS ($n = 5$). On the x-axis, a tape strip number of 0 refers to the SC surface (i.e. the peak area obtained after the surface wipe procedure). * denotes a statistically significant difference between the P_{MAX} obtained from treated and untreated SC ($p < 0.05$).

As mentioned in Section 7.1, the position of the CH_2 asymmetric frequency is sensitive to changes in the conformational order of the hydrocarbon alkyl chains of the intercellular SC lipids. Thus, it would appear that within the upper regions of untreated skin (between tape strips 0 to 4), the lipid alkyl chains became more ordered with increasing tape strip number (or SC depth) whereas in the lower regions of the SC (between tape strips 5 to 20), the conformational order of the SC lipids appeared to decrease with increasing SC depth. As all of the profiles shown in Figure 7.14 appear to follow the same trend, it would seem that similar changes to the conformational order of the SC lipids occurred within SC treated with either 95%v/v ethanol alone or 95%v/v ethanol containing OS.

Treating the skin with 95%v/v ethanol did, however, cause a very slight shift (-0.27 ± 0.01) to a lower wavenumber at the SC surface (compared with untreated SC). As

previously mentioned, this decrease may imply that ethanol exerts a slight ordering effect on the SC lipid alkyl chains (Section 7.4.1.1.2).

Treatment of the SC with 2.5 to 10%w/v OS resulted in significant shifts of the CH₂ stretching frequency detected at the SC surface to higher wavenumbers ($p < 0.05$ compared with control; peak shifts ranged from $+0.42 \pm 0.11 \text{ cm}^{-1}$ (at 2.5%w/v OS) to $+1.92 \pm 0.04 \text{ cm}^{-1}$ (at 10%w/v OS)³). A linear relationship was also observed between P_{MAX} and the applied concentration of OS ($r^2 = 0.984$ between 0 to 10%w/v OS), which is consistent with the data presented in Figure 7.5. As mentioned in Section 7.4.2.1.3, this trend may suggest that the ability of OS to induce SC lipid conformational disorder (or increase the number of *gauche* conformers in the lipid alkyl chains) is dependent on its applied concentration.

It is also apparent from Figure 7.14 that shifts of the CH₂ asymmetric stretching frequency were significant within the upper regions of the SC. In particular, treatment of the SC with 2.5%w/v OS elicited a significant peak shift only at the SC surface. However, the apparent lipid-disordering effect of OS seemed to be significant throughout the entire upper region of the SC (between tape strips 0 to 5) at higher applied concentrations (between 5 and 10%w/v). However, treatment of the SC with any concentration of OS seemed to cause only a marginal positive shift of the CH₂ stretching frequencies detected within the deepest regions of the SC (between tape strips 10 to 20), which may infer that the effects of OS on SC lipid conformational order are only significant within the upper SC layers. A possible explanation for this somewhat localised effect is provided in Section 7.4.2.3.

7.4.2.3. Changes in the properties of the stratum corneum as a function of increasing depth

The data presented for untreated SC in Figures 7.13 and 7.14 is consistent with the findings from previous research (31), which also demonstrated that in the upper regions of the SC (between tape strips 0 to 4) the SC lipids appeared to become more ordered and lipid content decreased as a function of increasing tape number (or SC depth). An

³ Due to reasons mentioned previously, it is likely that the peak shifts observed in Figure 7.5 and 7.14 were of different magnitudes due to inter- and intra-subject variations in SC lipid fluidity (28).

explanation that was proposed for these findings was that the lipids within the superficial SC layers represent a mixture of both intercellular and sebaceous lipids. As sebaceous lipids contain a significant amount of relatively low-melting-point fatty acids (68, 69), this explanation is supported by data obtained from tape stripping studies that were performed in conjunction with high-performance thin-layer chromatography (HPTLC), which revealed that the level of free fatty acids is highest within the upper layers of the SC (i.e. within the SC layers removed by 4 or 5 tape strips) (70, 71).

Further support for this notion comes from tape stripping studies that were conducted in conjunction with ATR-FTIR (28, 72). It was demonstrated from these studies that sebum is mostly responsible for carbonyl stretching frequencies located at $\sim 1710\text{ cm}^{-1}$ and $\sim 1740\text{ cm}^{-1}$. In addition, the stretching frequency located at $\sim 1710\text{ cm}^{-1}$ was found to be characteristic of carbonyl ester bonds within the polar head-groups of the free fatty acids whereas the IR band located at $\sim 1740\text{ cm}^{-1}$ was found to originate from carbonyl bonds within the polar head-groups of most other lipids (72). Not surprisingly, it was found that the peaks near $\sim 1710\text{ cm}^{-1}$ and $\sim 1740\text{ cm}^{-1}$ reduced or disappeared after removal of the superficial SC layers (by 2 to 4 tape strips) and that the magnitude by which the intensity of the $\sim 1710\text{ cm}^{-1}$ peak declined was greater than that by which the intensity of the $\sim 1740\text{ cm}^{-1}$ was reduced (a $\sim 30\%$ versus $\sim 13\%$ reduction was observed for the 1710 cm^{-1} and 1740 cm^{-1} bands, respectively) (28).

In addition to variations in fatty acid content, cholesterol and ceramide levels have also been found to change with increasing SC depth (71). While the level of free fatty acids was found to be highest, cholesterol and ceramide levels were the lowest in the upper SC layers (between tape strips 1 to 4). Thus, it has been suggested that the higher levels of free fatty acids may be due to the presence of sebaceous lipids or to an increased degradation of cholesterol and ceramide within the uppermost SC layers (71). Furthermore, whilst it has been found that the phase behaviour of isolated SC lipids remains essentially unchanged over a wide range of cholesterol/ceramide/free fatty acid molar ratios, it has also been shown that free fatty acids affect lipid phase behaviour by increasing the solubility of cholesterol in the lamellar structures (73). In particular, when the SC contains a relatively low amount of free fatty acids, a substantial amount of cholesterol exists in a crystalline form (74). Therefore, if the lipids located within the uppermost regions of the SC are a mixture of sebaceous and/or degraded lipids as well as intact intercellular lipids, it would follow that the average conformational

arrangement of these superficial lipids would be less organised than that of the highly ordered intercellular lipids located within the deeper SC layers.

Thus, the observation that OS appeared to elicit a greater lipid-disordering effect on lipids located within the upper regions of the SC may be partly explained by the possibility that, compared with the energy required to reduce the conformational order of the deeper SC lipids, less energy would be required to cause further changes to the order of the superficial SC lipids.

In addition to variations in SC lipid composition, it has been demonstrated that corneocyte cohesion gradually increases with increasing tape strip number (or SC depth) (75). Consequently, the corneocytes are "loosely bound" (i.e. minimal inter-corneocyte adhesion) within the uppermost SC layers, whereas in the lower SC regions they are tightly cohesive and appear more 'swollen' in appearance (75). As the intercellular lipid domain that surrounds the corneocytes is generally regarded as the major route for drug permeation through the SC and the corneocytes are thought to act as mechanical barriers that effectively increase the diffusional path length (26, 67, 76, 77), it would appear that due to the looser packing of the corneocytes there would be a greater area available for drug permeation through the intercellular domain within the uppermost regions of the SC. Thus, it would be anticipated that the SC accommodates a greater amount of the permeant within its upper layers. This notion is supported by the distribution profiles presented Chapters 5 and 6. In particular, it was evident from the distribution profiles presented in Chapter 6 that the concentration of either OS or PO within the SC declined exponentially as a function of increasing SC depth. Thus, it would seem that the lipid-reducing and/or lipid-disordering effects of OS and PO are significant within the upper regions of the SC, where the concentrations of OS and PO within the SC are greatest. This correlation is further exemplified by the distribution profiles presented in Figure 7.15.

The data presented in Figure 7.15 clearly shows that compared with distribution profile generated after the topical application of 2.5%w/v OS, the relative amounts of OS were significantly higher within the upper SC layers (between tape strips 1 and 5) following the topical application of higher (between 5 and 10%w/v) OS concentrations. Accordingly, the topical application of 2.5%w/v OS elicited a blue shift of the CH₂ asymmetric stretching frequency only at the SC surface whereas significant peak shifts were observed throughout the entire upper region of the SC (between tape strips 0 to 5)

following the application of higher (between 5 and 10%w/v) OS concentrations (Figure 7.14).

It is also worth mentioning some of the artifacts that may be associated with the experimental procedure that was employed. The observation that within the lower regions of the SC the lipids appear to become more disordered with increasing SC depth could be related to the fact that tape stripping the SC removes cell layers that originate from various depths because of macroscopic furrows in the skin (78). Thus, sequential removal of the SC layers by tape stripping may have eventually exposed the zinc selenide crystal to areas of the SC that are present within the furrows as well as the uppermost regions of the underlying epidermis (Figure 7.16).

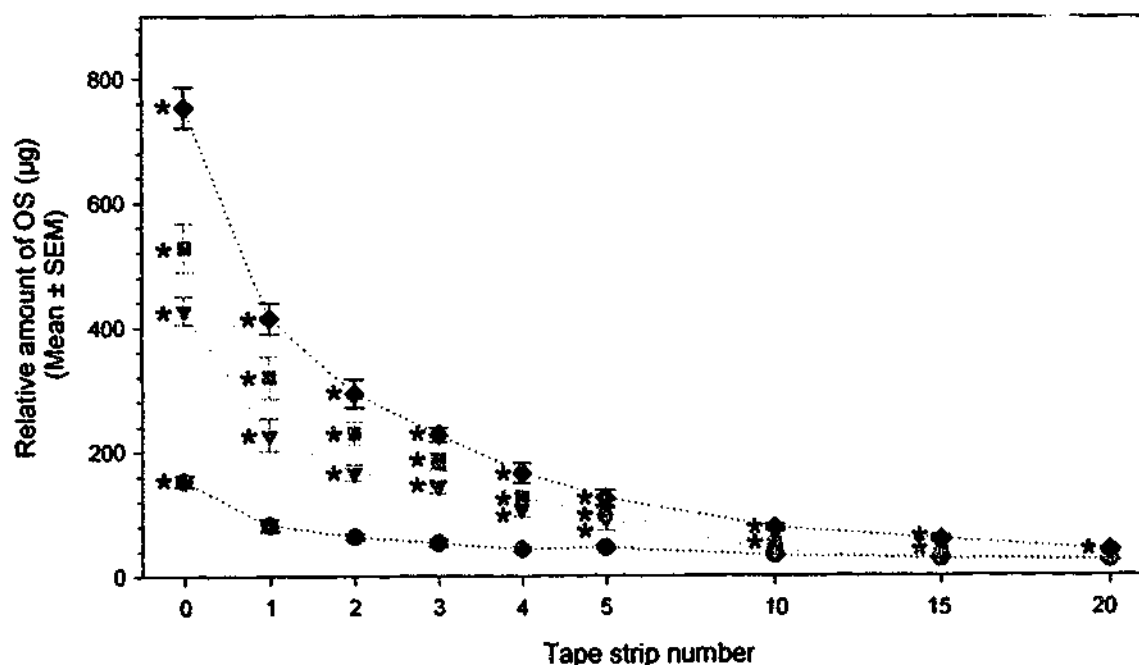


Figure 7.15. Amounts of OS present within the SC following the topical application of 2.5%w/v (●), 5%w/v (▼), 7.5%w/v (■) or 10%w/v (◆) OS ($n = 5$). The amount of OS is presented as a function of tape strip number (where a tape strip number of 0 refers to the SC surface). As the quantification of OS was performed using ATR-FTIR, these are only relative measurements. * denotes a statistically significant difference compared with the relative amount measured after the application of 2.5%w/v OS ($p < 0.05$).

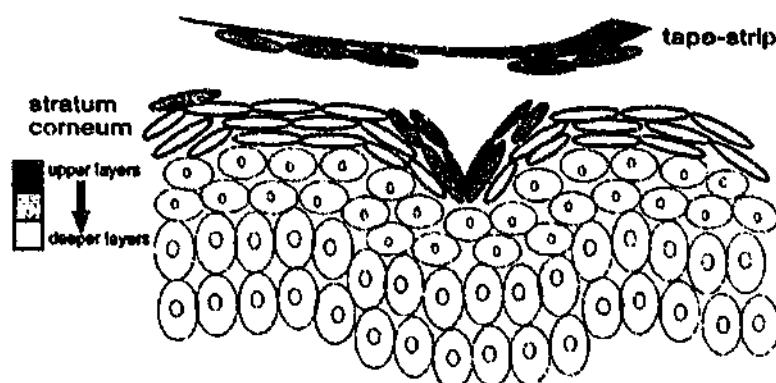


Figure 7.16. Schematic representation of how tape stripping the SC removes cell layers that originate from various depths because of furrows in the skin. Taken from van der Molen et al (78).

As the IR absorbances within an ATR-FTIR spectrum represent the average state of the chemical bonds within skin layers that are immediately in contact with the IRE, it is possible that the CH_2 stretching frequencies that were detected within the deeper SC layers actually represented a mixture of the intercellular lipids embedded within the SC furrows as well as the small amount of lipidic material present within the uppermost epidermal strata (67, 79).

Thus, the observation that neither OS nor PO significantly effected the signal intensities or peak frequency maxima of the CH_2 asymmetric absorbances detected within the lower SC regions may be partly explained by the fact that OS and PO are highly lipophilic and sparingly soluble in water and are therefore unlikely to partition into – and therefore interact with the lamellar bodies that are present within – the epidermis *in vitro*.

It is also evident from Figure 7.14 that compared with the CH_2 stretching absorbances detected within the upper SC regions (between tape strips 0 and 5), the CH_2 stretching frequencies obtained from the deeper skin layers (between tape strips 10 and 20) were centered at higher wavenumbers. Thus, another explanation as to why OS did not appear to effect the fluidity of the lipids located within the deeper skin strata could be related to the possibility that a large fraction of these lipids exist as a somewhat liquid-crystalline phase and therefore cannot be further perturbed.

Given that the hydration state of the SC has been related to the cohesive properties of SC corneocytes (where an apparent increase in SC hydration corresponded to increases

in corneocyte cohesion (75)) and that the removal of the SC layers by tape stripping would eventually expose the uppermost regions of the underlying epidermis, it should also be noted that water concentrations within the SC have been found to increase with increasing SC depth (22, 28). It was therefore not surprising to find that the O-H stretching frequency located at $\sim 3000\text{ cm}^{-1}$ increased as a function of tape strip number during the ATR-FTIR analyses that were conducted (data not shown). It has been previously reported that a large increase in the hydration level of the SC causes the CH_2 stretching frequencies to be located on the shoulder of the broad O-H band located at $\sim 3000\text{ cm}^{-1}$ – an effect which may shift the apparent peak maxima of the CH_2 stretching frequencies to higher wavenumbers (80). Thus, the relatively high level of hydration within the deeper SC layers could have artificially shifted the CH_2 asymmetric stretching frequencies detected within the region to higher wavenumbers and/or may have confounded the apparent effects of OS on the conformational order of the deeper SC lipids.

7.5. CONCLUSIONS

It would appear that both OS and PO extract lipids from the superficial layers of the SC. However, the lipid-reducing effect of OS seemed to be linearly dependent on its applied concentration whereas the potential for PO to reduce SC surface lipid content appeared to be saturated within the concentration range investigated. Differences were also apparent between the time-related effects of OS and PO on SC surface lipid content. While the degree by which OS seemed to reduce SC surface lipid content remained relatively unchanged over all exposure times (between 0.5 and 24 h), the maximum lipid-reducing effect of PO was not apparent until the exposure time was extended from 0.5 h to 2 h. However, the magnitude by which PO appeared to reduce SC surface lipid content remained relatively constant over longer exposure times (between 2 and 24 h).

It was also evident that OS rapidly partitioned into the upper layers of the SC after its application to the skin as maximal levels of OS were present within the SC after an exposure time of 0.5 h. On the other hand, the maximum amount of PO that was taken up into the SC surface layers was not evident until a 2 h exposure time. Thus, it would seem that the magnitude by which either OS or PO reduced SC surface lipid content may have

been related to the maximum amount of OS or PO taken up into the SC surface layers. However, as the uptake of either OS or PO into the SC surface layers subsequently declined over relatively long exposure times it would seem that – when they are left in contact with the skin – the lipid-reducing effects of OS and PO are not readily reversible *in vitro*.

It was also revealed from these studies that OS, but not PO, may reduce the conformational order of the lipid bilayers located within SC surface layers. As the magnitude by which OS shifted the CH₂ stretching frequencies declined exponentially over time and also appeared to be directly related to the applied concentration of OS, the apparent ability of OS to fluidise the SC surface lipids appears to be directly related to the amount of OS present within these superficial SC layers. It is possible that the different effects that OS and PO appear to elicit on the conformational order of the SC lipid alkyl chains could be related (or partly related) to differences in their chemical structures, the possibility that they are located at different regions within the lamellar structure, and/or their potential to modify hydrogen bonding between the SC lipid molecules.

Although it would appear that OS and PO exert different effects on the conformation of the lipid alkyl chains, neither seemed to alter the location of the carbonyl stretching frequency (located at $\sim 1740\text{ cm}^{-1}$) derived from the polar head-groups of the SC intercellular lipid bilayers and/or sebaceous lipids. This observation may suggest that neither OS nor PO form hydrogen bonds with the carbonyl moieties of the intercellular and/or sebaceous lipid polar head-groups. However, the vehicle that was used to deliver OS and PO to the skin surface was ethanol, which was found to elicit a blue shift of the carbonyl stretching frequency. Thus, it is also possible that hydrogen bonding between OS or PO and polar head-group carbonyls was offset by the presence of ethanol within the SC.

It was evident from the tape-stripping experiments that were performed that treatment of the SC with either OS or PO did not effect the areas or locations of the CH₂ asymmetric stretching absorbances detected within the deeper SC layers. This would indicate that the lipid-reducing or lipid-disordering effects of OS or PO are mainly confined to the superficial SC layers, where SC lipid content, SC lipid fluidity, and the concentrations of OS or PO within the SC are greatest.

7.6. REFERENCES

1. Golden GM, McKie JE, Potts RO. 1987. Role of Stratum Corneum Lipid Fluidity in Transdermal Drug Flux. *J Pharm Sci* 76:25-28.
2. Yamane MA, Barry BW. 1995. Effects of Terpenes and Oleic Acid as Skin Penetration Enhancers Towards 5-Fluorouracil As Assessed With Time; Permeation, Partitioning and Differential Scanning Calorimetry. *Int J Pharm* 116:237-251.
3. Leopold CS, Lippold BC. 1995. An Attempt to Clarify the Mechanism of the Penetration Enhancing Effects of Lipophilic Vehicles with Differential Scanning Calorimetry (DSC). *J Pharm Pharmacol* 47:276-281.
4. Khan ZU, Kellaway IW. 1989. Differential Scanning Calorimetry of Dimethylsulphoxide-Treated Human Stratum Corneum. *Int J Pharm* 55:129-134.
5. Cornwell PA, Barry BW, Bouwstra JA, Gooris GS. 1996. Modes of Action of Terpene Penetration Enhancers in Human Skin; Differential Scanning Calorimetry, Small-Angle X-Ray Diffraction and Enhancer Uptake Studies. *Int J Pharm* 127:9-26.
6. Ogiso T, Iwaki M, Paku T. 1995. Effect of Various Enhancers on Transdermal Penetration of Indomethacin and Urea, and Relationship Between Penetration Parameters and Enhancement Factors. *J Pharm Sci* 84:482-488.
7. Ogiso T, Iwaki M, Bechako K, Tsutsumi Y. 1992. Enhancement of Percutaneous Absorption by Laurocapram. *J Pharm Sci* 81:762-767.
8. Gay CL, Hadgraft J, Kellaway IW, Evans JC, Rowlands CC. 1990. The Effect of Skin Penetration Enhancers on Human Stratum Corneum Lipids: An Electron Spin Resonance Study. In Scott RC, Guy RH, Hadgraft J, ed. *Prediction of Percutaneous Penetration*. London: IBC Technical Services Ltd., pp 322-332.
9. Bouwstra JA, Gooris GS, White SH. 1997. X-Ray Analysis of the Stratum Corneum and Its Lipids. In Potts RO, Guy RH, ed. *Mechanisms of Transdermal Drug Delivery*. New York: Marcel Dekker, Inc., pp 41-85.
10. Cornwell PA, Barry BW, Stoddart CP, Bouwstra JA. 1994. Wide-Angle X-Ray Diffraction of Human Stratum Corneum: Effect of Hydration and Terpene Enhancer Treatment. *J Pharm Pharmacol* 46:938-950.
11. Engblom J, Engstrom S, Jonsson B. 1998. Phase Coexistence in Cholesterol-Fatty Acid Mixtures and the Effect of the Penetration Enhancer Azone. *J Control Release* 52:271-280.
12. Garrison MD, Doh LM, Potts RO, Abraham W. 1994. Effect of Oleic Acid on Human Epidermis: Fluorescence Spectroscopic Investigation. *J Control Release* 31:263-269.
13. Bommannan D, Potts RO, Guy RH. 1991. Examination of the Effect of Ethanol on Human Stratum Corneum *In Vivo* Using Infrared Spectroscopy. *J Control Release* 16:299-304.
14. Sen A, Zhao YL, Hui SW. 2002. Saturated Anionic Phospholipids Enhance Transdermal Transport by Electroporation. *Biophys J* 83:2064-2073.

15. Harrison JE, Watkinson AC, Green DM, Hadgraft J, Brain K. 1996. The Relative Effect of Azone® and Transcutol® on Permeant Diffusivity and Solubility in Human Stratum Corneum. *Pharm Res* 13:542-546.
16. Mak VHW, Potts RO, Guy RH. 1990. Oleic Acid Concentration and Effect in Human Stratum Corneum: Non-Invasive Determination by Attenuated Total Reflectance Infrared Spectroscopy *In Vivo*. *J Control Release* 12:67-75.
17. Konturri K, Murtomaki L, Hirvonen J, Paronen P, Urtti A. 1993. Electrochemical Characterization of Human Skin by Impedance Spectroscopy: The Effect of Penetration Enhancers. *Pharm Res* 10:381-385.
18. Tsai JC, Sheu HM, Hung PL, Cheng CL. 2001. Effect of Barrier Disruption by Acetone Treatment on the Permeability of Compounds with Various Lipophilicities: Implications for the Permeability of Compromised Skin. *J Pharm Sci* 90:1242-1254.
19. Hoogstraate AJ, Verhoef J, Brussee J, IJzerman F, Spies F, Boddé HE. 1991. Kinetics, Ultrastructural Aspects and Molecular Modelling of Transdermal Peptide Flux Enhancement by N-Alkylazacycloheptanones. *Int J Pharm* 76:37-47.
20. Bouwstra JA, Salomons-de Vries MA, van den Bergh BAI, Gooris GS. 1996. Changes in Lipid Organisation of the Skin Barrier by N-Alkyl-Azocycloheptanones: A Visualisation and X-Ray Diffraction Study. *Int J Pharm* 144:81-89.
21. Potts RO, Francoeur ML. 1992. Physical Methods for Studying Stratum Corneum Lipids. *Semin Dermatol* 11:129-138.
22. Naik A, Guy RH. 1997. Infrared Spectroscopic and Differential Scanning Calorimetric Investigations of the Stratum Corneum Barrier Function. In Potts RO, Guy RH, ed. *Mechanisms of Transdermal Drug Delivery*. New York: Marcel Dekker, Inc., pp 87-162.
23. Naik A, Kalia YN, Pirot F, Guy RH. 1999. Characterization of Molecular Transport Across Human Stratum Corneum *In Vivo*. In Bronaugh RL, Maibach H, ed. *Percutaneous Absorption: Drugs, Cosmetics, Mechanisms, Methodology*. New York: Marcel Dekker, Inc., pp 149-175.
24. Potts RO, Francoeur ML. 1993. Infrared Spectroscopy of Stratum Corneum Lipids. *In Vitro* Results and Their Relevance to Permeability. In Walters KA, Hadgraft J, ed. *Pharmaceutical Skin Penetration Enhancement*. New York: Marcel Dekker, Inc., pp 269-291.
25. Norlén L, Nicander I, Rozell BL, Ollmar S, Forslind B. 1999. Inter- and Intra-Individual Differences in Human Stratum Corneum Lipid Content Related to Physical parameters of Skin Barrier Function *In Vivo*. *J Invest Dermatol* 112:72-77.
26. Elias PM, Cooper ER, Korr A, Brown BE. 1981. Percutaneous Transport in Relation to Stratum Corneum Structure and Lipid Composition. *J Invest Dermatol* 76:297-301.
27. Lampe MA, Burlingame AL, Whitney J, Williams ML, Brown BE, Roitman E, Elias PM. 1983. Human Stratum Corneum Lipids: Characterization and Regional Variations. *J Lipid Res* 24:120-130.

28. Brancalion L, Bamberg MP, Sakamaki T, Kollias N. 2001. Attenuated Total Reflection-Fourier Transform Infrared Spectroscopy as a Possible Method to Investigate Biophysical Parameters of Stratum Corneum *In Vivo*. *J Invest Dermatol* 116:380-386.
29. Branagan M, Chenery DH, Nicholson S. 2000. Use of Infrared Attenuated Total Reflectance Spectroscopy for the *In Vivo* Measurement of Hydration Level and Silicone Distribution in the Stratum Corneum Following Skin Coverages by Polymeric Dressings. *Skin Pharmacol Appl Skin Physiol* 13:157-164.
30. Potts RO, Guzek DB, Harris RR, McKie JE. 1985. A Noninvasive, *In Vivo* Technique to Quantitatively Measure Water Concentration of the Stratum Corneum Using Attenuated Total-Reflectance Infrared Spectroscopy. *Arch Dermatol Res* 277:489-495.
31. Bommannan D, Potts RO, Guy RH. 1990. Examination of Stratum Corneum Barrier Function *In Vivo* by Infrared Spectroscopy. *J Invest Dermatol* 95:403-408.
32. Moore DJ, Rerek ME. 2000. Insights into the Molecular Organization of Lipids in the Skin Barrier from Infrared Spectroscopy Studies of Stratum Corneum Lipid Models. *Acta Derm Venereol Suppl (Stockh)* 208:16-22.
33. Potts RO. 1989. Physical Characterization of the Stratum Corneum: The Relationship of Mechanical and Barrier Properties to Lipid and Protein Structures. In Hadgraft J, Guy RH, ed. *Transdermal Drug Delivery Developmental Issues and Research Initiatives*. New York: Marcel Dekker, Inc., pp 23-57.
34. Ongpipattanakul B, Francoeur ML, Potts RO. 1994. Polymorphism in Stratum Corneum Lipids. *Biochim Biophys Acta* 1190:115-122.
35. Williams AC, Barry BW. 1998. Chemical Penetration Enhancement: Possibilities and Problems. In Roberts MS, Walters KA, ed. *Dermal Absorption and Toxicity Assessments*. New York: Marcel Dekker, Inc., pp 297-312.
36. Knutson K, Potts RO, Guzek DB, Golden GM, McKie JE, Lambert WJ, Higuchi WI. 1985. Macro- and Molecular Physical-Chemical Considerations in Understanding Drug Transport in the Stratum Corneum. *J Control Release* 2:67-87.
37. Casal HL, Mantsch HH. 1984. Polymorphic Phase Behaviour of Phospholipid Membranes Studies by Infrared Spectroscopy. *Biochim Biophys Acta* 779:381-401.
38. Krill SL, Knutson K, Higuchi WI. 1992. The Stratum Corneum Lipid Thermotropic Phase Behaviour. *Biochim Biophys Acta* 1112:281-286.
39. Golden GM, Guzek DB, Harris RR, McKie JE, Potts RO. 1986. Lipid Thermotropic Transitions in Human Stratum Corneum. *J Invest Dermatol* 86:255-259.
40. Potts RO, Mak VH, Guy RH, Francoeur ML. 1991. Strategies to Enhance Permeability via Stratum Corneum Lipid Pathways. *Adv Lipid Res* 24:173-210.
41. Potts RO, Golden GM, Francoeur ML, Mak VHW, Guy RH. 1991. Mechanism and Enhancement of Solute Transport Across the Stratum Corneum. *J Control Release* 15:249-260.
42. Golden GM, Guzek DB, Kennedy AH, McKie JE, Potts RO. 1987. Stratum Corneum Lipid Phase Transitions and Water Barrier Properties. *Biochemistry* 26:2382-2388.

43. Weigand DA, Gaylor JR. 1973. Removal of Stratum Corneum *In Vivo*: An Improvement on the Cellophane Tape Stripping Technique. *J Invest Dermatol* 60:84-87.
44. Schaefer H, Stüttgen G, Zesch A, Schalla W, Gazith J. 1978. Quantitative Determination of Percutaneous Absorption of Radiolabeled Drugs *In Vitro* and *In Vivo* by Human Skin. *Curr Probl Dermatol* 7:80-94.
45. Johnson ME, Blankschtein D, Langer R. 1997. Evaluation of Solute Permeation Through the Stratum Corneum: Lateral Bilayer Diffusion as the Primary Transport Mechanism. *J Pharm Sci* 86:1162-1172.
46. Knuston K, Krill SL, Lambert WJ, Higuchi WI. 1987. Physicochemical Aspects of Transdermal Permeation. *J Control Release* 6:59-74.
47. Clancy MJ, Corish J, Corrigan OI. 1994. A Comparison of the Effects of Electrical Current and Penetration Enhancers on the Properties of Human Skin Using Spectroscopic (FTIR) and Calorimetric (DSC) Methods. *Int J Pharm* 105:47-56.
48. Goates CY, Knuston K. 1994. Enhanced Permeation of Polar Compounds Through Human Epidermis. I. Permeability and Membrane Structural Change in the Presence of Short-Chain Alcohols. *Biochim Biophys Acta* 1195:169-179.
49. Zhao K, Singh J. 2000. Mechanism(s) of *In Vitro* Percutaneous Absorption Enhancement of Tamoxifen by Enhancers. *J Pharm Sci* 89:771-780.
50. Takahashi K, Sakano H, Yoshida M, Numata N, Mizuno N. 2001. Characterization of the Influence of Polyol Fatty Acid Esters on the Permeation of Diclofenac Through Rat Skin. *J Control Release* 73:351-358.
51. Zhao K, Singh J. 1999. *In Vitro* Percutaneous Absorption Enhancement of Propranolol Hydrochloride Through Porcine Epidermis by Terpenes/Ethanol. *J Control Release* 62:359-366.
52. Vaddi HK, Ho PC, Chan YW, Chan SY. 2002. Terpenes in Ethanol: Haloperidol Permeation and Partition Through Human Skin and Stratum Corneum Changes. *J Control Release* 81:121-133.
53. Rastogi SK, Singh J. 2001. Lipid Extraction and Transport of Hydrophilic Solutes Through Porcine Epidermis. *Int J Pharm* 225:75-82.
54. Ghanem AH, Mahmoud H, Higuchi WI, Rohr UD, Borsadia S, Liu P, Fox JL, Good WR. 1987. The Effects of Ethanol on Transport of β -Estradiol and Other Permeants in Hairless Mouse Skin. *J Control Release* 6:75-83.
55. Inamori T, Ghanem AH, Higuchi WI, Srinivasan V. 1994. Macromolecular Transport In and Effective Pore Size of Ethanol Pretreated Human Epidermal Membrane. *Int J Pharm* 105:113-123.
56. Peck KD, Ghanem AH, Higuchi WI. 1994. Hindered Diffusion of Polar Molecules Through and Effective Pore Radii Estimates of Intact and Ethanol Treated Human Epidermal Membrane. *Pharm Res* 11:1306-1314.
57. Krill SL, Knutson K, Higuchi WI. 1992. Ethanol Effects on the Stratum Corneum Lipid Phase Behavior. *Biochim Biophys Acta* 1112:273-280.
58. Knuston K, Krill SL, Zhang J. 1990. Solvent-Mediated Alterations of the Stratum Corneum. *J Control Release* 11:93-103.

59. Wertz PW. 1992. Epidermal Lipids. *Semin Dermatol* 11:106-113.
60. Hadgraft J, Peck J, Williams DG, Pugh WJ, Allan G. 1996. Mechanisms of Action of Skin Penetration Enhancers/Retarders: Azone and Analogues. *Int J Pharm* 141:17-25.
61. Lin SY. 1995. Direct or Indirect Skin Lipid-Ordering Effect of Pyrrolidone Carboxylate Sodium After Topical Treatment with Penetration Enhancers. *Biomed Mater Engineer* 5:9-20.
62. Fringeli UP, Gunthard H. 1981. Infrared Membrane Spectroscopy. In Grell E, ed. *Membrane Spectroscopy*. Berlin: Springer-Verlag, pp 170-232.
63. Naik A, Pechtold LARM, Potts RO, Guy RH. 1995. Mechanism of Oleic Acid-Induced Skin Penetration Enhancement *In Vivo* in Humans. *J Control Release* 37:299-306.
64. Harrison JE, Groundwater PW, Brain KR, Hadgraft J. 1996. Azone® Induced Fluidity in Human Stratum Corneum. A Fourier Transform Infrared Spectroscopy Investigation Using the Perdeuterated Analogue. *J Control Release* 41:283-290.
65. Hadgraft J. 2001. Skin, the Final Frontier. *Int J Pharm* 224:1-18.
66. Haberkamp MB. 1994. Skin Permeation Enhancement Reversibility. In Hsieh DS, ed. *Drug Permeation Enhancement*. New York: Marcel Dekker, Inc., pp 43-58.
67. Roberts MS, Walters KA. 1998. The Relationship Between Structure and Barrier Function of Skin. In Roberts MS, Walters KA, ed. *Dermal Absorption and Toxicity Assessment*. New York: Marcel Dekker, Inc., pp 1-42.
68. Imokawa G, Akasaki S, Hattori M, Yoshizuka N. 1986. Selective Recovery of Deranged Water-Holdinh Properties by Human Stratum Corneum Lipids. *J Invest Dermatol* 87:758-761.
69. Lampe MA, Williams ML, Elias PM. 1983. Human Epidermal Lipids: Characterization and Modulation During Differentiation. *J Lipid Res* 24:131-140.
70. Bonté F, Sauniois A, Pinguet P, Meybeck A. 1997. Existence of a Lipid Gradient in the Upper Stratum Corneum and its Possible Biological Significance. *Arch Dermatol Res* 289:78-82.
71. Weerheim A, Ponc M. 2001. Determination of Stratum Corneum Lipid Profile by Tape Stripping in Combination with High-Performance Thin-Layer Chromatography. *Arch Dermatol Res* 293:191-199.
72. Brancalion L, Bamberg MP, Kollias N. 2000. Spectral Differences Between Stratum Corneum and Sebaceous Molecular Components in the Mid-IR. *Appl Spec* 54:1175-1182.
73. Bouwstra JA, Gooris GS, Cheng K, Weerheim A, Bras W, Ponc M. 1996. Phase Behaviour of Isolated Skin Lipids. *J Lipid Res* 37:999-1011.
74. Lavrijsen AP, Bouwstra JA, Gooris GS, Weerheim A, Boddé HE, Ponc M. 1995. Skin Barrier Function and Stratum Corneum Lipid Organisation in Patients with Lamellar Ichthyosis. *J Invest Dermatol* 105:619-624.
75. King CS, Barton SP, Nicholls S, Marks R. 1979. The Change in Properties of the Stratum Corneum as a Function of Depth. *Br J Dermatol* 100:165-172.
76. Pugh WJ, Hadgraft J, Roberts MS. 1998. Physicochemical Determinants of Stratum Corneum Permeation. In Roberts MS, Walters KA, ed. *Dermal Absorption and Toxicity Assessment*. New York: Marcel Dekker, Inc., pp 245-268.

77. Abraham MH, Chadha HS, Mitchell RC. 1995. The Factors That Influence Skin Penetration of Solutes. *J Pharm Pharmacol* 47:8-16.
78. van der Molen RG, Spies F, van 't Noordende JM, Boelsma E, Mommaas AM, Koerten HK. 1997. Tape Stripping of Human Stratum Corneum Yields Cell Layers That Originate From Various Depths Because of Furrows in the Skin. *Arch Dermatol Res* 289:514-518.
79. Williams ML, Elias PM. 1987. The Extracellular Matrix of Stratum Corneum: Role of Lipids in Normal and Pathological Function. *Crit Rev Ther Drug Carrier Syst* 3:95-122.
80. Mak VH, Potts RO, Guy RH. 1991. Does Hydration Affect Intercellular Lipid Organization in the Stratum Corneum? *Pharm Res* 8:1064-1065.

CHAPTER 8

SUMMARY OF MAJOR FINDINGS AND CONCLUDING REMARKS

The primary objective of this research was to investigate the possible mechanism(s) by which OS and PO facilitate the percutaneous absorption of fentanyl *in vitro* under the “finite dose” conditions that would prevail if the non-occlusive transdermal delivery of a drug was applied to humans *in vivo*. Thus, the following is a summary of only the major findings that were relevant to this objective.

8.1. POSSIBLE MECHANISMS BY WHICH OCTISALATE AND PADIMATE O FACILITATE THE PERCUTANEOUS ABSORPTION OF FENTANYL *IN VITRO* UNDER “FINITE DOSE” CONDITIONS

A) Octisalate and padimate O may alter the thermodynamic activity of fentanyl in the applied vehicle

It was demonstrated that compared to ethanol alone, OS and PO significantly enhanced the *in vitro* percutaneous absorption of fentanyl under finite dose at concentrations at or above 1%w/v and 5%w/v, respectively. It also appeared that the enhancing effects of OS and PO were related to their ability to modify the kinetics of fentanyl absorption as:

- i. when ethanol alone was used as the vehicle, the time course of fentanyl absorption appeared to follow a trend that was typical of “finite dose” conditions (i.e. there was a subsequent decline in fentanyl absorption after fentanyl flux reached an apparent maximum)
- ii. although the time course of fentanyl absorption still appeared to follow a trend that was somewhat typical of “finite dose” conditions, the magnitude of and the time to reach maximum fentanyl flux were both increased, and the subsequent decline in fentanyl absorption was not as evident when relatively low concentrations (1 or 2.5% w/v) of OS or PO were added to the vehicle
- iii. when relatively high concentrations (i.e. at or above 5% w/v) of OS or PO were added to the vehicle, the time course of fentanyl absorption appeared to follow a trend that resembled “infinite dose” conditions: after an initial

nonlinear phase in which the rate of fentanyl absorption gradually increased, maximal fentanyl flux across the skin remained relatively constant (i.e. fentanyl flux eventually reached an apparent “steady-state”).

In agreement with these findings, it was also found that compared with ethanol alone, the presence of OS and PO in the vehicle modified the distribution of fentanyl across human SC. The areas under the fentanyl distribution profiles reached a “maximum” within 0.5 h after the “finite dose” application of fentanyl in ethanol alone. However, after this initial “burst effect”, fentanyl concentrations within the SC, and particularly within the upper regions of the SC, subsequently declined over longer exposure times. On the other hand, when fentanyl was applied with ethanol containing 5%w/v of either OS or PO, the areas under the fentanyl distribution profiles remained relatively constant at all exposure times, which could be attributed to the fact that relatively high concentrations of fentanyl were maintained within the upper regions of the SC.

Not surprisingly, it also appeared that when ethanol alone was used as the vehicle, the clearance of fentanyl from the SC surface declined by a two-compartment process in which the amount of fentanyl residing at the SC surface seemed to plateau after an initial rapid decrease. On the other hand, the clearance of fentanyl from the SC surface appeared to follow a first-order process when OS and PO were added to the vehicle, suggesting that in the presence of OS or PO, fentanyl was continually being cleared from the SC surface. It is likely that these findings can be partly explained in terms of the different compositional changes that occur following the finite dose application of a volatile or a volatile: non-volatile vehicle system.

As discussed in Chapters 3 and 5, the complete evaporation of ethanol from the volatile: non-volatile vehicle system would have resulted in the deposition of an “enhancer film” at the SC surface, which is likely to have been supersaturated with fentanyl. When relatively high ($\geq 5\%$ w/v) concentrations of OS or PO were added to the vehicle, this “enhancer film” may have contained a sufficient amount of OS or PO to reduce the tendency of fentanyl to precipitate out of solution.

As evidenced by the fentanyl distribution profiles, it is likely that the maintenance of a diffusable source of fentanyl at the SC surface (that is available for partitioning into the upper layers of the SC) coupled with the high thermodynamic activity of fentanyl in

the “enhancer film” maintains a favourable SC-vehicle partition coefficient and, therefore, a high chemical potential gradient across the SC.

It was also demonstrated that the enhancing capability of OS was generally superior to that of PO under finite dose conditions. However, in relation to the interactive mechanisms of action that were investigated in thesis:

- i. OS and PO appeared to enhance the partitioning of fentanyl between human stratum corneum (SC) and water to a similar degree (statistically significant differences were not detected between the $ER(K_{SC/V})$ or $ER(K_{SC/W})$ values generated from the infinite dose diffusion studies and the SC-water partitioning experiments, respectively, at any given concentration of OS and PO)
- ii. compared to OS, PO appeared to exert a greater enhancing effect on the partitioning of fentanyl between IPM and water ($ER(K_{IPM/W})$ values generated for any given concentration of PO were greater than those generated for the same concentration of OS)
- iii. compared to OS, PO appeared to extract a greater amount of lipids from the SC surface at any given concentration investigated.

Thus, as the saturated solubility of fentanyl in PO was found to be ~26% higher than its solubility in OS, it would seem that the superior enhancing activity of OS under finite dose condition may be related, or partly related, to the likelihood that the thermodynamic activity of fentanyl in the deposited “enhancer film” containing OS was higher than that of fentanyl in the film containing PO. However, it was also found that that OS, but not PO, may reduce the conformational order of the superficial SC lipid bilayers. Thus, the enhancing capabilities of OS may also be related to this effect.

B) Octisalate and padimate O may increase the solubility of fentanyl in the stratum corneum lipids

It was also demonstrated that, under infinite dose conditions, OS and PO significantly enhanced the permeability coefficient of fentanyl at all concentrations investigated. Analogous to the concentration-dependent trends that were evident under

finite dose conditions, the ability of OS to enhance fentanyl permeation of human epidermis appeared to be linearly dependent on its applied concentration whereas a parabolic relationship was evident between fentanyl permeation enhancement and the applied concentration of PO. As similar concentration-dependent trends were also evident for the enhancement of fentanyl partitioning between human SC and water, it would appear that the enhancing effects of OS and PO can be largely attributed to their ability to increase the partitioning of fentanyl into the SC.

Due to the fact that the infinite dose diffusion studies and the SC-water partitioning experiments that were conducted both involved the use of skin samples that were *pretreated* with either OS or PO, it was evident that interactive (i.e. vehicle-skin) interactions were responsible for the enhancement of fentanyl partitioning into the SC.

Using OCT and IPM to simulate the chemical environment of the SC lipids, it was demonstrated that:

- i. the saturated solubility of fentanyl in OS and PO was greater than that in either OCT or IPM
- ii. based on the differences between the partial solubility parameters of fentanyl and CER-6, OCT, IPM, OS or PO it would appear that the higher solubility of fentanyl in OS and PO may be related to hydrogen bonding and/or London dispersion interactions.
- iii. the intrinsic partition coefficient of fentanyl free base between either OS or PO and water was greater than that between either OCT or IPM and water. The rank order by which the intrinsic partition coefficients decreased was the same as that for the saturated solubility of fentanyl in each of the organic phases (PO > OS > OCT > IPM)
- iv. both OS and PO enhanced the intrinsic partition coefficient of fentanyl free base between IPM and water in a concentration-dependent manner.

These findings may suggest that the effects of OS and PO on fentanyl partitioning into the SC are not only related to their ability to modify the physicochemical properties of the applied formulation (under finite dose conditions) but also to their ability to increase the solubility of fentanyl within the SC lipids. It may also be reasonable to hypothesise that the ability of OS and PO to increase the solubility of fentanyl within this

domain may related to their ability to shift the hydrogen-bonding and/or London dispersion solubility parameters of the SC lipids in directions that are closer to those of fentanyl. However, this notion requires further investigation.

As it was apparent from the IPM-water partitioning studies that OS and PO enhanced fentanyl partitioning into IPM in a concentration-dependent manner, it was somewhat surprising to find that although the *in vitro* topical bioavailability of fentanyl (in the presence of OS or PO), OS and PO remained relatively constant at all exposure times investigated, the distribution phenomena of OS and PO across human SC was different to that of fentanyl. In particular, it was found that the AUCs calculated for OS and PO in the upper regions of the SC declined whereas those calculated for the lower regions of the SC concomitantly decreased with increasing exposure time. On the other hand, the AUCs calculated for fentanyl in the upper and lower regions of the SC remained relatively constant at all exposure times investigated.

Although the different time-related trends in OS or PO and fentanyl distribution across human SC could be attributed to the fact that these compounds possess different physicochemical properties, they may also indicate that:

- i. under “finite dose” conditions, the ability of OS and PO to maintain a favourable fentanyl concentration gradient across the SC can be largely attributed to the possibility that OS and PO maintain a diffusable source of fentanyl at the SC surface that is available for constant partitioning into the upper layers of the SC (i.e. under “finite dose” conditions, the contribution of this effect to fentanyl permeation enhancement may be more significant than that of the effect of OS and PO on the solubility of fentanyl in the SC lipids)
- ii. other mechanism(s) (in addition to increased fentanyl solubility within the SC lipid domain) may also be responsible for the effects of OS and PO on fentanyl partitioning

C) Octisalate and padimate O appear to alter the content and/or conformational order of stratum corneum lipids

The ATR-FTIR analyses that were performed in order to investigate the effects of OS and PO on SC lipids demonstrated that both OS and PO reduce the lipid content of the superficial SC layers. In addition, it was found that OS, but not PO, may also reduce the conformational order of the intercellular lipid bilayers located within the upper regions of the SC (refer to Section 8.2). However, neither OS nor PO appeared to interact with carboxyl groups of lipid polar head-groups.

As it was evident from the tape-stripping studies that were conducted in conjunction with ATR-FTIR analyses that neither OS nor PO affected the areas or locations of the CH₂ asymmetric absorbances detected within the deeper regions of the SC, it would seem that the apparent lipid reducing and/or lipid disordering effects of OS or PO were mainly confined to the superficial layers of the SC, where SC lipid content, SC lipid fluidity and the concentrations of OS or PO within the SC are greatest.

Although these findings may infer that OS and PO might reduce the diffusional resistance of the stratum corneum, it was apparent from the data generated from the infinite dose diffusion studies that neither OS nor PO significantly enhanced the diffusion coefficient of fentanyl within the SC. Interestingly, however, OS appeared to reduce the amount and the conformational order of lipids located in the SC surface layers in a manner that appeared to be linearly related to both its concentration within the applied vehicle and the amount taken up into the superficial layers of the SC. On the other hand, PO appeared to reduce the lipid content of the SC surface layers to the same extent, regardless of the concentration within the applied vehicle and the amount taken up into the superficial layers of the SC (after a 2 h pretreatment time). As these concentration-dependent effects are somewhat consistent with those observed for the enhancement of fentanyl partitioning between human SC and water, it is worth mentioning that SC lipid extraction and/or perturbation have also been reported to enhance solute partitioning into the SC (1-6). Thus, it is possible that the apparent effects of OS and PO on SC surface lipid content and/or conformational order also contributed to their ability to promote fentanyl partitioning into the SC.

However, the ability of the diffusion model to detect changes in the diffusivity of fentanyl within the SC was questioned as it was also demonstrated that neither oleic acid

nor Azone[®] enhanced the diffusion coefficient of fentanyl within the SC, which was somewhat unexpected given that i) relevant concentrations of the enhancers were used and ii) it is well established that both enhancers perturb SC lipids. Although a number of possible limitations of the diffusion model were discussed in Chapter 4, it is to be noted that:

- i. in Chapter 2, it was demonstrated that OS increased the diffusion coefficient of fentanyl under infinite dose conditions following a 12 h pretreatment time. Thus, it is possible that although the apparent effects of OS and PO on SC surface lipids were evident within relatively short (< 2 h) exposure times, longer exposure times may be required before these effects alter fentanyl diffusion within the SC
- ii. the diffusion model may have accurately depicted changes in the diffusion coefficient of fentanyl. In which case, as mentioned previously, it is possible that the apparent effects of OS and PO on SC surface lipids may have contributed to their ability to enhance fentanyl partitioning into the SC rather than its diffusivity within the SC lipids (i.e. it is possible that OS or PO do not perturb the sites(s) within the lipid lamellae that impose the greatest resistance to fentanyl diffusion).

D) Differences between the apparent mechanism(s) of action of octisalate and padimate O

Given that the enhancing effects of OS on fentanyl permeation through human epidermis appeared to be linearly dependent on its applied concentration and that its effects on:

- i. fentanyl partitioning between either IPM or isolated human SC and water
- ii. SC surface lipid content
- iii. the apparent conformational of the superficial SC lipid bilayers

also appeared to be linearly related to its applied concentration (and for the latter two effects, the amount of OS taken into the superficial layers of SC), it would seem that all

of these mechanisms may have contributed to the enhancing effects of OS. However, given that:

- i. a parabolic relationship was evident between the applied concentration of PO and the enhancement of fentanyl permeation and partitioning between human SC and water, with maximum enhancement observed at 5%w/v PO
- i. the effect of PO on surface SC lipid content appeared to be saturated within the concentration range investigated (1 to 10%w/v)
- ii. PO appeared to enhance the partition coefficient of fentanyl between IPM and water in a manner that was linearly dependent on its concentration in IPM

it would appear that although the latter mechanisms may have contributed to the enhancing effects of PO, other factors may have affected its enhancing capabilities when relatively high concentrations (i.e. > 5%w/v) were applied to the skin.

Although it was proposed in Chapter 4 that the partitioning of PO into the SC lipid domain may have become solubility-limited at high concentrations, it was later demonstrated in Chapter 7 that the uptake of PO into the SC was linear with respect to its applied concentration. However, the disposition of PO within the intercellular lipid lamellae cannot be determined from ATR-FTIR data. Thus, it is possible that:

- i. at high enhancer loadings, the partitioning of PO to its site of action may become solubility-limited and/or
- ii. at high enhancer loadings, other forces may come into play that counter-act the enhancing activity of PO.

Furthermore, the possibility that OS, but not PO, may reduce the conformational order of the SC lipid bilayers could also be related to:

- i. differences between the chemical structures of OS and PO and/or
- ii. the possibility that, compared with PO, OS can displace lipid molecules by forming relatively strong hydrogen bonds with adjacent lipid polar head groups (assuming that the OS intercalates between the lipid bilayers or at

another site within the lipid lamellae that allows for this interaction)

Evidently, the differences that have emerged between the concentration-dependent effects of OS and PO may provide further insight into some of the interactive forces that govern their enhancer activity and, in light of the above-mentioned hypotheses, it may be necessary to investigate structure-activity relationships for OS and PO (and relevant analogues) in order to gain a better understanding of their mechanism(s) of action and the factors that influence their enhancer activity.

In order to facilitate, or rationalise, the use of OS and PO as CPEs, it may also be necessary to investigate their effects on the permeation, partitioning, and diffusion of a series of homologous compounds with different lipophilicities. For instance, if a parabolic relationship is evident between the applied concentration of PO and the enhancement of the partitioning and/or permeation of other lipophilic compounds (i.e. this “parabolic trend” is not specific to fentanyl permeation enhancement), it could be that the “optimal” concentration of PO for such compounds is of the order of 5%w/v. Furthermore, if PO renders the SC less permeable to lipophilic solutes at relatively high enhancer loadings, would the use of high concentrations (i.e. >5%w/v) of PO facilitate the percutaneous penetration of hydrophilic solutes?

E) The possible mechanism(s) by which octisalate and padimate O facilitate the percutaneous absorption of fentanyl *in vivo* : the relevance of *in vitro* data

It was demonstrated that the distribution phenomenon of OS across human SC *in vitro* did not correlate with its distribution *in vivo* at relatively long exposure times. In particular, it was found that *in vitro*, the topical bioavailability of OS remained relatively constant at all exposure times up to 16 h. This was mainly due to the fact that there was an accumulation of OS within the deeper layers of the SC as the concentrations of OS within the upper regions of the SC concomitantly declined. On the other hand, the topical bioavailability of OS *in vivo* decreased with increasing exposure time, which was due to the simultaneous depletion of OS from the upper and lower regions of the SC. Not surprisingly, it was found that the poor correlation between the distribution of OS across human SC *in vitro* and *in vivo* was in part due to a greater loss of OS from the SC surface *in vivo*.

Although the distribution of PO and the mechanism(s) of action of OS and PO were not investigated *in vivo*, it is apparent from these findings that a number of biological factors that influence percutaneous drug absorption *in vivo* would not exist (or exist to the same extent) *in vitro*. Consequently, it is difficult to extrapolate the significance of the mechanism(s) by which OS and PO enhance fentanyl permeation *in vitro* to that of the mechanism(s) that might prevail during the percutaneous absorption of fentanyl *in vivo*.

Given that the enhancing effects of OS appeared to be linearly related to its applied concentration and/or the amount taken up into the SC, it would seem, based on the *in vitro-in vivo* data generated from this research, that some of the mechanism(s) by which OS enhances fentanyl permeation of human epidermis *in vitro* may operate to some extent *in vivo*. On the other hand, the correlation between the *in vitro* and *in vivo* mechanism(s) of action of PO may be confounded by the fact that the enhancing activity of PO does not appear to be linearly dependent on its applied concentration and/or the amount taken up into the SC. For instance, given that PO appeared reduce SC surface lipid content to the same extent *in vitro* regardless of the amount taken up into the SC, it would be interesting to investigate this particular mechanism of action *in vivo*.

8.2. SUGGESTIONS FOR FUTURE RESEARCH

As numerous avenues for future research have been proposed throughout this work, the following paragraphs elaborate on some of the main suggestions that have been made and include some additional suggestions.

It has been particularly evident from this final discussion that further studies are required in order to clarify the mechanism(s) of action of OS and PO. As discussed in Chapter 7, further ATR-FTIR investigations may need to be conducted, using the perdeuterated analogue of OS, in order to confirm whether or not OS perturbs the organisation of the SC lipid bilayers and if so, by what mechanism(s) of action (for example, by increasing the fluidity of the SC lipids, by forming separate fluid phases in the "gel like" lipids, or by other mechanism(s) of action). Future investigations into the mechanism(s) of action of OS and PO would also be assisted by the use of other analytical techniques, such as DSC or X-Ray diffraction.

The possibility that the *in vitro* activities of OS and PO may not be entirely predictive of their enhancing capabilities *in vivo* highlights the importance of conducting future mechanistic studies *in vivo* – not only to elucidate the efficacy of OS and PO *in vivo* but also to establish whether the *in vitro* mechanism(s) of action of OS and PO are predictive for their activities *in vivo*. If further ATR-FTIR investigations are to be carried out *in vivo*, it should be noted for future reference that – as mentioned in Chapter 6 – the IR absorbances arising from human forearm SC *in vivo* were found to be ~10-fold less intense than those generated from excised human abdominal SC. Thus, as OS and PO generate strong IR absorbances that may interfere with those arising from components of the SC, it is advisable to use deuterated analogues during *in vivo* ATR-FTIR investigations¹.

Although some pertinent drug-vehicle-skin interactions were investigated in this thesis, it is likely that the “finite dose” application of a volatile: non-volatile transdermal formulation will result in a complex array of such interactions. Thus, in order to gain further insight into some of the possible mechanism(s) involved in the enhancement of fentanyl permeation under “finite dose” conditions, it may be necessary to investigate the interplay between the dynamics of each vehicle component (7). Investigations of this nature may also be aimed at achieving synergistic enhancement of fentanyl permeation. For instance, given that the enhancing capability of OS appears to be related to the amount taken up by the SC, can the vehicle be modified in order to increase the thermodynamic activity of OS in the applied formulation and hence promote its partitioning into the SC? What effect would this have on the kinetics of fentanyl percutaneous absorption? Given that the current research suggests that OS and PO enhance the partitioning of fentanyl into the SC, could the skin penetration of fentanyl be further enhanced by incorporating a CPE that has known effects on the diffusion coefficient of fentanyl within the SC? It is evident that this area of research will involve extensive investigations.

As previously mentioned, it may be necessary to investigate the enhancing effects of OS and PO on a series of homologous compounds with different physicochemical properties in order to facilitate their future use as CPEs. However, in relation to the scope

¹ It is for this reason that ATR-FTIR investigations into the effects of OS and PO on SC lipids *in vivo* were not conducted during this research.

of this research, it would also be interesting to investigate the feasibility of using OS and PO to enhance the skin permeation of other opioid analgesics that are structurally related to fentanyl. For instance, in terms of efficacy and safety, sufentanil is a good candidate for TDD as it possesses physicochemical properties that are amenable to TDD, due to its high potency, it would be expected that relatively small doses would need to be applied to the skin, and it has a very high therapeutic safety index.

Finally, as it was demonstrated in Chapters 5 and 6 that:

- i. a large portion of the initial dose of fentanyl, OS, and/or PO that was applied to the skin *in vitro* or *in vivo* remains on the skin surface after relatively long exposure times
- ii. losses in fentanyl, OS, and/or PO recovery could not be accounted for after relatively long exposure times

it may be necessary to investigate whether the non-occlusive transdermal delivery system can be optimised such that minimal amounts of drug and/or enhancer need only be applied to the skin surface in order to achieve the required transdermal delivery rate of the drug.

In conclusion, it is apparent that although this work has identified a number of areas for future research, it has also increased our understanding of some of the possible mechanism(s) of action of OS and PO and, in particular, some of the likely mechanisms by which they enhance the percutaneous absorption of fentanyl. It is also anticipated that the present research will assist the future design, development and optimisation of a non-occlusive transdermal delivery system that delivers a therapeutically relevant amount of fentanyl to the systemic circulation, and has the potential to provide sustained relief of chronic pain.

8.3. REFERENCES

1. Phillips CA, Michniak BB. 1995. Transdermal Delivery of Drugs with Differing Lipophilicities Using Azone Analogs as Dermal Penetration Enhancers. *J Pharm Sci* 84:1427-1433.
2. Surber C, Wilhelm KP, Hori M, Maibach HI, Guy RH. 1990. Optimization of Topical Therapy: Partitioning of Drugs into Stratum Corneum. *Pharm Res* 7:1320-1324.
3. Surber C, Wilhelm KP, Maibach HI, Guy RH. 1990. Partitioning of Chemicals into Human Stratum Corneum: Implications for Risk Assessment Following Dermal Exposure. *Fundam Appl Toxicol* 15:99-107.
4. Walter K, Kurz H. 1988. Binding of Drugs to Human Skin: Influencing Factors and the Role of Tissue Lipids. *J Pharm Pharmacol* 40:689-693.
5. Kurz H, Fichtl B. 1983. Binding of Drugs to Tissues. *Drug Metab Rev* 14:467-510.
6. Ogiso T, Iwaki M, Paku T. 1995. Effect of Various Enhancers on Transdermal Penetration of Indomethacin and Urea, and Relationship Between Penetration Parameters and Enhancement Factors. *J Pharm Sci* 84:482-488.
7. Hori M, Maibach HI, Guy RH. 1992. Enhancement of Propanolol Hydrochloride and Diazepam Skin Absorption *In Vitro*. II. Drug, Vehicle, and Enhancer Penetration Kinetics. *J Pharm Sci* 81:330-333.

APPENDICES

APPENDIX I.

Table A1. Technical feasibility of some opioid analgesics

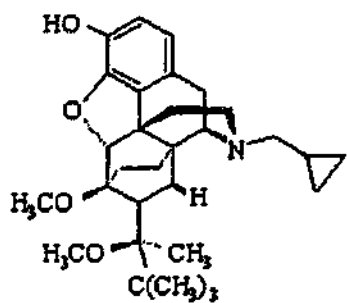
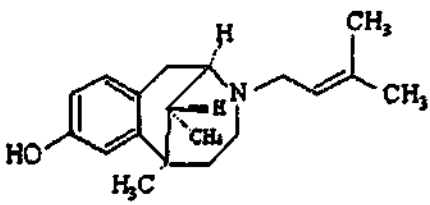
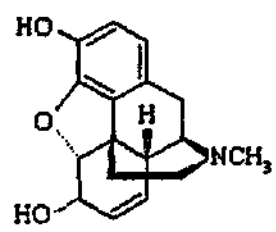
	Chemical structure	Daily dose	MW (Da)	MP (°C)	pK _a	Log K _{oct/w}	δ (MPa ^{1/2})	t _{1/2β} (h)	LD ₅₀ /ED ₅₀
PARTIAL AGONISTS Buprenorphine		0.9 – 2.4 mg IV/IM ^a	467.6 ^a	209 ^b	8.5, 10 ^c	3.08 ^d	20.7 ^e	1 – 7 ^e	7933 ^f
MIXED AGONISTS-ANTONISTS Pentazocine		180 – 360 mg IM ^a	285.4 ^a	~146 ^b	8.9 ^a	4.64 ^a	N/D	2 – 3 ^a	4 ^f
AGONISTS-Phenanthrene derivatives Morphine		10 – 330 mg IV (no standard dose in cancer pain) ^a	285.3 ^a	254 ^b	8.1 ^h	0.89 ^h	26.8 ^h	~1.7 ^a	71 ^f

Table A1 (cont). Technical feasibility of some opioid analgesics

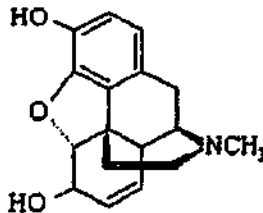
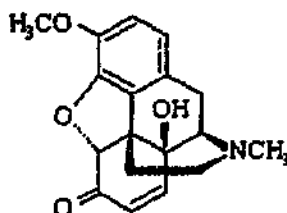
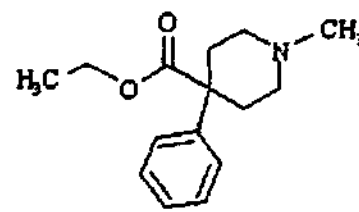
	Chemical structure	Daily dose	MW ^c (Da)	MP (°C)	pK _a	Log K _{OCTW}	δ (MPa ^{1/2})	t _{1/2β} (h)	LD ₅₀ / ED ₅₀
Hydromorphone		4 – 12 mg IV/IM ^a	285.3 ^a	~266 ^b	8.1 ^h	0.93 ^h	23.9 ^h	~ 2.5 ^a	LD50 (mice) (mg/ kg) = 61 – 96 IV ^f
Oxycodone		~20 mg PO ^a	315.4 ^a	~219 ^b	N/D	0.66 ^g	N/D	2 – 3 ^a	N/D
AGONISTS- Phenylpiperidine derivatives									
Pethidine		150 – 600 mg IV/IM ^a	247.3 ^a	35 ^h	8.5 ^h	1.6 ^h	19.6 ^h	3 – 6 ^a	8 ^f

Table A1 (cont). Technical feasibility of some opioid analgesics

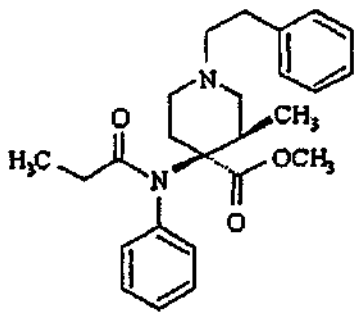
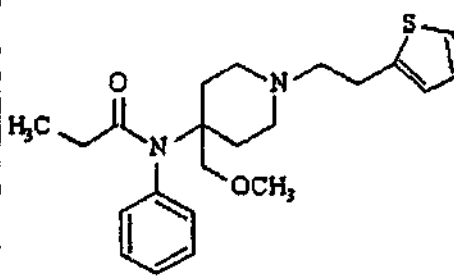
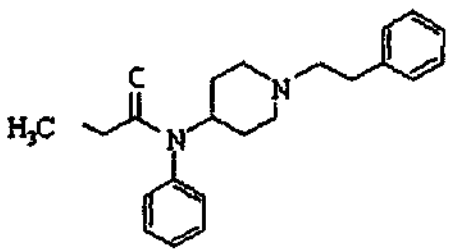
	Chemical structure	Daily dose	MW (Da)	MP (°C)	pK _a	Log K _{oct/w}	δ (MPa ^{1/2})	t _{1/2β} (h)	LD ₅₀ /ED ₅₀
Lofentanil		0.001 mg IV ¹	408.5 ¹	177 ¹	7.8 ¹	4.22 ¹	N/D	N/D	112 ¹
Sufentanil		0.08 – 0.8 mg IM (dose in cancer pain not established) ¹	387.5 ^h	97 ^h	8.5 ^h	3.45 ^h	19.8 ^h	~ 2.7 ^k	26716 ¹
Fentanyl		0.1 – 0.6 mg IV ¹	336.5 ^h	~84 ^h	8.9 ^h	2.91 ^h	20.0 ^h	~ 3.7 ^k	2727 ¹

Table A1 (cont). Technical feasibility of some opioid analgesics

ABBREVIATIONS

N/D Not determined

REFERENCES

- ^a Martindale The Complete Drug Reference, 32nd Edn, Pharmaceutical Press, London UK, 1999.
- ^b The Merck Manual An Encyclopedia of Chemicals, Drugs, and Biologicals, 12th Edn, Merck & Co., Inc, Rathway, NJ, USA, 1996.
- ^c Clarke's Isolation and Identification of Drugs in Pharmaceuticals, Body Fluids, and Post-Mortem Material, 2nd Ed, Pharmaceutical Press, London UK, 1986.
- ^d Roy SD, Roos E, Sharma, K. 1994. Transdermal Delivery of Buprenorphine through Cadaver Skin. *J Pharm Sci.* 83:126-130.
- ^e Stinchomb AL, Dua R, Paliwal A, et al. 1995. A Solubility and Related Physicochemical Property Comparison of Buprenorphine and its 3-Alkyl Esters. *Pharm Research.* 12:1526-1529.
- ^f Freye, E. 1987. Opioid Agonists, Antagonists and Mixed Narcotic Analgesics : Theoretical Background and Considerations for Practical Use. Berlin, Springer-Verlag.
- ^g Estimated using EPI Suite (v.3.11) computer software package (U.S. Environmental Protection Agency).
- ^h Roy SD, Flynn GL. 1989. Transdermal Delivery of Narcotic Analgesics: Comparative Permeabilities of Narcotic Analgesics Through Human Cadaver Skin. 6:825-832
- ⁱ Davis PJ, Cook DR. 1986. Clinical Pharmacokinetics of the Newer Intravenous Anaesthetics Agents 11:18-35.
- ^j Monk JP, Beresford R, Ward A. 1988. Sufentanil. A Review of its Pharmacological Properties and Therapeutic Use. 36:286-313.
- ^k Willens JS, Myslinski NR. 1993. Pharmacodynamics, Pharmacokinetics, and Clinical Uses of Fentanyl, Sufentanil and Alfentanil. *Heart Lung* 22:239-251.
- ^l Muijsers RBR, Wagstaff AJ. 2001. Transdermal Fentanyl. An Updated Review of its Pharmacological Properties and Therapeutic Efficacy in Chronic Cancer Pain Control. *Drugs* 61: 2289-2307.

APPENDIX II.

Table A2. Weight change of dessicated samples of isolated human stratum corneum before (dry weight) and after (wet weight) 24 h stratum corneum-water fentanyl partitioning experiments: skin left untreated or pretreated with ethanol alone or ethanol containing octisalate (per Chapter 4 (Section 4.4.2)).

Pretreatment details	No.	Dry SC weight (mg)	Wet SC weight (mg)	Fentanyl uptake ^a (µg)	Corrected weight change ^b (%w/w)
Untreated	1	3.00	4.70	49.91	55.00
	2	3.15	5.13	52.46	61.19
	3	3.32	5.73	49.60	71.10
	4	2.81	4.65	44.54	63.90
	5	3.07	5.05	48.87	62.98
0%w/v OS (Ethanol alone)	1	3.38	5.52	59.49	61.55
	2	3.23	4.02	55.70	22.73
	3	3.33	4.51	53.63	33.82
	4	3.45	5.78	57.45	65.87
	5	3.35	4.96	52.28	46.53
1%w/v OS	1	3.17	5.02	58.14	56.53
	2	2.72	4.50	53.10	63.49
	3	3.23	5.57	54.75	70.75
	4	3.56	5.91	44.52	64.76
	5	3.17	5.25	59.06	63.75
2.5%w/v OS	1	3.36	4.41	48.45	29.81
	2	2.96	4.22	46.74	40.99
	3	3.39	4.58	54.09	33.51
	4	3.05	4.98	44.58	61.82
	5	3.19	4.55	48.46	41.04
5%w/v OS	1	3.07	4.6	53.67	48.09
	2	3.44	4.33	51.72	24.37
	3	3.20	4.33	56.43	33.55
	4	3.32	4.98	56.28	48.30
	5	3.26	4.56	56.56	38.25
7.5%w/v OS	1	3.42	4.86	57.31	40.43
	2	3.45	4.28	60.48	22.30
	3	2.66	4.55	64.02	68.65
	4	2.98	4.66	63.72	54.24
	5	3.13	4.59	57.10	44.86
10%w/v OS	1	2.96	4.98	63.55	66.10
	2	2.95	4.33	68.42	44.46
	3	3.02	4.32	61.82	41.00
	4	2.99	4.54	58.92	49.87
	5	2.98	4.54	61.60	50.37
Mean ± SEM				49.88 ± 2.44	

^a Calculated amount of fentanyl taken up into stratum corneum after 24 h (refer to Chapter 4, Section 4.3.3.2)

^b Corrected for fentanyl uptake into stratum corneum

Table A3. Weight change of dessicated samples of isolated human stratum corneum before (dry weight) and after (wet weight) 24 h stratum corneum-water fentanyl partitioning experiments: Skin left untreated or pretreated with ethanol alone or ethanol containing padimate O (per Chapter 4 (Section 4.4.2)).

Pretreatment details	No.	Dry SC weight (mg)	Wet SC weight (mg)	Fentanyl uptake ^a (µg)	Corrected weight change ^b (%w/w)
Untreated	1	2.76	5.09	25.22	83.51
	2	2.69	3.8	19.93	40.52
	3	2.75	6.62	26.50	139.76
	4	2.73	5.17	23.88	88.27
	5	2.70	5.18	23.88	90.97
0%w/v PO (Ethanol alone)	1	2.84	6.79	26.03	138.17
	2	2.80	4.62	32.20	63.85
	3	2.91	6.62	28.58	126.51
	4	2.85	6.01	28.94	109.86
	5	2.85	6.01	29.91	109.83
1%w/v PO	1	2.73	6.21	31.47	126.32
	2	3.38	6.87	29.61	102.38
	3	2.94	4.64	20.76	57.12
	4	3.02	5.91	27.28	94.90
	5	2.98	5.90	25.88	97.12
2.5%w/v PO	1	2.83	5.6	45.30	96.28
	2	3.17	4.75	25.64	49.03
	3	3.55	5.57	43.34	55.68
	4	3.10	6.62	34.34	112.44
	5	3.16	5.64	37.16	77.01
5%w/v PO	1	3.24	8.8	40.90	170.34
	2	3.29	5.98	46.72	80.34
	3	3.55	5.19	52.21	44.73
	4	2.96	5.03	39.82	68.59
	5	3.26	6.25	44.91	90.34
7.5%w/v PO	1	3.04	5.83	43.34	90.35
	2	3.68	8.24	39.46	122.84
	3	3.48	7.29	50.51	108.03
	4	3.00	5.87	37.41	94.42
	5	3.30	6.81	42.68	104.99
10%w/v PO	1	3.32	7.70	42.35	130.65
	2	3.25	7.89	37.12	141.63
	3	3.02	6.06	42.24	99.26
	4	2.99	7.22	40.57	140.00
	5	3.15	7.22	39.98	128.19
Mean ± SEM				99.26 ± 5.21	

^a Calculated amount of fentanyl taken up into stratum corneum after 24 h (refer to Chapter 4, Section 4.3.3.2)

^b Corrected for fentanyl uptake into stratum corneum